REPORT DOCUMENTATION PAGE

Form Approved OMB No. 0704-0188

1. AGENCY USE ONLY (Leave blank)	2. REPORT DATE	3. REPORT TYPE AND DATES COVERED
	30 September 1995	Final Report

4. TITLE AND SUBTITLE

Experiemental Investigation of Supersonic Flows with Separated Regions in Ducts

5. FUNDING NUMBERS

F6170895W0266

6. AUTHOR(S)

Dr. Viacheslav Penzin

7. PERFORMING ORGANIZATION NAME(S) AND ADDRESS(ES)

Central Aerohydonamics Institute (TSAGI)
1 Zhukovsky St.1 Zhukovsky St.
140160 Zhukovsky

Moscow, Russia

8. PERFORMING ORGANIZATION REPORT NUMBER

N/A

9. SPONSORING/MONITORING AGENCY NAME(S) AND ADDRESS(ES)

EOARD
PSC 802 BOX 14
FPO 09499-0200

10. SPONSORING/MONITORING AGENCY REPORT NUMBER

SPC-95-4017

11. SUPPLEMENTARY NOTES

12a. DISTRIBUTION/AVAILABILITY STATEMENT

Dist "A"

12b. DISTRIBUTION CODE

13. ABSTRACT (Maximum 200 words)

As applied to supersonic diffusers of different purpose and scramjet engines separation flows in various geometry ducts are investigated. Flow Mach and Reynolds numbers at the entrance to the ducts ranged from 1 to 6 and from 4.10^5 to 7.10^7, respectively. The transition from supersonic flow to subsonic flow efficiency defined by the transition region length and pressure recovery. Separated and non-separated flow boundaries are determined. Hydraulic diameter concept expediency for separation flows analysis is appraised. Scramjet separation flows of different kinds were simulated. The influence on separation flows of such factors as off design modes of diffuser, combustors, non-uniformity of flow interaction of separated regions initiated by back pressure, secondary jets, cavities, struts and other kinds of elements of scramjet combustors are investigated. Several methods of separation control promoting flow stabilization and decreasing separated region lengths are offered.

14. SUBJECT TERMS	15. NUMBER OF PAGES 236
	16. PRICE CODE N/A

17. SECURITY CLASSIFICATION OF REPORT	18. SECURITY CLASSIFICATION OF THIS PAGE	19, SECURITY CLASSIFICATION OF ABSTRACT	20. LIMITATION OF ABSTRACT
UNCLASSIFIED	UNCLASSIFIED	UNCLASSIFIED	UL

NSN 7540-01-280-5500

Standard Form 298 (Rev. 2-89)
Prescribed by ANSI Std. 239-18
298-102

EXPERIMENTAL INVESTIGATION OF SUPERSONIC FLOWS WITH SEPARATED REGIONS IN DUCTS

V.I.PENZIN

Abstract

As applied to supersonic diffusers of different purpose and scramjet engines separation flows in various geometry ducts are investigated. Flow Mach and Reynolds numbers at the entrance to the ducts ranged from 1 to 6 and from $4\ 10^5$ to 7.10^7, respectively. The transition from supersonic flow to subsonic flow efficiency defined by the transition region length and pressure recovery . Separated and non-separated flow boundaries are determined. Hydraulic diameter concept expediency for separation flows analysis is appraised. Scramjet separation flows of different kind were simulated. The influence on separation flows of such factors as off design modes of diffuser, combustors, non-uniformity of flow interaction of separated regions initiated by back pressure, secondary jets, cavities, struts and other kind of elements of scramjet combustors are investigated. Several methods of separation control promoting flow stabilisation and decreasing separated region lengths are offered.

Table of contents

Symbols

a-velocity of sound
$\bar{b}$ -aspect ratio
c_f -skin friction coefficient.
H, h-step height, jet penetration depth.
L, l -duct length
M Mach number
n- index of power, number of orifices
p-pressure
Re-Reynolds number
S-asymmetry coefficient, distance between orifices
T-Temperature, Integral time scale
t-time
c_p-specific heat of constant pressure
D, d-diameter
x-co-ordinate
β-mass increasing coefficient
δ-thickness of boundary layer
δ^*-displacement thickness of boundary layer
ε_p-relative pressure pulsation intensity
ρ-density of fluid
λ-velocity coefficient
$Z = \lambda + 1/\lambda$ - impulse function
τ-shear stress
ζ-impulse loss coefficient

Subscripts

s-separation
w-wall
h-hydraulic
a-nozzle butt section

INTRODUCTION

A large number of scientific papers ,monographs [1,2] are devoted to the problem of the separation of fluid flows. This kind of flow take place in all branches of engineering connected with liquid and gas flows. Of particular complexity are inner separation flows.

Transition of supersonic flow to subsonic flow in ducts-supersonic diffusers - is an example of such flows. The aim of supersonic diffusers is to transform flow kinetic energy into potential energy and to increase pressure recovery. This pressure increase helps to discharge gases into atmosphere from aerodynamic facilities or gas-dynamic lasers and thus to ensure their operation under low pressure and rate of gases and in case of air breathing propulsion helps to increase thrust. However, pressure increase along the viscous gas flow creates conditions for flow separation and aggravates efficiency of the process. Systematic studies of transition from supersonic flow to subsonic flow in circular tubes (the process named afterwards 'classical' pseudo-shock) were initiated by the Neumann-Lustwerc's research [3]. Later a number of works connected with pseudo-shock were made. Complexity of the pseudo-shock flow is attested by the absence of methods to calculate structures of such flows. Available methods [2,4-7] can define only pseudo -shock approximate integral characteristics and in practice are not used because it is more convenient to use empirical formulas. As experimental investigations [8-10] have shown the complexity of deceleration of supersonic flow process sharply grows if rectangular ducts of large width to height ratio are used. The flow becomes non symmetrical with a train of three - dimensional boundary-layer separations along the narrow duct walls. The intensity of pressure oscillations grows considerably. Pressure recovery falls and the supersonic diffuser length required for the deceleration process completion sharply grows.

A variety of types and peculiarities of separation flows increases many times in scramjets and especially in dual-mode scramjets. Inlet, combustor and nozzle of this engine may have constant and variable geometry and section area , steps non streamlined bodies which are elements of the combustor. The front narrow part of the combustor at low Mach numbers is used as a supersonic diffuser and at high Mach numbers is used as a supersonic combustor. The supersonic/subsonic transition regions changes its place in the duct when flight Mach number changes and this process can be both in the narrow and wide part of the combustor. This leads to the change of flow conditions in front of these zones and behind them and accordingly to the change of the separated flow type. Interactions between separation regions due to heat release back pressure and separation regions due to steps, cavities, struts, secondary jets ets. may take place.

It should be noted that jet injection in scramjet may have different objective. So, blowing in gaseous fuel jets must provide good air-fuel mixing with air at minimal total pressure losses and separation region length. On the other hand if the objective of gas injection is the creation of a local region with high pressure and temperature, necessary to ignite fuel, separated flow zones and losses must be maximal at fixed gas rate in jets. Inner separation flow complexities make direct application of boundary layer theory or external flow stable viscous solutions impossible.

Present numerical and theoretical investigations are concentrated on Navier-Stokes solutions. Nevertheless, there are no satisfactory calculation method solutions for inner separation flows and experimental methods will hold their value for long. Unfortunately there is not enough experimental data about supersonic/subsonic transition flows that differ from classical pseudo-shock. There is also a lack of investigations of separated flows in ducts with steps, cavities , projections, secondary jets, etc. All this makes it difficult to calculate losses in a scramjet engine and its performance, to define

optimal engine geometry. The present work tends to somewhat fill up a gap in our knowledge of separation flows in ducts. Accumulated experimental materials on structure and particularities of separated flows on one hand can be useful for the elaboration of models and separation flow calculation methods in ducts and on the other hand can be useful in practical applications.

This work present an overview of author's experimental investigations published in articles and papers [11...34]. The sequence of the described investigations is as follows: at first, separation flows in constant area ducts with different, mainly, oblong section configurations. Influence of different flow parameters on the duct length which provides maximal pressure recovery is investigated. This parameters are: Mach and Reynolds numbers, boundary layer thickness, non uniformity of the flow at the duct entrance, different conditions of back pressure creation, hydraulic diameter concept application to separated flows in ducts. Possibilities of blowing in secondary jets with maximum and minimum total pressure losses, influence of jets on deceleration of flow in ducts are also examined.

The next part of this paper treats separation flows in ducts which have local widening and narrowing of cross section area. This duct cross section change are caused by idealised ramjet combustor parts intended for fuel injection ,air- fuel mixing and burning stabilisation. At first completely supersonic flows characteristics and momentum losses evoked by cavities, struts etc. are determined. After that supersonic/subsonic transition zones and nonsteamlined bodies and secondary jets interaction is analysed. Also as in the previous parts of the paper pressure pulsation characteristics are investigated.

The next part of the present paper is devoted to supersonic flow deceleration in diverging ducts. In scramjets these ducts may be smooth- widening and stepped ones. In the last case the separated flow behind the step can interact with separated flow evoked by thermal choking. Base pressure level in various geometry stepped ducts for different flow parameters is determined. Supersonic/subsonic transition flow in rectangular smoothly-diverging ducts is investigated in detail. Availability of subsonic flow in widening parts of the ducts allowed to consider these parts as a subsonic diffusers and to estimate the pressure recovery in them.

The analysis of supersonic flow deceleration permitted to suggest several methods of flow control which promote separated zones shortening, pressure recovery increasing.

The last part of the present paper is an annex in which several secondary effects initiated by separation flows and that can be used with profit are considered. In particular secondary jets influence on starting up flow-through modes and decreasing the duct drag are examined.

1. TEST METHODOLOGY

Separation flow investigations as applied to supersonic diffusers and scramjet combustors foresee specific approach to duct geometry and mode of flow selection. Reliable scramjet geometry and mode simulation is difficult to carry out due to absence of accomplished real scramjet engines. Therefore separation flow investigations were conducted with simplified models that permit nevertheless, we hope, to include most of the types of separation flow into consideration. The main aim of the exploratory experiments is to assist evaluating of the optimal performance of gas handling devices such as supersonic diffusers, scramjet combustors, etc.

1.1 Experimental models and apparatus.

Gas dynamic devices geometry is very diverse. So wind tunnel diffusers are invariably close to an axisymmetrical design i.e. either circular or square. Gas dynamic lasers and scramjet diffusers have oblong split-like cross section geometry. Scramjet combustors may be smooth or stepped diverging. Separation flows also can be induced by the combustor elements -steps, cavities, struts etc. This combustor elements and secondary jets in its turn change flow parameters in front of supersonic/subsonic transition separation zone. Separation flow properties depend on initial flow parameters including boundary layer thickness, shock systems. Gas dynamic laser diffuser initial flow is rather homogeneous, boundary layer is thin. Scramjet irregular flow is induced by the engine inlet, boundary layer is thick. Those factors not to be missed, the ducts were tested as in the free stream and

on direct connect technique. Experimental model and facility schematic diagrams are shown in Fig. 1.1.1 To make easier the comparison of flow deceleration efficiency of different geometry ducts it seems expedient to use at least in a first approximation the hydraulic diameter concept. This concept was a success in a drag law expression for non compressible liquid flow in various cross section ducts. To check this concept it is expedient the ducts of different cross section shape have equal hydraulic diameters and surface roughness. Rectangular duct cross section aspect ratio $\bar{b}$ determine effect of two-dimensionally of the flow on the pseudo-shock mechanism. Let us define $\bar{b}$ for all oblong cross sections as a duct cross section area S divided by the maximum height H raised to the second power. In rectangular cross section case $\bar{b}$ is a width to height ratio, in annular cross section- length of mean circle to the difference of radiuses ratio. The length of the duct of a supersonic diffuser must not be less then supersonic/subsonic transition region length the beginning and end of which is defined by the incipient pressure rise and the pressure maximum point respectively. But because of pressure recovery zone length strongly depends on geometry of duct cross section and is not known beforehand the duct length must be chosen with some excess. This excess to some extent does not affect the supersonic/subsonic transition zone flow. Figure 1.1.2 explains an approach to some near optimal constant area supersonic diffuser length determining. At low back pressures supersonic flow along all the duct length can be present only if it is not more then some maximal value -Lsm (supersonic maximal).Static pressure along the duct grows due to wall friction (curve 2). Duct length increasing above Lsm leads to formation of pseudo-shock which is travelling upstream till the entrance to the duct (curve 1). The length of the pseudo-shock in the aft part of the duct is small due to small Mach number there . It is maximal in forward position together with the required duct length- l_{max} . The pressure at the end of the duct practically does not change if the duct length varies in the range l_{smax}- l_{max} because of in this case duct outlet Mach number M=1 and velocity cross section profile is near uniform.

Pseudo-shock pressure distribution analogues to curve 1 can be received in short ducts under corresponding back pressures (curve 3). In this case the diffuser length is optimal, l_{opt} .So diffuser pressure recovery if it is evaluated on the pressure build-up in the duct end can change greatly if the diffuser length varied from l_{opt} to lmax and be lower then pressure recovery in an optimal diffuser. The limiting value of pressure drop corresponds to the ratio of pressures behind the normal shock wave at the duct entry and at the end of the duct where the flow accelerates to critical velocity value. Duct length shortening below l_{opt} also leads to pressure recovery drop. There is no necessity to define optimal duct length changing it step by step during experiments. It is enough to use a duct with a bit shorter then maximal length to define optimal diffuser length. Experiments show that pseudo-shock pressure distribution character does not change even if the duct length became less than optimal. It implies to ducts near axysimmetrical. In the case of ducts with oblong cross sections and non uniform flow fields such conclusion is not evident but as experiments show that it is also possible in some cases. In present work the duct length was equal or shorter then $40d_h$. It was enough to accommodate all kinds of separation zones which can occur at any flow conditions. Maximal length of duct section with supersonic flow depends on Reynolds number. In Fig. 1.1.3 distribution of average Mach number along the 45 calibre long tube is presented. It is seen that the increase of Re from 2.10^6 to $3.2.10^6$ leads to supersonic section increase by 15d. The pseudo-shock existence is caused exceptionally by friction. The length of pseudo-shock is less than 4d due to small M at the end of the tube.

Supersonic flows were formed by contoured nozzles having exit cross section diameter d=81.4 mm. The nozzles were connected either with the tube of the same diameter or the tubes with D = 134 mm. In direct connect tests the duct consisted of cylindrical and conical sections. The half angles of the conical sections were: 0.5, 11, 90^0. (stepped duct). The tube wall roughness was equal to k =15 mcm. In the case of free jet tests models were mounted in the 134 mm. diameter tube. The front model edges were sharpened on the external side so the flow entering the model was disturbed minimally. Geometrically defined nozzle Mach numbers were: 1.0, 1.5, 2.2, 2.6, 3.0, 3.08, 3.2, 3.8, 4.2, 4.5, 5.0, 5.5, 6.0. In the range Ma =2.2-3.8 the nozzles were contoured. The nozzles with Ma =1.5, 4.2 were conical with half angles 14^0. The rest nozzles were formed from the nozzle Ma =3.8 which was rearranged into ring-shaped nozzles by the use of conical bodies inserted along the nozzle axis. Mach

number fields in this case were non-uniform especially at Ma >5 due to air condensation and pressure shocks arising. A butterfly valve at the duct outlet allowed the pressure build-up in the duct to be controlled. The ejector helped to enlarge the Reynolds number range to Re = (0.4-7.0).10^6 . The air entering the nozzle had ambient temperature

The ducts with equal hydraulic diameters d_h=19 mm were considered basic. In their number there were three rectangular ducts with cross sections: 19 by 19 ,12,5 by 37.5 and 10.8 by 65 mm . They had aspect ratios $\bar{b}$=1, 3, 6 respectively. The ducts with segmental and circular-sector cross section also were basic. The duct sector angle was equal to =49^0 and 108^0 and aspect ratio $\bar{b}$=3, 6 respectively. The greater radius of the sector models was equal to that of the nozzle so model could be attached in such a way that the model wall became the continuation of the nozzle wall. In this case along the wide wall thick boundary layer (δ /r>0.1) entered the model. All basic ducts had identical length, l=600 mm. Inner duct wall roughness was k =3.0 mcm for rectangular ducts and k=5.2-5.5 mcm for the others. The ducts formed out of the main, 81.4 mm. duct (segmental, sectored) had near to basic duct parameters. Annular ducts were formed by mounting tubes of lower diameter into main tube concentricity. The inner tube entries were located either at the nozzle exit (tubes with sharp leading edges) or in the plenum chamber (tubes passed through the nozzle (M = 2.2)critical section and boundary layer accumulated on both walls). The second segmental duct was formed by means of the plate mounted parallel to tube axis. The plate was 450 mm long and this duct had 15 mm hydraulic diameter. The rectangular ducts with d_h<19 mm were formed out of basic 12.5 by 37.5 mm duct by placing on the lower wide wall plates of different geometry. There were plates making ducts with constant area and wedge-like inserts forming diverging ducts. The inserts geometry is given below. To evaluate the effect of corner shape on flow deceleration the duct with rounded corners was tested. Radius of rounding was equal to the half of the duct height. Besides, facility with changeable nozzles wind tunnel with variable nozzle was used. Mach number range of this facility was M=1.5-3.5. In Fig. 1.1.1 only part of ducts used is shown. Other types of ducts are described in the following chapters.

1.2 Flow modes and characteristics.

There are different ways of determination supersonic diffusers efficiency. In present paper it was evaluated by the ratio of maximal diffuser pressure to total pressure at the duct entrance $\overline{p_{\max}}$. Sometimes instead of total static pressure beyond normal shock wave was used. Pressure recovery in the case of direct-connect tubes due to friction is 5-8% lower then in the normal shock wave and practically equal to it in the case. of free flow tests. Pressure recovery drastically falls at high Mach numbers and d < 19 mm. This fact is connected with Reynolds number influence and discussed below. If wind tunnel and gas dynamic laser diffusers are used at design-mode of operation the dual mode scramjet with fixed geometry usually have off-design regime. In this case separation flow region can be far from the duct entrance, its location depends not only on the back pressure level but also on the duct geometry, availability of some protrusions and surface outline breaks. At equal back pressures the separation region location and its length in different ducts can change considerably. Taking this into consideration back pressure was changed in such a way that separation zone moved along the whole duct length. In ducts where pseudo- shock fixation was noticed small steps in back pressure changing were used.

Besides the throttling valve at the duct outlet cross jet injections was used -another way to simulate separation flows evoked by gaseous fuel jets injected into scramjet passage. Geometry and location of orifices for blowing in jets are given in the paragraph dedicated to the principle flow-secondary jets interaction. The static pressure distribution was measured along one, two or three duct walls in dependence on cross section geometry. The total pressure fields were measured by separated probes and rakes. In addition fields of intensity, and spectral characteristics of turbulent pressure pulsation were measured. For pressure measurements were used the complexes ИКД6ТДА. The precision of pressure measurements was + 1%. A traverse gear with a probe to measure pulsation characteristics was installed in the measuring unit. Figs. 1.2.1, 2- show parameters that characterise properties of flow expanding from the nozzles and spreading along the duct. These Figures illustrate Mach numbers

profiles in various duct sections for the two nozzle Mach numbers. At the bottom part of the Figure average and core Mach numbers defined using mass rate and static pressure are plotted as a function of relative distance from the nozzle. It is seen that at M =2.6 the duct length $l = 30d_h$ is near to maximal since average flow Mach number at the end of the duct outlet approaches the unit. In Fig. 1.2.2 the values of $\overline{\delta}$, $\overline{\delta^*}$, $\overline{\delta^{**}}$ are plotted as a function of $\overline{x}$. In some methods of pseudo-shock calculation (Ref. 6) the value of $\overline{\delta^*}$ is of importance. The profiles of turbulent pulsation intensity are shown in Fig. 1.2.2 for two stations of the duct and two values of M. In the flow core $\overline{\varepsilon_p}$=0.8-1.2%. Maximal values of $\overline{\varepsilon_p}$=4-5% are at $\overline{r}$ = 0.03-0.1 and depend mainly on wall roughness. .

The velocity profile measurements in the boundary layer (Fig. 1.2.3) showed that they are near to power dependence with exponent equal to n=1/6-1/8. The flow parameters in rectangular ducts including pulsation characteristics are presented in paragraphs 3.5, 4.3. The friction characteristics for supersonic and transonic modes of flow in ducts are investigated in Refs. 35 - 37. The nozzles with M >4 have peculiarities. They are annular, non contoured and there is possibility of air condensing in them. In Fig. 1.2.4 Mach number profiles at Ma = 5.5 received with the use of the total pressure rake are shown. The measured Mach numbers are noticeably lower than the designed values. The Mach numbers defined on wall static and plenum pressure ratio (dash line) are nearer to design Mach number. Fig. 1.2.5 illustrate Mach number fields at the end of the duct consisting of M 3.08 nozzle, lengthenig tube and conical section.

2. Separated flows in ducts with constant cross area.

Separation regions in supersonic flows in ducts arise, as in external flows, at sufficiently high positive pressure gradients. However, the length of separation zones in ducts lesser and recirculation may be absent. The angles of velocity inclination, except in short regions, are small and the flow can differ not much from one-dimensional one. For instance, blowing in cross gaseous jets into main stream evoke local flow separation with recirculation the length of which is only several diameters of jets. The jets rate growing above some limit results in disruption of flow mode and occurring of a pseudo shock flow in which recirculation in some cases may be absent.

2.1 Deceleration of a supersonic flow in ducts with various cross section configuration.

The flow structure strongly depends on duct cross section geometry. The development of separations in a circular tube is restricted and predicted most of all. The flow character in ducts with oblong cross sections depends on many factors such as aspect ratio, boundary layer thickness, initial flow non uniformity, etc. The rectangular ducts supersonic flow investigations (Refs. 8-10) showed that the flow deceleration in them can differ substantially from the flow deceleration in a circular tube where pseudo-shock realises in all cases. The flow becomes non symmetrical, three-dimensional separations occurs along the duct corners. In addition to high frequency oscillations low frequency oscillations the source of which is separation regions at the narrow side walls are added. However, notwithstanding to such deep alteration in the flow character the integral characteristics of flow such as pressure recovery and pressure recovery region length stay relatively small changed at a certain range of Mach number and aspect ratio change. Only at a certain combination of M and $\bar{b}$ there is almost shock-like change of flow character, long separation regions appear, pressure recovery drops and necessary for deceleration of flow the length of the duct rise.

Flow character change in a duct with oblong cross section resembles to some extent a flow character change in the subsonic diffuser when its diverging angle varies. When the angle is small there is non separated flow. After that, at greater angles the three-dimensional separation of the intermediate type with large pulsation occurs. At last, at still more greater angles there is stationary completely developed separation formed by turbulent reversed-circulate flow which in some cases can occupy all the duct. The reason of the difference in the flow character can be explained by the conditions of arising and developing of the boundary layer separation. The simplest case of a separation flow in a circular tube will be our initial concern

2.1.1. Ducts with circular cross section.

The separation flow of pseudo-shock type has been investigated most utterly in circular tubes. The beginning of the systematic investigations was laid by the work, Ref. 3 . At sufficiently large boundary layers and back pressures the flow which sometimes is called as "classical pseudo-shock" occurs. This symmetrical flow has two-layer character. As a result of interaction of the boundary layer and the central stream in the latter the train of oblique shocks occurs. The character of this flow depends on Mach number and boundary layer thickness. The main loss is concentrated in the near wall dissipation region. The pressure recovery in a pseudo-shock is near to that in the normal shock wave calculated using average flow parameters in front of it and the pressure recovery region length thanks to viscosity influence can reach ten and more tubes calibre. At the end of pseudo-shock the flow becomes near uniform.

Several integral methods were proposed for the flow parameters calculation in classical pseudo- shock , Refs. 4-7. The value of this methods is restricted because of impossibility to use them for calculation of non symmetrical flows with boundary layer separations which are common in practice. Besides, since parameters of classical pseudo-shock being investigated experimentally in detail, simple empirical relations are available. Some of this methods use an assumption about long separation regions presence in pseudo-shocks, others -about their absence. Nevertheless calculation results based

on both methods produced very near results having in mind pressure recoveries and the length of pseudo-shock. This fact can be interpreted in the sense that pseudo-shocks have both separation and non separation features. However, as experiments indicated, there are no long separation regions with reversed flows in "classical" pseudo-shock. The difference between separation and non separation flows can be easily established by comparison of static pressure distributions in these flows. For this purpose let us compare two flows in the same cylindrical tube: pseudo-shock and obviously separation flow in front of circular projection with rectangular cross section mounted on the tube wall. Fig. 2.1.1.1 presents the pressure profiles in both cases. The tube diameter is 81.4 mm, the step height is 4.2 mm. The flow Mach numbers at the entry to the tube are 2.6, 3.2, 3.8. The step was mounted on the various distances from the tube entrance section (l/d= 1.5-18) and was flown by the boundary layer with $\delta/d = 0.1\text{-}1.0$. In the last case the boundary layers closed. The pressure profiles in front of the circular step practically coincide with profiles in front of the analogues step on the flat plate which are well investigated (see Ref. 38). This fact disclose the character of the flow in front of the circular step. Independently of the step location in the tube the flow in front of it is of a separation type with the reversed flow the parameters of which are determined by Mach number. The plateau pressures in both cases also practically coincide. Analogues results were received with steps which heights were 1.2, 2.7, 5.7 mm. Then the step was removed and on this place the head of a pseudo-shock was moved by increasing the back pressure. So the pressure distribution was measured by the same apparatus through the same ports in the tube wall. The pressure distributions in pseudo-shocks are also shown in Fig. 2.1.1.1 The pressure profiles differ substantially. The pressure gradient in the case of separation flow in front of step is about three times as large as that in a pseudo-shock. There is also difference in the influence of Mach number on pressure profiles. In the case of pseudo-shock, in distinction from the separation flow, pressure distributions practically do not depend on M in the examined range on this number. In Figs. 2.1.1.2-4 pressure distributions in front of annular step and in pseudo-shock at different step heights and Ma are compared. Fig. 2.1.1.5 shows relative 'plateau' pressure dependence on mean Mach number.

Direct measurements of the flow fields in pseudo-shocks, Ref. 36, did not noted reverse flows. Lower pressure gradients in the head part of a pseudo-shock make it possible to state that in this case the inclination angles of the frontal part of the dissipation layer are lesser than in the case of Separation. To estimate this angle an oblique rake of total pressure tubes was manufactured. The entrance ports of this tubes were located on a straight line inclined to the wall at the angle of 6^0. The spacing between tubes was equal to 5 mm. At some value of back pressure the dissipation region begin to capture the rake. If the angle of the dissipation region is larger than the rake angle then the drop of pressure will begin earlier in the tubes located downstream (in the tubes distant from the wall) The distance between the two pseudo-shock positions in which in one case the dissipation region only toughed the rake and in other case occupied it in full lets to estimate the slope of this region. Evidently the rake pressure measurements were made with some errors thanks to the tube mutual interference but for the purpose of determination of the fact either the rake is in the dissipation region or not it does not matter. In Fig. 2.1.1.6 the results of experiments in which the rake was located at the distance of $14.5d_h$ from the tube entrance are presented. In this figure besides total pressure fields measured by the rake static pressure distribution are given.

Some characteristic positions of the pseudo-shocks and corresponding curves that are marked by the figures 1-3. can be noted. At the position 1 the rake is located in front of the pseudo-shock. The total pressure profile is determined by the boundary layer. The position 2 corresponds to the case when the rake is partially captured by the pseudo-shock. At last, at the third position the rake is captured by the pseudo-shock in full. Small movement of the pseudo- shock produces sharp change in pressure. The curve 2 existence says that the dissipation region slope is somewhat larger than the rake inclination angle but since for the full rake accommodation in the dissipation region the necessary pseudo-shock transition takes not more than 20-25 mm., it can be concluded that dissipation region angles do not surpass 8 or 9^0. It is evident that this estimation is very rough and determine only an average slope. Nevertheless this result confirm the suggestion that pseudo-shock dissipation region angle is less in comparison with separation region angle which is about 13^0. The absence of long regions with reversing flows confirm the test results in which friction force was measured. (Ref. 36) It was found

that resulting friction force in a pseudo-shock is directed downstream and approximately equal to the friction drag in the tube the length of which is equal to the length of pseudo-shock and in which flow is subsonic with the downstream the normal shock wave velocity. Local friction force measurements made by us using swimming element indicated in particular case negative value of this force. However, the analysis showed that in conditions of large pressure gradients the results of measurements are not dependable. This can also be said about analogues tests made in Ref. 39. The arguments stated above let to conclude that classical pseudo-shock can not be identified with free separation. It is more convenient to consider pseudo-shock separationless flow in contrast to the non symmetrical separation flow which occurs in ducts with oblong cross sections (see later).

In reality pseudo-shocks can contain short separation regions at certain Mach numbers and boundary layer thickness. Therefore carbon-oil visualisation shows the lines of separation and attachment (Ref. 9). The conditions at which separation regions in cylindrical ducts exit can be easily estimated. Suppose the cylindrical tube ends with the diverging section. In this section separation occurs if the back pressure rises. The flow in this case is the same as in an over expansion nozzle (Ref. 4). With the back pressure increasing the separation region shifts upstream and reaches the cylindrical section of the duct. If the walls in the diverging section do not restrict the separation region arising, the cylindrical section walls do it. Should the free symmetrical separation region in the tube with thick boundary layer occurred the choking of the flow would be inevitable. Stream line deviation contract the stream tube. The classical free separation region could exist only when its height is small (thin boundary layer) and there is no choking of the duct. The rise of the height of the separation region above certain limit invariably results in the flow rebuilding. The central high energetic stream interacting with the separation region presses it. The reversing flow zone dimensions reduces and at last fully disappear. At further pseudo-shock moving upstream the separation region can arise again as soon as the boundary layer become thin, not enough to chock the duct. Let us estimate the value of the boundary layer thickness at which free separation can exist. The separation region dimensions at a given Mach number and intensity of the incident chock that separate the boundary layer depends on the boundary layer thickness in front of it. It is known (Ref. 1) that the height of a separation region can be much more then the boundary layer thickness. On the other hand the height of the separation region that define the contraction of the flow can not be higher the value that define the choking. It is evident that the height of the symmetrical separation region must be wittingly lower than $h = R\,[1 - q(M)]$, where $q(M)$ is gas dynamic function, M - is mean value of Mach number in front of the separation region. This expression corresponds to the flow shockless decelerating up to the sonic speed in the channel formed by the circular separation region. The elementary calculation shows that for the range $M = 2.6$-6.0 the conditionally free separation can exist at $\delta < (0.08$-$0.15)R$, e.g. $\delta < 3$-6 mm. Suppose further that the length of the separation region can not be higher than the length of the free separation region. In this case, as it follows from Ref. 38 the height to length ratio $h/L = \sim 0.1$. That means that the length of the separation region can not be higher than 5-8% of the developed pseudo-shock length. If the dimensions of free separation region does not correspond to possible dimensions in the tube the flow rebuilds into one with a set of small local separations. This set is a source of intensive pressure pulsation's.

The zones with reversing flows in pseudo-shocks can be detected with the use of small probes of total pressure turned down the flow. In present experiments the 0.8 mm. diameter probes were located along the wall at the distance of 1 mm. from it. At the probe entry section static pressure p was measured at the wall. When the flow was not separated and there was no reversed flow the probes measured the base pressure - p_b . Total pressure fields at the end of the tube were measured as well. Fig. 2.1.1.7 shows distribution of p/p_t , $\Delta p = (p_b - p)/p$ and p_b/p along the tube at different back pressures. Here p_t is plenum pressure. Positive value of Δp at any section of the tube means presence of the reverse flow and separation. As it is seen from Fig. 2.1.1.7 when there is no separation the tubes turned down the flow register base pressure smaller than the ambient static pressure. The base pressure is in good agreement with the base pressure downstream of axisymmetric bodies in supersonic flow known from reference literature. Flow picture changes when there is a pseudo-shock in the tube. The build-up pressure region at the end of the tube contains separation which moves up the flow when the back pressure rise. However, even small propagation of the separation deep into the tube force it to divide into small parts. The picture resemble known from the Reference 6. At the further moving of the

pseudo-shock up the flow separation regions with reverse flows can disappear at some section and arise again when the boundary layer become thin enough. This supposition is confirmed by the pressure curve character in Fig. 2.1.1.7 which correspond to front part of the tube. This curves have gradient greater than that in classical pseudo-shock. When boundary layer is thick and Mach number is small reverse flows are absent. This follows from Fig. 2.1.1.8 analysis. In this Figure the curves are analogous to that in Fig. 2.1.1.7 but at $M = 2.6$ and $L = 11$. Using the diagrams of Fig. 2.1.1.7 it is possible to define the length of the separation region but very roughly due to small value of Δp and large distance between pressure tubes. The last circumstance might lead to exceeding the length of this region due to combining of two or several small regions or omission one of them. Nevertheless, it can be stated that the length of the separation region estimated in such a way is a little greater than that of free separation. This fact manifests more expressively in the case of short ducts when there is thin boundary layer (see later). Thus, it can be supposed that the length of separation region as in free flow depends on thickness of boundary layer but its height is lower. When concept of free interaction is working the separation angle and relative dimension of interaction region $\Delta x/\delta$ is practically independent on what causes the separation as well as Mach and Reynolds numbers. Should the pseudo-shock be a sort of a free separation its characteristics would not depend on the fixed back pressure of the duct geometry behind it. But it is not so.

Figs. 2.1.1.9 and 2.1.1.10 display results of experiments in which behind the tested tubes diverging sections were located. The diverging angles were $\theta = 0.5, 11, 90^0$.(sudden expansion). The tube length $l = (5\text{-}5.5)$ d. The thin boundary layer allows the separation regions exist. It was detected by the pressure tubes turned down the stream. In Fig. 2.1.1.9 experimental results are shown for two first values of θ at $M = 3.8$. It is seen that the flow character in the same tube, equal flow parameters at the tube entrance and back pressures which was assumed as static pressure on the wall at the end of the cylindrical tube depend on the geometry of the channel downstream of this tube. The angle θ increasing leads to pressure gradient and pressure recovery decreasing. The difference between curves becomes greater when boundary layer gets thinner, when location of separations is near the tube entrance. When the separation is at the back part of the tube the curves are practically merge. That says about small influence of the channel geometry on flow character in the case of thick boundary layer. as far as the possibility of separation is restricted. Thus it can be stated that at certain flow modes the flow structure in the tube is defined by vortex structure of flow downstream the tube and free interaction concept does not work. The pressure values measured with the use of Pitot tubes turned down the flow exceed static pressure at the tube wall. This indicates that separation region near the tube wall exist. If static pressure at the end of the tube is considered as back pressure it appears that the length of pressure upstream influence depends on the channel geometry behind the duct. At the lower part of Fig. 2.1.1.9 the curves $\Delta\bar{x}(p_b)$ are given. Here p_b is the value of back pressure. It is seen that at the duct length 5.5 d the difference in the upstream influence can reach one calibre. The character of curves $\Delta\bar{x}(p)$ is also different. In the curve corresponding to $\theta=0.5^0$. there is a loping region which says about flow transformation at certain back pressure that leads to some delay of separation transference. This kind of fixation takes place in the smooth cylindrical tube and is determined solely by inner structure of the flow.

In Fig. 2.1.1.10 analogues to Fig. 2.1.1.9 diagrams are presented. The decrease in Mach number (Ma= 2.6) assist in decrease of difference of curves and pressure upstream influence. At maximal back pressure there is a separation in the head part of the pseudo-shock) which is located in the region of thin boundary layer. As pseudo-shock moves down the flow in the region of lower Mach numbers and thick boundary layers the reverse flow disappear. This conforms with earlier made analysis. The scramjet passages are usually made slightly diverging for flow stability increasing. In Fig. 2.1.1.10 at $M = 3.8$ the pressure distribution in the conical duct with half angle $\theta = 0.5^0$. is presented. Downstream this duct the length of which is 5d the diverging section followed. In one case there was conical section with half angle 11.7^0. and in other case there was sudden expansion, $\theta = 90^0$. As in previous case the section angle increasing leads to pressure gradient and pressure recovery decreasing. The reverse flows are noted at all back pressures. The maximal exceeding of pressure measured by the Pitot tubes turned down the flow over the static pressure in the same section occurs at $\theta = 90^0$. that says about more

intensive vortex flow. . The filled total pressure profiles at supersonic speeds gradually transform into separating profiles with back pressure increase. However, in all cases the tube located at the distance h =3 mm from the wall showed the absence of reverse flow. This result confirm the previous estimates of the heights of separation regions.

To finish the description of special features of pseudo-shock in a tube describe in brief the flow separation directly behind the sharp cowl of the tube which has only indirect attitude to pseudo-shock. The flow with such a separation was investigated in Ref. 46 on the simple scramjet model. It was a section of a tube of 18 calibre long with sharp edge installed in supersonic Mach 2.5 flow. At the distance of 3d from the entrance there were orifices through which self igniting gas was supplied. The fuel equivalence ratio varying allowed to change back pressure and transit the separation upstream to be fixed on the sharp edges of the duct. Naturally there is no boundary layer upstream the separation. This is a basic difference of this separation flow from pseudo-shock. As the fuel supply increased the pressure in the separation region near the entry raised and reached the value three times larger than in the free stream separation (normal shock mode does not considered). This fact says about different nature of this flow, unlike the pseudo-shock which is defined by boundary layer. In greater detail this flow is investigated in Ref. 47 where indicated that if at the entrance of the duct there is some narrowing then the pressure rise in the separation can reach the value which correspond to maximal pressure behind oblique shock and clearly does not depend on viscous effects. In ducts with non axisymmetrical cross sections the flow of deceleration differ essentially from that in circular tubes. Even in the case of rectangular ducts with supersonic flow without shocks there is a pair of secondary vortexes which rotate in contrary direction and located symmetrically relative to bissectrise of the corner. As experiments with rectangular ducts showed there was no fixation analogues to that in the circular tube. In the corners of the duct there appear three-dimensional separations of boundary layer which can unite with outer flow. Trough these corners part of gas discharge out.

2.1.2 Rectangular ducts.

In distinction to a circular duct the limitation on separation arising in a rectangular duct is removed the more the aspect ratio is. Near narrow side walls and corners the thick boundary layer is accumulated. There a non symmetrical separation can occur when back pressures rises. The pressure rise in this kind of three dimensional separation is smaller than in a two dimensional separation. This separation can be considered as free separation if aspect ratio is large and because of this restricting influence of the opposite narrow side wall is not manifested. Notwithstanding to the large height of this one-sided separation narrowing of the cross section area it is not big enough to choke the flow. The more Mach number is the more probability of such a flow occur. It is possible that another separation zone can arise down the flow near the opposite side wall. Thus there is another, different from pseudo-shock, flow. To illustrate specific features of this flow let us consider static pressure distribution in the rectangular duct aspect ratio of which $\bar{b}$ = 6, hydraulic diameter d_h = 19 mm. and length l = 600 mm (Fig. 2.1.2.1). Mach number at the entrance of the duct was 3.8. Different curves correspond to different back pressures. The dashed curves correspond to the ducts with $\bar{b}$ = 3 and 1. They are placed for comparison and resemble pressure distribution in pseudo-shock in a circular tube very well. The curve character at $\bar{b}$ = 6 differ sharply. The pressure distributions measured along different sides does not coincide. For example, as it follows from Fig. 2.1.2.1b ,the pressure along the middle of the wide wall at the distance of $\bar{x}$ = 4-11 coincides with the pressure along the left narrow wall and at the distance $\bar{x}$ = 11-18 with the pressure along the right narrow wall. At the distance $\bar{x}$ = 18-20 it again coincides with the pressure of the left wall. The difference in position of separated regions along the left and right walls can be about two calibre's. In the curves there are some kind of plateau noted. If we symbolise the maximum plateau pressure as p_p and the pressure in front of separation as p_1 than for different variants of non symmetrical flow it appears just algebraic expression p_p/p_1 = 1 + M while for two-dimensional separation the expression is p_p/p_1= 1 + 0.5 M. (Ref. 4).

The flow character is very sensitive to pressure disturbances induced for instance by Pitot tube. The dashed curve in Fig. 2.1.2.1 corresponds to the case when a tube is absent. The length of pressure

recovery region in this case is much bigger than in the case of pseudo-shock (dashed lines). The duct length l = 30 d_h at M = 3.8 was not enough for accommodation of the pressure recovery region as a whole the pressure distribution in which has clear expressed maximum. One of the reasons of this lays in impossibility to bring the separation up to the duct entrance in contrast to circular tube. A small additional rise of pressure leads to swift upstream separation transition and flowing out some of the air into outer flow. More dependable data on the pressure recovery region length were received in the duct of 40 calibres length. The pressure maximum point in this duct was present in all cases and region length was determined. The examination of pressure distributions allows to make one more conclusion: the transition of the pressure recovery region downstream the tube where the boundary layer is thick and Mach number is small the transition of separation into pseudo-shock does not occur. Should there been thin boundary layer and the same average Mach number the pseudo-shock could be possible. Analogous results were received at Ma = 3.2 , 4.2 and $\bar{b}$ = 6. Only at smaller values of $\bar{b}$ (for instance at $\bar{b}$ = 3.9) the downstream transition of the separation region lets the pseudo-shock to occur. The estimates show that at $\bar{x}$ 10-20 the boundary layers are closed. Thus it can be concluded that arising of separation is affected not only by M and $\bar{b}$ but also by the non uniformity of the flow in front of separation. So an average Mach number can not be used in full measure as it done in circular tubes. The necessary length of the duct is larger than the separation region length. The difference between lengths is larger if the duct is tested in the free stream in contrast to connected pipe tests. In first case there exists laminar boundary layer in front of the tube.

It could be expected that if the duct corners are rounded off the transformation of the separation into pseudo-shock would be possible. However, the expectations did not realised. In Fig. 2.1.2.2 the pressure distribution along the duct remake of the rectangular, $\bar{b}$ = 6, duct is presented. The corners of the duct were rounded off over the all length except the front section. The duct entrance cross section was rectangular and than the radius of the rounding changed from zero to half height of the tube linearly. The dashed line correspond to the unaltered rectangular duct and is given for comparison. The presence of transient section induced a set of shocks initiating. In general the picture of flow with separations does not change. There is plateau and the length of he pressure recovery region is about 25 callibres. It is well to bear in mind that the curves presented in Fig. 2.1.2.2 are taken at Mach 3.2 which is near to that at which pseudo-shock occurs. As expected, at greater M the flow character did not changed. The pivotal role for the flow separation in the duct with oblong cross section has not the shape of the narrow side wall but the presence of the wall itself and thick boundary layer accommodation about it. The pressure recovery in this altered duct reduced due to the set of oblique shocks. In ducts with oblong cross sections the flow is more unsteady than in circular ducts and pressure pulsation's are higher.

The total pressure fields and dependences of total pressure pulsations on separation region position are presented in Fig. 2.1.2.3 The flow conditions are the same as in Fig. 2.1.2.1 . Here the pressure and its pulsation are related to the plenum pressure and local static pressure respectively. The pressure tubes were mounted stationary and pressure recovery region was moved due to back pressure change. So it was possible to measure the pressure pulsation in characteristic sections, say in a plateau region. The analysis of total pressure fields (Fig. 2.1.2.3 , $\bar{x}$ = 22) show that they are not symmetrical, near the side walls there are regions with zero velocities. The width of this regions is near 15 percents of the duct width. The presence of this regions to a large measure define the flow character. The dashed line corresponds to the open throttling valve and indicates that boundary layers are closed in the inspected section (critical mode occurs at $\bar{x}$ > 40). The supersonic flow core maintains up to the distance about 14 callipers (the average Mach number before separation is about 3) that is much more than in pseudo-shock. The total pressure pulsation measurements were taken in two sections: $\bar{x}$ = 15 and 22 .In the first section there were two total pressure tubes. One was located at the distance of 10 mm from the side wall and the other in the middle of the wide wall. In the second section the only Pitot tube was placed in the plane of symmetry. All the tubes were located at the distance of 4 mm. from wide wall. In Fig. 2.1.2.2 the values of relative pressure pulsation versus the distance between the tube and beginning of the pressure rise in separation are plotted. In the case when the pressure recovery region is located downstream the tube the values of x were considered positive and when it was located

upstream - negative. In the first case the values of $\overline{\varepsilon_p}$ were determined by initial flow turbulence induced by cowl edges and mainly by friction-of flow against walls. In the second case the tube lies in the region of boundary layer separation where total pressure pulsation increase sharply and vary with Pitot tube position - near the side walls they are on half order greater than in the middle of the duct. Maximal values of $\overline{\varepsilon_p}$ are equal 1.5 and 0.25 successively. In a pseudo-shock pulsations do not exceed $\overline{\varepsilon_p} = 0.2$. Such high values of $\overline{\varepsilon_p}$ near the side walls point to mighty pulsations of total pressure in the separation regions with reverse flows. At further upstream separation movement the relative intensity of pulsation drops but still remain rather high ($\overline{\varepsilon_p} < 0.2$).

The length of pressure recovery region is an important parameter characterising the effectiveness of flow deceleration. It is a regret that most experiments with oblong rectangular ducts as it justly said in Ref. 10 were conducted in ducts with not enough lengths to accommodate the developed separation regions. A long duct was investigated in Ref. 10 but there was only one combination of Mach number (5) and aspect ratio (3.8). It stayed unclear whether the separation flows indicated in Refs. 9 and 10 were determined by the M and $\overline{b}$ combination or by the duct length. In present investigations the duct lengths were enough to accommodate the full length of the pressure recovery region l including the sections with maximum pressure and negative pressure gradient for all combinations of M and $\overline{b}$. In Fig. 2.1.2.4 the length $\Delta\overline{x}$ is plotted as a function of $\overline{b}$ for indicated in Table nozzle Mach numbers Ma. Besides, there were used additional data corresponding to intermediate average Mach numbers in the region of $2.6 < M < 3.0$. These Mach numbers were received due to lengthening tubes put between the nozzle and the tested tube. The boundary layer increase resulted in average Mach number decrease. It should be also noted that the nozzle core Mach number was by about 0.1 lower than Ma. Fig. 2.1.2.4 large data disperse comes from difficulty of determining the longitudinal co-ordinates which correspond to pressure maximum and from impossibility to place the pressure recovery region exactly in the same position. Notwithstanding to this data scatter it is possible to do some conclusions. At Mach number Ma < 2.6 the pressure recovery region length $\Delta\overline{x}$ increases little when aspect ratio $\overline{b}$ grows from 1 to 7.4 and has the value of $\Delta\overline{x}$ = 10-15. At the same time in the region of Ma > 3 and $\overline{b}$ > 3 there occurs a sharp growth up to $\Delta\overline{x}$= 25-28. It allows to say about pseudo-shock transformation into the flow with separation. An additional increase in Ma or $\overline{b}$ does not change the length $\Delta\overline{x}$ significantly.

It was noted in Ref. 9 that at Ma = 4.5 the value of $\overline{b}$ = 3 is that at which the flow character changes. This result was received in a relatively short duct. The results of present work indicate that the decisive effect on the flow character has M and b combination but not the duct length. The results described above are true at number Re > 1x 0^6. At Re = 0.7x 0^6 a there occurs a laminar separation and the length of pressure recovery region grows up to $\Delta\overline{x}$ = 35. Fig. 2.1.2.5 presents the dependence of pressure recovery ratio Pmax/P_1 on aspect ratio $\overline{b}$. The increase of $\overline{b}$ leads at constant Ma and d_h (open symbols) to pressure recovery drop. This decrease can be estimated by the approximate relation: Pmax/P_1 = (Pmax/ P_1) $\overline{b}$=1x (1 - (M-2)/360x($\overline{b}$ - 1)) . Thus, hydraulic diameter concept can be used only for approximate estimates. The hydraulic diameter decrease (shaded symbols , dash-dotted lines) leads to additional decrease in ratio Pmax / P_1 for the most part due to effect of Re, relative displacement thickness of boundary layer δ^*/h and compatible with it non-uniformity of flow. The effect of δ^*/h on Pmax/P_1 was noted in Ref. 41. Equal drop in Re induced by total pressure drop or d_h reduction has different effect on Pmax/P_1.

2.1.3. Annular, Sector, Segmented ducts.

The characteristics properties of non symmetrical separation flows in rectangular ducts which are different from pseudo-shock on principle were analysed earlier. The same properties as three-dimensional separations of boundary layer and sharp lengthening of the pressure recovery region take place in the ducts having other shapes of oblong cross sections. At the same time in annular ducts the

height of which is many times smaller than their width the flow is near to pseudo-shock in circular tubes at all Mach numbers. On the upper diagram in Fig. 2.1.3.1 there are distributions of relative static pressure along the circular and annular ducts. The longitudinal co-ordinate x is related to the diameter of the outer tube. The open symbols and dashed lines correspond to supersonic flow along the whole duct and shaded symbols and solid lines - to pseudo-shock. There are two groups of curves which correspond to different back pressures. The inner tube installing which separates circular flow from the nozzle into two parts leads as expected to shortening of the pressure recovery region due to hydraulic diameter d_h drop. The difference between curves reduces if longitudinal co-ordinates are related to d_h of each duct but still remains. That says about hydraulic diameter concept restrictiveness. It should be noted that inner tube diameter change leads to average flow parameters change due to difference in the ratio of displacement thickness of boundary layer and the duct height. So for the ducts with d = 36, 48, 60 mm the average entrance Mach number calculated on static pressure and flow rate are 2.48, 2.36 and 2.15 respectively that corresponds to near 15% drop in pseudo-shock pressure recovery. A longitudinal partition mounted in the annular duct transforms it into a annular sector with the central angle of $\varphi = 360^0$. In the lower part of Fig. 2.1.3.1 there are pressure distributions along the two generatrixes of the annular duct (connected pipe) one of which is located just at the partition and the other on the opposite side of the tube (curves are marked by triangle symbols).At low back pressures when the front part of the pseudo-shock is located in the aft part of the tube with thick boundary layer the flow is non uniform. There is a tongue of boundary layer separation moving up the flow along the corner. When the head of the pseudo-shock is located in the front part of the tube where the boundary layer is thin the flow becomes even, the pressures on both generatrixes coincide, the classical pseudo-shock realises.

The pressure distributions in the annular sector ducts with other central angles are shown in the lower part of Fig. 2.1.3.1. The flow parameters at the ducts entrances are equal since their heights are equal. The duct cross section geometry can influence the flow character through different friction force due to different wetted surfaces. There are two types of curves: one is at equal back pressure ($\bar{p}$= 0.22) the other - at the same position of the pseudo-shock in the forward part of the tube. The curves correspond to the developed pseudo-shock. It can be concluded that at equal back pressures and hydraulic diameters the curve positions does not coincide. So, the hydraulic concept can not be used in full for pseudo-hock length determination. If the beginning of pseudo-shocks is placed at the same point ($\bar{x}$ = 3.3) the pressure distributions differ insignificantly. Because of friction influence the pressure recoveries does not coincide. The pseudo-shock length for all the ducts is about the same, $\Delta x/d_h = 7.7$. It can be noted that the pseudo-shock length in the annular duct at M =2.5 and $\delta^* / h = 0.022 - 0.026$ (Ref. 49) was about 7.2- 7.9. This says that results received in direct-connect and free-jet tests do not differ substantially. The influence of δ^*/h on pseudo-shock length is also small. In our case δ^* / h = 0.22.

The supersonic flow deceleration in the annular-sectoral duct free stream tests can be considered as an intermediate one between flows in rectangular and circular ducts. The flow can be as of separation and non separation type depending on the boundary layer thickness. It is clearly seen from Fig. 2.1.3.2 where the pressure distribution in the duct with cross section of annular sector ($\bar{b}$ = 6) is given. This is free stream tests at M = 3.8. The flow changed even if the pressure probe taking only 3% of area was inserted. When pressure recovery region is located in the front part of the duct where there is no pressure probes (curve 1) the flow is near to pseudo-shock. When the back pressure drops the character of pressure distribution changes (curve 2). In the forward part of the curve the pressure gradient does not differ from that of pseudo-shock. However, somewhere downstream the forward part there is some kind of plateau analogues to that in rectangular ducts. The pressure probe installed at one of the side walls assist in transition of pseudo-shock into separation flow (solid curves with symbols). The reason of flow character change is possibly bound with additional disturbances in the duct corners. The separation flow in forward part of the duct could be expected if the boundary layer thickness is increased. However, superposition of surfaces of the aerodynamic nozzle and the duct (larger radius) and increasing of relative boundary layer thickness up to $\bar{\delta}$ = 0.1-0.2 at the beginning of one of the wide walls does not change the character of flow deceleration (as well as in the case of annular duct,

see above). So an increase in boundary layer thickness on the wide wall does not lead to flow transformation because the reason of it is thick boundary layer at the narrow walls. The insert in Fig. 2.1.3.2 shows the total pressure fields measured by the pressure rake. An examination of the curve faired through the symbols indicates that at throttling valve fully open the boundary layer thickness in the direction normal to the narrow wall is equal to one and a half of the duct height. At some back pressure the stagnation zone occurs where static and total pressures are near equal. The root-mean square pulsation of the total pressure in this zone as experiments showed are lower than in analogues zones in rectangular ducts with $\bar{b} = 6$ and does not exceed 25% of static pressure of the incoming flow. This lends support to the validity of guesses that the flow in this type of duct is intermediate between flows circular and rectangular ducts. In Fig. 2.1.3.3 at M = 3.8 and 4.25 the pressure distributions along the duct which cross section is segment are given. At selected duct length ($l = 40d_h$) and inner surface roughness there is supersonic flow along the whole duct length. At Ma < 3.2 the duct does not start. At Ma > 3.8 in the forward part of the duct there is supersonic flow. The length of the pressure recovery region is in the range $\Delta\bar{x} = 21 - 27$ that is in accordance with the date for rectangular ducts with the same Ma and $\bar{b}$.

The length of the pressure recovery region in the segment duct formed by the tube surface (d = 81.4 mm) and a longitudinal plate at Ma = 3.8 and $\bar{\delta} = 0.1$ can be determined from Fig. 2.1.3.3 . There the pressure distribution in the sector duct (dashed line) at the same boundary layer thickness is also plotted. It is seen that in the segment duct separation flow is realised. Really, the beginning of pressure rise take place at $\bar{x} = 4$ (curve 1) and at the end of the segment duct the pressure only approaching the maximum. So the duct length chosen was not enough for the whole pressure recovery region accommodation. The region length was $\Delta\bar{x} > 26$. The increase in boundary layer thickness to $\bar{\delta} = 0.2$ made the flow unstable. Any small back pressure rise leads to the duct unstart , the leap of separation zone along the whole length of the tube. The pressure level in this case is near constant, $\bar{p} = 0.035$. The transition of pressure recovery region from the back position to the forward one or the other way circular makes the pressure distributions differ (curves 1 and 2).So, there is some kind of hysteresis. It should be noted one more particularity of the flow in the segment duct placed at the tube surface. If longitudinal co-ordinates are related not to d_h but to d then the curve 1 will be changed by the dash-dotted line which is near to pressure distribution in the pseudo-shock (two-dotted-dashed line). Is it simple coincidence?

2.1.4. Non uniform supersonic flow deceleration.

In technical devices the flow is always non uniform. It can occur due to models presence in wind tunnels, fuel struts in scramjet combustion chambers etc. Let us examine the influence of flow non uniformity on supersonic flow deceleration at first in circular tubes and then in the ducts with oblong cross sections. A pseudo-shock occurs when there is rather thick boundary layer and consequently the flow is not uniform in the section. The Ref. 3 investigations were made on the whole when the boundary layers were closed. Nevertheless it turned out that the pressure recovery is near to that in the normal shock calculated on average Mach number and depends little on boundary layer thickness. The influence of d on pseudo-shock length $\Delta\bar{x}$ is more substantial but still for approximate evaluations it can be considered as average Mach number function. It can be expected that the more powerful disturbance take place in the flow the more difference in pressure recovery and the length of this region is. In Fig. 2.1.4.1a the pressure distribution in the pseudo-shock in front of which the flow contains axisymmetrical pressure shocks is presented. Non uniform supersonic flow is formed behind the section of sudden expansion of the duct. The flow discharges from the nozzle d = 81.4 mm and M = 2.6 into the tube D = 134 mm. The average Mach number in the tube comes to 3.65. In the other case (Fig. 2.1.4.1b) with the nozzle Mach number 3.8 the tube d = 81.4 mm. was connected. The non uniform flow was formed due to injection of normal air jets through orifices placed evenly along the duct perimeter. Close arrangement of the orifices to one another produced circular separation of boundary layer and conical pressure shock. As distinct from the first case the flow average Mach number depends on injection mass rate. The non uniformity of the flow is made not only by the shocks but by

the jets themselves which turn in by 90^0 while interacting with the flow. The depth of penetration of the jets into the flow is about of 10% of the tube radius. The influence of the shocks on the flow parameters can be estimated when comparing pressure distributions in flows with different rate of non uniformity and equal average Mach number. The pressure distribution in Fig. 2.1.4.1a corresponds to the case when the pseudo-shock is located near the separated region induced by the step but does not join it. Comparison with the curve corresponding to pseudo-shock in uniform flow shows that incident shocks penetrates up to the wall distorting the usual character of pressure distribution but not the region length. The pressure distribution downstream the step or normally injected high-pressure jets has saw-like character. At lower pressure jets the pressure peaks are smoothed over, the oblique shocks in the core stream as in the classical pseudo-shock does not reach the wall, they are swallowed up by the dissipation layer.

Injection of normal jets leads to an increase in pressure recovery length (about 30%) and small decrease in pressure recovery. Thus it can be concluded that symmetrical disturbances of supersonic flow in circular tube does not transform pseudo-shock into separation flow. In Fig. 2.1.4.2 pressure distributions in the annular duct is presented. The non-uniform flow was produced by the conical, $\theta = 14^0$. nozzle. The pressure distribution is analogues to the case in which the flow from the contoured, Ma =3.8 entered. Examine now the influence of non symmetrical disturbances on pseudo-shock. It can be expected that in zones with low pressure the tongues of separations of boundary layer can penetrate and make the flow non symmetrical. The pressure distribution in circular tube with obstacle in form of segment and without it (dashed line) at Ma = 3.8 are given in Fig. 2.1.4.3 . The pressure in peaks exceed static pressure of incoming flow by 2.5 - 3.0 times. The pseudo-shock smooths out the pressure distribution like it take place in the case of axisymmetrical disturbances. But when the pseudo-shock is near the obstacle the pressure distribution keeps the saw-like character as it is at jet injection. The average pressure gradient in curves is near the same though there is some tendency of gradient decreasing in non uniform flows. The obstacle mounting decreases average Mach number from 3.5 to 3.3 and pressure recovery by 8%. The pseudo-shock length increased approximately by 20%.

The pressure distributions in Fig. 2.1.4.4 correspond to flow in tube with longitudinal partition of 450 mm. length which form segmented duct. The partition was mounted either just after the nozzle or at the distance of 450 mm from it so the boundary layer thickness in front of segmented duct was 4 and 8 mm. respectively. The length of segmented duct was $30d_h$ so the flow in it decelerated up to small supersonic velocities. The pressure at the outlet of the duct is nearly three times as much as ambient pressure. As it is seen from Fig. 2.1.4.4 the pressure distributions are near in all the cases. The pressure recovery region length nearly 20% larger then in the duct without a partition. Summing up the results of experiments in the tube with non symmetrical disturbances it can be concluded that this disturbances does not induce the transition of pseudo-shock into separation flow. The pseudo-shock length increase does not exceed 20-30%. At lower Mach numbers the changes in character and parameters of the flow are still smaller. Analogues results were received with the square duct. The unevenness of the flow in the duct with $\bar{b} = 1$ was created due to its inclination in by 2.5^0, (Fig. 2.1.4.5). The results of these tests were also used in methodical sense: the influence of an error in tube installation was estimated. It was shown that the angle of attack availability (Ma = 3.8) does not change the flow character. The pressure recovery dropped by 6%.

In the case of the duct with oblong cross section the influence of initial unevenness of the flow on flow character increases and there is possibility of transition of pseudo-shock into separation flow. This phenomenon can be shown while examining the flow in rectangular $\bar{b}$ =3 duct. When the flow at entrance is uniform the pseudo-shock is realising. The non uniformity of the flow was created by the wedges with the angle of 6^0. and height of 2 mm. mounted on the wide and narrow walls in the entrane section. The system of oblique shocks induced by the wedges speared down the flow. The width of the wedge was equal to the width of the wall (12.5 or 37.5 mm.). Besides, in another tests, on the wide wall a wedge of 15 mm. was mounted. In the last case the forces acting on this wedge were equal that acting on the narrow walls wedges. In Fig. 2.1.4.6 pressure distributions in the pseudo-shock in the duct with $\bar{b} = 3$ and wedges on wide and narrow walls are presented. These tests were intended to understand the orientation of shocks influence on flow deceleration. The curves in Fig. 2.1.4.6 indicate that the placing of wedges on wide walls produces nearly the same non uniformity of static pressure

like that made by wedges on the narrow walls. However, in the last case pressure recovery is smaller and the deceleration region is larger. The dashed-dotted line corresponds to the duct without wedges. It is seen that pressure gradients in both cases differ little. The pressure distributions that correspond to the wedges of 15 mm. and 37.5 mm. long have inflection points that is distinctive for separation of turbulent boundary layer by wedge and interacting shock. In these cases there is maximal divergence in pressure distributions along wide (open symbols) and narrow (shaded symbols) walls. In the duct without wedges there is no such divergence. The interacting shocks induce the pressure divergence even in the back part of the pseudo-shock where an average velocity is near critical. The difference in static pressure preserves when pseudo-shock moves down the flow.

In Fig. 2.1.4.7 the pressure distributions along wide and narrow walls of the duct ($\bar{b}$ = 3) with a wedge on the narrow wall at Ma = 3.2 and 3.8 are presented. The dashed line corresponds to the duct without wedges. From these Figs. one can see that mounting of a rather small wedge on the back wall caused large pressure unevenness especially along this wall (shaded circular symbols) at supersonic flow. When there is pseudo-shock (square and triangular symbols) the pressure distribution differ substantially from that in the duct without wedges (dashed line).

At Ma = 3.8 the flow can be considered as transitional from pseudo-shock to separation flow. There is an inflection point, the pressure recovery region length is about $18d_h$. In separation flow this value is near equal to 25d and in a pseudo-shock lesser than $15d_h$. The pressure recovery drops nearly by 20% in comparison with the case of wedge absence. The analogues picture is observed at Ma = 3.2 though the flow is near to pseudo-shock. Nevertheless, the length of the pressure recovery region because of the wedge presence increases approximately by 50%. The pressure recovery drops by 10%. Thus, it can be concluded that the boundary between pseudo-shock and separation flow received for uniform flow (see below) can somewhat change in the case of non uniform flow. The presence of shocks by the side wall can expand the region of separation flow in the direction of lower values of M and $\bar{b}$. The non uniformity of flow in front of the region of supersonic flow deceleration reduces pressure recovery.

2.1.5. About the boundary between separation and non separation flows in the ducts with oblong cross sections.

In Fig. 2.1.5.1 the values of lengths of pressure recovery regions are plotted as a function of flow Mach number in ducts with different cross sections tested in present work. The values of Mach numbers in front of pressure recovery region were calculated using static pressure and flow mass rate. When the pressure recovery region was located near the entrance to the duct it was considered that M = Ma. From Fig. 2.1.5.1, it is seen that in spite of large scatter of data due to difficulty to establish typical longitudinal co-ordinates the two branches of functions $\Delta\bar{x}$(M) can be selected. This branches correspond to pseudo-shock and non symmetrical separation flow. For both modes of flow the value of $\Delta\bar{x}$ practically does not depend on cross section shape. Thus, if the flow mode is known then the length of pressure recovery region in the investigated ducts can be approximately determined using the hydraulic diameter concept. The length of pressure recovery region of pseudo-shock first branch) is defined by relationship $\Delta\bar{x}$ = 15x(1- 1 / $M^{1.7}$) It should be noted that relation $\Delta\bar{x}$(M) for annular and circular ducts lays a little lower (dashed-dotted line in Fig. 2.1.5.1). For the regime of turbulent non symmetrical separation flow (second branch) it can be assumed: $\Delta\bar{x}$ = 25. At laminar flow(third branch) this value can reach $\Delta\bar{x}$ = 35-40.

In Fig. 2.1.5.2 the pressure recovery in examined ducts is plotted as a function of M. In the duct with square cross section pressure recovery is near to that in normal shock wave. As the aspect ratio $\bar{b}$ increases the pressure recovery reduces. Moreover, at some combinations of M and $\bar{b}$ there can be sudden change of flow character and transition of pseudo-shock into separation flow (compare curves with $\bar{b}$ = 3 and 6). For approximate definition of pressure recovery in different ducts ($\bar{b}$ = 1-6) the following relation can be used:

$p_m/p_1 = p_s/p$ x [1-0.015x (M - 1)] / [1- 0.006x($\bar{b}$ -1)] where p_s/p is pressure recovery in normal shock wave. If the flow regime is rated by the length of pressure recovery region (at $\Delta\bar{x}$ = 10-15 it is

pseudo-shock and at $\Delta\bar{x}$ = 20-30) then the results of experiments with ducts having oblong cross section allow define the regions of existence of pseudo-shock and separation flow. In Fig. 2.1.5.3 the open symbols correspond to pseudo-shock and shaded ones-to the separation flow. In this Figure. the reference data are also presented. From Fig. 2.1.5.3 it is clear that at $M < 2.5$ and any $\bar{b}$ only pseudo-shock is possible. It realises also if $\bar{b} < 3$. The transition region occupies narrow zone and it can be approximately substituted by the line:

$$M = 2.5 + 150.\bar{b}^{-4}$$

2.2 Separation flows caused by injection of secondary jets into supersonic flow in ducts.

As applied to scramjet the injection of secondary jets into supersonic flow can be considered in several aspects. First of all it is gaseous fuel injection from the orifices on combustion chamber walls or fuel struts. The jets can be inclined or normal to the principal flow. In this case the main objective is to get good air-fuel mixture at minimal total pressure loss. Then the injection of jets can pursue goals of formation of separation regions with increased pressure and temperature. In the first case the flow in diverging chamber can approach to the flow in constant area duct that assist to more stable chamber operation. In the second case the separation is created only for short time for inflaming the mixture e.g. for beginning of combustion. The objective of this operations is creating of separation region of maximal size at minimal flow rate in secondary jets. The secondary jets interaction with principal flow can have side effects So, the injection of high energetic jets from the duct walls allows to increase pressure recovery in the flow core. This can assist starting of models in wind tunnels or reducing of model's drag. The injection of low energetic jets approaching to injection through porous surface can contribute to reduction of wall friction and heat flux. At last, jet injection allows to simulate supersonic flow in ducts including pulse characteristics, mean Mach number and boundary layer thickness. From the said it follows that the way of jets injection, the size and location of orifices can vary essentially. Injection of isolated jets into free or half restricted space are investigated by many authors. In present work the interaction of group of jets that amalgamate on the short distance with the principal flow was analysed.

2.2.1. Injection and suction of secondary jets from the duct wall.

The separation flows induced by jets in ducts at low jet mass rates differ little from separations induced by jet's injection from surface in the free stream. An increase in mass rate can cause the pressure rise behind the jets and pseudo-shock appearing. The jets can be placed in front of a pressure recovery region, inside it and at last downstream of it. In the first case it can be fuel jets that reduce flow Mach number, making it non-uniform. The pressure shocks on the jets can be more strong then that in the core of the pseudo-shock being formed by the interaction of this core flow with dissipation layer at the wall. The local zones of higher pressure in front of a single jets are not obstacles that can restrict pseudo-shock upstream transition when back pressure increases. If jet is injected through an annular aperture it will induce circular separation region that can in certain range restrict the pseudo-shock transition, its shortening like it was with circular step. When jets are injected directly into pseudo-shock the depth of jet penetration reduces due to higher pressure however, there can be local contraction of flow and pseudo-shock splitting into several parts. Maximum pressure in each part is lower than in single pseudo-shock. The jets injected into supersonic flow and causing a pseudo-shock in front of them can be considered as a variant of throttle, fluid throttle. As applied to scramjet this effect can be useful for realising of inflammation of the fuel-air mixture in the combustion chamber. The gaseous throttle is maximally efficient at such arrangement of orifices that induce pseudo-shock at minimum jet mass rate. If through the orifices in the duct wall not to inject jets but to suck them then it can be expected that the pseudo-shock length gets shorter. It is known that full suction of boundary layer transforms pseudo-shock into normal shock wave. It can be expected that partial boundary layer suction through orifices in the duct wall can shorten pseudo-shock.
Experimental facility scheme is given in Fig. 2.2.1.1. The normal jets injection was performed from special injection section. The orifices were located evenly along the circumference in several rows (from 1 to 25). The number of orifices in the row- changes from 6 to 51, the orifice diameter from 1.7 to 3.5 mm. The distance between rows was from 5 to 120 mm. The scheme of arrangement of orifices is put in Fig. 2.2.1.1 and the number and dimension of orifices - in Table 1.

Table 1

varian	orifice dia	number of ori	N of orifices	number of	distance bet
1	2.0	51	51	1	-
2	2.9	51	51	1	-
3	3.5	51	51	1	-
4	2.0	51	17	3	5
5	2.9	255	51	5	5
6	1.7	153	51	3	120
7	2.9	255	51	5	60
8	1.7	150	6	25	5

Varying of the orifice diameters at equal mass rate allows to change jet total pressure as much as 8 times. The range of Mach number in front of jets was M = 1.8-3.8 and the ratio of boundary layer thickness to orifice diameter changed from 20 (closed boundary layers) to 1 when the jets were located near the duct entrance. The hot air (To = 800K) jets were injected from the set of orifices No. 4. At the end of the tube there was a conical section with the halfangle of divergence of 11.7^0. The plenum pressure was high enough to maintain supersonic flow along the whole duct. The axis jets injection was carried out from the circular step face 1.2 and 4.2 mm. height. The 4.2 mm. step was used for evaluating of the body" equivalent" to jets. Effect of jet injection on wall friction was investigated with the tube installed on the tension resistor balances. The air mass rate in the secondary jets was evaluated by the coefficient of heat and mass delivery $\beta\sqrt{\tau}$ Here β is a coefficient of mass increasing $\beta = (G+Gb)/G$, where G is mass rate in principal flow and Gb- mass rate in secondary jets $\tau=(T_s(\beta-1)+T_P)/\beta/T_P$ where T_s and T_p are total temperatures of secondary and principal flows respectively.

Experiments showed that four regimes occur as the jet mass rate increases. At small injection of low energetic jets the influence of walls can be ignored. (first mode). The flow approaches to the flow with air injection through porous wall i.e to separationless flow. As the jets injection increases the separation region in front of them arises. This separation does not differ from that on the plate and the pressure rise does not exceed the pressure rise in boundary layer separation (second mode). Oblique shocks caused by the jets can in some cases cause change in the picture of flow (curves 2, 3, 4 in Fig. 2.2.1.2, mode 3). Further increase in jet injection leads to regime 3 at which increased pressure is transmitted upstream at the distance greater then it take place in free flow and the pressure in front of jets can surpass the pressure downstream the normal shock wave. Still further increase in jet injection does not increase pressure in front of jets substantially but moves pseudo-shock upstream at large distances (mode 4). Depending on the jet total pressure duct pressure distribution character can change considerably (Fig. 2.2.1.3)

Depending on jet position pseudo-shock can arise up or downstream of jets orifices, be splitted on parts. (Figs. 2.2.1.4-6). Maximal pressure rise is reached when orifices are located at the duct end, minimal- when the pseudo-shock is splitted. The static pressure downstream the injection section can be essentially higher than the pressure in incoming flow. This is a distinctive feature of this flow in comparison with the jet injection from the plate in free stream. Fig 2.2.1.7 illustrate pressure distribution along fixed pseudo-shock depending on mean Mach number downstream the jet injection at different β. The pressure level at the end of the pseudo-shock is in good agreement with 1D calculations (Fig. 2.2.1.8). M-fields at the end of the tube and wall pressure distributions along diverging sections are shown in Figs. 2.2.1.9, 11. The pressure distributions upstream the step are in good agreement with those upstream the jets. This allows to use the model of equivalent body for evaluation of jet penetration depth . Fig. 2.2.1.12 shows the dependence of length of increased pressure region upstream the jets- $\Delta \bar{x}$ on the value of $\beta\sqrt{\tau}$ for several M_1. In the observed region of jet temperature the value of $\Delta \bar{x}$ does not depend on temperature. It is determined by the complex $\beta\sqrt{\tau}$. An exception is a regime with large $\beta\sqrt{\tau}$ (approaching to choking) at which the throttling effect of hot jets is higher. For evaluating of the length of the increased pressure region at $\beta\sqrt{\tau} > 1.05$ it can be used an empirical correlation:

$M_1/(M_1\text{-}1)\ \Delta\bar{x} = M_1\ [74(\beta\sqrt{\tau}\ \text{-}1.05)]$ here M_1 is Mach number in front of jets.

At $\beta\sqrt{\tau} < 1.06\text{-}1.08$ the flow picture is near to the case of free stream. The maximal value of $\beta\sqrt{\tau}$ (1.08) corresponds to orifice's set with maximal distance between orifices along the tube circumference. In this case the jets closing occurs later. So orifices disposition exercise influence on flow regime. The tube wall influence on flow character begin display at $\beta\sqrt{\tau}$ much less than that corresponding to sonic flow. At $\beta\sqrt{\tau} = 1.05\text{-}1.20$ the value of $\Delta\bar{x}$ increases from 0.2 to 5.5 and corresponds to pseudo-shock formation. At $\beta\sqrt{\tau}$ greater than $(\beta\sqrt{\tau})_{cr}$ the flow in front of jets is subsonic. Let us pay attention to influence of injection orifices disposition on flow regime. In Fig. 2.2.1.4 there are specific pressure distributions along the tube of 23.6 and 12.5 calibres long are shown. The jets were injected in several parts of the tube. The values of β larger than $(\beta)_{cr}$ correspond to pseudo-shock ($\Delta\bar{x}$> 0.8d), lower- to pseudo-shock absence. The curves scrutinising lets to conclude that chosen duct lengths at Ma = 3.08 do not restrict the transition of free separation into pseudo-shock. The latter arise earlier than the choking of the duct (in one-dimensional flow) occurs. Pseudo-shock arises in front of jets, then the flow accelerates just downstream the injection section and at last decelerate in the aft part of the tube. If this part is long enough there the second pseudo-shock occurs which up to certain value of $\beta\sqrt{\tau}$ does not interact with the first. The distances between orifices in variants 1-3 and 5-7 were near (s/d = 1.5) so jets merged and their influence on principal flow was the same as if the jets were injected from annular aperture. At bigger distances between orifices the jets acted as separate ones. The values of $\beta\sqrt{\tau}$ which limit the pseudo-shock arising at different s/πd (variants 1,3 and 8) are placed in Fig 2.2.1.13. Open symbols corresponds to pseudo-shock presence and shaded ones- to pseudo-shock absence. The symbols with dashes correspond to heated (T = 600-800 K) jets. The dashed lines restrict the region of values of $\beta\sqrt{\tau} = (\beta\sqrt{\tau})_{cr}$. Fig. 2.2.1.13 shows that the distance between orifices have large influence on pseudo-shock forming. In the examined range of s/πd variation (0.02-0.12) the jets mass rate at which pseudo-shock occurs changed more than by three times. Pseudo-shock at near placed orifices (s/πd =0.02) arose at mass rate three times lesser than maximal mass rate in one-dimensional flow (at M_1= 2.75, $(\beta\sqrt{\tau})cr$ =1.205). This orifices disposition is most favourite for flow throttling, for making the biggest separation region. It can be used for ignition of air-fuel mixture in scramjet, for instance. Another limiting regime at which the total pressure losses are minimal take place when the orifices are dispersed. But even at s/πd = 0.168 it was not possible to decelerate flow to sonic speed without pressure shocks. The separation flow in front of jets correlates rather well on $\beta\sqrt{\tau}$ and depends little on pressure and temperature of jets. In Fig. 2.2.1.7 the values of $(\beta\sqrt{\tau})cr$ are adduced. They can be considered as corresponding to injection through the aperture of different width. The sum orifices area changed by 10 times and total pressure in jets provided sub and supersonic gas exhaust.. The orifices area change have little effect on $(\beta\sqrt{\tau})_{cr}$ if distances between them are small. In Fig. 2.2.1.14 earlier received average values of $(\beta\sqrt{\tau})_{cr}$ are plotted as a function of Mach computed using mass rate and measured static pressure. It is seen that variants 1-4 differ relatively little in the observed range of Mach numbers and cause the pseudo-shock arising at $(\beta\sqrt{\tau})_{cr}$ much lesser than it could be in one-dimensional flow. In other words, because pseudo-shock springs up due to critical section existence, it can be concluded that the beginning of duct choking due to boundary layer separation start at mass supply in jets much less than it predicted by one-dimensional calculation. Fig. 2.2.1.15 illustrates the dependence of duct friction force on jet injection. There is a good agreement between experiment and 1D calculations.

The injection of longitudinal jets causes much less total pressure loss in comparison with normal injection. However, in this case pseudo-shock can also arise. It can occur due to expansion of jets after discharge and leaking the gas upstream that causes flow separation. It is possible that vortex structure downstream the injection section influences the flow separation like it was in the tube ending with diverging section (see above). As it is known (ref. 4) the full sucking out the boundary layer transform pseudo-shock into normal shock. In fact it corresponds to fluid streaming past the simple circular inlet

placed in the wind tunnel by supersonic flow on the regime of small mass rate trough it. It can be expected that sucking out of boundary layer not only in front of pseudo-shock but also inside it can shorten the length of region of transition of supersonic flow into subsonic. It can easily be done because of high pressure in this region. In experiments boundary layer was sucked through the set of orifices No. 4 (see Table 1). As it seen from Fig. 2.2.1.16 where pressure distribution is presented for the case without sucking and with it (about 2% of principal flow) the influence of sucking is small. The shortening of the region is not more than 15%. Sucking rate increasing up to 3% (due to larger orifices diameter) did not resulted in detectable change in pressure distribution. So the sucking of air out of the pseudo-shock is not effective means for shortening of its length and of increasing its pressure recovery.

2.2.2. Interaction of transverse jets with separation flow in ducts with oblong cross sections.

We will enlarge on the subject of the annular ducts. Let us pay attention at first on circular ducts. The scheme of experimental facility is shown in Fig. 2.2.2.1. Inside the tube, coaxial with it the tube of lower diameter is installed forming an annular nozzle and duct. The tube diameter, d_1 =26, 34, 49 mm, were chosen in such a way that Mach number calculated using ratio between areas of critical and exit section would be the same as in circular nozzles (Ma = 2.6, 3.2, 3.8). The section of transverse jets was installed either directly downstream of nozzle or behind lengthening pipe So the distance between the nozzle cut and the jet injection section could change discretely. The inner tube can move along and rotate around the axis in such a way that orifices on inner and outer tubes can be put in one or different cross sections, in the same or different meridian planes. The static pressure measurements were made along two generants. Because the number of orifices was odd the pressure distributions in one test can be measured in planes passing as through orifices and between them. It was done to discover the separation tongues coming between orifices. Maximal length of annular duct was 600 mm. Downstream this duct there was mechanical throttle installed. Hydraulic diameter of this ducts d_h used for normalisation of all dimensions was d_h = 55.4, 46.4, 32,4 mm.

We dwell first on characteristic features of flow in annular duct without jets injection. It was shown above that at Re < 0^6 the length of pseudo- shock is getting longer. Analogous effect has place in an annular duct. As one can see from Fig. 2.2.2.2 the length of pseudo-shock at Re = 1x 0^6 is three calibre's longer than at Re = 1.8x 0^6 which corresponds to automodel flow. The back pressure increasing and pseudo-shock approaching the entrance of the duct (curve 3) leads to boundary layer separation which transits to nozzle just as in the case of circular tube. The pressure distribution in pseudo-shock can change depending on whether it comes to specific position upstream or downstream, there is a gysteresis of flow. When moving from the nozzle down the flow the pseudo-shock length (curve 4) is larger.

Make now an estimate of influence of back pressure control technique on pressure distribution. It is known that in the case of free boundary layer separation the pressure distribution does not depend on the type of disturbance. The solid curves in Fig. 2.2.2.3 correspond to jets injection case. The place of injection is marked by the arrow on the axis x. The dashed lines correspond to the case of mechanical throttling and are taken from Fig. 2.2.2.2 (curves 1,2,3,5). Fig. 2.2.2.3 shows that at all values of mass increase coefficient β the pressure distribution character corresponds to separation flow in the ducts with oblong cross sections (see paragraph 2.1). As the back pressure grows the interaction region transits upstream and reaches the nozzle at β = 1.2. The tongues of separated flow between orifices were not detected. The use of mechanical throttle at Ma = 3.8 also can cause flow separation. However, pressure distribution characters differ substantially (compare curve 3 with curve β=1.17). At other β curves differ more. So, in an annular duct e.i. in a duct with oblong cross section but without corners (as, for instance, in a rectangular duct) possible separation of flow can occur depending on the back pressure control type. The existence of corners in the ducts with oblong sections is not the only reason for separation with reversed flow arising. Apparently, the flow stability, the possibility of separate parts of the region with increased pressure move upstream have some impact on separation of the flow . Analogues to Figs. 2.2.2.2 and 2.2.2.3 combination of curves but at Ma = 3.2

are placed in Figs. 2.2.2.4, 5 . Flow Mach number in front of jets due to friction drops to 3.0. Relatively low Mach number leads to pseudo-shock arising the length of which is, as in circular tubes, equal to $\Delta\overline{x} = 10$. The pressure distributions in both cases of back pressure way of control coincide. At equal numbers of orifices on inner and outer surfaces of the annular duct the distance S between them is different. So at n = 5 and orifice diameter d = 4.4 mm. the value of d/S = 0.086 and 0.145 for outer and inner surfaces respectively. At n = 11 and d = 3 the vale of d/S is approximately 1.5 times larger and at such close disposition the jets close quickly and the flows became two-dimensional. The increase or decrease of β can transform the flow from separation into non separation flow. The disturbed region of flow in front of jets has tongues of separation pushed forward only at small β. At larger β the jets operate as a single throttle, the influence of orifice disposition is small. At n = 11, jet injection from one or both surfaces simultaneously at Ma = 3.2 does not change the flow character. As in the case of circular tube the parameter $\Delta\overline{x} = \Delta x/d_h$ that characterise the supersonic flow and transverse jets interaction is used In Fig. 2.2.2.6 the relation $\Delta\overline{x}(\beta)$ is given for conditions Ma = 3.2 and n = 11 and two values of Re (scales along x are shifted). As Fig. 2.2.2.6 shows the increased pressure region length, as in the case of circular tubes, occurs at values of β much lesser than that of choking at one-dimensional flow ($\beta = 1.2$). The place of injection (inner or outer surfaces) have small influence on $\Delta\overline{x}$ - this value does not exceed 0.5-0.7 at $\beta < 1.15$. The change of Re in analysed range changes $\Delta\overline{x}$ only little. The comparison with data received in the circular tube (dashed line, Ma = 3.08) says that hydraulic concept is justifiable in this case. This conclusion is true for Ma = 3.8 as well. The position of orifices on the outer surface relatively to the orifices on the inner surface was changed due to longitudinal and rotate moving of the inner tube. The distance between injection plains was chosen equal to 0, 15 and 25 mm. At n = 5 the angle of rotating φ = 36deg. and at n = 11, φ= 16deg. Experiments showed that any change of relative positions of orifices comparatively little influence the value of $\Delta\overline{x}$. Nevertheless, it can be noted that at the fixed rate in jets the placing of orifices in one plane or in one section, one orifice opposite the other leads to separation region length increasing.

The rectangular duct investigations were carried out in free stream scheme. The injection of transverse jets was realised either through orifices in the duct walls or through the tubes projecting over the wall surface. In the duct with aspect ratio $\overline{b}$ = 3 the tubes were placed in one plane, 5 tubes on each wide walls. The tube height was 3 mm., the jets were distributed evenly (each tube supplied its square of area). In the duct with $\overline{b}$ = 6 all 10 tubes were placed on one wide wall. The tube height comprises h = 0, 3 and 5 mm, the tube diameter d = 1.5 and 2.0 mm., the tube wall thickness,- 0.15 mm. There also was investigated the injection through 20 tubes (10 tubes on each wall). The pressure taps were placed along three generants. The supposed internal flow model as with and without injection tubes is sketched in Fig. 2.2.2.1... It can be expected that jets-main flow mixing can take place at a shorter distance in the case of jet injection through tubes than through orifices in the duct wall due to larger surface of mixing. In present case the length of the duct downstream the injection section was more than 25 diams and there was full mixing for all variants of injection. As the injection increases the distance between pseudo-shock and jets decreases and interaction between separation regions induced by jets and pseudo-shock became possible. At the first sight it seems that this interaction must be more strong in the case of wall injection because of expanding jets that can cause more vast separation region than it exists before tubes.

The tube installing leads to additional total pressure loss and Mach number decreasing. At Ma = 2.6 and the tubes presence there critical regime occurs and pseudo-shock occupies essential part of the duct. With the tubes removed the supersonic flow along the whole duct length was maintained.. It is also seen from Fig. 2.2.2.7 that there is a point of tangent discontinuity at the place of tubes installation. The drag coefficient of cylinders mounted on the wall was C_x = 1.0-1.2. on conditions of present work. . There is no difficulty to calculate the flow parameters change downstream the tubes or jets using one-dimensional analysis. So full flow impulse downstream the struts and impulse function is given by respectively:

$$I(\lambda_2) = p_1 . F_1(1/r(\lambda_1) - C_x k M_1 . \overline{F_d}/2), \quad Z(\lambda_2) = Z(\lambda_1)/\beta$$

Here p_1, M_1, F_1, $\overline{F_d}$ are pressure, Mach number, duct area, and relative duct area. Knowing I(λ_2) and Z(λ_2) it is simple to define the value of M_2 and the degree of pressure rise p_2/p_1. This values are presented in Fig. 2.2.2.8 at various $\overline{F_d}$.The dashed line corresponds to the boundary of transfer from pseudo-shock to separation flow using relation $M = 2.5+150\bar{b}^{-4}$. As seen from Fig. 2.2.2.8 the struts installation or jet injection decreases Mach number and creates conditions at which flow separation at $\bar{b} = 6$ becomes impossible. At 10% duct area contraction by struts and $\beta >$ 1.1 simple one-dimensional analysis indicates that pseudo-shock can exist. A comparison between calculated and experimental pressure rises downstream the struts ($C_x = 1.2$, $\bar{b} = 3$, Ma = 3.2) is made in Fig. 2.2.2.7. There is fairly good agreement between both cases. Fig. 2.2.2.7 shows that pressure rise downstream the struts does not, as in the case of circular tube, influence the flow in front of struts as far as this flow keeps supersonic. The separated region induced by struts or jets prevents upstream pressure influence. Let us analyse now the interaction between pseudo-shock and separated regions in front of tubes and jets exhausted out of them. The pseudo-shock motion in present tests was also produced by throttling. Thus the full spectrum of possible flows with pseudo-shock was investigated. The coefficient β changed from 1 to β_{ma} at which subsonic flow dominated along the whole length of the duct. The curves of pressure distribution in a pseudo-shock at various β. are placed in Fig. 2.2.2.9 as an example. As tests show the tube installing does not prevent pseudo-shock up flow transition both in the cases of jets presence or absence and consequently does not shorten pseudo-shock length. The pressure gradient in pseudo-shock practically does not change when it crosses the section of injection. The high pressure regions are local, shock intensity sharply decreases in the space between struts where tongues of pseudo-shock apparently penetrates. It can be expected that at a more close strut spacing pseudo-shock fixation will be noted but such a spacing is not likely to have practical application. The jet injection from the wall instead the struts does not bring any qualitative alteration in the flow character. As at the struts presence the pressure increase behind jets does not influence up the stream at the injection section and at the same time jets are not an obstacles to pseudo-shock. Thus struts presence does not give any advantage in the sense of pressure influence up the stream in comparison with jet injection through orifices in the tube wall. As stated above in the duct with $\bar{b} = 3$ the struts presence and jets injection always secure pseudo-shock arising. At $\bar{b} = 6$ the situation changes and there is possibility of separation flow origin. The jet injection and struts mounting from one side promotes pseudo-shock arising due to decrease of Mach number and from the other side contribute to flow separation due to flow non uniformity increase. Fig. 2.2.2.10.. presents the pressure distribution along the duct with $\bar{b} = 6$ and struts placed at one of the walls at Ma = 3.8. At low back pressure here is a pseudo-shock (curve 1) at the end of the duct because the flow Mach number in front of it is lower than 3. At larger back pressures the pseudo-shock transform into separation flow due to larger Mach number in front of it. The pressure distributions along different generants (see dashed line) indicates that static pressure is not uniform in cross sections along the whole duct. It is clear that struts presence and jets injection through it does not lead to the separated flow transformation into pseudo-shock. Apparently the initial flow non uniformity has decisive effect on flow character compare to average Mach number decreasing. Considering the flow as one-dimensional in this case is not admitted. At Ma = 4.25 the separation flow character aggravates. Struts mounting at $\bar{b} > 3$ conduce to flow transition from separation into pseudo-shock. However, for realisation of this phenomenon the decreasing of Mach number must be bigger than in the case of uniform flow. The jet injection from the orifices in one wall unlike the injection through tubes induces flow separation. It can be supposed that the region of high pressure reaches corners with thick boundary layer and through it influences upstream at the injection section. So one-sided injection from the orifices in the wall at Ma > 3.8 does not change the flow character but conduce to its preservation. The jet injection from two wide walls (10 orifices on each wall) has better results. Figs. 2.2.2.11a, b (β=1 and 1.1) presents the pressure distributions along the duct with $\bar{b} = 6$ at Ma = 4.25 and at such throttle positions at which pressure influence distances are near the same. At the disturbances caused only by the throttle there are plateaus in the curves and pressure distributions along the different walls

do not coincide. When there is jets injection the pressure gradient increases, pressure distributions coincide. In other words the jet injection from two walls brings to flow transforming in pseudo-shock. However, this transformation take place at larger injection than it could follow from one-dimensional analysis. At this injection there is a pseudo-shock at the end of the duct even at the fully open throttling valve. Above the rectangular ducts in the uniform free stream were discussed. These ducts can be used as supersonic diffusers of gas dynamic lasers. The rectangular ducts can be also used as component parts of scramjet passage. In this case the incoming flow will be non uniform, with pressure shocks, thick boundary layer with separated regions. Still more complicated flow take place when there used not two-dimensional but three-dimensional inlet. The investigation of such flows deceleration in ducts with oblong cross section and jet injection presence have definite interest.

2.3 The use of hydraulic diameter concept for evaluating of supersonic diffusers parameters.

To express the drag law for turbulent flow of incompressible fluid in the ducts with non circular cross sections the drag coefficient related to hydraulic diameter (four times cross section area divided by the circumference) was introduced. In this case the drag laws for straight tubes with circular and non circular areas coincides notwithstanding to different velocity distribution. For instance, in corners of rectangular ducts rather high velocities due to secondary flows occur. The situation changes substantially if the flow is compressible and especially if the duct has oblong cross section. As was shown in Ref. 8 the supersonic flow deceleration in rectangular ducts at large Mach numbers leads to flow separation and the use of hydraulic diameter concept becomes unacceptable. At larger duct length as was shown above the length of pressure recovery region in first approach does not depend on the cross section shape and equal to $\Delta\bar{x} = (20\text{-}25)d_h$. This result can be interpreted as a particular case of hydraulic diameter concept display. It can be expected that the same can happen if the velocity go down and there will not be separations. Let us analyse the three possible flow sections in a supersonic diffuser. First of all consider the first section in which there is natural deceleration due to friction. The pressure distributions are not smooth due to nozzle profile defects and pressure shocks induced by the duct lips. Therefore the use of pressure coefficient $k_p = 2\mathrm{d}(p - p_1)/\rho w\ x$ which is usually applied for evaluations of incompressible flow characteristics in principle is inexpedient. However, the pressure oscillations at Ma> 2.6 take place around straight lines and pressure to a great extent smoothers at $\bar{x}>15$. That is why the pressure deceleration in ducts with different cross sections we shall evaluate in terms of p/p_{xo} in sections $\bar{x} = 15$ and 25. Here p_{xo} is static pressure at the beginning of the duct. In Fig. 2.3.1 the values of p/p_{xo} are given in terms of incoming flow Mach number. On the whole there are considered ducts with hydraulic diameter $d_h = 19$ mm. Besides there are data corresponding to connected pipes, $d_h = 19$ mm and also to rectangular ducts in free steam with $d_h = 9\text{-}15$ mm. As seen from Fig. 2.3.1 the dependence of p/p_{xo} on Ma as at $\bar{x} = 15$ and at $\bar{x} = 25$ laminate. The more d_h the more p/p_{xo} is. Besides the greater values of p/p_{xo} come out for circular duct with $d_h = 19$ mm (dashed line) the surface roughness of which is approximately twice to that of rectangular ducts. Several factors explain this lamination. As distinct from incompressible flow case the main part of the duct is occupied by the initial section of the flow. Because of boundary layer rise at this section the increase of pressure have to be greater than on the main section of the flow. At thin boundary layer at the duct entrance (duct in free stream) the roughness displays whereas at the back of the duct where the boundary layer is thick the duct surface can correspond to technically smooth surface. At tests on connected pipe scheme, a part of initial section is excluded that leads to the decrease in pressure rise as it follows from Fig. 2.3.1. The decrease in relative roughness due to big tube diameter is also conduce to pressure drop. The value of k_s/d_h can be considered as one of the principal factors defining the pressure increase in supersonic flow in ducts. The analysis of Fig. 2.3.1a allows to conclude that at Ma>2.6 the hydraulic diameter concept can be used for rough evaluations of pressure increase in the ducts with different cross sections only at similar relative surface roughness and flow parameters at the duct entrance. At low Mach numbers at which the flow approaches to blockade the pressure distribution along the duct becomes curved. In Fig. 2.3.1b the pressure distributions are plotted along

the circular duct and the ducts with circular sectors cross sections which were formed out of circular one with the use of longitudinal partitions. The annular duct was generated from circular tube due to thin-walled tube of smaller diameter co-axis installation at some distance from the nozzle end. The boundary layer accumulated in front of the circular duct entrance, so average Mach number of incoming flow was about 2.1 at Ma = 2.6. Hydraulic diameters of four ducts including circular and sector with angles φ = 360, 180, and 90^0 were successively equal to d_h=15.4, 15.0, 14.3, and 13.6 mm. The surface roughness, boundary layer thickness and Mach number for all ducts were similar. Nonetheless the difference in pressure distributions at large $\bar{x}$ is substantial notwithstanding to small difference in d_h (less than 14%). Thus, the use of hydraulic diameter concept is expedient if at Ma < 2.6 the length of supersonic section is larger than 3-4 duct calibre. Apparently, besides the relative surface roughness the value of p/p_{xo} is affected by the corner flow (see later).

Move on to the main section of diffusers- the pressure recovery section. In Fig. 2.3.2 the pressure distributions in the same ducts as in Fig. 2.3.1 at Ma = 2.2 and 2.6 are adduced. The back pressure was chosen in such a way that pressure recovery regions were near the duct entrance as much as possible and their beginning coincided for all ducts. The examination of Fig. 2.3.2 indicates that at Ma = 2.2 the pressure distributions practically coincides and, consequently, hydraulic diameter concept can be used as for pressure recovery and the length of this region evaluation. Somewhat comes out of general tendency the case of sector duct. It can be explained by larger surface roughness of this duct. At Ma = 2.6 the difference in pressure distributions is much greater. It can be said only about pressure gradients coincidence at the initial section. The increase in aspect ratio leads to pressure gradient and recovery decrease. The pressure recovery region length grows a bit. Now we move on to third section - the section with subsonic speed. The pressure distributions after the maximum pressure point depends on the length of the section from this point to the end of the constant area duct. If this length is big enough the pressure curve is near to straight line and apparently does not depend strongly on Mach number and duct cross section shape. This explains by relatively uniform and slow speed flow at the end of pseudo-shock. In the examined range of Ma = 2.2-4.2 this speed corresponds to M = 0.54-0.42. In Fig. 2.3.3 the pressure gradients dp/dx for third flow section are presented for ducts with d_h = 19 mm (free stream) and 81.4 mm (connected pipe). The data scatter is rather great and it is impossible to determine the gradient function of Mach number and duct geometry. The hydraulic diameter concept can be used only for rough estimations. The difference of pressure gradients at large difference of d_h is very substantial. It is possible that the main influence on pressure gradient exercises the value of relative surface roughness behind pseudo-shocks because the boundary layer thickness can be considered equal to zero irrespective of weather it is connected-pipe or free-jet tests. The value of dp/dx taken from Ref. 4.. is plotted in Fig 2.3.3. asa well. Agreement between the two results is not bad taking into consideration the tube diameter (25.3 mm). The possibility of hydraulic diameter concept use for pseudo-shock upstream transition evaluating as experiments showed is very poor.

2.4 The influence of Re number on flows in supersonic diffusers

It can be different depending on the duct cross section shape and length as well as on whether the duct is tested in free-stream or direct-connect scheme. As was shown in Ref. 50 the direct-connect tests of slot like rectangular ducts at M = 2.5-4.5 and Re < 10^6 the availability of thick boundary layer significantly impairs the pressure recovery. At Re < 10^3 there is no pressure recovery at all. The flow behaviour is analogues to subsonic one -the pressure contrary to supersonic flow drops along the duct. In this case the duct can not be considered as a supersonic diffuser. As Re gradually increases from 10^4 to 10^6 the pressure recovery increases being considerably lesser than in the normal shock wave. As rectangular duct flow investigations indicated (Ref. 39, $\bar{b}$ = 2, M = 3) this drop can be as high as 40%. This decrease in pressure recovery is possibly connected not only with thick boundary layer incoming from the nozzle but also with length of transition region due to laminar boundary layer separation. Unfortunately in Refs. 9, 10 there are no flow structure analysis.

In present tests the flow Re changed in the range of 4.10^5-5.10^6. We will enlarge first on the flow deceleration in circular and square ducts. In Fig. 2.4.1 the pressure distributions at the front part of the

tube direct connected to the nozzle are presented for two values of Re. The influence of Re is the more manifested the thinner the boundary layer is. In the rear part of the tube the boundary layer is thick and the influence of Re is small. The solid lines correspond to Re = 3.9 10^6 and dashed one -to Re = 7.10^6.As is readily apparent from 2.2.1 paragraph,- boundary layer separation is possible. It is seen from Fig. 2.4.1 that an increase in Re leads to pressure gradient increase in front part of the pseudo-shock. This high gradient keeps on if there is some shock moving downstream. The change in pressure profiles is most pronounced in its front part. It should be noted that pseudo-shock pressure distributions cited in references have as a rule smooth character with small variation in pressure gradient that can be explained partly by the absence of detailed pressure measurements. Pressure distributions of Ref. 49 is an exception. It was received at the front part of the rectangular duct with sharp edges in free M1.4 flow. This profile is much the same as in Fig. 2.4.1, Re = 3.9 10^6. At Re = 7.10^5, the same figure, in curves there are regions of small pressure rise or some kind of plateau. Possibly the shape of this curve segment is explained by the interference of pseudo-shock and boundary layer in the nozzle. Pressure gradients are minimal. At Re >1.5 10^6 the boundary layer is turbulent and pressure profiles change relatively little with Re increasing. At first profiles are of S-shape. Then they are continuously getting more monotone and at last , when pseudo-shock is near the entry to the duct there occurs some kind of plateau. Fig. 2.4.1 analysis allows to conclude that prehistory of generation and direction of pseudo-shock moving influences the flow character as well. The dashed lines correspond to pressure profile generated at downstream pseudo-shock movement and solid lines- at upstream moving. It is seen that in the first case the longitudinal gradients are lesser and pseudo-shock longer than in the second case. So, there is some kind of hysteresis. With boundary layer thickness increasing the value of hysteresis discrepancy falls. However, this phenomenon is detected at Ma> 3.8 up to δ< 0.5R.

It is observed in Fig. 2.4.1 that with increasing Re the pressure recovery increases. However, the difference in it is small as well as difference in pseudo-shock length. The pressure distribution in ducts with circular and square cross sections, d_h = 19 mm in free stream tests at Re = 5 10^5 and 6 10^5 are presented in Fig. 2.4.2. It is seen that transition to Re = 5.10^5 leads to sharp change of flow character, the pressure gradients fall. . Pressure recovery drops. It can be explained by the flow laminirisation. The duct length appeared small a little for full flow deceleration. However, an increase in length up to 60dh had failed to give positive result due to chocking of the flow that depends on duct length and surface roughness. So, at M>3.8, Re< 10^6 there is special type of limitation on pseudo-shock existence in the constant area duct. This limitation is connected with sharp increase of duct length required for flow deceleration at which invariably occurs the flow chocking due to friction against the duct walls. Another special feature of the pseudo-shock at Re<10^6 and Ma>3.2 is the possibility of the rise of such flow type at which more intensive pressure shocks exist. This phenomena is illustrated by Fig. 2.4.3 in which pressure profile is rather sow-like than monotonous. The average gradient falls and transition region length increases up to Δx=(20-25).d_h e.i. to values corresponding to the separation flow in slot-like ducts. Such kind of flow occurs at Ma = 3.8 at reverse throttle moving and at Ma > 3.8 at the straight throttle moving as well.. In Fig. 2.4.4 the pressure distribution along the duct with $\bar{b}$ = 3 (d_h=19 mm) at Ma = 4.25 are presented. Earlier it was indicated that at $\bar{b}$>3 and Ma>3 separation flow occurs if back pressure rises. The value of $\bar{b}$=3 is near to the ultimate value of $\bar{b}$ at which the required duct length is still be as high as 10-15d_h. Fig. 2.4.4 illustrates that at Re = 5.10^5 the length of required duct is above 20.d_h and there is a plateau in the curve. It can be considered that number Re decreasing attests to flow character transition from pseudo-shock to separation flow at $\bar{b}$<3. But this transition is not distinct. From the developed pseudo-shock it differs by relatively small plateau (compare with Fig. 2.4.1). Besides, the difference between pressure levels along different generatrixes is smaller then in separation flows described earlier.

Finally we shall deal with Re number influence on flow character in ducts with b>3 at Ma>3. In this case at any Re there is non symmetrical, separation flow region, 20-25 d_h length. Additional decrease in Re was gained by the sacrifice of the duct height with the duct width fixed. The drawback to this technique is in impossibility to determine Re influence uniquely. As it was shown earlier the increase

in $\bar{b}$ at constant Re leads to pressure recovery drop. Concurrent increase in $\bar{b}$ and decrease in Re makes the pressure recovery drop more sharp. In Figs. 2.4.6 and 2.4.7 pressure distribution along the duct with $\bar{b}>3.9$ and d_h = 15-8.8 mm at Re = (0.7-1.5) 10^6 are presented. There were two variants of ducts, 400 and 600 mm long. In the first case the duct was stepped and the throttle opened. There was supersonic flow along the whole duct. Inspection of curves corresponding to the mode with raised back pressure discloses that all values of $\bar{b}$ (>3) the flow is separated. The length of transition region is $\Delta x = 20\text{-}25\ d_h$. At larger values of $\bar{b}$ separation region exists at any part of the duct (see Fig. 2.4.7 , $\bar{b}=7.4$). At lower $\bar{b}$ the transition of this region downflow makes flow transformation possible (see Fig. 2.4.4)

At Re<1.10^6 another type of transition exists. In Figs 2.4.8 and 2.4.9 pressure distributions at Ma = 4.25, $\bar{b}=6$ and 7.4 are also included. The duct heights were 5.2 and 8.8 mm successively. There was no throttling. The change of Re was performed due to total pressure change. Pseudo-shock moved upstream when the total pressure got down. Pressure data in Figs. 2.4.8, 9 reveal that an increase in static pressure take place along the whole duct length $\Delta x = 40 d_h$. At $\Delta x = 60\ d_h$ the pressure recovery region moves upstream and becomes open to the outer flow. So, the duct length $\Delta x = 40\ d_h$ in this case is near to critical one. The same phenomena at this Re, as was shown earlier take place with circular and square ducts. The use of the duct with $\bar{b}=7.4$ has brought about additional change in the flow character. This duct was 5 mm height and 400 mm long at front part and 12.5 and 200 mm at the rear. As in the case of $\bar{b}=6$ in the section of sudden expansion there is flow acceleration and then flow deceleration in the set of shocks. But in the case of $\bar{b}=7.4$ the pressure increase takes place when the pressure in the wide part of the duct is lower than in the narrow part. This says that pressure rise in case of $\bar{b}$ = 6, 7.4 is not connected with back pressure in directly but occurs due to internal processes taking place in the narrow part of the tube.

Figs. 2.4.5 and 2.4.10 summarise the influence of Re and $\bar{b}$ on diffuser efficiency. At the last diagram the values of pressure recovery normalized by that in normal shock wave versus Re are presented for rectangular ducts with different $\bar{b}$. Due to large scatter of data it was impossible to select curves for each value of $\bar{b}$.The field was broken up into four envelopes- $\bar{b}$ = 1-3, 3-4, 5-6, 7.4. It is seen that pressure recovery in the ducts with $\bar{b}$ 1-3 in all the range of Re is near to pressure recovery in the normal shock wave (90-100%). The influence of Re is more substantial for the ducts with $\bar{b}>3$ and Re $< 2.10^6$. At $\bar{b}=3\text{-}4$ and 5-6 pressure recovery comprises 80 and 70% successively. At $\bar{b}=7.4$ pressure recovery drops considerably and comes to only 25% of the normal shock recovery. At Fig. 2.4.5 the lengths of pressure recovery regions versus Re are plotted for differet Ma and $\bar{b}$. It is seen that sharp increase of Δx takes place at Re $< 0.7.10^6$.

3. Supersonic flow deceleration in ducts with local area contractions and widening.

As discussed above, the scramjet air-gas passage can contain cavities and ledges that are elements of combustion chamber and intended for fuel injection and combustion stabilisation. Under passage operation as supersonic diffuser these elements make alterations in flow parameters in front of the region of transition from supersonic flow to subsonic one. Besides, the interaction of this region with these combustion chamber elements can change the flow deceleration character. So, of particular interest is the investigation of supersonic and transition flows in the ducts with variable area. We dwell on the supersonic flow first. In the paper (Ref. 36) it was depicted that skin friction stress in straight constant area tubes at supersonic velocities invariable along the whole length and the influence of wall roughness exhibits in the same manner as in the core of incompressible flow. This effect is possible if local cavities or ledges are small. Their location in the different parts of the duct will not change the wall friction force. However, if friction does not lead to flow transition for real scramjet passages the presence of local area contractions of real proportions (for instance fuel struts) can induce the flow choking and separation at certain flight Mach numbers. The flow around the struts vary with its position due to different boundary layer thickness.

3.1. Supersonic flows in tubes with conical and wedge-like bodies and grid of struts installed.

For the purpose of elucidating of flow characteristic properties in non constant area ducts and drag force defining two series of tests were carried out: 1.Measurement of total force imposed to inner surface of the ducts including wedge lake bodies, 2.Measurement of pressure distribution around wedge-lake bodies permitting to determine the forces imposed to these bodies. Besides, the static pressure distribution along the ducts and the total pressure fields at the end of the ducts where static pressure across the duct can be considered constant were measured. This fact allows to use one-dimensional analysis for momentum change and total drag evaluating. The scheme of the duct mounted on the balances is shown in Fig. 3.1.1. The supersonic flow arrives from the contoured nozzles (Ma = 2.6, 3.2, 3.8) into 81.4mm diameter cylindrical duct assembled from sections. The tests were carried out at two relative duct length-l = 23.7 and 15.4d. The Reynolds number changed in the range Re = $(1.5-4.5)x10^{6}$. The wedge-lake bodies were mounted in special section that was installed between the duct sections. Several types of models were tested. The schemes are presented in Fig. 3.1.1. Type 1- The conical cowl is located directly on the tube wall. The inclination angles of cowl generants were $4,^{0}$ 8^{0},and 90^{0} . In this case the boundary layer is deflected to the axis direction and effects the pressure distribution including base pressure. Type 2 -The conical cowl is located concentric to the tube wall and in accordance with the distance from the wall can be located either in the boundary layer or above it. The cylindrical cowls were fastened by the two wedges to the wall. The halfangles of these wedges was 8^{0}. Type 3 - The wedge crossing the tube along the diameter. The wedge was flown by the boundary layer near the duct wall and by non disturbed flow in the centre of the tube. Type 4 - The set of 16 struts. The strut location scheme is sketched in Fig. 3.1.14. Cylindrical and rhombus-shaped struts had diameter or thickness of 2 and 3mm (in special case d = 4mm). Rhombus half angles come to 8^{0}. The strut height was equal to 15mm. It was examined three variants of strut housing: in one, two and three rows. The distance between rows comprised S1 = s1/d = 0.25, and the distances between struts in a rows along the tube circumference S = s/d = 0.16, 0.32, 0.48 respectively. The strut set width for the three variants makes up to L = l/d = 0, 0.25, 0.5. Here d is the tube diameter. The static pressure distributions in model (Types 1-3) were measured along the cowl generatrixes, on the pylons in the middle of the annular aperture , and on the wedge of Model 3. The pressure taps were placed at a distance at 2.7 and 20.7mm from the tube surface. The base pressure was measured on the butt-ends of Model surfaces-

behind pylons and between them. These models were manufactured with one value of relative cross section blockage that was equal to F\f = 0,195. The models designed to get weighted had additional values of F\f = 0,125 and 0,26. The force exerted to the model was determined as the difference of forces operating in cases of the duct with and without a model. The change in momentum and pressure recovery coefficient was determined by one-dimensional analysis:

$\Delta I= F (p_1/r(\lambda_1)- p_2/r(\lambda_2))$

$\zeta =\Delta I/I_1$

$\nu = p_2\ \pi(\lambda_1)/p_2/\pi(\lambda_2)$

Here $r(\lambda)$ and $\pi(\lambda)$ - gas dynamic functions, ζ- momentum loss coefficient. The total pressure probes were placed on the rake to determine the arithmetic-mean of the results. The value of p_{0m} was defined for several types of flow, having as supersonic and subsonic zones. The duct length downstream of the local area contraction was enough for placing a developed pseudo-shock. The pressure loss level, evoked by a local contraction is uniquely determined by the pseudo-shock peak pressure. Thus the amount of Pmax= Pmax/Po is an additional parameter characterising the model drag. Fig. 3.1.2 presents the results of the total force measurement (momentum loss coefficient) exerted to the inner surface of the tube and inserts of different kind. Here ζ=f/Ih,where f is a force and Ih is a total momentum of the incoming flow. From Fig. 3.1.2 follows that the duct drag is essentially affected by the body's shape at the same duct area contraction. The function $\zeta(x)$ character varies noticeably with the tube length in front of the contraction section. So, the value of ζ for the tube with blunt cowl (θ = 90 deg.) changes little with the tube length increasing until the choking occurs. An increase of the duct area blockage does not augment the drag in proportion to the step height (h = 2.4, 4.2, and 5.7 mm).The value of ζ for the smooth duct is plotted in Fig. 3.1.2 by the dashed line and the difference between it and ζ for the duct with a cowl can be considered in proportion to the cowl drag. As noted above the flow around plane and circular steps practically does not differ if flow average Mach number in front of step is used. A decrease in the cowl height by 1.5 times (2.7 mm. instead of 4.2 mm.) leads to decrease in drag near 2.5 times. This can be explained by the boundary layer influence. The 35% increase in h (5.7 mm) causes a six-fold drag rise. The reason for this increase in drag lies in a pseudo-shock influence. The experimental and computed drag data are in good agreement suppose a normal shock is in front of the model. A characteristic property of the relation in the case of sharp cowl is the existence of pressure maximum at x = 5-10d. The reason of this phenomenon is in boundary layer influence which contrary to previous case flows the cowl without separation. However, when the height of the cowl is increased up to 5.7 mm there is a sharp rise in drag. The placement of the wedge across the flow leads to drag increase because the central part of the wedge is in the region of the flow with high total pressure. The different flow character around different parts of the wedge could result in ζ decrease at some wedge downstream position. The value of Xmax can be determined only approximately because of monotonous flow character change. At low cowl angles the flow in converging duct section can be considered isentropic. With a knowledge of the mean Mach. number in front of this section and Mach number distribution along the smooth duct it is simple to calculate Xmax. So, at Ma = 3.2 and converging rate Fm/Fa =0.195 (M in front of converging section M = 1.59) the value of Xmax = 17. The experiments with 10^0. cowl indicated that at X = 15 the flow around the cowl is supersonic and at X = 18 the flow chokes. So at $\theta< 10^0$ the values of Xmax can be determined on a basis of Mm. For the cowl with $\theta =90^0$ and wedge with $\theta = 10^0$ the pairs of X at which there is supersonic and subsonic flow are equal to 12.5, 14.0 and 10.0, 12.5 respectively. This means that values of Xmax decreased by 20 and 50%. At Mach number decreasing the difference between measured and calculated Xmax increases and at M increasing - decreases. So, at Ma = 3.8 the supersonic flow around the cowl with blunt nose exists at X =16 , while Xmax =19. Fig. 3.1.3 illustrates the pressure distribution along the cowl and wedge with $\theta = 8^0$ at Ma =2.6, 3.2, 3.8 for three values of X . From Fig. 3.1.3a

follows that the measured pressure on the forward part of the conical cowl is near to calculated on the basis of mean velocity . The pressure distribution on the conical surface is in good agreement with one-dimensional theory. As is seen from Fig. 3.1.3b the pressure distribution along pylon taken at the distances of 2.7 and 20.7 mm from the duct wall are nearly the same. When X changes from X =0.7 to X = 4.4 the wedge mean pressure decreases a little just as in the case of the cowl at Ma = 3.2 that have to assist the drag decrease. Fig. 3.1.4. presents the pressure distribution along the circular ledge (cowl with θ=90 deg.) of 5 mm and 60 mm length and 4.2 mm height at three values of Ma and three ledge positions. Further inspection of this Figure discloses that ledge transition down the flow changes the pressure on the forward looking butt-end relatively insignificantly. There are regimes when this transition produces the increase of this pressure (see Fig. 3.1.4b, Ma = 3.8). The pressure on this butt-end practically does not depend on the ledge length until the regime of choking comes (see Fig. 3.1.4b, l =60 mm, Ma =2.6).

The base pressure on the down facing step face is more sensitive to the ledge length , especially when the flow is approaching to choking. So at Ma = 3.2 and X > 4.4 the base pressure rises sharply, whereas at Ma = 3.8, the base pressure for both examined ledges is practically the same. So the pressure shocks caused by the front step of the ledge and the flow choking have an important bearing on the base pressure. Fig. 3.1.5 depicts the relationship between mean pressure Pm on the wedge and cone-like surfaces of models (for ledge- pressure in front of step) and X at Ma = 3.2. Almost for all models at X =5 there is minimal pressure noted that has to result in drag reduction. At X = 0.7 the mean pressure corresponds to pressure calculated on the basis of mean flow parameters for all models. At X = 4.4 the mean wedge pressure is in exes of calculated one. The duct crossing by the wedge , apparently, gives rise to such shock systems and boundary layers separations that causes premature choking. The mean pressure rise at X > 5 when choking is absent can be explained by the flow static pressure increase due to friction. The pressure distribution in the tube without any contractions is presented by the dashed line. The relationship of Pb and X for conditions examined is given in Fig. 3.1.6. It is seen that transition of any model down the flow leads to base pressure increase that corresponds to duct drag decrease while its minimum is reached at certain value of X (see Fig. 3.1.2) The most sharp pressure rise take place at the flow choking with the wedge and annular ledge of 60 mm long.

Analysing of Figs. 3.1.5 and 3.1.6 helps to establish the reason of minimum existence in the relationship of drag from local contraction position. Such analysis does not take into consideration the tube friction force change because it is small and can be determined in one-dimensional theory. Quantitative analysis discloses that a friction force at certain position of contraction in the tube also can have minimal value. If we divide the tube flow into two parts, in front of and after the local contraction (Fig. 3.1.1) and accept that mean friction coefficient Cf along this section is determined by the Mach numbers at the beginning of sections then equation connecting the velocity change along the tube of constant area with the work done by the friction force, and also the impulse equations that take into account the velocity change at the area contraction, will be:

$F_1 = Z(\lambda_1)(1-\zeta) - Z(\lambda_2) = 0$

$F_2 = Z(\lambda_1) - f - Z(\lambda_2)$

$F_3 = Z(\lambda_3)(1 - \zeta) - Z(\lambda_4)$

Here λ, $Z(\lambda)$ -are velocity coefficient and impulse function

$\zeta = f/I = Cf\, 4k/(k+1) x \lambda / Z(\lambda) x X$ - impulse coefficient

$Cf = Cfo\, (1-0.05\, \lambda^3)$ - Coulse experimental data approximation for plates.

X - relative tube length.

Minimal friction force value at fixed model drag force corresponds to maximal velocity coefficient at the duct end or to condition: $d\lambda_4 / dx$ Using rules of differentiating of

implicate and complex functions we receive $\frac{d\lambda_4}{dx} =$

$$\frac{2k}{k+1} l \frac{\zeta - \zeta \left[\frac{\lambda_2}{\lambda_3} - \frac{2k}{k+1} \bar{l} \cdot X \frac{\lambda_2}{2 \cdot \left(1 - \frac{1}{\lambda_3^2}\right)} \cdot \frac{d\zeta_2}{d\lambda_4} \right]}{\frac{2}{\lambda_4} \cdot \left(1 - \frac{1}{\lambda_4^2}\right)}$$

The fraction denominator is positive at all flow conditions, that is why the sign of derivative is determined by the numerator which after substitutions and cancelling (at x =0) can be written

$$\frac{1 - 0.05 \cdot \lambda_3^3}{1 + \frac{1}{\lambda_3^2}} - \frac{1 - 0.05 \cdot \lambda_1^3}{1 - \frac{1}{\lambda_1^2}}$$

The function $(1 - 0.05\lambda^3)/(1 + 1/\lambda^2)$ has maximum at $\lambda = 1.5$

At $\lambda < 1.5$ the numerator and with it the value of $d\lambda_4 / dx$ are negative, the deduction of which is that at low minimal drag achieved when the local contraction is placed at the tube beginning. At $\lambda > 1.5$ $d\lambda_4 / dx > 0$ and consequently it is expediently to transit the local contraction down the flow The relation in square brackets is seen to rise as $\bar{x}$ increases and at certain combinations of $\bar{x}$, and l the value of $d\lambda_4 / dx$ can become negative. In other words the minimal friction drag can be achieved at $0 < \bar{x} < 1$.

3.2 The supersonic flow around a circular cavity

In the scramjet air-gas passage comprising supersonic diffuser and combustion chamber there can be arranged some local enlargements of sectional area or cavities used for combustion stabilisation. This cavities can affect pseudo-shock as directly when they are in the region of it and indirectly, throughout the change of flow parameters before it. The cavity and pseudo-shock interaction depends on the cavity geometry and the flow regime in it. Much attention is given to the flow in cavities in a plane. Detail experimental investigations of the flow in a two-dimensional is performed in Ref. 51. The difference between flows in the duct circular and plane cavities supposedly displays only at low Mach numbers when disturbances evoked by the front part of the circular cavity reflect from the duct axis and hit the cavity. The flow in a cavity can be influenced by the incoming flow non uniformity induced among other factors by the jet injection (for instance by the gaseous fuel jets in a scramjet) or by pseudo-shock occurring at the duct thermal choking.

The experimental facility scheme is sketched in Fig. 3.2.1. The uniform supersonic flow entered 23.6 calibre length connected pipe that was mounted on the balances. The circular cavities of rectangular cross section were formed by installing between pipe flanges cylindrical inserts of different diameters and length. The cavities length and depth were l = 20, 40, 60 and 90 mm, h = 2, 4 and 12 mm respectively. Experiments were carried out at Ma = 2.6, 3.2 and 3.8 and Re = $(1.5\text{-}4.5)\times10^6$. It was measured static pressure distribution along the tube and cavity and the drag force applied to the inner tube surface. The cross jet injection was effected by a special duct section with various sets of orifices. The essentials of orifices location were discussed above. In some cases an injection of atmospheric air in the cavity in addition to high pressure jets injection before it was carried out. The atmospheric air rate control was effected by the change of incoming flow total pressure or by the number or diameter of orifices. Maximal value of the flow mass increase coefficient was $\beta = 1.05$.

When the flow is consistent with the closed cavity flow ($l/h>10$) the pressure distribution across the both cavity butts is near uniform (Ref. 51). That allows to estimate the drag force produced by the cavity and the flow parameters downstream. This force can be also gained by subtraction of the drag applied to the smooth pipe from the drag applied to the pipe with a cavity. The change of the friction force induced by the cavity presence is negligible (Ref. 36). The cavity drag is characterised by the momentum loss coefficient $\xi = X/I$ where I = p+mv - total momentum of the incoming flow. Cavity drag coefficient is expressed by: $Cx=2x/kpM\ F$,where F - cavity bottom area, p and M- static pressure and Mach number before cavity.

Let us consider the flow in the 60 mm length cavity placed at a distance of l = 4.7d and 21d from the entrance to the weighted section of the tube. In the first case the boundary layer is rather thin ($\delta/r=0.2$) and in the second case --$\delta/r>0.5$ (at Ma = 2.6, l/d=21 and δ/r = 1). In Fig. 3.3.2 the pressure distribution curves along the cavity are plotted for l/h=5 (open cavity) and l/h=15 (closed cavity). x- is a distance counted from the front cavity wall. Open symbols and solid curves correspond to the case l/d=4.7 and shaded symbols and dashed lines to l/d=21. Mach number at the entrance to the tube can change due to jet injection from M = Ma till M = 2. In the last case critical velocity is set at the end of the tube. Low pressure jet injection does not lead to strong shocks and flow non uniformity formation .

As follows from Fig. 3.2.1a the pressure curves at l/h = 5 correspond to the two-dimensional open cavity flow: the bottom pressure is equal or a little higher (at thick boundary layer) to the pressure of incoming flow. The curves have slightly expressed minimum at the middle. Flow Mach number decreasing due to jet injection somewhat increases the relative bottom pressure. The pressure distribution character does not change even if the flow velocity is near the critical one (l/d = 21, β = 1.1). At the closed cavity regime (l/h =15, Fig. 3.2.1b) after the first step there is the first separation region. The second flow separation (compression) region came into existence before rearward cavity step. The pressure curves with the plateau segments hold its shape in the range of $\beta < 1.062$ (flow Mach number Ma > 2.4). At $\beta > 1.062$ the flow transforms nearing to the open cavity

regime. Such a change of flow regime is likely to be induced by the flow disturbances. Analogues effect take place at large duct length (l/d = 21, no injection, Fig. 3.2.1b). In this case the average Mach number before the cavity is near 2 and two extreme types of pressure distribution are possible (in Fig. 3.2.1 they are traced by the dashed lines). So, for the special case (l/h = 15 and l/d = 0.74) the cavity flow rearrangement from closed to open separation flow begins with $M \cong 2.3$. It does matter what method of M reducing was chosen. It is possible that additional increase of cavity length can increase extreme M before cavity at which the closed mode is preserved. At $\beta = 1.1$, l/d =21 and l /h =15 the cavity flow corresponds to fully open cavern mode.

Fig. 3.2.2 indicates the pressure level at the step faces p_1 and p_2 in points located at a distance of 3 mm from the bottom surface in terms of l /h at $\delta/R = 0.2$. Analogues curves obtained in Ref. 51 for the two-dimensional cavity are plotted in the same Fig. 3.3.2 . A rather good agreement is noted. It can be expected that critical length of cavern closing for both cases is near. In Fig. 3.2.3 a comparison of drag coefficient Cx obtained in Ref. 51 using pressure distribution and Cx obtained in present work by balance is performed. Double symbols connected by a line indicate the range of Cx received at various cavity settings in the tube, various β and ,consequently, various M before a cavity (M = 3-1.5). Single open (l/d = 2.7) and shaded (l/d = 21) symbols correspond to $\beta = 1$.

Fig. 3.2.1 analysis depicts that in spite of considerable data scatter the results agreement for plain and circular cavities at l/h > 10 is satisfactory. At small values of l/h (open cavity) the plane cavity drag is smaller than that of circular.

The cavity pressures P_1 and P_2 are plotted as a function of l/d at different Re in Fig. 3.2.4. It is seen that forward face step pressure does not depend on Re only if $Re > 2.6x10^6$ that corresponds to Ref. 51 data about laminar to turbulent Re transition (and corresponding reducing of separation region length) that in the case of axisymmetrical flow take place at greater Re comparative to the plane case. The dashed line in Fig. 3.2.4 corresponds to base pressure, Ref. 1, obtained at M corresponding to core flow Mach number. A comparison between axisymmetrical and plane cases shows that the difference is small. At $Re = 1.4x10^6$ and l/d = 2.7 the value of P_1 approachs to P_2 that says about distraction of closed type flow because at laminar flow the critical cavity closing length is greater than 15. The noted delay of laminar to turbulent flow transition is manifested on a large duct distance l, at least up to l/d = 5, where $Re_l > 7x10^6$. At l/d = 10 and 15 the effect Re on P_1 can be explained by average Mach number decreasing in front of cavity.

An injection of high pressure jets causes pressure shocks that can hit into cavity and change flow mode in it. The change in jet rate can displace shocks and modify the flow mode again. The cycling change of pressure at the step faces when injection rate changes is clearly seen in Fig. 3.2.5 (solid line). Dush-dotted lines correspond to low pressure jet injection. The curve is near to monotonous one. The base pressure at the downstream facing step corresponds to plane flow, Ref. 1., if use mean M for comparison. Air injection in open cavity leads to pressure increase along the whole its length. the cavity drag somewhat decreases. Air injection in closed cavity, see Fig. 3.3.6, curve 4, $\beta = 1.05$) activates the rearrangement of closed type flow into open one. The rearward facing step pressure comparatively little.

3.3 The pseudo-shock interaction with an obstacle

As was illustrated above, the pseudo-shock head gradient is much lower than that in free boundary layer separation. Thus, if possible to realise local pressure rise in a duct and join the pseudo-shock to that circular region it can be expected that total length of supersonic/transonic transition region can be reduced even at the same pressure in the aft part of pseudo-shock. The presence of circular bodies placed on the duct wall give rise to circular regions of high pressure. These regions, depending on bodies position and its shape, can occur as up and downstream these bodies. The increased pressure regions can arise due to boundary layer separation in front of step or as a result of flow deceleration in pressure shocks. This overview section discusses different variants of high pressure regions occurring and pseudo-shocks joining them. Different nonstreamlined bodies were placed in various tube sections. Fig 3.3.1 gives pressure distributions around the obstacles that are conical and blunt step cowls mounted on the tube wall. In the first case the flow is non separated, in the second-separated.

The circular ledges with rectangular cross section had length of l/d=0.0615, 0.37, 0.74 and height of h/d = 0.0515. The distance between the weighted duct entrance and the front ledge face run between l/d= 0.52 and 0.185. In Fig. 3.3.1 the front step faces are made coincide for the sake of comparison convenience. The curves plotted in Fig. 3.3.1 correspond to two limit modes : maximal throttling and no throttling. At first mode pseudo-shock does not cross the obstacle (solid lines). Additional rise in back pressure leads to pressure leap ahead the obstacle and subsonic flow ahead of it. Farther inspection of Fig. 3.3.1 (Ma = 3.8) discloses that in the case of 4^0 cowl the front part of pseudo-shock can be positioned on the conical part of the cowl. The pressure gradient in this case is the same that in free boundary layer separation. The pressure distribution in pseudo-shock in smooth tube is presented by the dash-dotted line for comparison. The Ma = 3.2 and 2.6 tests gave the analogues results. The cowl angle rise up to 8^0 (Ma = 3.8) caused maximal pressure decrease by two times. It seems likely that it is connected with impossibility of stable position of separated region in converging channel having large cowl angle. The use of circular blunt ledge (Fig. 3.3.1b) cause the boundary layer separation that exists no matter what position pseudo-shock takes. The front part of the pseudo-shock can be placed stable at a grater distance from the forward face step than it takes place with free separation region, but the difference does not exceed 30% of the step height. The pressure gradients in both cases coincides. So, it is possible to create local high pressure region in front part of pseudo-shock. The pressure distribution in the boundaries of the ledges is affected by the length of it, whereas the pressure distribution in front of the ledge does not depends on it (Fig. 3.3.1)

The pressure distributions differ most substantially in the case of transition from the cowl with l/d = 0.37 to cowl with l/d = 0.0615. In the last case maximal pressure behind cowl at the distance of 10h. stayed almost constant and does exceed the pressure upstream the step. The comparison of Fig 3.3.1a and 3.3.1b- shows that both types of obstacles give approximately identical pressure rise. However, the use of blunt ledge gives some rise in required duct length and total pressure loss. Experimental results shown in Fig. 3.3.1 correspond to the case when the height of the obstacle is approximately equal to the boundary layer thickness. The obstacle downstream displacement makes the pressure build-up at the rear facing step drop. At δ>2 h the positive obstacle influence on pseudo-shock length disappears.

Simultaneously with the duct drag force the pressure force at the rectangular ledge was measured. The dimensions of this ledges were l/d=0.74 and h/d = 0.033, 0.0515, and 0.07. The relationship $\zeta(\zeta_l)$ for noted models are given in Fig. 3.3.2 Here ζ and ζ_l are forces normalised by the flow total momentum at the duct entrance and exerted to the duct with an obstacle (balance measurements) and obstacle (pressure measurements) respectively. Vertical

sections of curves correspond to pseudo-shock moving from the end of the duct (ζ decreasing due to friction decreasing). The inclined sections of curves correspond to pseudo-shock fixed at the obstacle or to pseudo-shock compression regime at which base pressure increases. As seen from Fig. 3.3.2 the curve inclination is near to 45^0. That indicates on week dependence of friction force on back pressure level in the case when pseudo-shock is joined to obstacle. At maximal obstacle height h/d = 0.07 the curve comes much lower comparative to other curves. This can be explained by the long separation region downstream the obstacle that decreases the friction force. However, maximal back pressure and force applied to the rear facing step herewith decreases. Flow deceleration effectiveness drops. So, optimal ledge height exists. Downstream obstacle moving leads to duct drag increasing at both limiting modes of flow. Maximal increase is noted at maximal throttling.

Negative drag (thrust) at rectangular ledge as it seen from Fig. 3.3.2 was not achieved. In the case of conical, 4^0 cowl, as estimates indicate, the applied force could have negative meaning (ξ =-0.1) Balance experiments supported conclusions about pseudo-shock compression or mean pressure gradient increasing. These experiments allow to select optimal cowl shape.

Fig. 3.3.3 presents pressure distributions for limiting regimes in a tube with ledges. Conical cowl, $\theta=8^0$, $d_c/d = 0.85$, was installed concentric in the tube. The tests were also performed for $d_c/d = 0.7$ and 0.5. The local high pressure region was caused by the circular core stream exhausted from the cowl and interfering with the annular flow and the tube wall. When nearing to the limiting regime the flow in the cowl becomes separated, analogues to the case with conical cowl placed on the tube wall. Maximal pressure rise and pseudo-shock compression at Ma>2.6 is found to be small. In the case of wedge crossing the tube the high pressure regions occur due to shock interactions with the tube walls. However, the pressure distributions along the circumference of the tube are not uniform. There is possibility for pseudo-shock tongues to penetrate into the zones with low pressure. Obstacle pseudo-shock fixing ability falls. Smaller wedges are no obstacle to pseudo -shock upstream transition.

Fig. 3.3.4 present limiting pressure distributions for different obstacles. It is seen that forward obstacle position ($\delta/r = 0.1$) restricts pseudo-shock upstream transition. Its compression occurs both as a consequence of pseudo-shock forward portion substitution for portion with higher pressure gradient as well as due to mean pressure gradient growing in the rest pseudo-shock part. Of all the obstacles most effective is 4^0. cowl because it provides practically maximal pseudo-shock compression and has small drag in supersonic flow. The more maximal pressure at the aft part of an obstacle can be reached the more pseudo-shock compression can be expected. Fig. 3.3.5 displays the dependence of pseudo-shock length on maximal base pressure p_b/p_1. Here p_1 is static pressure in non disturbed flow in front of obstacle. Fig. 3.3.5 examination confirms the hypothesis about the presence of correlation between $\Delta x/d$ and p_b / p_1. The curves in Fig. 3.3.5 are extended to the left in such a way that at $p_b/p_1=1$ the pseudo-shock length was equal to that in the smooth tube, and to the right so that at l = 0 the pressure ratio p_b/p_1 correspond to that in normal shock.

We will enlarge now on pseudo-shock and cavity interaction. The incoming Mach number decreases in forward near wall part of pseudo-shock up to M = 0.1-0.2 at a distance of 1.5d and then increases to values corresponding to velocities downstream the normal shock (Ref. 36). Clearly at pseudo-shock different position over the cavity that is wittingly shorter than pseudo-shocks, the interactions of flows will be different. The pseudo-shock flow around the cavity can be as subsonic and supersonic. The difference in subsonic velocity can be very essential. Fig. 3.3.6 presents pressure distributions along the tube with circular cavity for different pseudo-shock positions and jet injection rate. Curve 1 corresponds to supersonic flow over the cavity. When the pseudo-shock reaches the cavity (curve 2) the flow in it changes -the closed flow rearranges into open.

Fig. 3.3.6 illustrates the fact that a cavity is not an obstacle to pseudo-shock upstream movement at back pressure rise. When a cavity is positioned in pseudo-shock subsonic part the pressure distribution in the cavity does not change from that received in Ref. 51 for

subsonic flow over cavity at M = 0.6. Curves 3 and 5 correspond to an intermediate pseudo-shock position at which flow over cavity has near wall Mach number equal M = 0.1-0.2. The changes in the flow induced by the cavity are small. Air injections into the cavity does not change the interaction between the cavity and pseudo-shock.

3.4 Jet injection from annular step face

Earlier there were analysed separation supersonic and pseudo-shock type flows over struts and ledges. They were considered as simplified elements of scramjet combustion chambers. These separation flows can change in the case of jet injection from these elements. The temperature of jets also can influence the separation flow character. The total pressure loss induced by jets depends on jets orientation and mass rate coefficient β. The impact of this parameters can be detected on pressure distribution and axial force acting on diverging duct installed downstream of ledge.

The experimental model scheme is presented in Fig. 3.4.2. M 3.08 nozzle was used. The maximal duct length was 23.6d, the cone angle of diverging duct-11.7^0. The length of annular ledge was 93 and 137 mm and step height-1.2 and 4.2 mm. The jet injection took place at 0 and 7^0. to axis successively. The secondary jets heating took place in gas heater. The injected gas rate was defined by the critical section of Ventury tube. positioned before the gas heater and did not depends on gas temperature. Maximal jet flow rate comprises 25% of the main flow rate. The pressure distribution was measured along one directrix of cylindrical tube and two directrix along conical one. Integral axial force impressed on conical section was normalised by the nozzle total impulse Ip. The variation of annular jut position make it possible to investigate three flow types in front of the step- free separation of boundary layer, pseudo-shock arising and developed regimes.

The experiments showed that jet injection in the observed rate range and pressure build-up downstream the jut does not influence the flow upstream the step if it positioned at the distance of 5.5 d from the nozzle when there is free separation of boundary layer. In the second regime (l = 11d) long separation region in front of jut occurs even with no jet injection. In Fig. 3.4.1 pressure distributions are presented. Open symbols correspond to cold jets and shaded symbols - to heated ones. Jet injection results in separation region increase. With hot jets this effect is lower due to larger jet ejecting. So in the second case the jut with jet injection can not fix the upstream pressure propagation. As in the first case the heating of jets leads to pressure increase downstream the jut and makes pressure distribution more even. Fig. 3.4.1c corresponds to developed pseudo-shock. The length of transition region in front of step can reach 10 calibres and pressure - to pressure downstream of normal shock. Jet injection leads to noticeable increase of upstream influence. So, in the case of second and third regimes there occurs “liquid throat”, the area of which can change in the dependence on flow conditions downstream the jut that leads to change of upstream influence. As experiments with jet injection from rather small jut, h = 1.2 mm, l = 5.5d showed at $\beta = 1.1$ and Tt = 800K there is no disturbance propagation upstream the jut. In Fig. 3.4.2a pressure distributions along conical section at different jut dispositions and jet temperatures are presented. The injection of hot jets led to pressure distributions along two generatrixes drawing together, e. i. to flow becoming more even.

In Fig. 3.4.2b the dependencies of axial force R are plotted as a function of $\beta\sqrt{\tau}$ for two positions of the two values of jut heights and different β. Dashed lines correspond to the case of normal jet injection from the wall of smooth tube. In contradiction to this last case the jet injection from jut have following specific features: 1 Curves $R(\beta\sqrt{\tau})$has lower inclination and reaches smaller maximal values, and 2.- there is essential stratification of curves for different β. This phenomenon is connected with some change of flow impulse in front of conical section at heated jet injection.

3.5 Pressure pulsations downstream the strut cascade.

Pressure pulsation measurements in ducts are of practical significance and in some cases- standard procedure. In particular it refers to inlets of airbreathing engines. The pressure pulsation level can defined the boundary layer state, duct mechanical robustness, turbo machine stable operation and so on. The pressure pulsations exert some action on mixing and combustion processes among other factors. The duct flow turbulence to a large measure defined by the duct geometry. At supersonic flow deceleration in ducts with oblong cross sections the pressure pulsations can far exceed the pulsations in axisymmetric ducts (see sec. 2.1) As it was indicated earlier the pressure pulsations become more sensitive to Re in diverging ducts. The sets of struts designed for fuel injection are representative of scramjet combustors. The air-fuel mixing being the main purpose of the set of struts, their drug force have to be minimized, their strength should be reasonably high, they must assist to comustion stabilisation. These demands to the struts mentioned being conflicting result in large variety of strut geometry, their position and size. The vortex motion and flow separation generate velocity and pressure pulsations which superpose on the turbulent back ground produced by an inlet. The flow turbulence, besides the duct geometry, is defined by the combustion chamber mode of operation. It can work at a regime of supersonic flow. Besides there are modes at which the struts are blown by subsonic and mixed flow (with pseudo-shock positioning in the duct) It is apparent that level and nature of pulsations in these modes will be different. The interference between struts exerts some action on pulsations as well.

The objective of experiments performed was investigation of strut configuration, size and disposition impact on static and total pressure pulsations downstream the set of struts in ducts with different flow mode. The cylindrical and rhomb-like struts were chosen. They were arranged evenly along the tube radiuses. It is apparent that no simulation of real incoming flow is possible in this case. The situation is simplified due to possibility to consider measured pulsations as a sum of pressure pulsations produced by struts and incoming background pulsations. The facility and strut disposition schemes are presented in Fig. 3.5.1. Nozzle Mach numbers were 2.6, 3.2, 3.8, Re = (1.5-4.5) 10^6, P_t = 10-30 bar. The two types of experiments were carried out. The first one, balance measurements (total force was normalised by total flow impulse), were described earlier. The pressure distributions (along one generatrix from the nozzle end) and pulsations were measured in the direct-connect pipe tests. Static and total pressure pulsations were measured in two sections positioned at $\bar{x}$ = 1.85 and 3.7 downstream the front row of struts. The total pressure probes were placed at the distance of h/r = 0.37 from the surface in the first measuring section and at h/r= 0.49 in the second that was outside of the boundary layer. The probe internal and external diameters and transitional tube length were of 2, 3 and 70 mm respectively. The measurements were made relatively close to the struts that was desirable having in mind the real combustion chamber construction. At the same time the flow downstream the struts was not uniform that caused data scatter.

The used equipment ensured uniform amplitude-frequency characteristics up to f = 5000 Hz. The signals arriving from sensors after amplification were recorded on magnitograph and oscillograph. Experimental data for pressure pulsations were presented as a root-mean square values related by the plenum pressure. Five regimes were investigated (Fig. 3.5.1): 1. The throttling valve is fully open and supersonic flow exists. 2. Back pressure rises and pseudo-shock head occupies second measurement section. The probes are in a dissipation zone of pseudo-shock. 3. The pseudo-shock head is located upstream the first measuring section. The probes of first measurement section are in initial part of dissipation zone and the probes of second position - in the developed part. 4. The pseudo-shock catchs

the root part of struts and they are flown by mixed supersonic/subsonic flow. The drag of struts is decreasing a little. 5. The pseudo-shock is at the entrance of the tube. The struts are in fully subsonic flow. For getting some data about pulsation background experiments without struts were carried out. The arranging of needed flow regime was made approximately using the pressure distributions. Because of that some data scattering was present. It concerns especially to total pressure pulsation measurements due to probe orifice could get into different parts of the oscillation front.

In Fig. 3.5.2 the static pressure distributions along the tube and total pressure fields at the end of it for different regimes are presented. They are numbered by 1-5. To gain a better understanding the symbols are retained only in the case of the duct without struts. Four variants of ducts were chosen: 1. Smooth duct, 2. One row of rhombus struts, d = 3 mm, 3. One row of cylindrical struts, d = 3 mm, 4. Three rows of cylindrical struts, d = 3 mm. This set of variants allows to estimate the impact of strut geometry (at the same strut disposition and thickness) and strut disposition (at the same geometry) on the flow character . The curve corresponding to the above mentioned regimes are numbered by 1-5. Fig. 3.5.2 analysis says that supersonic flow (1) is nonuniform. The pressure peaks correspond to weak pressure shock system. The presence of struts makes the flow still more non uniform. On the existing shock system the another system is superimposed. The mean pressure level in the tube with struts increases due to additional pressure loss and M decreasing. Maximal pressure level corresponds to cylindrical struts and their cascading is responsible for interference pressure rise. Dashed line corresponds to one-row and dotted one to three-row strut grate. The back pressure build up causes pseudo-shock generation. 2 and 3 curve groups correspond to pseudo-shock head location in front of second and third measurement sections respectively. It is seen from Fig. 3.5.2 that pseodo-shock in smooth duct offers maximal pressure recovery. One row rhombus strut grate decreases pressure recovery a little. Three rows of these struts leads not only to additional pressure recovery drop but also to change of pressure distribution character which become non monotone due to strong pressure shocks arising.. 4 and 5 curve groups correspond to pseudo-shock capturing struts partly or fully. The difference in flow character for these cases is large. If pseudo-shock head is positioned in front of strut grate and flown by mixed flow (group 4) then distribution character is near to curve groups 2 and 3. Pseudo-shock moving to the beginning of the tube (group 5) makes the flow in the strut region fully subsonic that serves to sharp loss decrease. The pressure distributions in the tube with or without struts practically coincide. Similar conclusions can be received at total pressure fields analysing.

In Fig. 3.5.3 the curves correspond to groups 1 and 3. The distance from the duct wall normalised by the duct diameter is arranged along abscissa. It is seen that pressure level sequence in the case of supersonic flow and pseudo-shock are the same as in Fig. 3.5.2. The use of cylindrical struts results in P_t drop in the near wall region and an increase in the flow core in comparison to rhombus strut grate case. The strut cascading offers some P_t evening that is possibly connected with turbulent velocity pulsation and friction stresses increase. The influence of rhombus strut interference on the flow character readily illustrated by at low M and thick struts. In Fig. 3.5.4 the pressure distributions correspond to Ma = 2.6 and two variants of 4 mm thick struts positioned in one and three rows. The curves corresponding to the flow regime 1 are differ cardinally. The cascade disposition leads to such loss increase that the tube duct length downstream of struts becomes too long for supersonic flow realisation. As a result, at fully open throttle, a pseudo-shock arises (dashed line 1). This regime is near to regime 2. The differences in curve character in groups 2 and 3 for two variants of strut disposition remains substantial. Further pseudo-shock transition brings to practically coincidence of pressure distribution curves. The comparison of total pressure fields at the end of the tube, Fig. 3.5.5, confirms earlier described result-supresonic flow realises only if struts are positioned in one row. When pseudo-shck is present the flow fields are getting more uniform due to intensive turbulent velocity pulsations. The total pressure

level is lower at three-row rhombus grate. One-row disposition of struts of different thickness (2 and 4 mm) as experiments show does not result in substantial difference of curve character. Any way of drug increase (due to geometry dimension or interference) leads to pressure recovery decrease in supersonic flow and pseudo-shock.

We are coming now to pressure pulse analysis. As was mentioned earlier there is strong dependence of pressure pulsations on duct geometry and particular on size and shape of struts, their cascade relative position to the duct entrance. The last factor is connected with the boundary layer thickness on the boundary of which pulsations increase considerably. In Fig. 3.5.6 for three values of Ma the dependences of relative pulsation intensity of total pressure $\overline{\varepsilon_{Po}}$ along the smooth duct at the distance of h/ r = 0.37 and 0.49 from the duct wall (disposition of probes for pulse measurements). The analysis of this curves shows that at the measurement sections I and II (marked by vertical dashed lines) the influence of boundary layer is not exhibited and the values of $\overline{\varepsilon_{Po}}$ are in the range of $\overline{\varepsilon_{Po}}$ = 0.6-1.1%. The nearer to the wall probe position could increase $\overline{\varepsilon_{Po}}$ four times at Ma = 3.8. The boundary layer factor must be taken into account at strut grate influence on pulsations. The more the grate drug the more boundary layer thickness and region with intensive pulsations is. It can be expected that time scale will change as well if the grate parameters change. Let us call attention now to pressure pulse downstream of the struts in regime 3. It is seen that maximal amplitude of total pressure change ΔP_{max} relatively weakly depends on strut disposition. However, pulse frequency caused by pseudo-shock changes noticeably. So, if regular oscillations at one-row strut grate are approximately 50 Hz then at two-row grate oscillations with f = 15Hz can be detected. At three-row grate the oscillations are approximately the same (20 Hz). The low-friquency oscillations in two sections of measurements are very near. That testifies that pseudo-shock is oscillating as a whole. As was shown earlier the pressure distribution downstream the strut grate depends on strut disposition. In the case of pseudo-shock swallowing the grate and total pressure probe placed in dissipative region of pseudo-shock (regime 5) the low frequency pulsation is about 100 Hz irrespective of strut position. This result accords to pressure distribution analysis.

As was mentioned above the objective of these investigations was in elucidation of pressure pulsation dependence on strut geometry, position, pressure loss induced by them and also on flow mode. The impulse loss coefficient is determined from relationship ζ=x/I. Where x-force exerted across the grate, I-flow full impulse. In Fig. 3.5.7 the relative maximal amplitude of total pressure oscillation, derived from oscillograms are plotted as a function of impulse loss coefficient ζ. ΔP_{max} corresponds to grates of rhombus and cylindrical struts placed in one, two, and three rows at M = 3.2. The thickness of all the struts was 3 mm. The values of ΔP_{max} are given for supersonic (1), mixed (4) and subsonic (5) flow regimes in the strut region. Fig. 3.5.7 indicates that at the supersonic flow around strut grate the increase of strut drug leads to ΔP_{max} increasing due to strut interference. This implies as to rhombus struts in the range of ζ = 1.7-3.5% and cylindrical struts in the range of ζ = 6.5-7.7% in both measurement sections. At the same time the drug coefficient increase due to strut shape and dimensions does not result in such noticeable pulsation increase. Therefore, the value of ζ is not the only and most important factor that define the pressure pulsation change. The strut interference has greater impact on pressure pulsation level. In present case this difference is about half an order.

Further, as Fig. 3.5.7 demonstrates, the total pressure pulsation level in first and second sections of measurements differ sharply. In the section 2 it is 3-4 times higher than in the section 1. This fact, presumably, can be explained by close location of pressure probes to the strut grate and by high level of non uniformity of flow in front of struts. The pulsation pressure level dependence on impulse loss coefficient (defined at supersonic flow) changes

substantially at passing from 1-3 to 4-5 regimes at which the strut grating is occupied fully or partially by pseudo-shock. If a strut echeloning leads to ζ increase then the transition from rhombus to cylindrical struts contrary to supersonic flow case reduces the total pressure pulsation level. Total pressure pulsation level in the second section, as in the case of supersonic flow surpass that in the first one. At the regime 5 this difference decreases. We dwell now on influence of ζ on a total and static pressure pulsations root-mean square deviations ε_{p1},ε_{p2} at the different flow modes. In Fig. 3.5.8 the values of $\overline{\varepsilon}_{Po}$ and $\overline{\varepsilon}_{p}$ are plotted as a function of ζ for regimes 1 and 3 for all variants of geometries and Mach numbers. Fig. 3.5.8 analysis lets to conclude that relationship $\overline{\varepsilon}_{p}(\zeta)$ character is analogues to curves $\Delta p(\zeta)$, plotted in Fig. 3.5.7. There is a tendency for an increase in pressure pulsations when rhombus struts are substituted for cylindrical ones and pressure probes are flown by supersonic flow. Another tendency- decrease of pulsations is noted when the probes are flown by subsonic flow. Taking into consideration that this tendency occurs as at supersonic and subsonic flow (Fig. 3.5.7) over strut grating it can be explained by pseudo-shock properties in the region at which the probes are placed. A root-mean square deviations of static and total $\overline{\varepsilon}_{Po}$ pressure pulsations at supersonic flow (outside of boundary layer) is 0.05-0.3% and 1-4% respectively. $\overline{\varepsilon}_{Po}$ for smooth duct is 0.6-1.1%. At regime 3 (pseudo-shock) the values of $\overline{\varepsilon}_{p}$ and $\overline{\varepsilon}_{Po}$ are 0.5-1.5% and 3.5-12%. At supersonic flow a decrease in M gives rise to $\overline{\varepsilon}_{p}$ and $\overline{\varepsilon}_{Po}$. At some cases this increase can be as high as 2-3 times, for example, when Ma decreases from 3.8 to 2.6. At subsonic flow over probes there is an opposite tendency, but due to large scatter of data the $\overline{\varepsilon}_{p}$-Ma relationship can not be established correctly. Maximal values of $\overline{\varepsilon}_{Po}$ downstream the strut grate at supersonic flow is approximately equal to maximal $\overline{\varepsilon}_{Po}$ in a smooth duct (see Fig. 3.5.6).

Let us call attention to analysis of dimensionless mean-root square values of pressure pulsations and autocorrelation functions which have been received at the interrogation frequency 10 kHz and realisation length not less than 2 seconds. Digital processing was made on computer using quick Furier transformation method. In Fig. 3.5.9-24 the power spectra density and autocorrelation functions are presented for regimes 1 and 3. The disposition of probes in the tube allows to analyse pressure pulsations at other regimes as well. These Figures allow to do comparative analysis of influence on pressure pulsations of: 1. Strut geometry at the same width and location, 2. Strut location (cascading) at the same strut geometry (d = 3 mm) and lastly 3. Strut dimension at the same location and geometry (rhombus struts of 2 and 4 mm). In Fig. 3.5.9 the relative power spectra density S(F)/Smax and autocorrelation functions R(r) for three variants of ducts are plotted as a function of frequency at Ma = 3.8. There pulsation spectrum for supersonic flow in the smooth (1), one row of 3mm width (2) and of cylindrical (3) ducts are compared. From Fig. 3 .5.9 it is seen that spectrums are of a wide band type. One would expect, taking into account the duct dimensions from which the vortexs are darted off, the real frequency band width can be much more than 5000 Hz. The analysis of Fig. 3.5.9 shows that some regular component of total pressure pulsation that increases the pulsation intensity several times, are contained in the smooth duct flow and saved when the struts installed. The pulsations caused by the struts are superimposed on the nozzle pulsation background. As in the smooth ducts and ducts with struts the maximal power spectra density of total pressure at supersonic flow is noted at low frequencies (f<500 Hz) and are probably connected with the used facility and occur in the duct before nozzle critical section. The installing of one-row strut grid decreases discreet pulsation components and by doing so produces equalization of spectra characteristics. But

the cylindrical strut grid leads to an increase in existing discreet component level and arising some new components.. The pulsation energy displaces towards the higher frequencies. This observation is reinforced by the R(T) function character for the observed variants of flow. In the case of cylindrical struts this function more fast decay says about time scale diminishing. Dimensionless spectrums of static pressure pulsations for the same variants of the flow are presented in Fig. 3.5.10 The spectrum band width is much less than for the total pressure pulsations. S(F) function for smooth duct decays practically at f = 1000 Hz and in the case of cylindrical struts due to vortexes behind them, up to f = 5000 Hz. The discreet component that presents in the smooth duct at frequency f = 750 Hz disappears when the strut grid installed, probably due to interference with the pulsations caused by struts. The autocorrelation function shapes are markedly affected by the strut configurations. The damping of R(T) functions occurs more severe when rhombus struts are changed by cylindrical ones. That corresponds to the time scale decrease at vortexs dimensions curtailment. In Fig. 3.5.11 and 3.5.12 the pulsation spectra of static and total pressure are plotted. This corresponds to ducts examined earlier at Ma = 3.8. and regime 3, at which pressure probes are located in the dissipation region of pseudo-shock. Fig 3.5.11 corresponds to total pressure pulsation spectra. The main pulsation energy is concentrated in the range of f<200 Hz and possibly is defined by oscillations of pseudo-shock as a whole. With the strut drag increasing this region is narrowed down.

The autocorrelation function shape for all analysed cases are near as well. These results correspond to conclusions based on pressure distributions analysis. made earlier. Fig. 3.5.12 illustrates the relationship of S(F) for static pressure at regime 3 The presence of cylindrical struts decreases the frequency band width from 5000 Hz in smooth duct till f = 500Hz in the duct with strut grid. The pressure peaks are practically flattened in the range of f = 100-800 Hz. In Figs. 3.5.13-3.5.16 pulsation spectra and autocorrelation functions are compared at three positions of rhombus struts in the tube at Ma= 3.2 and different flow modes. The objective of this investigations is to reveal the strut interference influence on flow pulsation characteristics. These Figures allow to compare pulsation characteristics received in two tube sections. It is seen from Fig. 3.5.13 that total pressure pulsation spectra change their character at the expense of rearranging of power spectra density at different frequencies at concerning in general the place of discrete pulsation components. The figures indicated in diagrams correspond to the number of rows in the grid. The two-row grid (curve smooth at some extent the discrete components) and three row grid increases the spectrum characteristic non uniformity and energy level in the high frequency region. So, the increase in strut drag impact spectrum characteristic whether it be on account of strut shape or strut interference is analogues. It was earlier noted that relative root mean square pressure pulsation deviation at the second measuring section is higher than in first section. The comparison of pulsation spectra in these sections (curves 1 and 4) indicates that pulsation levels grow in the second section at frequencies more high than 500 Hz and there is any reason to declare that the spectra frequency band width increases as well. In the second section the pulsation level at f> 2000 Hz is greater than for one row grid in the first section The autocorrelation function character for all cases presented in Fig. 3.5.13 is very near. Its decay occurs in the range of $\Delta T<10$ ms and takes place in a shorter time interval if the drug increases or if there is a transition from the measurement section 1 to section 2.That attests about power spectra density displacement into the region of high frequencies The analogues relationship S(f) and R(T) for static pressure pulsations at regime 1 are presented in Fig. 3.5.14. The two row grid of rhombus struts installation having higher drag induces an increase in pulsation energy and band widening Analogues effect, though in considerably lower scale, take place at the transition from section to section in the case of one row grid, when some discrete components disappear. Autocorrelation functions in the section 1 at struts present decays faster. In Fig. 3.5.15 and 3.5.16 the relationships S(F) and R(T) for the same variants of grids as depicted in Figs. 3.5.13 and 3.5.14 but for regime 3 are presented.

The spectra of Figs. 3.5.11 and 3.5.15 comparison indicates that for rhombus struts the decrease in Ma from 3.8 to 3.2 and corresponding increase of M downstream of pseudo-shock causes the spectra bend width to rise. Therefore, the sharp increase in mean square root deviation of pressure pulsations at transition from Ma = 3.8 to Ma = 2.6 noted before can be explained by high frequency pulsation intensities increase. The tendency for an increase of these pulsations is conserved at transition from section II. As is seen from Fig. 3.5.15 the grid type influence on S(f) function character is approximately the same as at supersonic flow but the level of change is not so high. The relationship R(T) are differ slightly from the supersonic flow case. However, as before an increase in the drag leads to more earlier decay of R(T) function. The spectra of Fig. 3.5.15 for one row strut grid analysis shows that the decrease in Ma from 3.8 to 3.2 for cylindrical struts, as opposed to rhombus struts does not tend to change spectra characteristics. However, in the case of rhombus struts the difference in frequency band width is much more greater than in the case of cylindrical struts that correlates well with the grid drag dependence on the strut disposition. The static pressure pulsation change at regime 3 and 1, Fig. 3.5.16, differ significantly. The two-row grid presence causes the discrete component arising at the frequency of 200 Hz. At three row grid this component is absent. In the second section the pulsation energy at high frequencies somewhat increases. The R(T) functions have special features at low frequency fluctuations. At three- row grid the R(T) function oscillates. Figs. 3.5.17- 3.5.20 correspond to different positions of cylindrical struts at Ma = 3.2. It is seen from Fig. 3.5.17 that cylindrical strut cascading leads at regime 1 to smoothering of spectra characteristics in contrast to cascading of rhombus struts. The spectra difference at various dispositions of rhombus struts, Fig. 3.5.14, is much greater as well as difference in drag. At the transition to the second section downstream the one-row grid the energy of discrete components with frequency more than 1000 Hz in contrast to rhombus struts decreases and low frequency oscillations keep their energy. R(T) functions differ little. Fig. 3.5.18 corresponds to static pressure pulsations, regime 1.The S(f) function character for all variants including rhombus struts, Fig. 3.5.14 is near with the exception of discreet component at f = 750 Hz for two-row grid of cylindrical struts. In total pressure pulsation spectra at regime 3, Fig. 3 .5.19, the spectrum corresponding to two-row grid that involves maximal impulse loss is prominent. In this case the frequency band makes more wide and in the frequency range 150-1000 Hz the pulsation intensity increases noticeably. The transition from the first to second sections of measurement for the case of one-row grid, as in earlier analysed cases, comes to spectra band widening in the direction of high frequencies. The static pressure pulsations downstream the cylindrical struts, Fig. 3.5.20 in contrast to rhombus strut case, differ very little whereas R(T) function for both cases are very near.

Finally stay on strut dimension influence in one-row rhombus grid on pressure pulsation. From spectrum analysis, Fig. 3.5.21, follows that the strut width increasing from 2 to 4 mm assists to smothering of spectra characteristics, to decreasing in pulsation energy at frequencies over 1000 Hz, due to vortex dimension increase. R(T) function changes relatively small. Analogues phenomena takes place in the spectra character of static pulsations, Fig. 3.5.22. A decrease in relative intensity of low-frequency pulsations at strut getting thicker is noted beginning from f = 200 Hz. An increase in strut width slow down the R(T) function decay. There is an opposite influence of the strut width at regime 3. The increase in strut width leads to essential increase in relative total pressure pulsation energy, Fig. 3.5.23 at frequencies f> 200 Hz and to widening of the frequency band. R(T) function decays quicker with strut thickness growing. The S(f) function changes in this case little, Fig. 3.5.24.

4. Separation flow deceleration in diverging ducts.

The use of a supersonic diffuser the duct of which is diverging is most probable with air breathing propulsion. In this case length shortening and stability of work can be more important than the maximal pressure recovery achievement that is characteristic of stationary gas dynamic facilities. In a scramjet that operates in a wide range of flight velocities the engine passage divergence provides necessary fuel supply without inlet stable operation disruption. In the upper part of Fig. 4.1 the air-gas passage of large scale dual-mode scramjet model HRE (Ref. 52) is presented. The diverging model passage consists of narrow and wide parts connected by sudden expansion section. The narrow part in its turn consists of annular ducts with constant and diverging area parts. The duct parts can be connected also by a smoothly diverging section. In this axisymmetrical duct taken as an example possible flow regimes in which supersonic flow transforms into subsonic one are schematically illustrated in Fig. 4.1. This regime analysis is the principle contents of supersonic diffuser's investigation. It is another matter that diffuser working conditions for scramjet and wind tunnel are different. Let us discuss special features that determine the direction and scope of experimental investigations.

Regime 1 corresponds to minimal flight Mach number. Subsonic combustion takes place in a wide part of the combustion chamber. The fuel supply is up or downstream of step. In the narrow passage part a pseudo-shock is positioned. In front of it there is non uniform supersonic flow induced by the inlet. Regime 2 is a transitional one. Pseudo-shock is not fully developed and realised at greater Mach numbers when the heat supply is not sufficient to create the necessary back pressure. There are interactions between the flow separation in the head of pseudo-shock and the flow separation downstream steps, cavities and elements of combustor. Regime 3 corresponds to the back pressure level at which upstream influence in the narrow part is absent. This regime depends essentially on the section geometry that connects the combustor parts and flow parameters in front of this section. At the same back pressure the position of the region of flow transition can differ essentially. Regime 4 corresponds to fully supersonic flow in narrow part and at the front part of the wide one. The transition region is positioned at the rear of the duct. The flow parameters in front of this region depend to a large extent on the character of flow separation and base pressure that in turn is defined by the flow parameters and duct geometry up and downstream of the step. Regime 5. Flight speed increases steel more. Fuel supply occurs in narrow part of the tube. Fuel can be ejected through orifices in the duct wall and in struts as well. The flow separation regions can occur both up and downstream of the fuel injection sections. Regime 6 corresponds to maximal flight speed at which the transition region still exists and is located in the narrow part of the duct downstream the fuel supply section.

4.1. Supersonic flow special features in stepped ducts.

The experiments were carried out in circular tubes with initial diameter of 81.4 mm. There was also used conical sections. The cylindric sections of 100 and 134 mm were installed at the aft part of the ducts. So, the ducts had sections of constant and diverging area including stepped ducts. There are fairly few investigations of flow propagation in stepped ducts. Results of some publication are not

dependable. Unfortunately, in investigations (Ref. 53) there were used only conical nozzles (θ= 15 and M > 2.55) and high expansion rate of the stepped duct (f > 4). It was shown that calculation of flow with such parameters by march method at known base pressure give results that are in a very good agreement with experiment. In scramjets the flow parameters differ essentially from analysed in

Ref. 53 .It is hardly probable that scramjet passage angles and expansion ratios could exceed θ =3-5 and f = 2 respectively. Mach numbers can be lower than 2.5 and thick boundary layer in front of diverging section can be present.

Let us compare at first the experimental pressure distributions with that computed by Ref. 54 method for conditions as near as possible to real scramjet conditions but at thin boundary layer (step is at the

nozzle exit).The experiments were carried out at Re > 7 0^6 at which the flow was automodel. The pressure distribution along the wide part of the duct has saw-like shape The static pressure in the first peak is essentially higher than in the following ones. Because of it the value of P_1 and position of it is of special interest. In Ref. 56 there was made an attempt to define general laws of flow propagation in the stepped tube on the base of dimension theory and generalisation of experimental and numerical investigations. In this work it was received that the position of second pressure peak X_2 and its value P_2/Pa are defined by impulse function $I_* = 0.35\ Z(\lambda)$. $Z(\lambda)=\lambda+1/\lambda$ Here $Z(\lambda)$- impulse function and λ-velocity coefficient

In Ref. 56 the values of P_2 and X_2 are used as scales of pressure and longitudinal co-ordinate for all the regions of supersonic flow in the duct. However, this work does not allow to determine the pressure level in the first peak and its location in conditions different to the case of θ =15 and f> 3.

The typical pressure distributions in the wide part of the duct for different Ma and $\theta = 0$ are presented in Fig. 4.1.1 In this Figure for the purpose of comparison the pressure distribution for θ = 19 is also shown. It is seen that an increase in Mach number leads to increase of relative maximal pressure P_1/Pa and distance of this peak from the step. So, if Ma changes from 1 to 3.8 than the distance X_1 increases more than three times and value of P_1/Pa more than 1.5 times. Special attention must be given to the fact that the peak positions at Ma = 1 and 1.6 practically coincide with peak position at Ma = 3.8, θ = 19 .Thin boundary layer is a common fact for both variants. So, it is not excluded that boundary layers getting thicker that take place at Mach increasing, would have some effect on pressure distribution smoothening. It should be also noted that if at Ma = 1 or 1.6 the first peak is clear expressed whereas at greater Ma it becomes more smoothed. At lower level of expansion rate (f =1.51) as experiments depicted P1 grows. In Fig. 4.1.2 the dependence of P_1/Pa and X_1/D on Mach number is shown for f = 2.72, 1.75, 1.51. The analysis of diagrams indicates that the level of X_1/D is only slightly affected by expansion rate. The influence of different parameters on second peak distance is in a good agreement with computed values for conical nozzle. A deviation from designed straight line is noted for contoured nozzles (pressure increases with Mach or impulse function- Jx increase). Thus, in the case of section with sudden expansion located directly downstream the contoured nozzle, the value of maximal pressure P_1 and distances X_1 and X_2 can be expressed: $P_1/Pa = 0.28+0.13Ma$, $X_1/D = 0.07+0.33Ma$, $X_2/D = I_* + 0.125 I_*^2$

The effect of length and geometry of narrow part of the duct on these parameters is illustrated by Fig. 4.1.3 The tube length increase leads to boundary layer growth and Mach number reducing. The use of slightly diverging duct allows to change δ at practically constant M in the flow core. The use of intermediate constant area duct with D = 100 mm decreases the duct expansion ratio in front of wide part (D = 134 mm) and creates two sections of sudden expansion. It is seen from Fig. 4.1.3 that the narrow part length increase leads to pressure P_1 growth. The value of X_1 changes little and can be estimated by the earlier given relation. The pressure distribution at the tube portion X = 0-X1 indicates a new pressure peak arising when l increases.

As experiments showed a decrease in Ma and increase in δ can effect in such a way that the pressure in the new peak can become larger than in the first one. The existence of slightly widening tube section practically does not change the pressure distribution at the front part of the tube but at greater X the pressure gradient becomes lower. Still more pressure smoothing is observed at the narrow part diameter increasing. In Fig. 4.1.3 the pressure profiles for two last variants (dashed line) are plotted. The experiments depicted that air injection through annular slot into the wake, as in Korst's experiments (Ref. 57) noticeably increases the base pressure. Calculation of flows in stepped ducts were made using method (Ref. 54) at the same flow parameters including base pressure $\overline{Pb}$ = Pb/Pa or off-designed expansion ratio $\overline{Pa}$ = Pa/Pb. So, for f = 1.65 and Ma = 1.5, 2.2, 2.6, 3.8 the values of $\overline{Pa}$ were: 8, 10, 14, 18 respectively. The calculated and experimental values of total pressure downstream of the normal shock differ substantially due to absence of boundary layer in calculations. The longitudinal pressure distributions obtained by both methods show good agreement. Fig. 4.1.4a

presents the pressure distribution along the wide section wall at R/r = 1.65 and two values of Pa. It is seen that 3.5 times change in Pa leads to 30% displacement of pressure peak position and practically coincide with experimental data. As comparison of calculated and experimental pressure distributions show at R/ra = 1.23, Ma = 3.8 the experimental value of Pmax appeared 20% greater than calculated. The increase of the number of cells from 30 to 60 practically does not change the result. In Fig. 4.1.4b pressure distributions corresponds to Ma = 2.6. The length of the narrow part is 5.5 d. In this case $\delta / r_a = 0.2$. The agreement between theoretical and experimental data is good. At Ma = 2.2 the discrepancy in curves noticeably increases. So, Ma = 2.6 can be considered as critical for the used method of calculation.

Below there are given the results of supersonic flow investigations in rectangular stepped ducts. The flow in the narrow part decelerates to near critical velocities. There were investigated three ducts with similar wide parts' sections (37.5 by 12.5 mm). The narrow parts had similar width while heights were equal to 7.5, 6.2 and 5 mm. So aspect ratio of these sections was 4.9, 5.6 and 7.4 and hydraulic diameters were 12.5, 10.6 and 8.8 mm respectively. The length of the wide section was 200 mm (l/d_h= 10.5) and the length of narrow one was 400 mm (l/d_h = 32, 38 and 45). The duct expansion ratios were equal to 1.67, 2.03 and 2.5. The experimental conditions did not change from that outlined in section 2. At Ma = 2.6 the flow choking takes place at all diffusers and at Ma = 3.2 it occurs at d_h = 10.6 and 8.8 mm, and at Ma = 3.8 there were supersonic flows at all the ducts. The static pressure distribution in the tube with two steps and the dependence of base pressure in them on Re are presented in Fig. 4.1.5. It is seen that pressure in stepped ducts strongly depends on Re at large M and expansion ratios. Fig. 4.1.6 presents pressure distributions in rectangular ducts with d_h = 12.5 and 10.6 mm at Ma = 2.6 and 3.2 successively (solid and dashed lines). Reynolds number variation in the range analysed changes the position of the pressure maximum relatively little. Critical flows occur in both cases, however at Ma = 2.6 in front of the step there is prolong region of subsonic flow ($\Delta x = 10 d_h$) and at Ma = 3.2 this region does not surpass $\Delta x = (3\text{-}4) d_h$. So, it can be expected some difference in velocity profiles in the critical section. Only supersonic flows in wide part were considered. Such regimes at Ma = 2.6 took place at Re > 1.6 10^6 Downstream of the first pressure peak flow acceleration was noted.

In Fig. 4.1.7 at Ma = 2.6 the pressure distribution is presented for the duct with $\bar{b}$ = 6. The static pressure in front of the step is near to calculated by using the rate equation and the condition that static pressures in the sections are even. In the immediate vicinity of the step the static pressure drops (shaded symbols correspond to the pressure in the narrow part and open symbols- to the pressures in the wide part) due to upstream pressure influence along the subsonic boundary layer. On the same diagram computed curves (code of Ref. 54) are presented. For initial static pressure it was taken P = Pw. Analysis indicates that in the case of rectangular ducts with flow deceleration in the narrow part up to critical speed due to friction, i. e. at wittingly non uniform flow in the section of sudden expansion, the flow in the wide part qualitatively corresponds to the flow in circular stepped ducts. The pressure peaks are present. The pressure distribution measured along the upper (without step) wall just downstream the step practically coincides with calculated distribution. As the distance from the step grows the difference between measured and computed data increases due to viscosity effect. The pressure in peaks along the duct grows contrary to calculated results. Still more discrepancies take place along the lower wall. In calculations the base pressure was taken from experiment. At x > 0 the curves do not coincide. The calculation was made for two-dimensional flow but in reality it is three-dimensional. The high pressure from the region of reattaching transmits along corners into base region. As a result the isobaric region, that exists in the case of axisymmetrical flows, in rectangular stepped duct does not realised. The pressure grows continuously along the length of $\Delta \bar{x}$ = 2 and than decreases. The maximal pressure is realised approximately at the same distance as in the case of ideal fluid, but the value of the pressure in the peak is about 40% lower. Thus, the two-dimensional computing programme can be used only at a restricted region lying near by the upper wall.

4.2 Influence of flow gasdynamic parameters in stepped ducts on base pressure

Gasdynamic devices, for example scramjet passages can have sudden expansions. The possible modes of operation are discussed earlier. The front part of the passage can be occupied by supersonic flow and supersonic/subsonic transition flow can occur in the rear part. In this case the flow deceleration character is affected by the pressure shocks with intensity depending on the base pressure - $\overline{Pb}$. The value of $\overline{Pb}$ in turn is defined by numbers M and Re, boundary layer thickness in front of the step, by the duct shape up and downstream of the step, by the secondary jets injected into base region. The base region flow has been the objective of much research, their overview is given in Ref. 1, 2. But at present, less emphasis is placed on inner flows. Some investigations, Refs. 55-61, do not bear evidence of systematic character and their results sometimes lead to conflicting conclusions, excessive base pressure levels, Ref. 58, 59 and 62, that can be explained by methodological errors induced for example by non hermetically sealed experimental models. The present base pressure investigations in the ducts were carried out at the following flow parameters in front of the steps: Ma = 1-4, Re = (7-17)x10^6 ,relative boundary layer thickness-$\overline{\delta}$ = δ/h = 0.1-1.0 and duct expansion ratios f = 1.15-3.0.

The duct directrix angle inclination θ = 0-26 . These parameters can be considered near to possible for ramjets and scramjets. In the beginning let us take a look at the experiments with circular stepped ducts. The experimental facility (stepped ducts) scheme is sketched in Fig. 4.2.1. The length of narrow part of stepped duct varied in the range l = (0-22)d with the interval of Δl = 5.5d. The boundary layer thickness in this case comes to $\overline{\delta}$ = 0.1-1.0 (i. e. up to layer closing). The effect of inclination angle on $\overline{Pb}$ was investigated using conical nozzles (at l/d = 0). The rear of the stepped duct, which was connected with ejector in all cases was longer than 5D. That is much more than the possible separation region length downstream the step. This fact assured, at the vacuum existed at the back of the facility and designed Re, the automodel separation flow realisation.
The contoured nozzle Mach numbers were as follows: 1, 1.5, 2.2, 2.6, 3.2, 3.8. The diameters of first two nozzles were 49.6 mm and the others-81.4 mm. The conical nozzles with Ma = 3.8 had θ = 19 and 26 . and with Ma = 4.25, θ = 14 . The experiments were carried out with cold air (Tt = 250-260 K). The air was dried but factual humidity was not measured. Control tests repeatedly carried out and the fact that the base pressure values were not greater than minimal known in References at similar conditions allows to suggest that the effect of humidity was negligibly small.
The base pressure was measured on the step face directly, at the distances from the axis r_i/r = 1.12, 1.20, 1.30, 1.44 (r- nozzle radius) and on the surface of the wide part of the duct in the isobaric region. The base pressure was also measured in the plane parallel to the step face (0.5 mm from it) with the use of a transferring probe. The base pressures were normalised by static pressure in front of the steps-$\overline{Pb}$ = Pb/P . Here P is wall static pressure, 10 mm upstream the step. The pressure P and flow rate were used to calculate the average Mach number in front of the step. The wide parts of the ducts were replaceable (D = 134, 108, 100 and 89.5 mm). At d = 81.4 mm the expansion rates were f = 2.72, 1.75, 1.51, 1.2. At d = 49.6 mm the used diameters were 81.4 and 60 mm (f = 2.72 and 1.51). For the purpose of $\overline{\delta}$ effect estimation on $\overline{Pb}$ the cylindrical part was substituted for conical one with half angle 0.5 . The length of this narrow part is l = 4.9d, and the exit diameter-88 mm. In the combination with the tube diameters 108 and 134 mm this section formed steps with f = 1.51 and 2.3. The base pressure dependence on Reynolds number for axisymmetrical bodies with conical noses in free supersonic flow has complicated character (Ref. 1). As Re decreases the value of Pb at first decreases and reaches a minimum and then increases because of boundary layer laminirisation. Base pressure investigations of internal flow intended for ejectors and ejector nozzles at nought secondary flow rate (Ref. 2, 55, 62) indicated Pb rise at Re decreasing. In present work this effect is studied in detail. Fig. 4.2.2 gives base pressure distributions along the tube radius taken by the total pressure probe moving in the shade of step. Out of the shade this Pitot tube measured total pressure in the boundary layer at the nozzle exit. In the upper part of diagram, at r_i/r = 1-1.65 the values of $\overline{Pb}$ and in the bottom part, at r_i/r = 0.75-1.0-the values of $\overline{Pt}$ = Pt/p are plotted. Fig. 4.2.2 gives the results for

two variants of ducts: 1. Section of sudden expansion is placed: directly downstream the nozzle (open symbols) and 2.-downstream the lengthening tube (l/d = 5.5, shaded symbols). From Fig. 4.2.2 analysis it is apparent that at Ma = 3.8 and Re > 4.6 10^6 the boundary layer is turbulent since the velocity distribution is expressed by the corresponding power law. The curve shown by dashed line is taken for power degree n = 1/7. The values of $\overline{Pb}$ as opposed to $\overline{Pt}$ depend more strongly on Re. The decrease in Re at l/d = 0 leads to Pb decreasing. Base pressure distribution becomes less uniform. At l/d = 5.5 (δ /r =0.2) the transition from Re = $14\text{x}10^6$ to $4.6\text{x}10^6$ .changes the pressure distribution character in smaller degree than at l/d=0.

Further investigations showed that the dependence of $\overline{Pb}$ on Re is affected by M, expansion ratio f, and nozzle generatrix angle θ. Fig. 4.2.3 depicts in particular $\overline{Pb}$ dependence on Ma, Re, and f at l = 0, θ = 0, and r_i/r = 1.2. At this value of r_i/r base pressure is practically the same as on the wide tube wall in the isobaric region. This Figure also presents relationship of $\overline{Pb}$ and Re for the nozzle with θ =

14 . at f = 2.72.

As it follows from Fig. 4.2.3 the minimal value of Pb is reached at maximal Ma and f. At Ma < 3.8 and f = 2.72 the influence of Re on $\overline{Pb}$ decreases but its character does not change up to Ma = 1. When f changes the function Pb(Re) undergoes alteration. So, at f < 1.51 no matter what Ma is the value of $\overline{Pb}$ increases with Re drop, and at f = 1.75 either stay constant (at Ma = 3.8) or increase (at Ma = 2.6). An increase in boundary layer thickness (shaded rhombus) decreases influence of Re on Pb. The change of contoured nozzle to conical one (Ma = 4.25, θ = 14) at f = 2.72 does not change the function character but effect of Re on $\overline{Pb}$ becomes less essential. Referring to Fig. 4.2.3 it will be observed that an automodel flow regime take place at Re much greater than that corresponding to Remin at which turbulent nozzle flow as yet exists. For rough estimates ($\overline{\delta}$ = 0.1 and θ = 0) the following relationship can be used:

Reaut> (5xMa-4)(D/d-0.65)x10^6

Special features of the above discussed flows evidently can be explained by the sharp pressure drop (in 20 times) in the expansion fan. This pressure drop can change pressure pulsation characteristics in the wake downstream the step. With the aim to find Re effect on pressure pulsation appropriate experiments were carried out. The Ma = 3.8 nozzle was connected with the 134 mm tube so expansion ratio was 2.72. The remote control probe was mounted on the tube wall. The total pressure and its pulsation's were measured at a distance of 0.5, 20, 50 mm from the nozzle. The probe stroke was 50 mm and minimal pitch-0.2 mm. At X = 20 and 50 mm the probe moved in the shear layer. Maximal flow total pressure was 5.5 MPa, minimal- 0.5 MPa (at ejector working). For the purpose of understanding of incoming flow pulsation influence on the base pressure and pulsation characteristics downstream the step a turbulisator made in the shape of a disc with 6 holes was installed in subsonic part of the nozzle.

Fig. 4.2.4 presents dependencies of relative total pressure pulsation intensity on Re. As seen from this Figure maximal values of $\overline{\varepsilon}_p$, as was expected, are positioned in the region of maximal velocity gradients in the boundary layer and reach $\overline{\varepsilon}_{p,max}$= 6.5-7.5 %. Outside boundary layer the values of $\overline{\varepsilon}_p$, are in the range of 0.4-1.5 % and they increase with Re drop, as was in the shear layer. Besides, curves $\overline{\varepsilon}_p$ (h) stop being monotonous when Re reaches minimal values. The boundary layer at the end of the nozzle likely passes from turbulent into transient one. At Re decreasing the total pressure distribution becomes more non uniform.. The pressure pulsation intensity increases with the distance between measuring section and nozzle. However, the pressure pulsation dependence on Re is still present. This relationship is most pronounced in Fig. 4.2.5 whose data correspond to fixed probe positions. The values of $\overline{\varepsilon}_p$, in all the measurement sections and probe positions decrease by 1.5-2.0 times when Re increases from $5.\text{x}10^6$ to $12\text{x}10^6$. On further Re increase the values of $\overline{\varepsilon}_p$, increase. Thus, in all situations examined the decrease in Re makes pressure pulsation more intensive that can

result in mixing intensification. It is possible that this phenomenon is the reason for base pressure drop. However, $\bar{\varepsilon}_p$, increasing takes place not in the expansion fan or mixing layer but in the the supersonic part of the nozzle. At small duct expansion ratio, f = 1.51 and the same Ma = 3.8 there is no base pressure drop at the Re decrease. This can be explained by the short separation region and mixing layer. The comparison of pressure pulsation fields at the turbulizator present or removed is demonstrated in Fig. 4.2.6. The turbulizator placed at the subsonic part of the nozzle causes the value of $\bar{\varepsilon}_p$, to increase, however, the existed relationship $\bar{\varepsilon}_p$, and Re is conserved. This result allows to suggest that the flow rearrangement process take place in the supersonic part of the nozzle.

Figs. 4.27, 4.2.8 present data exhibiting effect of Ma, $\bar{\delta}$, and f on $\overline{Pb}$ and Reaut. parameters. This relationship at l = 0 and θ = 0 received at present (symbols and solid lines) and other works (θ > 0, dashed lines) are displayed in Fig. 4.2.7. The dashed line for Ma = 1.0 is taken from Ref. 63. and corresponds to many author results. We emphasise that all methodological errors, as facility non hermetic, air humidity and so on lead to $\overline{Pb}$ growing. These errors possibly are characteristic to a number of experimental works (Ref. 58, 59, 62).

Fig. 4.2.8 depicts the relationship between $\overline{Pb}$ and Ma for f = 2.72, 2.3, and 1.51. Different open symbols correspond to different nozzles at $\bar{\delta}$ = 0.1, l = 0, and shaded symbols (the same configuration) accords to the same nozzles but to more thick boundary layer (at l > 0). The symbols with dashes indicate that in tests was used slightly diverging duct that allows to receive core Mach number equal to Ma at $\bar{\delta}$ = 0.2. Transition from the right from one to the other symbol of the same configuration corresponds to duct lengthening by 5.5 calibre. The limiting left shaded symbol of each configuration corresponds to the lengthening tube of l = 22d.

The comparison of present base pressures with these received in Refs. 55 and 56 strongly suggest that $\overline{Pb}$ monotonously decreases independent of f and θ if Ma increases over 1.5. We dwell now on effects of $\bar{\delta}$ on $\overline{Pb}$. The increase in δ is limited from above ($\bar{\delta}$ < 1) that is why for given f the influence of $\bar{\delta}$ on $\overline{Pb}$ is also limited. The upper curve of each dashed envelope in Fig. 4.2.8 corresponds to maximal $\overline{Pb}$ that does not surpass $\overline{Pb}$min more than by 40-50%. At lesser M the effect of $\bar{\delta}$ on $\overline{Pb}$ decreases. The bulk of $\overline{Pb}$ increase occurs at the transition from $\bar{\delta}$ = 0.1 to $\bar{\delta}$ = 0.2, i.e. at the transition from l = 0 to l = 5.5d. Base pressure becomes practically maximal at $\bar{\delta}$ = 0.3-0.4 (l =11) and further increasing in l increases $\overline{Pb}$ only due to decrease in M. This phenomenon can be easily explained by small increase in δ** when boundary layer is nearing to closing. Practically linear relationship of $\overline{Pb}$ on δ** is exhibited in Fig. 4.2.8 insert

The effect of inclination angle θ on $\overline{Pb}$ was investigated at two values of f (2.72 and 1.51) at Ma = 3.8, l = 0, and Re near maximal. The test results including variant of conical, Ma = 4.25, θ = 14 . nozzle are depicted in Fig. 4.2.9. At the same Figure the data of different authors that were carried out at conditions not much different from present flow conditions considering the slight dependence of Pb on M (at M > 2.5). It is seen that for considered f the influence of θ on $\overline{Pb}$ is quite essential. So, the transition from θ = 0 to 26 . at f = 1.51 produces to near 10-times base pressure increase that becomes larger than the exit nozzle static pressure. There the flow rearrangement occurs: instead of expansion fan coming from angle point at the nozzle exit, there goes the weak pressure shock at θ = 26 .

In the range of θ = 0-10 . there is rather weak θ influence on $\overline{Pb}$. The relationship is near linear. The increase in duct expansion ratio up to f = 2.72 practically does not change the relative influence of θ on $\overline{Pb}$. These specific features of relationship $\overline{Pb}$(θ) can be explained as follows: it is known, Ref. 64, that stream and tube wall meeting angle in discussed range of Ma and f does not change considerably and does not surpass 30-35 . The initial stream inclination in conical nozzles decreases the flow

turning angle in the sudden expansion section and consequently increases $\overline{Pb}$. This reasoning was supported by the following experiment: The conical nozzle surface was directly followed by the short cylindrical ring having the width of 0.1d. Thanks to flow turning at the ring and pressure shock appearing the pressure at the end of the nozzle with the ring sharply increased. In spite of it the base pressure at this sharply decreased due to flow turning angle increase. Experimental data of Refs. 56 and 61 are in good agreement with present work data. The relationship was received as a result of experimental data development. It permits to estimate $\overline{Pb}$ as a function of basic parameters in the range of M = 1-4, f = 1.2-2.72, $\bar{\delta}$ = 0.1-0.3, θ = 0-20 .

$\overline{Pb} = 16[0.145\, e^{-0.49\,(M-1.3)} + 0.0085(M-1.3)^2 + 0.05(\bar{\delta}-0.1)(M-1.3)]x[0.0106 + 0.0624/f + 0.167/f^2]\,(1 + 7\; 10^{-2}\;\theta)$ Maximal error in base pressure determining according this formula, 20%, takes place at M = 1.7-2.3.

For completeness sake the negative angles θ effect on $\overline{Pb}$ was considered The experiments were carried out with sonic nozzles. The inclinations of conic surfaces were 0, 15, 30 and 45 . There was only one value of expansion ratio f = 2.72. As it proved to be base pressures in the range of θ = 0-30 . practically do not depend on θ. Only at θ = 45 . there is noted a slight drop in $\overline{Pb}$. The mass rate coefficient decreases by 6% due to "liquid" throat arising. The cylindrical section of 4d length installed between the sonic nozzle and the wide tube does not change the correlation between $\overline{Pb}$ and θ. Fig. 4.2.10 presents the pressure distribution along the lengthening section. It is seen from Fig. 4.2.10 that pressure drops at θ rise is displayed for the length of l < 0.5d. So, the effect of sonic nozzle geometry on $\overline{Pb}$ at large duct expansion rate practically does not note. At lower f the influence of boundary layer thickness on Pb can become more visible. This suggestion has found confirmation in tests in which conical cowl (Fig. 4.2.11) with half angle 4 . was placed in different parts of the tube. The expansion rate was in this case f = 1.24. Fig. 4.2.11 depicts the pressure distribution along the cowl and the tube in the isobaric section for three tube lengths and three values of Ma at the critical regime. Fig. 4.2.11 analysis shows an interesting feature : an increase in duct length in front of the cowl at a certain range leads to the base pressure decrease. This phenomenon does not correspond to general tendency and possibly can be explained by the change in flow velocity profile in front of the cowl. It can be expected that if analogues non uniform velocity profile is artificially created in front of expansion fan then lower pressure can be achieved downstream of it.

We dwell first on the flow characteristics in front the sudden expansion, the method of creating of critical regime, e.i. regime at which a supersonic flow becomes sonic one. The velocity profiles in cross section can be created by combined action of friction and secondary jet injection. It can be expected that jet injections in forward part of the duct produce more uniform profiles than the jets in the back tube section. Jet injection from the duct wall must provide profile with low velocities near the wall and jet injection in the centre of the tube will induce more uniform profiles, Fig. 4.2.12.

Fig. 4.2 13 illustrates the pressure distributions along the 12.5d length tube for different mass increasing coefficient β The jet injection was carried out in the front part of the tube. At β> 1.13 the supersonic flow at the back part of the tube becomes subsonic and the length of this region grows with β. The duct length increasing does not change the flow character. As indicated earlier the static pressure at the duct end depends on β. Once the boundary layer is thick the change in jet injection position does not have a pronounced effect on the Mach number profiles at the duct end (Fig. 4.2.14). At lesser duct lengths the influence of jet injection position is greater, Fig. 4.2.15, 16

Come back to the effect of history of critical regime rise on pressure distribution on the conic surface downstream the expansion fan. The character of this flow expansion will be the same as in the case of flow over a step. The pressure distribution along 11.7 cone surface is depicted in Fig. 4.2.17 for different variants of critical flow mode creating. The dashed line corresponds to one-dimensional analysis. The pressures are normalised by the static pressure at the duct end P_1 that was calculated

knowing flow rate, plenum pressure and value of β. As evident from Fig. 4.2.17 the influences of flow non uniformity in front of expansion fan manifest this property mainly at the front part of the conic surface, $r_i/r< 1.4$. The pseudo-shock transition due to β varying practically does not change the value of P_1. The most effect on this value is rendered by the jet injection at the back of the tube. This influence is increasing at thin boundary layer. At l = 1.35 the pressure distribution character changes, pressure drops below values corresponding to one and two-dimensional flow. At the same time the general relationship P(R) support Ref. 65 experimental results that indicate that the pressure directly downstream the angular point (at the distance of approximately equal to five boundary layer thicknesses) is higher then that in Prandtl-Mayer theory. Supersonic parts of the boundary layer expansion and flow directly downstream of it is in essence inviscous, e.g. caused from under the pressure forces. Ref. 65 depicts that at small flow turn the inclination angles of all flow lines mainly depends on initial Mach number and practically does not depend on the initial velocity profile.
As a supplement let us analyse the effect of jet injection into base region. The injected air had the same stagnation temperature as the main stream and added mass in the wake at the rate G. The dimensionless injection number H is defined by $H=\frac{G_b\sqrt{T_t}}{hP_t}\sqrt{\frac{R}{g\gamma}}$

where R is gas constant, g is gravity constant, h - height of step, P_t and T_t - are stagnation pressure and temperature of the main stream .The injection of air has little effect on pressure profiles. In any event the change in H = 0-0.01 is negligible. Still less change is noted at Re variation Re = (2-15) 10^6 . In Fig. 4.2.18 the relationship of Pb/P_1 vs. related injection flow density is plotted for variant f= 1.51 and Ma = 2.6. Here ρu= Gi/(G1+Gi) where Gi and G1 are air flow rates through slot and nozzle. The change of ρu was controlled by means of slot width and plenum pressure change. The curve character is analogues to curves for plain flows.
Earlier we discussed the effect of flow non uniformity on base pressure. The non uniformity can occur if in front of one step another step is present. Fig. 4.2.19 illustrates base pressure dependence on duct length for this case. As it seen from this Figure the split of one step by two at equal total expansion ratio leads to base pressure increase and correspondingly to axial force rise by 30-40%.

4.3 The effect of stepped duct cross section geometry on base pressure

The diverse duct geometry is governed by technical devices properties, requirements of minimal (ejectors) and maximal (scramjets) base pressures. The maximal base pressure is achieved in axisymmetrical inwards to the axis, and minimal base pressure - in axisymmetrical outwards from the axis, flows. The flow in the plane stepped duct takes intermediate position. In the present paper simple straight ducts with walls directed parallel to velocity vector and various cross sections up and downstream the step are considered. The surface in front of step was cylindrical (with different position of curvature radius) and plane. Fig. 4.3.1 sketched all the tested ducts - 7 groups. For the most of them the surfaces of contoured nozzle, M 2.6 and its butt were used as surfaces of stepped ducts. Schemes of the ducts are placed in the upper part of Fig. 4.3.1, 1-5 groups. The expansion flow corresponds to the flow outwards from the axis. In the middle part of Fig. 4.3.1 the ducts, group 6. with flow corresponding to the flow inwards to the axis are placed. In this case the model consisting of cylindrical surface with the radius 40.7 mm and the duct downstream of it was placed in the rhomb of uniform velocities of the nozzle (free jet tests). The plane ducts (side walls on the lower left scheme, Fig. 4.3.1, group 7 are not shown) were tested in the wind tunnel with variable geometry nozzle in the M = 2.7-3.5 range. The steps were produced by the wedge-like inserts installed on one or several rectangular duct (37.5 by 60 mm) walls.

In the general case (see for example duct 3.3) the duct consisted of lower wall adjoining to the 134 mm duct wall, side and upper walls. The upper wall could be moved between side walls, changing the expansion ratio of the duct f. If the upper wall was removed the duct transformed from closed into half open (group 2). In the case when side walls do not jut out over the nozzle surface and are in "shade" of the step, the ducts were called open ducts or shoots (groups 1 and 6) The duct flat walls were thin, their front edges projecting into the flow were sharpened from the external side to exclude disturbances coming into duct flows. The shape of shoots was determined by the angle of wall inclination to the symmetry plane and the shape of the closed ducts, in addition, by the inclination angle of the wall parts projecting over the step. Angle α took the values 45, 0, -22.5, -70^0 and angle β =45, 27, 0, -33^0. The part of the duct projecting over the nozzle surface and having area F_1, can be considered as a narrow part of the stepped duct and the duct downstream the step with the area F_2-a wide part. The expansion ratio of this duct is $f = F_2/F_1$. In the most cases the duct entrance was positioned in the sudden expansion section and only in separate cases, as it is depicted in Fig. 4.3.1, variant 3.3 the entrance was placed upstream this section.

Besides symmetrical closed ducts non symmetrical ducts were analysed (Fig. 4.3.1, group 5). The angle β for variants 5.2-5.5 was fixed and equal to 45^0., and angles between side walls and symmetry plane of the narrow part of the duct α_1 and α_2 were equal to -30^0 and 30^0, 53^0 and 0, 60^0 and -22.5^0, 75^0 and -80^0. The non symmetry of the figure can be characterised by eccentricity ε- the distance of centre of gravity from the symmetry plane of the initial duct (variant 5.2). In going from duct 5.2 to duct 5.4 the value of $\bar{\varepsilon} = \varepsilon/\sqrt{F}_2$ changes from 0 till 0.5.

The step edge length characterising the duct widths for groups 1-6 was equal to 1/8 if the nozzle circumference. The pressure taken as base pressure was measured on side walls near the step face (3 mm), on 134 mm duct surface (3 taps) and directly on the butt end of the step. The base pressure was normalised by the static pressure at the nozzle surface $\overline{Pb}$ = Pb/ P. The length of the ducts was 200 mm (in special cases 400 mm) that surpasses the length of the separation region many times and guarantee the existence of the automodel supersonic flow at the vacuum produced by the facility. The ducts placed over the nozzle perimeter were investigated by groups. The group 1 (6 ducts) and groups 3 and 5 (8 ducts) were tested simultaneously. The tests of ducts in blocks besides the save in time and volume of tests give one more advantage - all the ducts were blown by the flow having the same parameters including velocity, temperature, humidity, and boundary layer thickness. That makes it simpler to compare the results with different ducts. Arithmetic mean base pressures were used in all the following diagrams. It can be expected that base pressure distribution on the step face due three-dimensional flow can be non uniform. Very likely that the largest non-uniformity corresponds to variant 3.5. In Fig. 4.3.1 the disposition of four pressure taps on the step face is shown. Base pressure distributions measured at different expansion ratios are summarised in the accompanying table.

f	p_{b1}	p_{b2}	p_{b3}	p_{b4}
5.3	0.685	0.0665	0.064	0.067
3.8	0.108	0.100	0.096	0.100
2.8	0.i24	0.126	0.110	0.117
2.4	0.163	0.167	0.175	0.187

It is seen from the table that at large expansion ratios (f>3.8) the non uniformity of the base pressure is small and does not surpass 4%. At smaller f non uniformity increases with $\overline{Pb}$ at the walls (points 3 and 4) getting higher.

Fig. 4.3.2 illustrates the relationships $\overline{Pb}(\alpha)$. Three groups of ducts are investigated: shoots (groups 1 and 6), shoots with additional parallel walls (half opened ducts, group 2), and ducts with fixed shape of incoming streams and expansion ratios (groups 3 and 4). The base pressure levels correspond to plane and axisymmetric outwards and towards axis flows are depicted in Fig. 4.3.2 as well. The analysis of Fig. 4.3.2 lets to conclude that angle α is an important parameter of this separation flow. The change of α in the range from -30^0 to 30^0 increases p_b 3-7 times and this relationship is near linear with the inclination of lines to the horizontal $k = dp_b/d\alpha = 0.006$. p_b takes values correspondingly to axisymmetrical towards the axis, plane, and axisymmetrical outwards from the axis as α decreases. The lowest base pressures for open ducts correspond to duct groups 1 and 6. It can be supposedly explained by the flow expansion that takes place not only at the nozzle edge but also along the side walls. When this additional expansion at $\alpha = 0$ is excluded by the additional parallel walls installing (ducts 2.2 and 2.3) the flow is nearing to plane one and the value of p_b confirms this fact (compare ducts 1.3 and 2.3, Fig. 4.3.2).

More high base pressure level in group 3 (at f = 2.4) can be explained by pressure shocks and near wake interaction. More neat manufacturing of the duct front edges, upper and side wall junctions helped to decrease $\overline{Pb}$ approximately by 25% (lower shaded symbol for the duct 3.3). Additional confirmation of this conclusion is in experimental data for the duct 4.3 that has the same expansion ratio f = 2.4 but the movable upper wall removed. In Fig. 4.3.2 the value of $\overline{Pb}$ for this case is marked by the cross and it practically coincides with $\overline{Pb}$ for duct 2.3. Base pressure downstream the step in axisymmetrical flow can change several times depending on direction of expansion (towards or outwards axis). As one can see from Fig. 4.3.2 at the restricted duct width the angle α is the governing factor controlling $\overline{Pb}$ and direction of radius of curvature of duct edges practically does not effect this pressure (compare ducts 1.2, 1.3, 6.2, 6.3). The decrease in the width of the duct must in principle increase $\overline{Pb}$ due to increase of friction loss. As experiments with the ducts 1.3 and 1.4, the width of which was shorten by twice by installing a partition in the middle of the duct, showed that effect is very small, practically negligible. The conclusion about great influence of α on $\overline{Pb}$ is correct for symmetrical ducts. For non-symmetrical ducts, group 5 the change of α at fixed expansion ratio does not lead to essential change of $\overline{Pb}$. In the insertion of Fig. 4.3.2 the relationship $p_b(\bar{\varepsilon})$ is plotted. At $\bar{\varepsilon} = 0$-0.5 variation the base pressure changes approximately by 10%. So, the increase of α_1 at one wall and corresponding increase in flow deceleration is compensated within certain limits by the decrease in α_2 and flow expansion at the other wall.

In Fig. 4 3 3 the dependences of $\overline{Pb}$ on boundary layer thickness $\bar{\delta} = \delta/h$ for closed and opened ducts are plotted. The value of δ stayed fixed while h decreased due to plates installing at the bottom of the ducts 1.3, 4.2, 4.3, 4.4. For closed ducts there is a change in expansion ratio (f = 2.4-1.2). However, as it is shown below (Fig. 4.3.5) the change of f has little effect on p_b in the analysed range of f. Fig. 4.3.3 indicates that relationship $\overline{Pb}(\delta)$ is rather near to the plane flow (dash-dotted line, Ref. 2). Absolute value of $\overline{Pb}$ of ducts 2.3 and 4.2 are most close to the plane flow, as it was mentioned above. The relationship $\overline{Pb}(\delta)$ for ducts 4.3 and 4.4 differ insufficiently that says about little effect of incoming stream shape on $\overline{Pb}$ at fixed f. Increased level of $\overline{Pb}$ for this ducts is connected, likewise for duct 3.3, with interaction of shocks induced by duct leading edges with the near wake. At $\bar{\delta} = 1$ the values of p_b for this ducts are near and approximately

correspond to 2D flow over the step. The influence of walls restricting the flow is minimal in this case. In Fig. 4.3.4 the dependence of $\overline{Pb}$ vrs Ma for ducts with rectangular cross section (group 7) is presented. The duct was flown by free stream with Ma = 2.7-3.4 in the wind tunnel with smoothly variable plane nozzle. In Fig. 4.3.4 the relationship $\overline{Pb}$(M) for 2D flow is also plotted (the envelope restricted by dash-dotted lines, Ref. 2). Notwithstanding of disposition of steps along the perimeter of rectangular ducts the base pressure decreases with the increase of expansion ratio f. The sharp base pressure decrease for all the ducts at Ma > 2.7 can be explained by the transition of reflected shocks into region placed far from the near wake. The increase of the number of duct sides along which the steps are formed, e.i. nearing to the case of axisymmetrical flow, leads to decrease in p_b (compare ducts 7.2 and 7.4). For the ducts at which flow expansion occurs over main part of perimeter (ducts 7.3 and 7.4) an increase of M decreases the value of $\overline{Pb}$ down to values corresponding to axisymmetrical flow with expansion outwards from the axis.

In Fig 4.3.5 there are given the dependencies of $\overline{Pb}$ in stepped ducts on reversed value of expansion ratio - 1/f. The characteristic feature of the supersonic flow in closed stepped ducts lies in the fact that base pressure can be made as small as is wished notwithstanding on the duct cross section shape. At $1/f \to 0$, $P_b \to 0$. On the other hand at 1/f nearing to unit the base pressure have to approach to the 2D flow base pressure. In Fig. 4.3.5 for comparison by vertical fragments and dashed envelopes the range of $\overline{Pb}$ for different types of flow and Mach numbers are depicted. Solid lines connect the values of p_b for ducts with variable f. Dash-dotted line corresponds to relationship $p_2/p_1(1/f)$ for isentropic flow. Here p_1 and p_2 are static pressures at the beginning of the duct (M = 2.6) and at the end of it successively. The influence of 1/f on $\overline{Pb}$ is investigated in detail for the duct with rectangular cross section (3.3). From Fig. 4.3.5 is seen that at 1/f < 0.4 there is rather sharp drop in base pressure and an approaching to isentropic expansion. This can be explained by the interaction of the expansion fan and the near wake.

In the range of 1/f = 0.25-0.50 maximal scattering of experimental data is noted which is connected with interference of shocks initiated by duct wedges projecting into the flow (dashed region). At 1/f > 0.5 these disturbances do not hit near wake and base pressure stabilise and approaches to the base pressure downstream the plane step. Base pressure in the ducts 7.1 and 7.2 are near to the upper boundary of the plane flow. An increase in p_b in this case can be explained by the large number of shocks induced by the duct edges. An increase in α up to 30^0 (duct 3.2) makes the flow near to axisymmetrical with expansion towards the axis. So, influence of α on $\overline{Pb}$ develops quite essentially in all types of ducts at any values of expansion ratio. The relationship $\overline{Pb}$(1/f) for the duct 3.5 approaches as expected to zero at $1/f \to 0$, notwithstanding to some exotic shape of the duct, confirming the community of the phenomenon.

4.4 Base pressure in annular stepped ducts.

Base pressure downstream the step in internal flows as it evident from the foregoing discussion depends on the duct shape and at similar area expansion ratio can change many times over. It refers in full measure to the annular stepped ducts. Some factors can have a twofold effect on base pressure. So, an increase in the diameter of internal constant area tube at fixed external stepped tube at one hand will serve to decreasing of base pressure due to expansion ratio increasing and on the other hand it draw the flow near to the flat one that leads to base pressure rise.

Experimental facility scheme is presented in Fig. 4.4.1. Three tube sections having lengths of 450 mm each and diameters d_1 = 81.4, d_2 = 100 (or 134 mm) were successively attached to the nozzle (Ma =2.6 and 3.8). In the first case (d_2 = 100 mm) the duct had two steps. In the second section thin-walled tubes of 450 or 650 mm length were mounted. The external diameters of this tubes were - 48, 58 and 66 mm. Front edges of these tubes were sharpened inside to minimise disturbances in the annular supersonic flow. The flow in the internal duct was also supersonic. At l = 450 mm the tube entrance was placed at the end of 81.4 mm tube and at l = 650 mm part of the tube, 200 mm long, entered into this tube. In all the cases an annular stream was cut out from the circular flow passing from the nozzle. The height of this stream in front of step was $h_1 = (d-d_1)/2$ and downstream of it $h_2 = (D-d_1)/2$. the annular ducts dimensions are given in table:

N	D mm	d_1 mm	h_1 mm	h_2 mm	F_2/F_1
1	100	0	40.7	50	1.57
2	100	48	16.7	26	1.8
3	100	58	11.4	21	2.05
4	100	66	7.7	17	2.5
5	134	0	40.7	67	2.72
6	134	48	16.7	43	3.62
7	134	58	11.4	38	4.5
8	134	66	7.7	34	5.95

As it seen from the table the expansion ratios of annular ducts are far exceed the ones of circular duct tubes ($d_1 = 0$). This factor is favourable to base pressure decrease. At higher values of d_1 annular ducts look like narrow slot that differ little from flat slot. Base pressure must be higher than in the case of axisymmetrical, outwards from the axis, flow. Base pressure in the second section of a sudden expansion is influenced by more thick boundary layer as well. There is no internal tube that makes interaction of internal and external flows inevitable. Such numerous factors make it difficult to analyse their influences on base pressure individually and in combination. Therefore, the results can be considered as preliminary and can be used only for approximate evaluations.

In the section 4.2 it was shown that the increase of boundary layer thickness $\bar{\delta} = \delta/h$ in the range of 0.3-0.8 can increase base pressure approximately by 25-30%. Further increase of boundary layer thickness increases base pressure very little. The influence of $\bar{\delta}$ on $\overline{Pb}$ can be estimated by the mean Mach number in front of step. Let us consider that mass flow in the annular duct is lower by δ^* in comparison to uniform flow. Because the static pressure across the flow is constant the mean M can be defined from the mass flow equation. Impulse loss coefficients and boundary layer parameters can be taken from Ref. 36. When employing internal tubes of 650 mm length there is additional deceleration of supersonic flow before step due to boundary layer in these tubes. Besides, there is some change in conditions for expansion fan reflection from internal tube surface. Mach number drops at the step section can be very notable. At $d_1 = 48$ mm and Ma = 2.6 the internal tube does not start up (Fig. 4.4.2) and normal shock occurs in front of it transforming all the flow into some kind of pseudo-shock. However, this very sharp change in flow character relatively little change base pressure. It can be possibly explained by relatively small rise of pressure in front of step. Maximal pressure in the first peak increases approximately proportional to p_1 increase. At l = 450 mm, Ma = 2.6 supersonic flow exists at all tube diameters, Fig. 4.4.2 b). the presence of lengthening section of the duct does not change the character of flow, Fig. 4.4.3. Since the objective of the experiments was base pressure measurements at supersonic velocities the tests were carried out at maximal total pressures (maximal Re) possible in the facility. At $Re>2.10^6$ the automodel supersonic flow with closed separation regions was achieved along the whole duct. The base pressure was measured at the face step surface and also at the tube surface in the isobaric region. Fig. 4.4.3 presents pressure distributions for Ma = 2.6 and different d_1. The first step was placed downstream the lengthening tube with d = 81.4 mm and the second step downstream the tube with D = 100 mm. The dashed line corresponds to variant without internal tube. From Fig. 4.4.3 it is seen that internal tube installing leads to sharp (2-3 times) rise in base pressure notwithstanding expansion ratio increasing. This rise in the base pressures can be explained by the flow pattern nearing to the plane flow. The pressure rise in the second step section is favoured also by thick boundary layer and system of pressure shocks. At internal tube diameter increase the reattaching of the flow take place at smaller distances from the step and the first pressure peak displaces upstream. The distances between following peaks also decreases. The peak succession downstream the first and second steps changes depending on d_1/d. The difference of peak levels in the cases of presence and absence of internal tubes is greater in the first step section. The decrease in boundary layer thickness (no lengthening tube) is responsible for large (in first section) and small (in second section) decrease in base pressure. Dash-dotted line corresponds to $d_1 = 48$ mm.

Figs. 4.4.4 and 4.4.5 show that influence of M on $\overline{Pb}$ is small. So, sharp rise of $\overline{Pb}$ with f increasing from 0 to 0.5 can be explained mainly by the nearing of the flow to the plane pattern. It is seen from Fig. 4.4.4 that at $(d_1/d)^2 = 0.5\text{-}0.8$ base pressure is higher by 20-30% than in plane-flow case for which the values of p_1/p were

determined at thick boundary layer. This increase in base pressure can be explained by the difference in boundary layer thickness. So, for particular case (Ma = 2.6 and f = 2-2.3) the base pressure in the annular stepped duct is near to that of the plane step. At $F_2/F_1 > 2.3$, for instance at d_1 = 66 mm and f = 1.51 and at any d_1 and f = 2.72 the influence of expansion ratio begin prevail over the influence of nearing the annular flow to 2D flow and the base pressure begin decreasing.
The increase in Ma up to 3.8, Fig. 4.4.5, causes the base pressure at f = 1.51 approach to the 2D step base pressure at lower expansion ratios. At higher values of d_1/d the base pressure in annular stepped duct is much higher than that in 2D case. This can be explained by the boundary layer influence. At the same time, as it was shown above, this influence develops mainly when the boundary layer is thin. The additional tube section installation, l = 5.5 that corresponds to two times increase in boundary thickness, Fig. 4.4.5, influence the base pressure rather small, especially at $(d_1/d)^2$ = 0.5-0.6. At f = 2.72 the base pressure in annular stepped duct at all $(d_1/d)^{2is}$ is lower than in 2D flow.
In Fig. 4.4 6 annular duct base pressure is plotted as a function of circular duct expansion ratio at minimal δ and Ma = 2.6 and 3.8. There are given also analogues curves for circular stepped tube, which are lengthened to f = 1 value, at which the base pressure was assumed equal to the base pressure at 2D flow at thin boundary layer. The analysis of Fig. 4.4.6 shows that the character of base pressure relationship in annular duct practically does not distinguish from analogues relationship for circular stepped tube. For the fixed ratio of expansion of annular stepped tube f maximal base pressure is reached at d_1 = 66 and 58 mm for Ma = 2.6 and 3.8 respectively.

4.5 Deceleration of supersonic flow in stepped tube and annular duct.

The supersonic/subsonic transition region lay-out in scramjet depends on flight conditions, scramjet passage geometry and the intensity of heat release. In present experiments the lay -out of this region is determined by the flow throttling. To evaluate the influence of throttling valve position on flow deceleration character the latter was placed at different distances from the step (x/d =5-10). In Fig. 4.5.1 the pressure distributions along the tubes with two variants of narrow parts (cylindrical and conical) at characteristic regimes are given. The sections of sudden expansions are superimposed. The curve 1 corresponds to fully open throttle and supersonic flow along the main part of the tube. Dash-dotted lines correspond to places of stream reattaching and shock incidence (determined using method Ref. 54). The pseudo-shock occurs when the throttle valve gets practically closed (curves 2). Curves 3 correspond to maximal back pressure at which yet there is no interaction between pseudo-shock and separation region downstream the step. The pseudo-shock transition strictly speaking is not a monotonously increasing function of back pressure. The front part of the pseudo-shock is fixed when crossing the pressure peaks. However, these delays and length shortenings are small and in practical applications possibly can be ignored.
A mass-average value of M downstream the step is 3.65. Pressure distribution in pseudo-shock at near this Mach number (3.8) and uniform flow in front of it is plotted by the dushed line. It is seen that inclination of this curve on the initial part of it is smaller than in curves 3. Such special features of curves 3 is characteristic when the pseudo-shock transition is limited by the regions at higher pressure. However, in the middle part of the curves the pressure gradient sharply decreases and there is no region length shortening. The difference in curve shape is explained by the difference in flow non-uniformity in front of pseudo-shocks. The change in boundary layer thickness ($\bar{\delta} = \delta/r$ = 0.1 and 0.3 at l = l/d = 0 and 11 instead of $\bar{\delta}$ = 0.2 at l = 5.5) changes pressure distributions character little. The change of cylindrical narrow part to conical one changes the supersonic flow pressure distribution but makes practically no change in the in the case of pseudo-shock.
Next specific regime of flow is the regime of interaction of pseudo-shock and separation region downstream the step-curves 4. High pressure transmission from the pseudo-shock region into base region leads to noted changes of flow character. An increase of the pressure acting on the butt end results in flow momentum increase, lower stream overexpansion and loss. As this takes place the pressure level on the rather long distance, contrary to pseudo-shock in cylindrical tube, decreases. Curves 3 and 4 illustrate the said. On the distance more than 4d the pressure along curves 3 is greater than along curves 4. The change of boundary layer thickness, the duct shape of narrow part and positioning of the throttling valve does not change the flow character.

The Pitot pressure field measurements explain the specific features of this flow. Comparison of curves corresponding sections x/h= 0.8 and 2 downstream the step and base pressure downstream the cylinder (Pitot tube turned downstream) in the section x/h = 3 was carried out in the duct in which D = 134 mm tube was directly connected to the nozzle (l = 0). In Fig. 4.5.2a Pitot pressure profiles p_t/p_a and in Fig. 4.5.2b - p_b/p_a profiles are plotted for the flows corresponding to the regimes 3 and 4 in Fig. 4.5.1. It is seen that the transfer from regime 3 to regime 4 leads to sharp increase in total pressure in the range of y/D = 0.18-0.28 and decrease in shear layer thickness. Dashed lines correspond to pressure level on the duct wall in the sections of the pressure probe positions. It is seen that at transfer from regime 4 to regime 3 in the region adjoining to the step face (in the "shadow" of step) the difference between p_t and p, p_b and p_1 increases that indicates at the vortex flow downstream the step deceleration. The increase in back pressure causes the increase in base pressure that can become greater than static pressure in front of the step. Curve 5 (see Fig. 4.5.1) correspond to limiting value at which increased pressure does not penetrate to the duct section upstream the step In the case of cylindrical duct limiting value of p_b/p_1 approximately corresponds to critical pressure relation of turbulent boundary layer. In the case of conical duct in front of the step this limiting value is smaller.
Curves 6 and 7 correspond to pseudo-shock transfer to the narrow part of the duct and this process was analysed earlier. We will only point out that as the pseudo-shock moves upstream the curves for both ducts are brought together and then practically coincide at the entrance of the duct. The pseudo-shock transfer flow and the value of axial force acting on the duct are factors determining the supersonic flow deceleration effectiveness. This effectiveness is higher if the pressure in the step section is greater and the duct length shorter. In Fig. 4.5.3a the dependence of distance between pseudo-shock boundary and the place of throttle valve position on back pressure is shown. It can be noted six characteristic regimes that arise as the back pressure increases: 1,2-free separation and pseudo-shock formation in wide section of the tube. It is seen that the transfer law of pseudo-shock at the boundary layer thickness change at the duct length variation l = (0-11)d changes little. The curves moves in the direction of lower values of l, that can be explained by the decreasing of mean M and increasing of pressure level in the wide section of the duct. In fact there is decreasing of back pressure. 3-interaction of pseudo-shock and separation region downstream the step. The pseudo-shock boundary does move at the back-pressure increase, in curve there is a plateau. This plateau the more so as the boundary layer in the narrow part of the tube is thinner. The presence of conical narrow section cut down the length of the plateau.
4-5-Flow separation in front of step and pseudo-shock formation in the narrow section of the tube. From Fig. 4.5.3a it is seen that the pseudo-shock transfer gradient at this regime is lower than in the case of pseudo-shock formation in the wide section of the tube and it decreases as the boundary layer thickness grows. The transfer gradient change is connected with flow former history that is determined by the shape of the duct following the examined stepped duct (see below).
6-Developed pseudo-shock in the narrow part of the duct. Large transfer of it take place at the very low increase in back pressure. In Fig. 4.5.3b for four variants of the narrow parts of stepped ducts axial force R normalised by the full nozzle momentum is presented. It is plotted as a function of the pseudo-shock length. From Fig. 4.5.3b it is seen that at l<7 axial force in the cylindrical stepped duct and consequently the effectiveness of the flow deceleration is greater than in the duct containing conical section.. At l >7-8 the advantage is belong to the combined duct, containing cylindrical and conical sections. In the last case in the front cylindrical section there goes the deceleration of the flow up to subsonic flow and in conical section there is an additional deceleration that is more effective than that at sudden expansion.

4.6 DECELERATION OF SUPERSONIC FLOWS IN SMOOTHLY DIVERGING DUCTS

Experimental investigations of supersonic flow deceleration to subsonic in straight ducts with oblong cross sections at various backpressures showed that characteristic properties of the flow essentially depend on the flow Mach number M and the cross section aspect ratio $\bar{b}$ combination. At certain values of these parameters there is a transition from pseudo-shock where no region of appreciable stall exists to flow with long boundary layer separations. The transition to this flow pattern leads to a decrease in the pressure recovery and an increase in the supersonic/subsonic transition region length. The pseudo-shock

length versus changes of parameters predicted by computations are in good agreement with experiments. There is no such results in the case of ducts with oblong cross sections.

Detailed measurements of static pressure distribution, total pressure profiles, oscillation characteristics, made in ducts with different oblong cross sections , allowed the dependence of M on $\bar{b}$ to be determined, which establishes the line of division between separated and nonseparated flows. Flow will separate from the duct surface if the required conditions are met there. The correlation of pressure recovery, distance necessary to complete supersonic/subsonic transition and M , $\bar{b}$ were also analysed. Besides, it was shown that if the hydraulic diameter which was used as a scaling factor is decreased below a certain limit, pressure recovery diminishes substantially (combined effects of the Reynolds number and the displacement thickness of boundary layer).The principal cause of the flow transition from non-separation to separation mode in the ducts with long cross sections is associated with nonsymmetric separations. The flow is allowed to separate over a portion of the side wall surface and then reattaches. Owing to the reverse flow, the boundary layer thickens considerably. These separations are not suppressed by an opposite wall at high aspect ratios. In technical devices, for instance, in scramjets, an air passage can include a rectangular duct section with one of the wide walls inclined to axis. The backpressure can be the combustion pressure of a scramjet engine. Such diverging ducts provide more stable flow at various backpressures but lower pressure recovery due to greater Mach numbers at which deceleration occurs. However, the diverging of the rectangular duct leads to a decrease in the aspect ratio that can partly compensate for the drop in the pressure recovery. As a continuous effort of duct flow study the following issues will be emphasized in this section: 1) an investigation of the characteristic properties of the flow in diverging rectangular ducts at various backpressures, 2) definition of integral characteristics of flow (such as pressure recovery and supersonic/subsonic transition region length) as a function of a wall inclination angle, duct expansion ratio and hydraulic diameter at the duct entrance and 3) determination of separation transference along the duct as a function of the backpressure that characterizes flow stability.

The experimental facility consisted of replaceable contoured nozzles with exit diameter d = 81.4mm and a test chamber connected with an exhaust ejector. The nozzle Mach numbers Ma =2.6, 3.2,3.8 were calculated using the nozzle critical to exit area ratio. All the test ducts were formed from one basic 12.5 by 37.5mm cross section and 600mm length duct on the lower wall of which were mounted wedge-like inserts. The constant cross section basic duct became a combined one with three sections having constant, variable and again constant area. A schematic side view of the duct is sketched in Fig. 4.6.1. This configuration is a typical one for airframe integrated scramjet . The first section was 50mm long for all variants and the third one had constant cross section 12.5 by 37.5mm. The angle of inclination of the lower wall changed in the range of $\theta = 0.5\text{-}3^0$. The ducts geometry is given in Table 1.

Table 1.

duct	inlet cross sec mm	aspect ratio	wall inclinatio atio	duct expansion	inlet hydraulic
1	12.5x37.5	3.0	0	1	19
2	9.5x37.5	3.9	0.5	1.37	15
3	7.5x37.5	5.0	0.5	1.67	12.5
4	"----"	5.0	1.0	1.67	12.5
5	"----"	5.0	2.0	1.67	12.5
6	6.2x37.5	6.0	2.0	2.03	10.6
7	5.0x37.5	7.4	0.5	2.5	8.8
8	" ----"	"-----"	1.0	"-----"	"-----"
9	"----"	"----"	2.0	"-----"	"-----"
10	"----"	"----"	3.0	"----"	"----"

For the purpose of comparison there were investigations of flow in constant area planar ducts with cross section configurations corresponding to adduced in table 1. These ducts were formed from the duct 1 by mounting into it plates of various thickness. Duct-inner wall roughness in all cases was equal to k = 3 micrometers. A throttling valve at the duct outlet allowed the pressure build-up in the duct to be

controlled. The duct entrance sections were located at the nozzle outlet in the uniform free stream. The earlier done investigations of static pressure distributions are found to be particular useful in flow character diagnosis. Since flow integral characteristics were the main purpose of this investigation static pressure measurements were the only kind of measurements taken. Static pressure taps in duct 1 were located along the middle of the upper wide flat wall with the pitch of a half of the hydraulic diameter and along the narrow side wall (at the distance of 1/4 of duct height from the upper wall) with the pitch equal to the hydraulic diameter. There were no measurements along the wedge-like inserts. The pressure was measured by special complex and normalized by the plenum pressure. The relative pressure measurement accuracy was + 1%. The air stagnation temperature was T = 250-260 K. The flow Reynolds number range was $0.5 \times 10^6 < Re < 2 \times 10^6$ based upon average velocity entrance section at the duct and hydraulic diameter. Longitudinal dimensions were normalized by duct 1 hydraulic diameter i.e. by d_h =19mm.

At the flow Mach number 2.6, as it was shown earlier, the pseudo-shock type flow can be established in all the above ducts. At Mach 3.2 and 3.8 there is great possibility of flow separation, pressure recovery drop and an increase in the required duct length. There are two factors of the duct diverging effect on the flow character. On one hand, hydraulic diameter increase and aspect ratio decrease tends to the separation restriction and on the other hand, the duct expansion makes the flow similar to the separation flow in the over-exertion nozzle. The details involving these two factors are discussed later in this section. Nonseparation to separation flow transition is accompanied by the certain changes in static pressure distributions. For instance, in the pressure curve segments with small gradient, some kind of plateau appear and longitudinal static pressure distributions along the narrow and the wide walls do not coincide. A plateau in the pseudo-shock does not exist and the static pressure over the circumference of the cross section of a duct is constant. General behaviour of the pressure distribution subject to various backpressures is depicted in Fig. 4.6.1 . Typical internal wall pressure distributions in several ducts are shown for different Mach numbers. The upper diagram (duct 7, Ma =2.6, $\theta = 0.5^0$, f = 2.5) describes nonseparation flows. The static pressure distributions along the wide (shaded symbols) and the narrow (open symbols) walls coincide, the pressure curves are characteristic for pseudo-shock. The middle diagram (duct 5, M =3.2, $\theta = 2^0$, f = 1.67) include pressure curves characteristic of nonseparation and separation flows. At low backpressures pressure recovery region is located in the duct constant area section with $\bar{b} = 3$. The pressure curves are similar to those in pseudo-shock (curves 1,2),the transition region length is about 10 duct 1 hydraulic diameters. The curve with maximal pressure build-up is near to that of pseudo-shock (with average Mach 3.7 at the outlet of the diverging section). The dash-dotted lines correspond to duct 1 pressure build-ups (pseudo-shock) at Mach 3.8 and they are similar to curves 1 and 2 in the combined duct. If pressure recovery region approaches the diverging section (curve 2) Mach number before this region grows and, if it moves along this section (curve3) the aspect ratio grows and hydraulic diameter decreases. It is now observed that these factors assist in flow separation because there are plateaus in the pressure curves and they do not coincide. Dashed line fairings have been placed through the open-symbol data (narrow sidewall) and solid line fairings- through the shaded-symbol data (wide wall). The pressure build-up along the narrow sidewall moves upstream further then along the wide one. This phenomenon can be considered as the appearance of the separation tongues along the narrow walls. That would make physical sense considering the fact that three-dimensional separation of boundary layer at the duct corner occurs at the lower pressure ratio.

Now it is necessary to note one more characteristic property of the flow in a constant area section of the combined duct. If a supersonic/subsonic transition region is located in the constant area section (curves 1 and 2) then pressure build-up curves have the same character as pseudo-shock curves: there is negative gradient in the pressure curves after reaching the maximum which indicates subsonic flow acceleration. Such pressure distribution character, as it was shown earlier, practically does not depend on flow nonuniformity before the pseudo-shock. The flow nonuniformity created by the 2-D diverging duct is not an exception in this sense. But if the transition region is located even partially in the diverging section the pressure distribution (curve 3) has a pressure plateau and no pressure maximum notwithstanding the supersonic flow before the constant area duct section. Such curve character can be explained partially as a consequence of the back flow occurring. Thus, this kind of flow can be considered as a specific kind

of pseudo-shock. This tendency is also pronounced in stepped tubes in which a separation regions are present invariably.

Mach number increasing up to M = 3.8 (Fig. 4.6.1, lower diagram, duct 2, $\theta = 0.5^0$,f = 1.31) leads to the flow pattern at which the separation starts immediately downstream of the throat due to the large aspect ratio (more then 3). The pressure recovery region length reaches 20 and more calibres of the duct 1 hydraulic diameter. It occupies both diverging and constant area sections. There are pressure plateau segments in the curves. The dash-dotted lines in the lower diagram of Fig. 4.6.1 (curves 4, 5 and 6) are given for comparison and correspond to 9.5 by 37.5mm constant area duct. One can note the following flow characteristic properties: the pressure distributions in the front part of the diverging and constant area duct sections (curve 4) are very close and have separation character. However, pressure recovery in the combined duct is higher than in the constant area duct due to higher hydraulic diameter and lower aspect ratio. If the pressure recovery regions are at the aft part of the duct (curve 6)the picture is reverse-pressure recovery is higher in the constant area duct. It is explained by the higher Mach number before the pressure recovery region in the combined duct and consequently by the higher pressure losses.

Absence of the distinct pressure maximum in curves p(x) in the case of combined duct make it difficult to answer the question whether a diverging section permits the shortening of a required duct length for supersonic/subsonic process completion. However, as it follows from the earlier stated, the initial pressure gradient grows if a pseudo-shock is fixed and its length drops. Solid (combined duct) and dash-dotted (constant area duct) curves in Fig. 4.6.1 show that using of the diverging sections does not lead to growth in the pressure gradient and consequently the supposed duct shortening can not be expected. Only at a high Mach number and equal pressure recoveries (compare with curve 4 for the constant area duct) is there a small gain in the duct length due to lesser $\bar{b}$ and greater d_h. Maximal pressure build-ups for all the ducts at the three Mach numbers are outlined in Figs. 4.6.2-4. Maximal mass rate through the ducts existed while the static pressure at the duct entrance was independent of the backpressure. It can be supposed that maximal backpressure could be raised a little if static taps were located somewhat nearer to the duct entrance (nearer than 38mm). Experiments however show that this increment can not surpass 5-7%. Normal shock in front of the duct entrance arises at the greater backpressures. The extreme complexity of the flow, availability of separations and back flows at the beginning of the diverging section at the maximal backpressures is testified to by many investigations .

The curves of Figs. 4.6.2-4 are grouped in such a way that it can be traced the influence of the wall inclination angle at identical expansion ratio f and the effect of duct expansion ratio f at identical θ on the pressure distribution. For the first two groups of curves f = 2.5 and 1.67 and for the second two groups $\theta = 0.5^0$ and 2.0^0. Fig. 2 demonstrates the test results for Ma = 2.6 at which pseudo-shock is realised at all aspect ratios. Examination of the top curve group (scale I, f = 2.5, d_h = 8.8mm, $\bar{b}$ = 7.4) allows the following conclusions to be made: pressure recovery in the combined duct depends substantially on the wall inclination angle, its increase from 0.5^0 to 3.0^0 decreases the pressure recovery by 1.5 times. For Mach 3.2 and 3.8 this decreasing is approximately 1.35-1.3 times. A Mach number increase tends to a decrease in the flow stability displayed in the top pressure build-up position scatter at f = 2.5. At f = 1.67 the curves converge. At $\theta = 2^0$ and 3^0 the curve character testifies to the appearance of separation flow at the frontal part of the diverging duct. At $\theta = 0.5^0$ and 1.0^0 there is no such kind of flow. Thus, a decrease in $\bar{b}$ and an increase in d_h along the diverging duct at $\theta > 1^0$ was insufficient to check separation stimulated by the expansion itself due to Mach number increase. Fig. 4.6.3 and 4.6.4 (Mach 3.2 and 3.8) show that separations take place at all θ . At duct expansion ratio f = 1.67 (scale II) the wall inclination angle effect on pressure recovery appeared lower than at f = 2.5 though the character of influence remained. The deceleration process takes place to a greater degree than in the duct with f = 2.5 in the constant area section. The plateaus which indicate separation practically disappear. Decreasing of the duct expansion ratio at Mach 3.2 and 3.8 (Fig. 4.6.3 and 4.6.4) does not cause a change in the flow character.

Let us look now at the duct expansion ratio effect on flow character at identical wall inclination angles. The curve groups in Figs. 4.6.2, 3 and 4 are for various f at identical θ are located in the lower diagram parts (scales III and IV). Curve analysis indicates that the duct expansion ratio change carries no essential alteration in the pressure distribution along the initial part of the duct. It is defined by the M($\bar{b}$) relationship. Pressure recovery at various f differ substantially however, to define this effect quantitatively

was not possible. As it was noted earlier there is the combined effect of f, d_h and $\bar{b}$ on the pressure distribution. Influence of the hydraulic diameter should be noted separately. As experiments with a number of constant area rectangular ducts showed pressure recovery substantially decreases if d_h is less than d_h of the basic variant (19mm) due to change of Reynolds number and relative displacement thickness of boundary layer. The hydraulic diameters at the entrance and outlet sections of the combined ducts are d_h <19mm and d_h =19mm respectively. It is possible that pressure recovery can be dependant on some average hydraulic diameter. Maximal/minimal possible pressure recovery ratio scarcely can be larger than theoretical ratio of pressures after normal shocks located at the entrance and the exit of diverging duct

Fig. 4.6.3 and 4 presents as well curves related to the constant area duct (dashed lines) having the same cross section as that at the entrance to the combined ducts. Curve comparison (Fig. 4.6.3,scale III; Fig. 4.6.4,scale I) allows the conclusion that pressure recovery change in the combined duct at changing f can be explained mainly by d_h influence being consistent with previous results. The variation of θ effects only small changes in pressure distribution . At d_h >15mm the pressure recovery in both ducts are close (the upper dash-dotted line in Fig. 4.6.3 relates to duct 1). Analogues result take place at the rest of the Mach numbers. In practice it is useful to know the pressure recovery in short diverging rectangular ducts with a given duct entrance cross section and length and various wall inclination angles (duct expansion ratios). Some information can be derived from Figs. 4.6.2-4. Estimations made at x = 10 and 12 (corresponding to the outlets of the ducts 4 and 6 diverging sections) show that at identical x and $\theta = 1^0$ and 2^0 the pressure recovery is nearly the same and at $\theta = 3^0$ it is somewhat lower.

Thus, it can be concluded that in short diverging rectangular ducts the increase in the wall inclination angle above 1 does not lead to pressure recovery rise, notwithstanding the increase in the expansion ratio. Let us pay attention to the definition of the internal characteristics of the flow ,such as the pressure recovery. To evaluate the effects of θ and f on the pressure recovery it is necessary to exclude effect of d_h as much as possible. Let us mark the maximal static pressure at the end of the diverging section and the end of the constant area duct as p_v and p_c respectively. Fig. 4.6.5a presents p_v/p_c relation as a function of f for all θ, M combinations. As it follows from Fig. 4.6.5a there is no possibility to establish the effect of M on p_v/p_c. This is due to a big scattering of data caused by a certain indefinitely of selection of pressure distribution curves used for this relation determination, and also by the duct inlet geometry difference. At the same time there is obvious influence of and f on p_v/p_c noted. At $\theta=0.5^0$ and f>2 the value of p_v/p_c is greater then 1, e.i. demonstrating performance rivalling the constant area duct. It depends on flow mode in the ducts with long cross sections. Small wall inclination angle provides sufficient duct length for flow deceleration occurring at bigger average d_h and lower average $\bar{b}$ than in constant area ducts with the same inlet configurations that promote pressure recovery rise .

At greater angles θ the pressure recovery in diverging sections yields essentially to that in constant area ducts. The length of the diverging section is not enough to complete deceleration and the flow at that section exit is supersonic. The pressure recovery can be even lower than that after a normal shock stationed at the diverging section exit. For rough estimations of p_v/p_c an empirical relation can be used.

$p_v/p_c = 1.1 - 0.2\,x\theta + (f-2)\,(0.07+0.1x\theta\ )$

Let us mark the maximal pressure in the constant area section of the combined duct p_k .Then the ratio p /p characterizes the fraction of the summary pressure recovery belonging to the diverging section of the combined duct. In Fig. 4.6.5b values of p_v/p_k are plotted as a function of f for all combinations of θ and M .It can be seen that p_v/p_k is less than 1 for all the above ducts and consequently in not one diverging section is the deceleration process completed. To do these greater expansion ratios f (about 2.5-3.0) for ducts with $\theta=0.5^0$-3.0^0 are needed. An empirical relation for p_v/p_k intended for rough estimations is: $p_v/p_k = 1-0.15x(3-f)x\,\theta$.

Consider now the total effectiveness of the flow deceleration in the combined duct. The figure of merit for this effectiveness used here is p_k/p_d . p_d is the maximum expected calculated pressure recovery successively provided by the normal shock and by the ideal subsonic diffuser with fixed expansion ratio equal to each f of the combined duct from table 1. In Figure 4.6.6a the values of p_0/p_d are plotted as a function of f for θ= 0.5^0 and 2.0^0 and various M . Fig. 4 6 6a analysis permits the conclusion that the relative pressure recoveries in the examined diverging ducts are very low and at f = 2.5 (d_h = 8.8mm, $\bar{b}$ =7.4) can be lower then 50%. In "classical"pseudo-shock this value is about 95%. The main cause of such low

effectiveness in the supersonic flow deceleration is small hydraulic diameter d_h (small Re) and large cross sectional aspect ratio $\bar{b}$.

Effect of the wall inclination angle on p_k / p_d can be seen in Fig. 4.6.6b. For approximate estimation an empirical relation can be used:

$$p_k / p_d = (p_k / p_d)_{F=c} \, (0.55-0.05 x \theta).$$

Here $(p_k / p_d)_{F=c}$ is the relative pressure recovery in a constant area duct having a cross section which is equal to the entrance cross section of the corresponding combined duct. In analysing supersonic flow deceleration in ducts containing diverging parts with long cross sections it is possible to state that the pressure recovery in them is lower than in ducts with the same exit to entrance area ratio and consisting of constant area + subsonic diffuser sections. The analogous result was received in Ref. 3 in which the supersonic diffusers with square cross sections were investigated. In conclusion let us consider the conditions of propagation of pressure disturbances upstream in the combined duct due to backpressure rise. It can be connected with the flow stability, say in a scramjet passage. As was stated above the developed pseudo-shock in a constant area duct is very sensitive to pressure rise. A small backpressure change leads to the essential transition of the pseudo-shock that creates a danger of the duct unstart.

In technical applications the flow stability in special situations may be more important than the pressure recovery, but in all cases pressure losses must be as minimal as possible. The pseudo-shock propagation in a round tube can be restricted by creation of a local region of high pressure. In Ref. 9 that local region was created by circular ledges of different shape. A base in a stepped duct also is an obstacle to pressure disturbances which do not go upstream while the pressure at the step is lower than the pressure that occurs at incipient turbulent separation, corresponding to the flat plate-ramp (2-D). Methods of creating obstacles to pressure disturbance propagation are specific. Mounting of wedge-like bodies along the circumference of a duct of rectangular cross section , for instance, did not bring a pseudo-shock fixation as it took place for round tubes. Disturbances in this case propagate primarily along corners where there is a thick boundary layer and shock waves interact three-dimensionally. The back flow is not eliminated or reduced. In order to achieve an optimum design the vanes should be arranged in the vicinity of the inlet. In Fig. 4.6.7a, b, c the distances of upstream pressure influences $\Delta\bar{x}$ measured from the combined duct exit are plotted as a function of the backpressure. Curves correspond to Ma = 2.6, 3.2 and 3.8 , f = 1.67 and 2.5 and θ = 0.5- 3 . Open symbols are pressure data obtained along the middle of the wide wall and shaded symbols - along the narrow sidewall. The dash-dotted lines correspond to constant area duct 1 with 12.5 and 7.5 by 37mm cross sections. Horizontal dash-doted lines indicate the start of the section and horizontal lines on each curve - the end of it.

Inspection of Fig. 4.6.7 indicates that separation region transference along the constant area section of combined ducts resembles the transference along constant area ducts. This result corresponds to the above conclusion about nearness of pressure distributions for these two cases. The separation region transference into a diverging section leads to a decrease in the gradient $d(\Delta\bar{x})/dp$ in some cases to zero. That can be interpreted as a fixation of a separation at the upper flat wall surface. The greater the length of a plateau in curve $\Delta\bar{x}(p)$ the more stable the flow is. In this sense the duct with $\theta = 0.5^0$ may seem most prospective. However, the plateau in this case is located rather far from the diverging section inlet , which reduces the maximal pressure recovery. Hence, it is expected that the most favourite divergence angles lies between θ=0.5^0 and $\theta = 2^0$. It is possible that separation region fixation at the lower sloped wall could exist in a greater range of backpressure change as takes place at the base of a stepped duct Further backpressure rise leads to a quicker upstream separation transference and then to the flow disruption. As mentioned above the pressure disturbance front is irregular, there are tongues of separation regions along the side walls but their advance is not great. As it can be seen from Fig.4.6.7 the distance between incipient separations along side(dashed lines) and upper(solid lines) walls does not exceed one or two duct heights. It should be noted that an increase in the wall inclination angle makes the separation front more uniform and in the proximity of the wall breakline curves corresponding to side and upper walls practically coincide and even can change places. From an analysis of Figs. 4.6.7a and 7b it is possible to conclude that, at f = 1.67, an increase in the wall inclination angle promotes plateau transference upstream close to the wall breakline , but pressure recovery drops. At f = 2.5 curves displace to regions of lower backpressures that can be explained by the greater Mach number before the separation region and by the lower hydraulic diameter. At f = 2.5, $\theta = 1\text{-}3^0$ and maximal backpressure curves

practically merge, only the curve with $\theta = 0.5^0$ moves. At f= 1.67, $\theta = 0.5^0$ separation region can approach the wall breakline while at f = 2.5 stable supersonic flow aside. An failure occurs earlier. In Figs. 7a and 7b the dash-dotted lines correspond to duct 2 (f = 1.31 and $\theta = 0.5^0$), which are near to the dashed curves (duct 1,constant area).That means that at small θ and f diverging sections of combined ducts practically do not assist flow stabilization -there is no plateau in curves, gradient d $(\Delta\bar{x})$/dp is high. Some other conclusions could be made from Fig. 4.6.7c where curves are plotted for ducts with $\theta = 2^0$ and f greater then 1.31. It can be seen that curve parts with plateaus are located approximately at the same $\Delta\bar{x}$ values. However, the greater f, the greater these curves are displaced to the region of lesser backpressures(at Mach 3.2 and 2.6). Thus the data indicates that the highest performance in terms of maximal backpressure is obtained with a duct having small f (f = 1.67). However, this conclusion may prove to be premature because compared ducts had different hydraulic diameters.

4.7 Pressure recovery in subsonic diffusers

The operation of subsonic diffusers at low velocities and uniform flow at the entrance was examined in detail. There are many publications. The results of studies are generalised in Ref. 1. Maximal efficiency of pressure recovery in axisymmetrical conical diffusers is reached at expansion angle $2\theta = 7^0$. Such type of subsonic diffusers are used as a supplementary part of supersonic diffusers for receiving of additional pressure recovery. In the simplest case supersonic diffuser is a straight tube of constant cross section where supersonic flow decelerates up to subsonic velocity. The investigations of subsonic diffusers working together with supersonic diffusers are hampered by non-uniform flow in front of them. Taking into account that the fraction of the pressure recovery accounted for subsonic diffuser is small it usually is not separated out of the combined (net, integrated) pressure recovery.

The use of supersonic/subsonic diffusers in gasdynamic lasers or in scramjets have special features that are little studied. These features are related to duct geometry and regimes of operating. So, in Laser systems that have supersonic flow in resonators main interest lies in flow deceleration in slot-type ducts. In scramjet engines passages also can be of slot-type with expansion angles differ substantially from that of optimal subsonic diffusers. Besides, the flow at the entrance of this subsonic diffuser is a rule very non-uniform and contain supersonic zones and stratified. In Ref. 50 it is noted that at M>2.5 real contribution of subsonic diffuser in net pressure recovery is small and can be ignored. This conclusion evidently can be considered as a special and relevant to slot-type diffusers for Laser systems. In the case of scramjet it is not reasonable to ignore the pressure recovery in subsonic diffusers. It could led to some errors in the passage geometry selection and change in engine operation mode. The pressure recovery fraction can be noticeable if off-design supersonic regime is considered and pressure recovery in it falls down. From what has been said, it might be assumed that wide and detailed investigations of processes occurring in subsonic diffusers, having in mind its using in scramjets, is unlikely worthwhile. At the same time the receiving of approximate data about pressure recovery in subsonic diffuser will be very useful for estimating of scramjet efficiency. The objective of these investigations was to obtain findings about the range of pressure recovery change in the scramjet passage sections where subsonic flows occurs.

The duct diverging angles, as in the scramjet passage, changed in the range of $\theta = 0\text{-}90^0$, duct diverging ratio f = 1-3, flow Mach numbers M = 2-4. The facility was described earlier. It consisted of changeable contoured, 81.4 mm diameter nozzles, Fig. 4.7.1 . In the case of direct connect scheme the tubes of maximal length of 1350 mm were attached to the nozzles. These were supersonic diffusers. Downstream the cylindric tube diverging sections followed. These were subsonic diffusers, three types of them were considered: 1. Conical section, 400 mm long with $\theta = 0.5^0$. Downstream this section cylindric tube, 134 mm in diameter followed. 2. Conical section, 140 mm long, $\theta = 11.7^0$. 3. Cylindrical tube, 134 mm in diameter. This variant corresponds to sudden expansion case, $\theta = 90^0$.

In the case on free stream tests the tube of 134 mm in diameter was attached to the nozzle and was used as a camera wall on which models were mounted. The models were rectangular ducts, 37.5 by 12.5 mm, 600 mm long. At one wide wall flat plates, 400 mm long were fastened. The duct become stepped. Front, narrow part of the duct had cross sections 7.5 by 37.5, 6.2 by 37.5 and 5 by 37.5 mm. The expansion rates and hydraulic diameters were f = 1.67, 2.0, 2.5; d_h = 12.5, 10.6, and 8.8 mm respectively. the wall roughness of circular

ducts was k_s = 9 mcm, and rectangular-k_s = 3 mcm. The throttling of the ducts was effected by bodies that were moved at the end of the ducts. The tube inlet was placed in the uniform flow right at the end of the nozzle. The pressure taps and measurement devices positions were described earlier In Fig. 4.7.2 characteristic pressure distributions are presented for circular ducts with different subsonic diffusers. and different regimes of supersonic diffusers operation. The following variants of ducts were investigated: 1. Cylindrical tube, d = 81.4 mm, l = 16.5d (supersonic diffuser) and tube, D = 134 mm (subsonic diffuser). 2 and 3. The same, only l = 11d and 5.5d successively. 4. Cylindrical duct, l = 5.5d+conical section, $\theta = 0.5^0$. 5. The same as in point 4 only $\theta = 11.7^0$.

Possible flow modes (marked by figures in the diagrams): 1. Developed pseudo-shock is placed in the supersonic diffuser. The flow velocity in front of diverging section is critical., 2. The backpressure falls. The pseudo-shock moves downstream. Pressure maximum is disposed at the end of supersonic diffuser where the flow velocity is subsonic corresponding to the velocity downstream the normal shock, 3. Further backpressure drop leads to pseudo-shock transition partly into diverging section of the tube. There is non-uniform flow with supersonic zones at the entrance of the diverging section that can be called as a transonic diffuser, 4. Supersonic flow along all the cylindrical duct. The diverging section acts as supersonic diffuser. The transition of supersonic flow into subsonic take place in the diverging section and cylindrical, D = 134 mm tube. The supersonic flow deceleration in diverging ducts was analysed earlier in this overview. In present paragraph the regimes corresponding to the region between curves 1 and 2 are analysed. In this case the velocity in front of subsonic diffuser changes in the range between critical and following normal shock. In our case M = 0.47-1.0.

We will first look more closely at the pressure distribution special features. At the stepped duct, $\theta = 90^0$, at the initial part of the diffuser (solid lines, regimes 1 and 2) there are either pressure plateau or slight pressure drop. At the diverging angles θ = 11.7 and 0.5^0 the static pressure is built up along the whole diverging duct (dashed and dash-two dotted curves) and then additionally in the 134 mm cylindrical duct. Maximal deceleration (maximal pressure) is reached at the distance of 7-10 calibres of supersonic diffuser or 4-6 calibres of cylindrical, 134 mm tube. It is interesting to note another special feature of the pressure distribution. In spite of essential difference in flow conditions in front of subsonic diffuser at first and second regimes the pressure distribution characters differ insignificantly. The pressure ratios $\overline{p3} = p_3/p_2$ are as well near to each other. Here p_2 - static pressure at the end of the supersonic diffuser, and p_3-maximal pressure in the subsonic diffuser. This phenomena says that 1D estimations of flow parameters in this case are not correct. Apparently, at the pseudo-shock transition from position 1 to position 2 the flow parameters change comparatively little. When considering transonic and then supersonic flow regimes the p_3 value grows due to Mach number increase in front of diverging section (see paragraph 4.6).

The lengths of subsonic diffusers with θ = 0.5 and 11.7^0 for which expansion ratios were 1.2 and 2.72 successively turned out not enough for full subsonic deceleration. Substantial part of pressure increase occurs in the constant area duct, D = 134 mm, due to flow fields smoothing. A reduction in the supersonic diffuser length and corresponding decrease in boundary layer thickness leads at equal or smaller pseudo-shock length to pressure p_2 increase. However, the value of p_3 changes little. Mach number increase don't change the curve shape and conclusions made earlier for lower Ma are valid. The pressure distributions along rectangular stepped ducts are exemplifies in Figs. 4.7.3, 4.

Supersonic diffuser is 7.5 by 37.5 mm cross section duct, 400 mm long and subsonic diffuser following it has 12.5 by 37.5 mm, and 200 mm dimensions. The expansion ratio is 1.67. Ma = 3.8.and 4.25. The diagram's analysis shows that transition from circular to rectangular stepped duct does not lead to change in flow character. The pressure recovery occurs, as in circular duct, at the distance of approximately 10 calibres of hydraulic diameter. What is more, the flow character in subsonic diffuser does not change even if in the supersonic diffuser the flow deceleration, occurs with long separation region. In the last case ($\overline{b}$ = 7.4, Ma = 4.25) the separation flow can exist at the distance of approximately $30d_h$.

Let's call our attention to respective analysis of pressure recovery in subsonic diffuser of different shape. In Fig. 4.7.5 the values of $\overline{p3}$ are plotted as a function of expansion ratio. These values correspond to maximal pressure in all subsonic diffusers excluding the case of $\theta = 0.5^0$ in which $\overline{p3}$ corresponds to pressure at the end of the conical section, e. i. at expansion ratio 1.2. Square symbols correspond to rectangular ducts and round - to cylindrical ducts. Open symbols correspond to regime 1 and shaded- to regime 2. In order to distinguish

between values $\overline{p3}$ received at different Ma the symbols are displaced a little from their normal position. The symbols corresponding to Ma = 2.6 were shifted to the left on the value Δf = 0.04, and symbols for Ma = 3.8- to the right at the same small value. Data for Ma= 3.2 were shifted. Solid values in Fig. 4.7.5 are received as a result of 1D computation for velocity coefficients $\lambda = 0.4, 0.6, 0.8$ and 1.0 at the entrance to the subsonic diffuser. It is seen that the value of $\overline{p3}$ essentially depends on λ and comparatively little on f (at f>1.4). Dashed lines correspond to isentropic flow deceleration for the same values of λ.Fig. 4.7.5 lets to conclude that pressure recovery in subsonic diffusers placed directly downstream the supersonic one is considerably less than that computed at $\lambda = 1.0$. This concerns as to stepped and smoothly diverging ducts and possibly connected with large subsonic flow velocities at the end of supersonic diffuser and high level of non-uniformity of this flow. The experimental data are grouping dominantly between curves computed for $\lambda = 0.6$ and 0.8 both for circular and rectangular ducts. The values of $\overline{p3}$ depend little on f and $\underline{\bar{b}}$ and are equal approximately to 1.15 -1.2. If uniform flow with $\lambda = 1.0$ would be present in front of subsonic diffuser the pressure recovery might reach $\overline{p3} = 1.4$. Approximately the same value of $\overline{p3}$ might reach in conical ($\theta = 0.5^0$, f = 1.2) duct. Using of conical section with $\theta = 11.7^0$ as an alternative to subsonic diffuser with $\theta = 90^0$ produce but little increase in pressure recovery.

5. Some methods of duct separation flow control.

5.1 Transition from separation to non separation flow by means of partitions and wedge-like bodies installation into it.

It is clear that the means of pseudo-shock length reduction investigated earlier can not be used directly for the flows in ducts with oblong cross sections, especially if there nonsymmetrical separation flow exists. An decrease in length can be expected only if there is transition of separation flow into pseudo-shock. It is known that partition installation in rectangular ducts allows transform separation flow into pseudo-shock. Can it be achieved with short partitions? In Fig. 5.1.1 there are presented the pressure distributions in this duct. There realises flow of pseudo-shock type instead of separation flow.
In contrast to the case of circular tube the placing of wedges along the circumference of the duct at the entrance section does not lead to separation flow transformation into pseudo-shock due to flow non uniformity induced by the wedges. In this case one can tell about possibility to transit the separation region near the duct entrance but not about shortening of this region. This phenomena allows to shorten the required duct length and impede the separation region to be open to the external flow into which part of gas can bleed. In Fig. 5.1.1 the pressure distributions for this case along narrow and wide walls are presented. The curves correspond to limiting back pressure, the exceed of which leads to the flow upsetting. Sharp distinction in pressure distributions along narrow and wide walls is noted. There is the separation fixation at the narrow butt end of the wedge, where static pressure is neat to static pressure on the wedge blown by non disturbed flow. The pressure distribution along the wide wall reminds the pressure distribution in the front part of pseudo-shock. In Fig. 5.1.1 the pressure distribution along ducts with square and rectangular cross sections without wedges are presented for comparison. It is seen that the wedges presence allows to move separation upstream approximately by $5d_h$. Mach number increasing makes it more difficult to shorten the region of flow deceleration by this method.
The wedges positioned around the whole perimeter of the duct increased total pressure loss but did not shorten the flow deceleration region, Fig. 5.1.2. Non symmetric character of flow maintains, the plateau length is more than $5d_h$. So, wedge-like bodies mounting in rectangular ducts does not resulted in substantial shortening of the deceleration regions as it takes place in the case of circular ducts. To a large measure it can be assigned to the destabilising influence of shocks. Later we call attention on the possibility of shortening of flow deceleration region due to decreasing Mach number by installing another bodies into the flow.
In Fig. 5.1.3 and 5.1.4a pressure distributions and maximum pressures in duct, $\overline{b} = 6$, Ma = 3.8, are plotted as a function of partition length. Two variants of partition installation are depicted. In one case they are positioned at the entrance to the duct, in the second - 100 mm downstream. It is seen that there is no need to have long partitions, 8-10 d_h length is enough, e. i. approximately twice as small as the duct length in which the process of flow deceleration is completed. Methods of transforming separation flow into pseudo-shock similar to analysed earlier but in fact using another principle are depicted also. In the same duct and Ma short wedges with angle $\theta = 4^0$ were mounted. They formed side converging ducts. The pressure shocks induced by the wedges hit the side narrow walls and give rise to high pressure zones which retard the up flow transit of boundary layer separations.

5.2 Variation of cross section shape along the duct as a mean to transform separation flow into pseudo-shock.

Earlier it was shown that the duct with circular-sector cross section allows to realise the pseudo-shock type flow deceleration even at large value of $\overline{b}$. So, there is possibility to realise such process if the duct cross section changes smoothly from rectangular into circular-sector and in such a way shorten the required duct length. Fig. 5.2.1 presents at Ma = 3.8 pressure distributions in rectangular, $\overline{b} = 6$, dash-dotted line and in combined, rectangular-sectoral (central angle 106^0), solid lines, ducts. The

curve analysis confirms the justice of above made suggestion. The pressure recovery is approximately the same as in rectangular duct with a set of wires at the duct entrance (see later). At the duct length x = 18 d_h the pressure recovery approximately by 60% higher than in $\bar{b}$ = 6 rectangular duct.
Here is some simple explanation of this phenomenon. The presence of curved wall hanging over narrow wall restrict separation rise. The ratio of distance from the middle of the narrow wall to the large circle of the duct b_1 to the duct width H is approximately equal to 2. In this case as in the case of rectangular duct with $\bar{b}$ = 2 pseudo-shock type flow can be realised. This condition and condition of cross section area and values $\bar{b}$ and H being constant allows the sector angle defining. Conditions of cross section equality $bH = \pi(R^2-r^2)\varphi/360$ or $\varphi = bH360/(R^2-r^2)/\pi$ Thus, with b taken as 2H, we receive $R = 17H/4$, $r = 13H/4$, $\varphi = 15.3b/H$
In this particular case the duct with $\bar{b}$ = 6 was chosen. The central angle is equal to $\varphi = 92^0$. The transitional duct section (from rectangular to sectored) was chosen at the condition of space separation absence. The realisation of this condition is possible if side wall inclination is less than that at which three-dimensional separation occurs ($p_2/p_1 = 1.5$,.Ref. 48). Angle of inclination along the mean line: $\varpi = \text{atan}(H\sin(\varphi/2)2/l_2)$ - here l_2- length of transitional section, equal to $H\sin(\varphi/2)/2/\tan\omega$ or if it normalised by hydraulic diameter, $d_h = 2bH/(b+H)$, $l_2 = \sin(\varphi/2)x(1 + H/b)/4/tg\omega$.
The reason of separation region absence in circular-sector duct can be explained qualitatively by this consideration: The curved wall hangs over the plane side wall (equivalent to $\bar{b}$ decreasing) and prevents the separation. Considering the distance from the middle of side wall to the curved surface, b_1 as equivalent width of the duct one can expect that at $b_1 = b_1/H < 3$ the pseudo-shock will be present. It is simple to determine duct geometry if b_1 and duct area are fixed. If the duct has constant area than $b_1H = \pi(R^2-r^2)\varphi/360$ and $b_1^2 = R^2 - (r + H/2)^2$. The ratio of side wall and incoming flow pressures $p_1/p = 2k/(k-1)Ma^2\sin^2\alpha - (k-1)/(k+1)$. Taking $p_1/p = 1.5$ we calculate α and then, using shock polar, angle ω. As calculations showed in the range of Ma = 3-6 $\omega \cong 4^0$ and $\bar{b} \cong 2$-4. The experiments carried out indicate that the reduction of the deceleration region length is possible mainly due to flow transformation into pseudo-shock.

5.3 Mach number decrease due to additional pressure loss as a mean of separation flow transformation into pseudo-shock.

Chapters 2 and 3 showed that Mach number or aspect ratio deceasing allows transform separation flow into pseudo-shock at supersonic flow deceleration in ducts with oblong cross sections. One of these ways is installing of sets of wires into supersonic flow in the duct. If the wire drag coefficient is known the definition of their diameter and number for receiving the required Mach number according the relationship $M < 2.5 + 150b^{-4}$ in 1D theory is simple. The experiments showed that Cx = 1.1-1.3
Fig. 5.3.1 illustrates the pressure distribution in the duct , b = 6, Ma = 3.2 and 3.8, with and without wires. As this figure indicates five wires, 0.3 mm diameter transformed separation flow into pseudo-shock. The transition region shortened from 25d_h to 12d_h and pressure recovery increased practically to the level corresponding to pressure recovery in the duct with square cross section. The high effectiveness of flow deceleration in this case is connected with the fact that flow Mach number, 3.2, is near the boundary at which, M = 2.8-3.0, separation can occur. At Ma = 3.8, $\bar{b}$ =6, d_w = 0.3 mm, Fig. 5.3.1, pressure recovery was 25% less then in the duct, $\bar{b}$ = 1.0. The transition region length in both cases is near the same. The pressure distribution analysis in the case of d_w = 0.3 and d_w = 1.2 mm indicates that up to distance x = 20d curves go near. At Ma = 4.25 and d_w = 0.5 mm the flow corresponds to pseudo-shock and at d_w = 0.3 mm - to separation flow. At high Mach numbers flow transformation demands more thick wires then it follows from 1D theory.
Let us dwell now on another method - using wedges instead wires. The use of wedges at the duct entrance simultaneously with the set of wires did not give any advantages. The transition of the separation flow is realised as in the case of wires only but pressure recovery is lower. So, at Ma = 4.25 the installing the wedges with angle of 6^0 along the whole perimeter of the duct and 5 wires, d_w = 1.5 mm makes the transition region length equal to 8d_h. The presence of wires only makes Δx =14d_h but

the pressure recovery is 6% higher. In Ref. 10 conical bodies were installed into rectangular duct, $\bar{b}$ = 3.8, uniform across the duct with the aim of flow turbulisation and mixing increase and on this basis to shorten the required duct length. At Ma = 5 the required duct length is about $25d_h$. The conical bodies presence sharply decreased Mach number and with it -transition length So results of Ref. 10 confirmed present investigations.

Let us consider hysteresis phenomena in rectangular ducts the separation flow in which is transformed into pseudo-shock due to bodies insertion. In Fig. 5.3.2 pressure distribution is presented for the duct with $\bar{b}$ = 6 at Ma = 4.25 and d_w = 0.5 mm The solid lines correspond to experiment sequence at which pseudo-shock was moving upstream the supersonic flow (forward movement of throttle). The dashed line corresponds to downstream movement from the extreme forward position (back movement). It is seen that in the last case separation flow exists.

5.4 The effect of secondary jets on flow transformation and pressure recovery.

Jet injection leads to supersonic flow deceleration that in principle can transform separation flow into pseudo-shock. Using struts for jet injection still more decreases Mach number. In Fig. 5.4.1 pressure distributions along the duct, $\bar{b}$ =6, Ma = 3.8 are presented. It is seen that even without jet injection strut installation leads to pseudo-shock formation (curve 1) because in front of it Mach number is below 3.0. At back pressure increasing pseudo-shock moves upstream and Mach number in front of it increases. At some moment pseudo-shock transforms into separation flow. Jet injection makes new separation region in front of it and pressure distribution looks as if it was a pseudo-shock. However, there is no constant pressure across the duct in any section of the duct. It indicates on separation region presence and no pseudo-shock. Evidently, Mach number is not low enough for that or, what is more probably, the flow is extremely non uniform and 1D theory is not valid. At Ma = 4.25 the flow is separation one at almost any back pressure. The pressure loss induced by struts and jet injection is not enough for flow transformation.

So, it can be concluded that strut installation and jet injection assist to flow transformation. However, we have no enough data to state the number, shape and disposition of struts and values of jet injection rates at which flow transforms from separation to pseudo-shock. There are needed additional experiments.

Supplement

6.Secondary effects of supersonic flows in ducts due to flow separation.

6.1 Use of pressure increase in central part of flow initiated by normal jet injection for starting up flow-through models and deceasing duct drag.

As already noted the pressure difference of flow deceleration process can be explained by the presence of oblique shocks in front of jet injection and deceleration region. In Fig. 6.1.1 the total pressure fields at different distances from the nozzle, Ma = 3.08 without jet injection are presented. This diagram is an example of "natural" deceleration due to friction. The measured total pressure in the flow core corresponds to "shockless deceleration + normal shock" system. It is seen that the flow deceleration effectiveness is growing with the boundary layer thickness increasing. It is clear that the change of isentropic deceleration process by oblique shocks occurring with the jet injection leads to total pressure decrease. In Fig. 6.1.1 the mean values of p_t' averaged by the three central Pitot tubes are plotted as a function of increase mass coefficient β for injection orifices corresponding to low and high pressure head of injected jets. It is seen that in the range of β = 1.04- 1.14 the total pressure in the core of the flow for the first variant of injection is lower then for the second variant, and at lower and higher values of β , the values of p_t practically coincides. At β = 1.0-1.04 the oblique shocks are very weak in both cases, and at β > 1.14 the jet injection leads to flow blockade and pseudo-shock occurring in which total pressure loss is practically equal to normal shock loss (see p_t at β = 1). Normal jet injection

leads to total pressure increase in the core of the flow, notwithstanding of the distance from the injection section. However, the further increase in the duct length (L = 23.6 and l = 0) leads to p_t decrease at any value of β. The transition of the jet injection to the duct end again leads to total pressure increase in the core of the flow with the absolute value considerably higher then in the case of "natural" flow decreasing. In this case the system "isentropic deceleration + oblique + normal shock" is realised. In Fig. 6.1 2 the total pressure profiles in the duct at the distance x = 7d (M 3.08 nozzle) are presented. In the centre of the duct there is a pressure drop due to Mach disk. The cross jet injection can increase this drop (β = 1.04) and eliminate it (β = 1.24). In the last case maximum of p_t is reached due to oblique shock occurrence on the jets.
We call attention now to practical application of the noted phenomena. In particular it can be used for flow-through models starting and drag decrease. To confirm this proposition special experiments with cowls installed in tubes were carried out. This cowls formed internal converging channel In front of these cowls shock wave formed if there was no jet injection. The geometry of these cowls are indicated in Fig. 6.1.3. The pressure distribution was measured along the internal cowl surface, wedge-like pylons on which cowls were mounted and along the tube generatrix as well.
In Fig. 6.1.3, left diagram, pressure distribution along cone generatrix and base pressure at Ma = 3.8 are presented. It is sees that internal channel is not started and subsonic flow in it accelerate up to sound speed. Injection of high pressure jets leads at first (β = 1-1.036) to small pressure decrease and at β = 1.044 there is full start of the channel. Static pressure at the beginning of the channel corresponds to that at the wedge with angle of 8^0 and then smoothly increases due to flow deceleration in the converging duct.

6.2 Influence of jet injection on the drag of duct with circular cavity

The pressure shocks induced in particular by jet injection can hit cavity and change flow character in it. In particular they can destroy the close cavity flow mode, increase pressure at the front step and decrease pressure at the back step. An increase of secondary jet rate can transit shocks position, restore the mode of closed cavity and so on. Cyclic change of pressure at the step faces of the cavity due to change of β was shown in Fig. 6.2.1 (solid lines). It is evident that such change of pressure have to lead to change of cavity drag, ζ_c, and together with it-to drag of all the duct. In Fig. 6.2.1 solid lines and shaded circles correspond to drag of the tube with cavity, dotted line-to drag without cavity. Dashed line corresponds to cavity drag ζ_c received by balance measurements, and open circles - by pressure measurements. Rather near agreement of data says about validity of assumption about weak dependence of friction force on shock presence and uniform pressure distribution along the step face. The pressure shocks at the end of the tube are getting weak and transition of this cavity into this region decrease pressure amplitude and cavity drop. However, cyclic character of change remain, the number of cycles increases possibly due to disturbance wave length decreasing.
In Fig. 6.2.1 dashed-dotted lines correspond to case of low pressure jet injection It shows monotonous change of face step pressure and cavity drag. The front step pressure corresponds to 2D base pressure if for Mach number average tube Mach number is accepted. Open cavity flow practically is not influenced by the quality of incoming flow. This can not be said about cavity drag. It is known, Ref. 51, that pressure distributions along the height of the back step is non uniform. At the edge of the step the pressure gradient is high and depends on part of flow that hit the step. Longitudinal pressure gradients in the duct also can influence the cavity drag in the case of open type flow. The difference of pressures at the steps is defined by this gradient.

6.3 The depth of penetration of cross jets in ducts with supersonic flow and equivalent body.

Characteristic feature of jet injection in ducts unlike the jet injection in free flow is the depenence of pressure level of flow in which jet is injected on mass rate of secondary jets. This rate can change pressure at the existent flow regime and defines the duct flow mode as well. Schemes for different flow modes are depicted in Fig. 6.3.1. The values of $\beta = 1.01$-1.13 and 1.14 correspond to arising and developed pseudo-shock mode successively. At $\beta < 1.13$ the flow along the whole duct is supersonic in average and at $\beta > 1.14$ - in greater part - subsonic. Pressure distribution in case of circular jut presence corresponds to pseudo-shock arising regime. It is known, Ref. 65 and 68, that jet and main flow mixing is not essential only at the distance lesser than 10 diameters of orifices for jet injection. In our case average pressure downstream the injection section was defined at the position x = (40-120)d. So, mixing was substantial. Nevertheless, let us make an attempt to use the model of "equivalent" body, Ref. 65 and 68, that do not count mixing but gives good results..
It is impossible to use the computation scheme described in these References directly because pressure acting on jets is not known. Therefore, an closing condition yielding to experimental result about approximate conformity with computations (1D theory) was used (details see in Ref. 11). Comparison of test results and computations is given in Figs 6.3.2 and 6.3.3. The values of total pressure coefficients in the primary and secondary flows are plotted as a function of β. Experimental data of pressure recoveries, ν_3' and ν_3 defined on the basis of the total pressure fields measurements positioned in such a tube section at which static pressure is approximately constant. M-fields received at x = 7d distance from nozzle are given in Fig. 6.3.3. For the value of p_{t3} was accepted average total pressure in the flow core (segment with near constant M). For value of p_{t3}' were taken the readings corresponding to the tube positioned at the exterior boundary of the equivalent body (r = 0.47d). This value sufficiently depends on friction, not counted in the method. Because of that the comparison of computed and experimental values have qualitative character. There is good agreement for primary flow that says about possibility of using related method.
It is known that the height of equivalent body corresponds not to exterior boundary of jet but rather to line corresponding to maximal concentration or temperature. Temperature profile measurements in the duct were taken with the use of thermocouple rake. Measurements were done at the distance x = D that is much nearer to the duct entrance then in the case of total pressure fields measurements. In Fig. 6.3.2 calculated and measured temperature profiles are presented for two values of total pressure and constant temperature of jets (750K). Dashed-dotted line present maximal jet penetration at 2D flow, defined at the proposition that at the duct entrance normal shock exists and downstream of which flow accelerates isentropically to sound velocity in the cannel formed by jets. Near 100% increase in p_t showed small increase in jet penetration as at calculations and experiments. Analogues result was received in Ref. 69 at hydrogen jet injection into air flow. Said is valid generally speaking for regimes of developed pseudo-shocks when mixing intensity increases considerably.
The temperature profile measurements were not detail. Because of that Fig. 6.3.2 tells only about approximate correspondence of external boundary of equivalent body to the line of maximal temperature. It is interesting to note that jet penetration depth at $\beta = 1.11$-1.13 (Fig. 6.3.1) is near to 4.mm. and pressure distribution is near to that corresponding to annular jut, 4.2 mm height presence. This result, possibly, can be considered as a proof of equivalence body use validity.

6.4 Supersonic flow modelling possibilities using cross jet injection.

Artificial increase of boundary layer thickness have substantial interest for aerodynamics-experimentators. The difficulty concludes in necessity to obtain full imitation not only of average boundary layer characteristics (velocity profile, local friction coefficients) but pulse characteristics as well. The use of vortex generators applied for subsonic boundary layer modelling in supersonic flows in ducts through pressure shock system arising can be undesirable.
It is known that gas injection through porous surface increases the boundary layer thickness and do not induce strong disturbances in the primary flow. The possibilities of jet injection through perforated surface are not clear. It can be used for smooth decreasing of average flow Mach number which in 1D

flow is defined by equation $Z(\lambda_2) = Z(\lambda_1)/\beta$, where λ_1 and λ_2 are velocity coefficients up and downstream of jet injection.

We dwell first on relationship of flow parameters downstream the jet injection and secondary jet rate, disposition of orifices, jet total pressure and distance from the jet injection section. Naturally to assume that dispersed injection provide more uniform flow than concentrated injection. In Fig. 6.4.1 pressure distribution along the tube for the variant of dispersed injection is presented. Experiments showed that the most uniform flow take place for variant with 5 rows of orifices. At 25 rows, 6 directrixs, the smoothing of the flow take place at greater distance from injection section. At first let us look at natural pressure distribution in long tubes. In Fig 1.1.3 it is given for 50d long tube. In Fig. 6.4.2 Mach number fields at the end of the tube are plotted for two tube lengths and jet injection rates. These fields have only qualitative character because static pressure across the section was not constant. Dashed lines present velocity profiles for l = 26 and 50d. It is seen that jet injection in the duct L = 7d allows to receive velocity profiles characteristic to flows in long ducts. So, injection of 8% of air into primary flow makes it similar to profile in 50d long tube. In Fig. 6.4.3 the three curves $M(\beta)$ for three nozzles are plotted. Comparison of 1D calculations and experiments shows good agreement.

In Figs. 6.4.4-6.4.6 profiles of parameters (ε_p) are presented for different Ma and β. In Fig. 6.4.4 comparison of flow parameters for variants $l = 12.6$, $\beta = 1$, $l = 7$, and $\beta = 1.04$ is produced. It is seen that pulse profiles are very near. That says about possibilities of supersonic flow modelling with the use of jet injection. This process for different Ma is illustrated in Fig. 6.4.5 for Ma = 2.6 and 3.8. It is seen that by corresponding selection of β it is possible to get good nearing of artificial profiles to natural ones. In Fig. 6.4.6 there are given flow parameter comparison at the end of pseudo-shock created by two methods: due to flow throttling at the end and jet injection at the entrance of the tube. For natural chocking the length of the tube must be about 50d long. As one can see from Fig 6.4.6 parameter profiles are near notwithstanding sufficient difference of pseudo-shock creation methods.

Conclusions

To chapter 2

1.Comparison of pressure profiles in front of circular jut and pseudo-shock showed that pressure gradient in free flow separation three times greater then in pseudo-shock. The inclination angles of dissipating regions in this cases are also different. In pseudo-shock case it approximately twice as lower as in free separation. Micro Pitot tubes near wall measurements indicated that if boundary layer in the tube is thick then there is no separation regions with recirculating. At thin boundary layers separation regions have small length. The pseudo-shock surface friction measurements proved conclusion that pseudo-shock can not be considered as a separation of boundary layer. Separation flow in constant area tube is influenced by the shape of diverging duct that follows downstream of it. This phenomena is not detected in free separation.

2. Deceleration of separation flow in straight ducts with different cross sections, in contrast to non compressible liquid do not follow to hydraulic diameter concept due to influence on flow character of boundary layer separation, depending on M, Re, surface roughness and cross section shape. Hydraulic diameter concept can be used only at low Mach numbers <2 and Re.$>10^6$.

3. Deceleration of supersonic flow can be divided conditionally on two types: non separation (pseudo-shock) and separation. The first is characterised by absence of long boundary layer separation regions with reversed flows. The length of pressure recovery regions is about 10-15 hydraulic diameters and pressure recovery level about that in normal shock. The transition from non separation to separation flow occurs uneven and defined by the duct aspect ratio $\bar{b}$ and M relationship. In this range of M = 2-5 and b = 1-8 the conditional boundary of transition can be evaluated by formula $M_b = 2.5 + 150\bar{b}^{-4}$. At $M > M_b$ the flow is separation one and the length of pressure recovery region depends little on M, Re, d_h, δ and approximately equal to $(20\text{-}25)d_h$.

4. In ducts close to axisymmetrical the initial non uniformity influence but little on integral flow parameters. The increase of transitional region length does not exceed 20-30% and pressure recovery regress-7-10%. In ducts with oblong cross sections the initial non uniformity can result in pseudo-shock transition into separation flow and essential growth of this region length.

5. In ducts with annular-sectoral cross sections having, as in rectangular, corners in the range of M< 4.25 and b<6 there can exist pseudo-shock type flow. Such essential difference of flow from flow in rectangular ducts can be explained by some restrictions laid on separation and connected with the curvature of the walls. Pseudo-shock type flow in annular sectored ducts realised only if there is thin boundary layer, when pressure recovery region is positioned at the beginning of the duct. At lower back pressures these regions are positioned at the depths of the ducts and the flow becomes separation. So, boundary layer thickness influences flow character considerably. Analogues phenomena- the existence of separation flow at rather small M, but thick boundary layers take place in rectangular ducts with high $\bar{b}$.

6. The change of Re influences on flow differently depending on $\bar{b}$. At Re $< 10^6$ the transition region in square duct at Ma = 4.25 grows one and half times. The pressure distribution character at this did not change. At $\bar{b} >$ 3 the same Re drop leads to flow character transformation. At $\bar{b} > 6$ and Ma = 4.25 there is upstream pressure influence at all duct length, Δx = 30-40d that possibly can be explained by laminar boundary layer separation. The decrease of hydraulic diameter lower than 19 mm at $\bar{b}>3$ and Ma = 4.25 leads to pressure recovery drop. That does not noted at corresponding decrease of Re due to pressure decrease. This fact, possibly, connected with the change of relative thickness of boundary layer. At Re $< (0.5\text{-}0.8)10^6$ and Ma = 3.2 for circular ducts and Ma> 3.8 for square ducts the length of pressure recovery region can increase more than twice. The smooth pressure distribution transform into saw-like. This phenomena can be explained by laminar separation occurrence. At this Ma there hysteresis take place depending on the way of movement of separation in the tube.

7. Four character flow regimes can occur in dependence of secondary jet injection rate: separationless, separation type analogues to free stream separation, regime of pseudo-shock arising, and regime of developed pseudo-shock. The injection of normal jets in ducts leads to flow choking at injection rate much lesser than at 1D assumption. Maximal choking effect take place in the case at close injection orifices disposition. acting like slot. The transition from free separation to pseudo-shock at fixed M is defined in general by the heat/mass increase coefficient and depend little on total pressure, temperature in jet injection and boundary layer

thickness in ducts. At heights of equivalent body and jut equal the last has bigger throttling effect. Jet injection into flow at critical regime leads to substantial change of flow character. The jet injection in the middle of the duct lets to split the pressure recovery region into parts and decrease of pressure maximum and length of region.

8. In ducts with oblong cross sections at $M < 3$ the means of back pressure creation (mechanical valve or jet injection throttling) exerts essential influence on the flow character upstream the section of disturbance source. It is known that free separation is independent on disturbance type. The change of orifice disposition in the annular duct, their diameter, that define the level of total pressure in them, exerts rather small influence on the pseudo-shock length and is defined mainly by the jet injection rate. Nevertheless, it can be noted, that disposition of orifices on the only one wall, at the same section, promote pressure recovery region growth.

9. The pressure influence distances in pseudo-shock normalised by hydraulic diameters differ little. It allows to use empirical relationship $\Delta(M, \beta)$ for different ducts. The use of tubes for jet injection in rectangular ducts promotes separation flow transition into pseudo-shock. The value of these tube drag coefficients is $C_x = 1.1$-1.3. The change of the tube length, their diameter, tube disposition on one or two walls do not lead to noticeable errors in total pressure loss evaluations. Jet injection from one wall at $b = 3$ rectangular duct at $M > 3$ saves flow separation. In front of jets there occurs separation flow that creates additional non uniformity that prevents the pseudo-shock forming. Jet injection from two walls assist to flow transformation into pseudo-shock.

To chapter 3

1. Approximate drag evaluation of ducts with local widening and narrowing can be done using 1D theory. Supersonic flow depends little on the length of a jut The length of annular cavities defines two essentially different flow regimes with opened and closed cavities. An increase of cavity length leads to drag increase. The flow mode in duct with cavity longer than critical essentially depends on non-uniformity level and average Mach number. Relatively small changes in non-uniformity can result in transformation from separation flow to pseudo-shock.

2. In axisymmetrical ducts with thin boundary layers ($\delta<0.1R$) the pseudo-shock two or more times shortening is possible. It can be done by creating local zones of high pressure. These zones can be created for example by annular juts. At more thick boundary layers this advantage decreases and at $\delta>0.2R$ disappears. The separated local zones of high pressure induced by struts do not fix the pseudo-shock upstream transition. In ducts with oblong cross section the increasing of pressure recovery region is possible only in the form of separation flow transformation into pseudo-shock.

3. The fixation of pseudo-shock at the high pressure zones done without boundary layer separation, for example with the use if conical juts, is preferable due to smaller drug as at supersonic and subsonic modes of flow. There are correlation relationships of minimal pseudo-shocl lengths and maximal pressure around the obstacle. Pseudo-shock pressure profile in front of the obstacle depends little on obstacle shape. The base pressure downstream the obstacle essentially depends on obstacle disposition in the tube and can reach the values lesser than at sudden expansions of sonic flow.

4. The flow character in the tube with circular jut at axial jet injection essentially depends on the flow regime in front of the jut. At the regime of free separation there is no disturbances propagations upstream the jut. In the case of pseudo-shock position in front of jut the jet injection leads to pseudo-shock upstream transition. The heating of injected jets smooth the pressure distribution and increase its level just downstream the jut. The flow reaction on the diverging section of the tube R at small values of β decreases R and at large β - increases.

5. The different geometry strut grid installation in the duct with supersonic flow, $Ma = 2.6$-3.8, that produce flow impulse loss $\zeta = 1$-8% causes total pressure pulsations having intensity $\varepsilon_{p0} = 1$-4% in comparison to $\varepsilon_{p0} = 0.6$-1.1% in smooth duct. An increase in strut grid drag due to interference occurring at strut cascading leads to essentially more pulsation intensity increase than in the case of grid drag increase due to strut geometry change. The transition from rhomboid to cylindrical struts flown by the front part of pseudo-shock leads to rather small change, in contrast to supersonic flow, in pulsation intensity. The pulsation intensity of static and total pressure increases at transition grid position from $x = 1.85d$ to position $x = 3.7d$. The spectra band widens and high frequency oscillation energy increases. Pressure pulsations depend little on strut geometry and

disposition if pseudo-shock occupies all the duct. The installation of two or three row grid of rhomboid struts in supersonic flow leads in comparison to one row grid, to rise of high-frequency of static and total pressure pulsation energy. At the pseudo-shock regime total pressure high frequency pulse energy grows at an increase in the number of rows. The opposite situation occurs with static pressure pulsations. An decrease in supersonic Mach number apart from the increase of mean square toot deviations of pressure pulsation leads to spectra band widening in the case of rhomboid struts. In the case of cylindrical struts this effect develops little.

To chapter 4

1. Pressure distribution along the duct wall positioned downstream the section of sudden expansion at given M essentially depends on conical nozzle directrix angle θ. In the case of contoured nozzle the pressure peak gets far from the step. The pressure in the region of stream reattaching decreases. The calculations made using transparent code showed that the angle between flow direction and duct wall changes little at M = 1.5-2.6 and approximately equal to 30^0. The increase in M up to 3.8 decreases this angle. Using of this code shows good agreement between calculations and experiment in the case of conical nozzles at M>2. The use of contoured nozzles makes this agreement worse.
2. Static pressure at the beginning of the widening of the tube consisting of cylindrical and conical sections has greater value than computed in the suggestion that obtuse angle is flown by uniform supersonic flow with Mach number equal to average Mach number. None of examined velocity profiles of flow in front of conical section exerted essential influence on the pressure distribution in this section. The influence of velocity profile on pressure distribution and base pressure in stepped duct at critical regime is also small. For approximate evaluations it is possible to accept uniform profile and M = 1. Most of velocity profile influence is noted at small expansion ratios (f = 1.24) and jet injection near critical section.
3. Investigations in the stepped ducts (f = 2.72, Ma = 3.8) showed that the decrease in Re (12.10^6.-5.10^6) leads to pressure pulsation increase approximately in 1.5-2.0 times. This is possibly the reason of base pressure drop. The installation of an turbulisator in the subsonic part of a nozzle did not change the relationship ε_p(Re).This confirm suggestion that subsonic part of the nozzle is not the source of changes of ε_p. The ratio of ε_p up and downstream of expansion fan does not depend strongly on Re. This points out on absence of some reconstruction of flow. The increase of ε_p at Re decrease take part possibly in supersonic section of the nozzle due to transition of turbulent boundary layer into transitional.
4. The division of the flow in the stepped duct into two parts, circular and annular with the use of thin wall cylindrical tube leads to base pressure increase. This can be explained by the flow nearing to 2D type. Base pressure in stepped annular ducts, as in circular stepped duct is defined by expansion ratio. The presence of thinwalled cylindrical tube leads to growth of peak pressure and decrease in distance between peaks.
5. The dependence of relative base pressure in stepped ducts on Re at turbulent supersonic flow in front of step has complex character and defined mainly by M and f. The reason of such specific feature is in boundary layer laminarisation at swift acceleration of flow around the step. At f = 2.72 in the curve p_b(Re) there is a fragment at which p_b decreases with Re at M = 1-3.8. This fragment displaces into region with smaller Re at Ma decreasing. It is necessary to rise Re 5-10 times to save automodel regime in comparison of saving turbulent flow in the supersonic nozzle. The increase of boundary layer thickness in 2-3 times, the change of one section of sudden expansion into two does not change the dependence p_b(Re) qualitatively.
6. The shape of duct cross section at equal duct expansion ratios exerts substantial influence on base pressure. The partition disposition that leads to flow lines converging makes base pressure increase and diverging of lines to p_b decrease. The distortion of duct axis downstream the step leads to p_b increase which however is not great. At f < 2.4 in the relationship p_b(Re) there is no minimum. A f.> 2.4 such minimum is present.
7. There are 6 flow regimes in stepped duct depending on throttling level, flow parameters in narrow and wide parts of the tube, pseudo-shock interference with separation region downstream the step, pseudo-shock fixation at the step. The shape of narrow part of the tube exerts substantial influence on pseudo-shock propagation, its fixation. Stepped duct consisting of cylindrical sections provides minimal pseudo-shock length at given back pressure. The transition of higher pressure from pseudo-shock into base pressure region leads to flow impulse growth and flow regimes arising at which the increase of back pressure leads to static pressure decrease along the surface of wide part. The supersonic flow deceleration effectiveness in stepped ducts depends on narrow

section shape and length. At $l < 7d$ maximal axial force is achieved in case if this part is cylindrical. At larger lengths of this part and inserting in it slightly diverging duct allows to increase the deceleration effectiveness. In cylindrical part there occurs deceleration of supersonic flow and in diverging part -additional subsonic deceleration

8. The diverging of rectangular duct with oblong cross section does not remove the possibility of transforming of separationless flow into separation notwithstanding of decreasing of $\bar{b}$ and d_h increasing, e.i. to factors preventing the boundary layer separation. Additional deceleration of, partly decelerated, vortex flow in diverging section of combined duct, of supersonic flow in constant area duct take part downstream practically at constant pressure that make it different from pseudo-shock flow type.

9. Pressure recovery in rectangular diverging ducts with oblong cross sections can surpass a little the pressure recovery in constant area duct with cross section equal to entrance section of diverging duct. It occurs at $\theta = 0.5^0$ due to greater d_h and lower $\bar{b}$. At $\theta > 0.5^0$ the duct diverging leads to greater, in comparison with duct F=const, decreasing in efficiency the more θ is due to M increase at which the deceleration take place. Pressure recovery in diverging sections of the ducts with given length depends little on θ if $\theta < 3^0$. The received dependence of pressure recovery on diverging angle depends little on M in examined range. The length of rectangular diverging duct necessary for supersonic flow deceleration into subsonic in examined range of $\bar{b}$ is $f = 2.5\text{-}3.0$. In all tested combined ducts the concluding flow deceleration took part in constant area duct. The pressure recovery in examined combined ducts decreases substantially at f increasing and can be less 50% from pressure recovery in normal shock. The basic reason of it is in fact that at f increasing the value of d_h can reach of values at which deceleration effectiveness of all duct types decreases.

10.The presence of diverging section in the rectangular duct assist to flow stabilisation, developing in pressure upstream influence decreasing and pseudo-shock movement fixation. The most near to entrance pseudo-shock position take place at $\theta = 2^0$ ($f > 1.6$). At $f < 1.3$ there is no separation fixation.

11. Pressure distribution character in subsonic stepped diffuser positioned directly downstream supersonic diffuser with $M = 0.5\text{-}1.0$ at its exit practically does not depend on flow Mach number at the entrance of supersonic diffusers, their length, cross section geometry and expansion ratio. Immediately downstream the step there is a segment in the curve with small drop of pressure. Then, the pressure grows and reaches maximum at the distance of 7-10 calibres of supersonic diffuser hydraulic diameter. Installation of $0.5\text{-}11^0$ conical subsonic diffuser instead of stepped one does not lead to pressure recovery rise corresponding to calculated for this expansion ratio. Additional pressure rise take place in cylindrical duct following conical duct due to velocity profile smoothing. Pressure recovery in subsonic diffuser is much lower than calculated by 1D theory. This fact is possibly connected with high subsonic velocities and high non uniformities of flow at the entrance to subsonic diffuser. Data characterising pressure recovery are grouping in general for circular and rectangular ducts between curves computed for stepped ducts at velocity coefficients at the entrance to subsonic diffusers $\lambda = 0.6$ and 0.8 and depends little on Ma and f.

To chapter 5

1. Smooth change of cross section shape along the duct from rectangular to annular sector allows to rearrange separation flow into pseudo-shock flow and shorten the required length of supersonic diffuser and increase pressure recovery level.

2. The length of pressure recovery region in rectangular ducts with $\bar{b} > 3$ can be shorten if wire grid will be installed ar the entrance of the duct. The flow transforming from separation to pseudo-shock type flow.

3. The installation of wedge-like bodies at the narrow walls at the entrance to the duct makes zones of high pressure and fixes the separation region. The length of pressure recovery region shortens.

References

1. Chang Separation of flow
2. Gogish L.V., Stepanov G.Yu. Turbulent separation flows. Nauka, 1979.
3. Neumann E.P., Lustwerk F. Supersonic diffusers for wind tunnels- J. Appl. Mech.,1949, Vol. 16, No.2
4. Crocco L. In Fundamentals of Gas Dynamics. Editor Emmons H.W., 1958
5. Zimont V.L., Ostras V.N. Calculation of pseudo-shock in cylindrical duct. Uchenye Zapiski TsAGI (TsAGI Scientific Notes- TSN) 1974, v.5, No.3
6. Ikui T., Matsuo K.,Nagai M. The mechanism of pseudo-shock waves. Bull. of the JSME, 1974
7. Tamaki T. et al Bull. JSME, v.13, No.55, 1970
8. Hasinger S.H., Miller D.K. Two-Dimensional supersonic diffuser experiments. AIAA Journal,v.13, No.4, 1975
9. Kusmin V.A. Deceleration of supersonic flow in rectangular ducts. In Coll. Gas dynamics of engines for vehicles. v.1, Kasan, 1978
10. Ktalcherman M.G. et al Pseudo-shock in rectangular constant area duct. In Coll. Gas dynamics of flows in nozzles and diffusers. IPTM SOAN SSSR Novosibirsk 1982
11. Penzin V.I. Experimental investigation of normal jet injection into supersonic flow in ducts. TSN v.4,No.6,1973
12. Penzin V.I. Experimental investigation of supersonic boundary layer separation in a cylindrical duct TSN, v.5, No.4, 1974
13. Penzin V.I. Separation flow incircular cavity. TSN v.7, No.6, 1976
14. Penzin V.I. Pseudo-shock and obstacle interaction. TSN v.14, No.5, 1983
15. Penzin V.I. Influence of gasdynamic and geometric parameters of flow in stepped duct on base pressure. TSN, v.14, No.6, 1983
16. Penzin V.I. Duct with wedge-like bodies drag estimation at supersonic velocities. Tsander transactions. (TT), 1980
17. Penzin V.I. Some features of supersonic flows in stepped ducts. Astronautical conference transactions (ACT) , 1981
18. Penzin V.I. Supersonoc stream spreaing in stepped duct. ACT ,1983
19. Penzin V.I. Pseudo-shock in stepped duct. ACT, 1984
20. Penzin V.I. Supersonic flow deceleration in ducts with annular and circular cross sections. ACT, 1985
21. Penzin V.I. Base pressure dependence on the shape of the duct with sudden expansion. TSN, v.17, NO.1, 1987
22. Penzin V.I. Pseudo-shock and separaion flow in rectangular ducts. TSN, v.19, NO.3, 1988
23. Penzin V.I. Influence of cross section geometry on supersonic flow deceleration. TSN,v.19, No.3, 1988
24. Penzin V.I. Separation flow rearranging into pseudo-shock in rectangular duct. Coll. UAI, 1987
25. Penzin V.I. Influence of initial flow nonuniformity on pseudo-shock . Coll. UAI, 1987
26. Penzin V.I. The use of hydraulic diameter concept for estimation of supersonic flow parameters in rectangular ducts. ACT, 1986
27. Penzin V.I. Influences of differencies in means of back pressues build up on flow separation in constant area dact. ACT, 1993

28. Penzin V.I. Experimental investigation of supersonic flow deceleration in diverging rectangular ducts. Preprint TsAGI , No.80, 1993
29. Penzin V.I. Experimental investigation of drag of set of struts installed in the duct. ACT, 1993
30. Penzin V.I. Pressure pulsations behind the set of struts. ACT, 1994
31. Penzin V.I. Experimental investigation of cramjet model elements. TsAGI conference transactions, 1994
32. Penzin V.I. Supersonic flow deceleration in diverging ducts. IAC, 1994
33. Penzin V.I. Subsonic diffuser following the supersonic diffuser. ACT, 1995
34. Penzin V.I. Duct flow transformation induced by partitions and wedges. ACT, 1995
35. Ostras V.N., Penzin V.I. On duct flow character changes at supersonic flow throttling. TSN No.3, 1976
36. Ostras V.N., Penzin V.I. Experimental investigation of friction force in ducts with pseudo-shock. TSN, No.2, v.5, 1974
37. Ostras V.N.,Penzin V.I. Experimental investigation of friction force in ducts with non-uniform supersonic flows produced by conical nozzles. TSN v.3, No.4, 1972
38. Gurilev V.G., Penzin V.I. Tansition of supersonic flow into subsonic in a tube with short confusor section. TT, 1981
39. Merkli P.E. Pressure recovery in rectangular constant area supersonic diffusers. AIAA J., v.14, 1976, pp 168-172
40. WaltrupP.J., Billig F.S. Prediction of precombustion wall pressure distribution in scramjet engines. Journal of Spacecraft and Rockets. v.10, No.9, 1973
41. Waltrup F.J., Billig F.S. The structure of shocks waves in cylindrical ducts. AIAA J. v.11, 1973
42. Bogdonoff Kepler Turbulent boundary layer separation in supersonic flow. AIAA J., v.22 ,No.6 , 1955
43. Zukoski E.E. Turbulent boundary layer separation in front of a forward facing step. AIAA J., No. 10, 1967
44. Waltrup P., Cameron J. Wall shear and boundary layer measurements in shock separated flow. AIAA J.,v.12, No.6, 1974
45. Pavlenko A.M. Experimental investigations of flow separations in ducts. TsAGI Transactions No. 1592, 1974
46. Chernov V.A., Kiseleva E.N. In Coll. Kinetics and aerodinamic process of fuel combustion. M. Nauka, 1969
47.Gurilev V.G,, Trifonov A.K. Transition of supersonic flow into subsonic in ducts with diverging forward sections TSN v.6, No.4,1980
48.Korkegi Comparison of shock-induced two-and three-dimensional incipient turbulent separation. AIAA J.,1975, v.13, No. 4
49. Zubkov A.I., Sorkin L.I. Viscosity influence on flow in the vicinity of normal shock wave. Isvestia AN SSSR No.1, 1967
50. Krause S. Experimental investigation of supersonic diffusers with high aspect ratio and low Re mumbers. AIAA 79-1491R
51. Charwat A.F., Roos J.N., Dewey F.C., Hits J.A. An investigation of separated flows - Part 1: The pressure field. JASS, v.28, No.6, 1961
52. NASA CR 132654, 1975

53. Blagosklonov V.I. , Khomutov V.A.. Sudden expansion of supersonic in cylindrical duct. TSN, v.6, No.3 , 1975
54. Blagosklonov V.I., Ivanov M. Ya.Algorithm and computing programm for two-mode flow of ideal fluid. TsAGI Transactions No 1660, 1975
55. Grodsovsky G.L. On gas ejector with large compression in cylindrical mixing chamber theory. Isvestia AN SSSR, MJG, 1968, No.3
56. Leytes E.A.., Nesterov Ju.N. , Khomutov V.A. Supersonic flow propagation in the duct with sudden expansion. TsAGI Transactions, 1975, No. 1672
57. Korst H.H. A theory for base pressure in transonic and supersonic flow. New York, 1956 Paper No.56-ARM-30
58. Davidson V.E., Neshcheret P.A. On underexpansion supersonic stream discharge into pipe. In coll. Hydromechanic and springing theory. Dnepropetrovsk university. No.16, 1973.
59. Davidson V.E., Neshcheret P.A. Wall pressure in the wide part of the stepped tube at supersonic flow. In coll. Hydromechanic and springing theory. Dnepropetrovsk university. No.21, 1976.
60. Fabri J., Siestrunk R. Rev. Generale des sciences appliquees.,2, 1955
61. Vagramenko Yu.A. , Puchkova A.F. On base pressure determination at supersonic axisymmetrical strem discharge into ducts. Isvestia AN SSSR MJG, 1973, No.6
62. Lavruchin G.N., Yagudin S.V. An investigation of flow mode transition in ejector nozzles. TsAGI Transactions , 1979, No. 1995
63. Glotov G.F., Moroz E.K. An investigation of axisymmetrical flows with sudden expansion. TsAGI Transactions , 1975. No. 1672
64. Sirieix M., Delery J., Mirande J. Recherches experimentales fondementals sur les economlements separes et applications. ONERA, T.P. 520, 1967
65. Weinbaum S. Rapid expansion of supersonic bundary layer and its application to the near wake AIAA J., No. 2, 1970
66. Zukosky E.E, Spade F.W. Secondary injection of gases into supersonic flow. AIAA J., V.2, No.10, 1964
67. Zukosky E.E. Spade F.W. A study of the interaction if gaseous jets from transwerse slots with supersonic ezternal flows AIAA J. v. 1, No. 2,1966
68. Schetz J.A., Billig F.S. Penetration of gseous jet injection into supersonic stream., J. Spacecraft v.3 , No 11, 1966
69. Orth R., Funk J.A. An experimental and comparative study of jet penetration in supersonic flow J. Spacecraft, v. 4, 1967
70. Wu Chan-Min, Kinia Aoiama Transverse injection into supersonic flow in duct JASS No.11, 1968
71. Cohen L.S. Measurements of the penetration and mixing of gases injected into subsonic and supersonic air streams. AIAA Paper 70-714
72. Shetz J.A. Interaction shock for transverse injection in supersonic flow. Spacecraft and Rockets, No.2, 1970

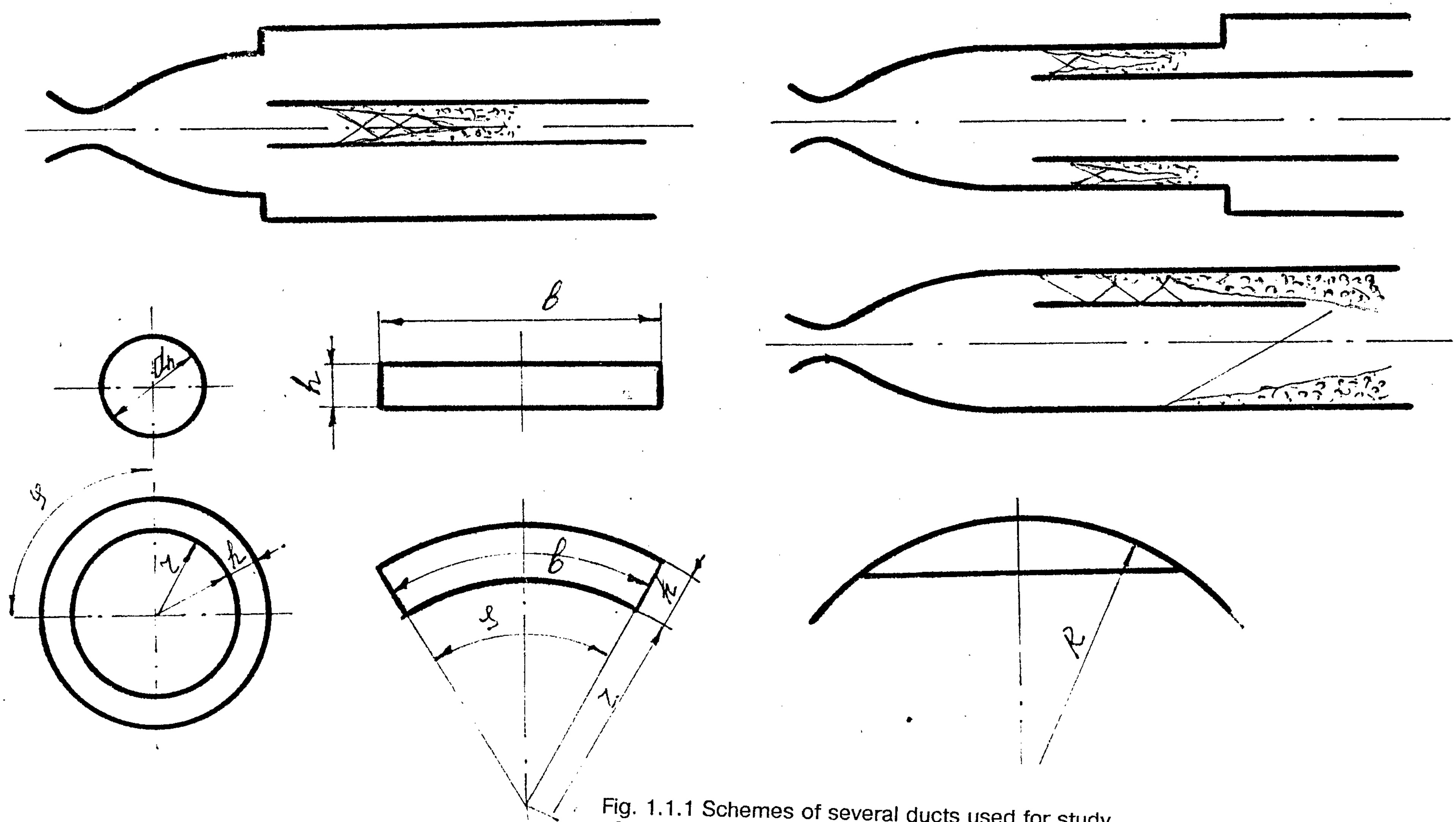

Fig. 1.1.1 Schemes of several ducts used for study of supersonic flow deceleration.

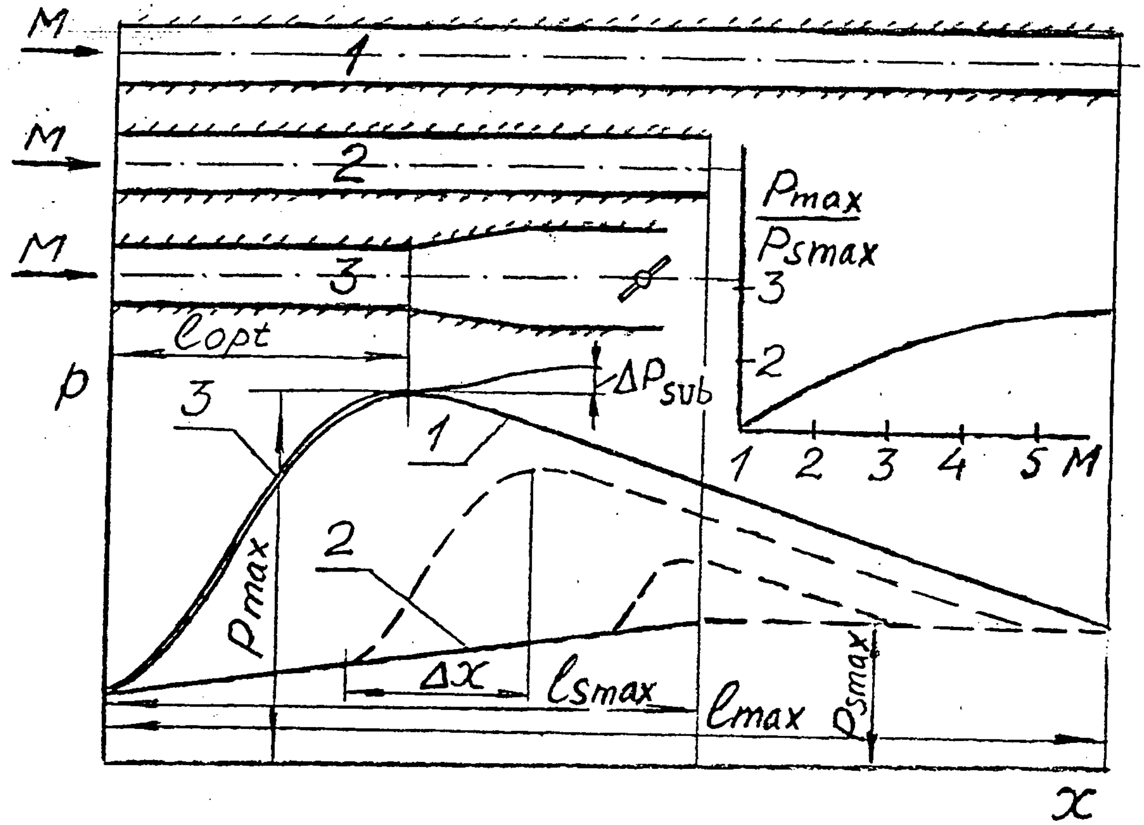

Fig. 1.1.2 Diagrams explaining an approach to duct length selection.

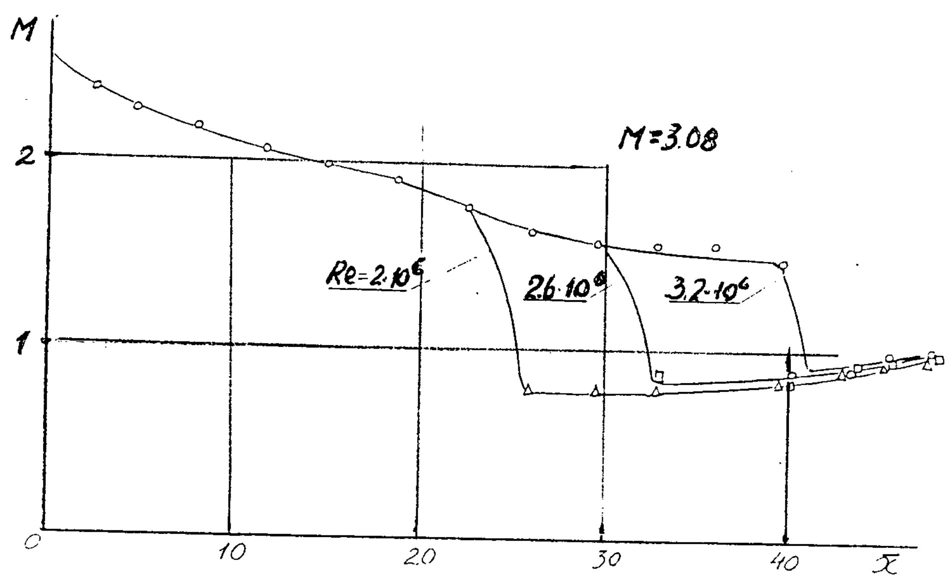

Fig. 1.1.3 Avarage Mach number distribution in circular duct at different Re

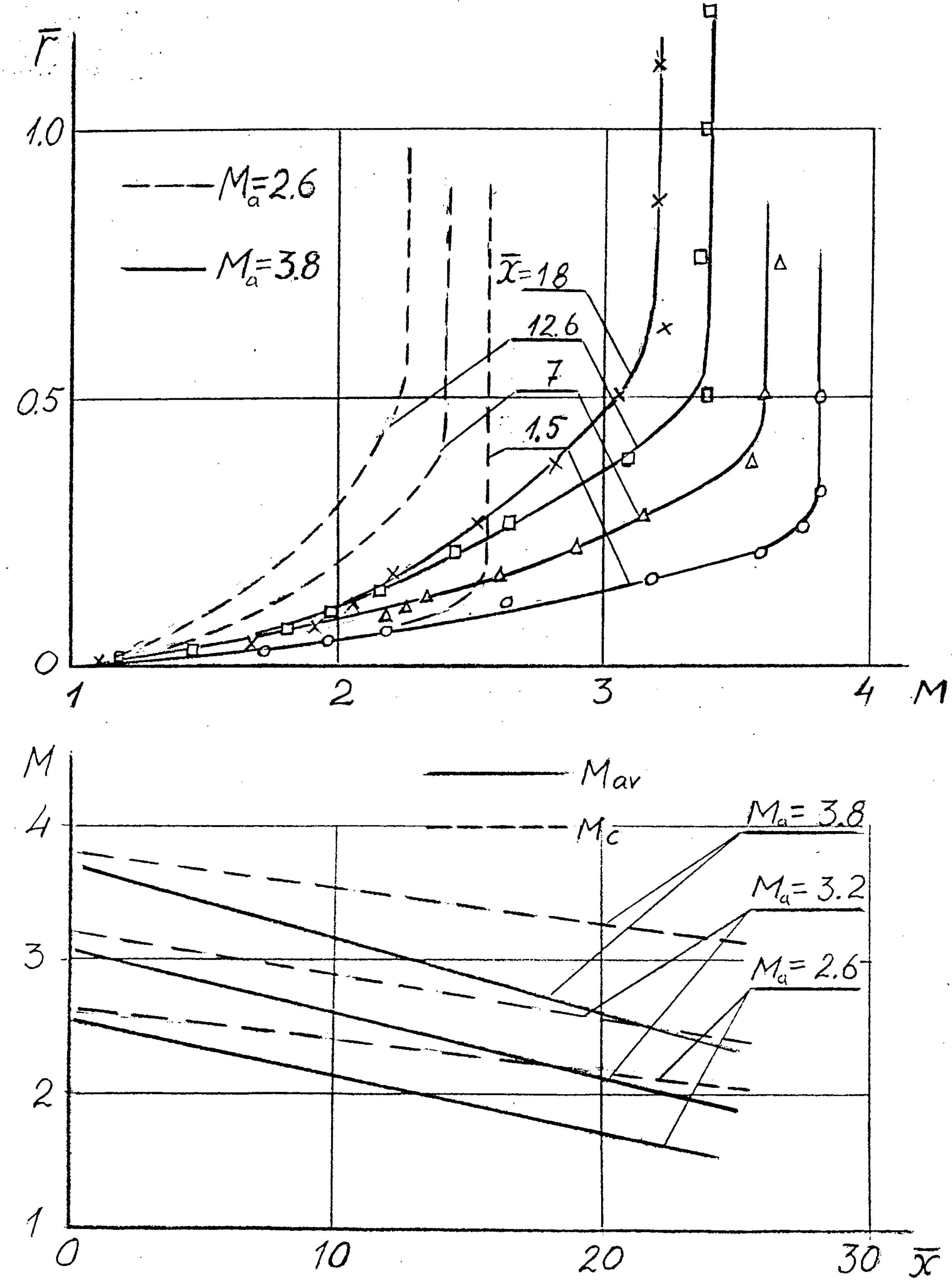

Fig. 1.2.1 Duct flow parameters

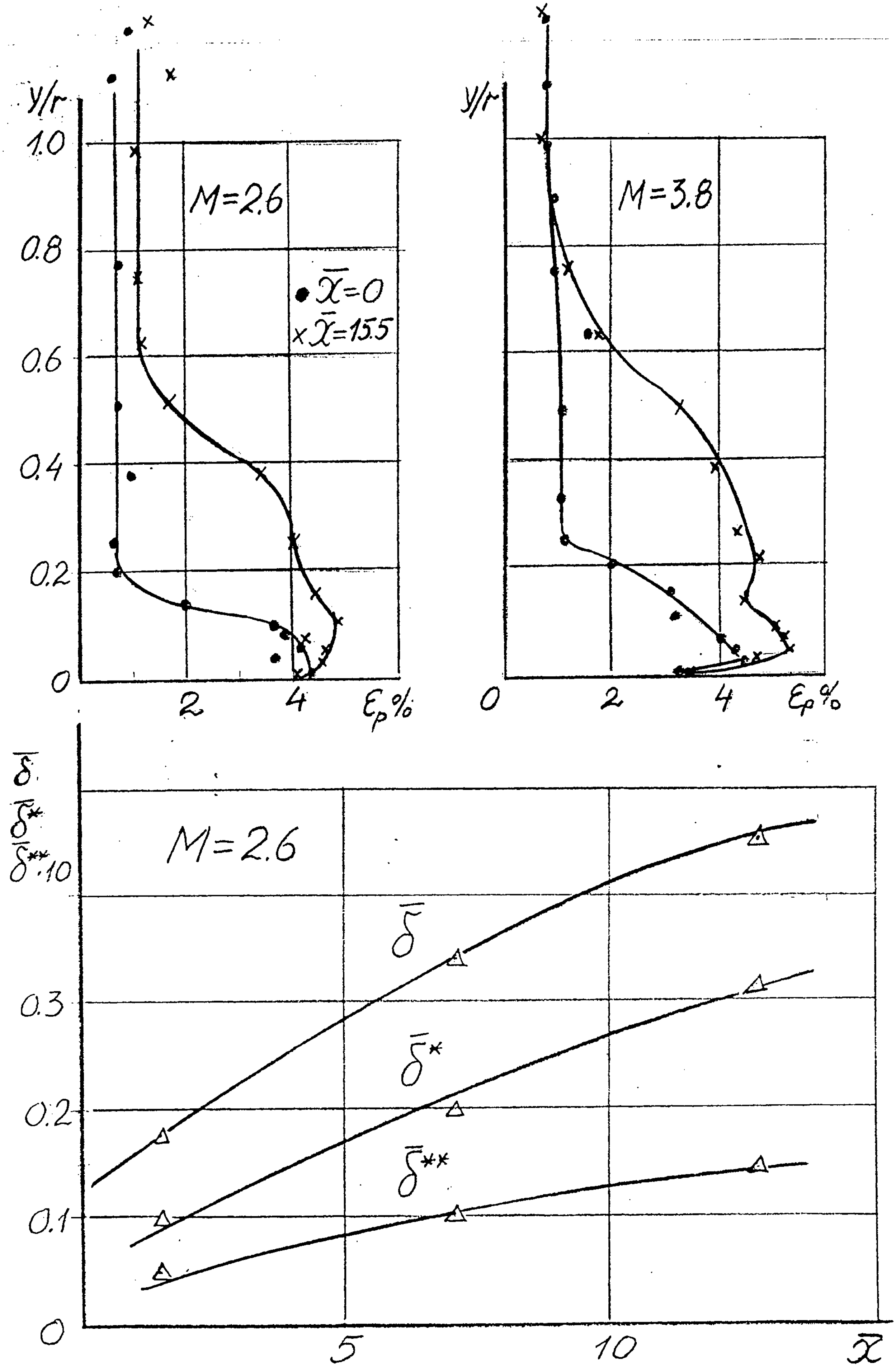

Fig. 1.2.2 Duct flow parameters

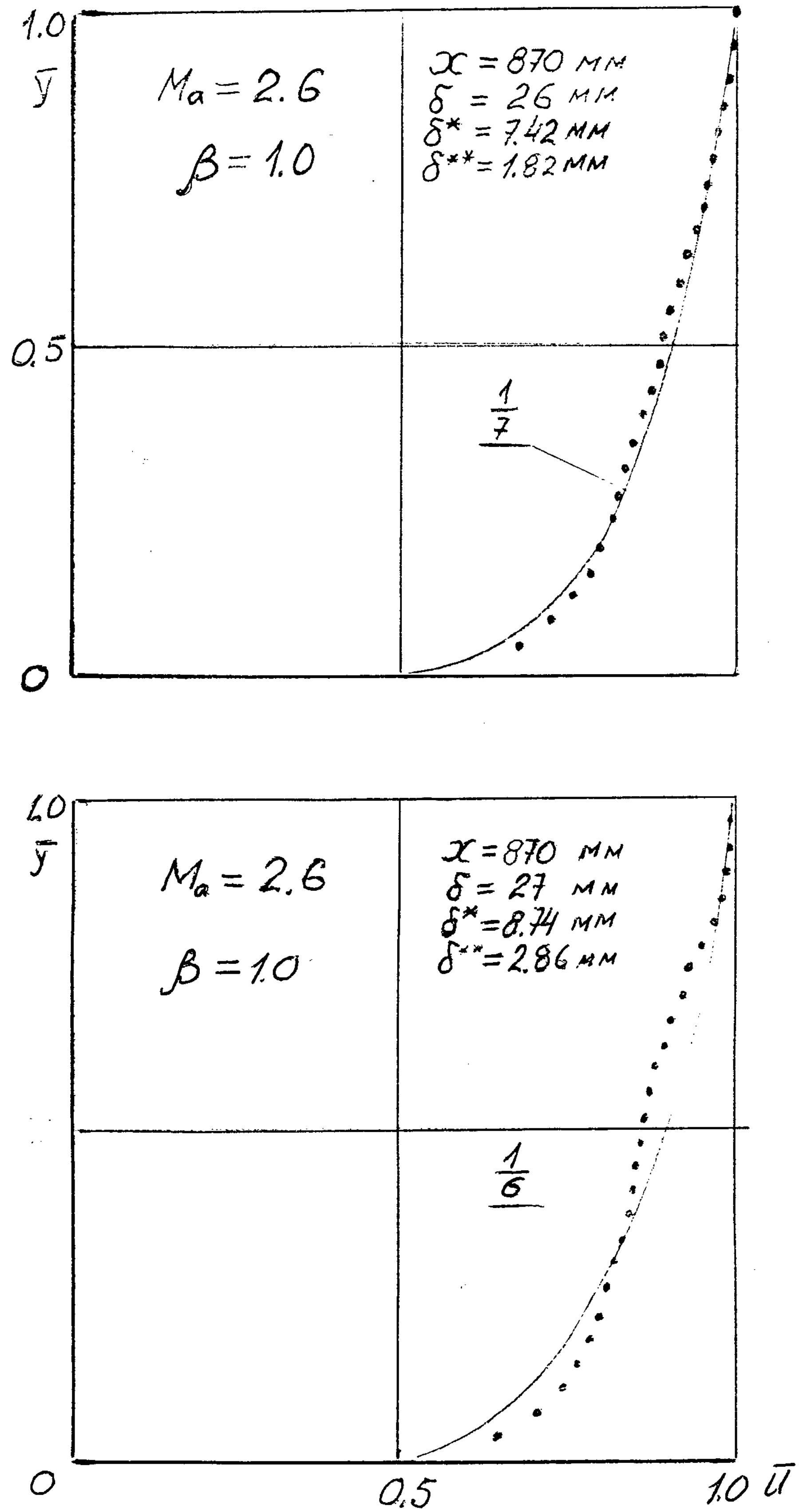

Fig. 1.2.3 Velocity fields in tube boundary layers.

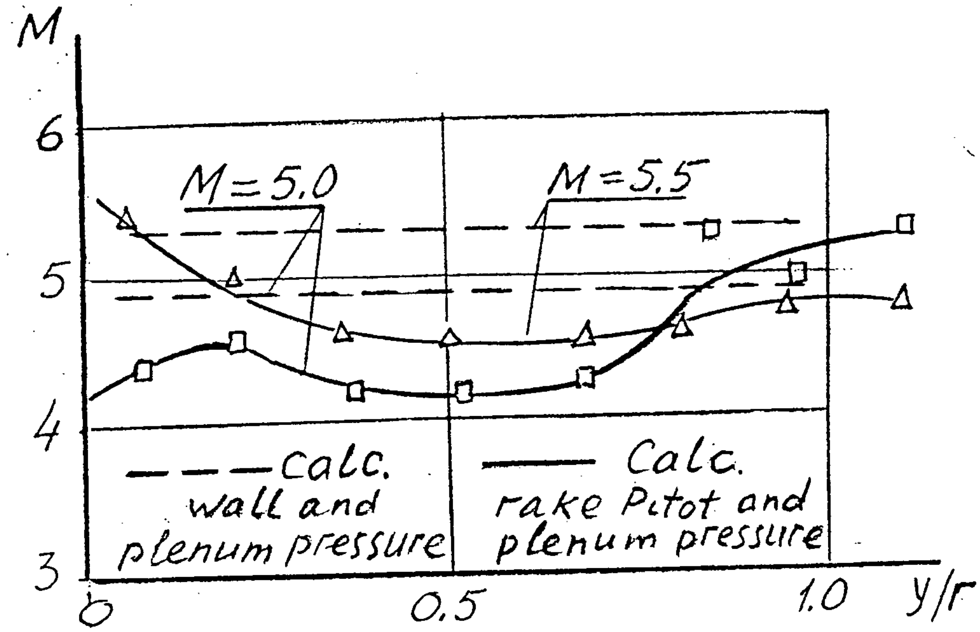

Fig. 1.2.4 Mach number fields
in M5.5 and M6.0 nozzles.

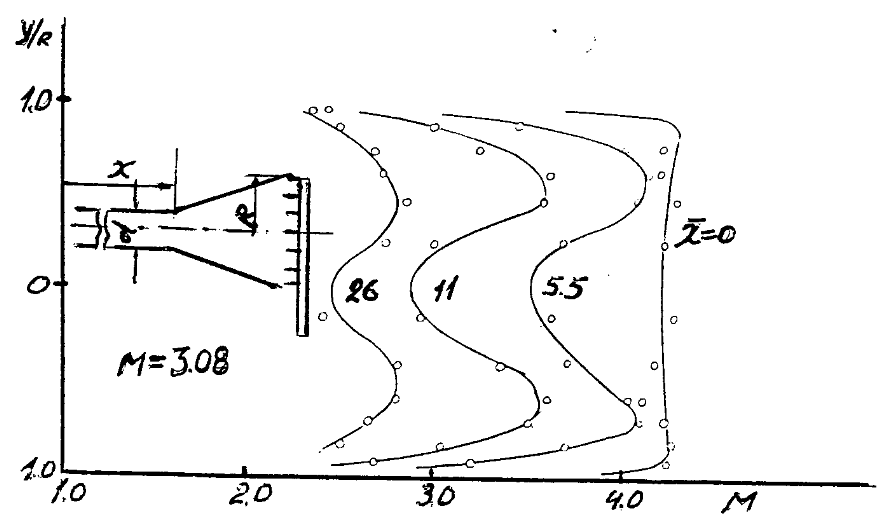

Fig.1.2.5 Mach number fields at the end of the duct
consisting of M 3.08 nozzle, lenghening tube and
conical section

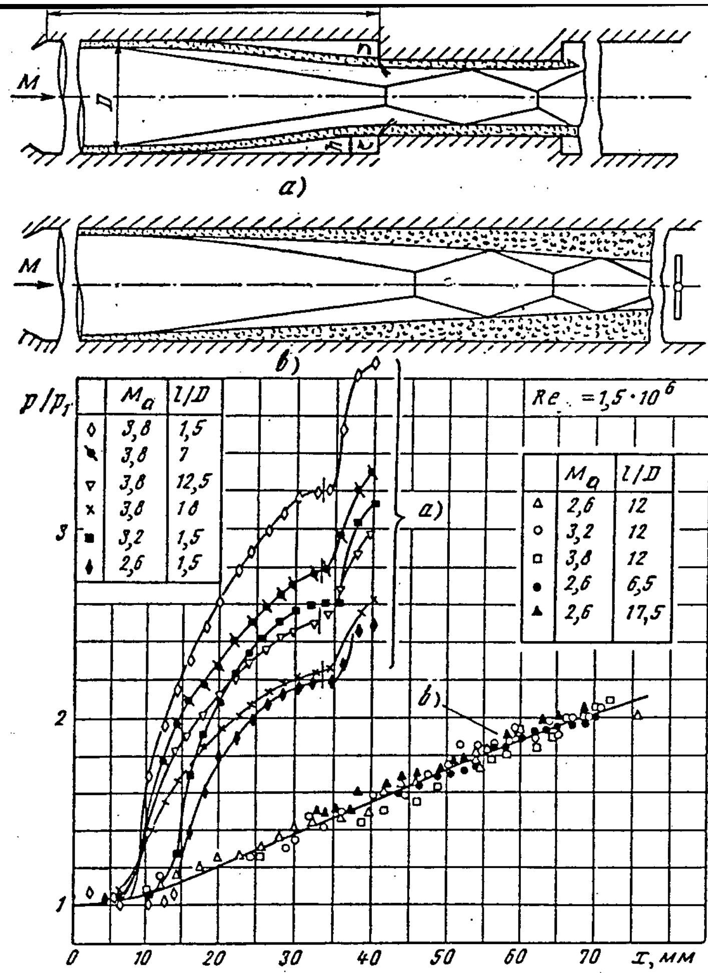

Fig. 2.1.1.1 Comparison of pressure distributions in front of the step and in pseudo-shock.

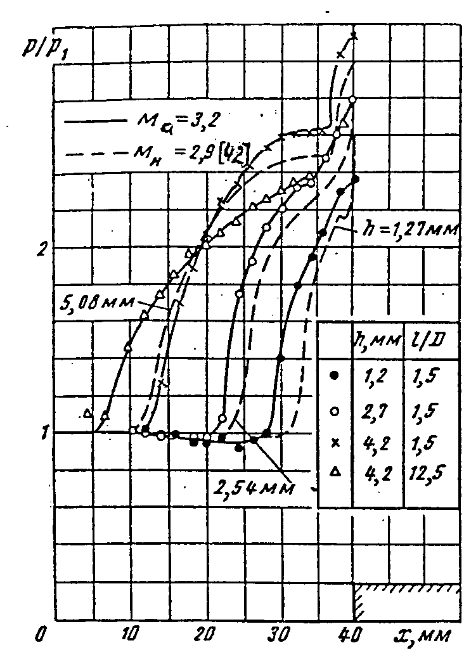

Fig. 2.1.1.2 Pressure distribution in front of annular and plane steps of different heights and duct lengths at Ma = 3.2.

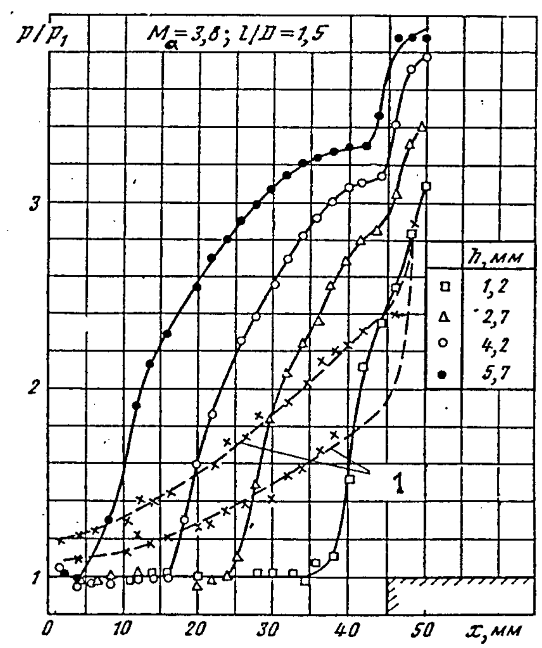

Fig. 2.1.1.3 Pressure distribution in front of annular step and in pseudo-shock at different step heights at Ma = 3.8, 1-pseudo-shock

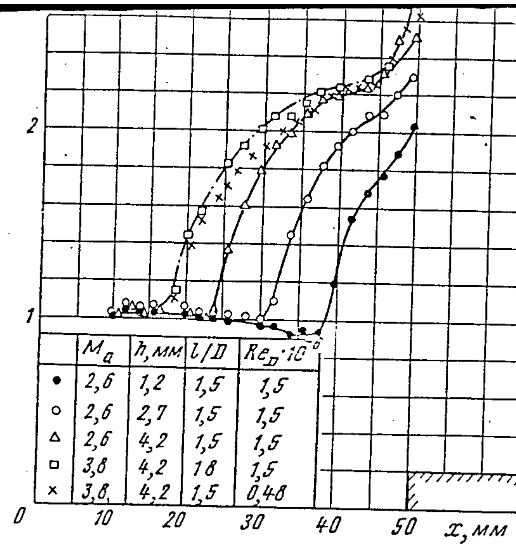

Fig. 2.1.1.4 Pressure distribution in front of annular step and in pseudo-shock at different step heights at Ma=2.6 and 3.8

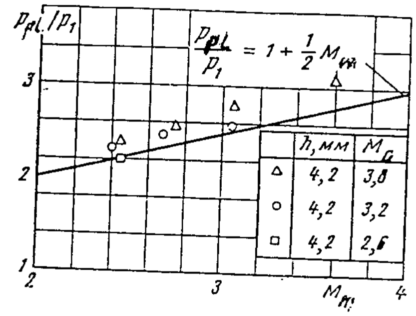

Fig. 2.1.1.5 Relative "plateau" pressure vs. mean Mach number.

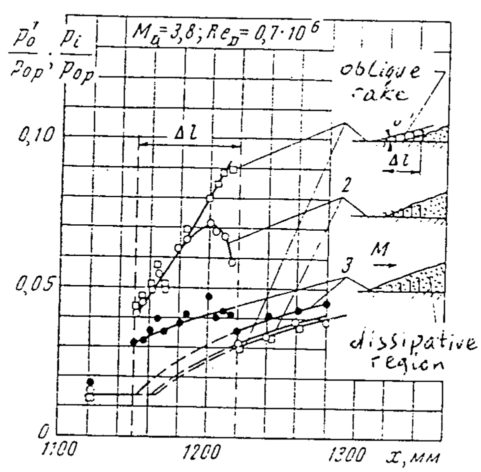

Fig.2.1.1.6 Pseudo-shock measurements with the use of the oblique rake.

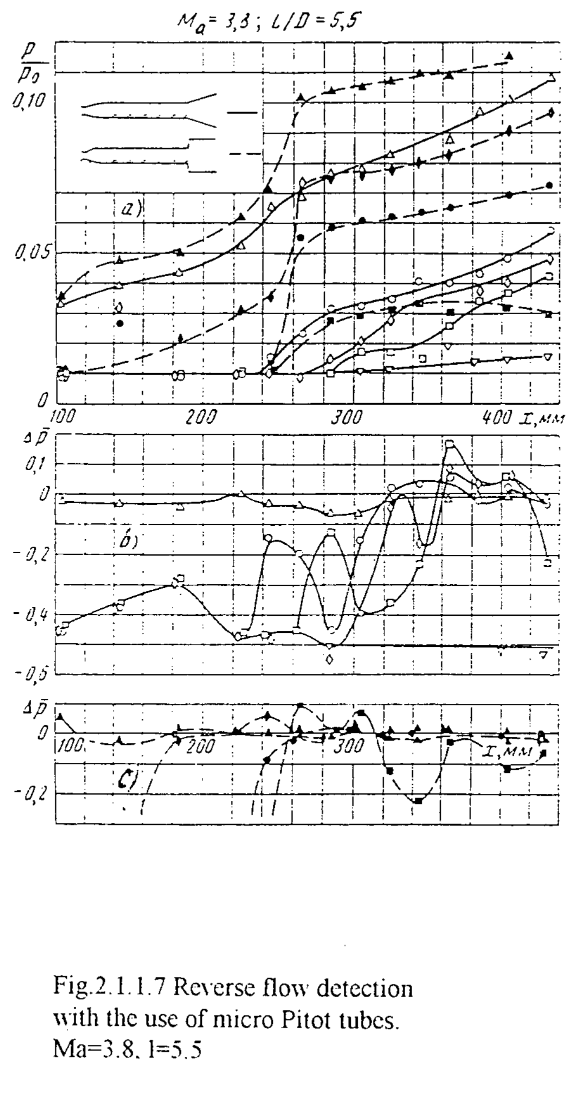

Fig.2.1.1.7 Reverse flow detection with the use of micro Pitot tubes. Ma=3.8. l=5.5

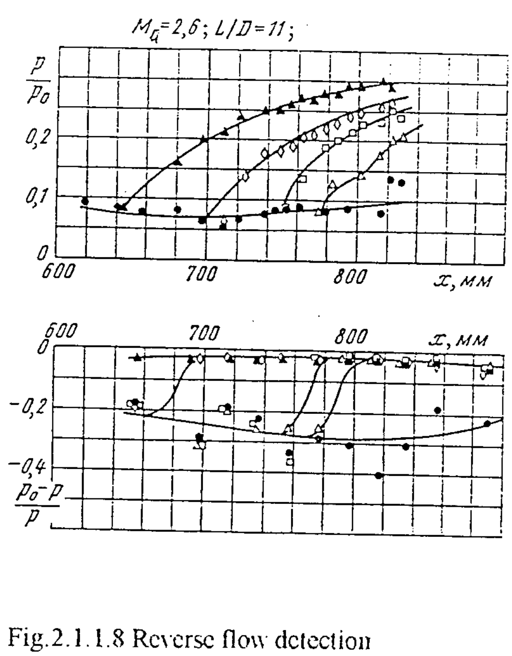

Fig.2.1.1.8 Reverse flow detection with the use of micro Pitot tubes.

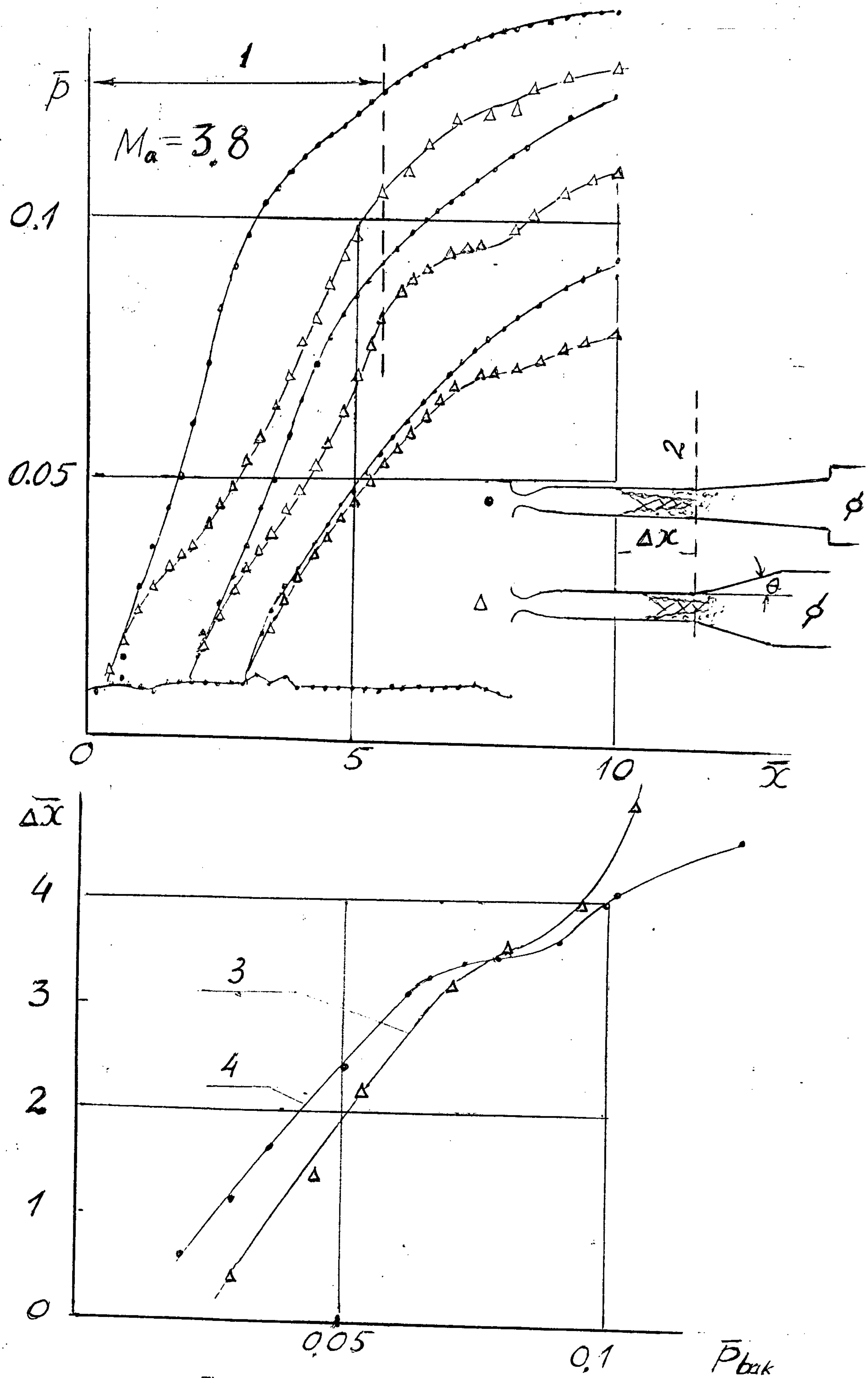

Fig.2.1.1.9 Impact of duct shape downstream the cylindrical tube on upstream pressure influence. Ma=3.8, 1- cylindrcal duct, 2- section of back pressure

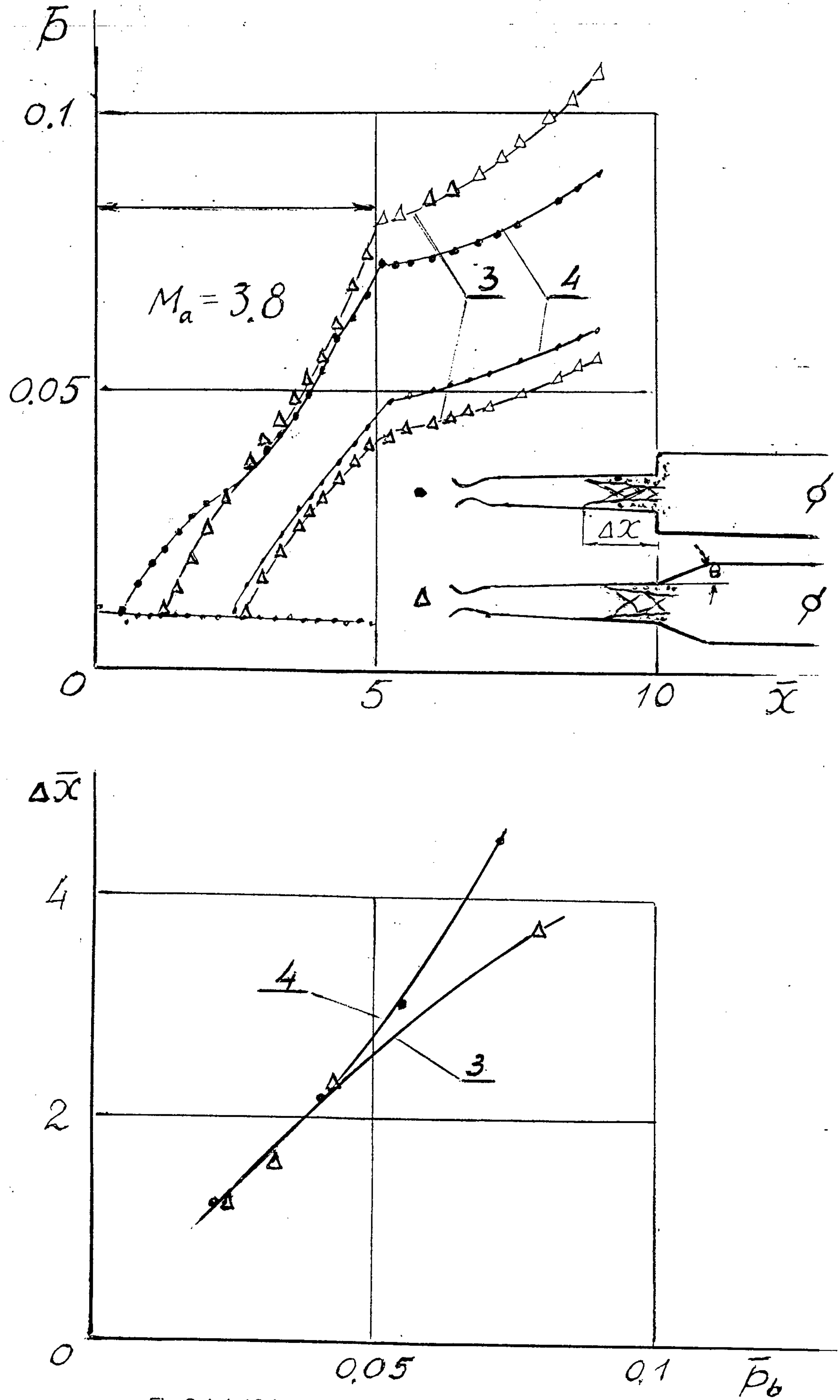

Fig.2.1.1.10 Impact of duct shape downstream the cylindrical tube on upstream pressure influence. Ma=3.8, 1- conical duct, 2- section of back pressure measurement, 3-θ=11^0, 4- θ=90^0

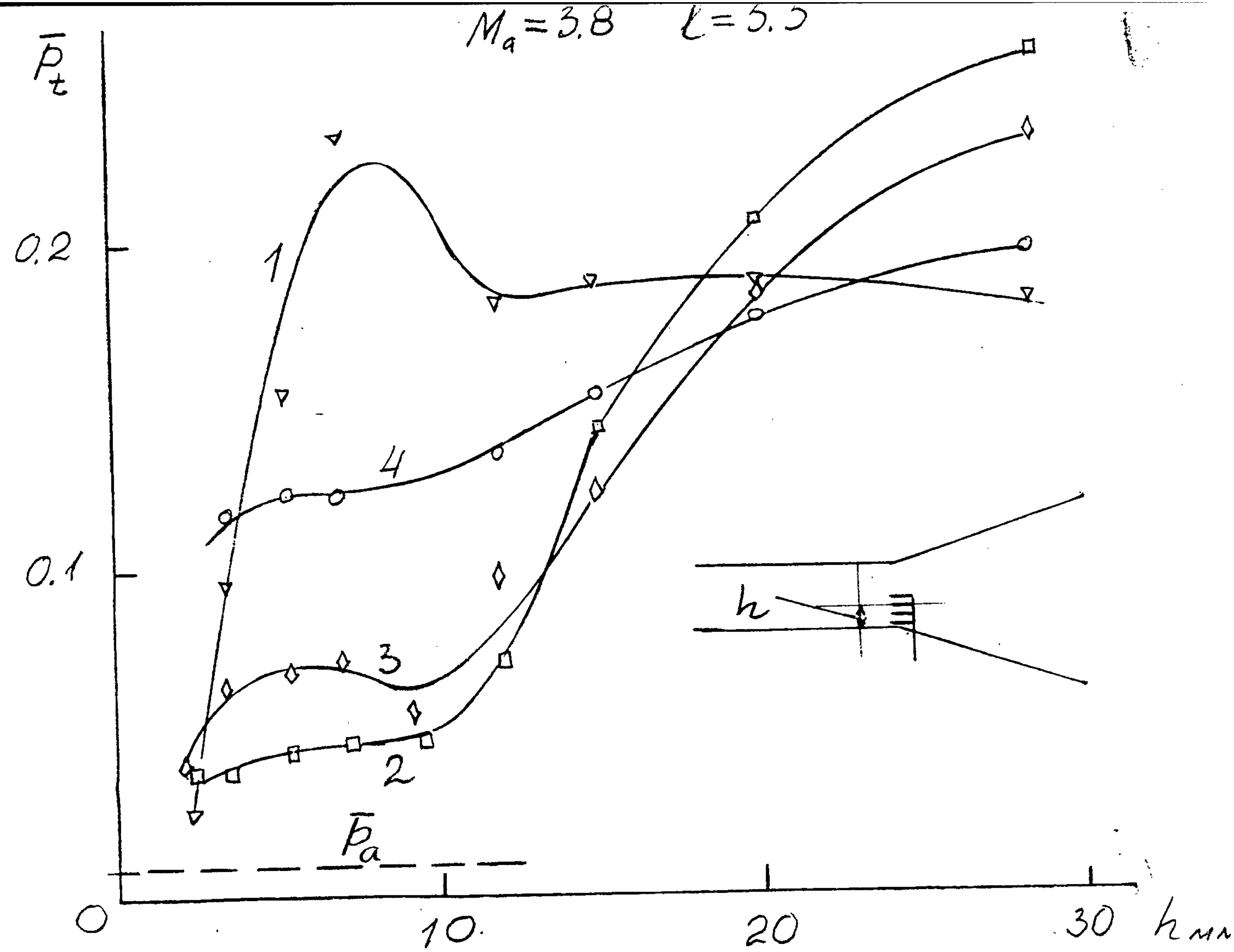

Fig.2.1.1.11 Pt profiles at the end of the tube at different modes of flow.

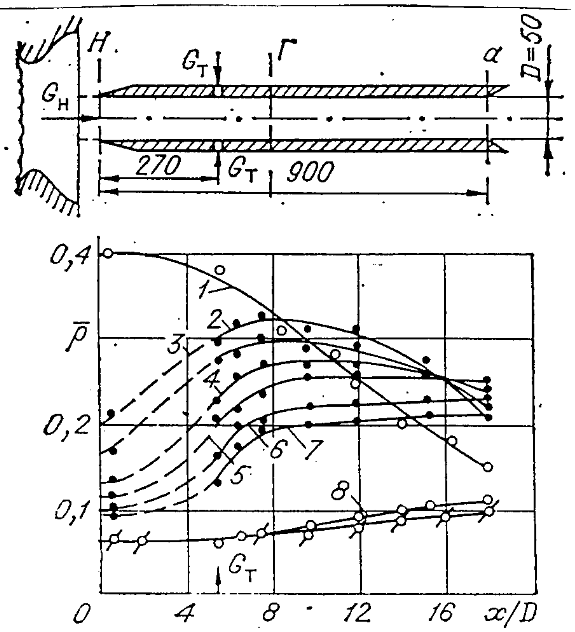

Fig.2.1.1.12 Pressure distribution in cylindrical duct in free stream, Ma=2.5 at different supplies of gas from generator 1-β=1.03, 2-1.22, 3-1.019, 4-1.016, 5- 1.015 6-1.012, 7-1.009, 8-1.0

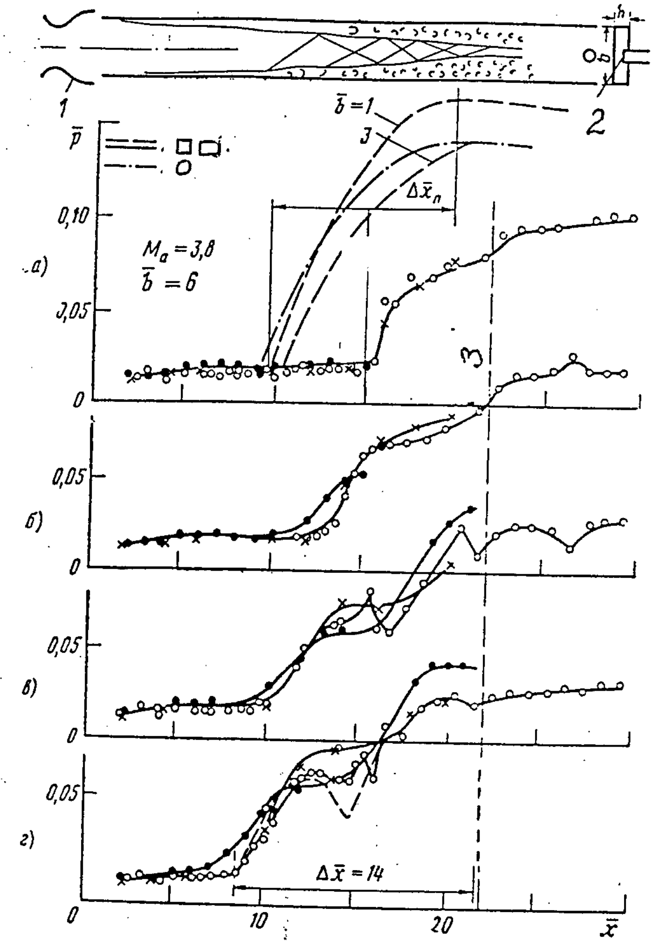

Fig.2.1.2.1 Pressure distribution in pseudo-shock in rectangular duct, b = 6, Ma = 3.8. ----,—rectangular duct. — • — circular duct, O-wide wall, •-narrow wall (right), x-(left), 1-nozzle, 2-throttle, 3-rake P_t^1

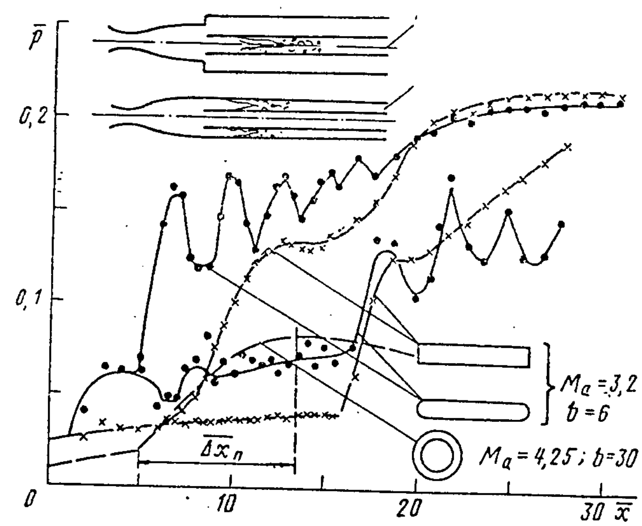

Fig.2.1.2.2 Pressure distribution in ducts with oblong cross sections. 1-plane or sector duct, 2-annular duct.

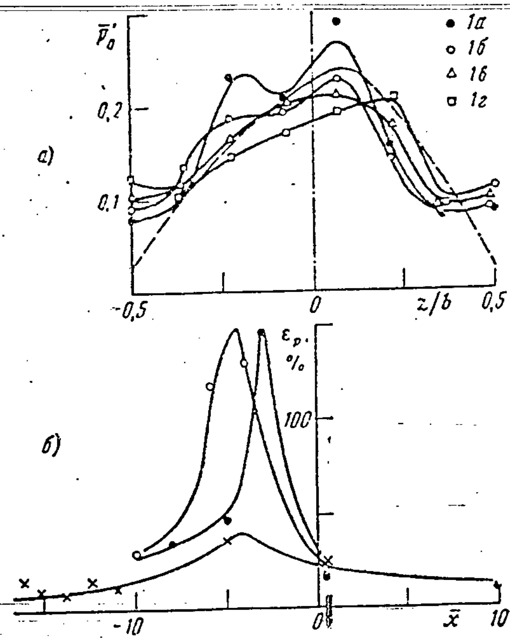

Fig.2.1.2.3 Total pressure fields and pressure pulsation intensity dependencies on separation region position. O-left, ●-right, x-middle probes

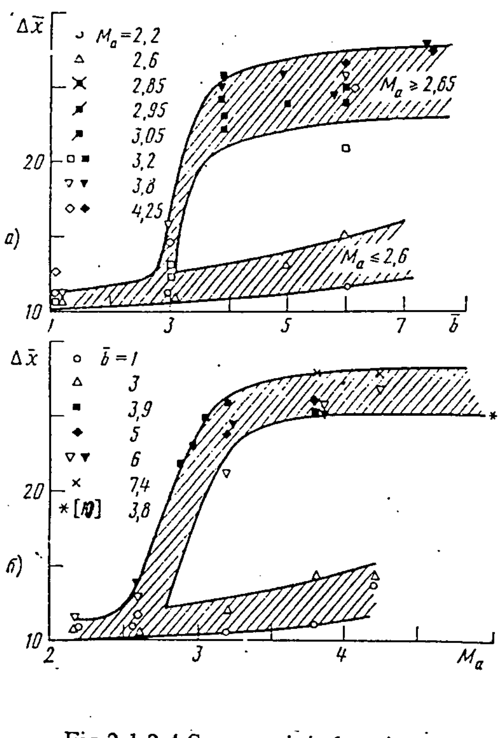

Fig.2.1.2.4 Supersonic/subsonic transition lengths versus Ma and b.

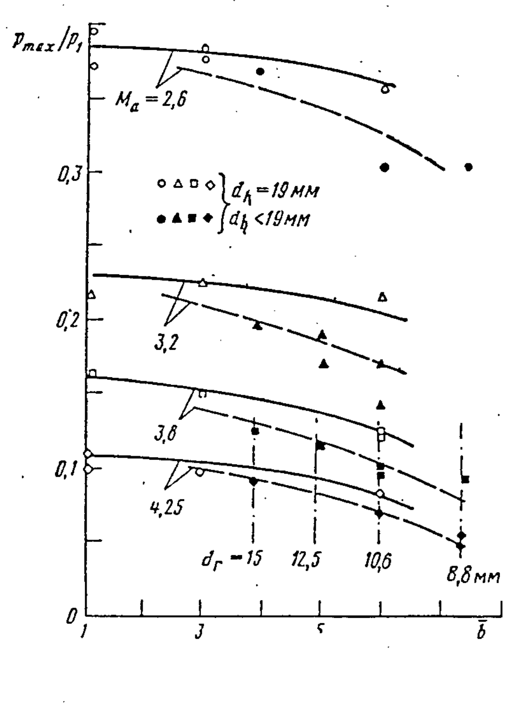

Fig.2.1.1.5 Pressure recovery versus b for different d_h.

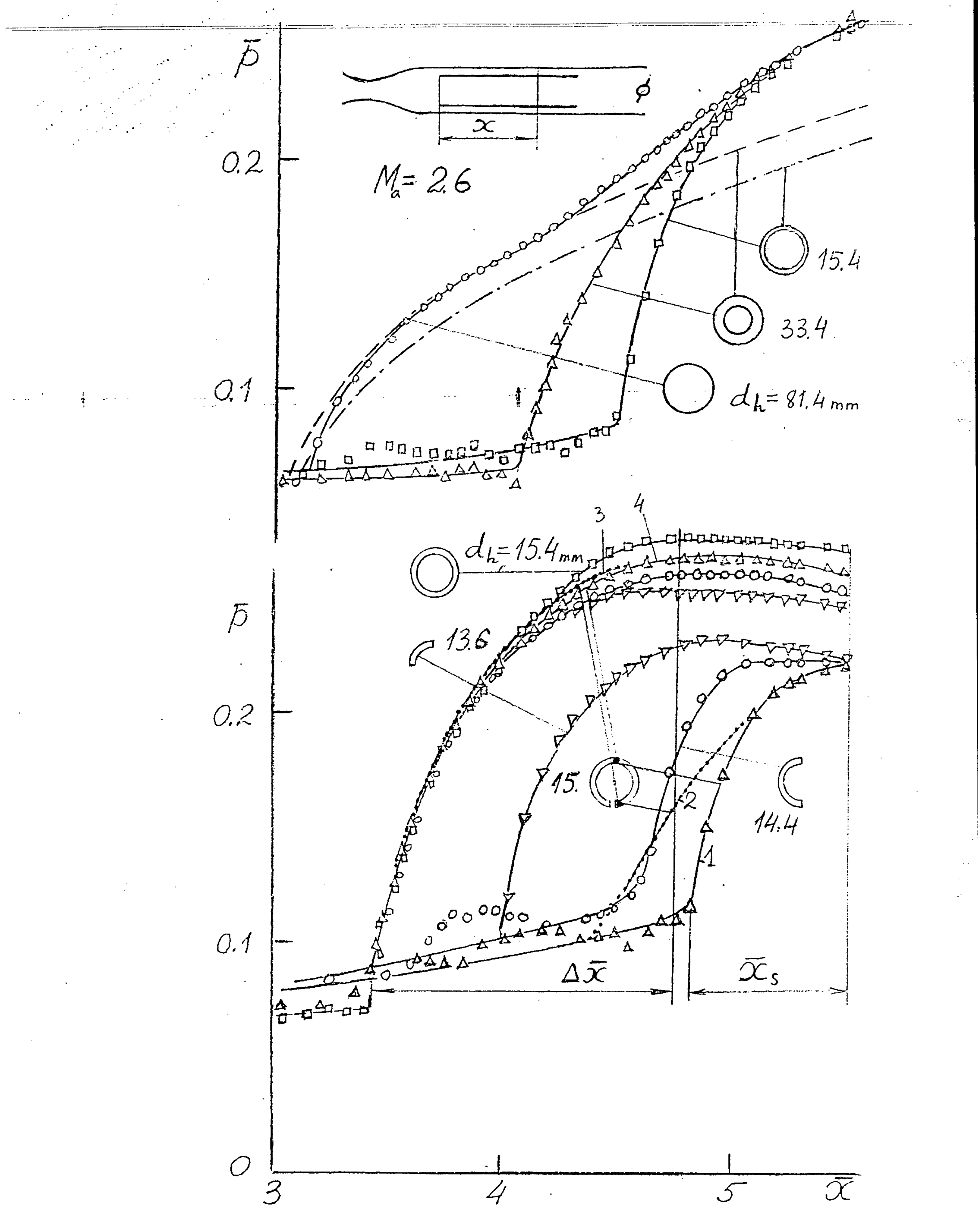

Fig.2.1.3.1 Pressure distribution along the ducts (annular and circular - a, annular sector - b)

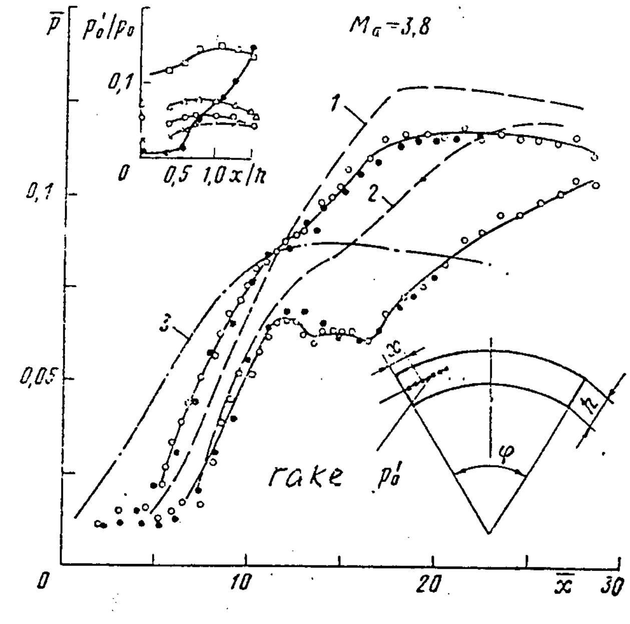

Fig.2.1.3.2 Free-stream tests of annular sector ducts.

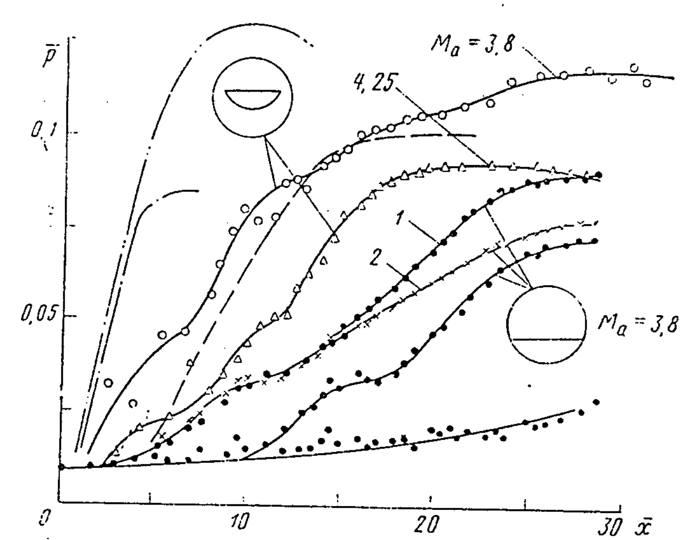

Fig.2.1.3.3 Pressure distribution along segmental duct (free stream and direct-connect tests)

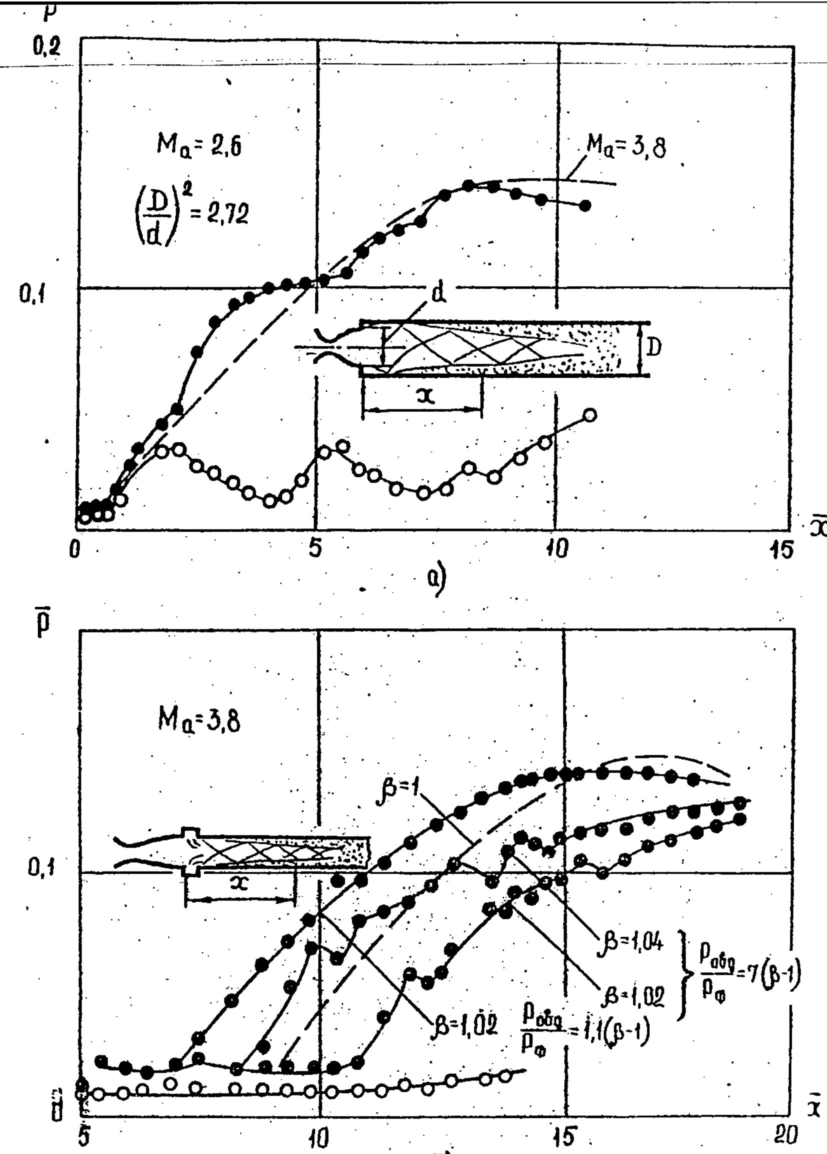

Fig.2.1.4.1 Pseudo-shock in non-uniform flow produced by step and jet injection

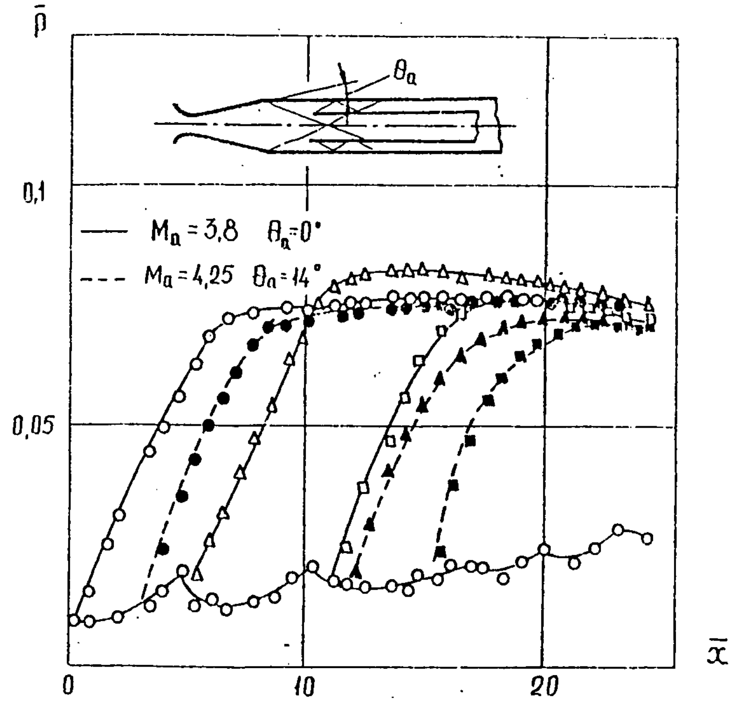

Fig.2.1.4.2 Pseudo-shock in non-uniform flow produced by conical nozzle.

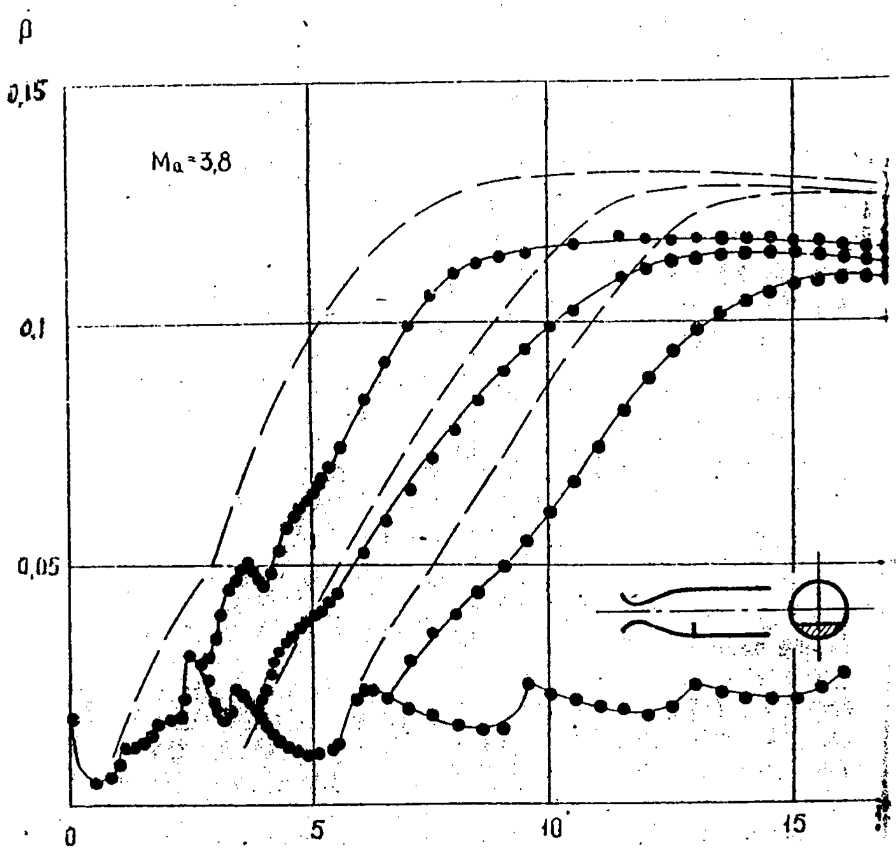

Fig.2.1.4.3 Pseudo-shock in non-uniform flow produced by segmental partition.

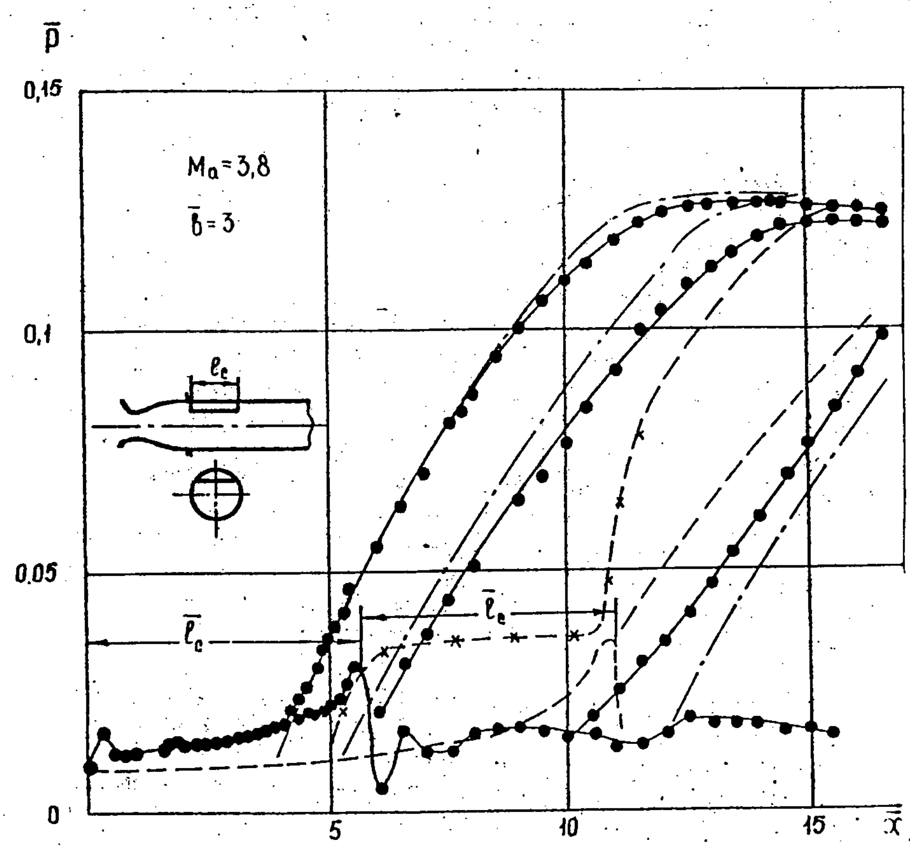

Fig.2.1.4.4 Pseudo-shock in non-uniform flow produced by segmental section.

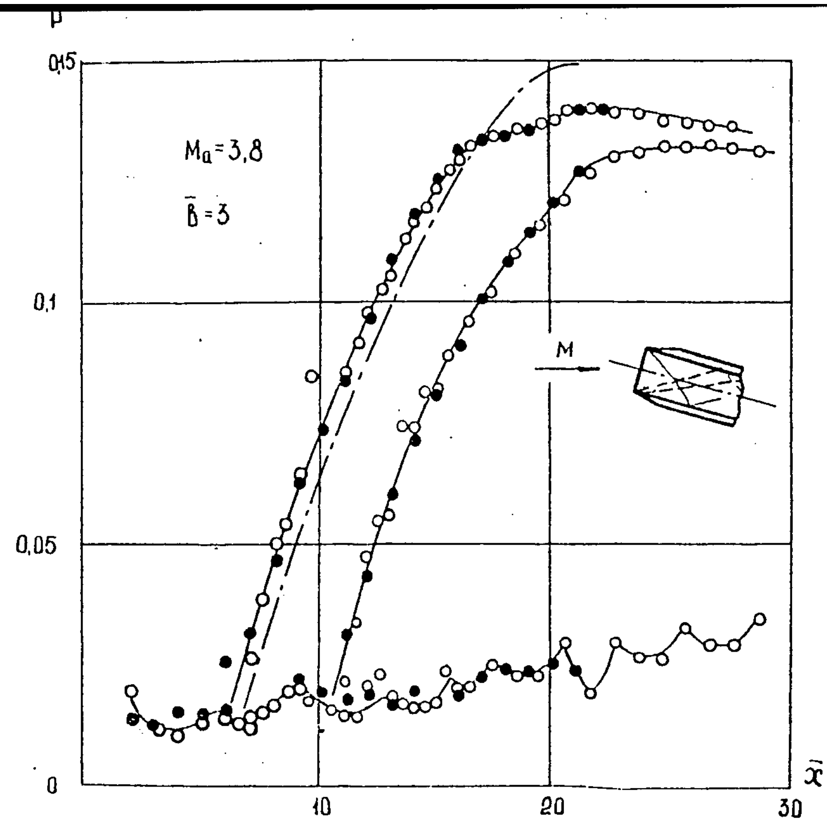

Fig.2.1.4.5 Pseudo-shock in rectangular duct.
2.5 deg. angle of attack.

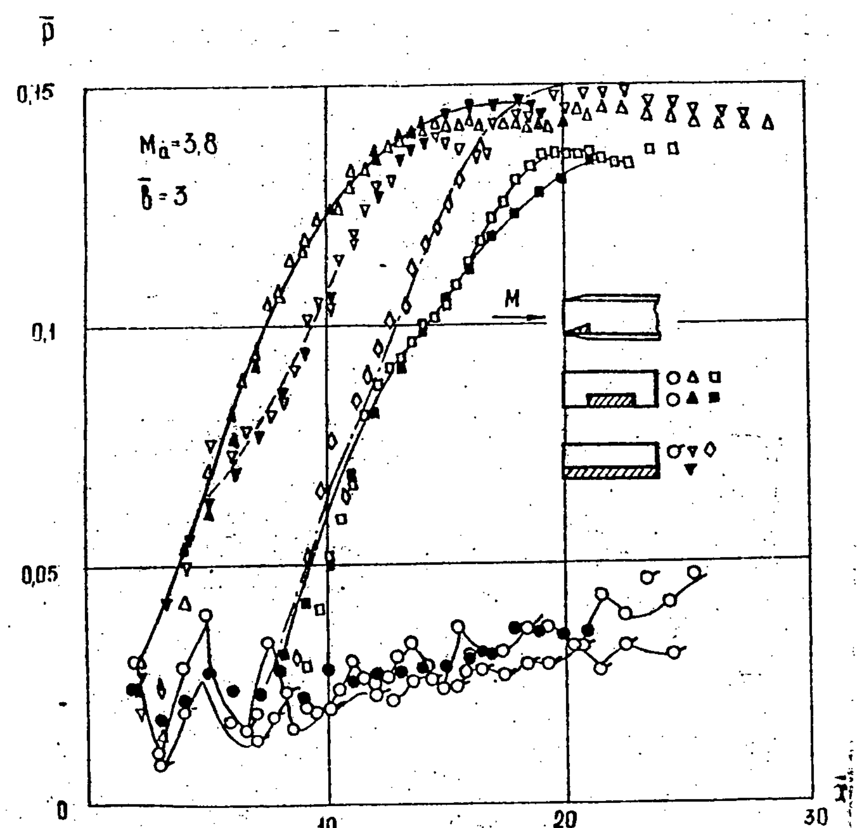

Fig.2.1.4.6 Pseudo-shock in rectangular duct, b = 3, with wedges installed on the walls.

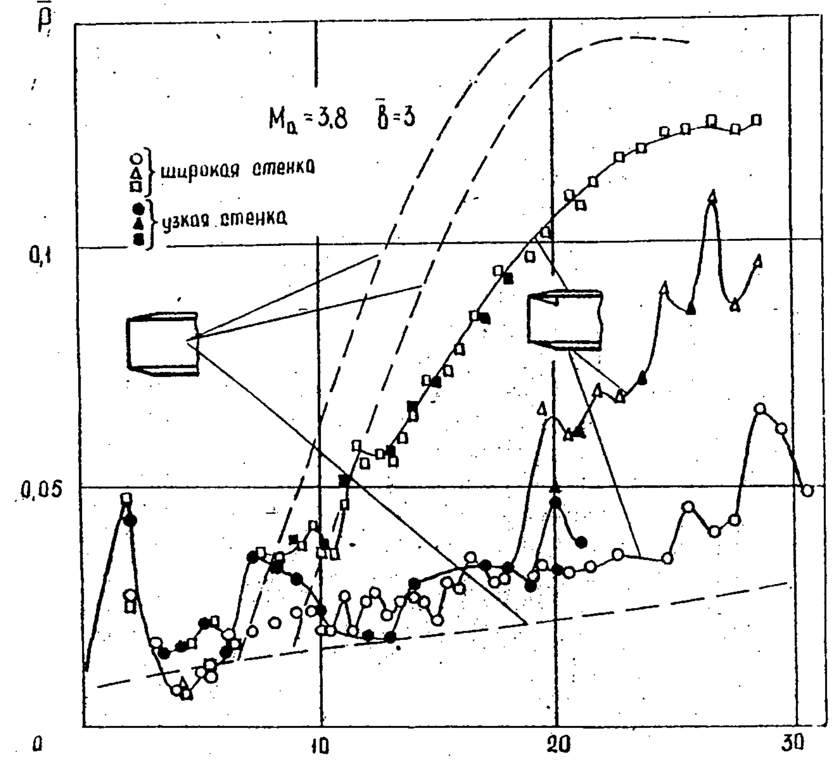

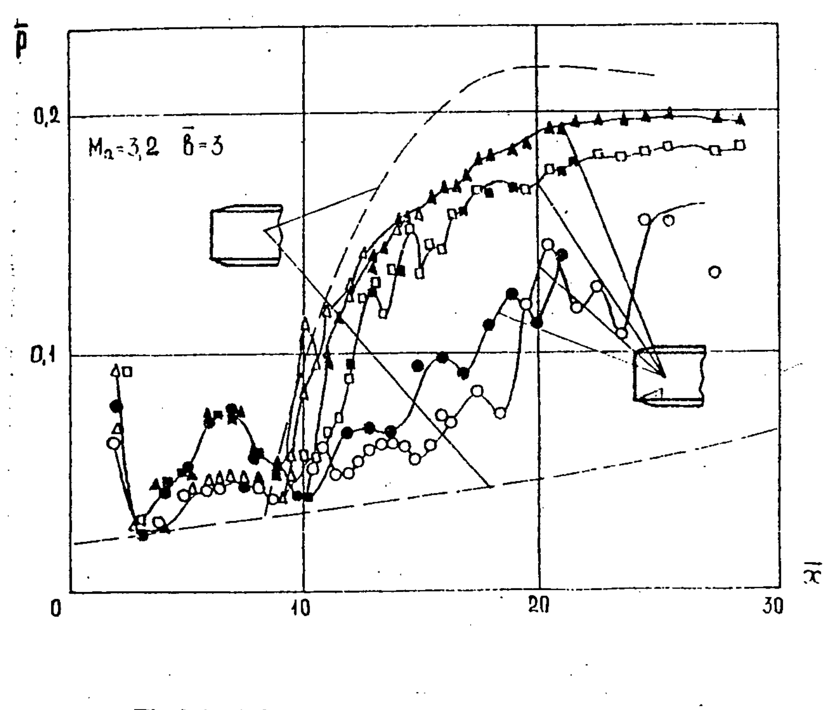

Fig.2.1.4.7 Separation flows in rectangular duct with wedges, ○, □-wide wall, ●,■-narrow wall.

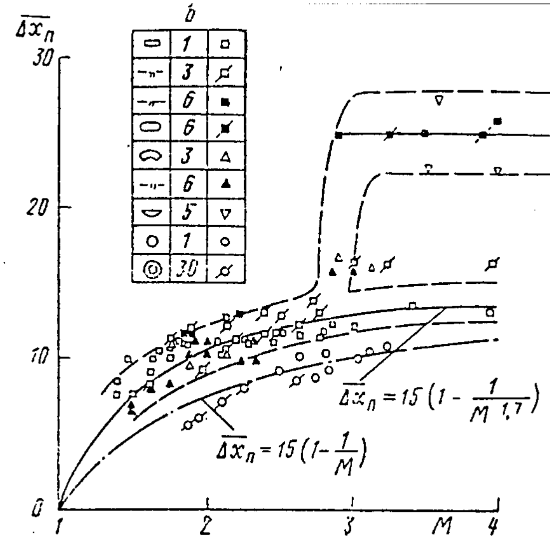

Fig.2.1.5.1 Supersonic/subsonic transition region lengths in ducts with oblong cross sections vs. Ma.

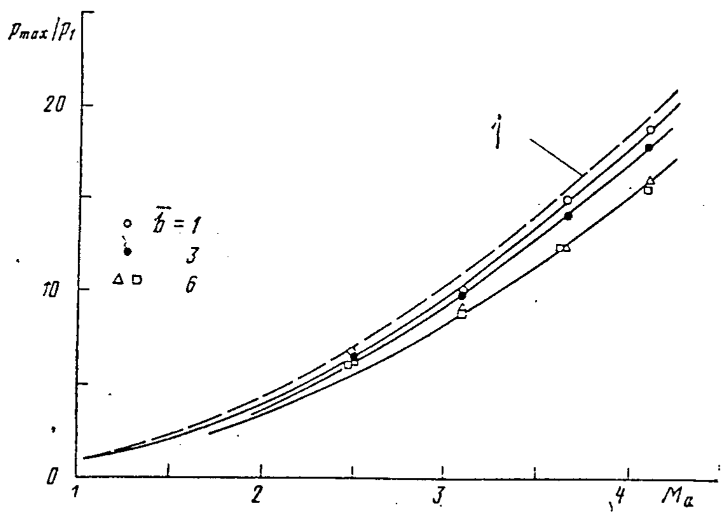

Fig.2.1.5.2 Pressure recovery in supersonic/subsonic flow transition in ducts with oblong cross sections vs. Ma
1-normal shock, ●,○ rectangular, □-sectoral ducts.

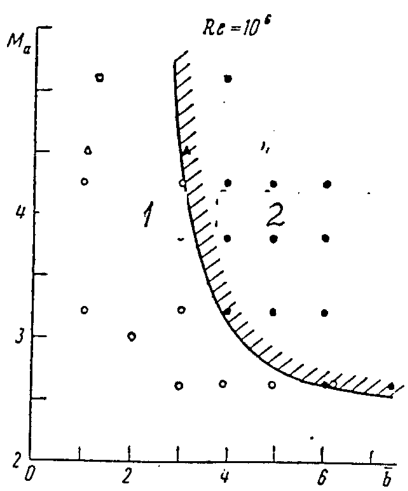

Fig.2.1.5.3 Boundary between pseudo-shock and non symmetric separation flow in ducts.
1-pseudo-shock, 2-separation flow

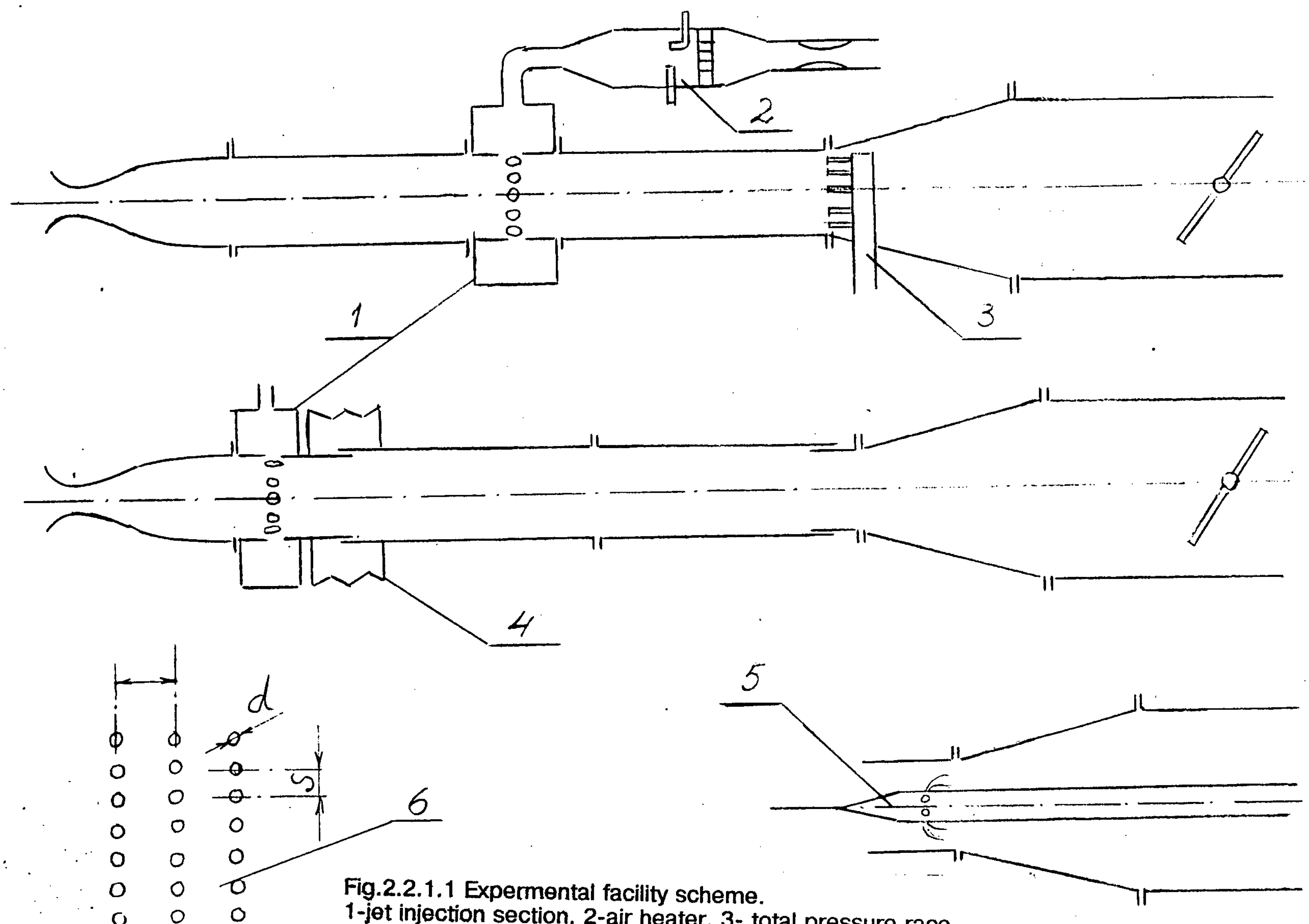

Fig.2.2.1.1 Expermental facility scheme.
1-jet injection section, 2-air heater, 3- total pressure race,
4-balances, 5-axial injector, 6-set of orifices.

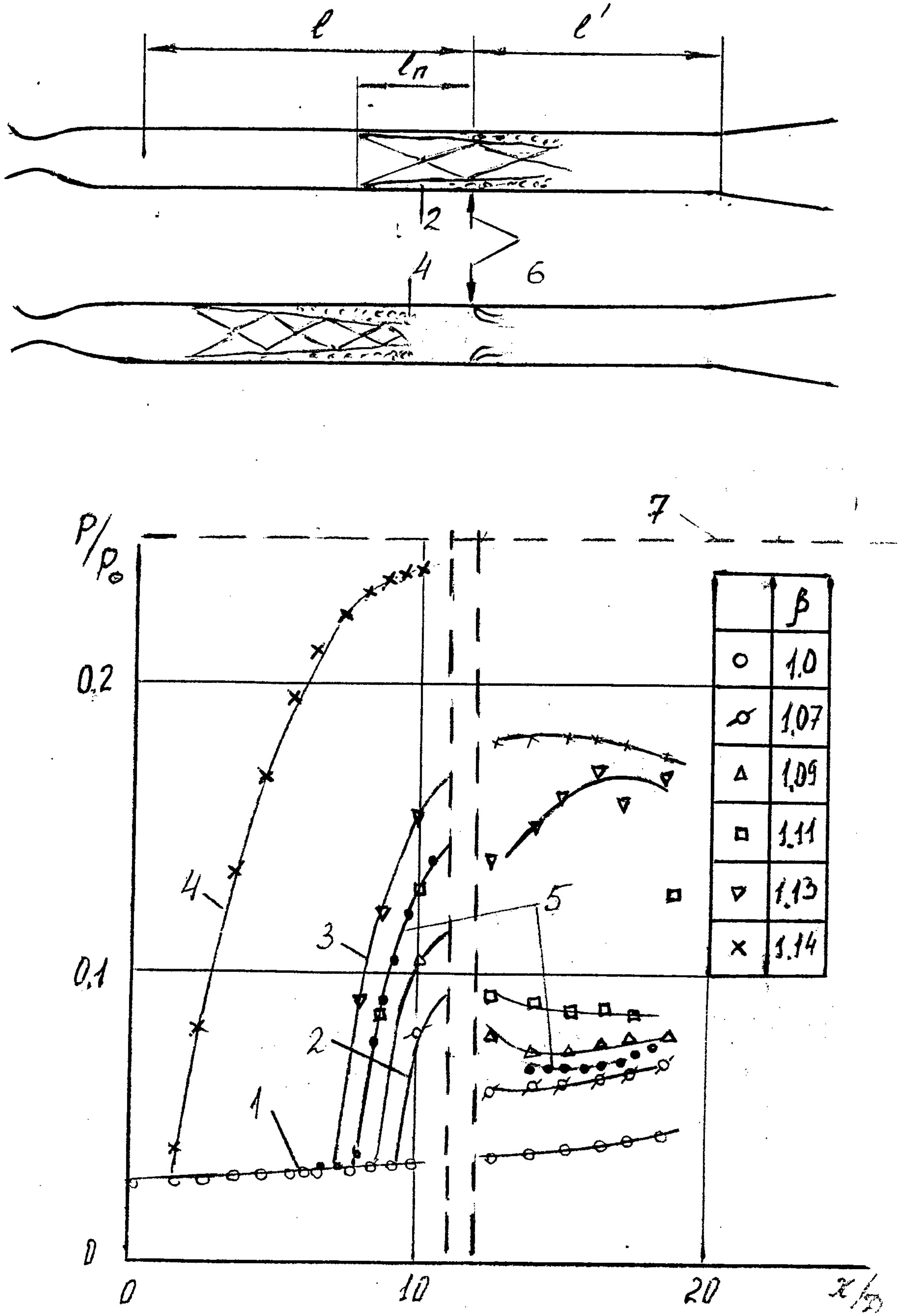

Fig.2.2.1.2 Prewssure distribution along the tube at different jet injections.
1-supersonic flow, 2,3-pseudo-shock rise, 4-developed pseudo-shock, 5-pressure distribution up and downstream of annular jut, h = 4.2 mm, 6-jet injection section, 7-pressure downstream of normal shock, M = 2.8.

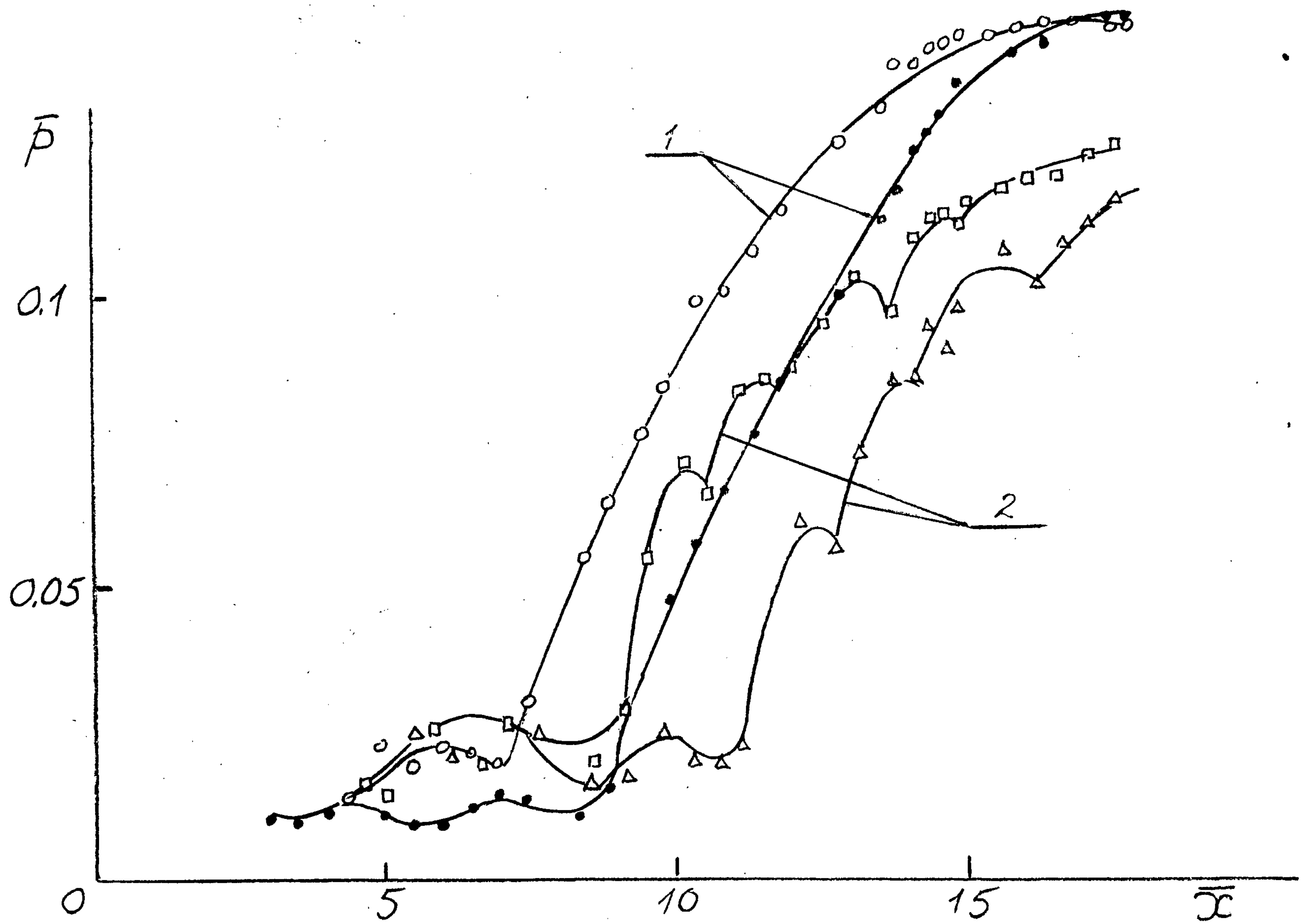

Fig.2.2.1.3 Pressure distribution along the tube, L = 23.6, Ma = 3.08 at high and low jet injection pressure, -low pressure, 2-high pressure

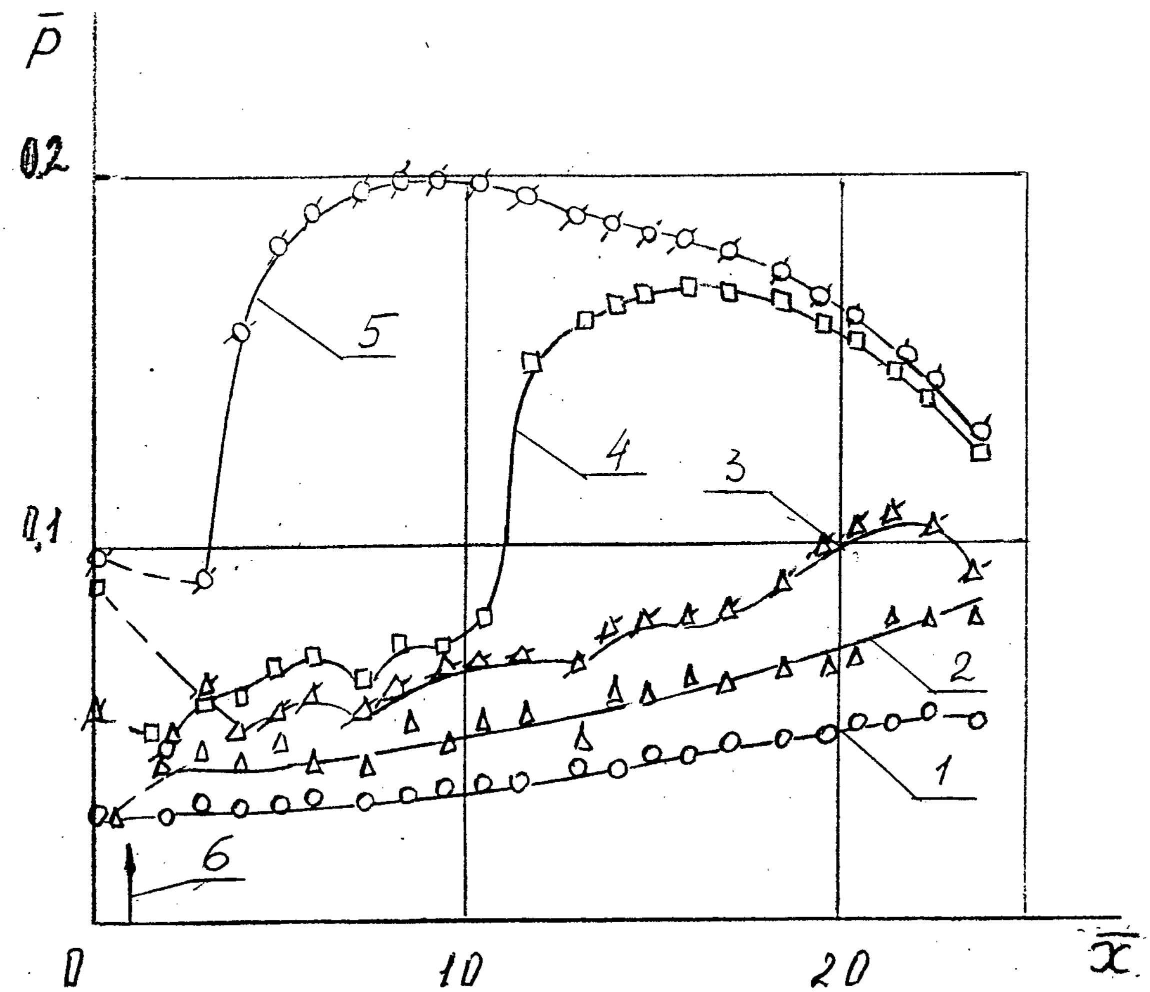

Fig.2.2.1.4 Pressure distribution at different front jet injections.
1- β = 1.0, 2-1.054, 3-1.086, 4-1.112, 5-1.132, 6-injection section
Ma = 3.08, L = 23.6

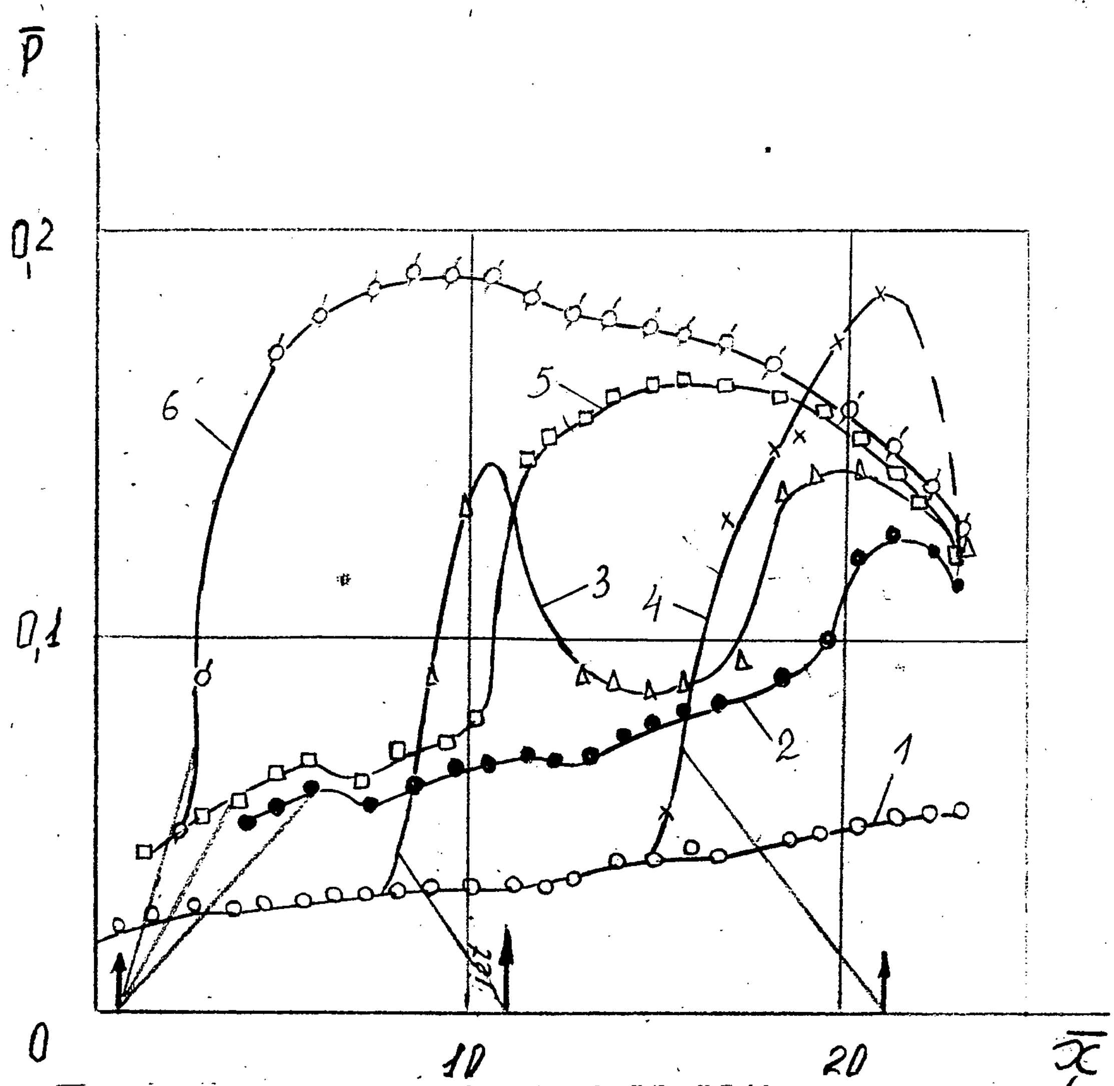

Fig.2.2.1.5 Pressure distribution at different middle jet injection.
1- β = 1.0; 2-1.09, l = 0.5; 3-1.11, 11.5; 4-1.13, 22.5; 6-1.13, 0.5
Ma = 3.08, L = 23.6

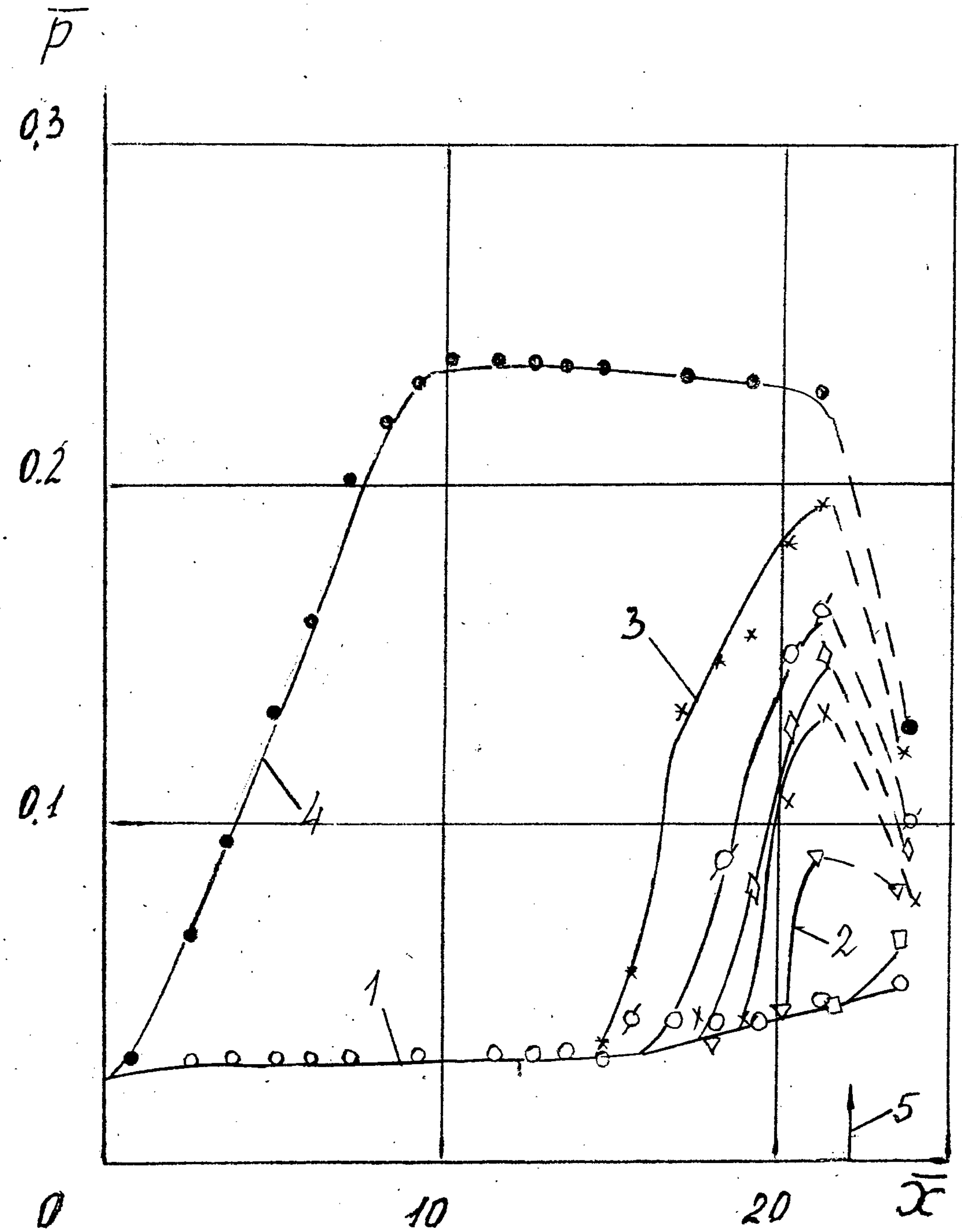

Fig.2.2.1.6 Pressure distribution at different back jet injection.
1- β = 1.0, 2-1.055, 3-1.078, 4-1.159, 5-injection section.
Ma = 3.08, L = 23.6

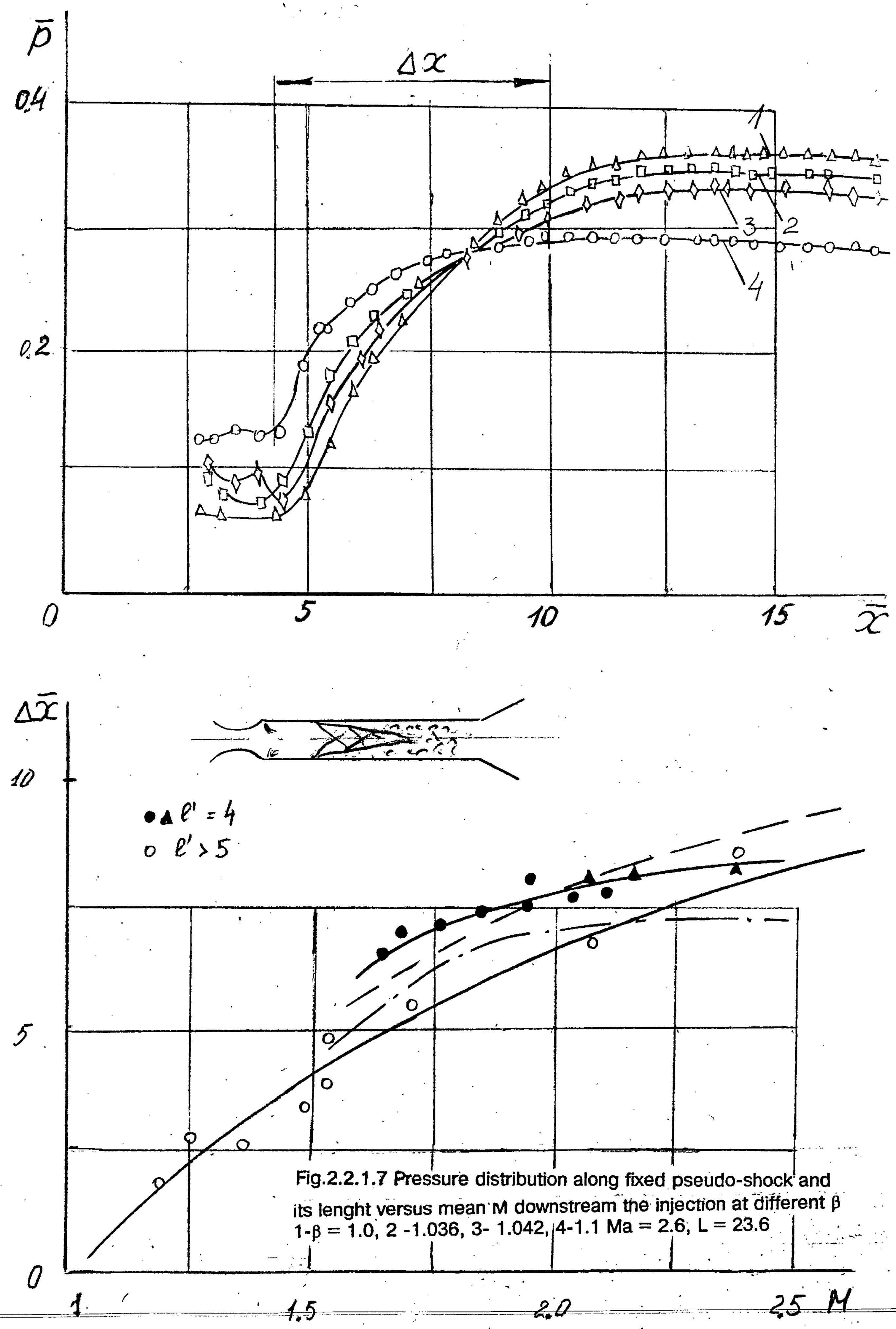

Fig.2.2.1.7 Pressure distribution along fixed pseudo-shock and its lenght versus mean M downstream the injection at different β 1-β = 1.0, 2 -1.036, 3- 1.042, 4-1.1 Ma = 2.6, L = 23.6

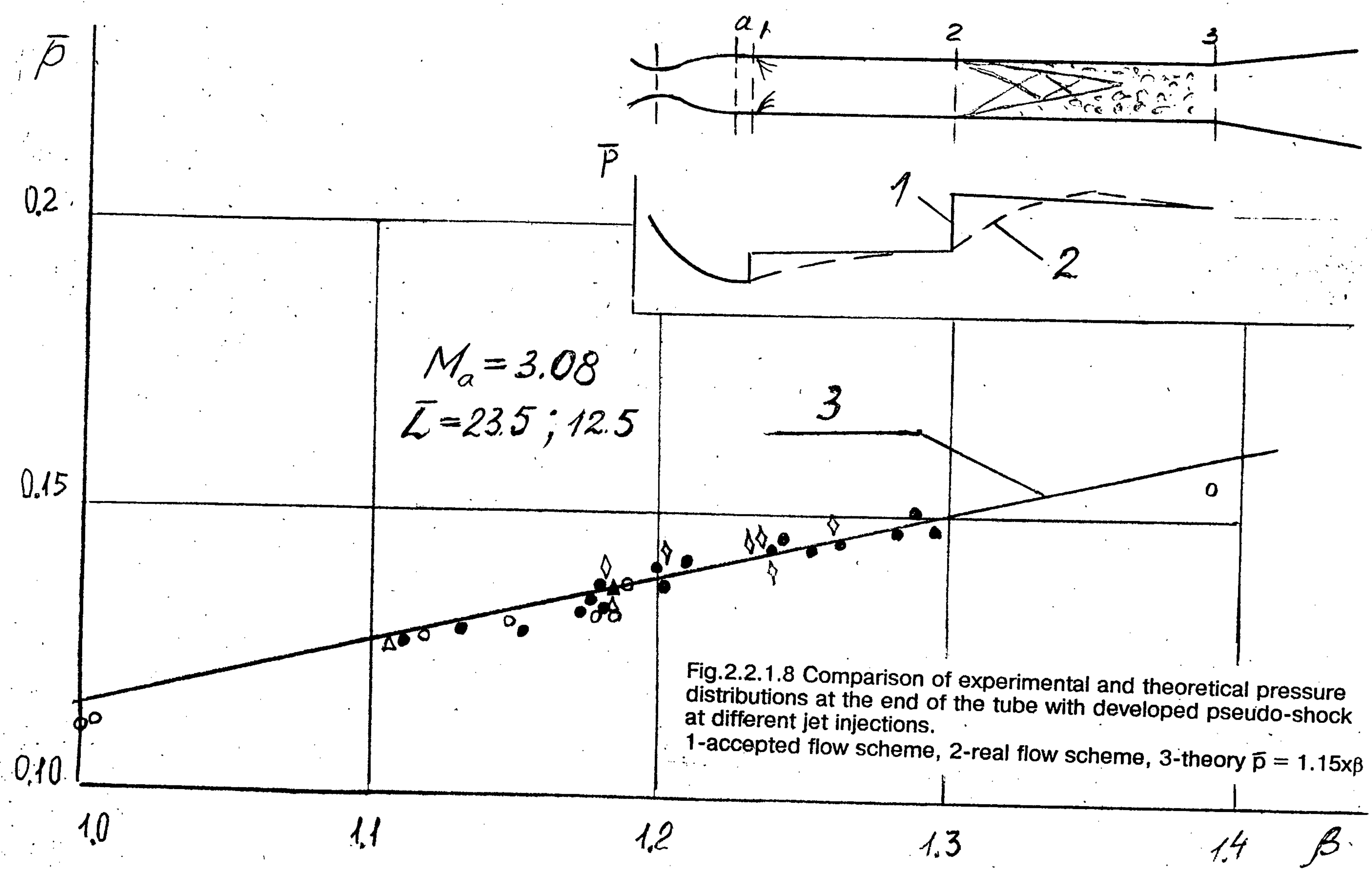

Fig.2.2.1.8 Comparison of experimental and theoretical pressure distributions at the end of the tube with developed pseudo-shock at different jet injections.
1-accepted flow scheme, 2-real flow scheme, 3-theory $\bar{p} = 1.15 \times \beta$

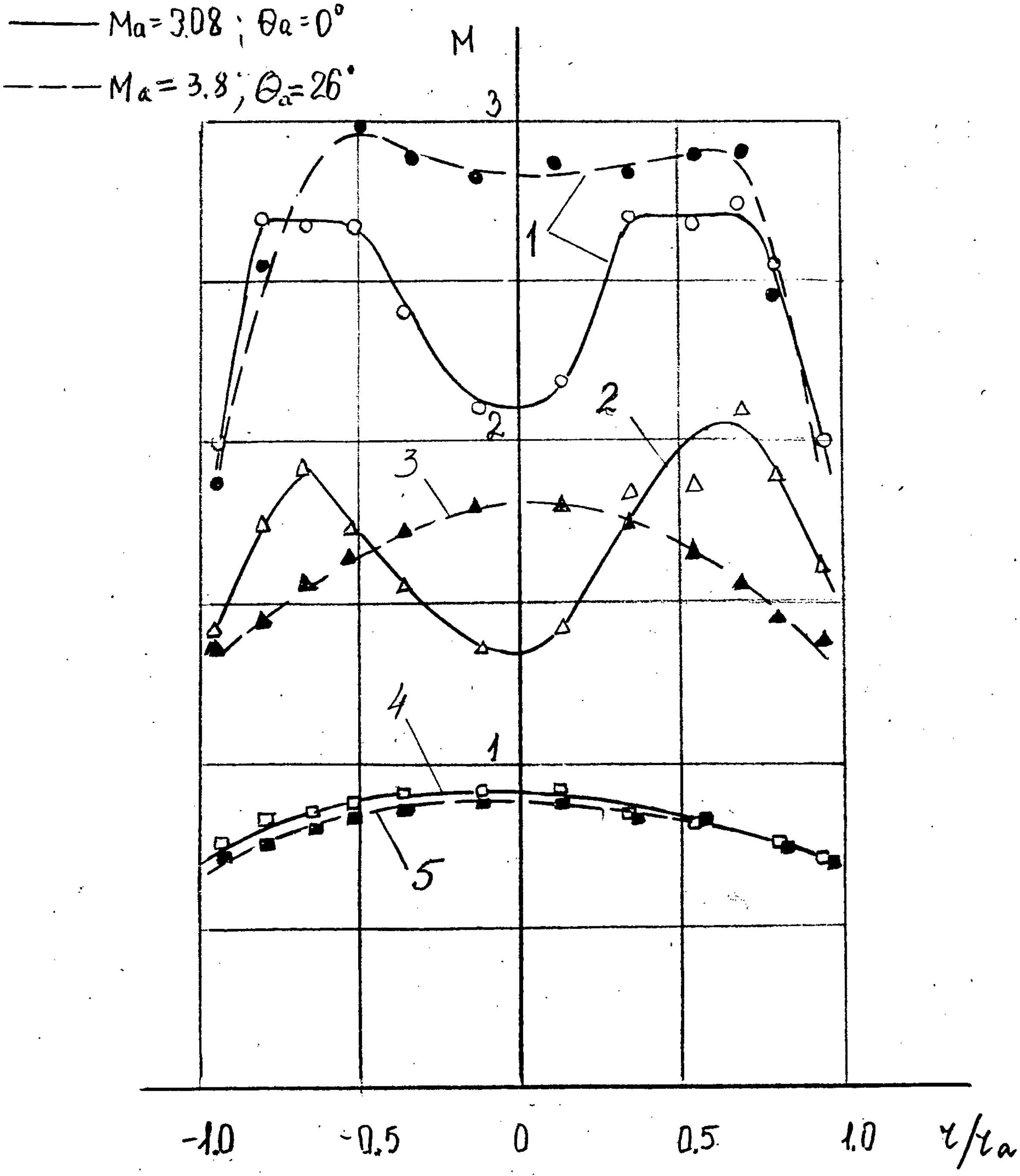

Fig.2.2.1.9 M-fields at the end of the tube, l = 7 for two two nozzles-
Ma = 3.08, θa = 0, Ma =3.8, θa = 26 deg.. 1-β=1, 2-1.09, 3-1.14, 4-1.26, 5-1.24

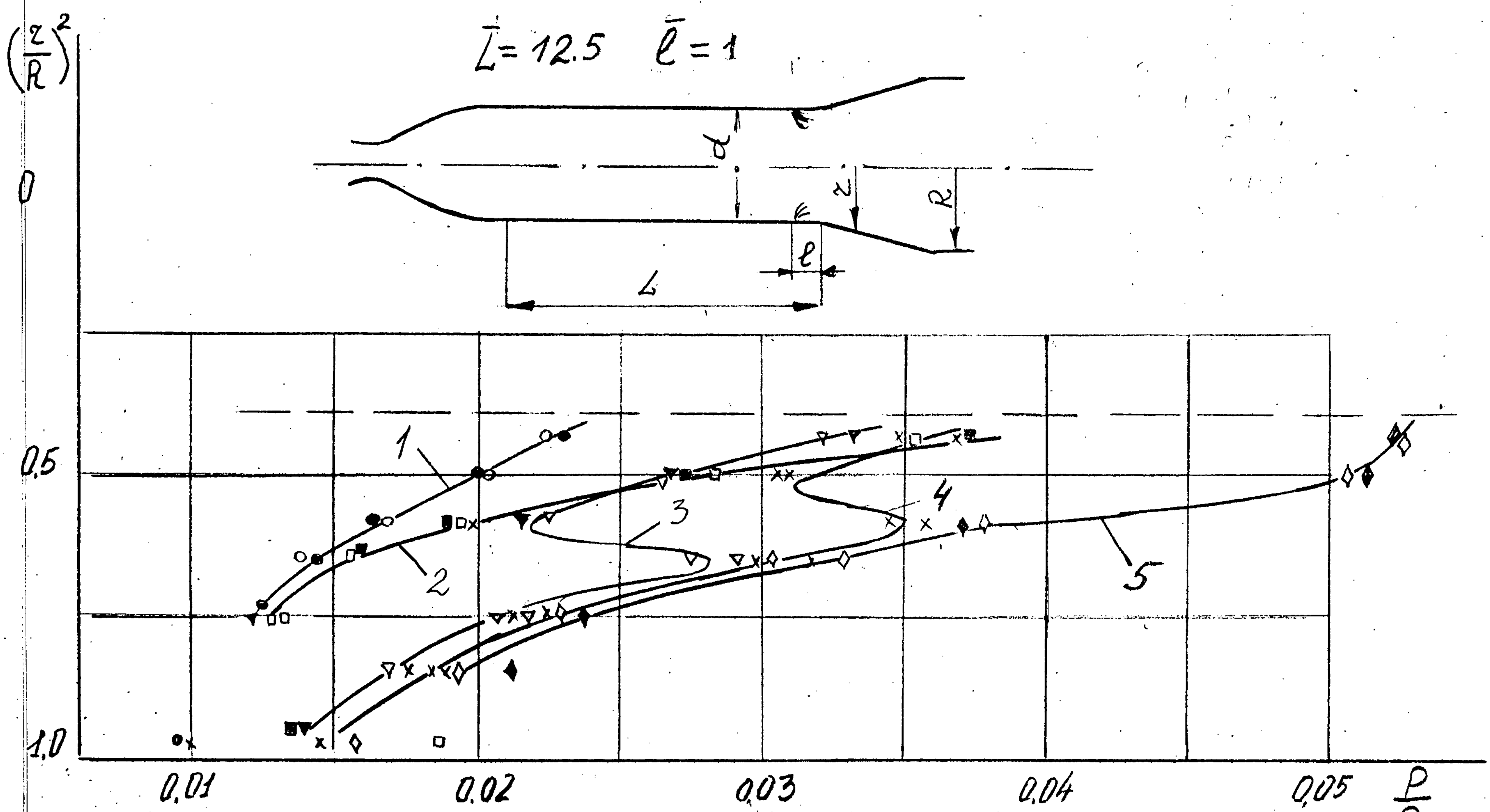

Fig.2.2.1.10 Pressure distribution along the conical section of the duct at different jet injections. L=12.5, l=1, Ma=3.08, 1-β=1.0, 2=1.034, 3-1.061, 4-1.089, 5-1.139

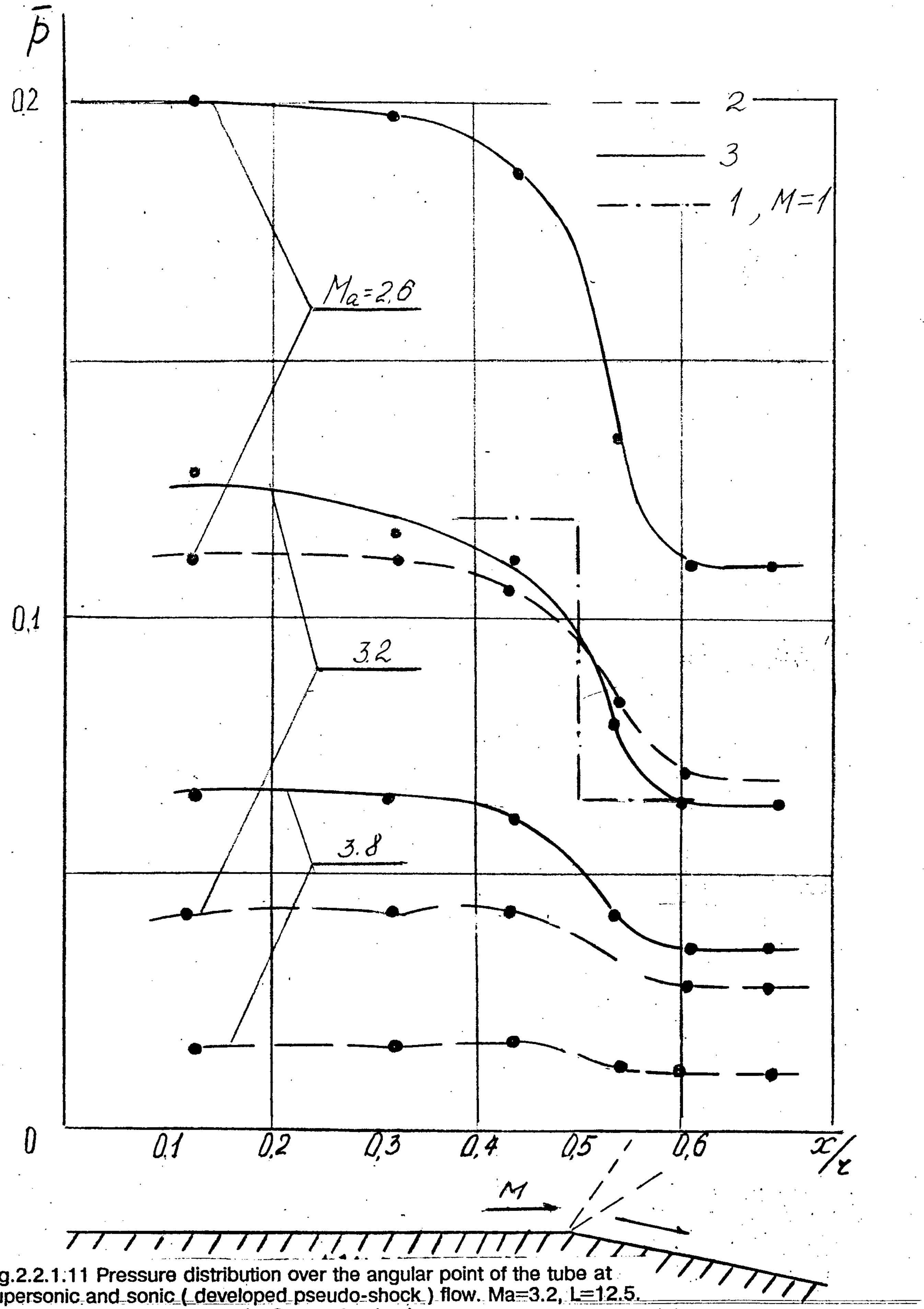

Fig.2.2.1.11 Pressure distribution over the angular point of the tube at supersonic and sonic (developed pseudo-shock) flow. Ma=3.2, L=12.5.
1-Prandtl-Mayer, 2-supersonic, 3-pseudo-shock

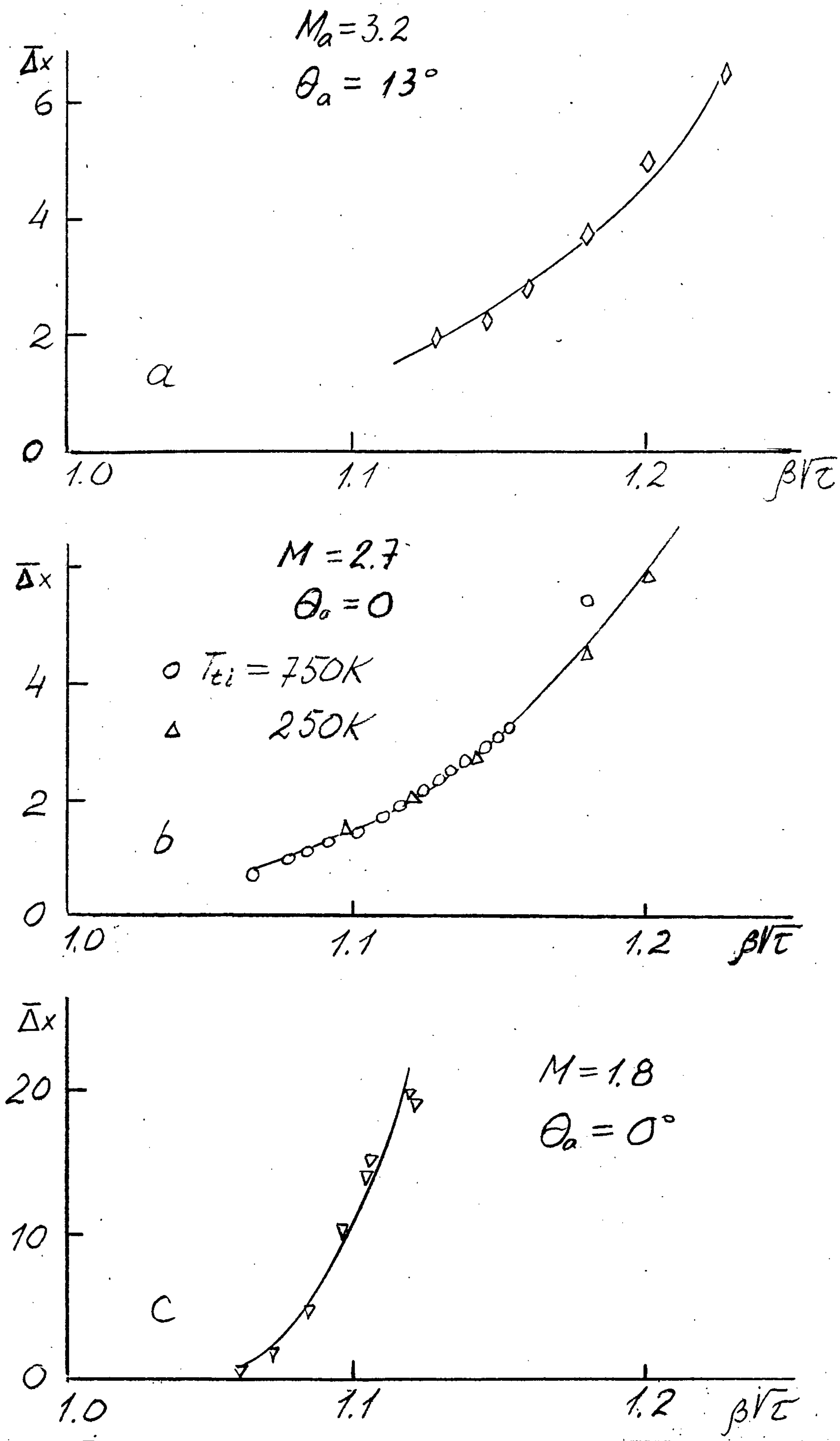

Fig.2.2.1.12 Distance of upstrem influence versus $\beta\sqrt{t}$ at different M

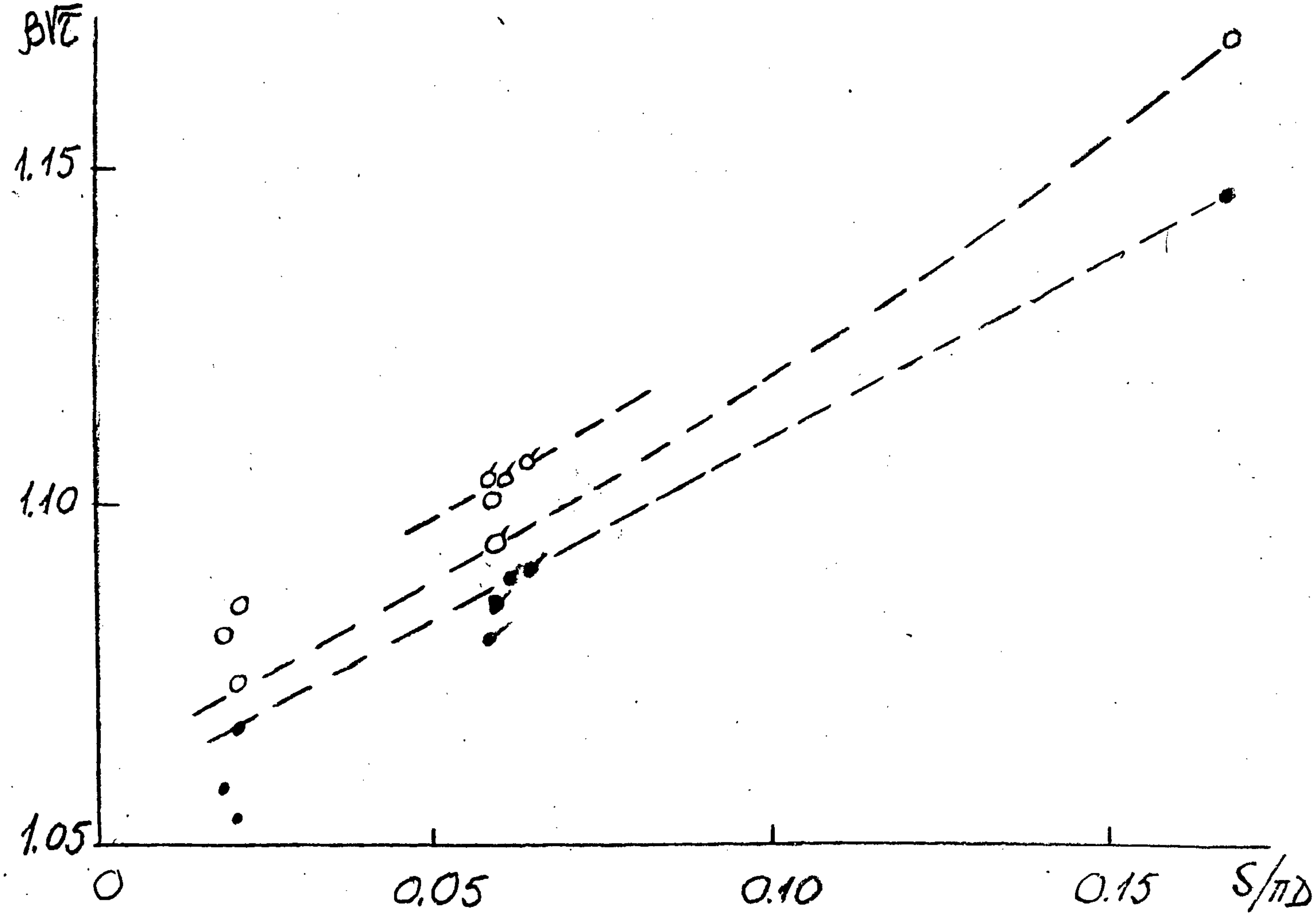

Fig.2.2.1.13 Limiting values of $\beta\sqrt{7}$ vs. $s/\pi D$

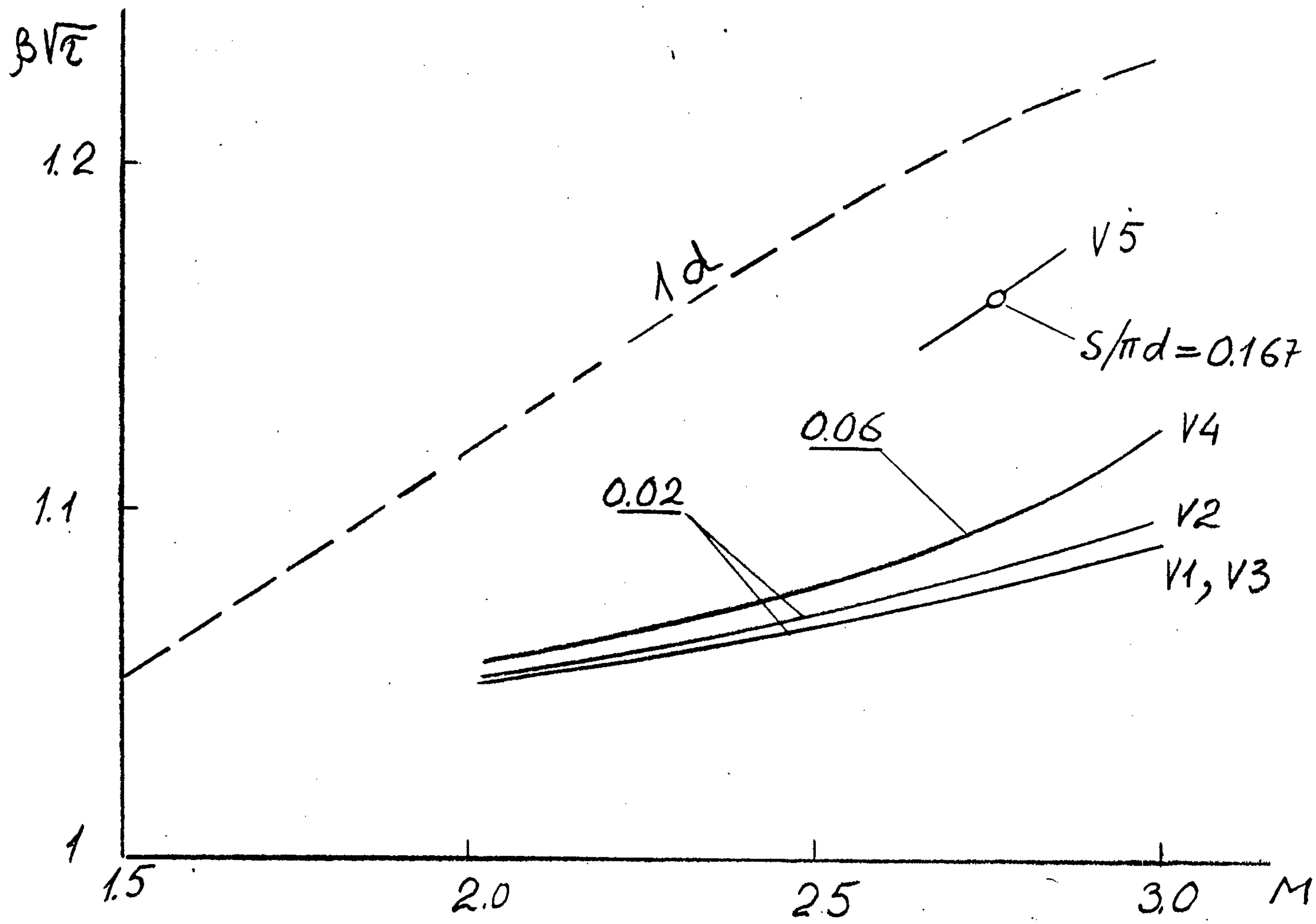

Fig.2.2.1.14 Dependence of limiting $\beta\sqrt{\tau}$ on M for different variants of orifice's disposition

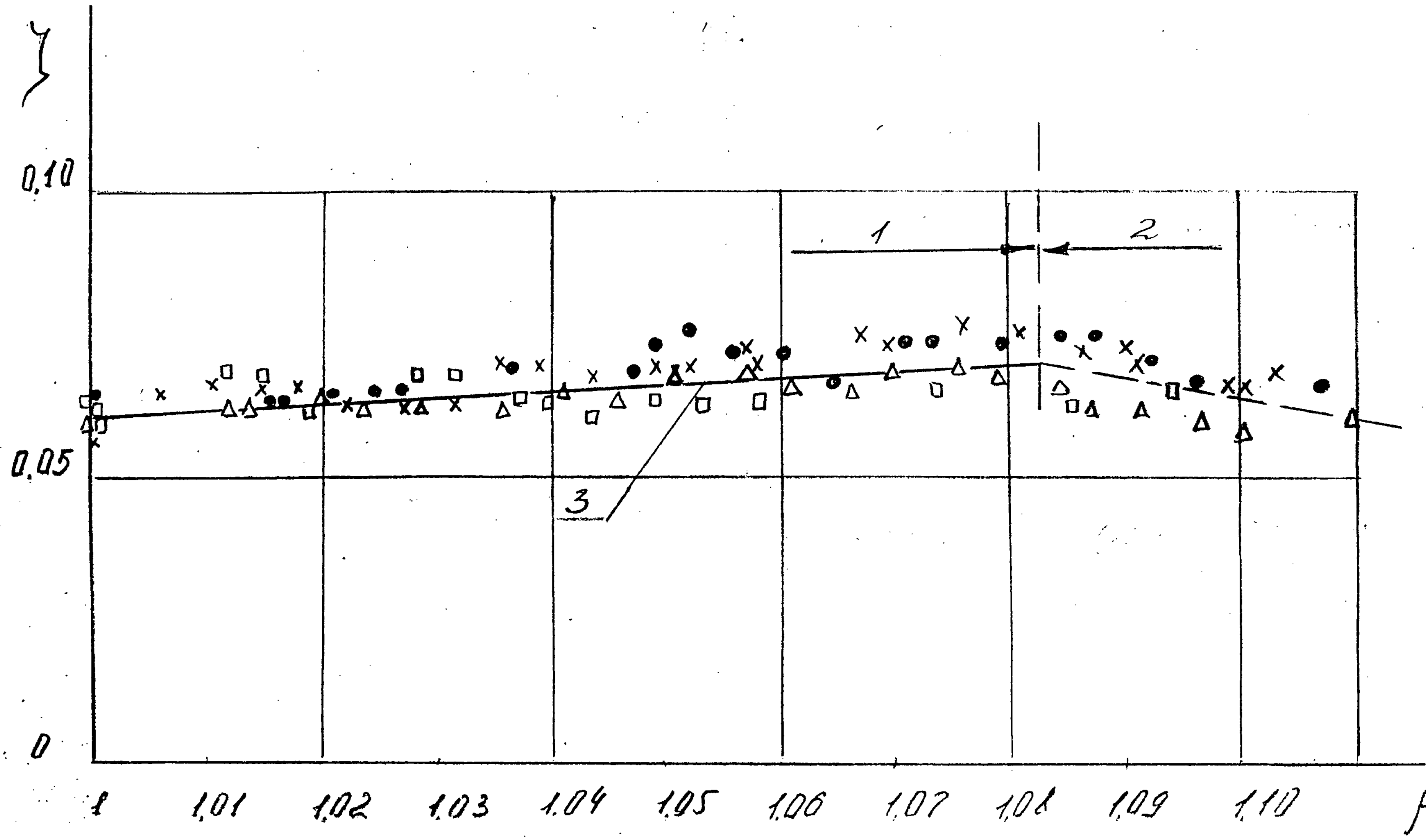

Fig.2.2.1.15 Friction force dependence on β. Ma=3.2, L=23.2, v1.
1-supersonic flow, 2-mixed flow, 3-calculation.

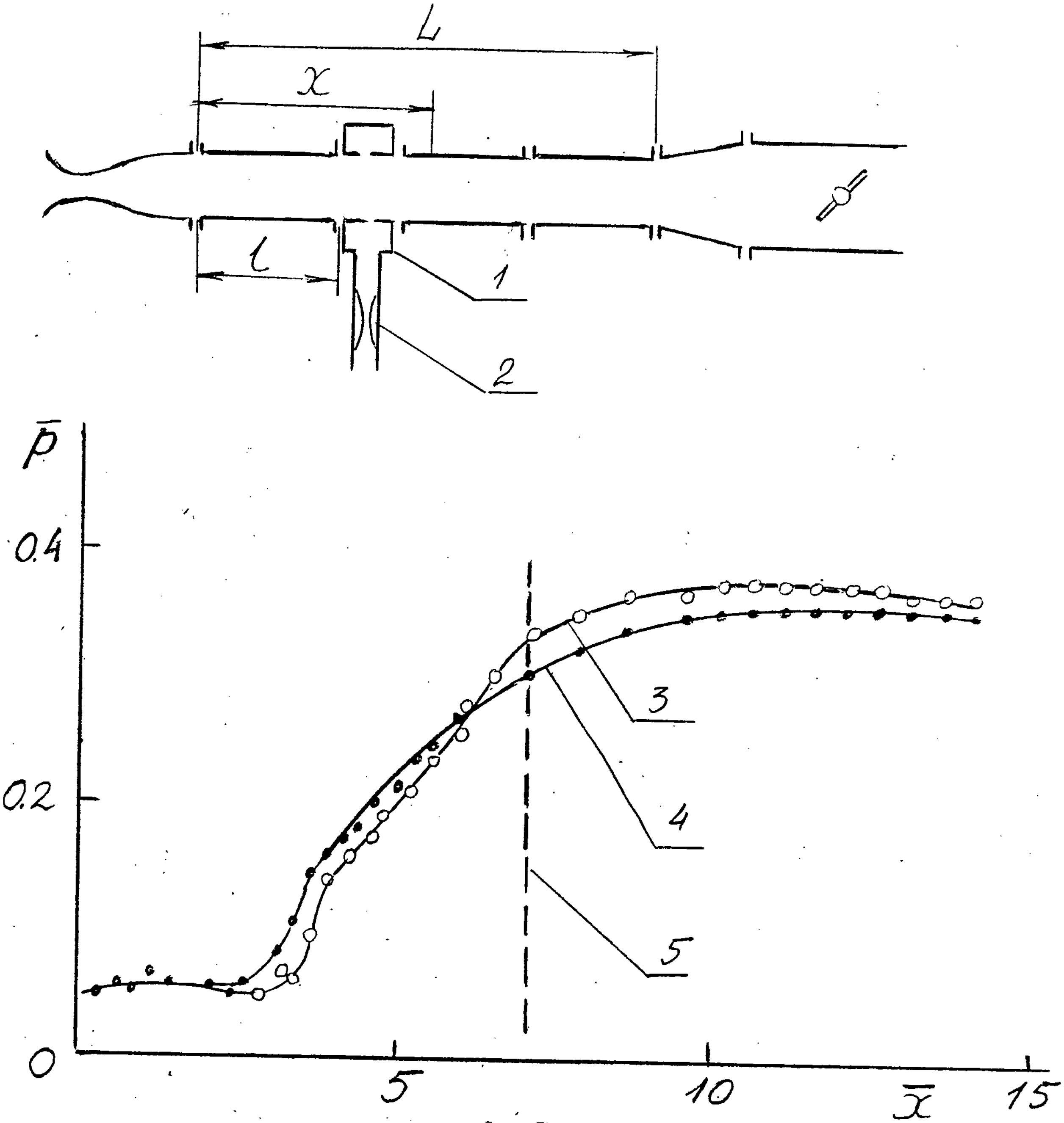

Fig.2.2.1.16 Comparison of pressure distribution along pseudo-shock with and no bleeding.
1-bleeding section, 2-rate meter, 3-no bleed, 4-bleed, 5-section of bleeding.

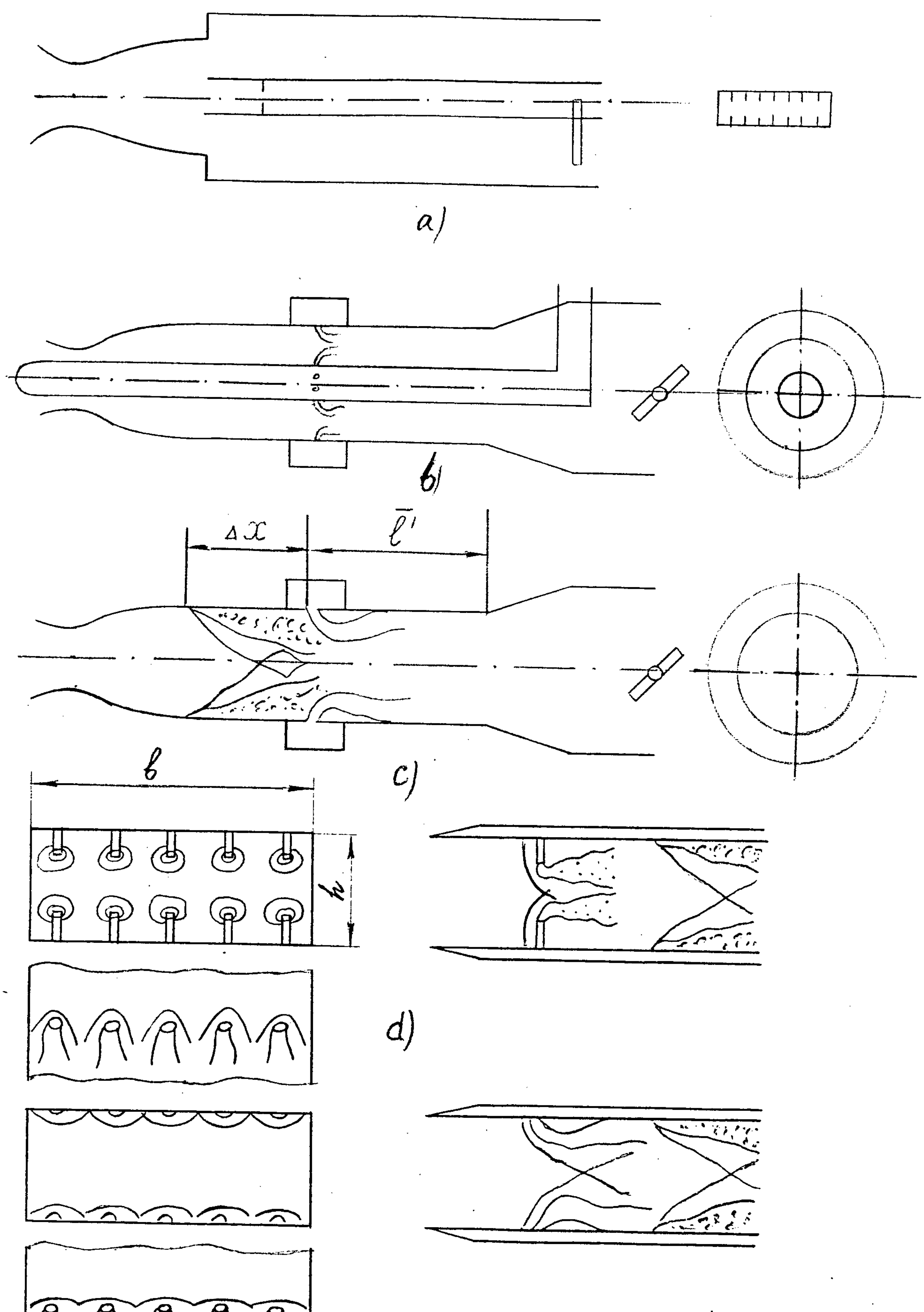

Fig. 2.2.2.1 Experimental facility scheme.

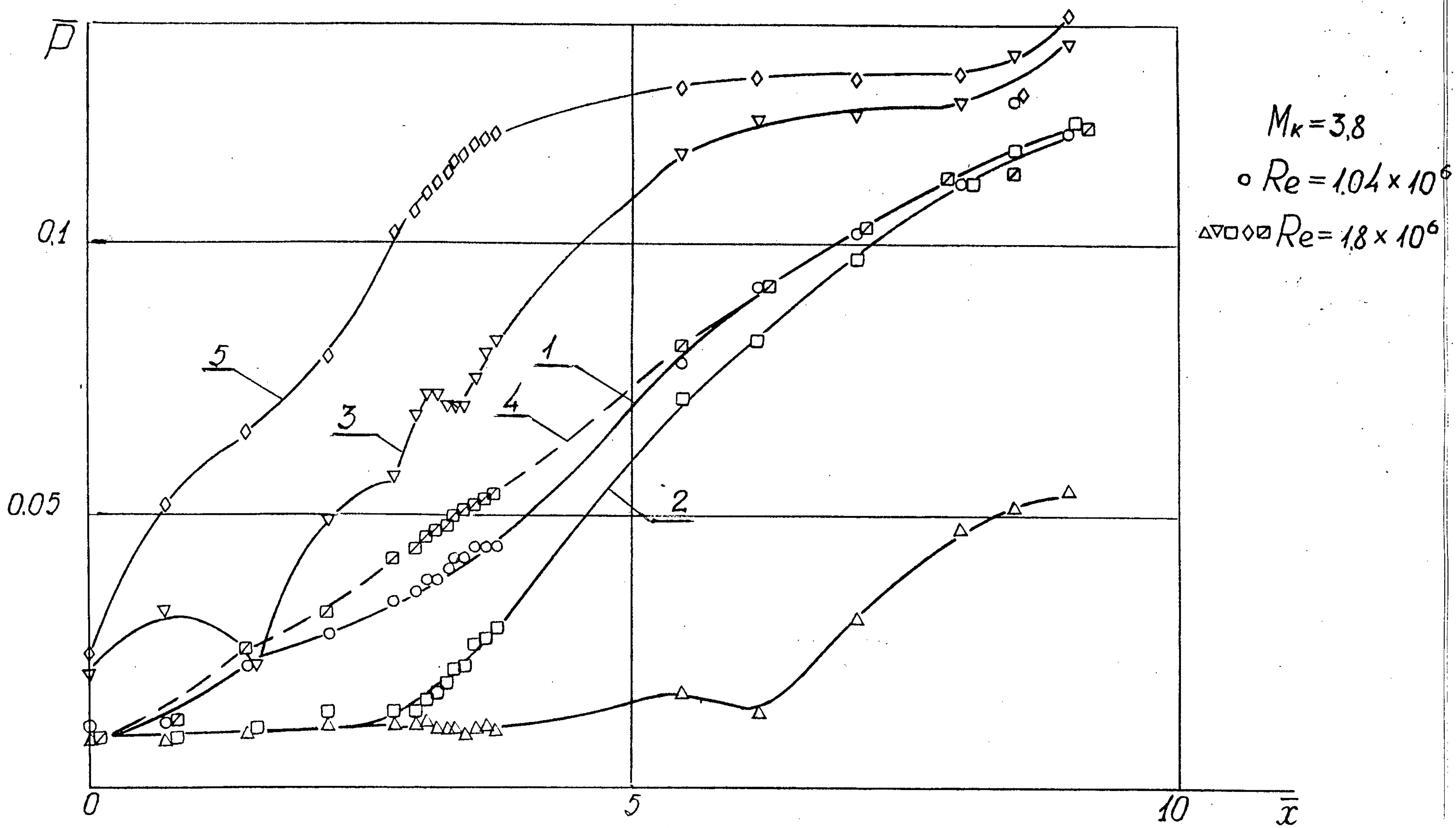

Fig. 2.2.2.2 Pessure distribution along the annular duct.
Ma=3.8, different Re, no injection. 1-5-numbers of regime

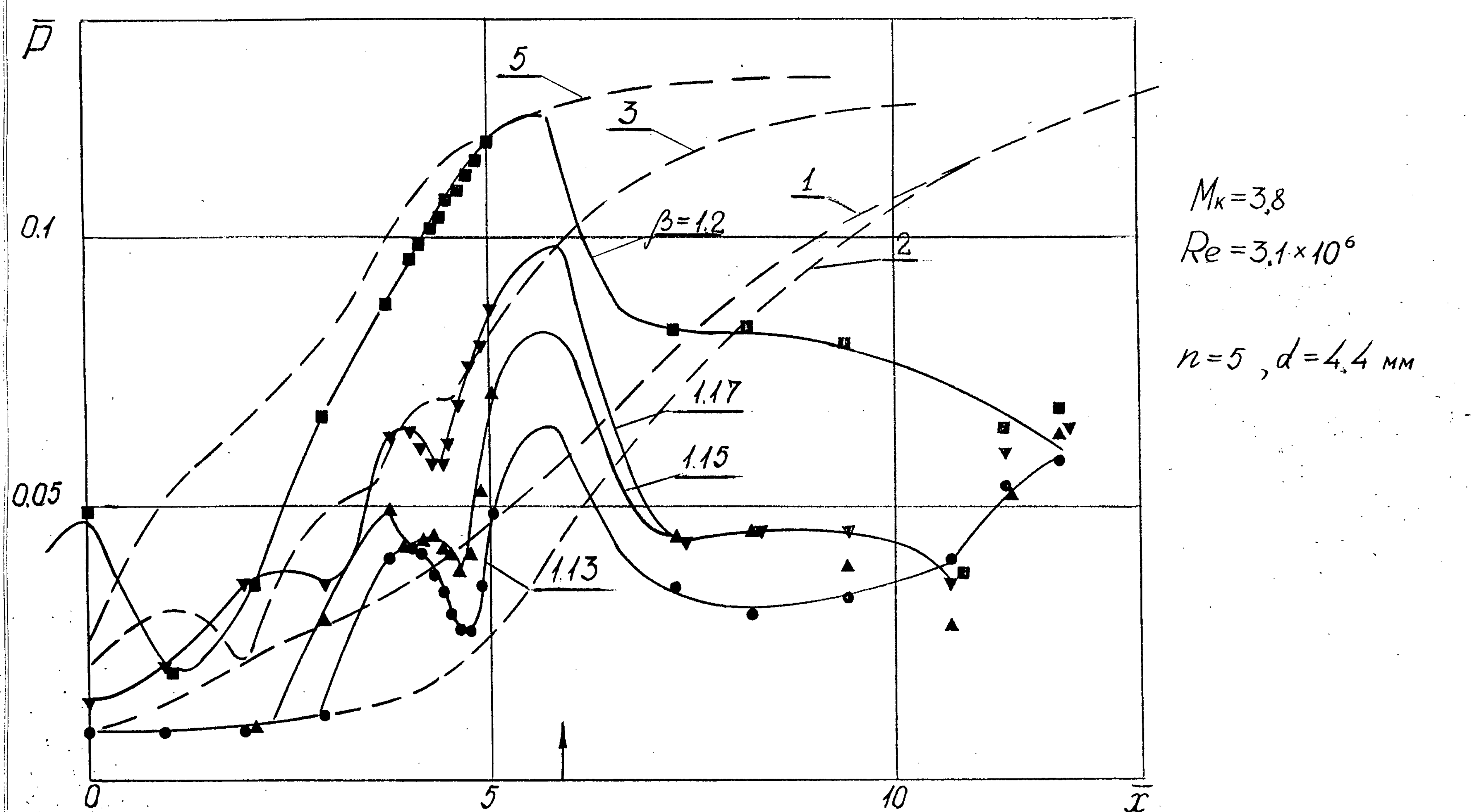

Fig. 2.2.2.3 Pessure distribution along the annular duct.
Ma=3.8, Re= 3x10⁹, jet injection from two walls.
1,3,5-numbers of regimes,----throttling, —-injection

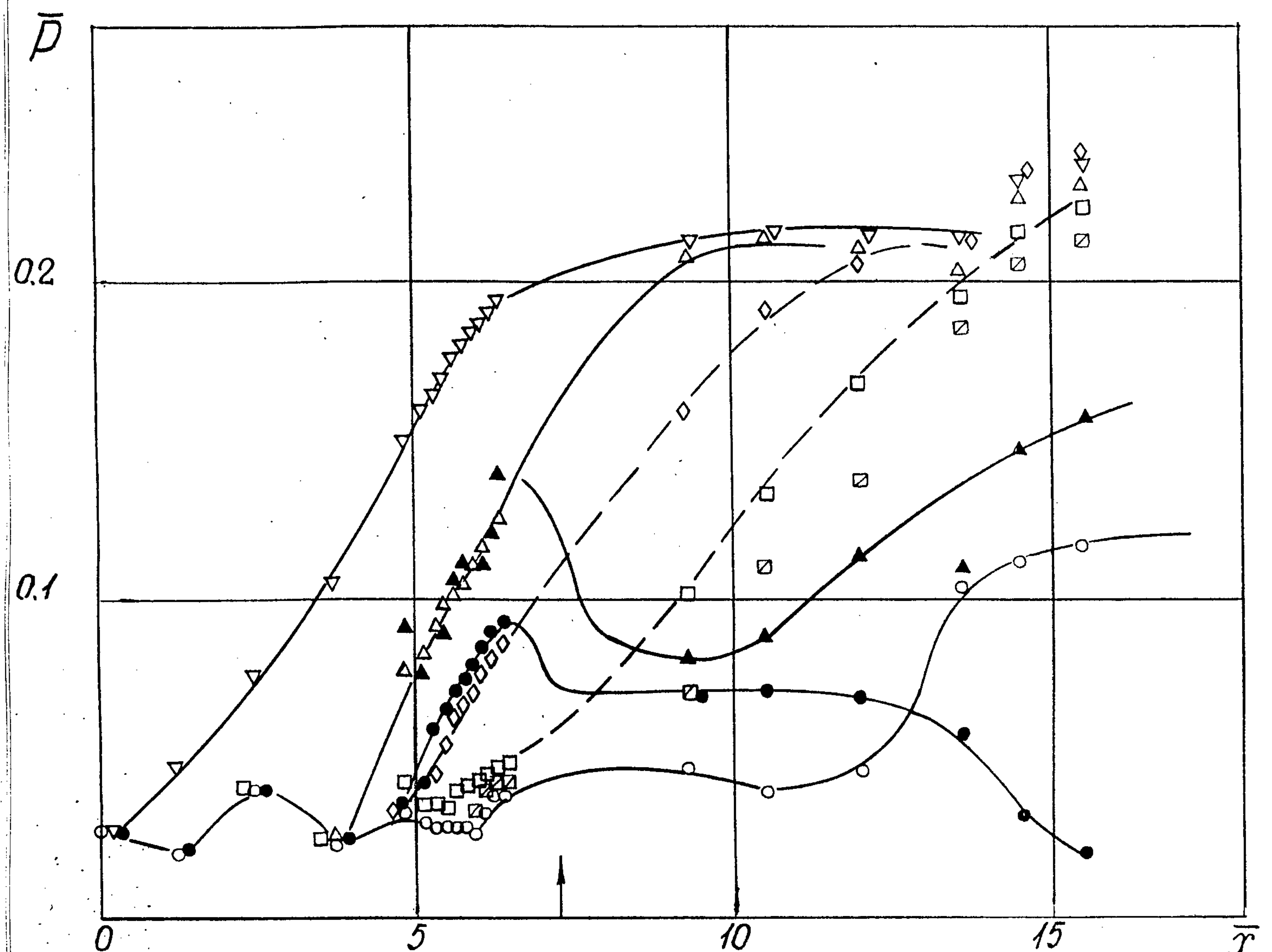

Fig. 2.2.2.4 Pressure distribution along annular duct at Ma=3.2 jet injection from the two walls, n=5, d=4.4 mm, ----throttling, —injection

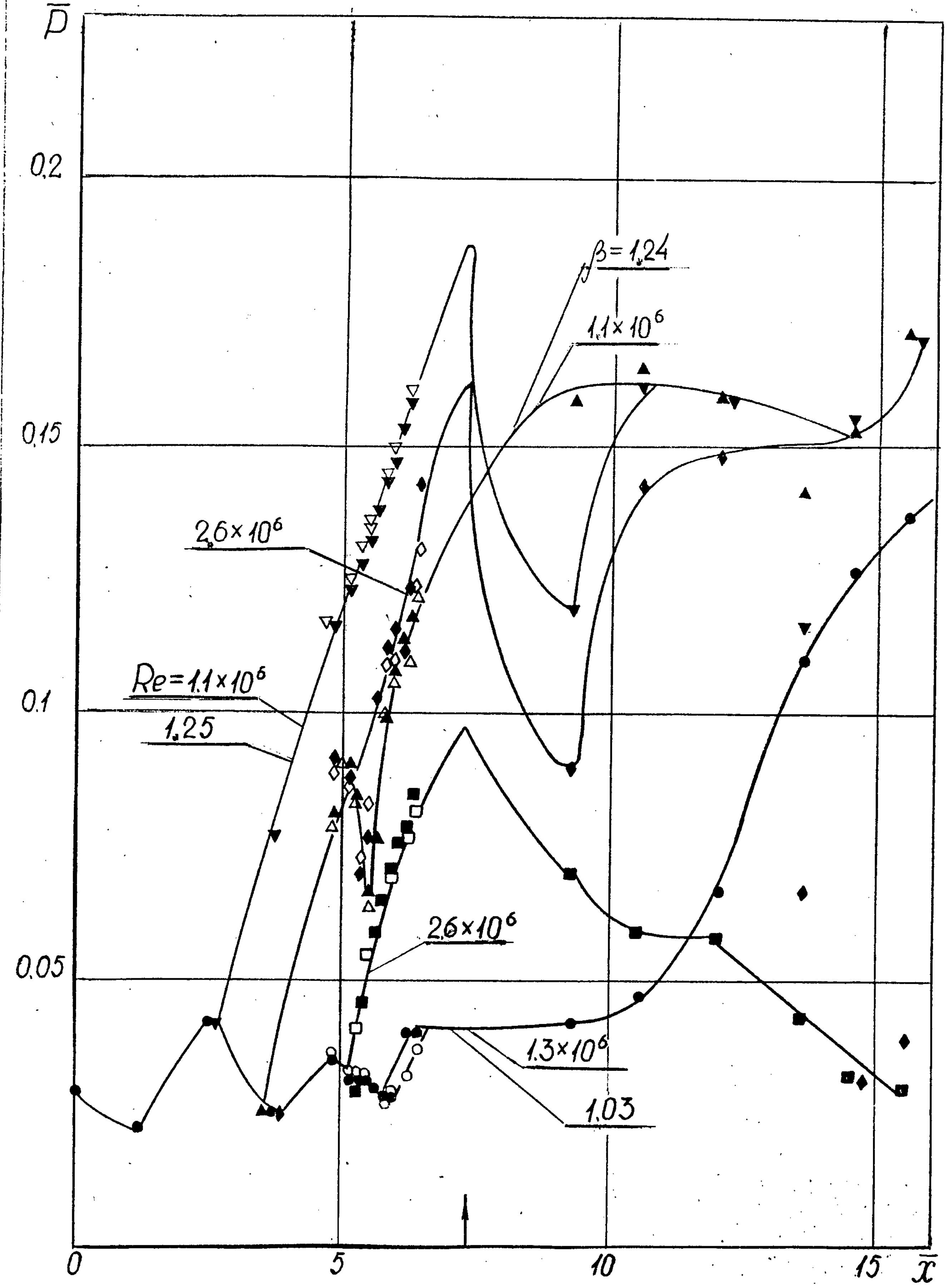

$\overline{P}$
0,2
0,15
0,1
0,05
0
5
10
15
$\overline{x}$
$\beta = 1,24$
$1,1 \times 10^6$
$2,6 \times 10^6$
$Re = 1,1 \times 10^6$
1,25
$2,6 \times 10^6$
$1,3 \times 10^6$
1,03

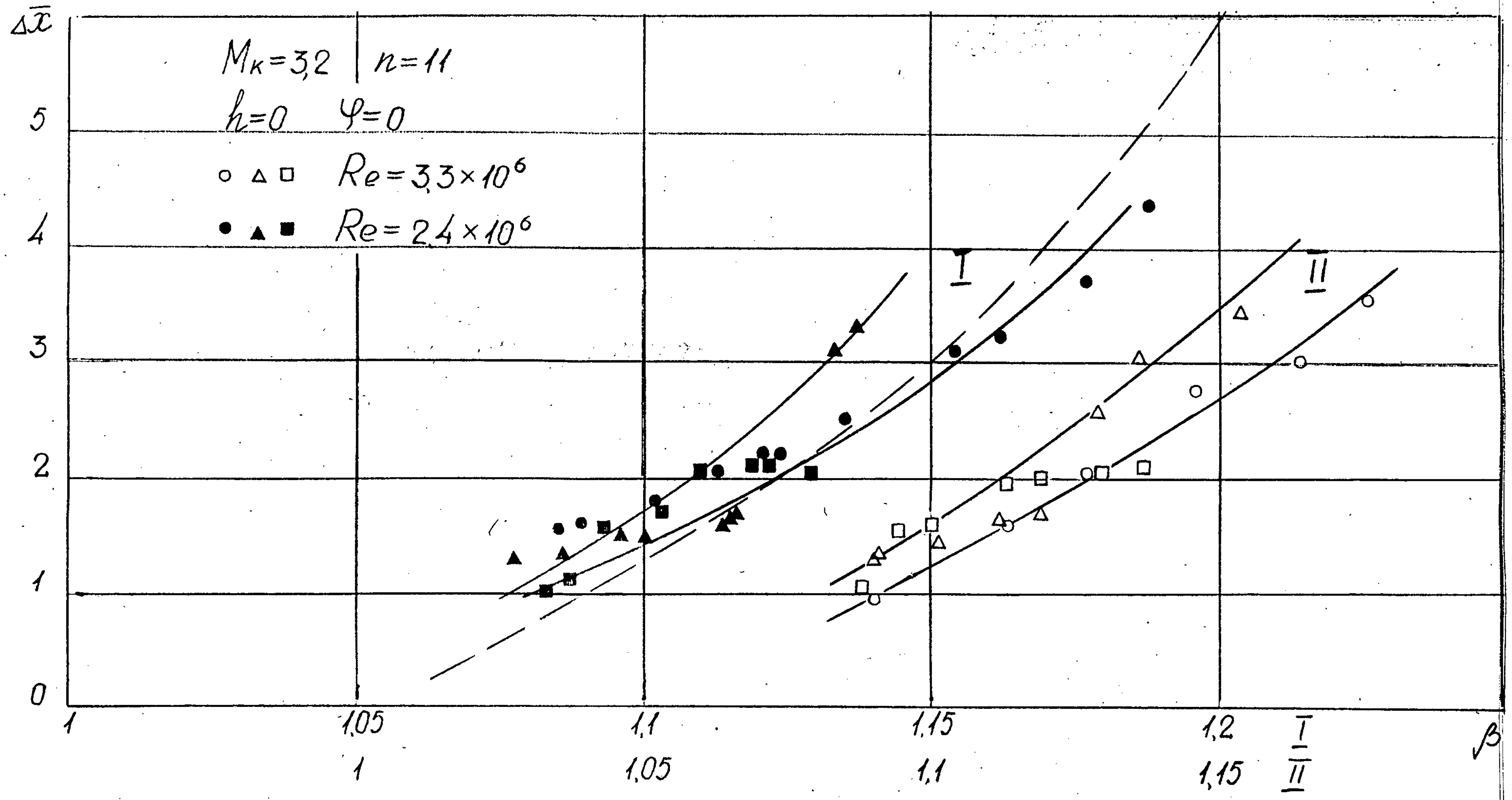

Fig. 2.2.2.6 Distancies of upstrem influence vs β
Ma=3.2, n=11, h=0, ●, ○-injection from two wall, Δ, Δ -outer wall, ■, □-inner wall, 1- Ma=3.08 circular tube

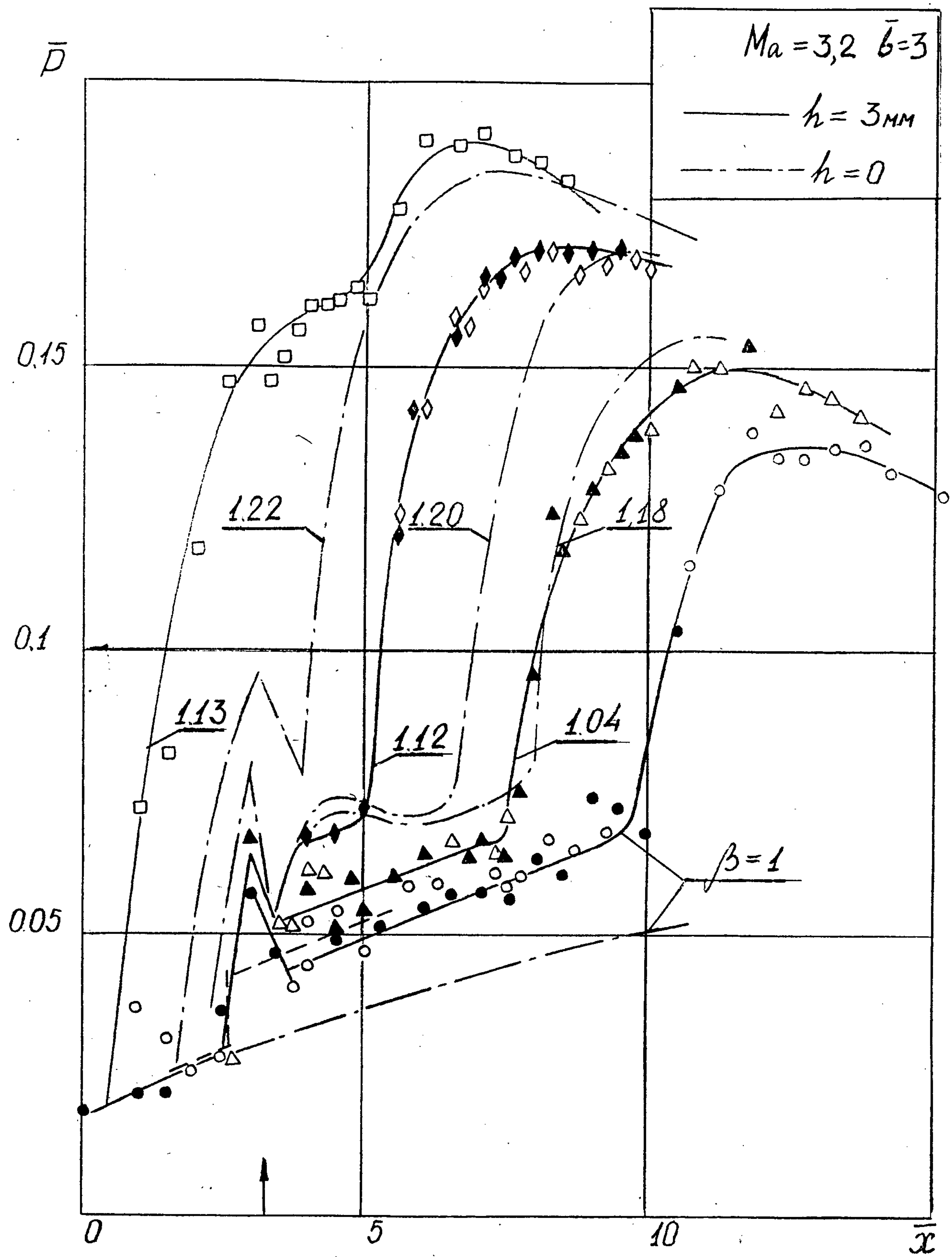

Fig. 2.2.2.7 Pressure distribution along rectangular duct with a set of struts, Ma=3.2..

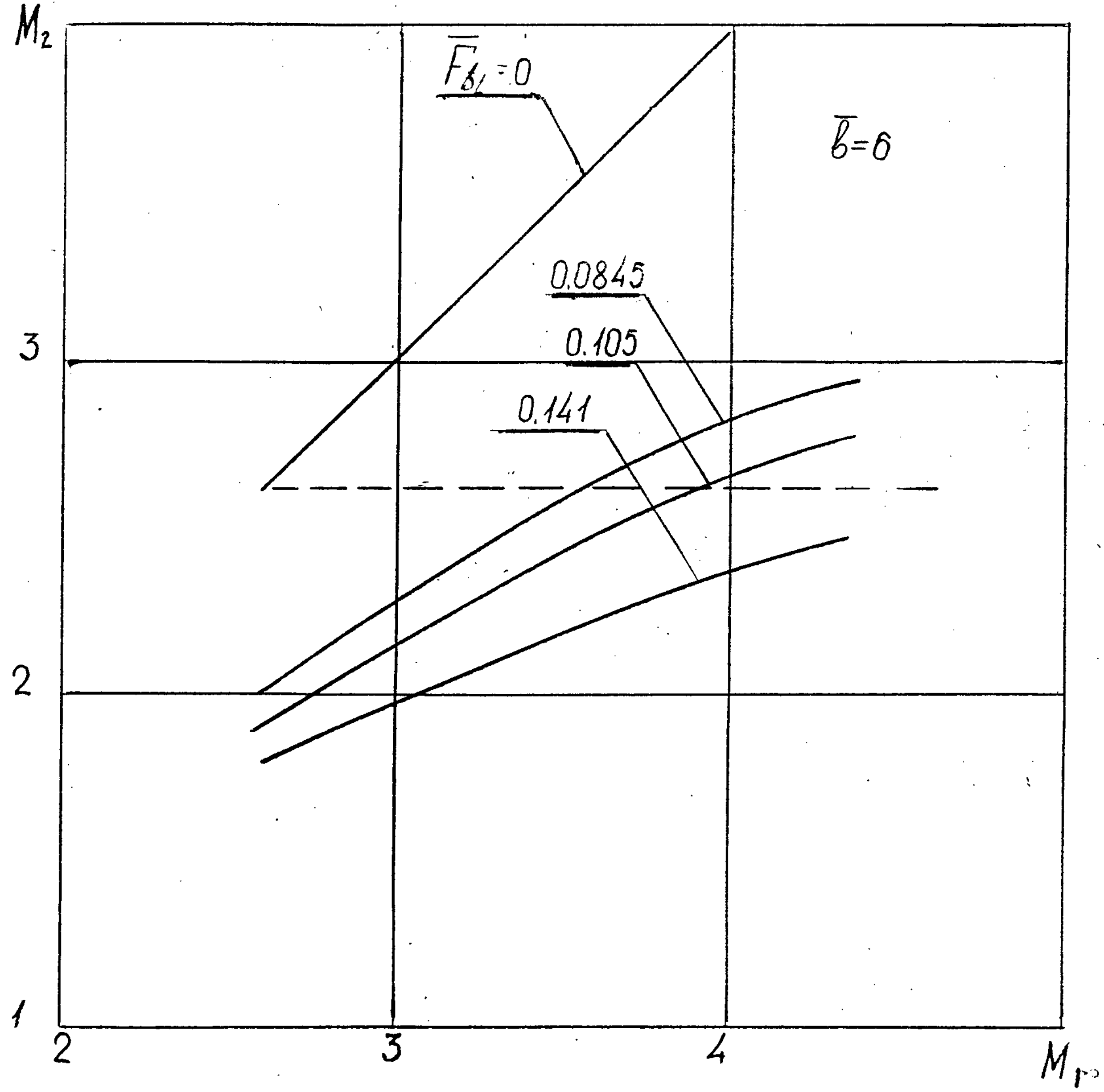

Fig. 2.2.2.8 $M_2(M_1)$ relationship at different blocages of the duct and β, —theory

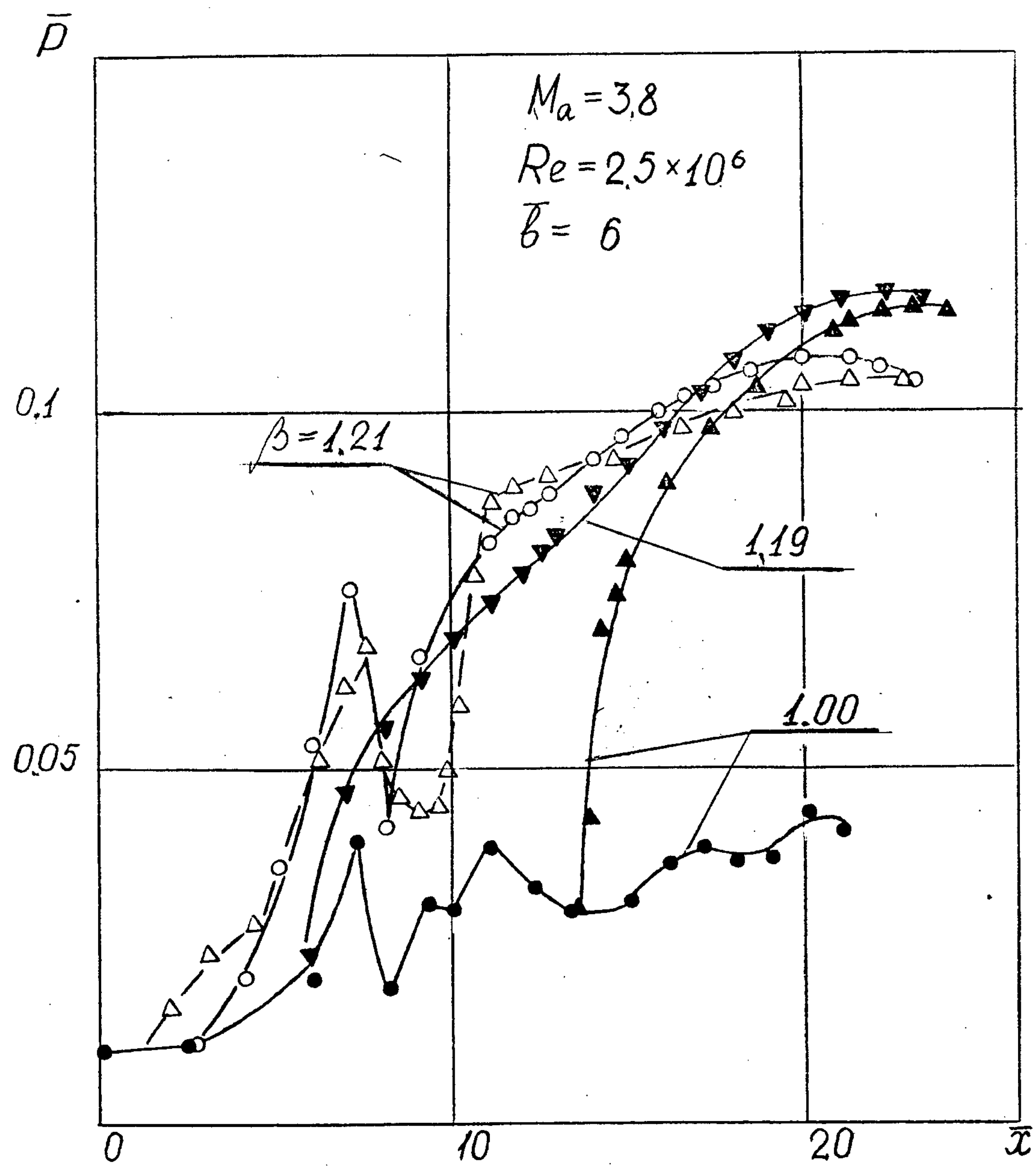

Fig. 2.2.2.9 Pressure distribution along rectangular duct, b=6 with struts at one wall, Ma=3.8

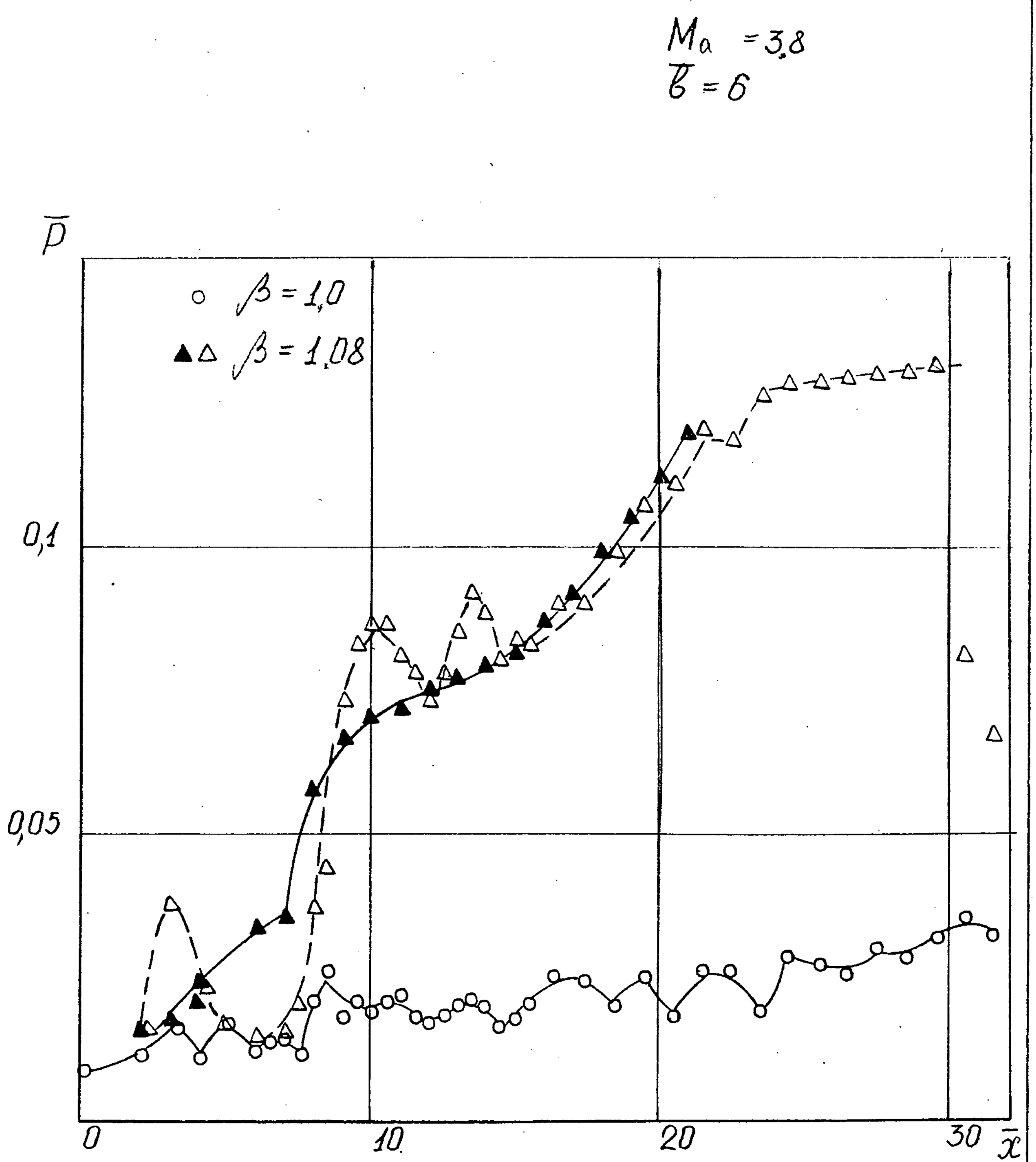

Fig. 2.2.2.10 Pressure distribution along rectangular duct, b=6
Ma=3.8, with jet injection from one wall

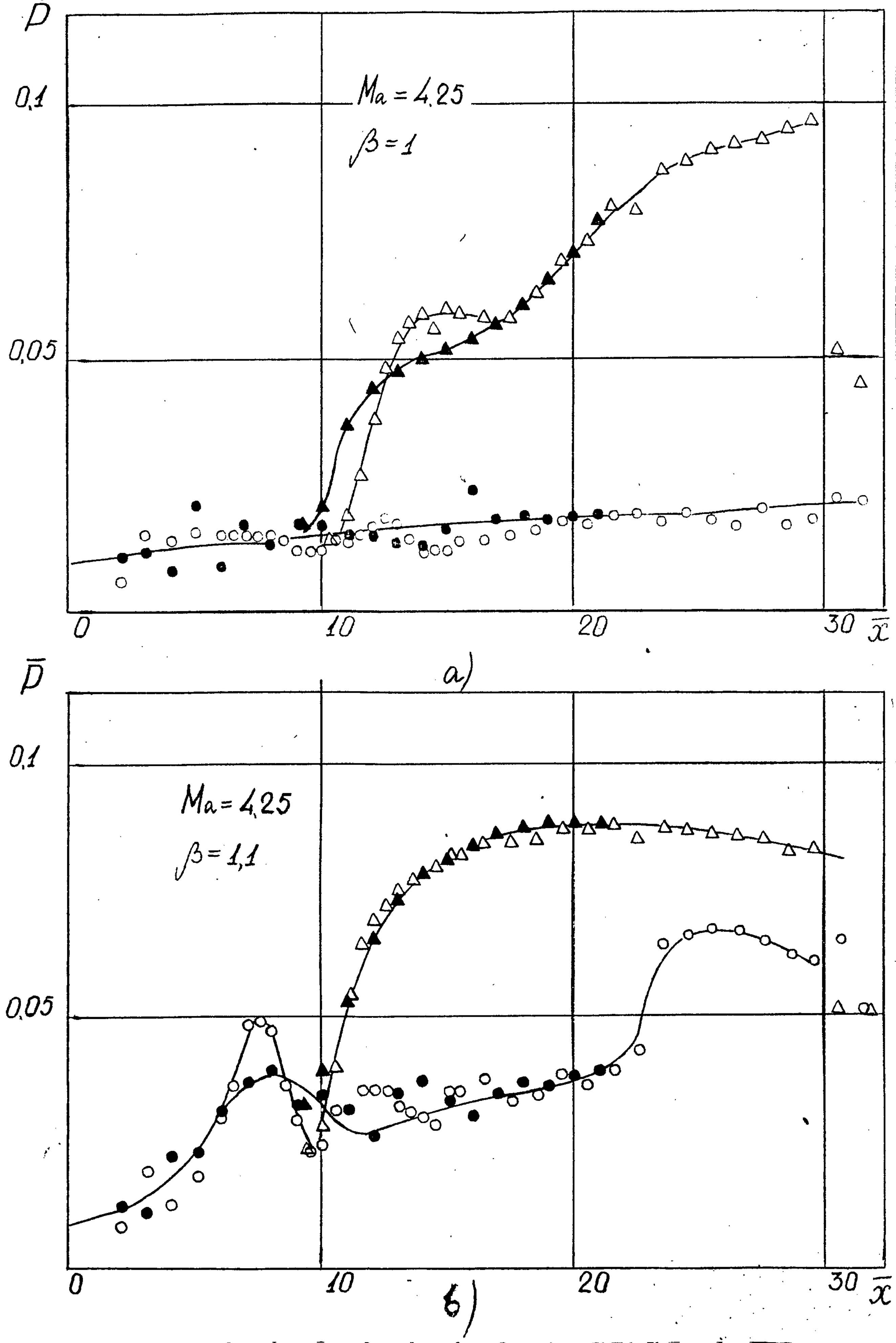

Fig. 2.2.2.11 Pressure distribution at jet injection from the wall, Ma=4.25, b=6.

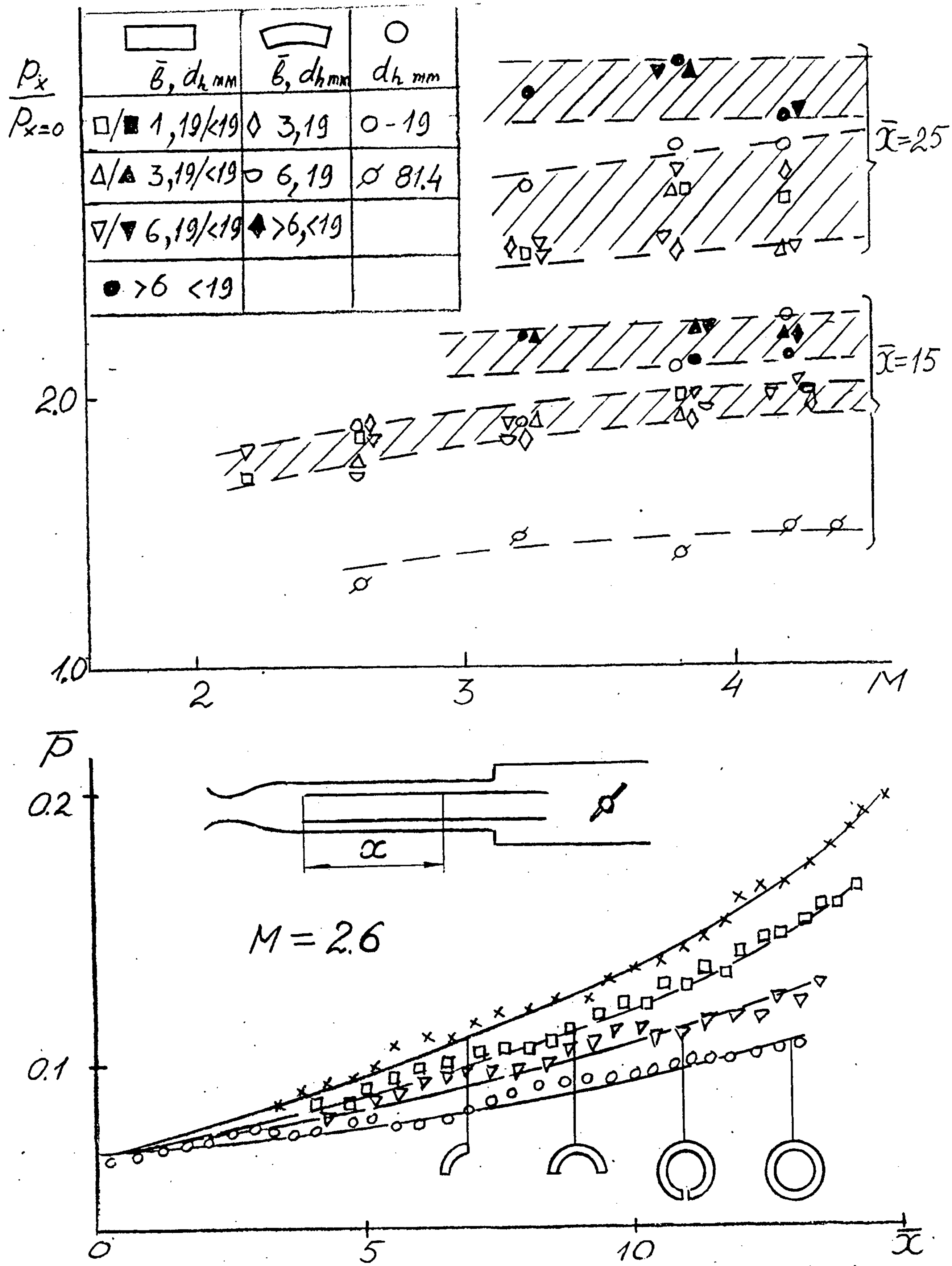

Fig. 2.3.1. a) $P_x/P_{x=0}$ dependance on Ma.
Initial stage, supersonic flow, Ma=3.8, b) Pressure distribution along annular sector duct, Ma=2.6.

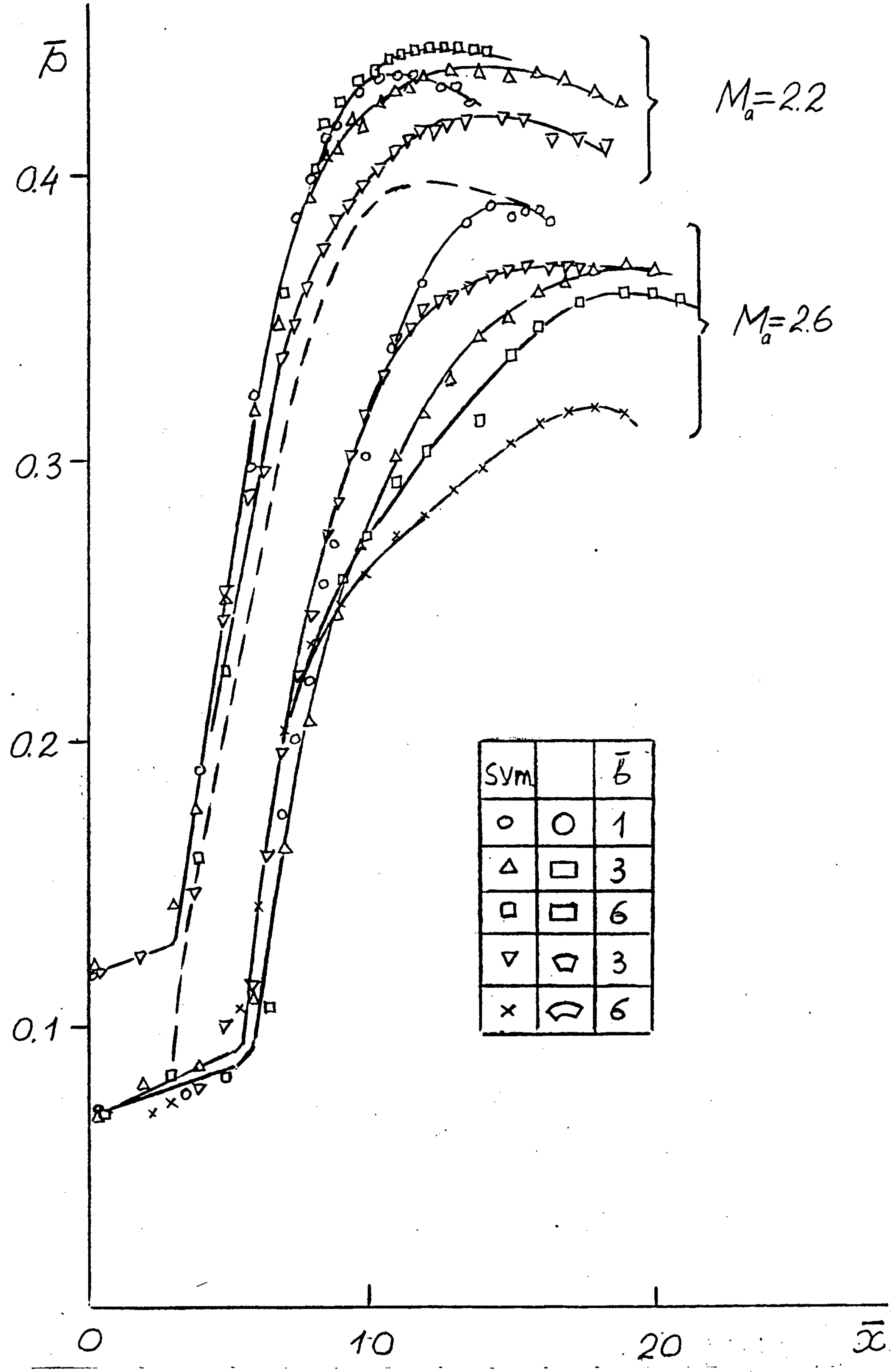

Fig.2.3.2 Pressure distribution at maximal back pressure. Second, basic stage of flow. Ma=2.2, 2.6

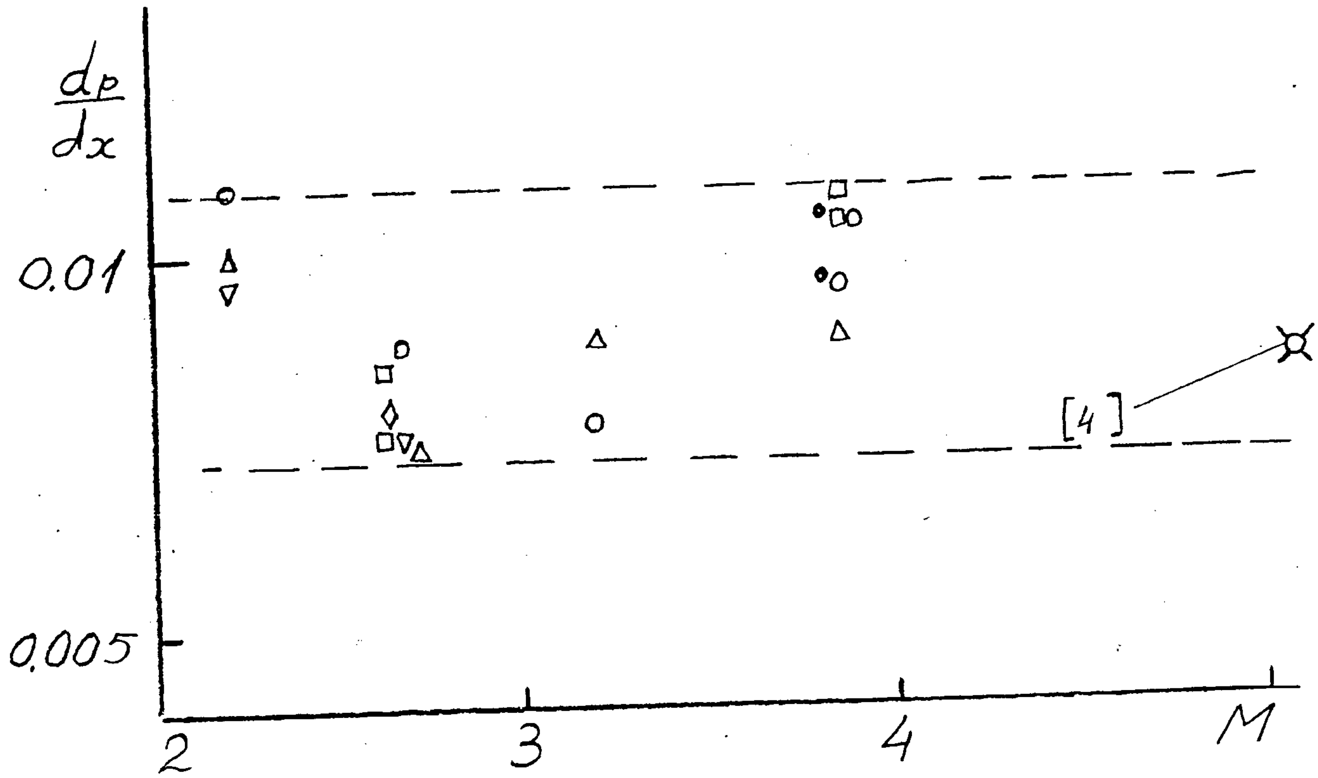

Fig.2.3.3 Third stage flow pressure gradient dependence on Ma.

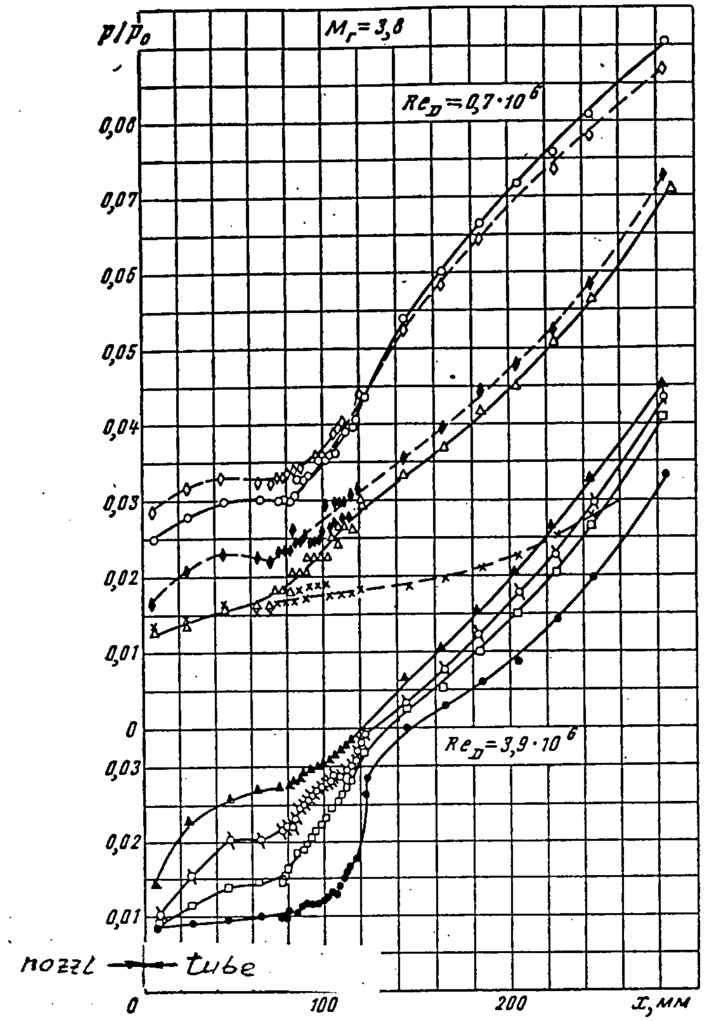

Fig.2.4.1 Pressure distribution in cylindrical tube with pseudo-shock, direct-connect tests.

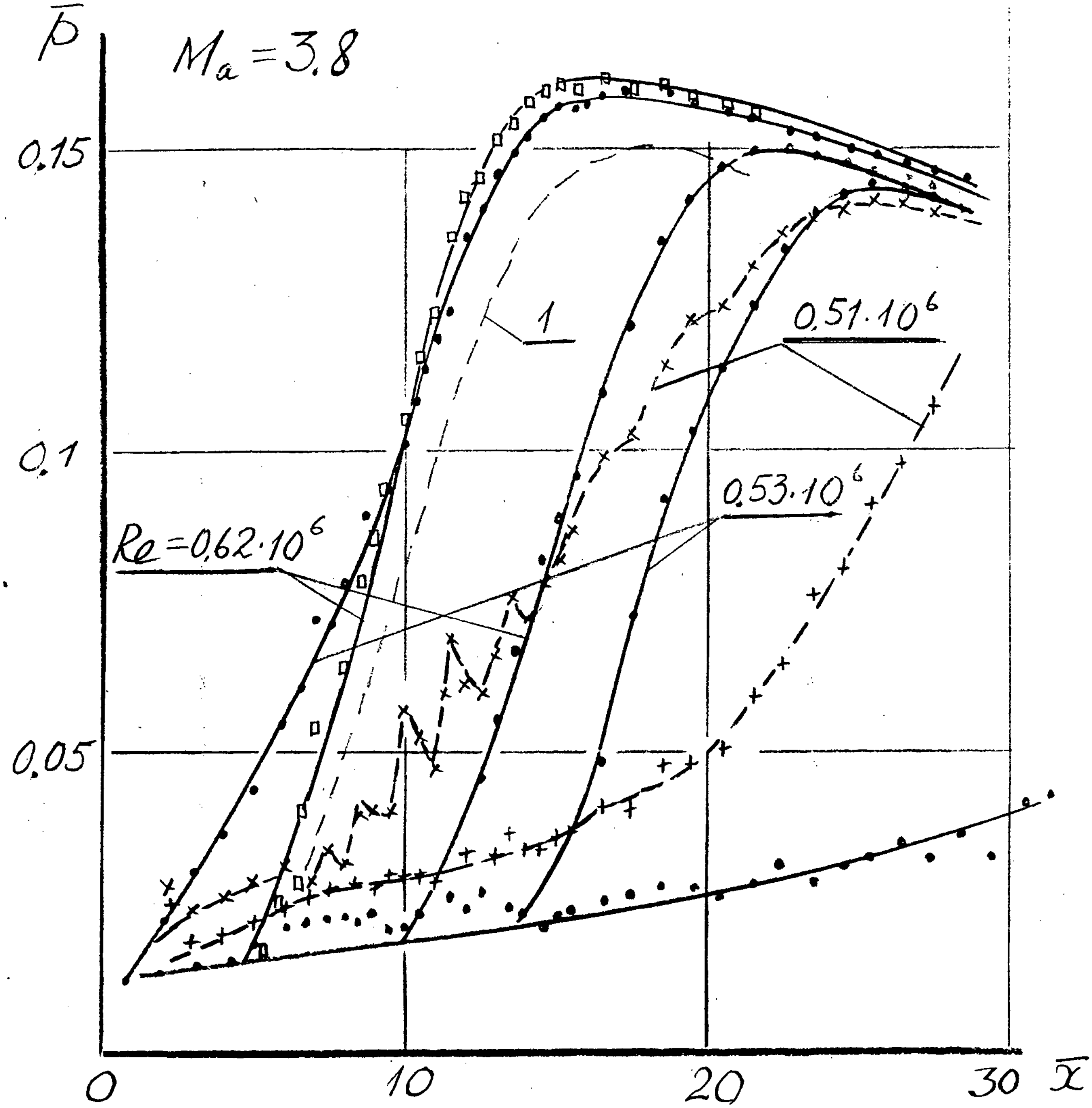

Fig. 2.4.2 Pressure distributions in ducts with ~~circular~~ and square cross sections, dh = 19 mm in free-stream tests. 1 – $\bar{b} = 1$

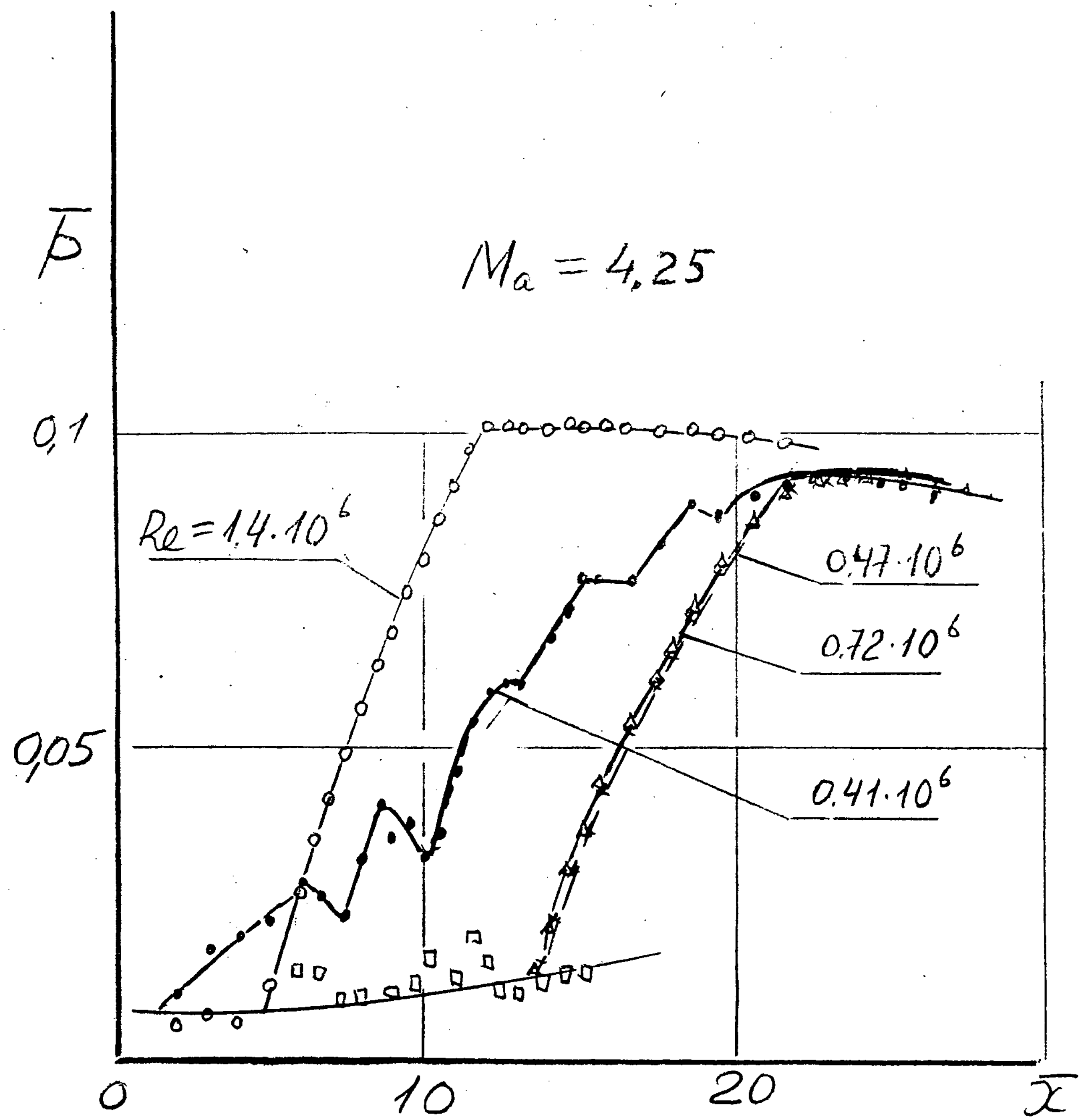

Fig. 2.4.3 Pressure distributions in rectangular ducts, b = 3, Ma = 4.25, dh = 19 mm.

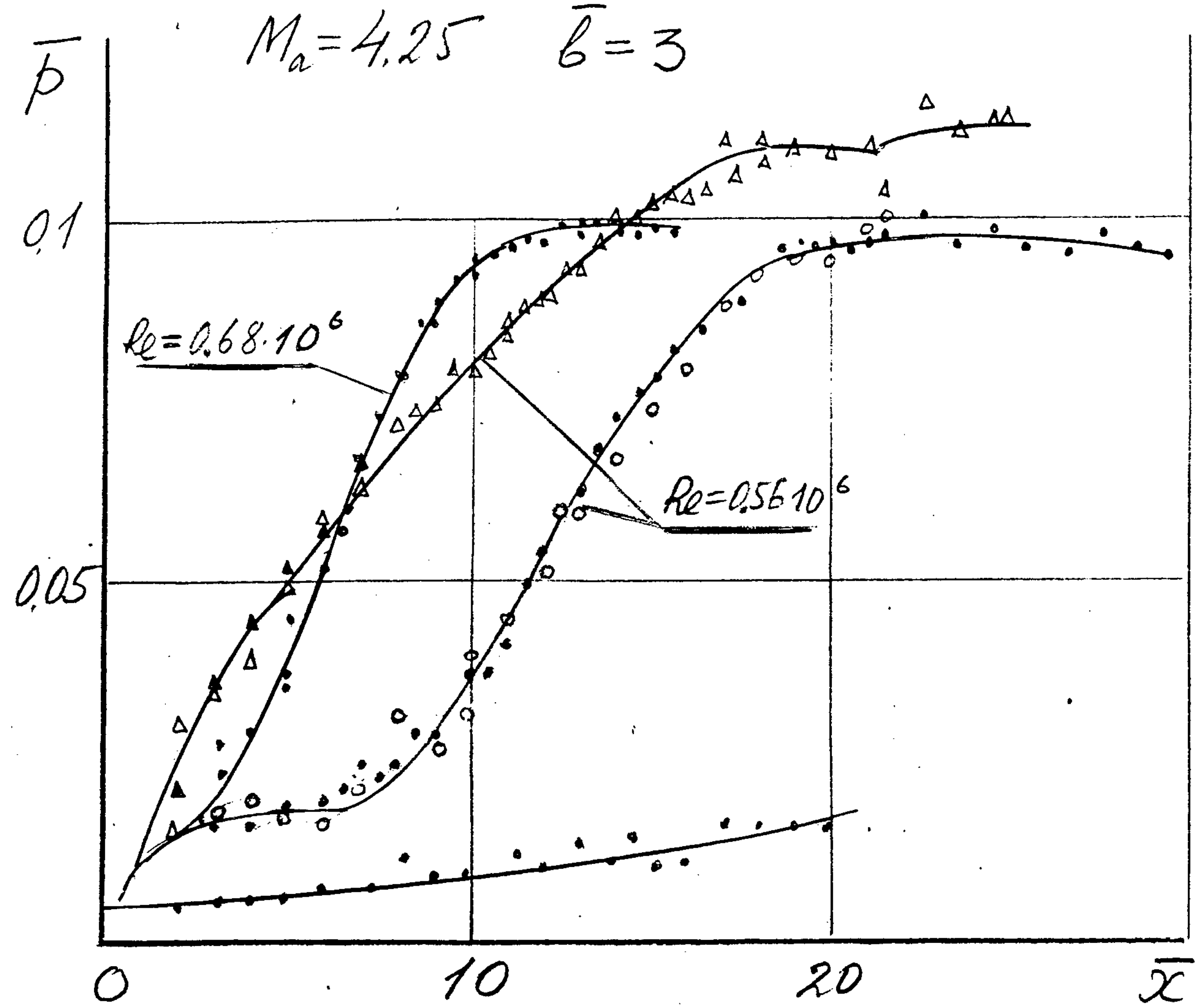

Fig. 2.4.4 Pressure distributions in rectangular duct b=3, Ma=4.25 at different Re.

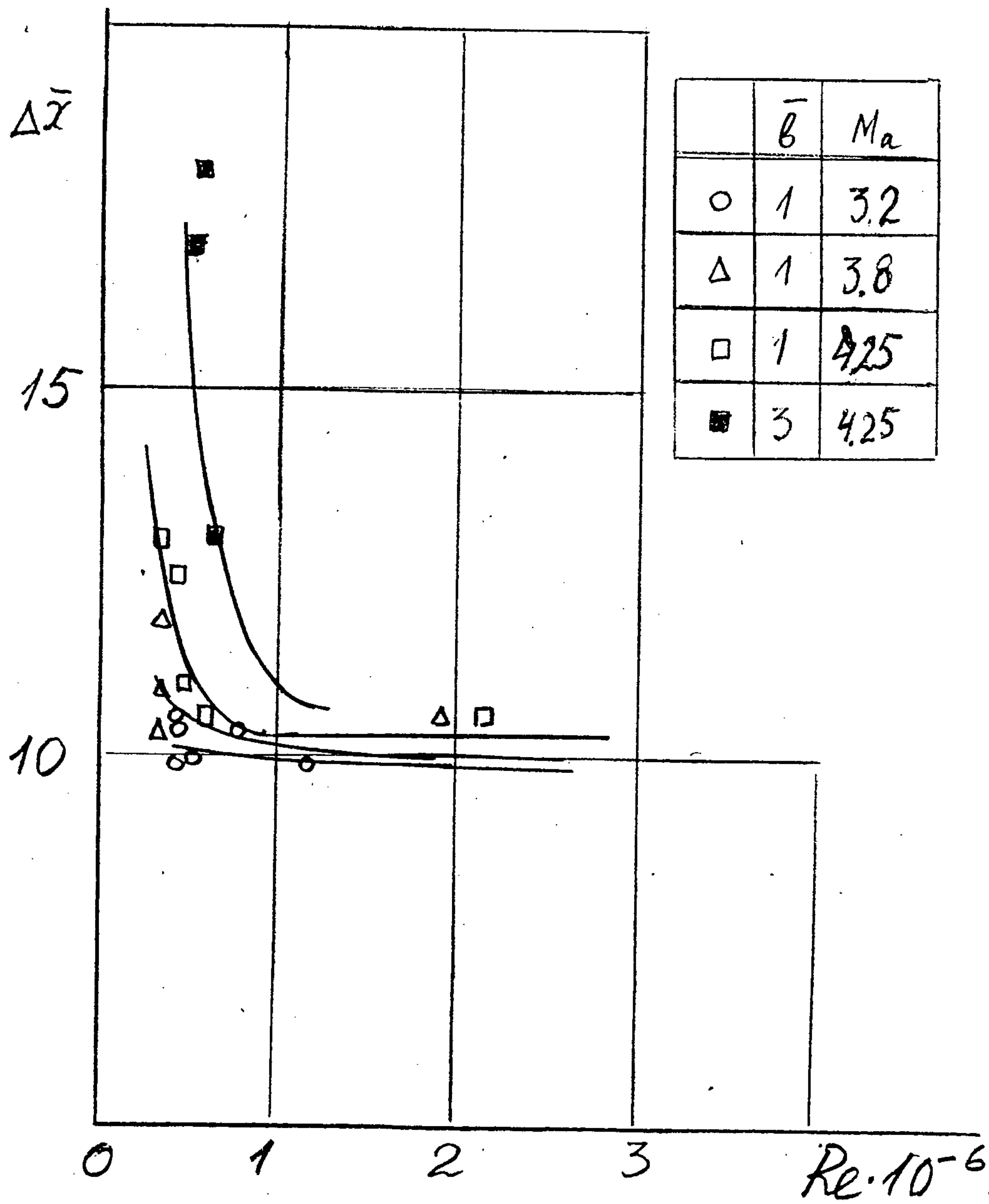

Fig. 2.4.5 Supersonic/subsonic transition length depenence on Re at b<3

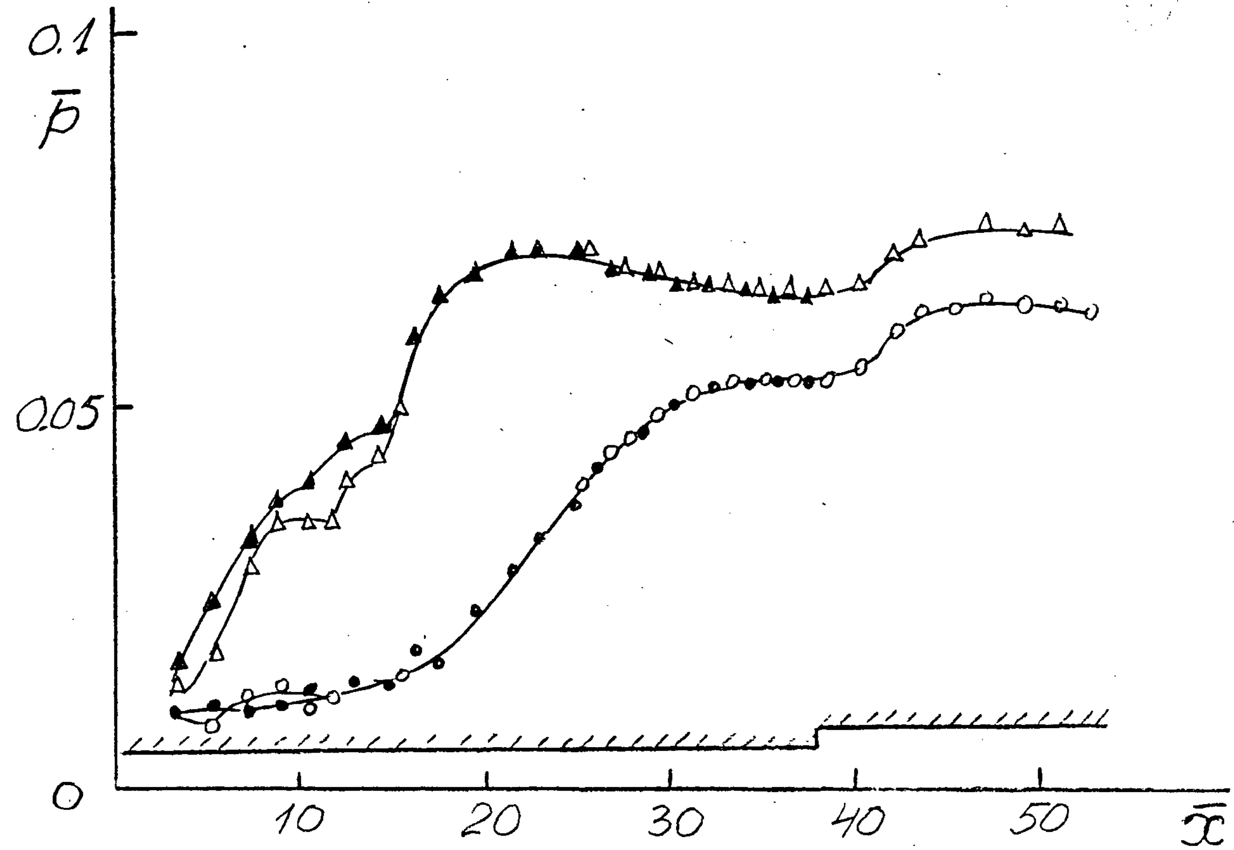

Fig. 2.4.6 Pressure distributions in rectangular duct
b=6, dh=10.6 mm, Ma=4.25, Re=10^6
○△ wide wall
●▲ narow wall

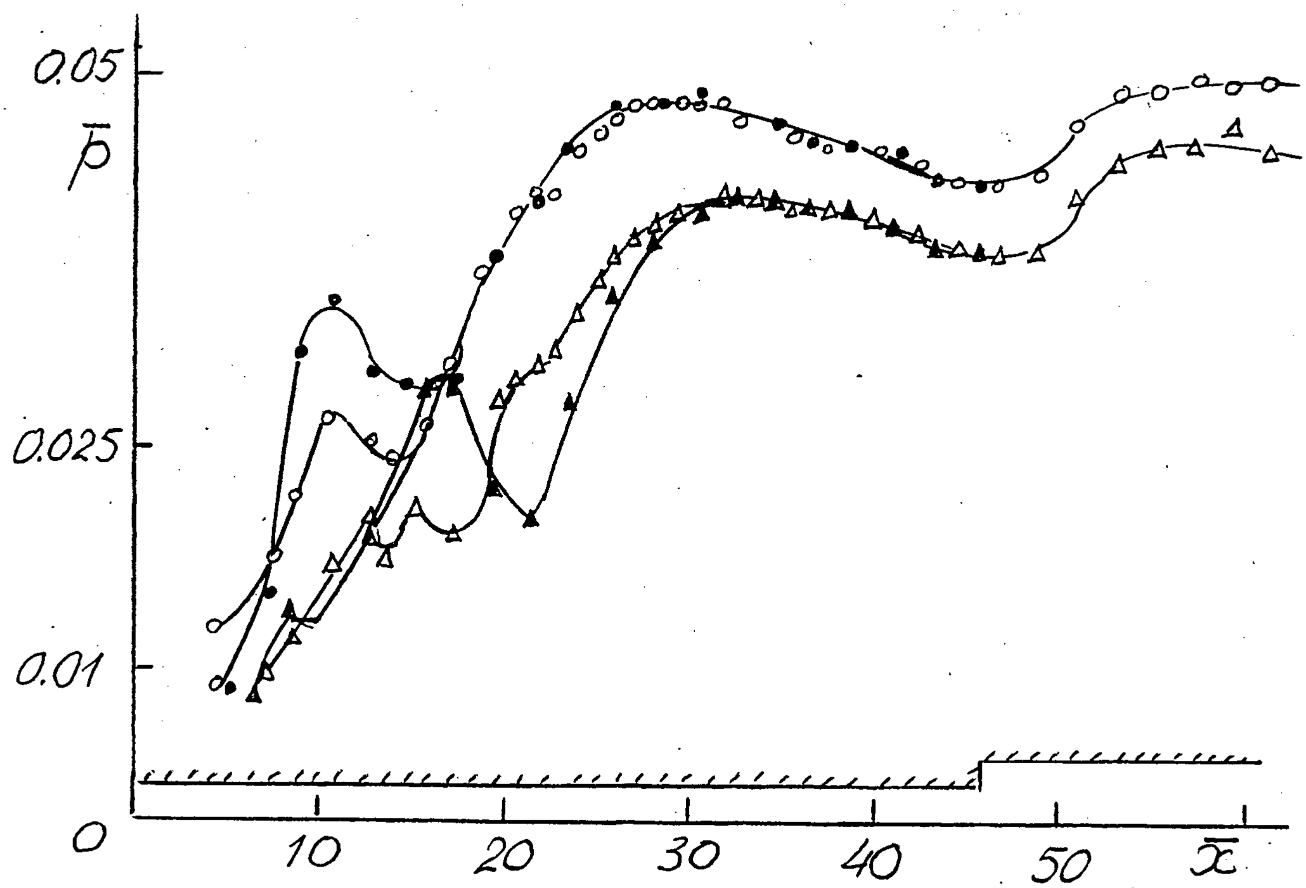

Fig. 2.4.7 Pressure distributions in rectangular duct
b=7.4, dh=8.8 mm, Ma=4.25 ○△ wide wall, ●▲ narrow wall.

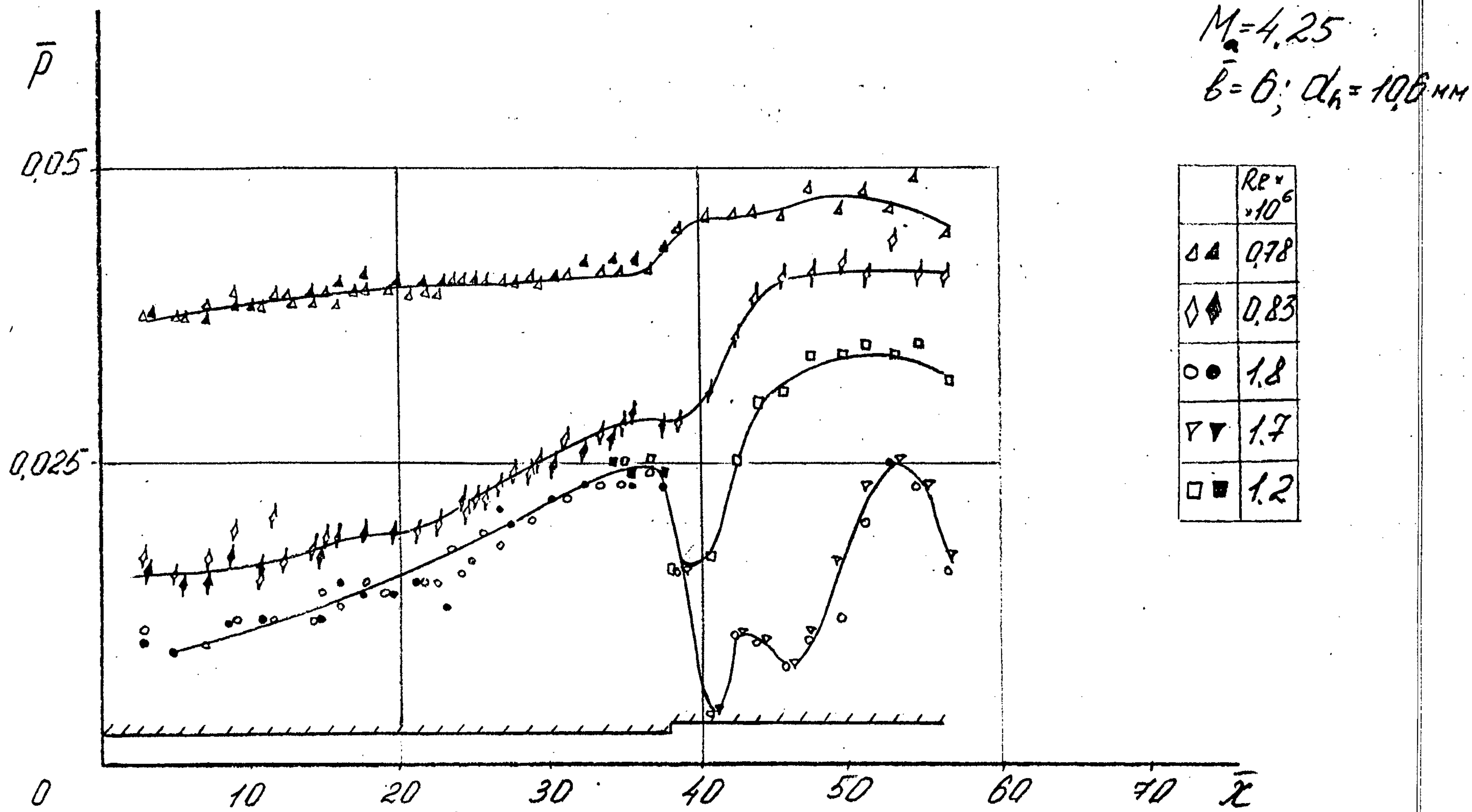

Fig. 2.4.8 Pressure distributions in rectangular duct

b=6, dh=10.6, Ma=4.25 at different Re<10^6

○△□◊▽ wide wall, ●▲◆■ narrow wall

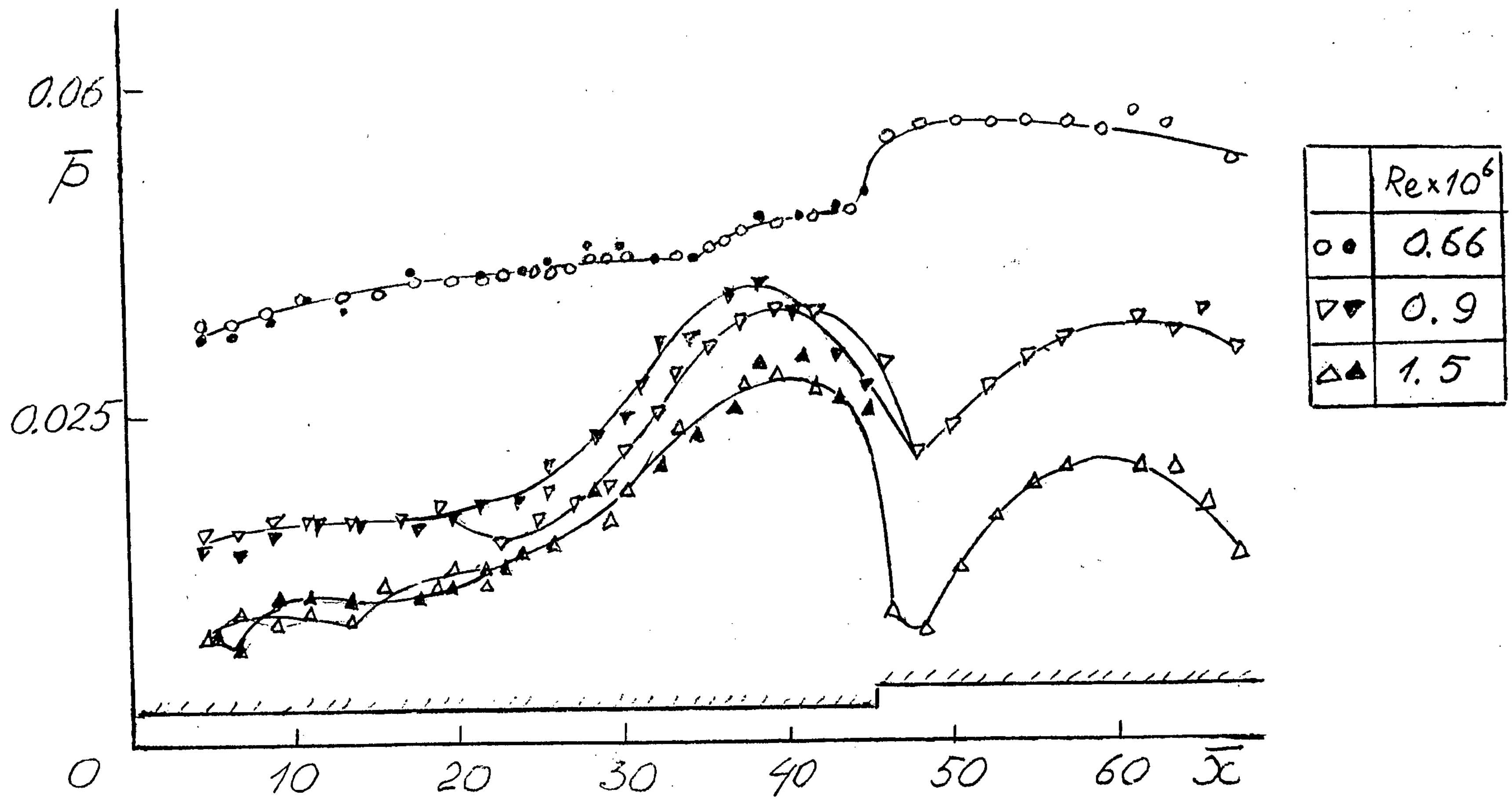

Fig. 2.4.9 Pressure distributions in rectangular duct
b=7.4, dh=8.8 mm, Ma=4.25 at different Re.
○△▽ wide wall, ●▲▼ narrow wall

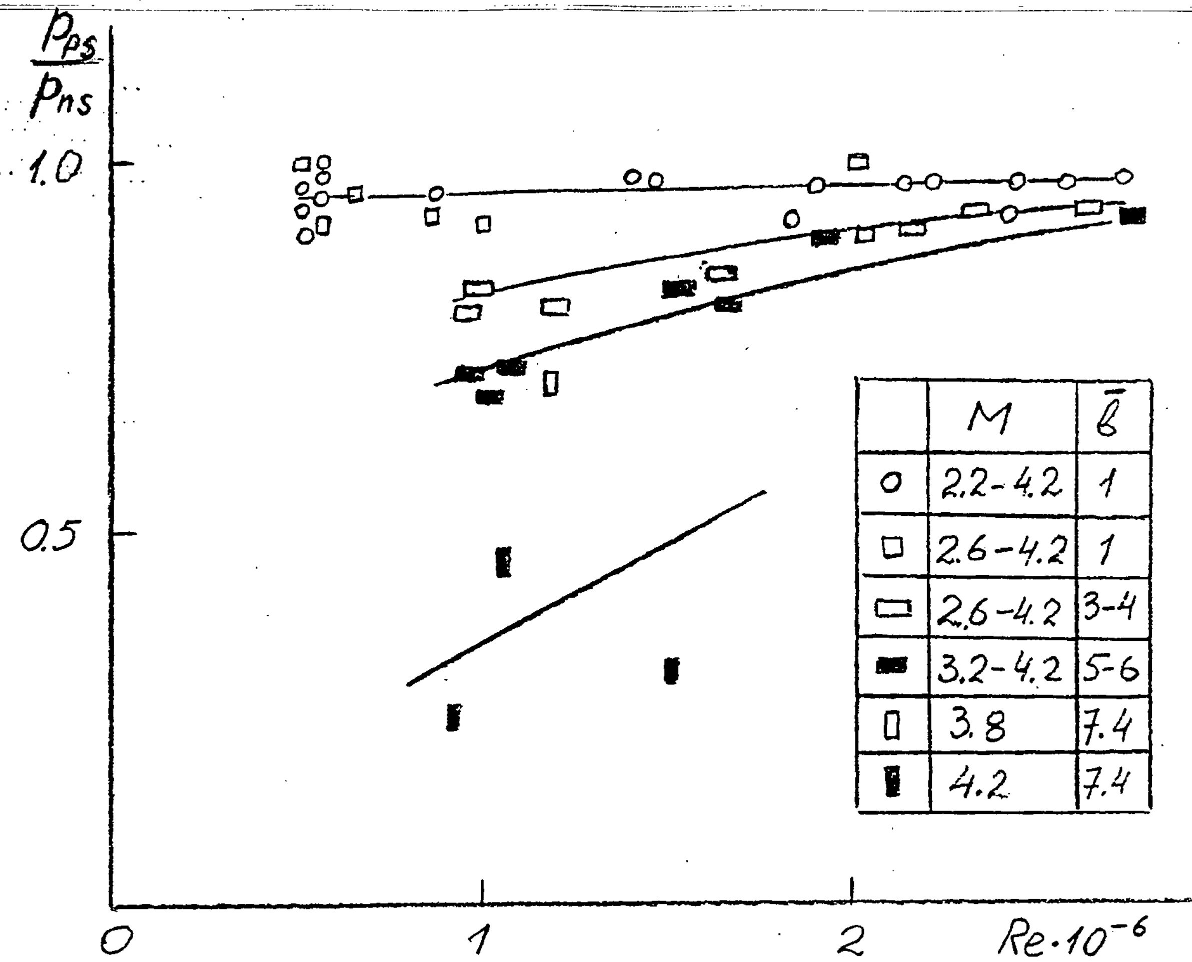

Fig. 2.4.10 Pressure recovery in rectangular ducts with constant cross sections vs. Re.

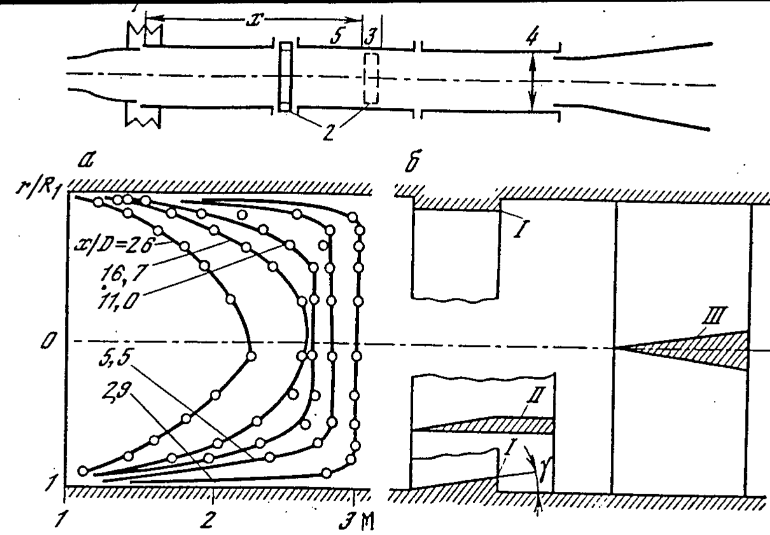

Fig. 3.1.1 Experimental model schematic.
1-balances, 2,3-wedge-lice bodies, 4-telescope junction
5- cylindrical section, M-profile in the ducts
I-III-variants of steps and wedge-like bodies

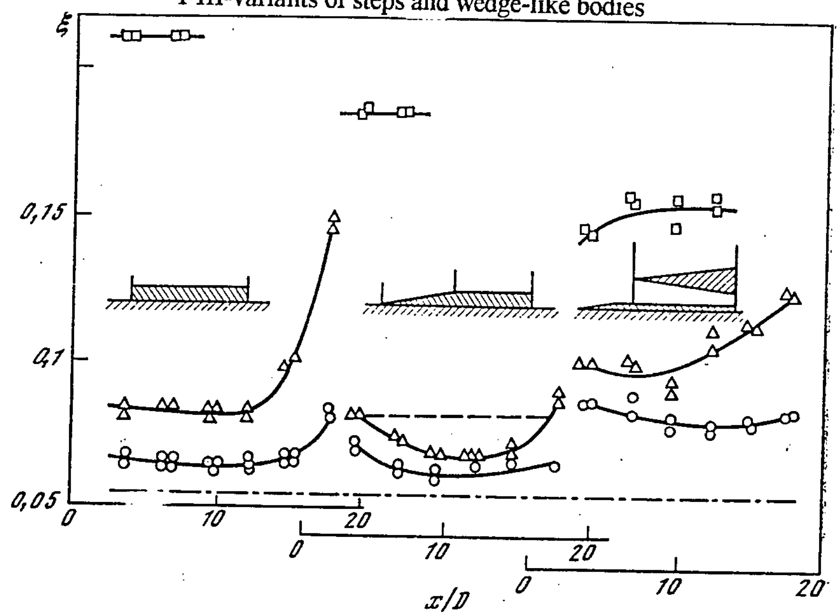

Fig. 3.1.2 Impulse loss coefficients for different models.
square symbols-Fm/Fd = 0.26, triangles-0.195, circles-0.125.

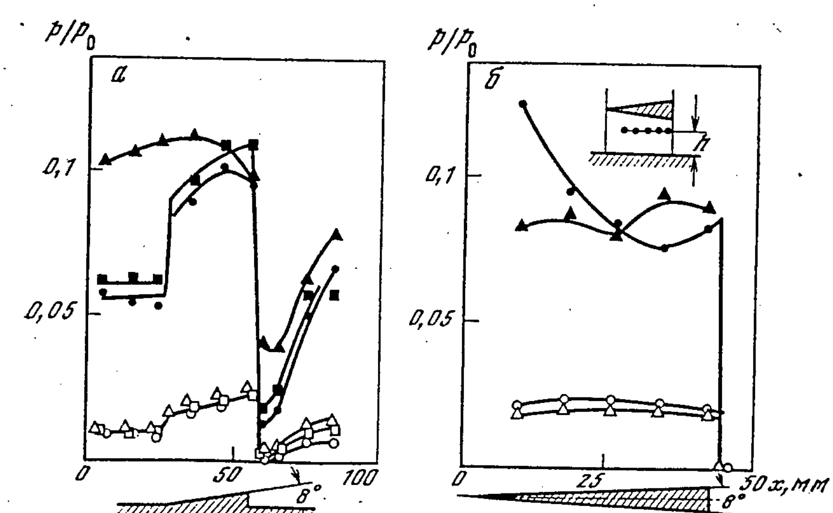

Fig. 3.1.3 Pressure distribution along cowl (a) and wedge (b).
open symbols-Ma = 3.8, shaded-2.6
a: circles-x/D = 0.7, square-4.4, triangles-10.1
b: circles-h = 20.7 mm, triangles-2.7 mm.

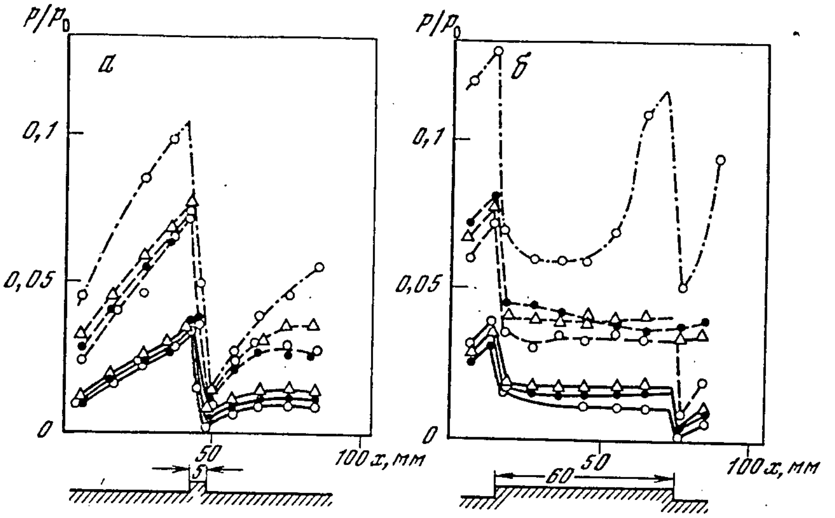

Fig. 3.1.4 Pressure distribution along the annular jut.
a- jut length-5 mm, b-60 mm. Open circles for x/D = 0.7
shaded-4.4 mm, open triangles-10. Solid line for Ma = 3.8,
dashed-3.2, dashed-dotted-2.6.

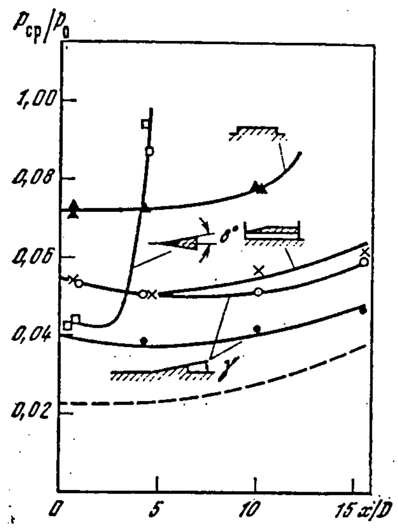

Fig. 3.1.5 Average pressure distribution along the surfaces
of tested models at Ma = 3.2. open circle-t - 8 deg.,shaded-4.

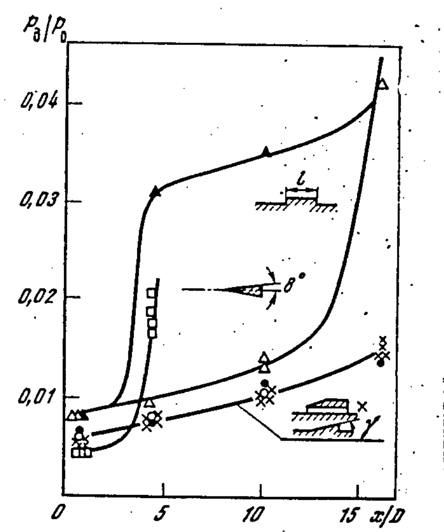

Fig. 3.1.6 Base pressure at Ma = 3.2
open circles- t = 8 deg., shaded-4, Open triangles -for jut of
l = 5 mm, shaded -for l = 60 mm.

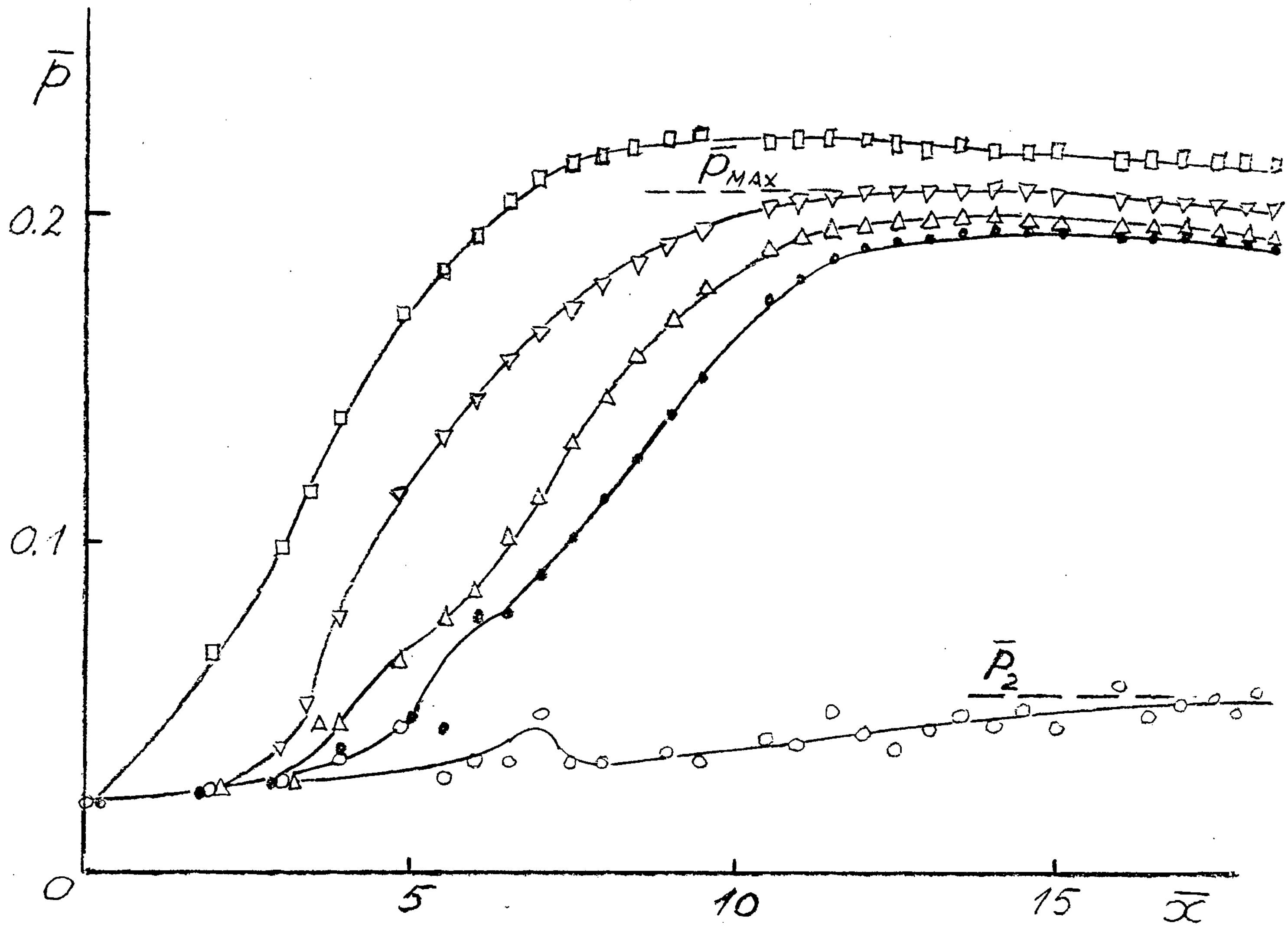

Fig. 3.1.7 Pressure distribution along tube with cylindric struts, Ma=3.2, 3 rows, d=3 mm at different back pressure.

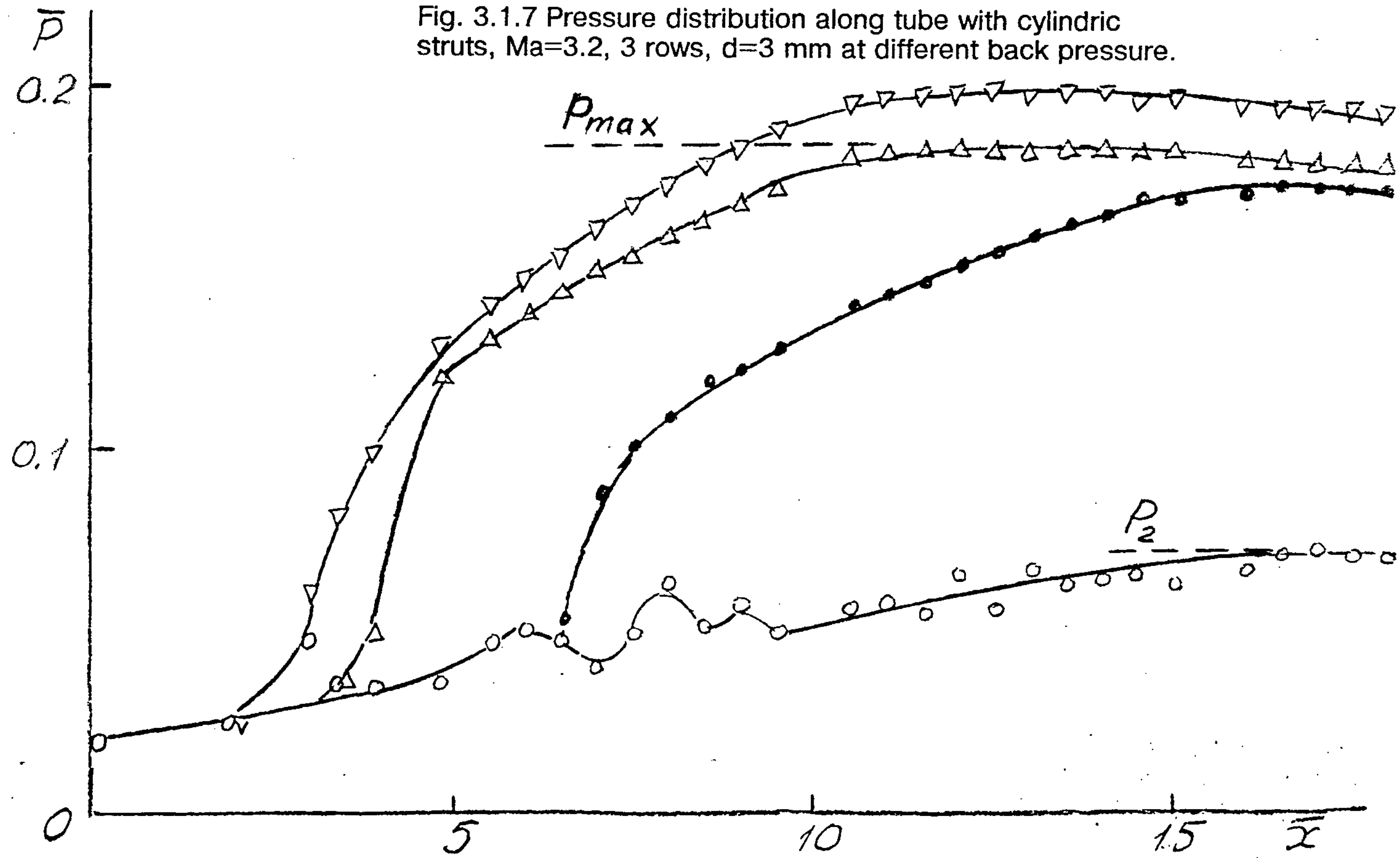

Fig. 3.1.8 Pressure distribution along tube with rhombic

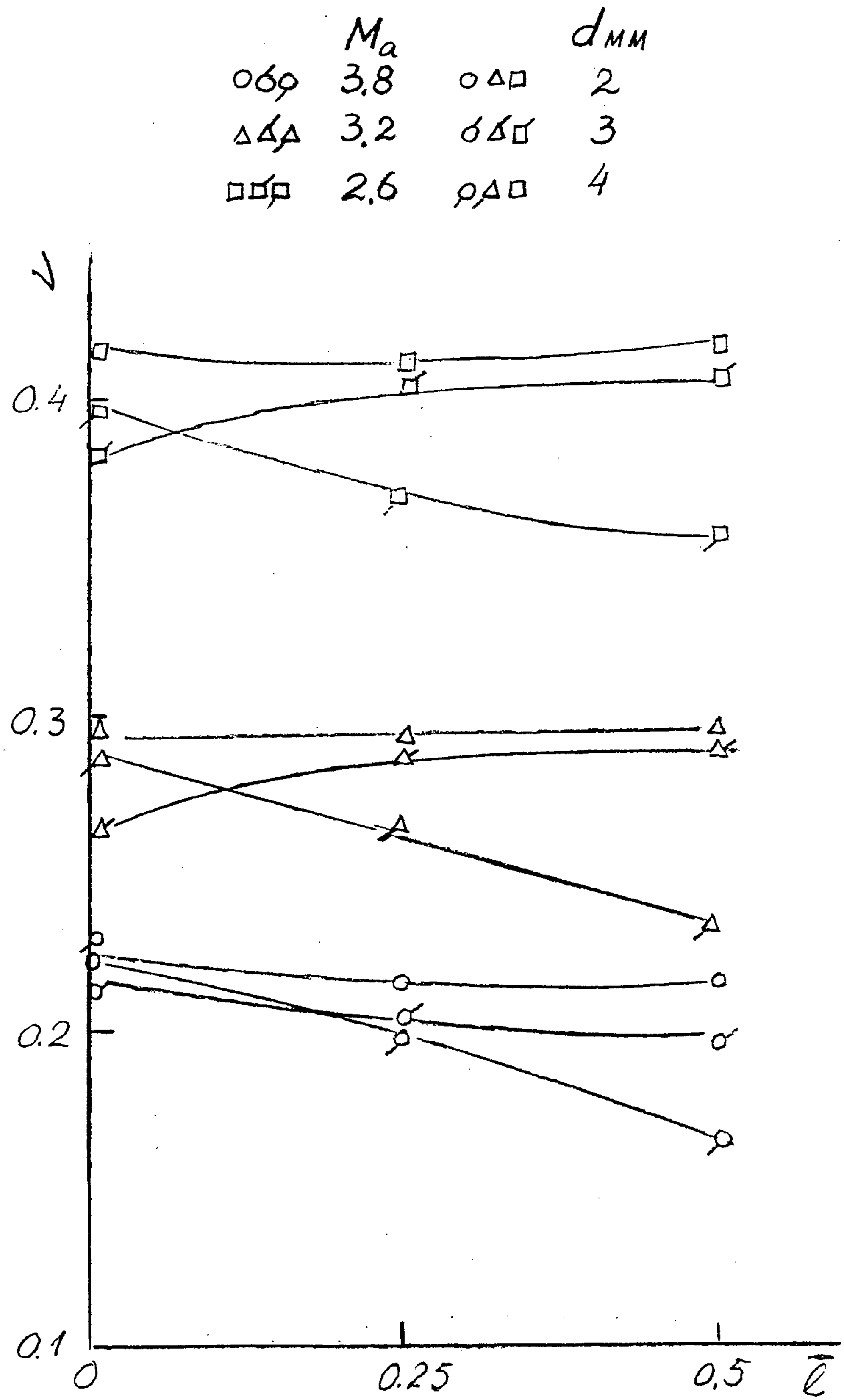

Fig. 3.1.9 Total pressure recoveries dependence on the grate width. Rhombic struts.

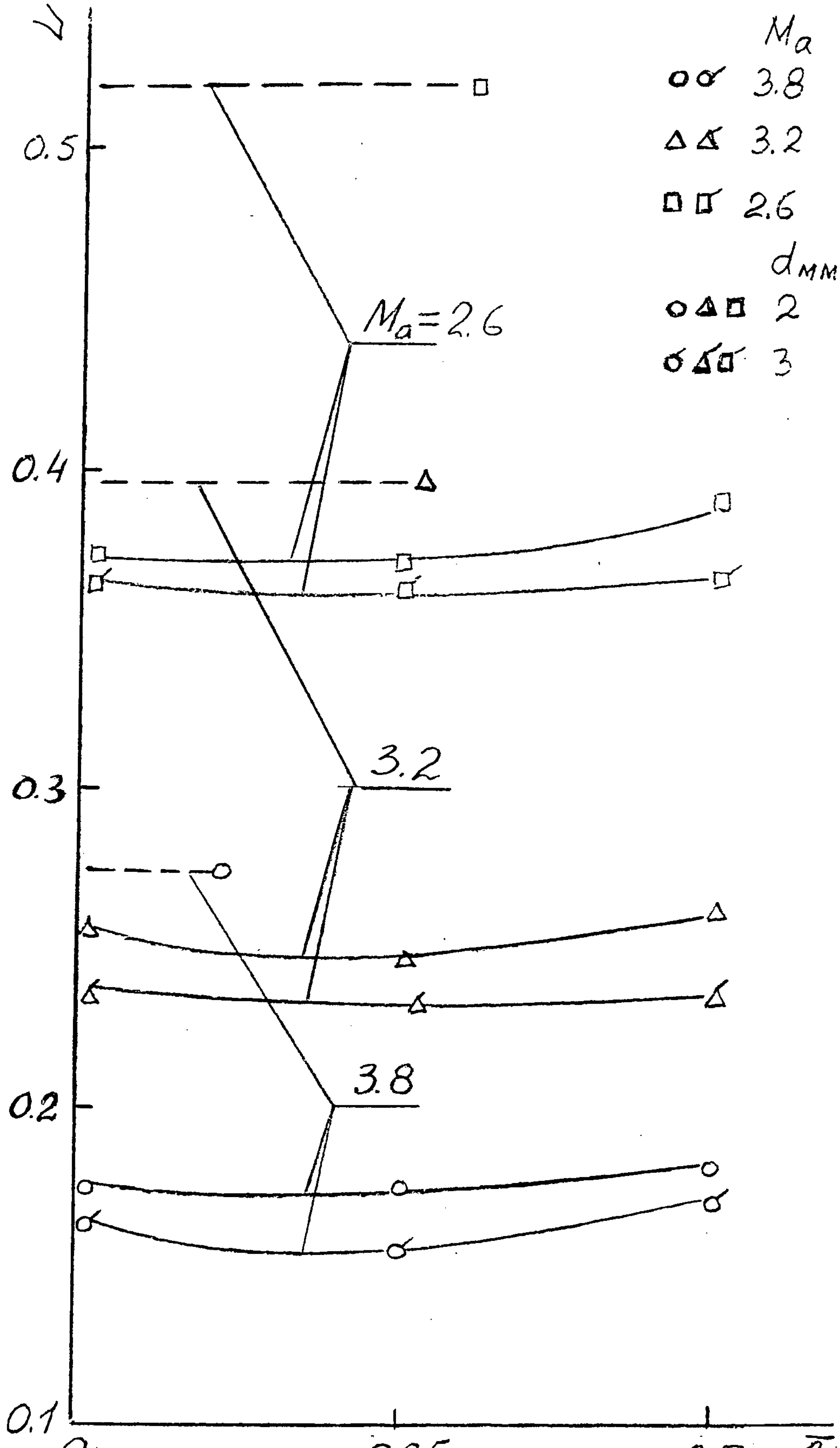

Fig. 3.1.10 Total pressure recoveries dependence on the grate width. Cylindric struts. - - - -no struts.

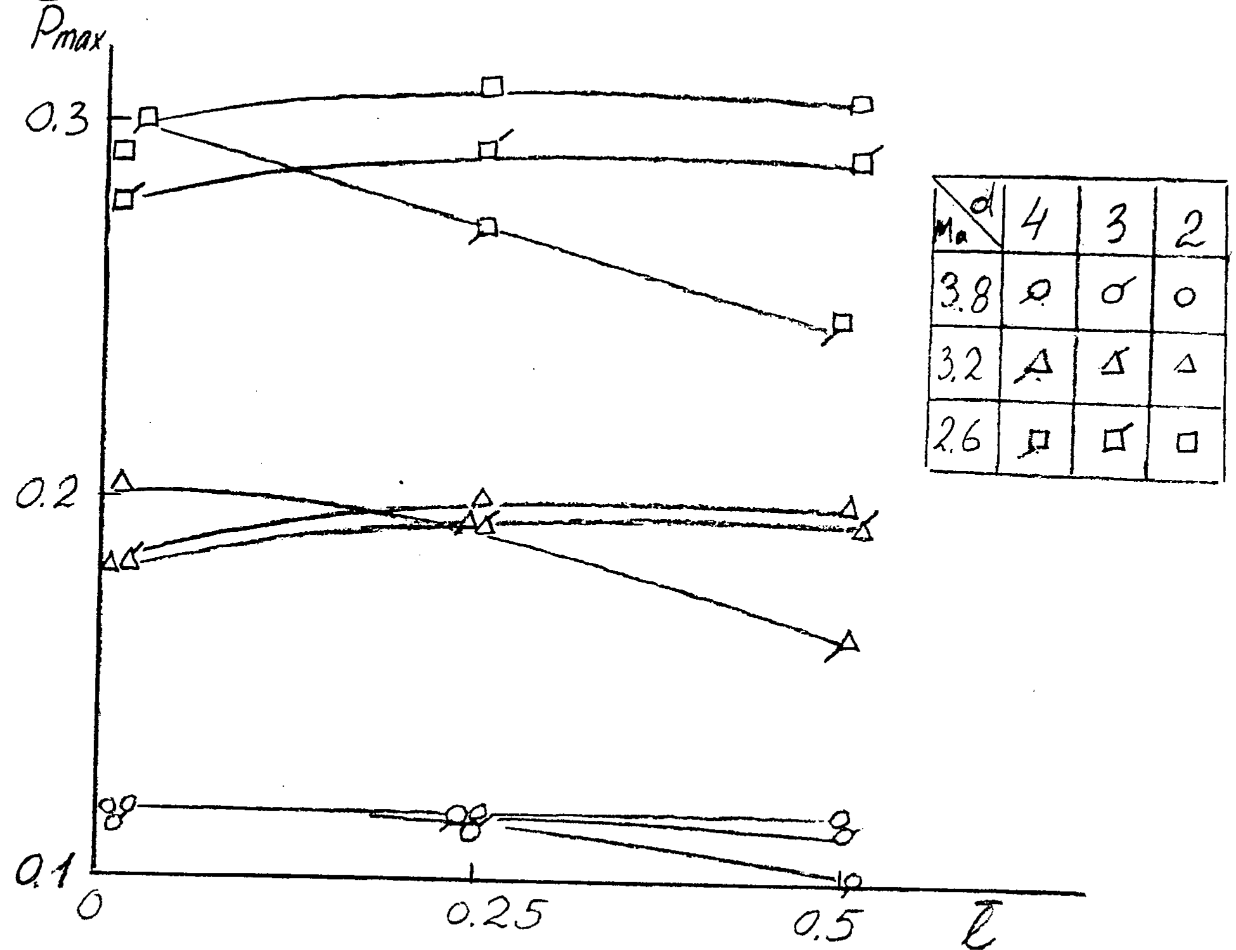

Fig. 3.1 11 Pmax dependence on the grate width.
Rhombic struts.

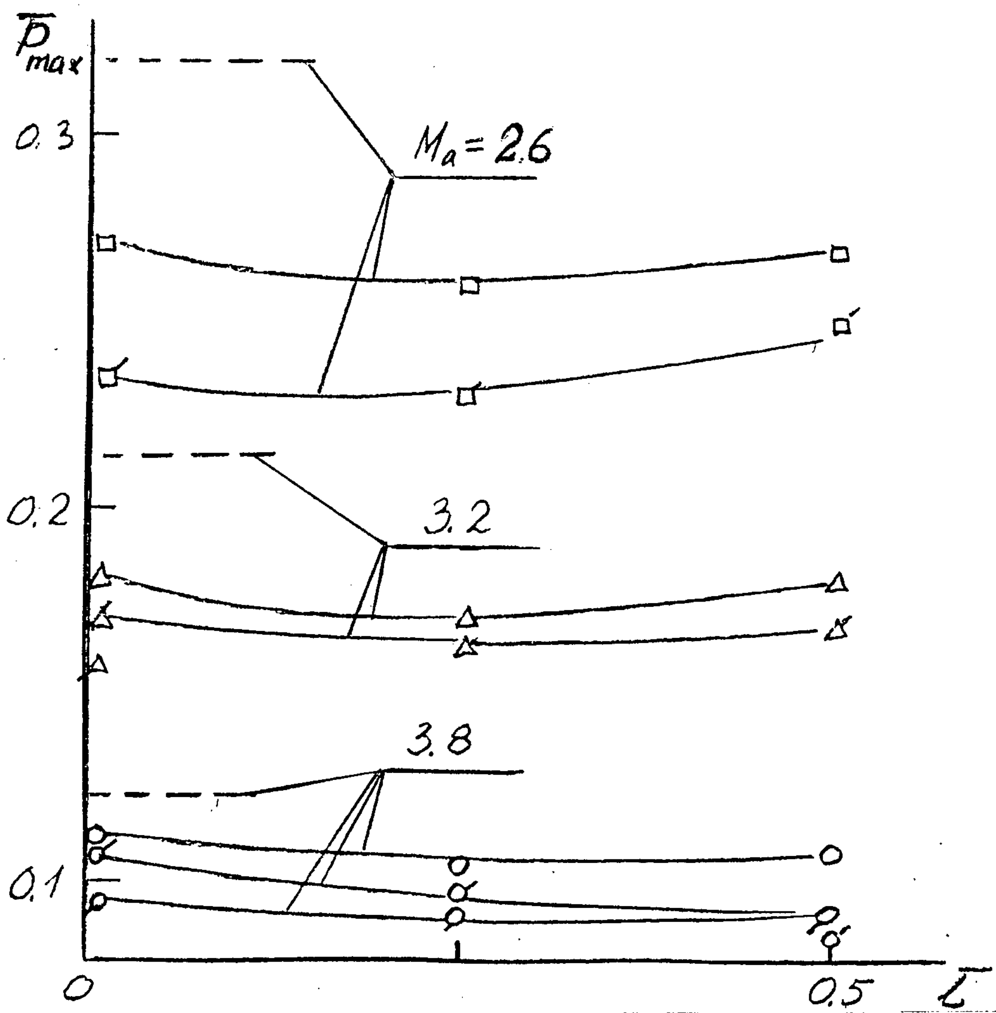

Fig. 3.1 12

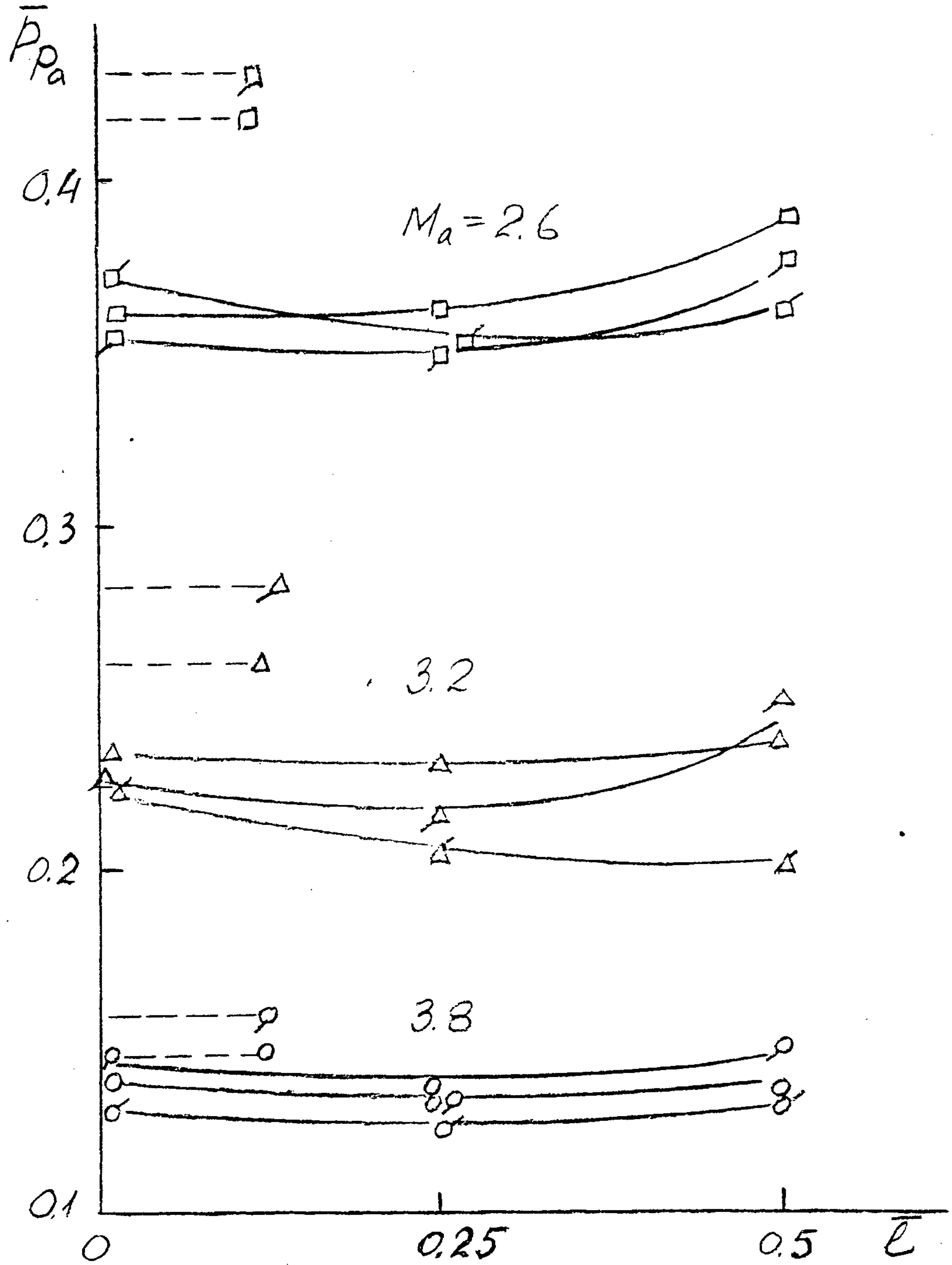

Fig. 3.1.13 Mean total pressure dependence on the grate width. Cylindric struts.
supersonic flow, pseudo-shock, - - - no struts.

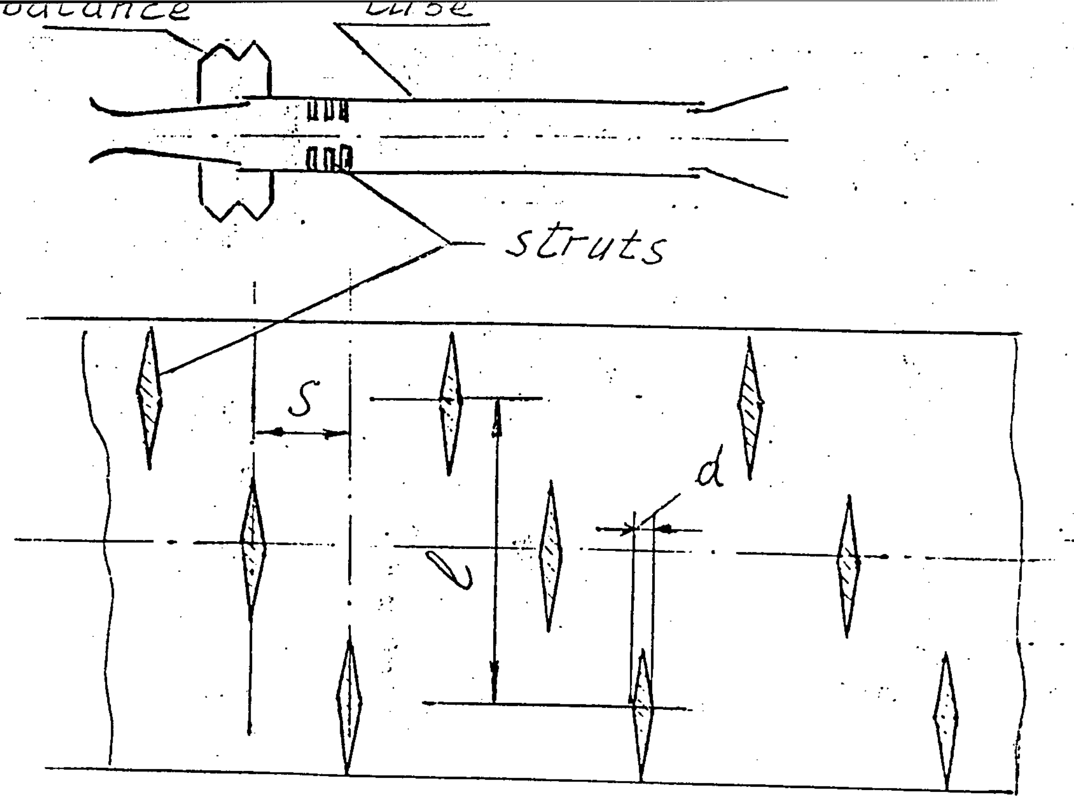

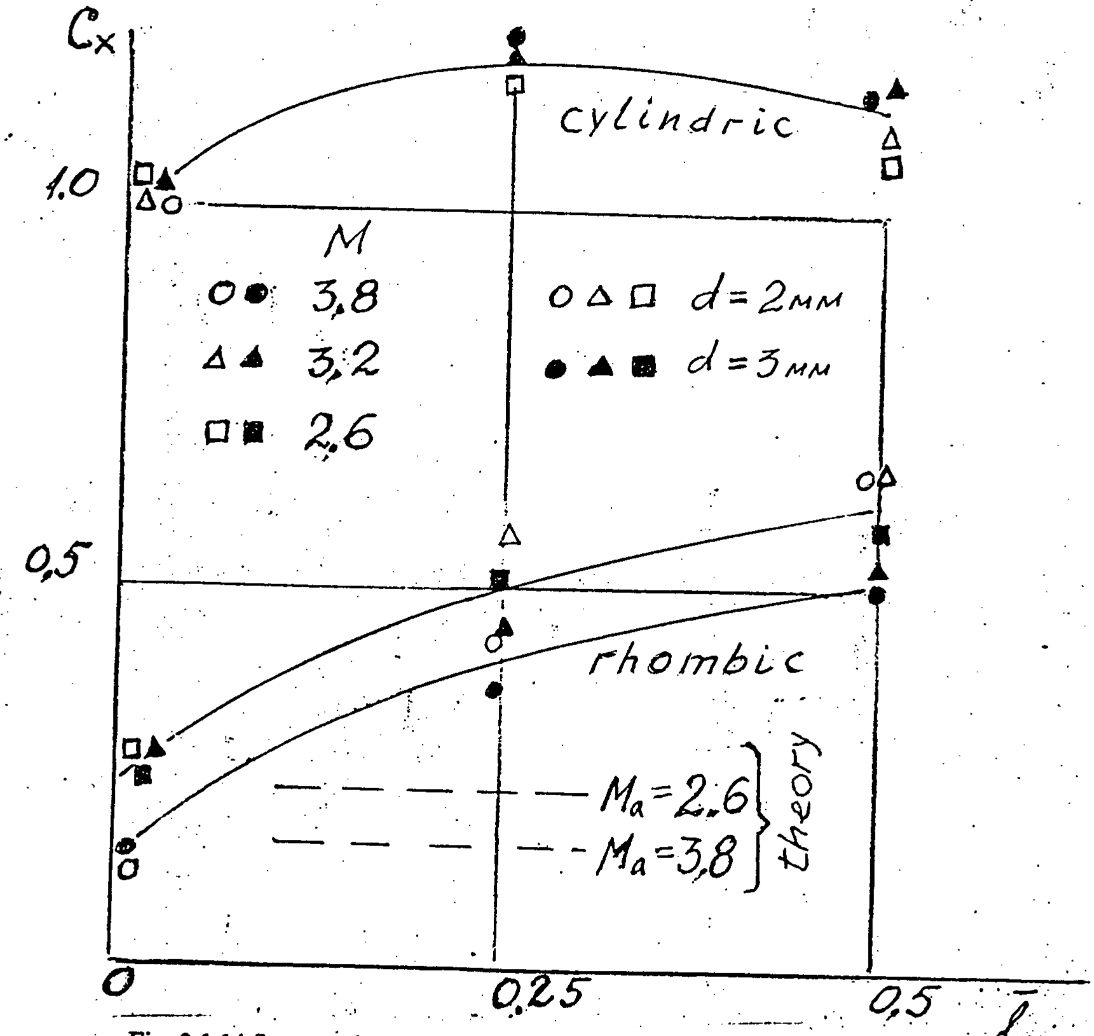

Fig. 3.1.14 Strut set drug coefficients versus width of the grate.

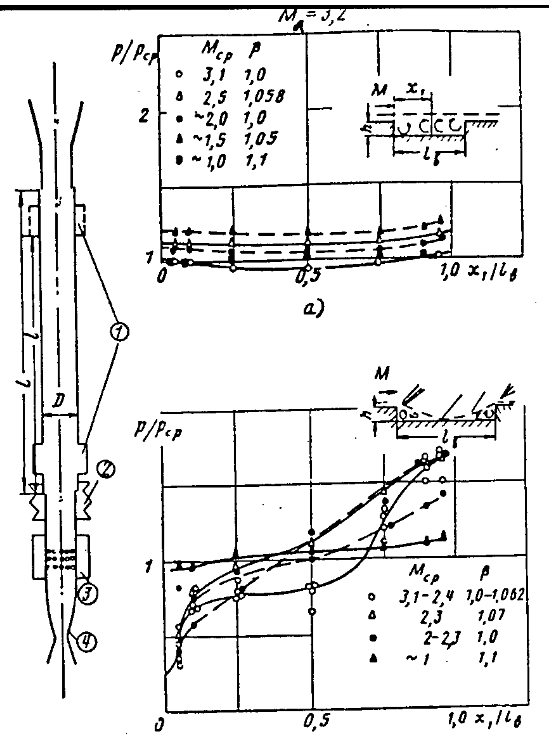

Fig. 3.2.1 Modele schematic. Pressure distribution along the cavity

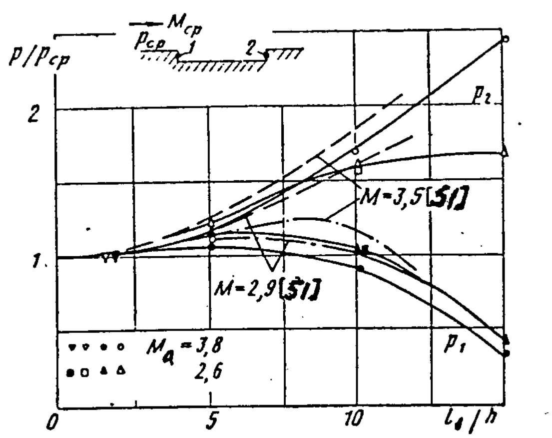

Fig. 3.2.2 Cavity forward and down facing step pressure versus l/h at d/R=0.2

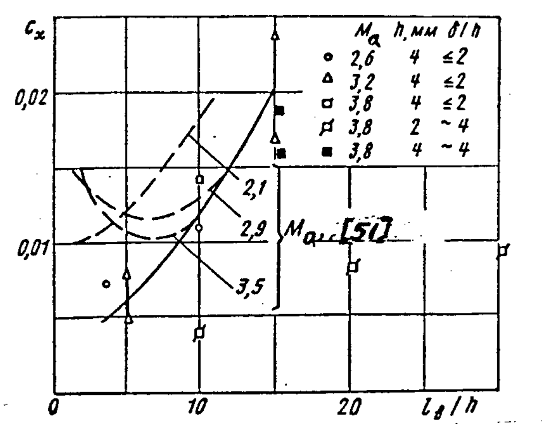

Fig. 3.2.3 Cavity drag coefficients comparison.

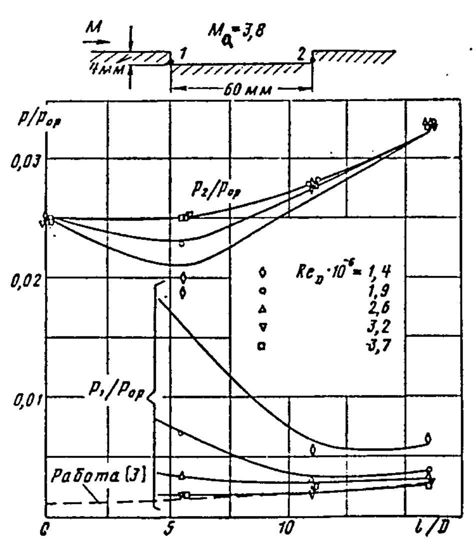

Fig. 3.2.4 Cavity forward and down facing step pressure at different Re.

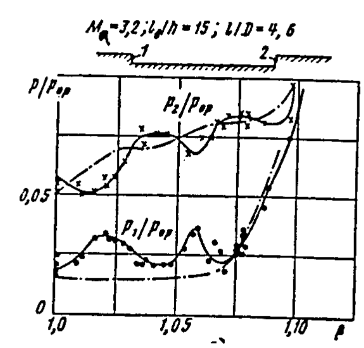

Fig. 3.2.5 Flow mode transformation due to jet injection in front of cavity.

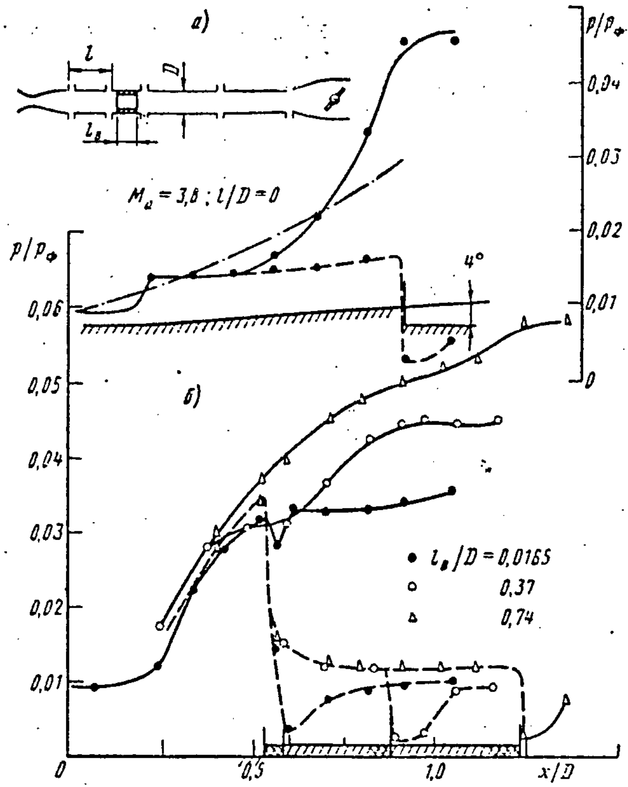

Fig. 3.3.1 Pressure distribution along obstacles.

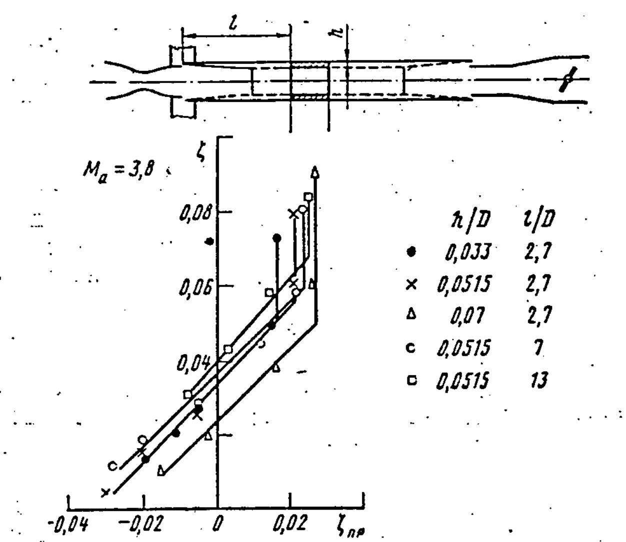

Fig. 3.3.2 Dependence of total force exerted to the tube on force exerted to the obstacle.

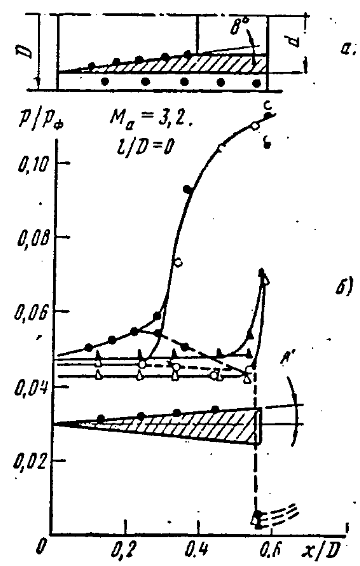

Fig. 3.3.3 Limiting pressure distributions along cowls.

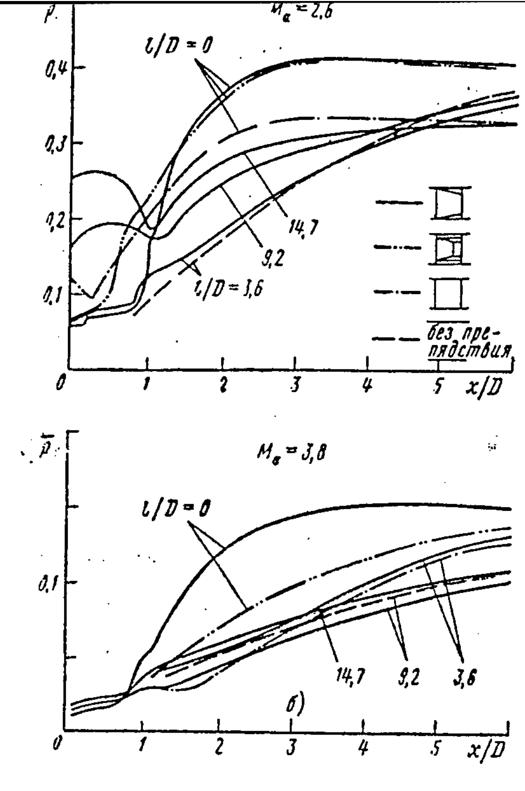

Fig. 3.3.4 Pressure distribution along tubes with obstacles.
1-obstacle removed.

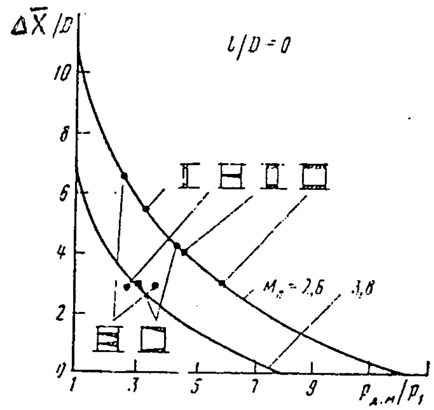

Fig. 3.3.5 Pseudo-shock length dependence on maximal pressure in the base region.

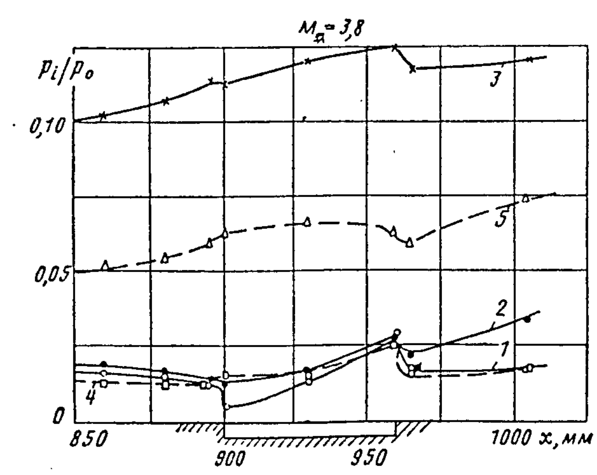

Fig. 3.3.6 Pressure distribution along the tube with a cavity.

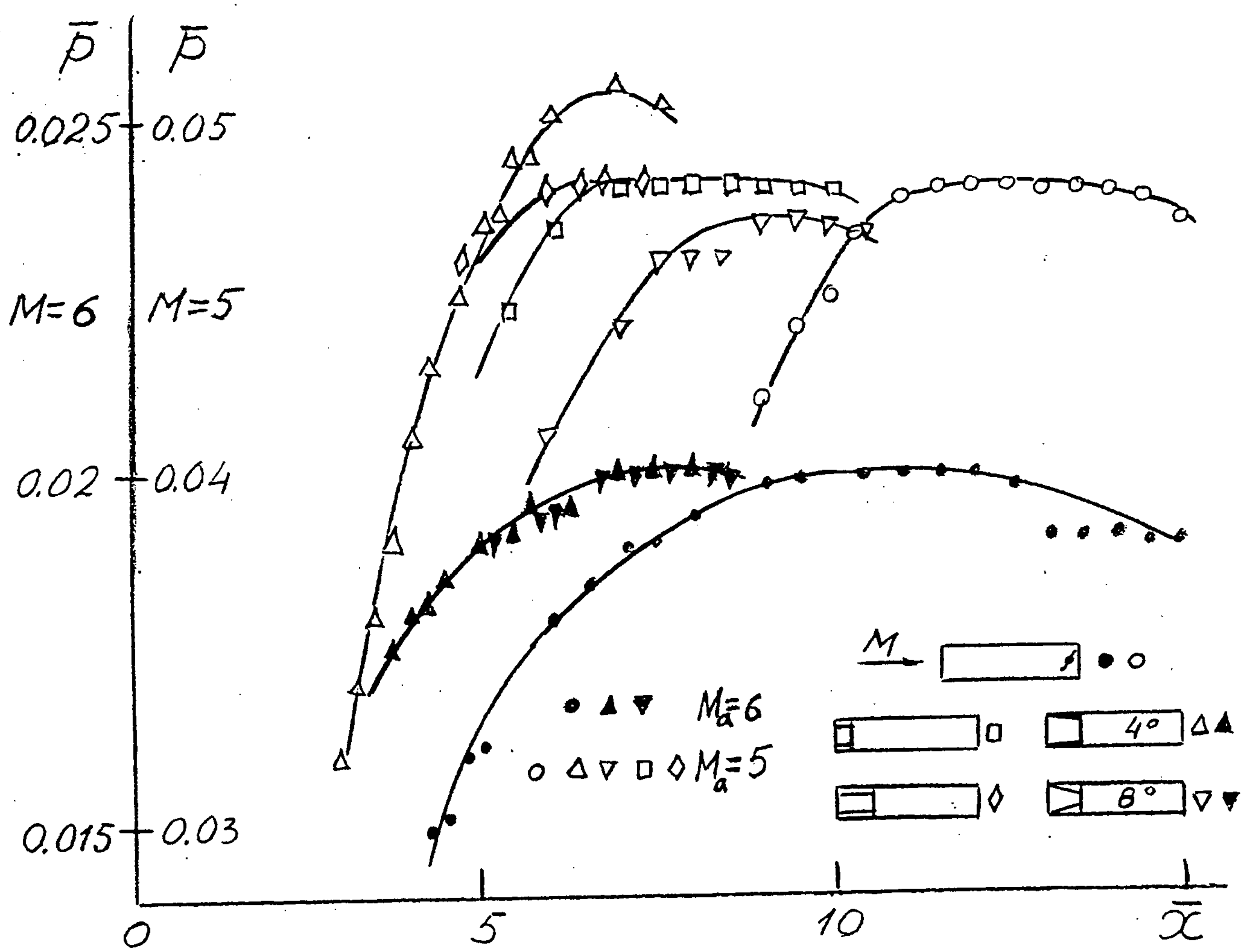

Fig. 3.3.7 Pressure distribution along rectangular duct with wedges installed on the walls.

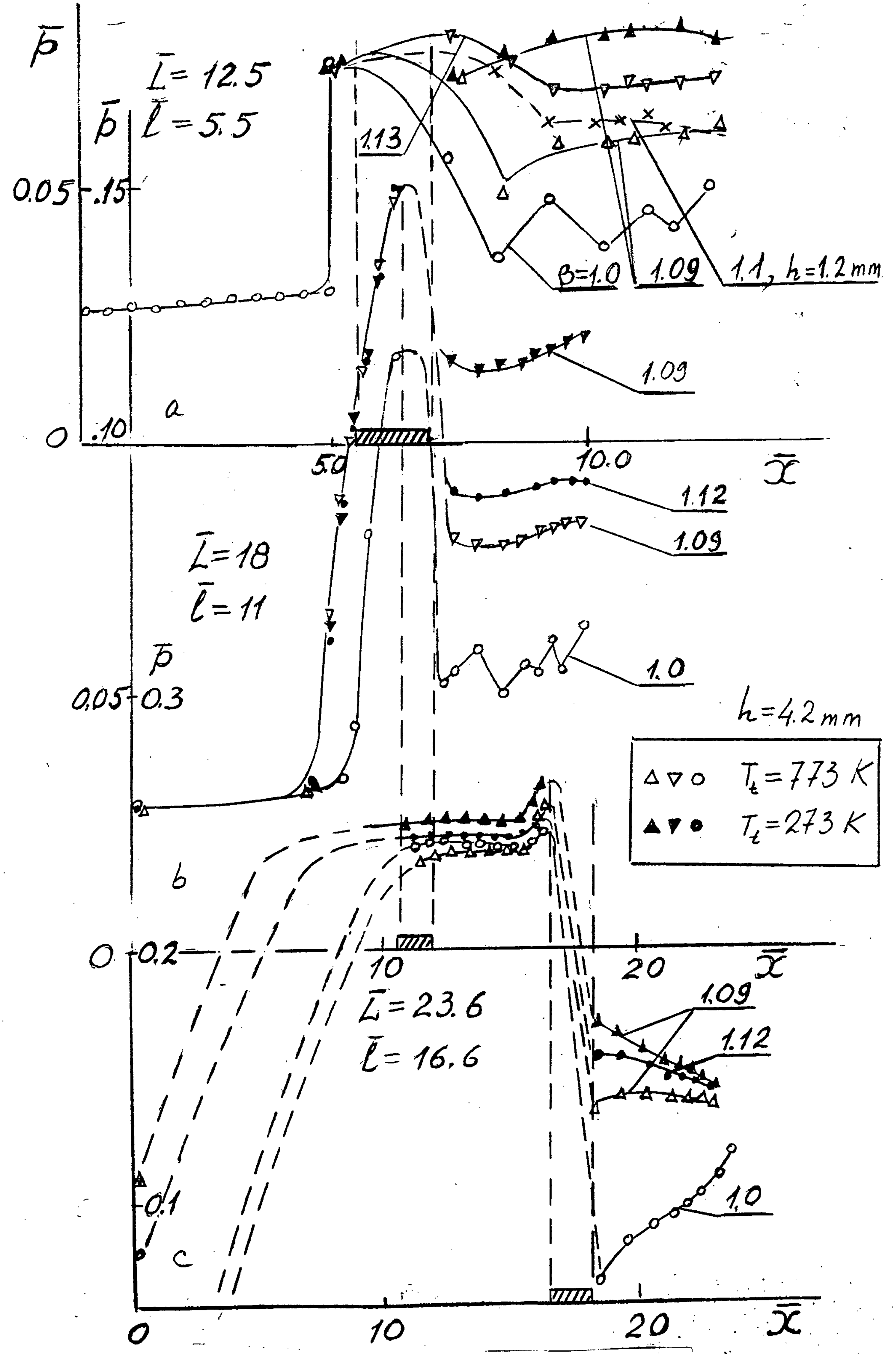

Fig.3.4.1 Pressure distribution in front of jut positioned at different parts of the tube and different β, Tt of jet

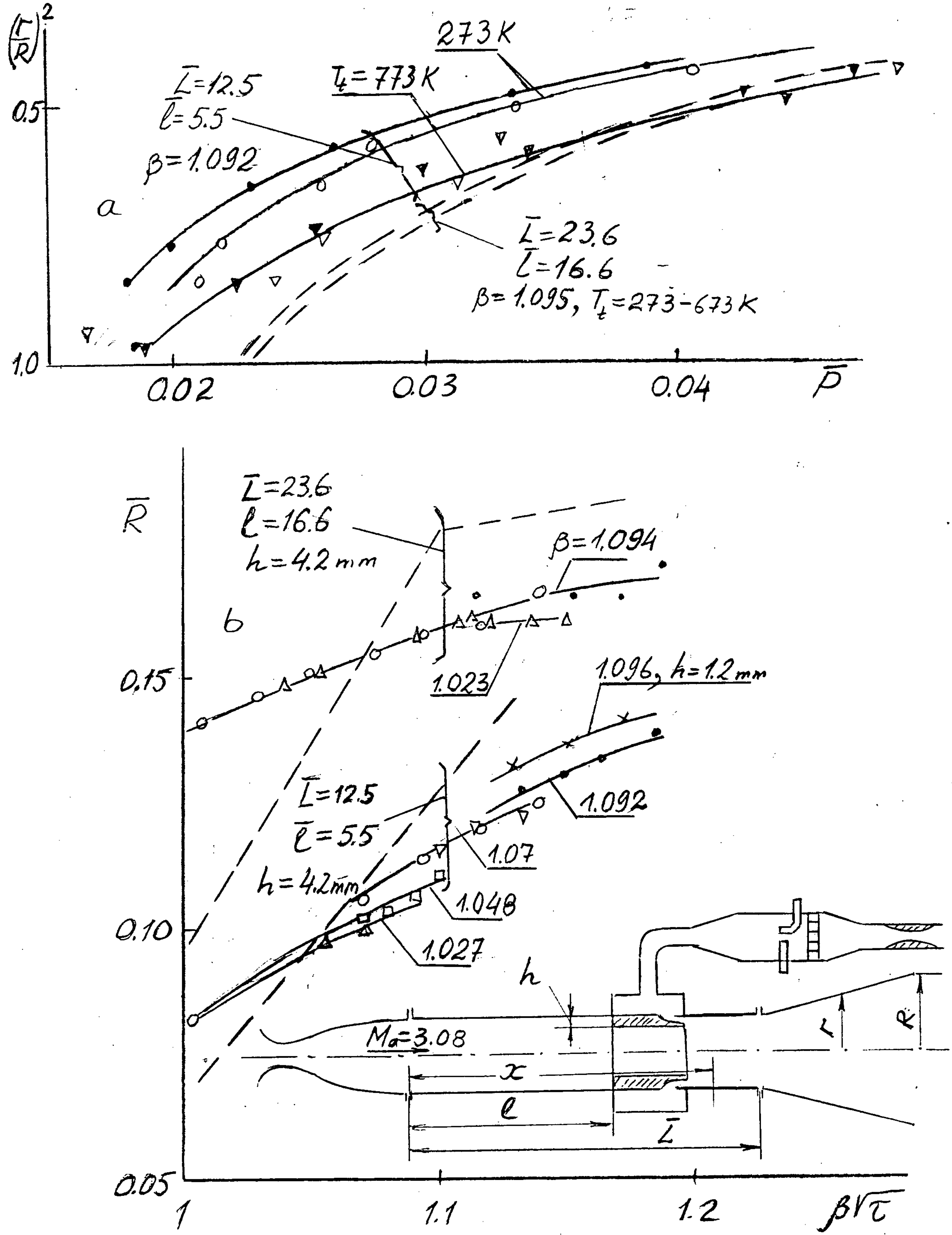

Fig.3.4.2 Pressure distribution and axial force acting on the conical section.

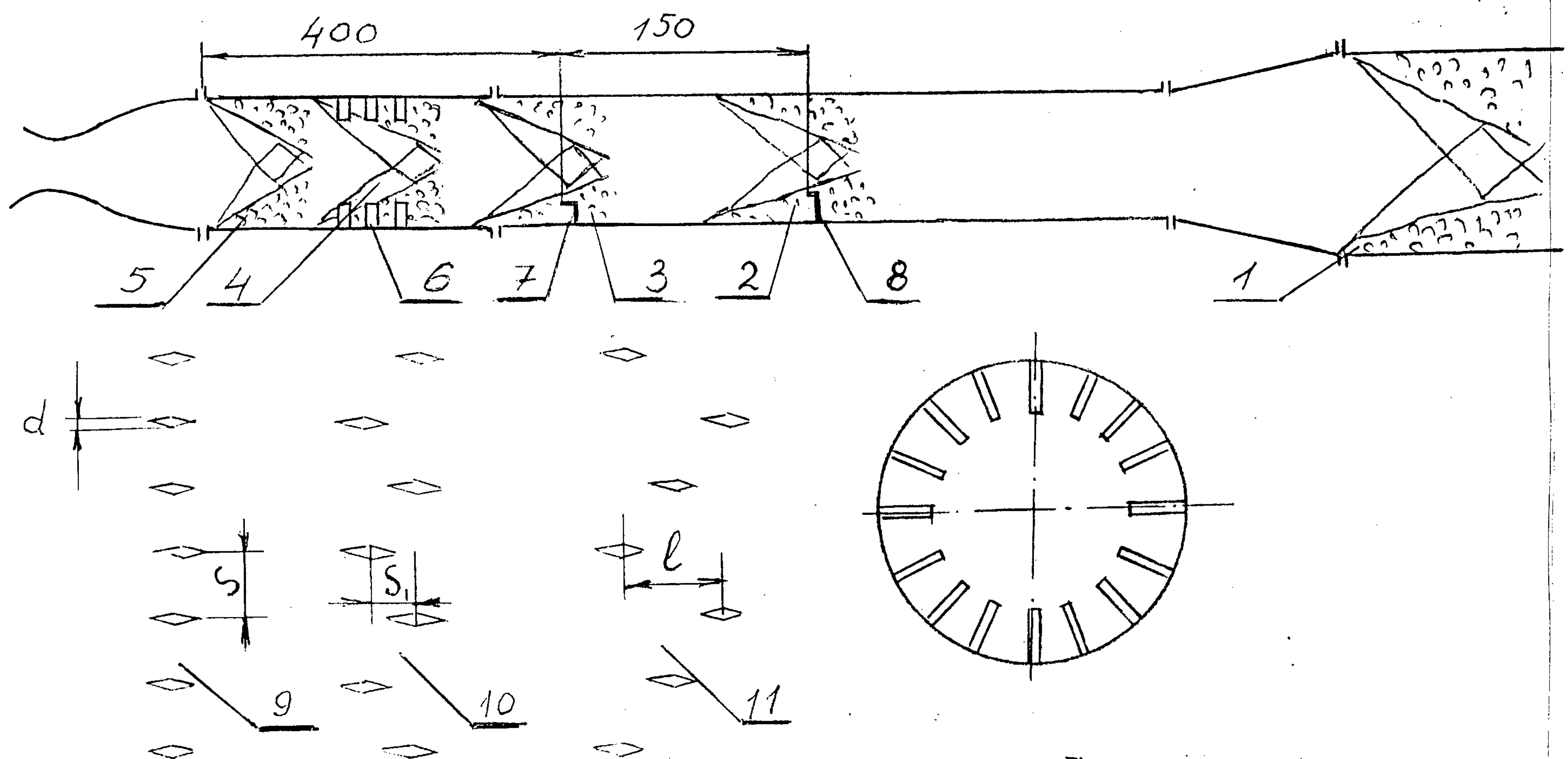

Fig.3.5.1 Model scematic.

1-5-numbers of regimes (pseudo-shock location)
6-set of struts, 7 - total pressure probe, first measurement section, 8 - second section, 9-11 -one, two, three- row strut sets

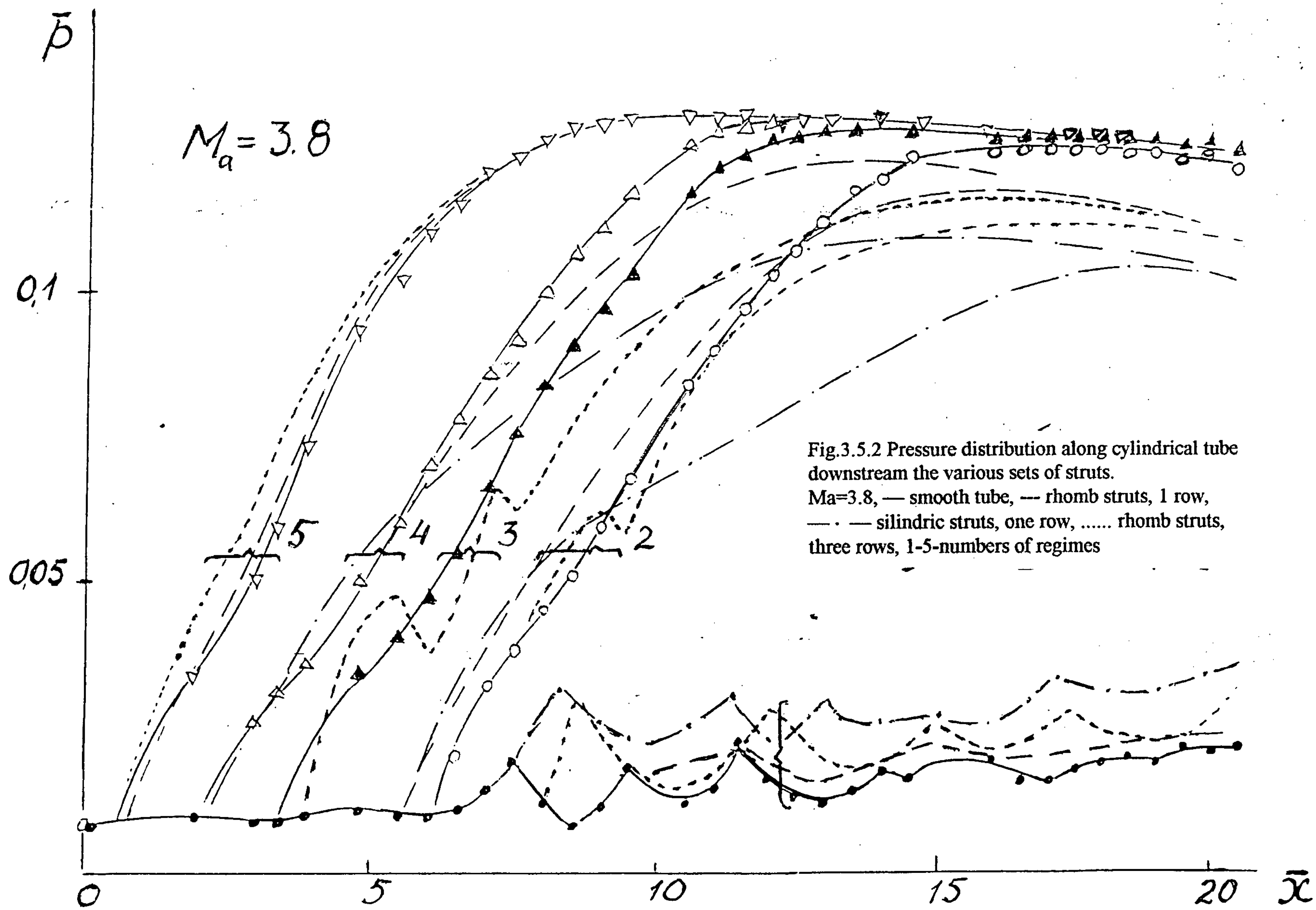

Fig.3.5.2 Pressure distribution along cylindrical tube downstream the various sets of struts.
Ma=3.8, — smooth tube, --- rhomb struts, 1 row, —·— silindric struts, one row, ... rhomb struts, three rows, 1-5-numbers of regimes

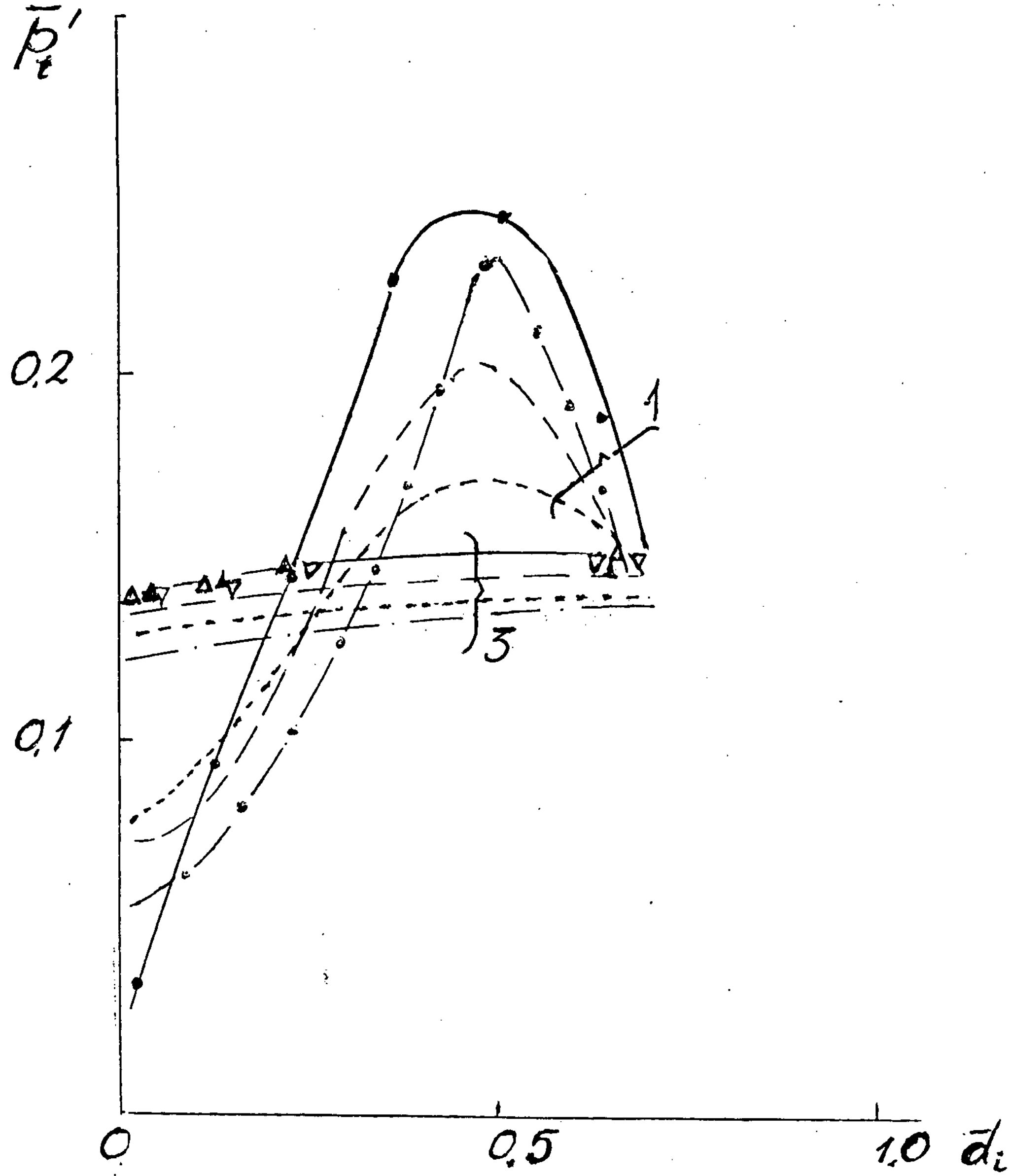

Fig.3.5.3 Total pressure fields at the end of the tube. Ma=3.8, — smooth tube, --- rhomb struts, 1 row, — · — silindric struts, one row, ... rhomb struts, three rows, 1, 3-numbers of regimes

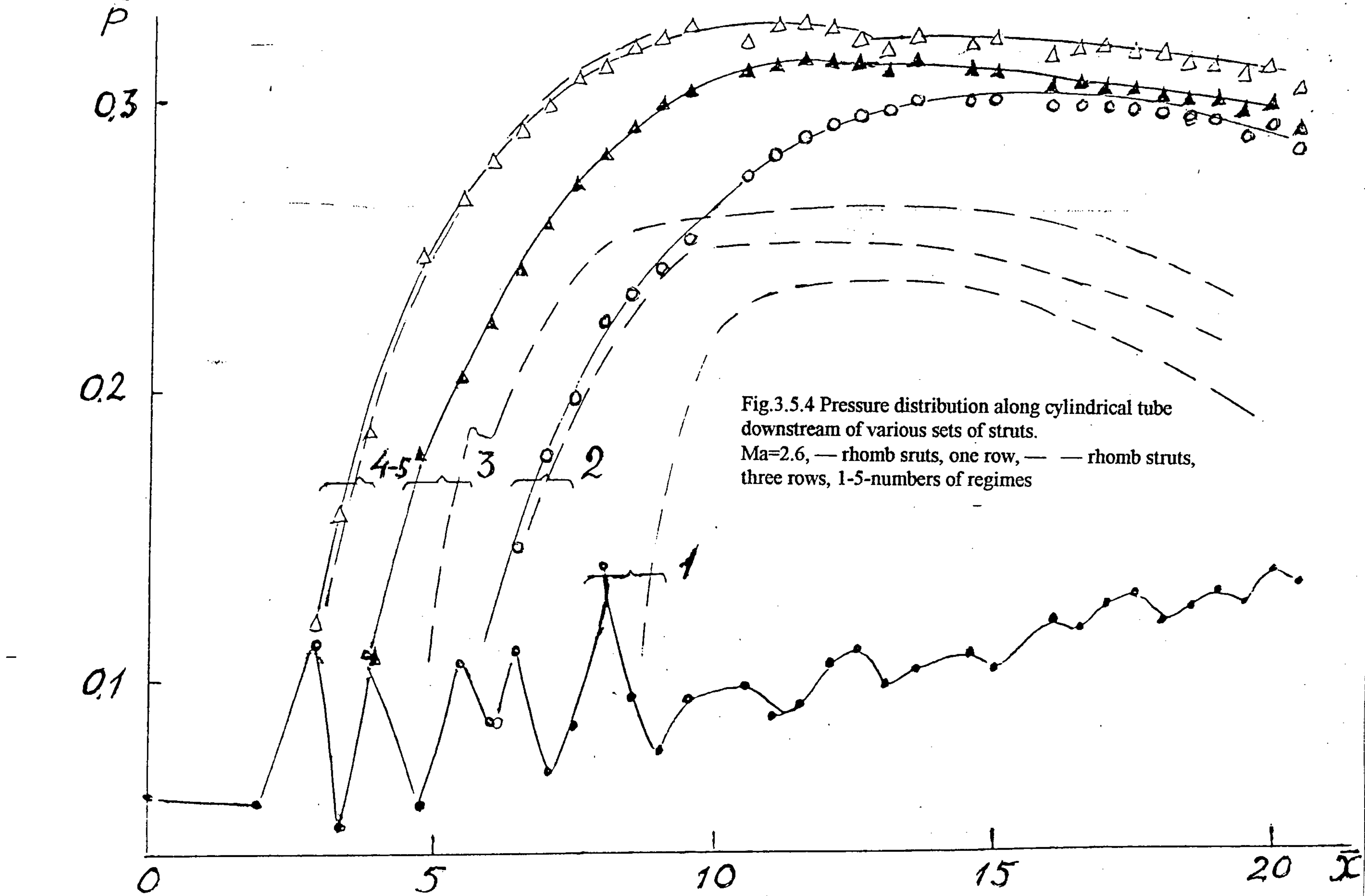

Fig.3.5.4 Pressure distribution along cylindrical tube downstream of various sets of struts.
Ma=2.6, — rhomb sruts, one row, — — rhomb struts, three rows, 1-5-numbers of regimes

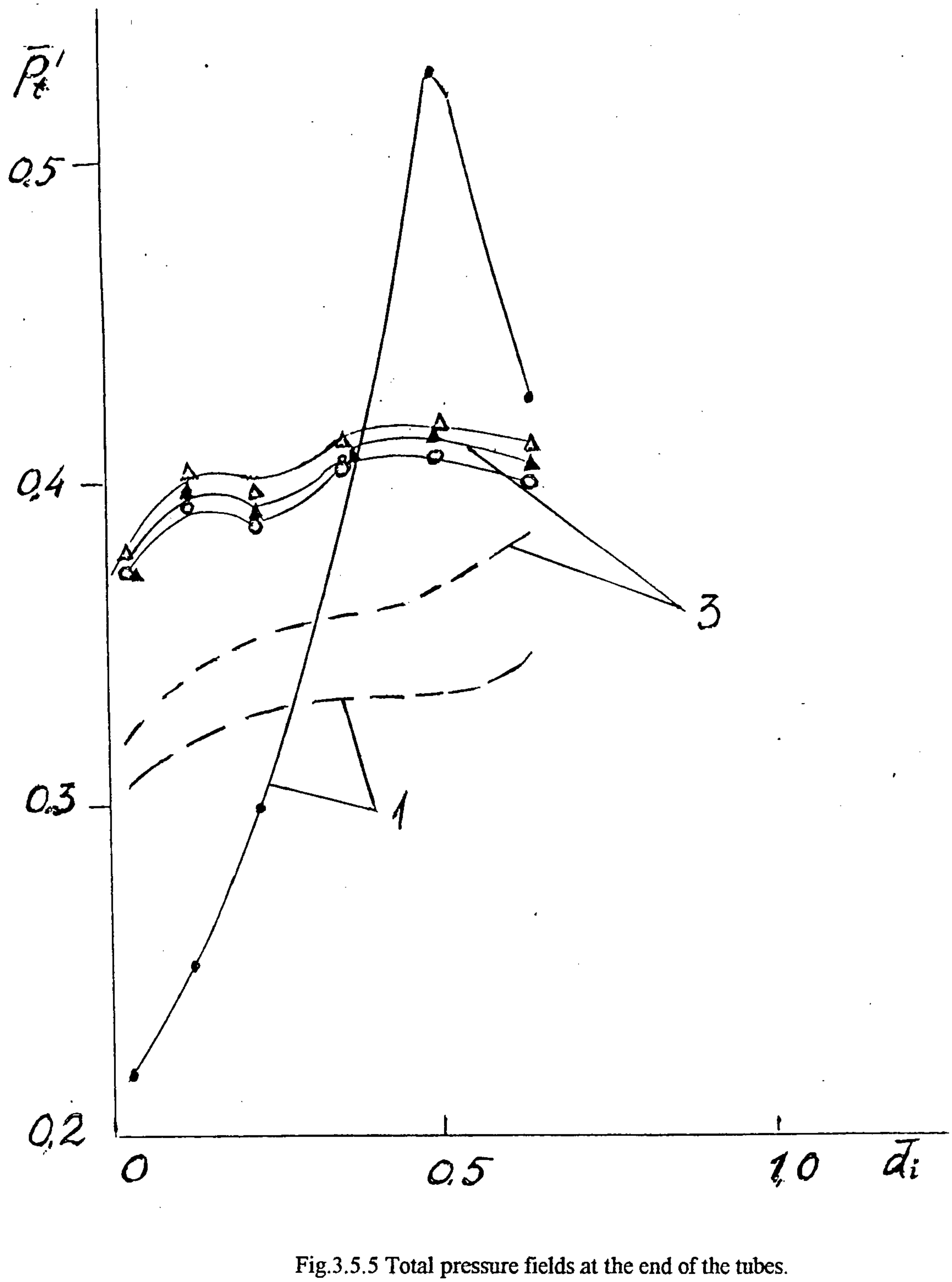

Fig.3.5.5 Total pressure fields at the end of the tubes. Ma=2.6, — rhomb sruts, one row, — — rhomb struts, three rows, 1-5-numbers of regimes

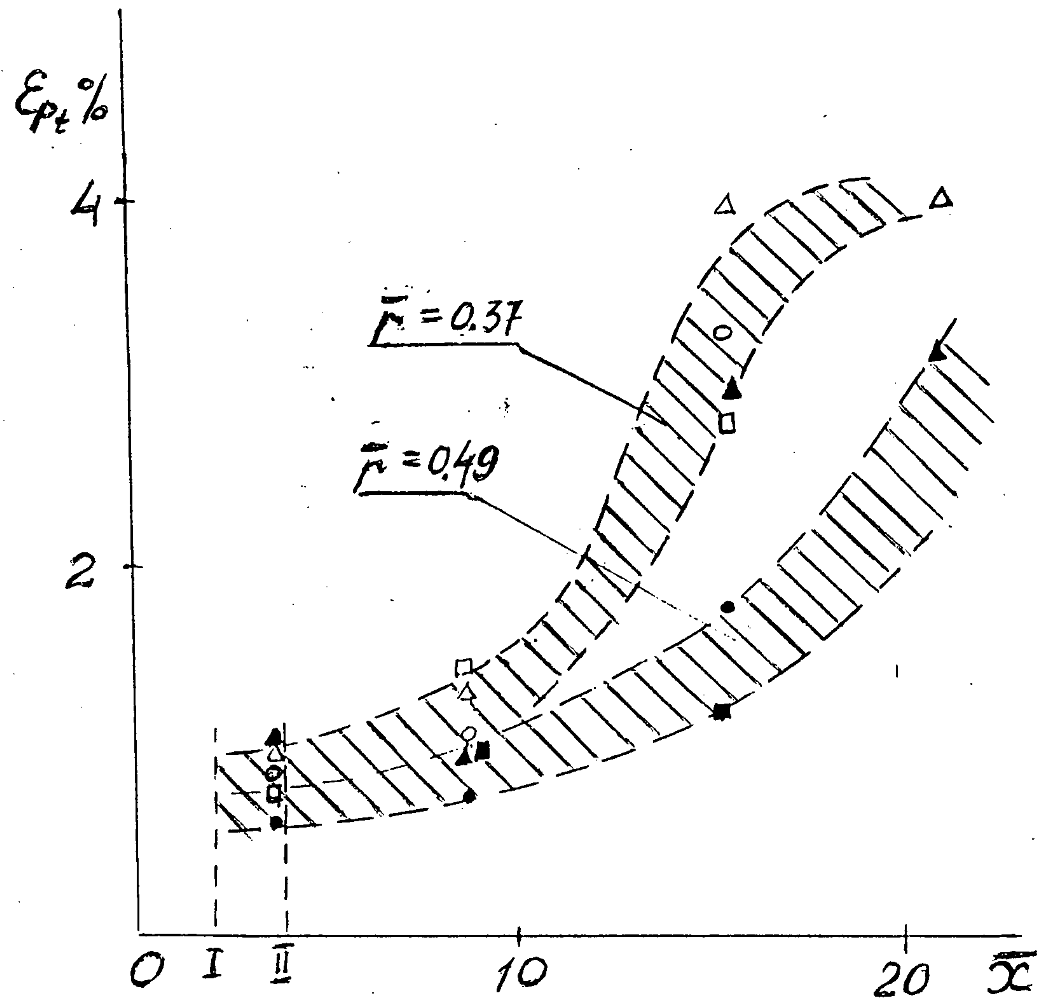

Fig.3.5.6 Total pressure pulsation intensity - e_{p_t} along the tube at two distances from the wall.
smooth tube,○● -Ma=2.6, □■ -3.2, △▲ 3.8

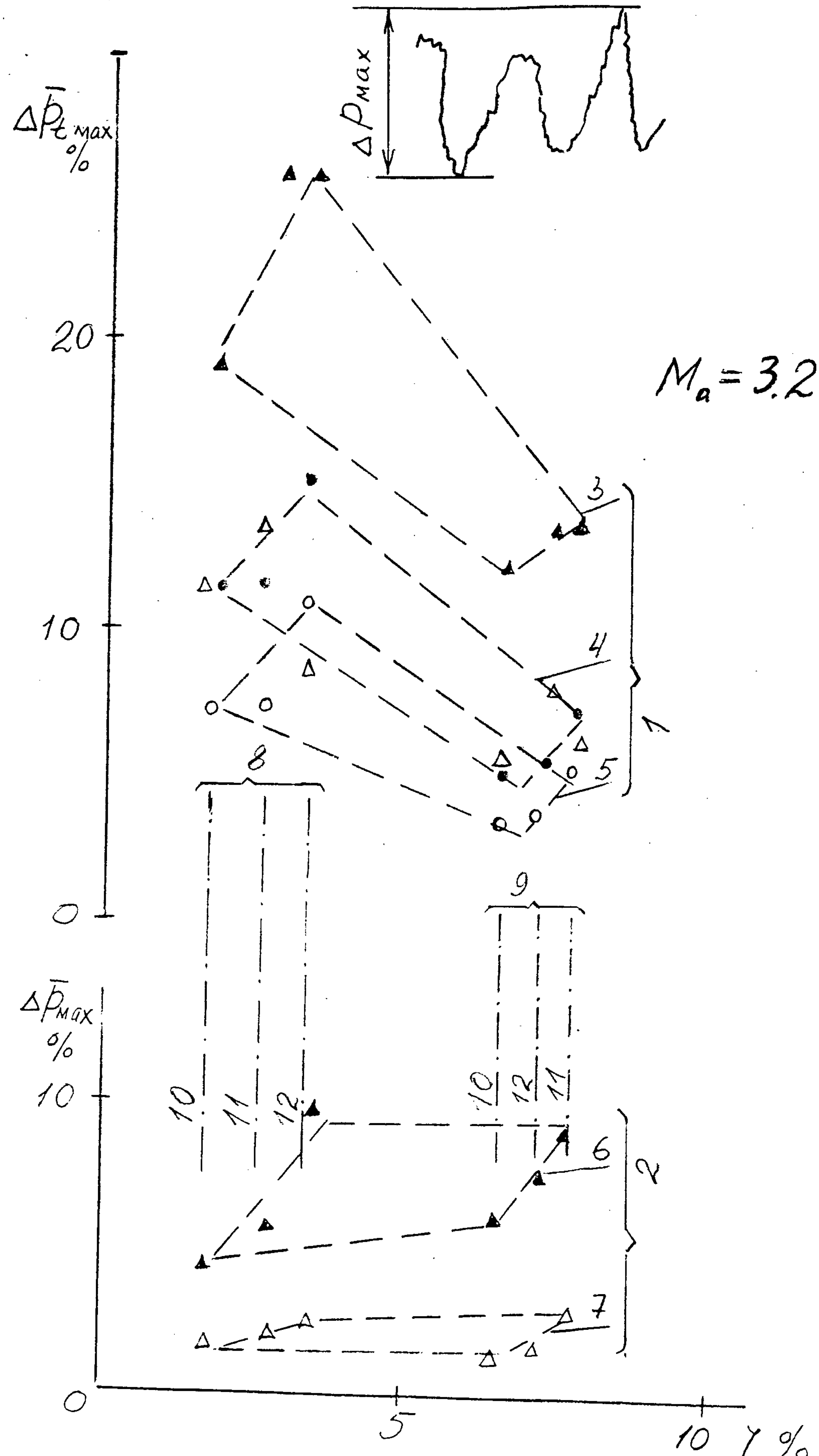

Fig.3.5.7 Maximal pressere pulsation amplitude versus impulse loss coefficient.
1-pseudo-shock, 2-supersonic flow, 3-regime 4, section 2, 4- r.4, s.1, 5- r.5, s.2, 5-r.5, s.1, 6-sec. 2, 7- s.1, 8- rhombs, 9- cylinders, 10- 1 row, 11-2 r, 12- 3r.

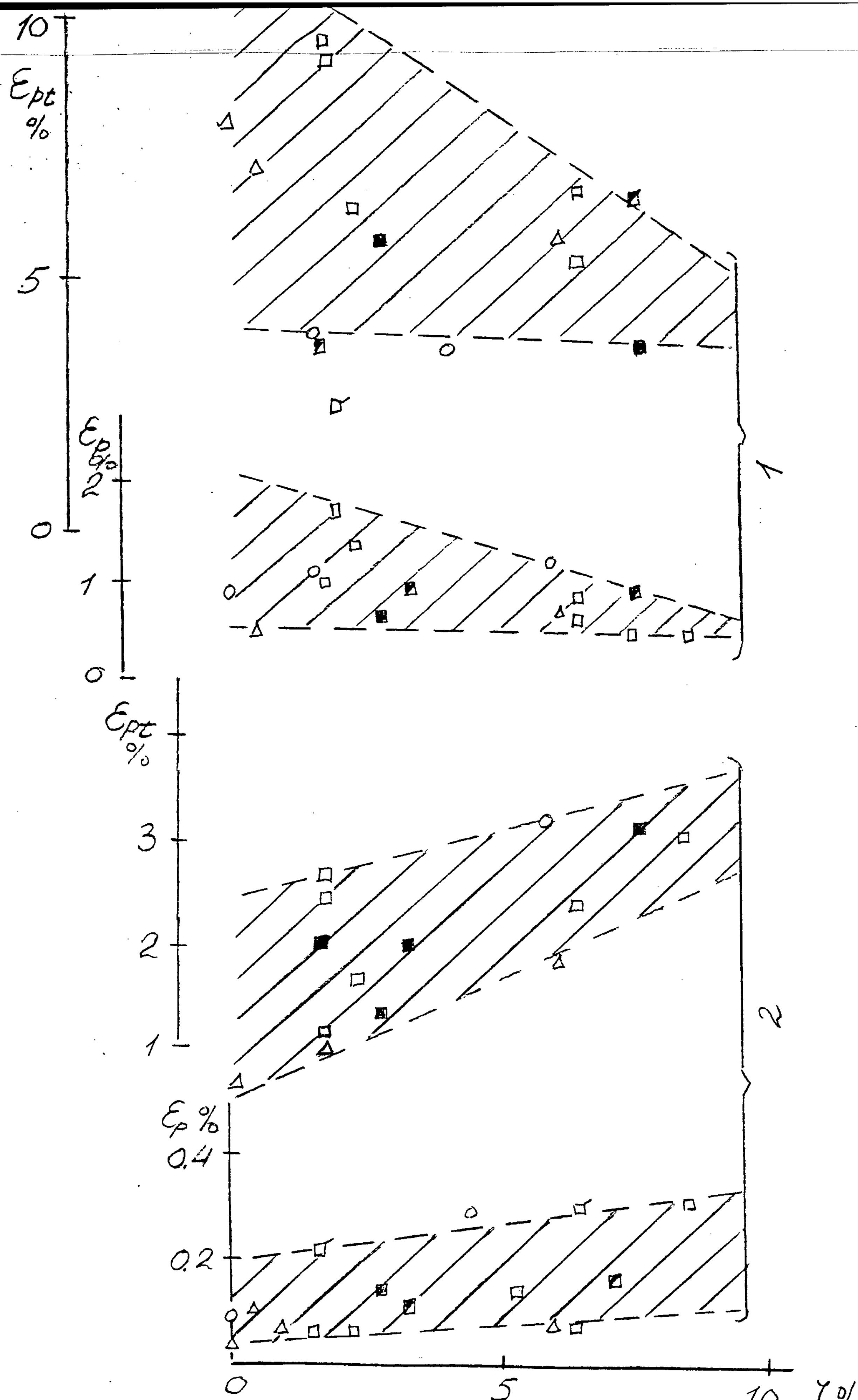

Fig.3.5.8 Pressure pulsation intensity versus impulse loss coefficient
1- pseudo-shock, 2- supersonic flow

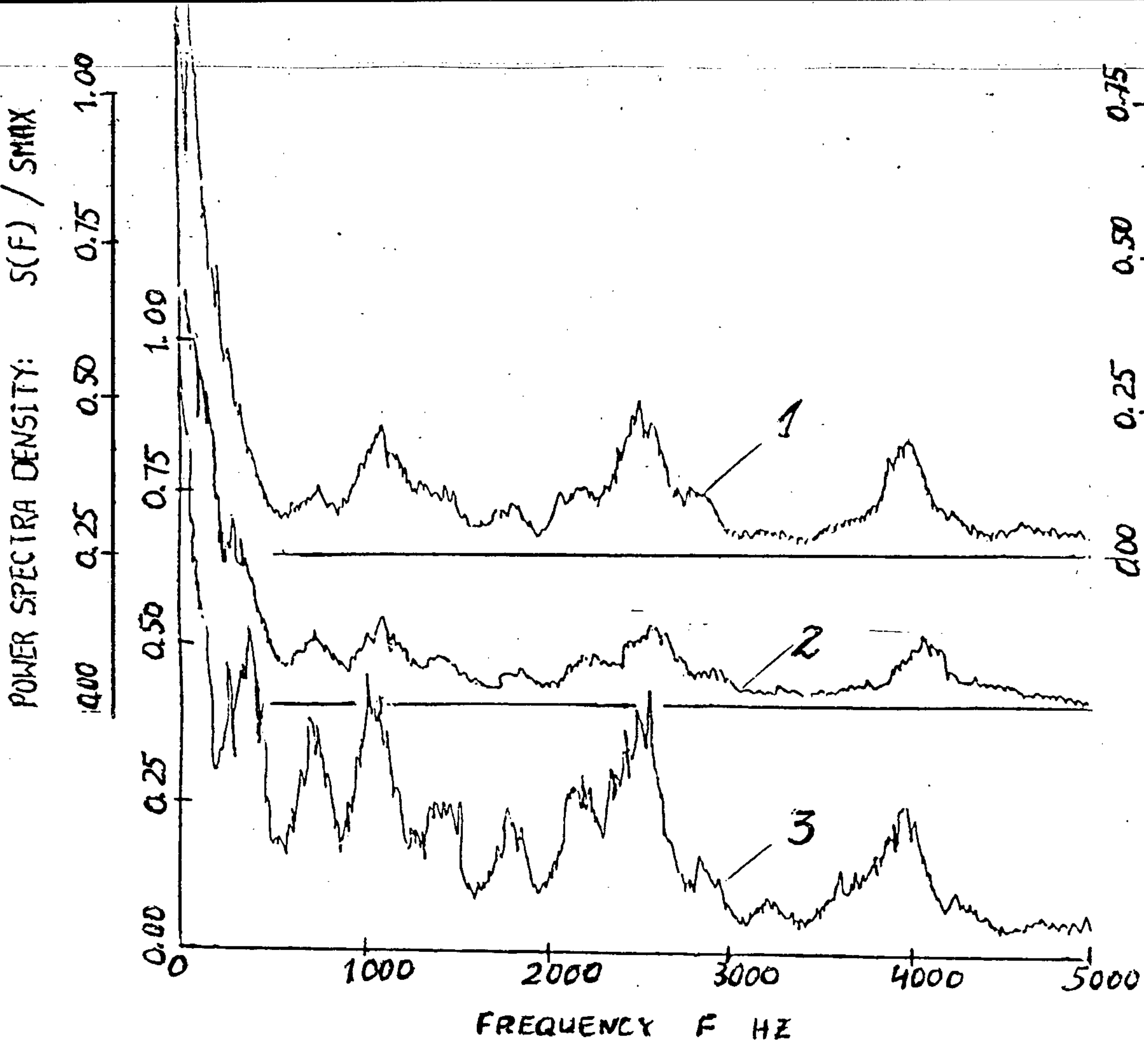

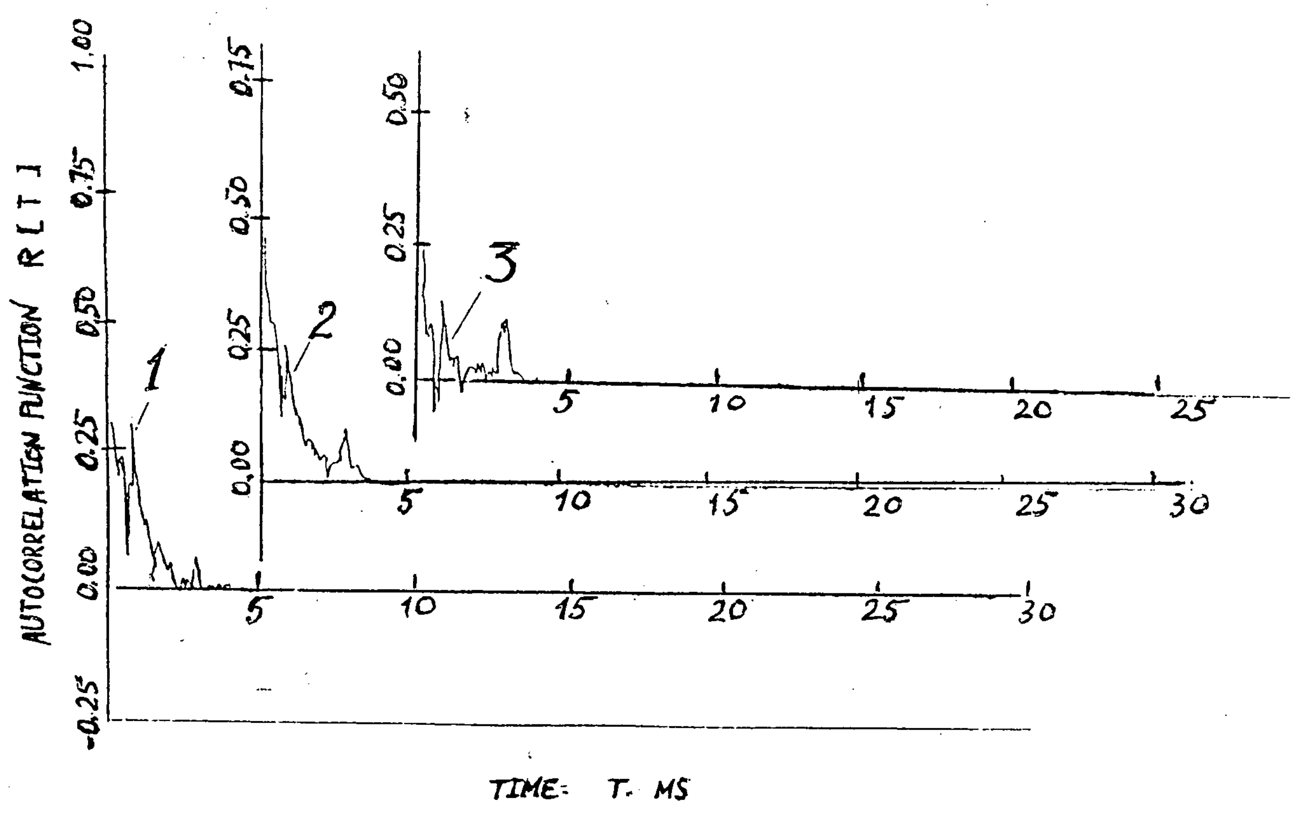

Fig.3.5.9 Power spectra density vrs. frequency.
Autocorrelation function vrs. time.
1- no struts, 2- rhomb struts, 1 row, 3- cilindric struts, 1 row
Ma=3.8, supersonic flow, total pressure pulsations, I section

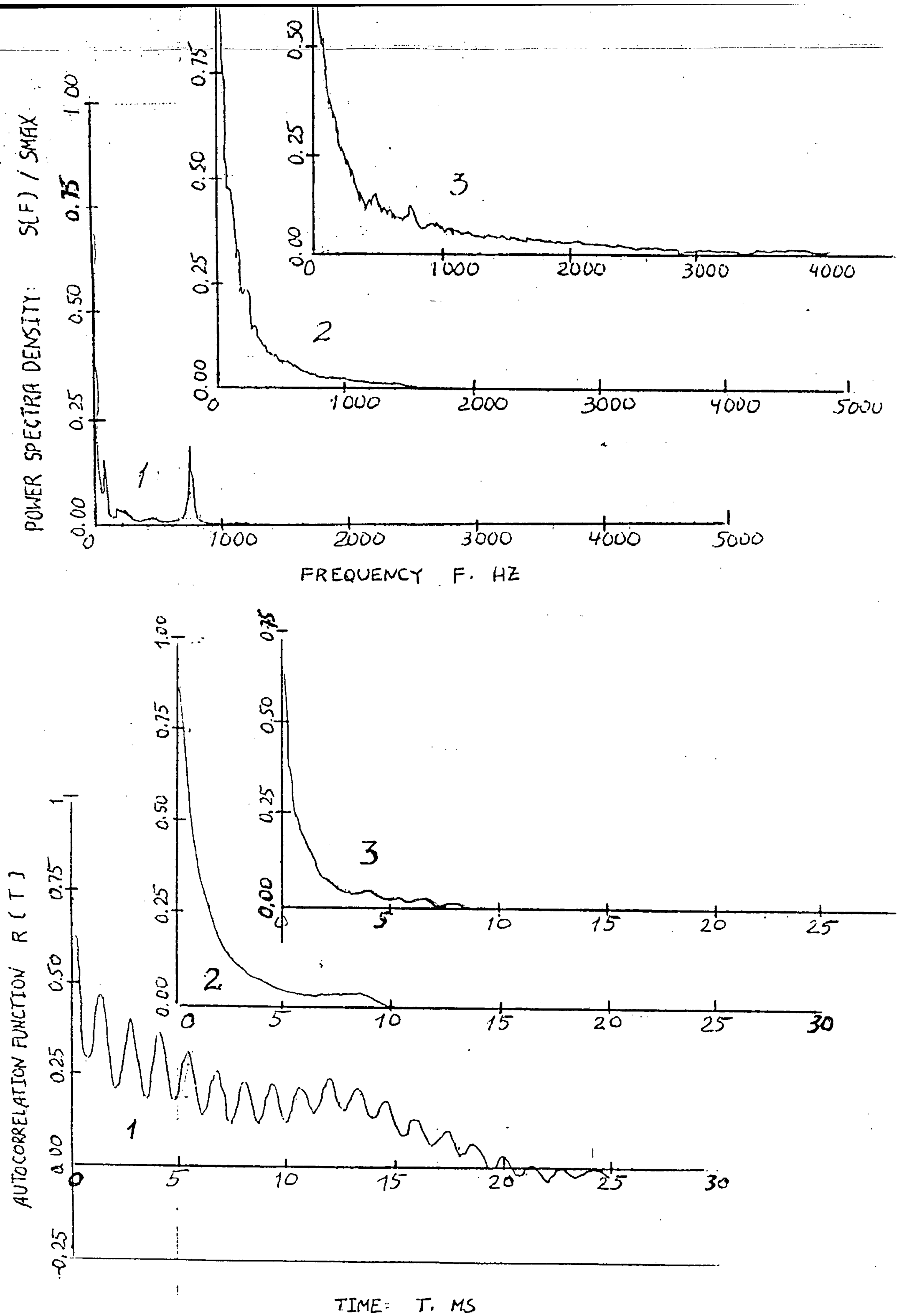

Fig.3.5.10 Power spectra density vrs. frequency.
Autocorrelation function vrs. time.
1- no struts, 2- rhomb struts, 1 row, 3- cilindric struts, 1 row
Ma=3.8, supersonic flow, static pressure pulsations, I section

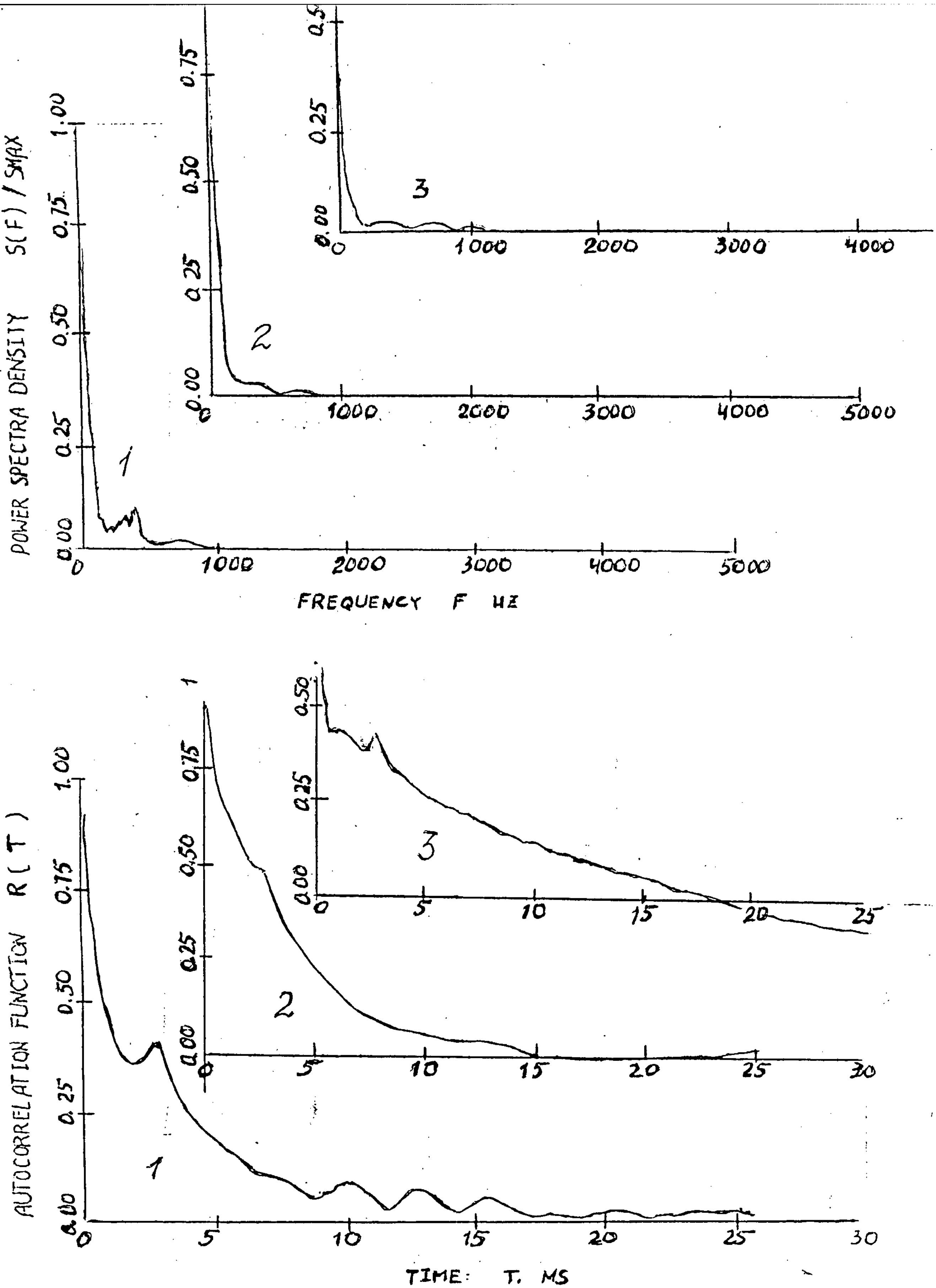

Fig.3.5.11 Power spectra density vrs. frequency.
Autocorrelation function vrs. time.
1- no struts, 2- rhomb struts, 1 row, 3- cilindric struts, 1 row
Ma=3.8, pseudo-shock, r.3, total pressure pulsations, I section

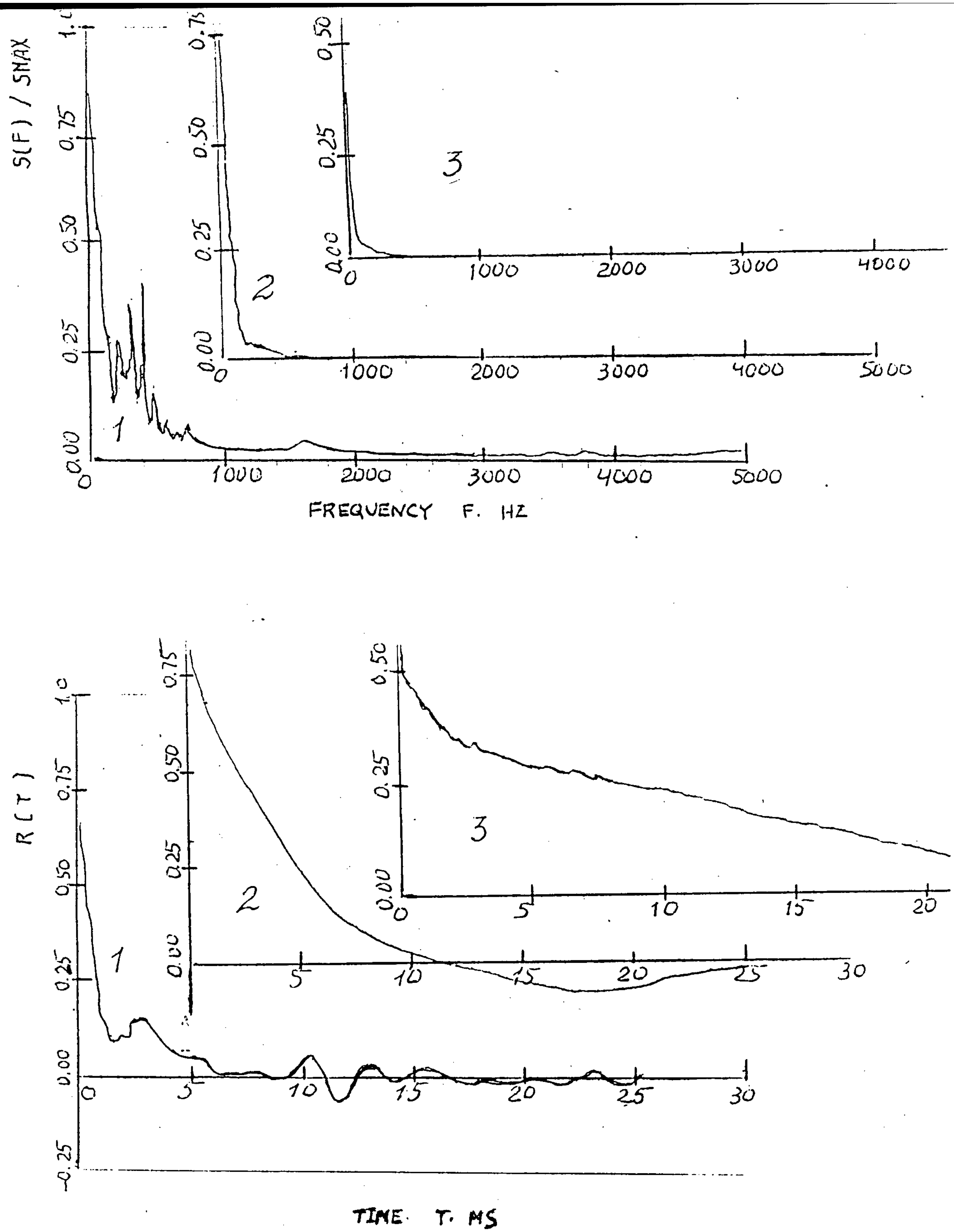

Fig.3.5.12 Power spectra density vrs. frequency.
Autocorrelation function vrs. time.
1- no struts, 2- rhomb struts, 1 row, 3- cilindric struts, 1 row
Ma=3.8, pseudo-shock, r.3, static pressure pulsations, I section

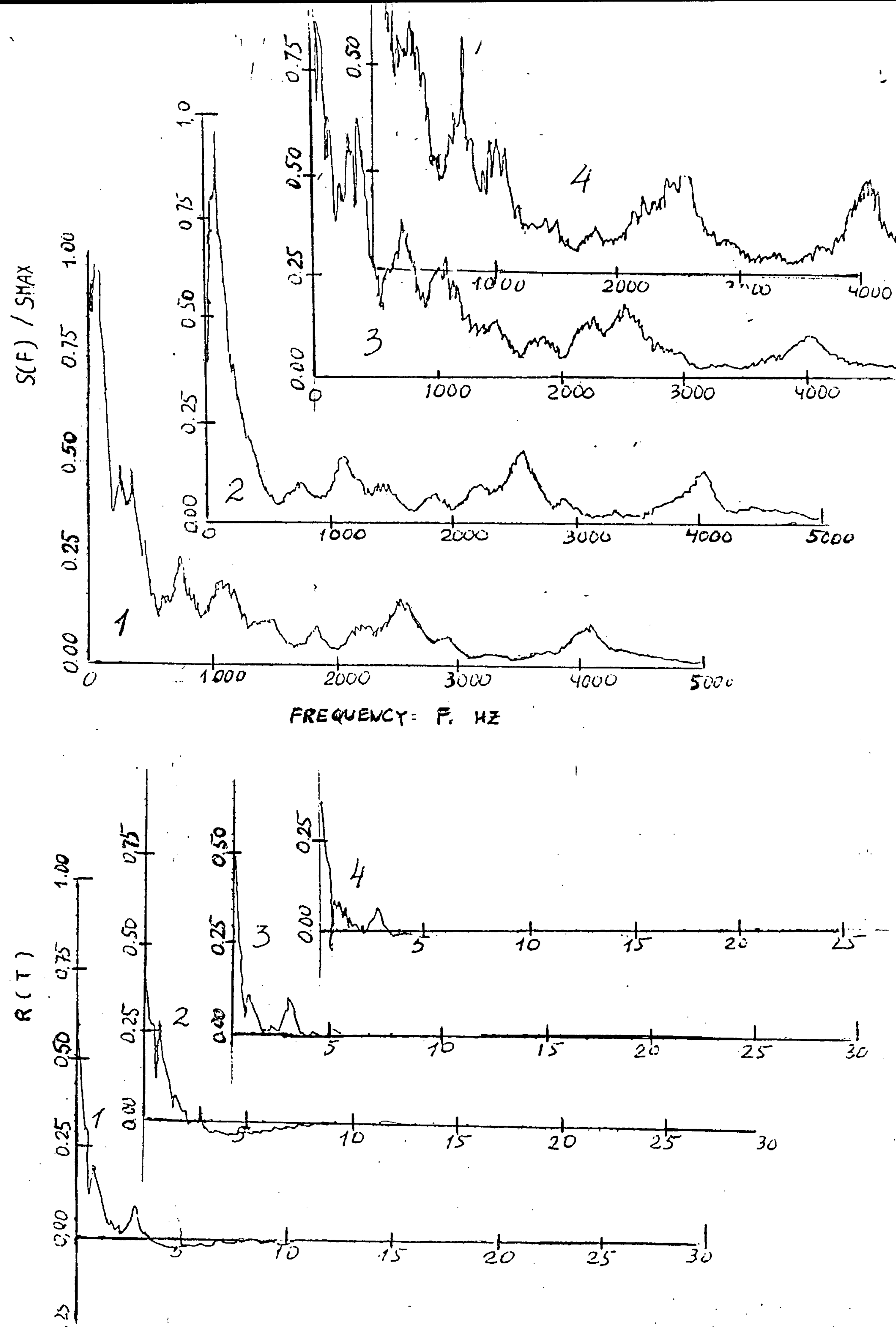

Fig.3.5.13 Power spectra density vrs. frequency.
Autocorrelation function vrs. time.
rhomb struts, 3 mm,1- 1 row, 2 two rows, 3- three rows
4- one row, II section

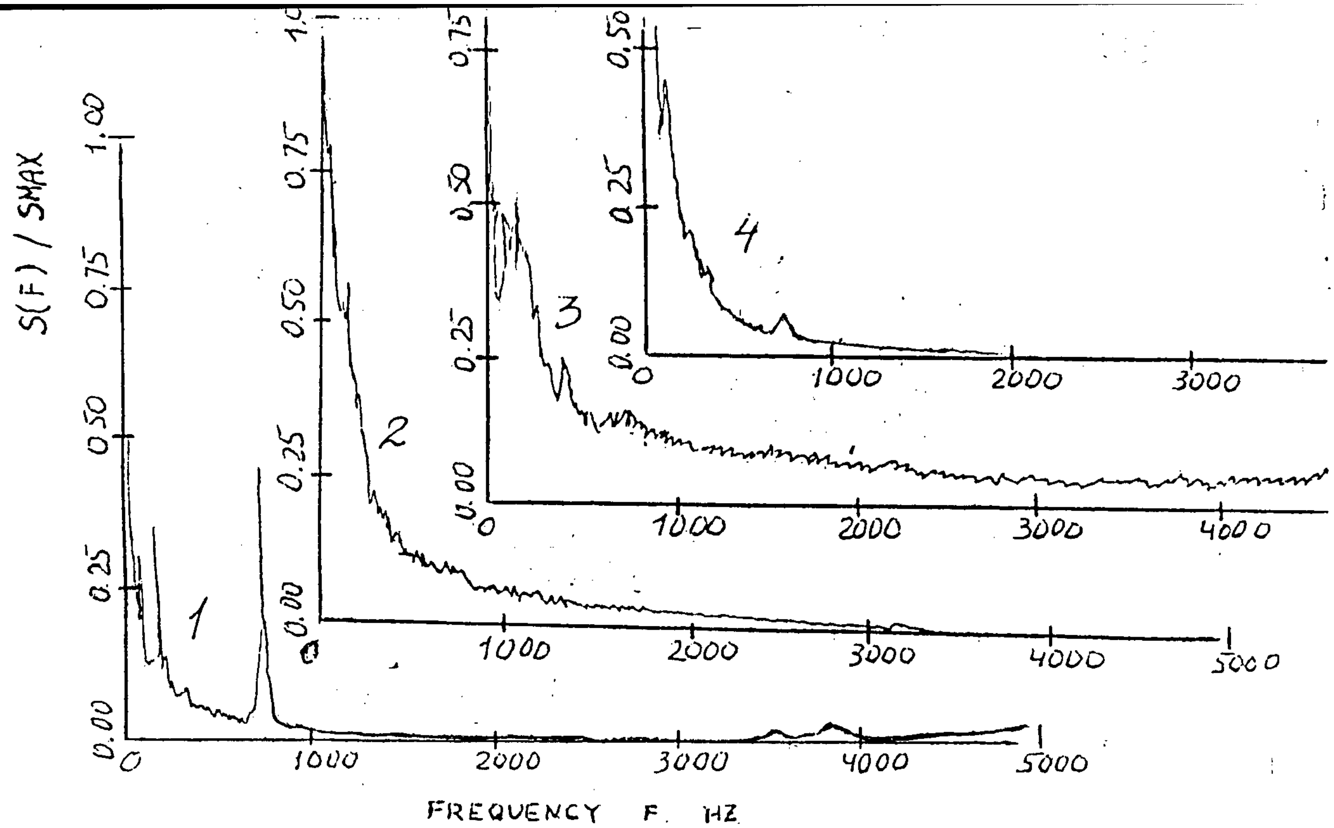

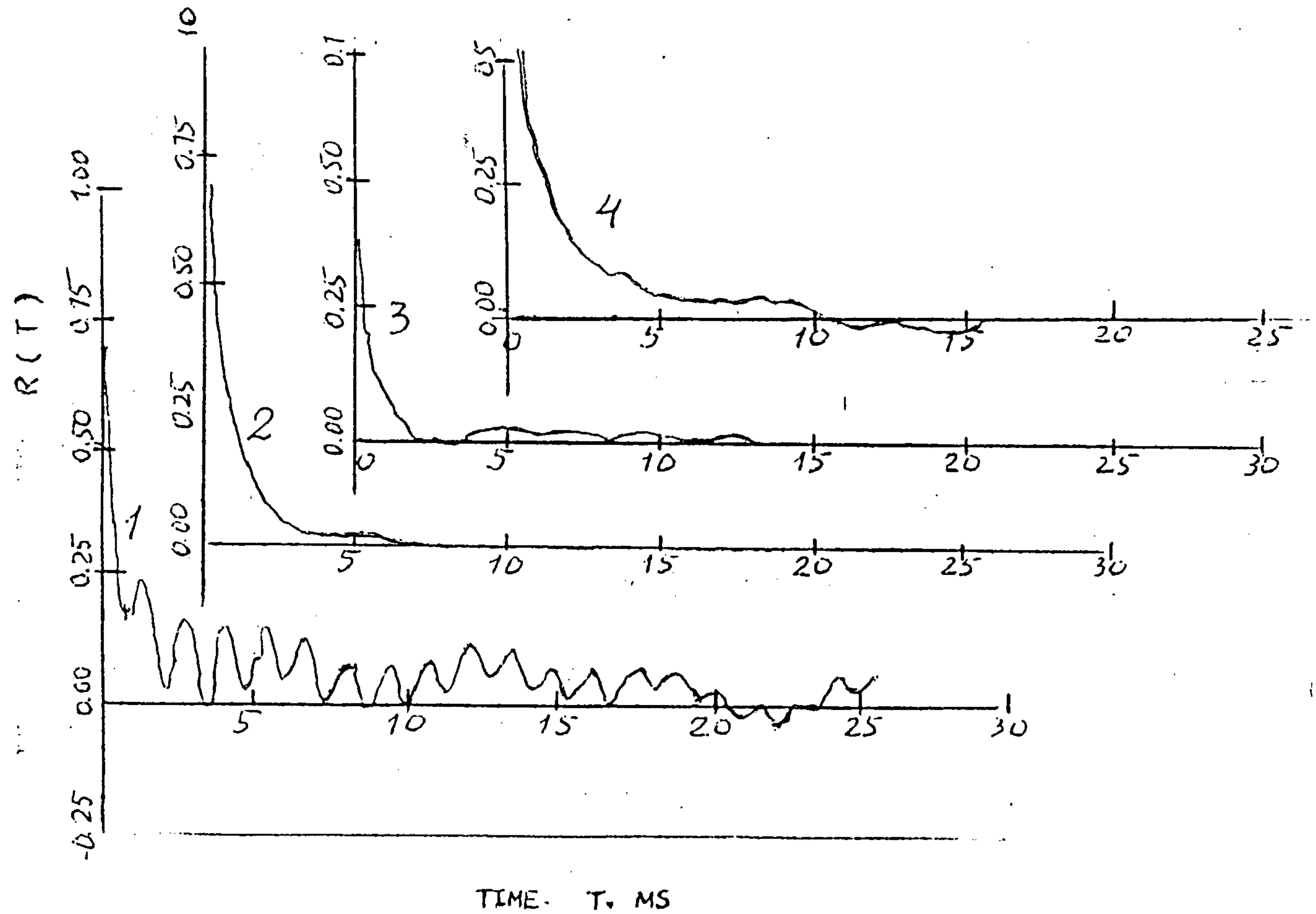

Fig.3.5.14 Power spectra density vrs. frequency.
Autocorrelation function vrs. time.
rhomb struts, 3 mm,1- 1 row, 2 two rows, 3- three rows
4- one row, II section
Ma=3.2, supersonic flow, static pressure pulsations, I section

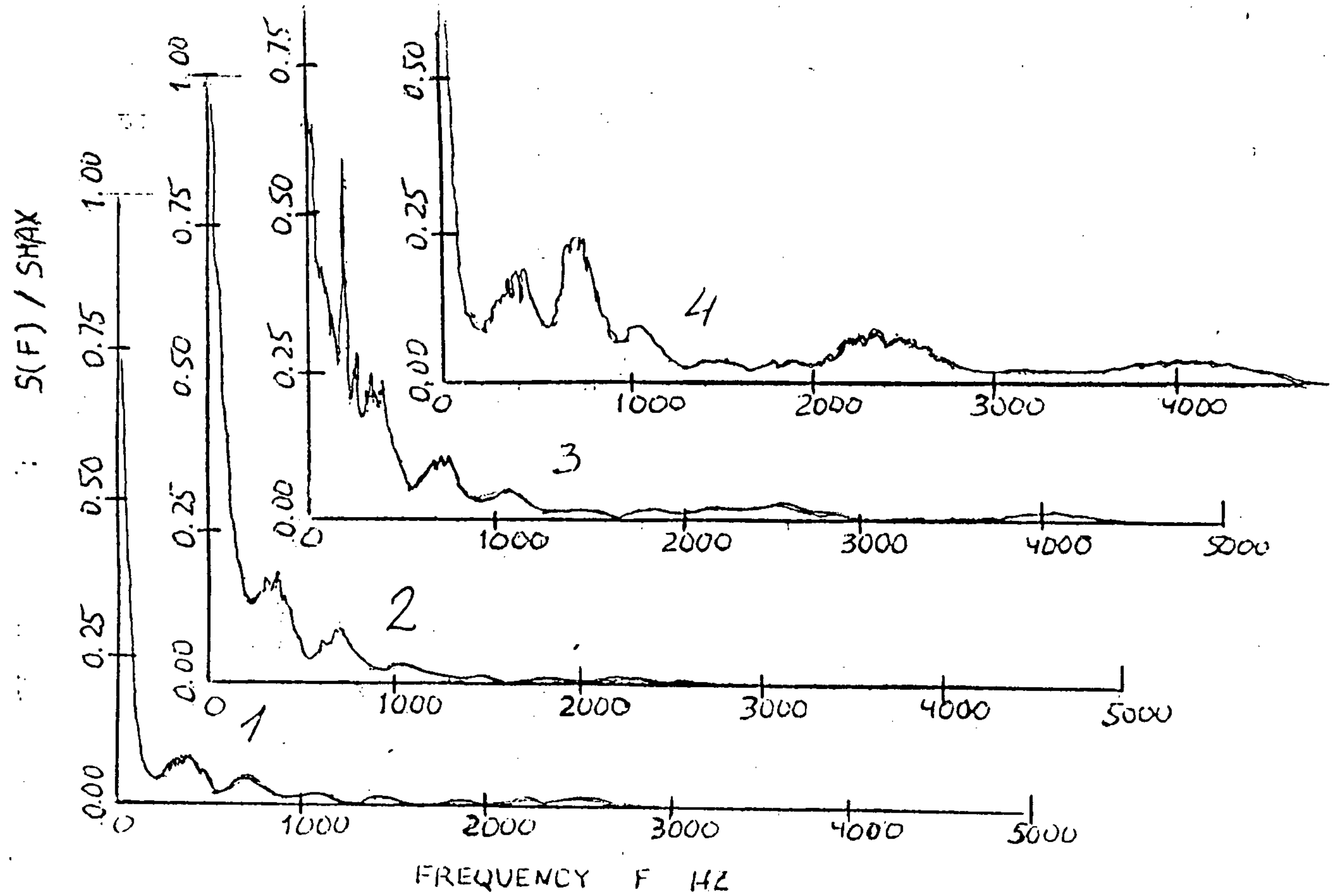

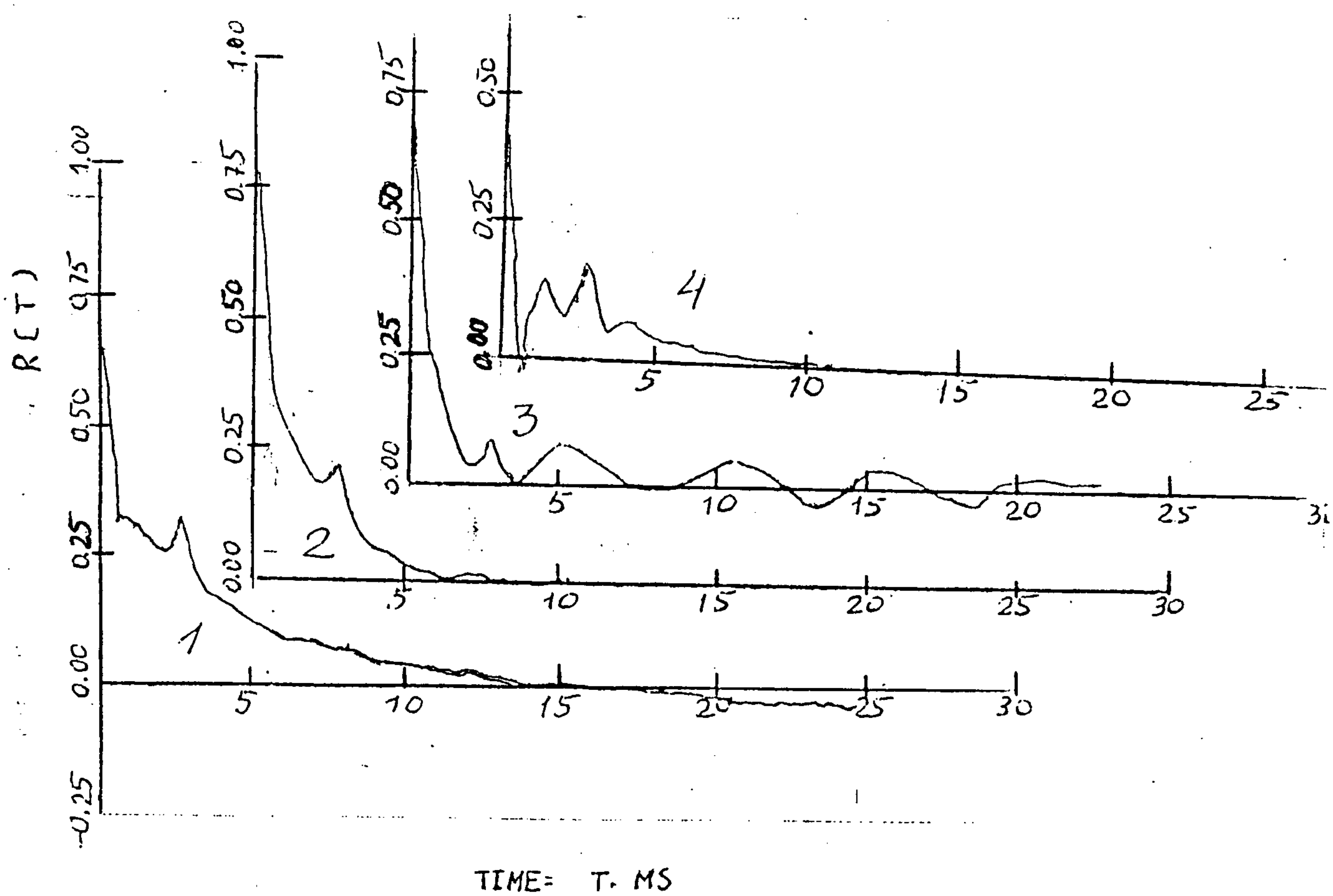

Fig.3.5.15 Power spectra density vrs. frequency.
Autocorrelation function vrs. time.
rhomb struts, 3 mm,1- 1 row, 2 two rows, 3- three rows
4- one row, II section
Ma=3.2, pseudo-shock, r.3, total pressure pulsations, I section

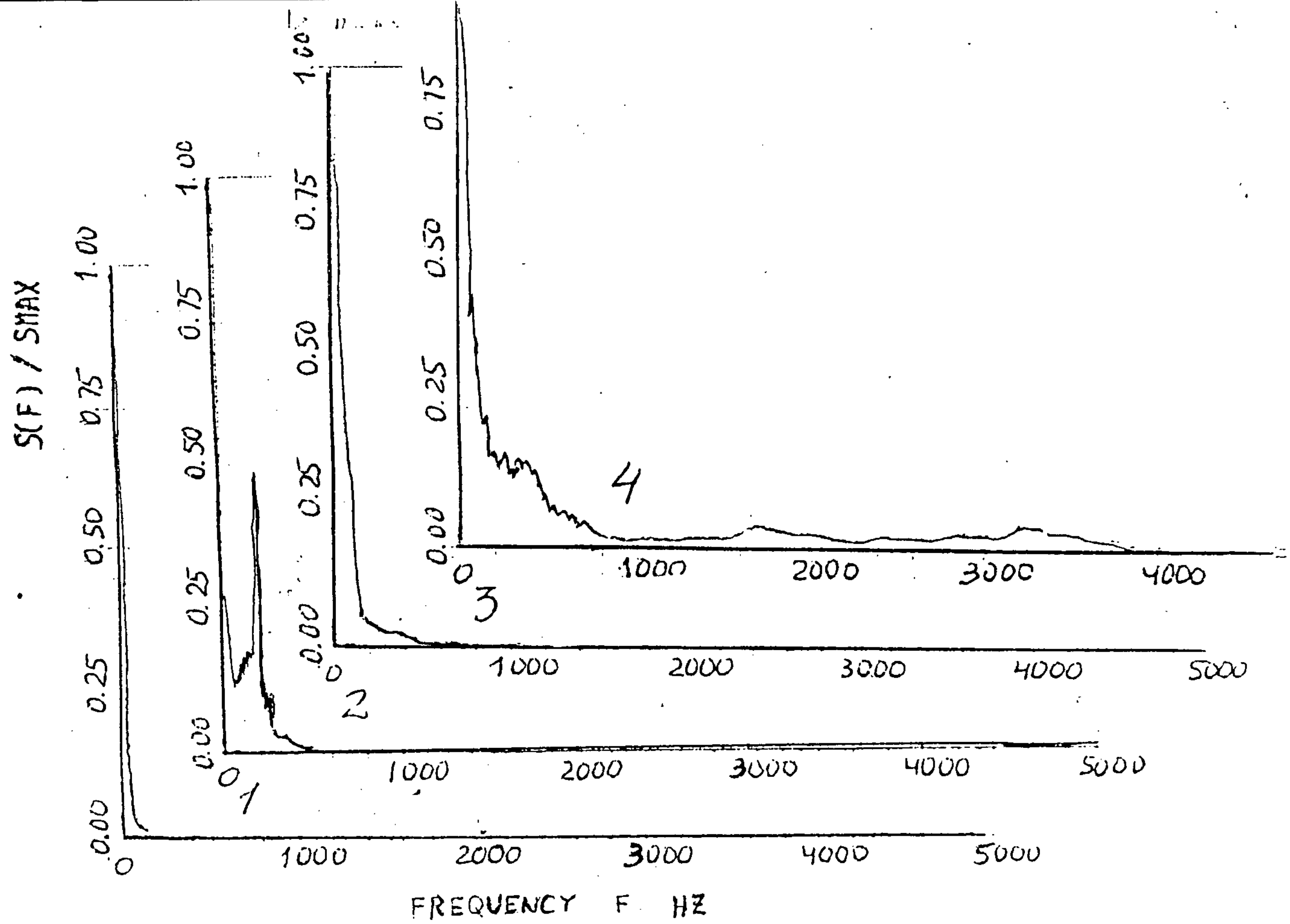

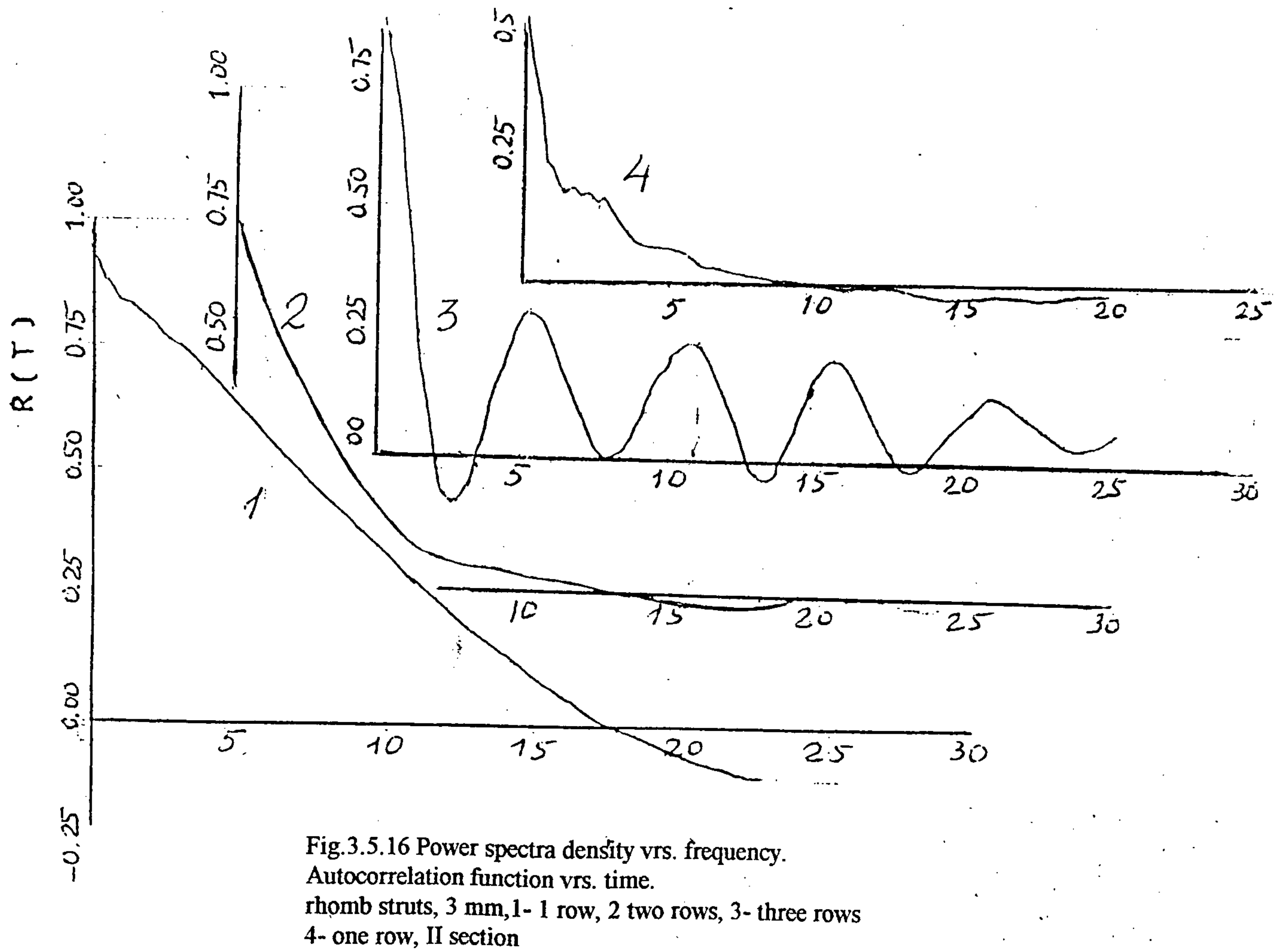

Fig.3.5.16 Power spectra density vrs. frequency.
Autocorrelation function vrs. time.
rhomb struts, 3 mm,1- 1 row, 2 two rows, 3- three rows
4- one row, II section
Ma=3.2, pseudo-shock, r.3, static pressure pulsations, I section

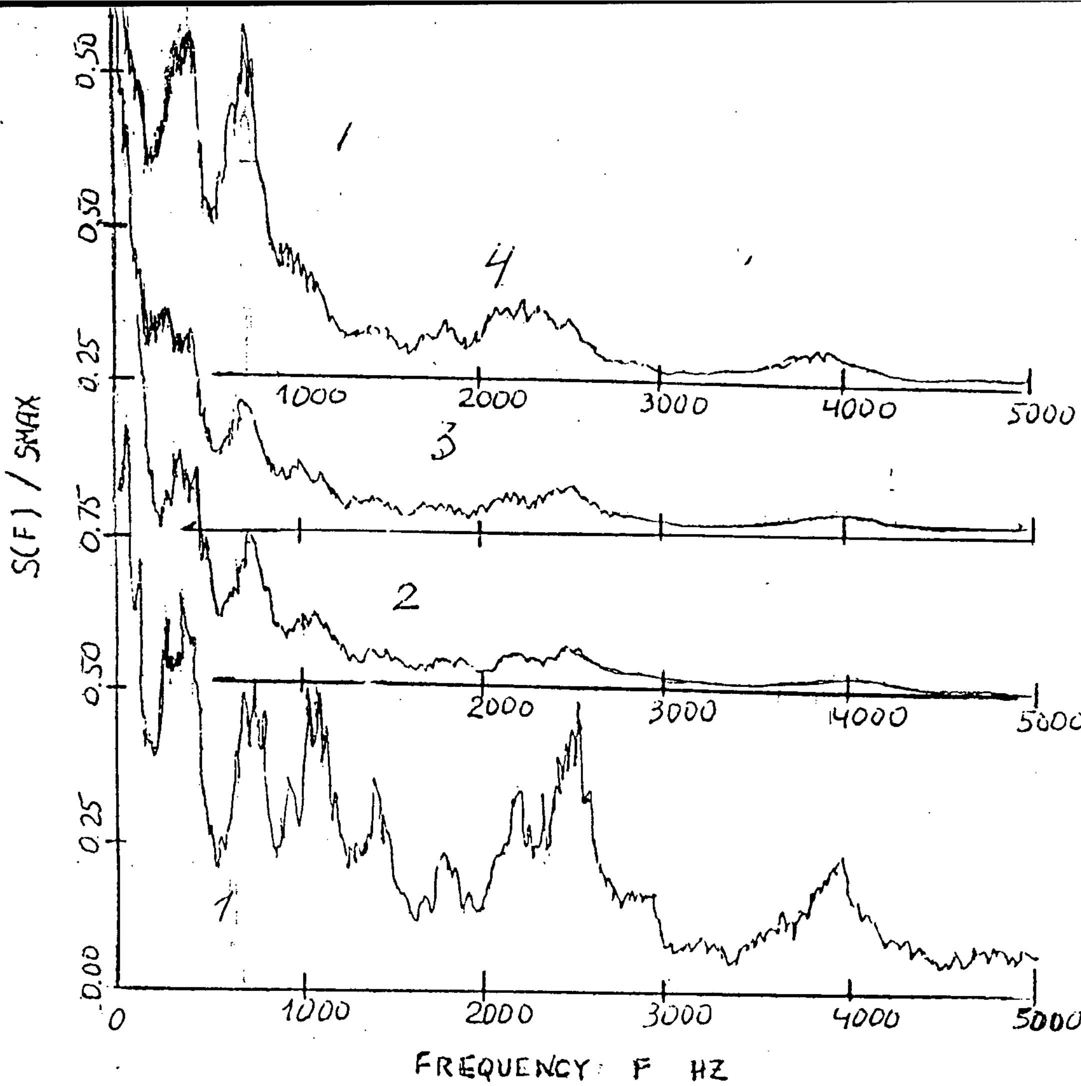

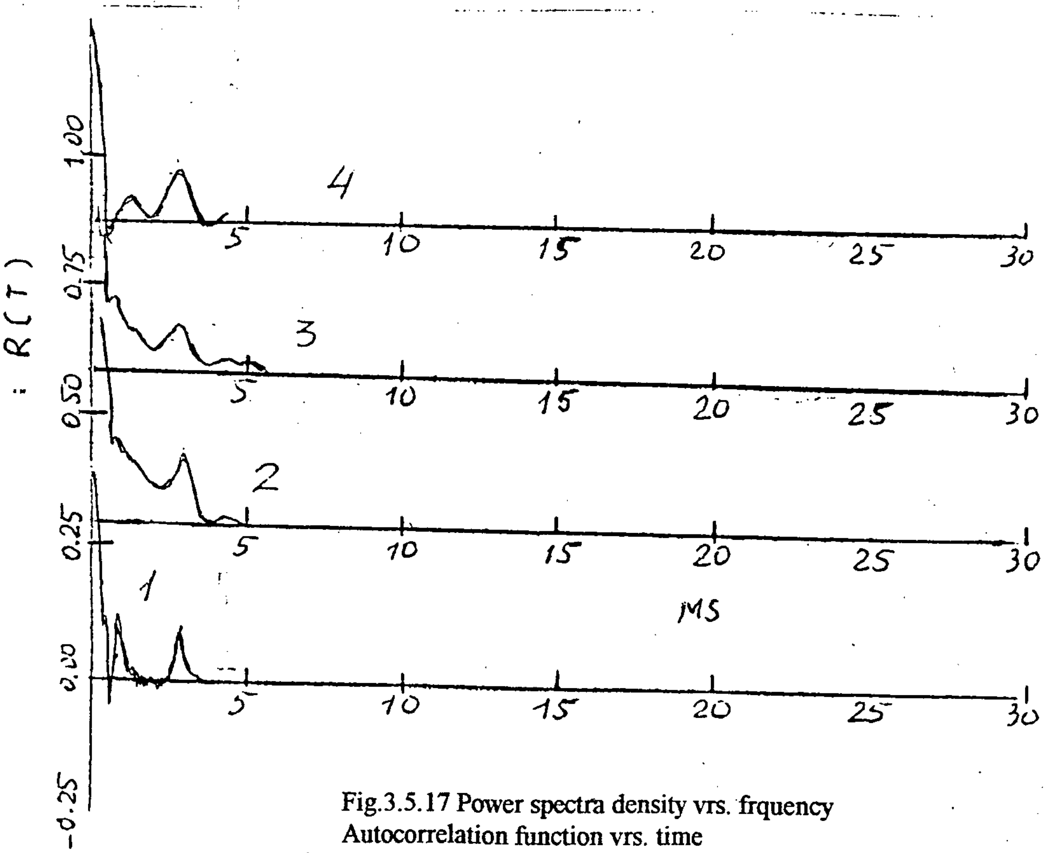

Fig.3.5.17 Power spectra density vrs. frquency
Autocorrelation function vrs. time
cilindric struts, 3 mm,1- 1 row, 2 two rows, 3- three rows
4- one row, II section
Ma=3.2, supersonic flow, total pressure pulsations, I section

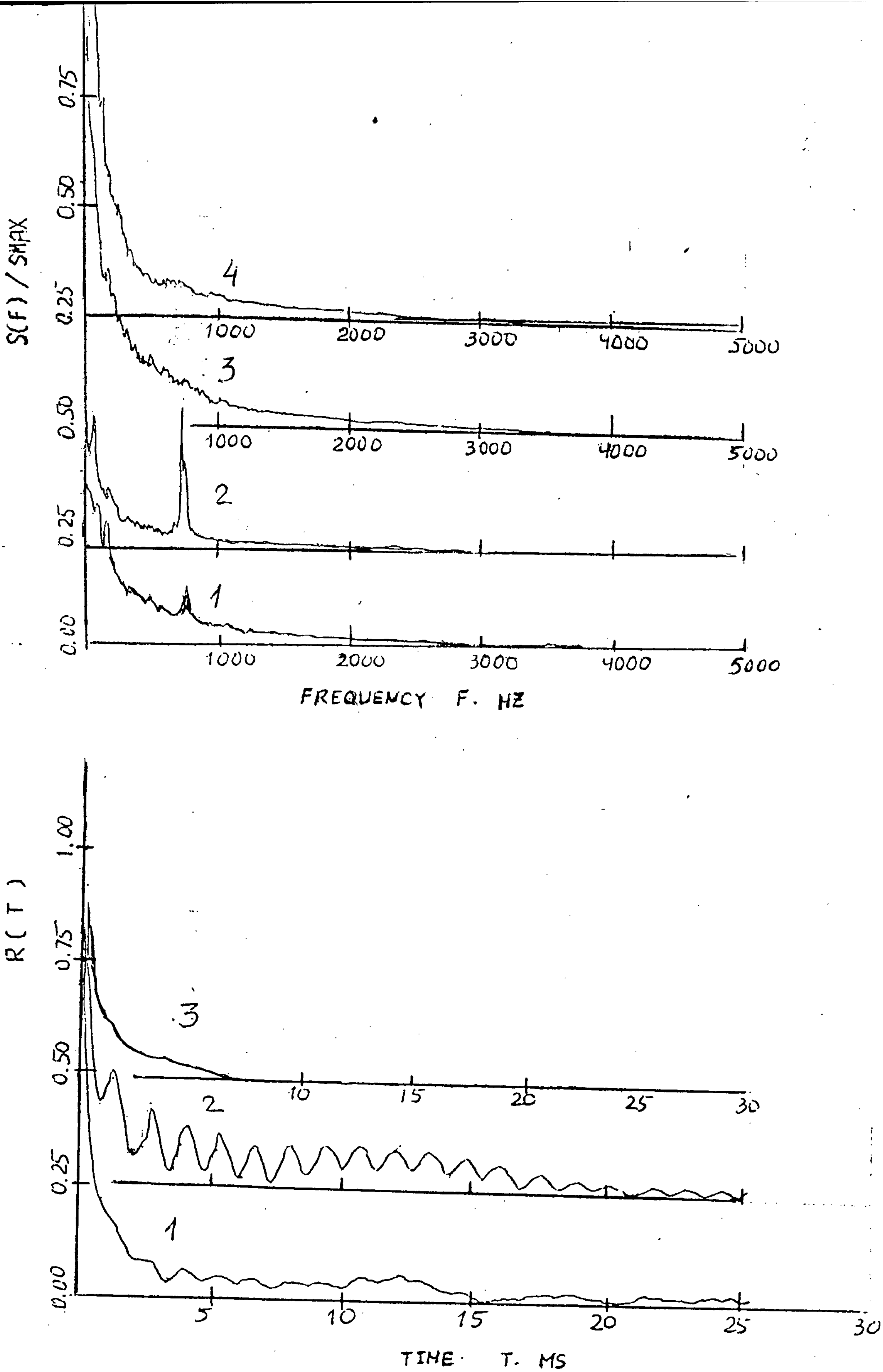

Fig.3.5.18 Power spectra density vrs. frequency.
Autocorrelation function vrs. time.
cylindric struts, 3 mm, 1- 1 row, 2 two rows, 3- three rows
4- one row, II section
Ma=3.2, supersonic flow, static pressure pulsations, I section

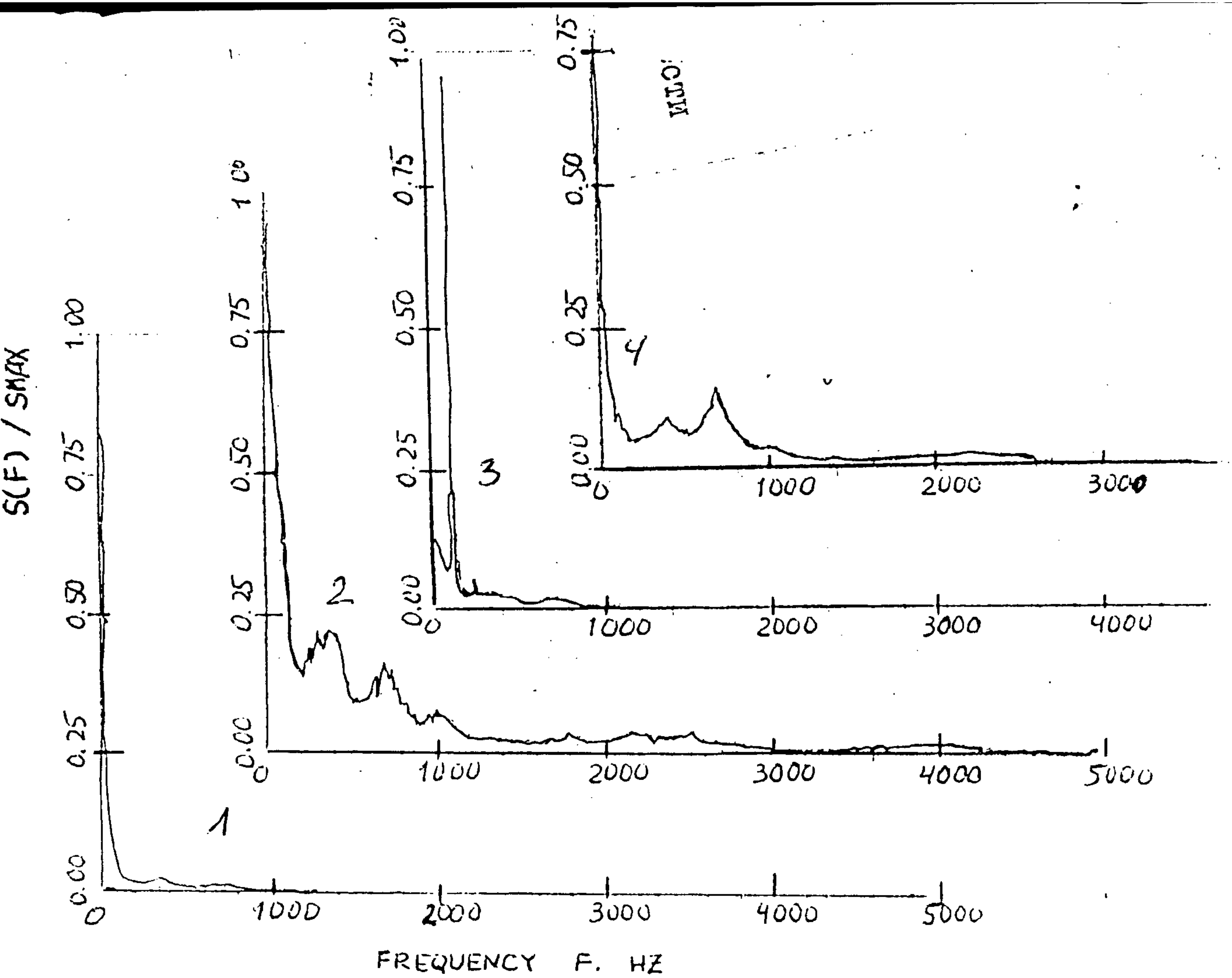

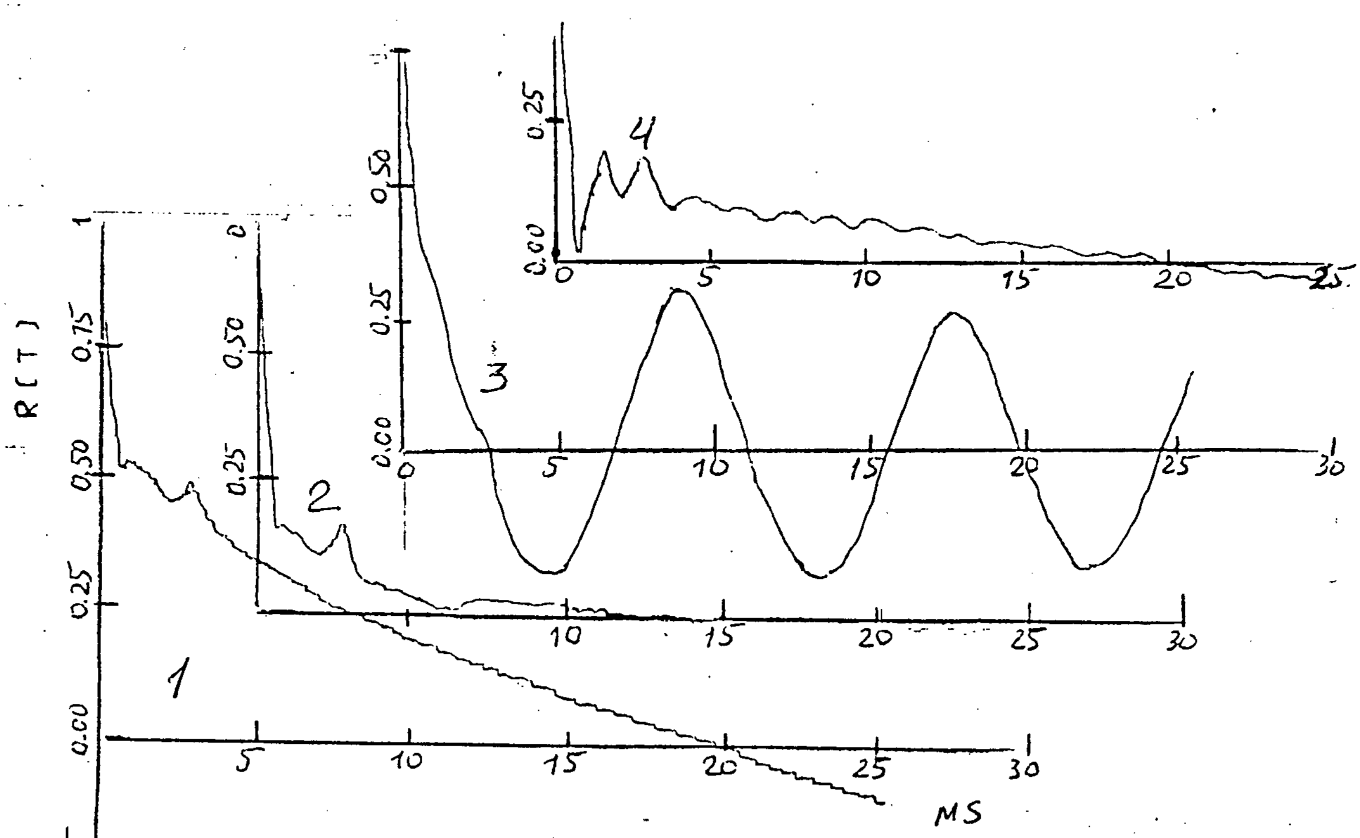

Fig.3.5.19 Power spectra density vrs. frequency.
Autocorrelation function vrs. time.
cylindric struts, 3 mm,1- 1 row, 2 two rows, 3- three rows
4- one row, II section

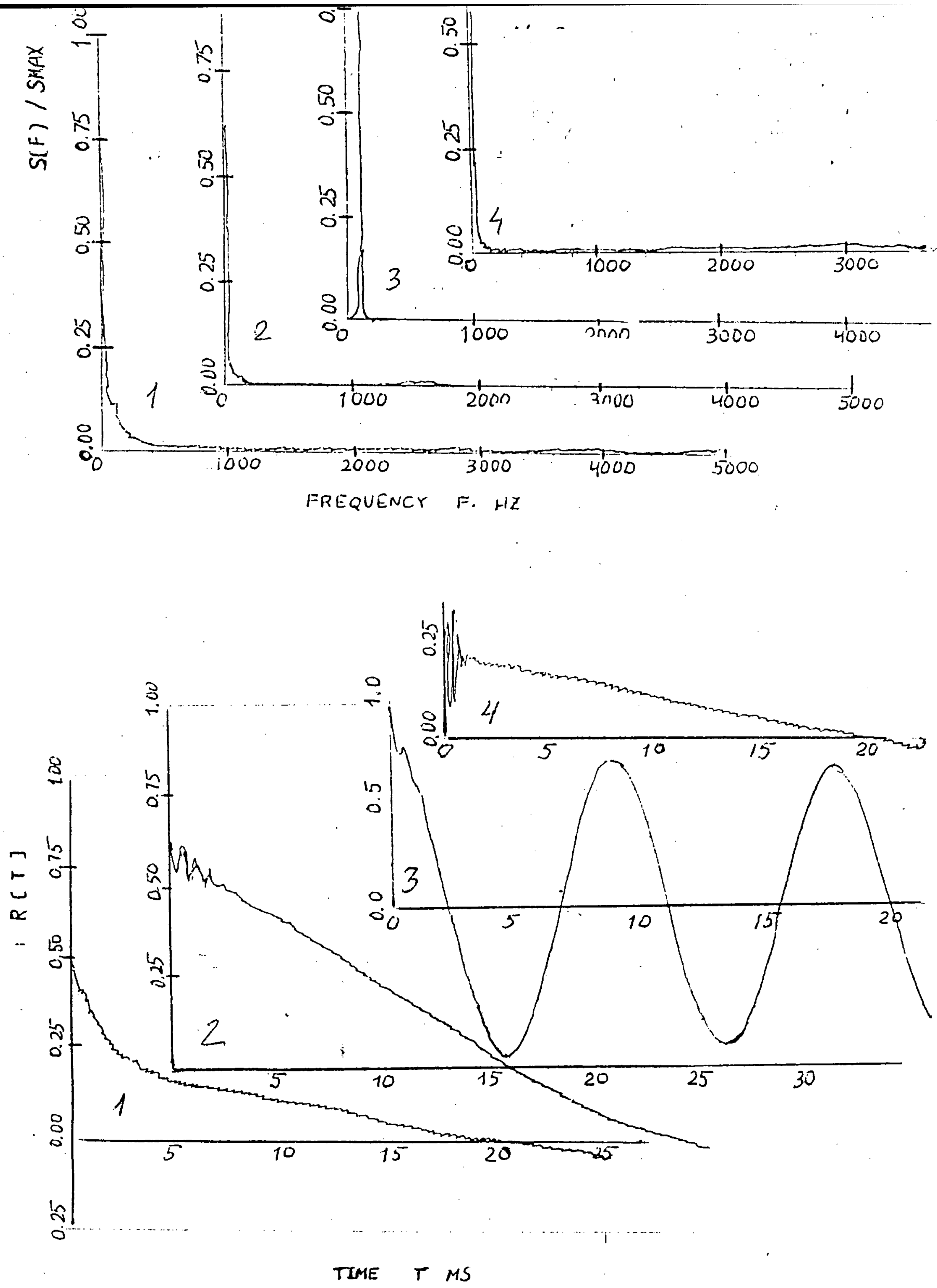

Fig.3.5.20 Power spectra density vrs. frequency.
Autocorrelation function vrs. time.
cylindric struts, 3 mm,1- 1 row, 2 two rows, 3- three rows
4- one row, II section
Ma=3.2, pseudo-shock, r.3, static pressure pulsations, I section

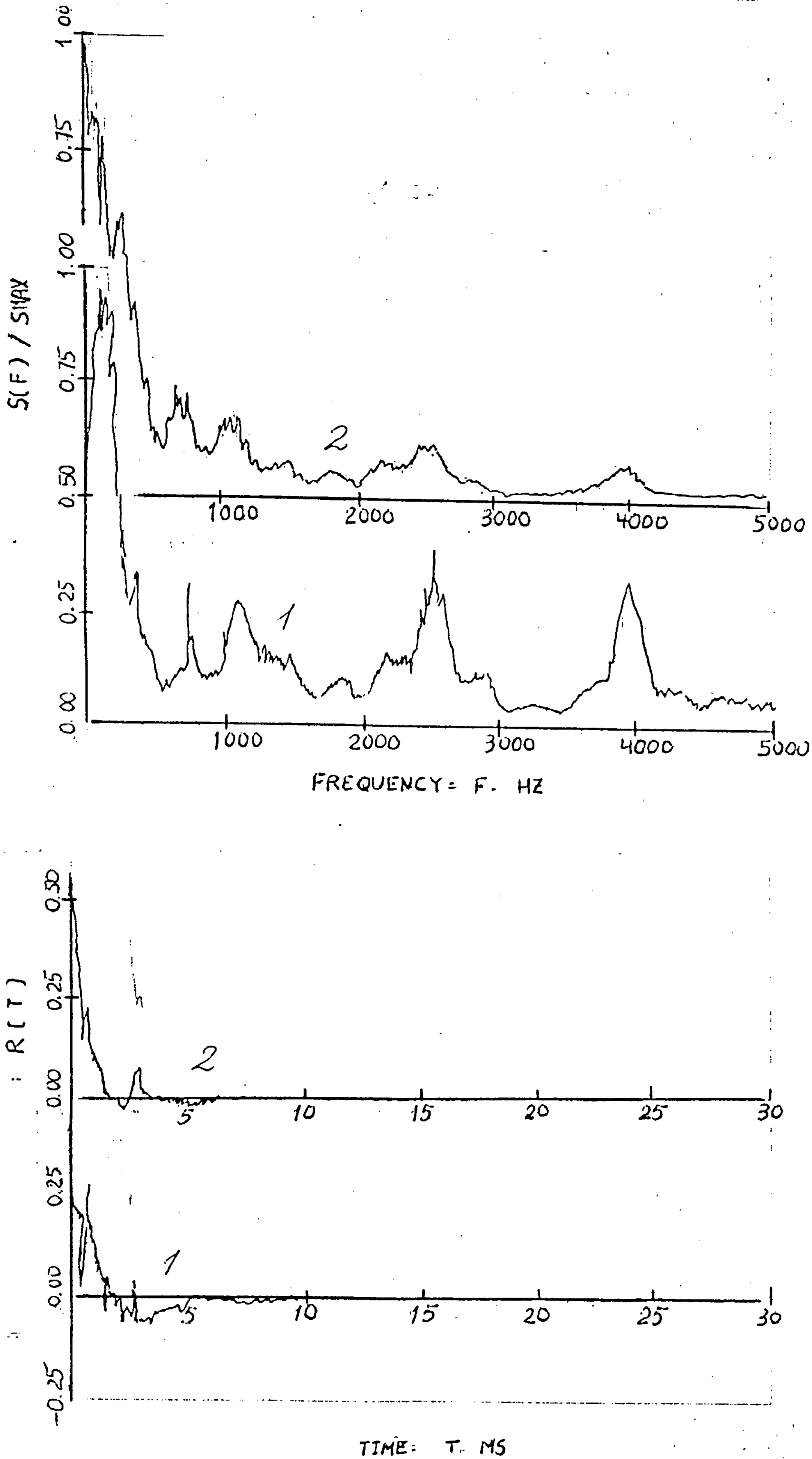

Fig.3.5.21 Power spectra density vrs. frequency.
Autocorrelation function vrs. time.
rhomb struts, 3 mm, 1 row, 1-d=2 mm, 2- d=4 mm.

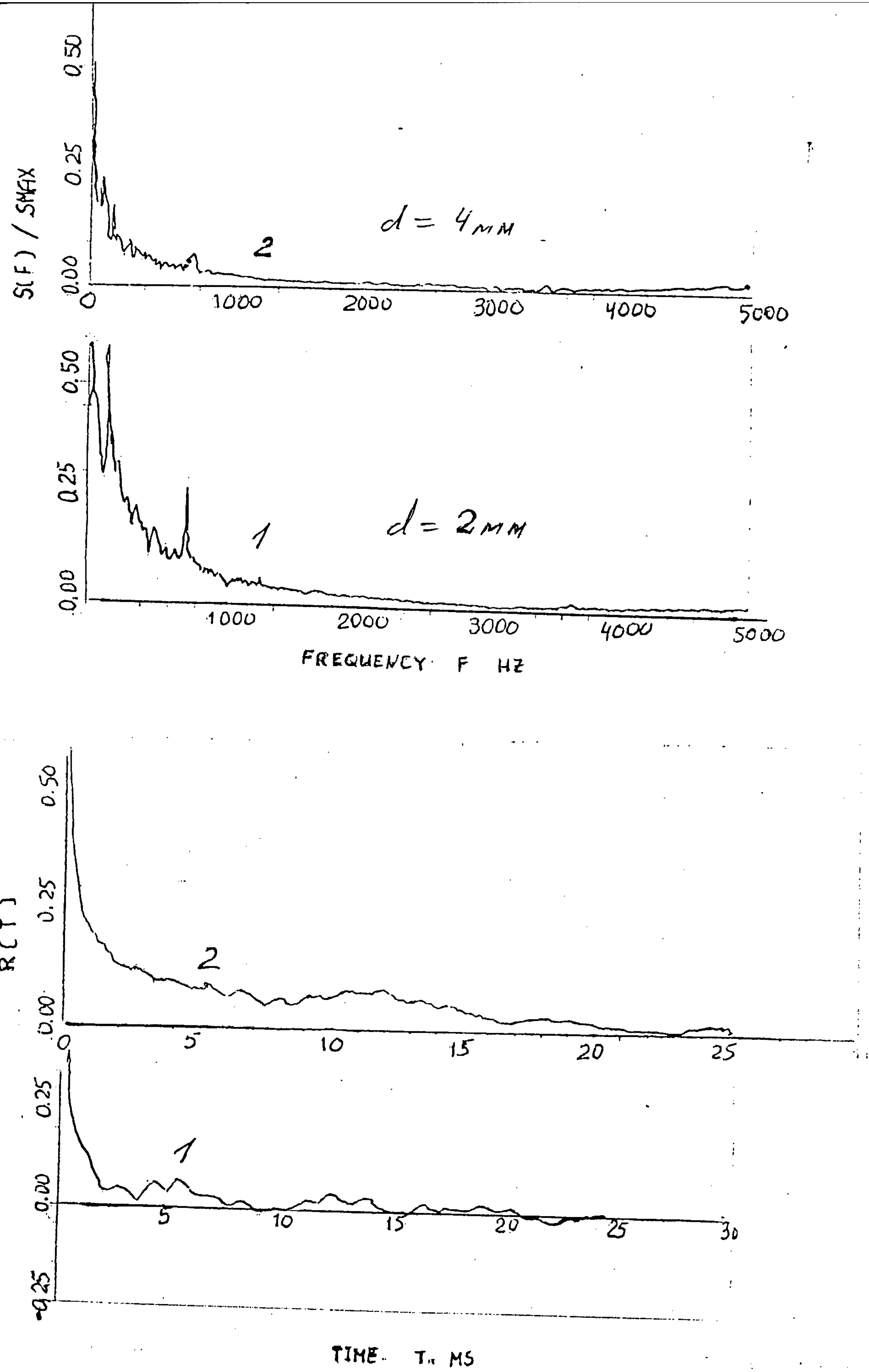

Fig.3.5.22 Power spectra density vrs. frequency.
Autocorrelation function vrs. time.
rhombic struts, 1 row,
Ma=3.2, supersonic flow, static pressure pulsations, I section

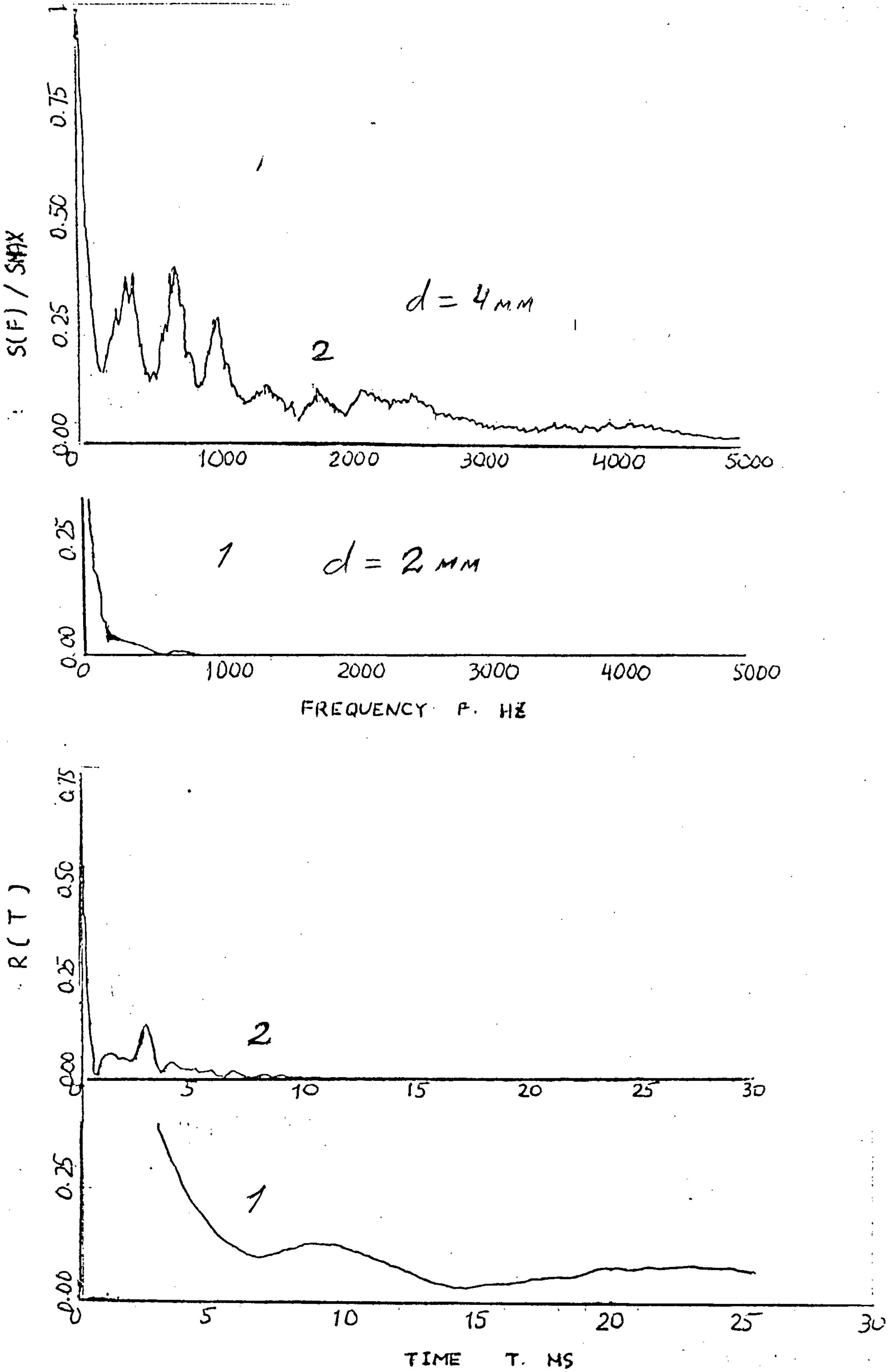

Fig.3.5.23 Power spectra density vrs. frequency.
Autocorrelation function vrs. time.
rhomb struts, - 1 row,
Ma=3.2, pseudo-shock, r.3, total pressure pulsations, I section

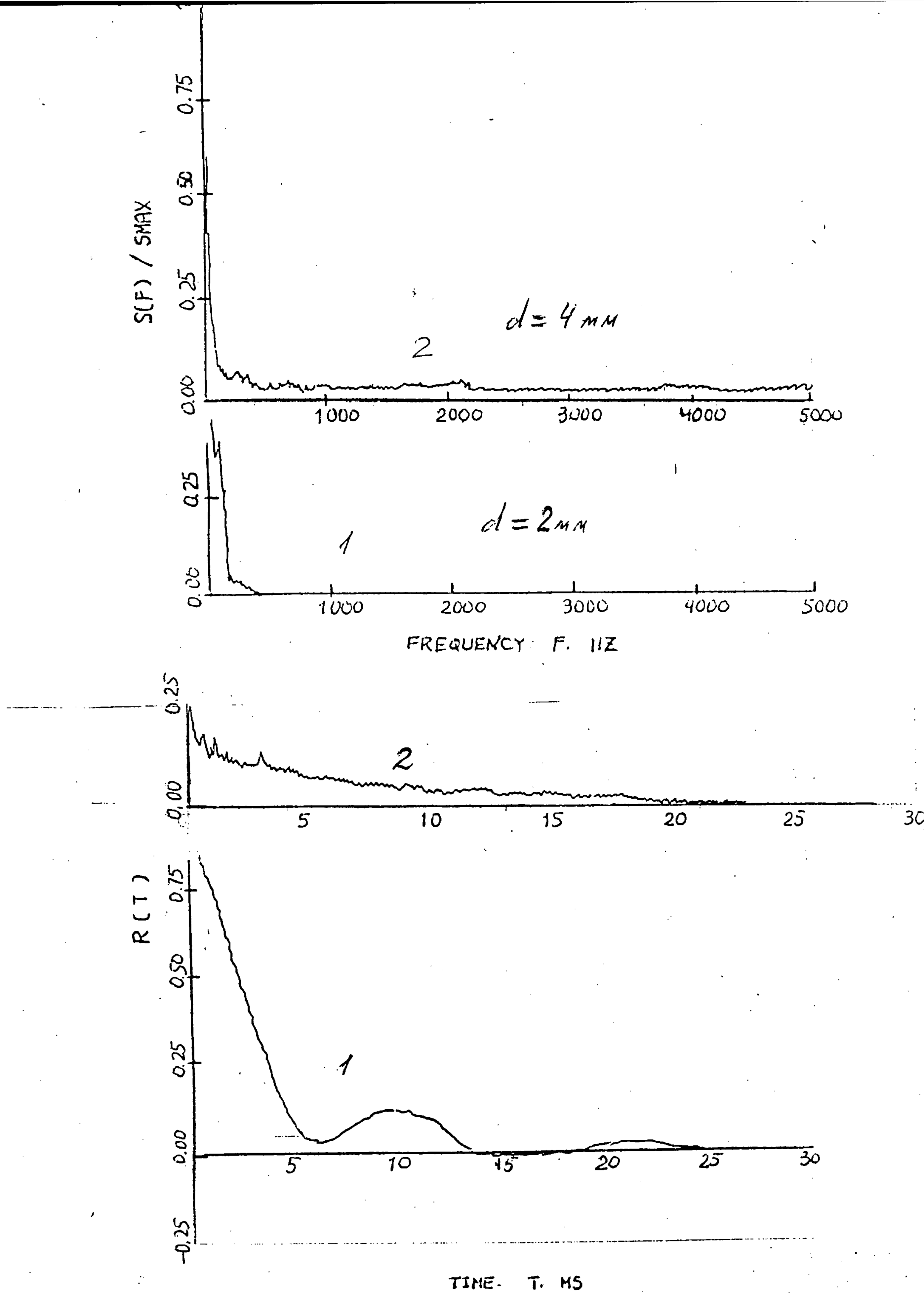

Fig.3.5.24 Power spectra density vrs. frequency.
Autocorrelation function vrs. time.
rhomb struts, 1 row,
Ma=3.2, pseudo-shock, r.3, static pressure pulsations, I section

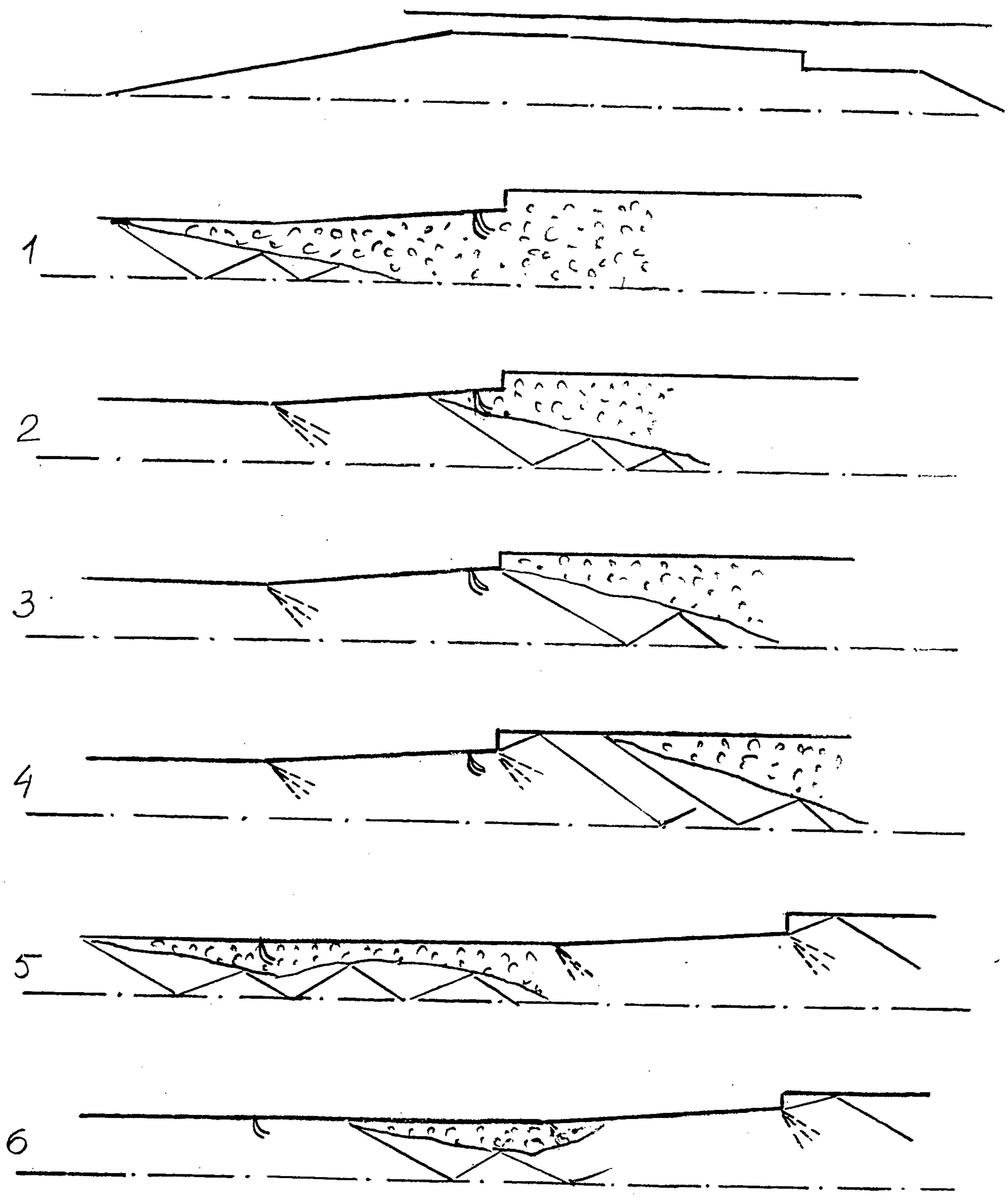

Fig. 4.1 Caracteristic flow mode schematic in diverging ducts.

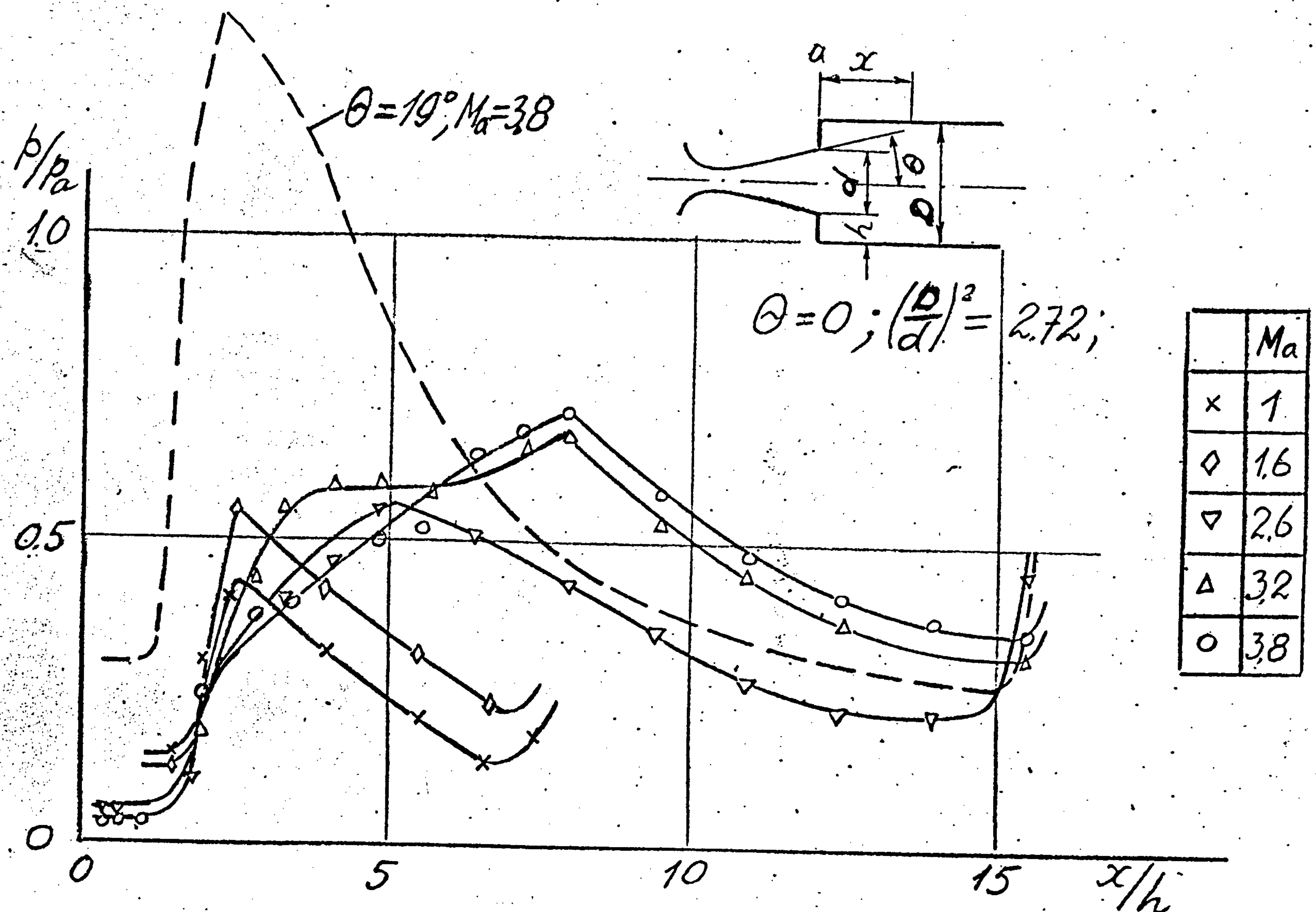

Fig. 4.1.1 Typical pressre distributions on wide part of stepped duct

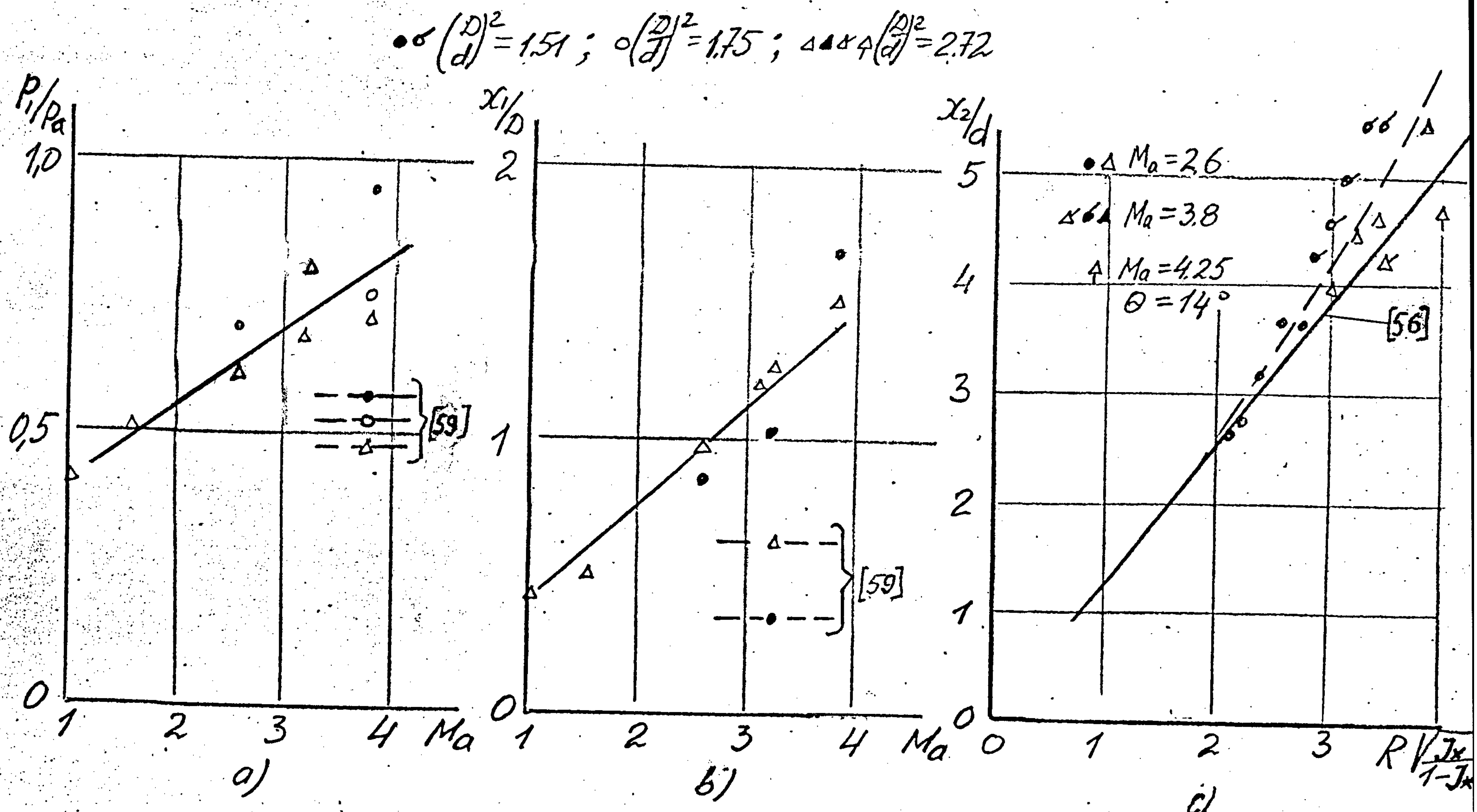

Fig. 4.1.2 Relative pressure peak dependence on Ma
for different expansion ratious.

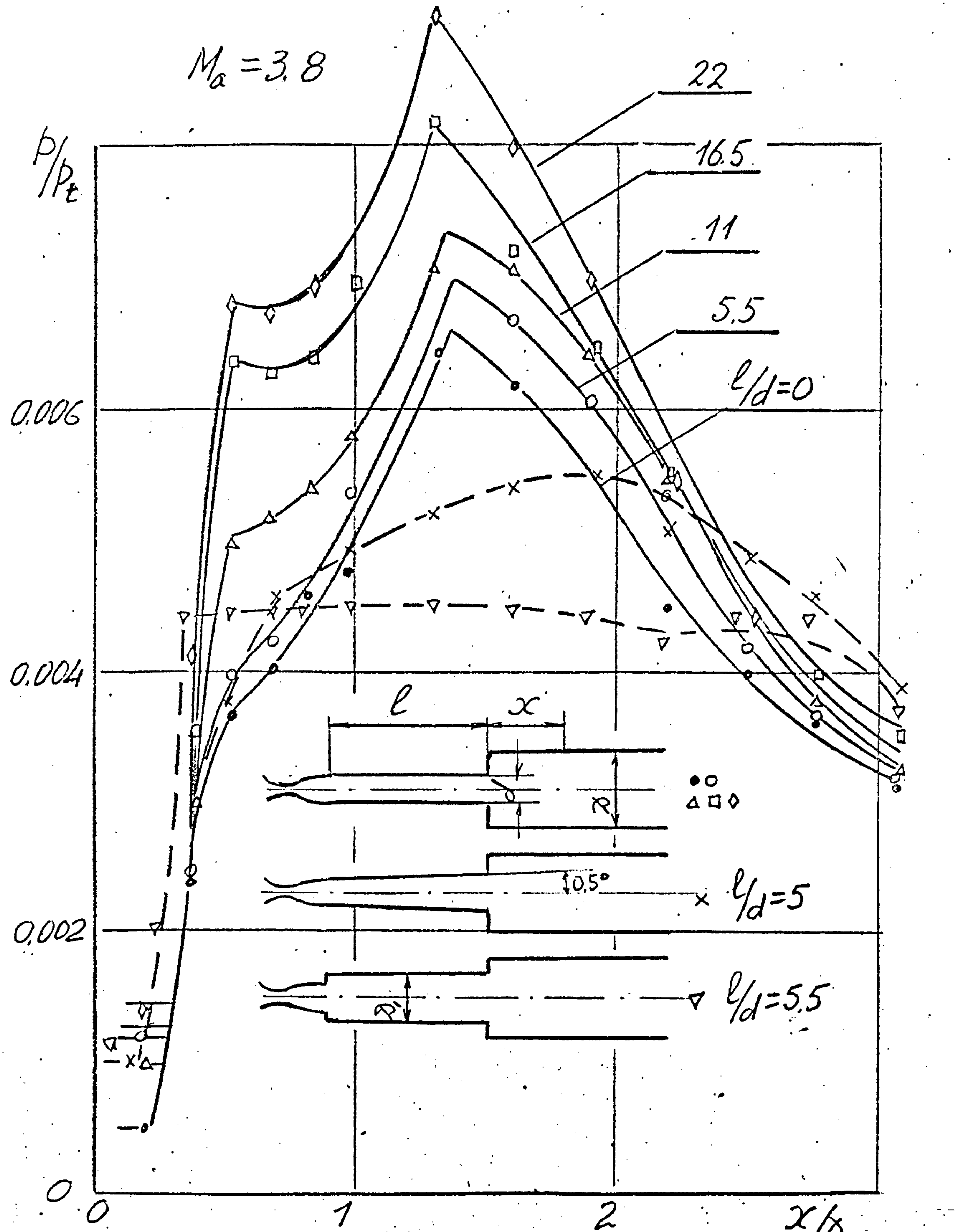

Fig. 4.1.3 Ifluence of duct geometry upstream of the step on pressure distribution.

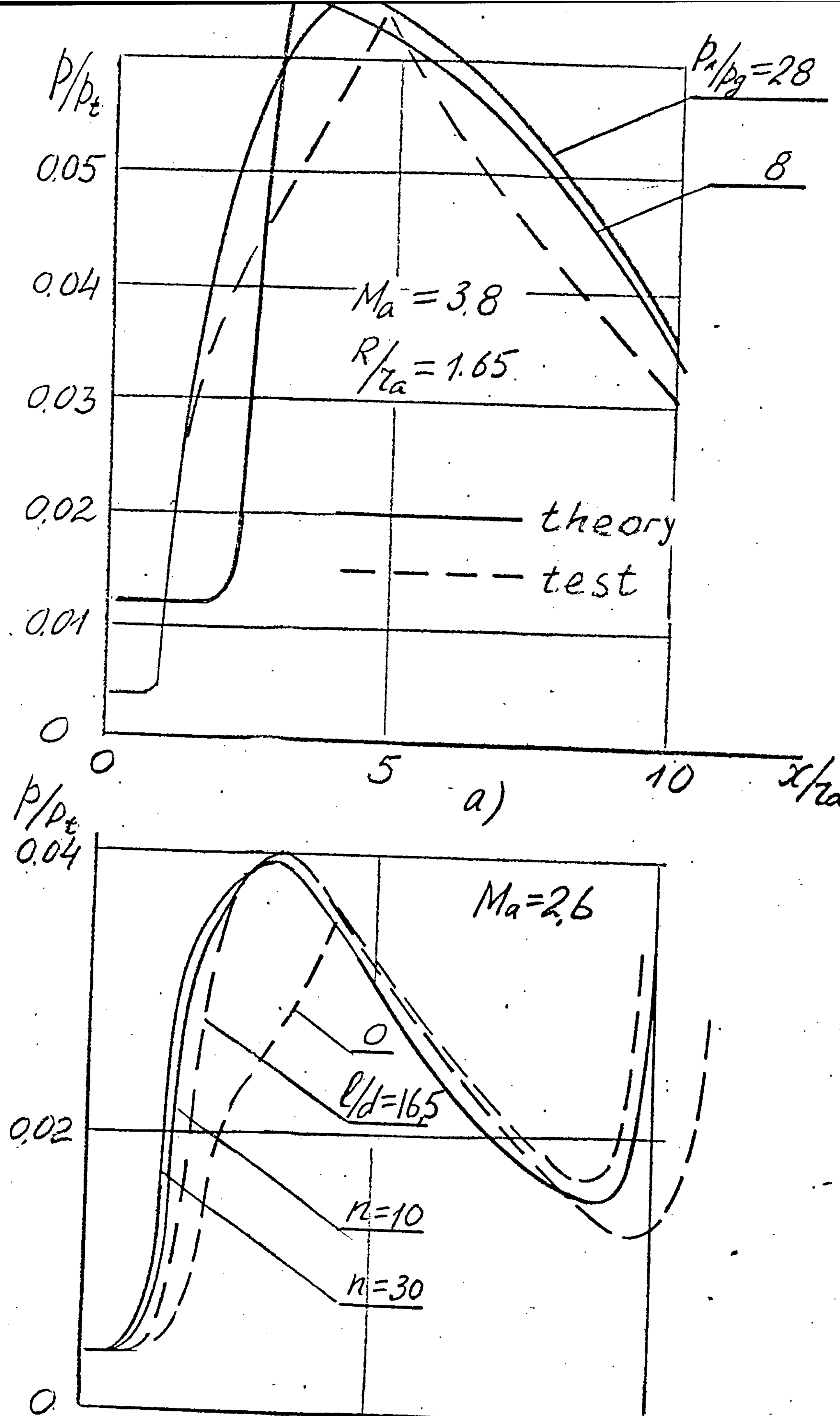

Fig. 4.1.4 Experimental and calculated pressure distributions along stepped duct

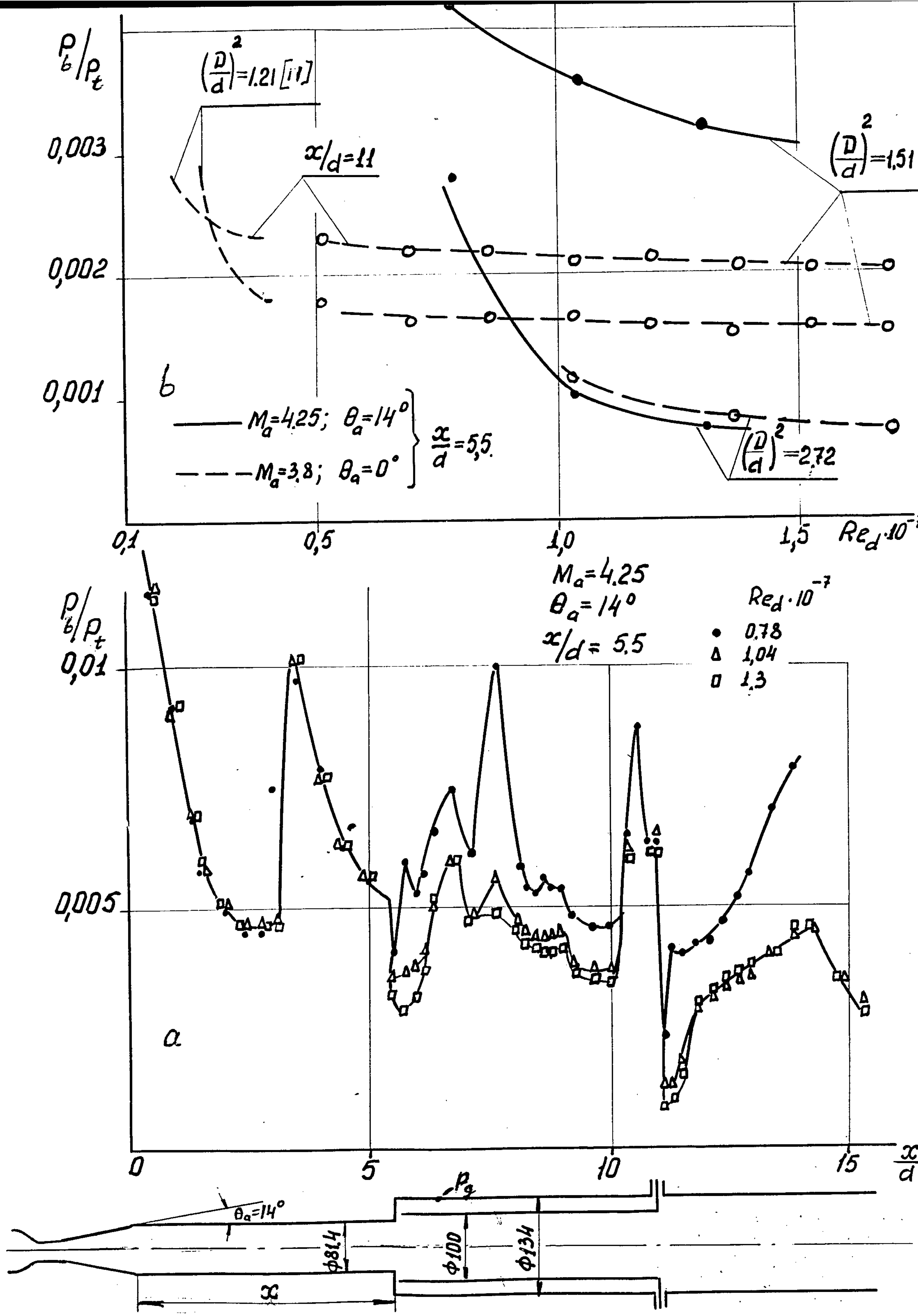

Fig. 4.1.5 Pressure distribution along the two-stepped duct-a
Base pressure dependence on Re-b

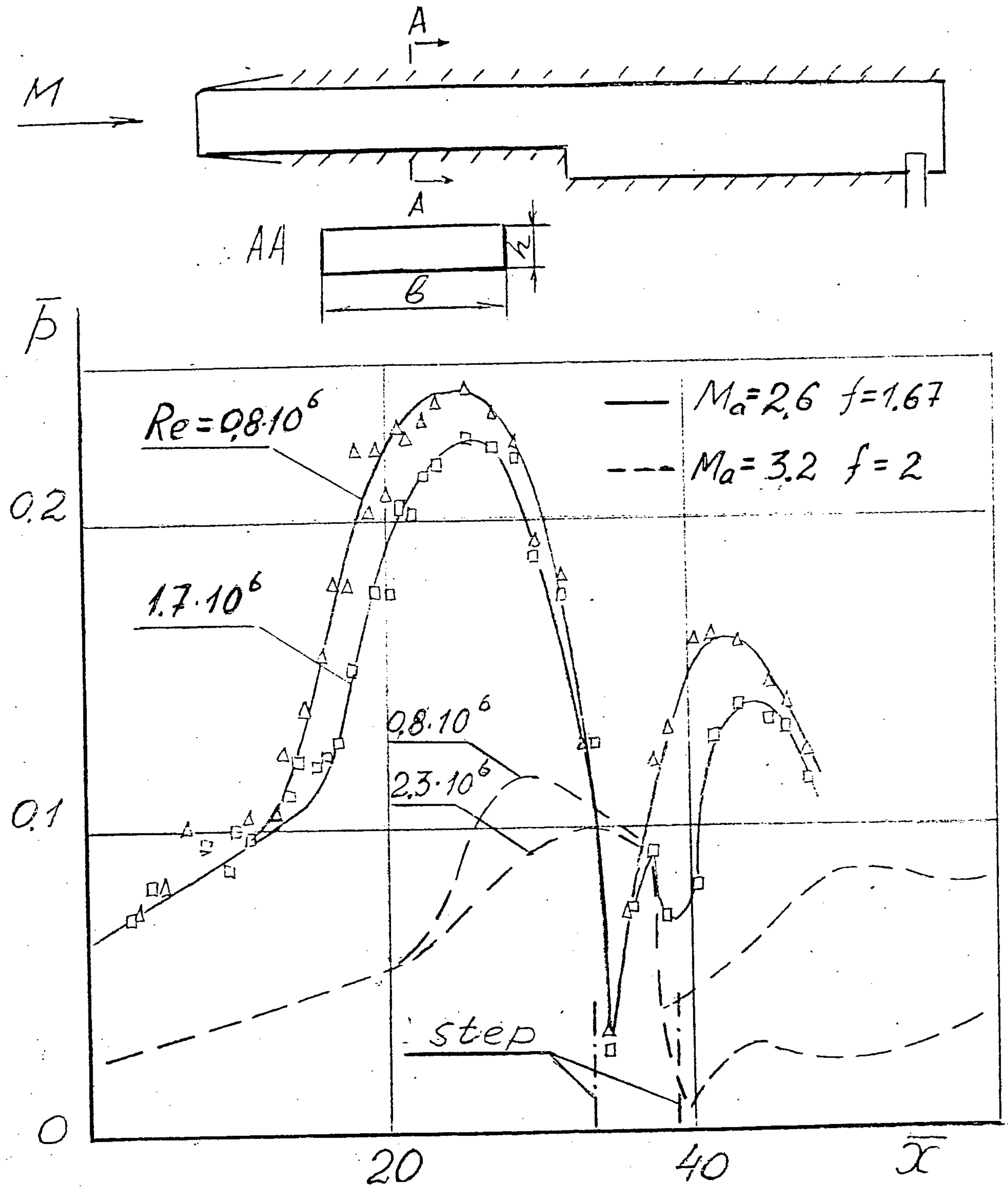

Fig. 4.1.6 Pressure distribution along rectangular stepped duct at different Ma, Re, f.

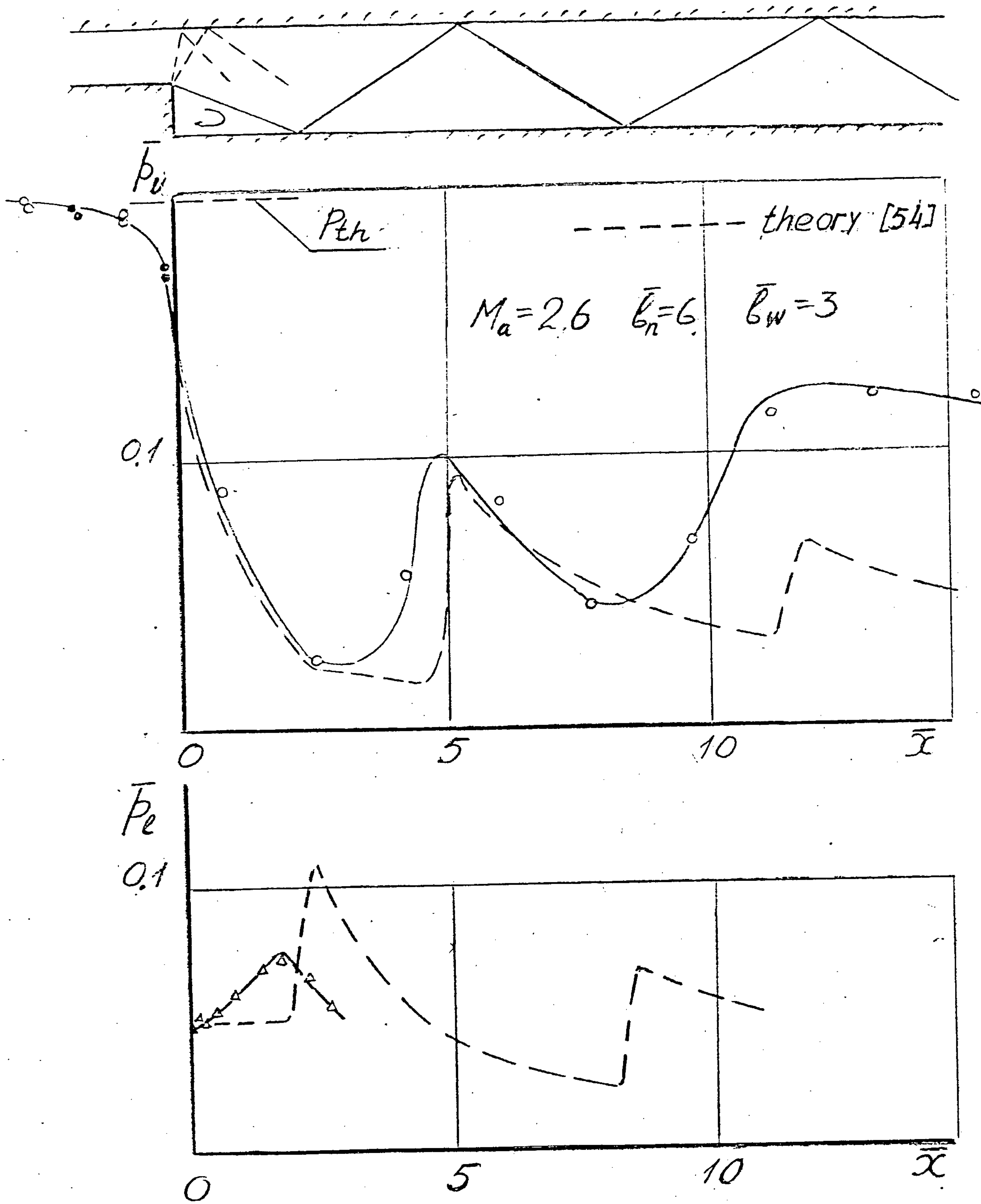

Fig. 4.1.7 Comparison of experimental and theoretical pressure distributions along the rectangular stepped duct. at Ma=2.6

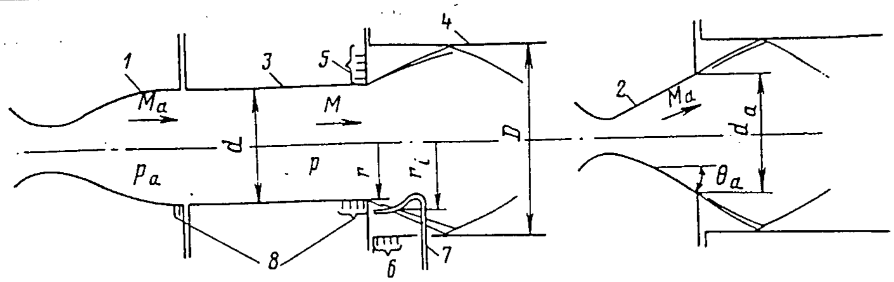

Fig. 4.2.1 Experimental module schematic.

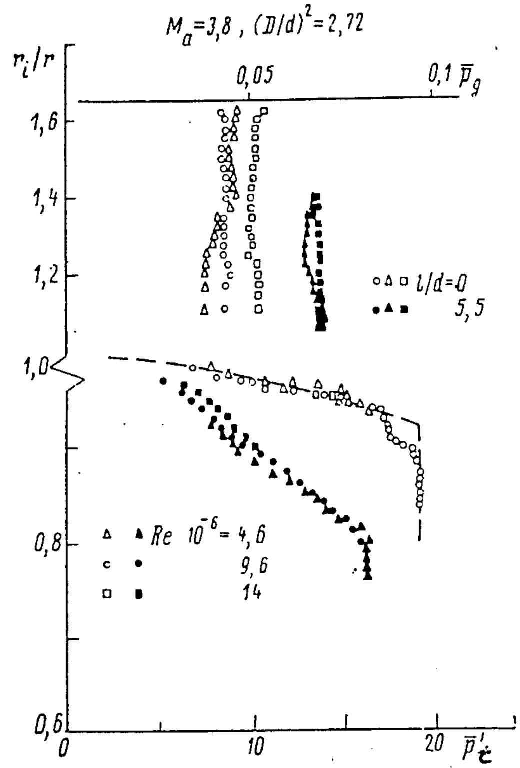

Fig. 4.2.2 Base pressure distribution over the step face at different Re and l/d

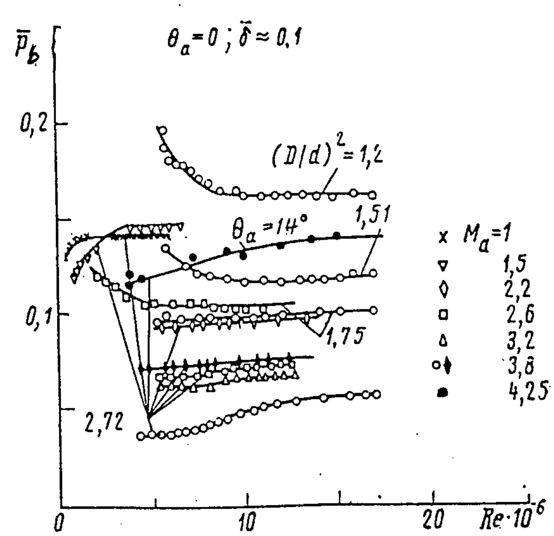

Fig. 4.2.3 Base pressure dependence on Re

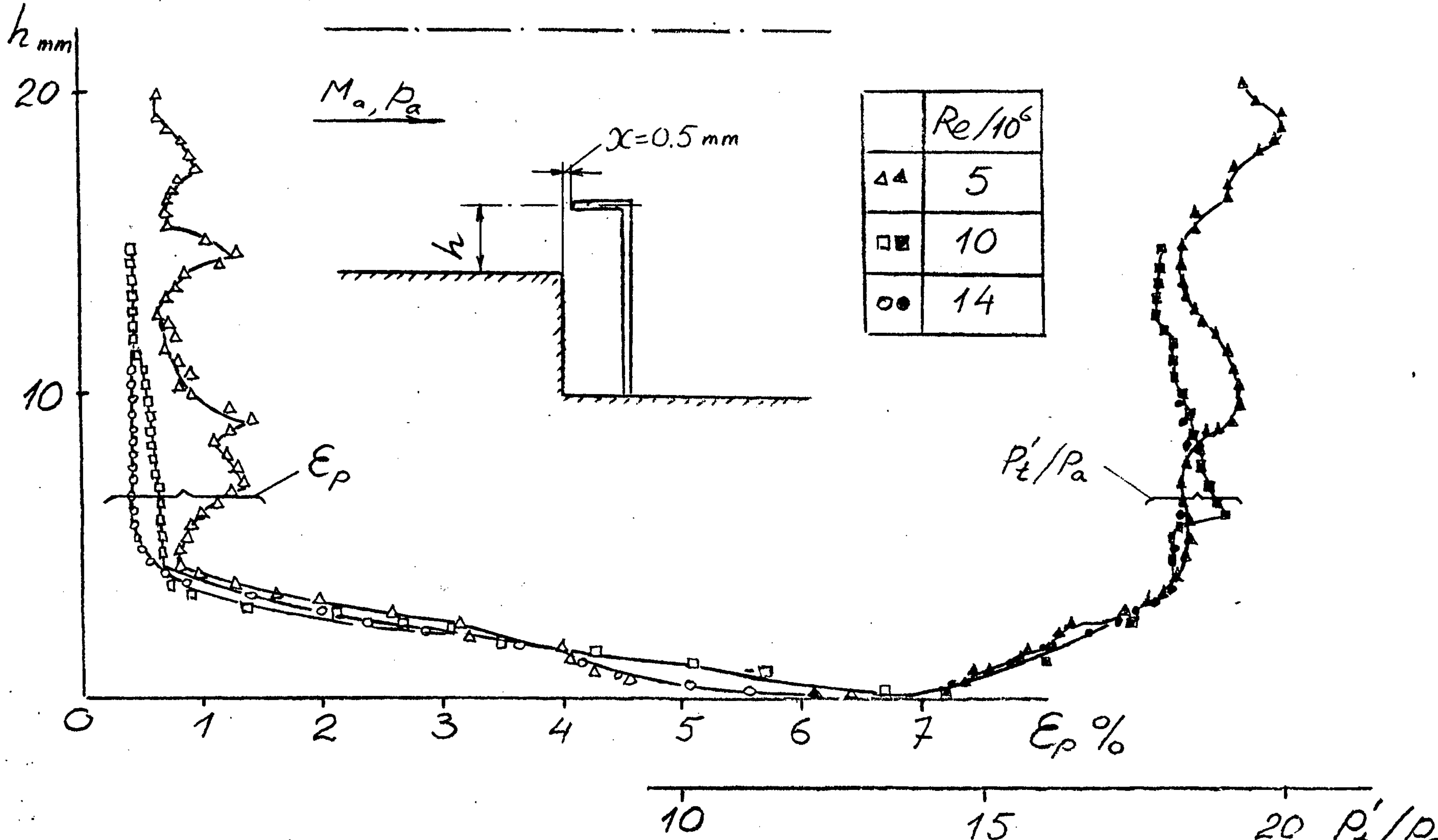

Fig. 4.2.4 Profiles of pressure pulsation intensities at different Re

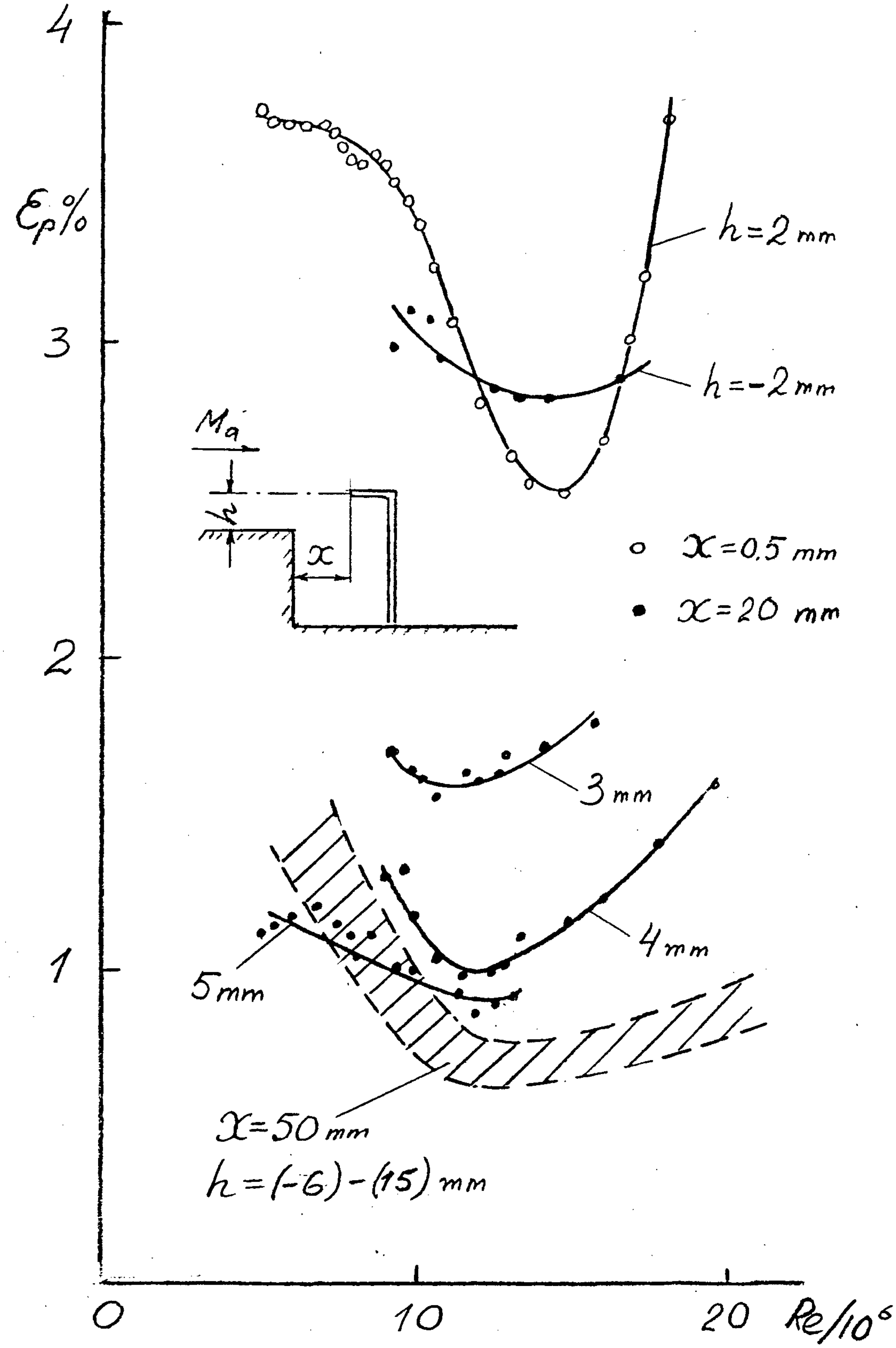

Fig. 4.2.5 Pressure pulsation intensitiy dependencies on Re

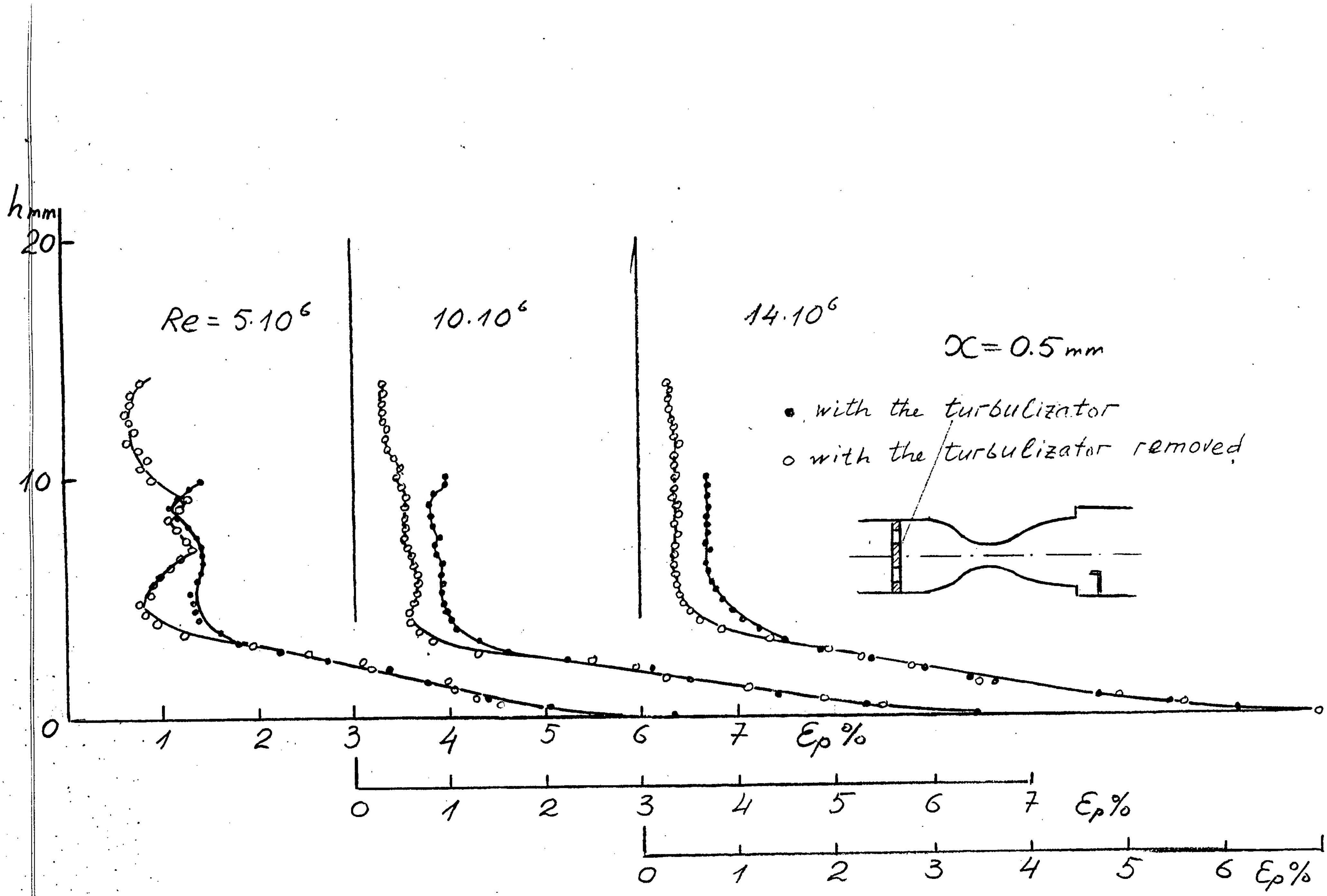

Fig.4.2.6 Comparison of base profiles
of Ep in duct with and without turbulisator

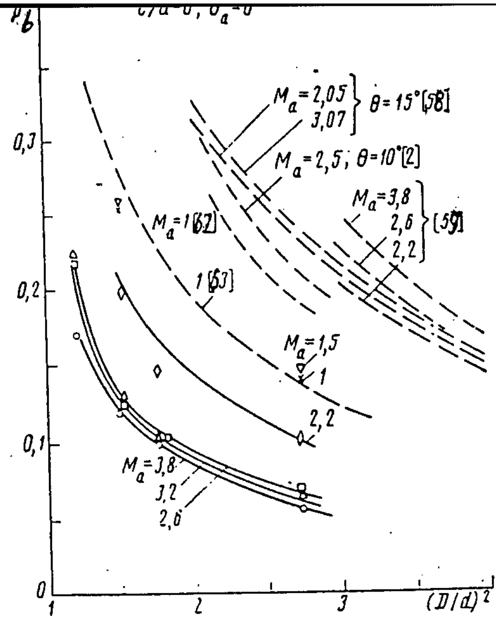

Fig. 4.2.7 Base pressure dependence on expansion ratio f.

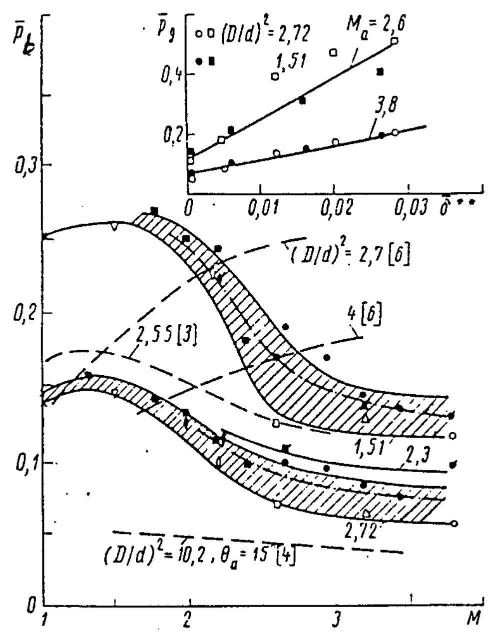

Fig. 4.2.8 Base pressure dependence on M

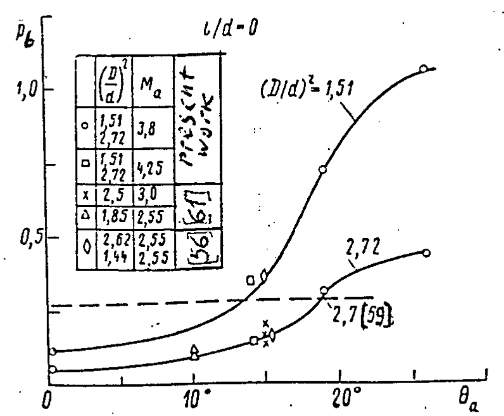

	$(D/d)^2$	M_a	
o	1,51 2,72	3,8	present work
□	1,51 2,72	4,25	
x	2,5	3,0	[61]
Δ	1,85	2,55	
◊	2,62 1,44	2,55 2,55	[56]

Fig. 4.2.9 Base pressure dependance on θ

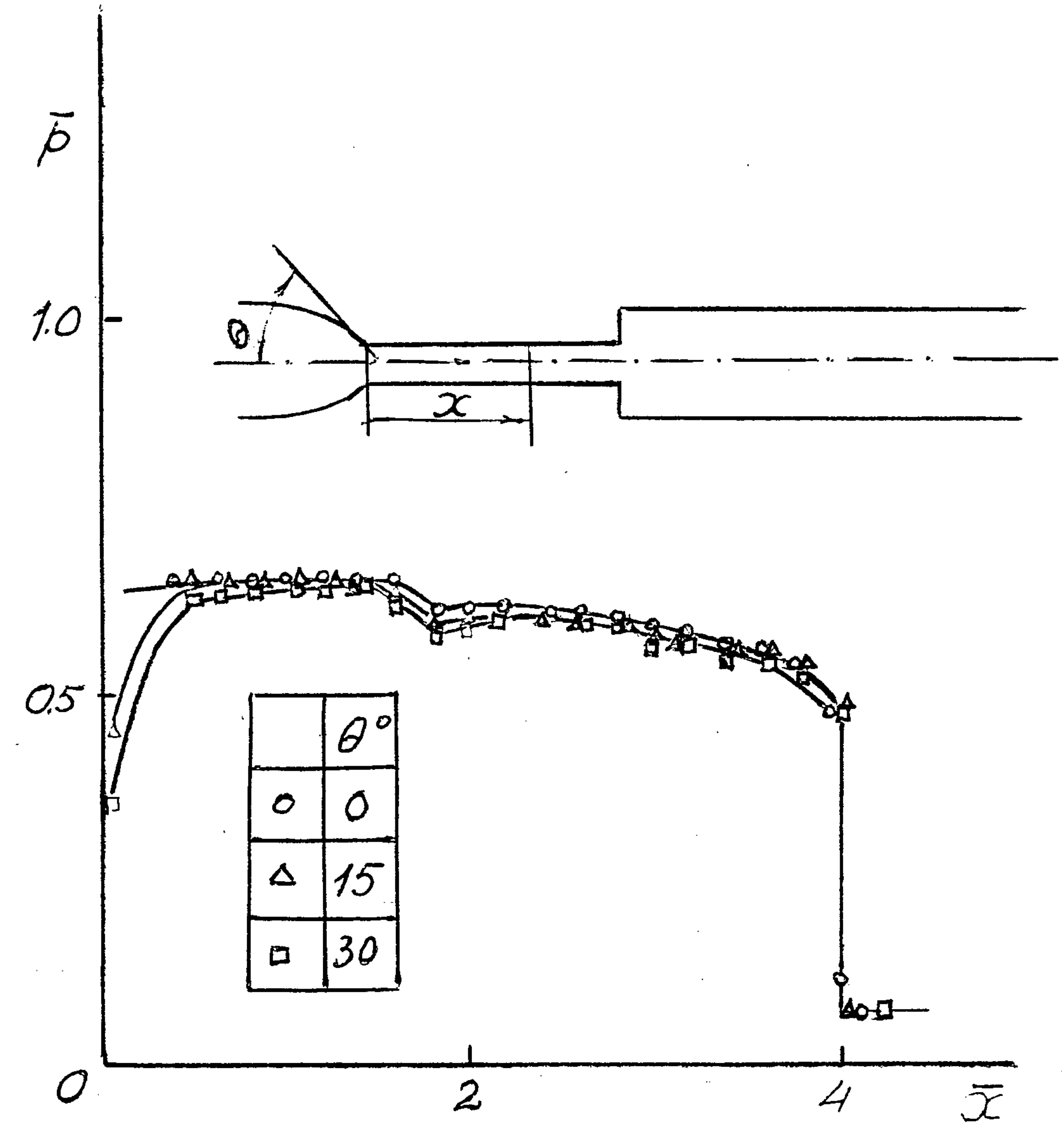

Fig. 4.2.10 Pressure distribution in tube
downstream the sonic nozzle

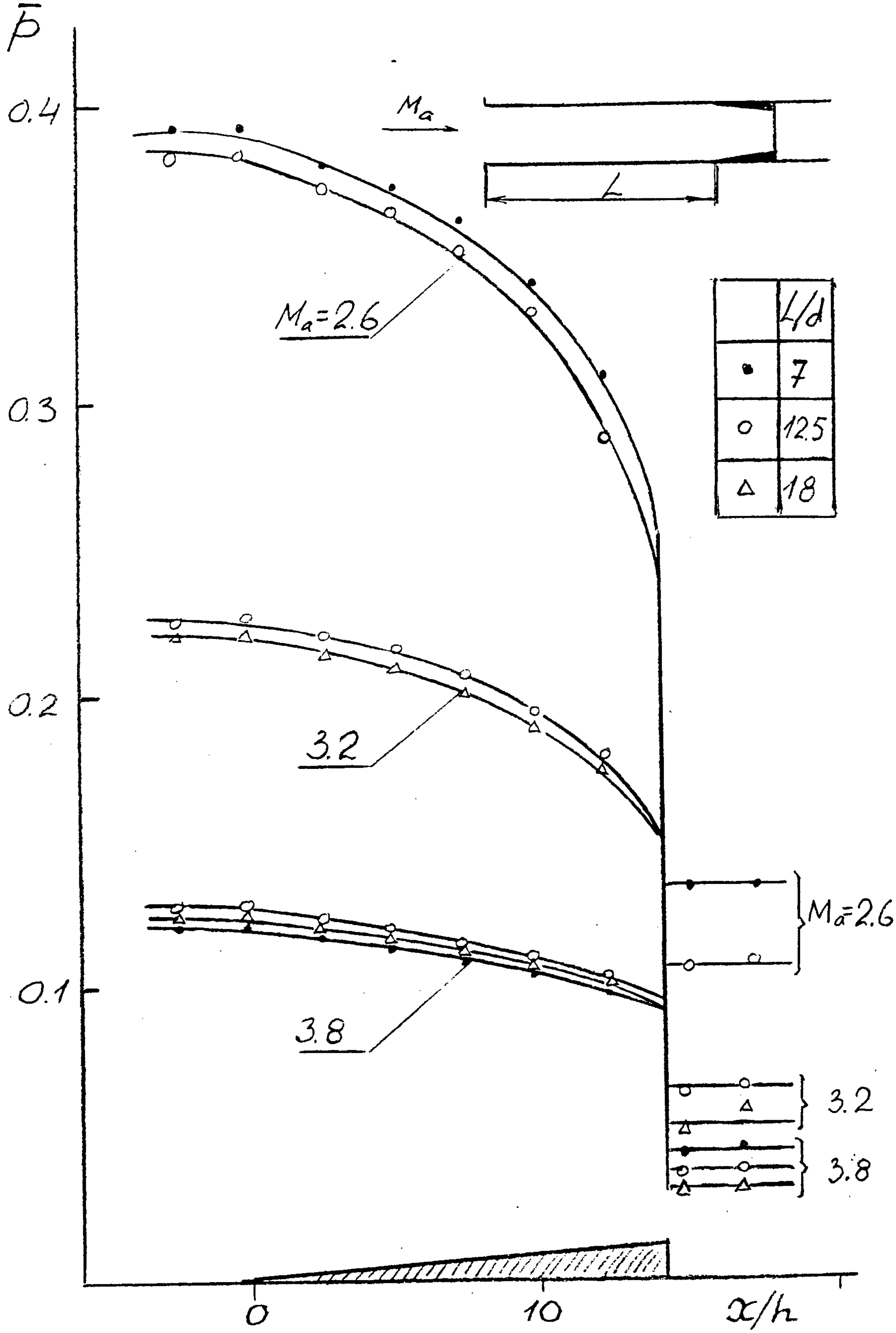

Fig. 4.2.1(Pressure distribution along the circular jut at different Ma and lengths of ducts installed between step and nozzle

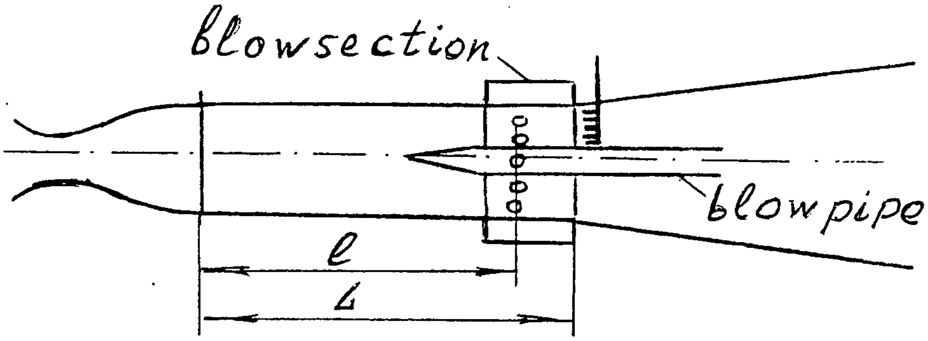

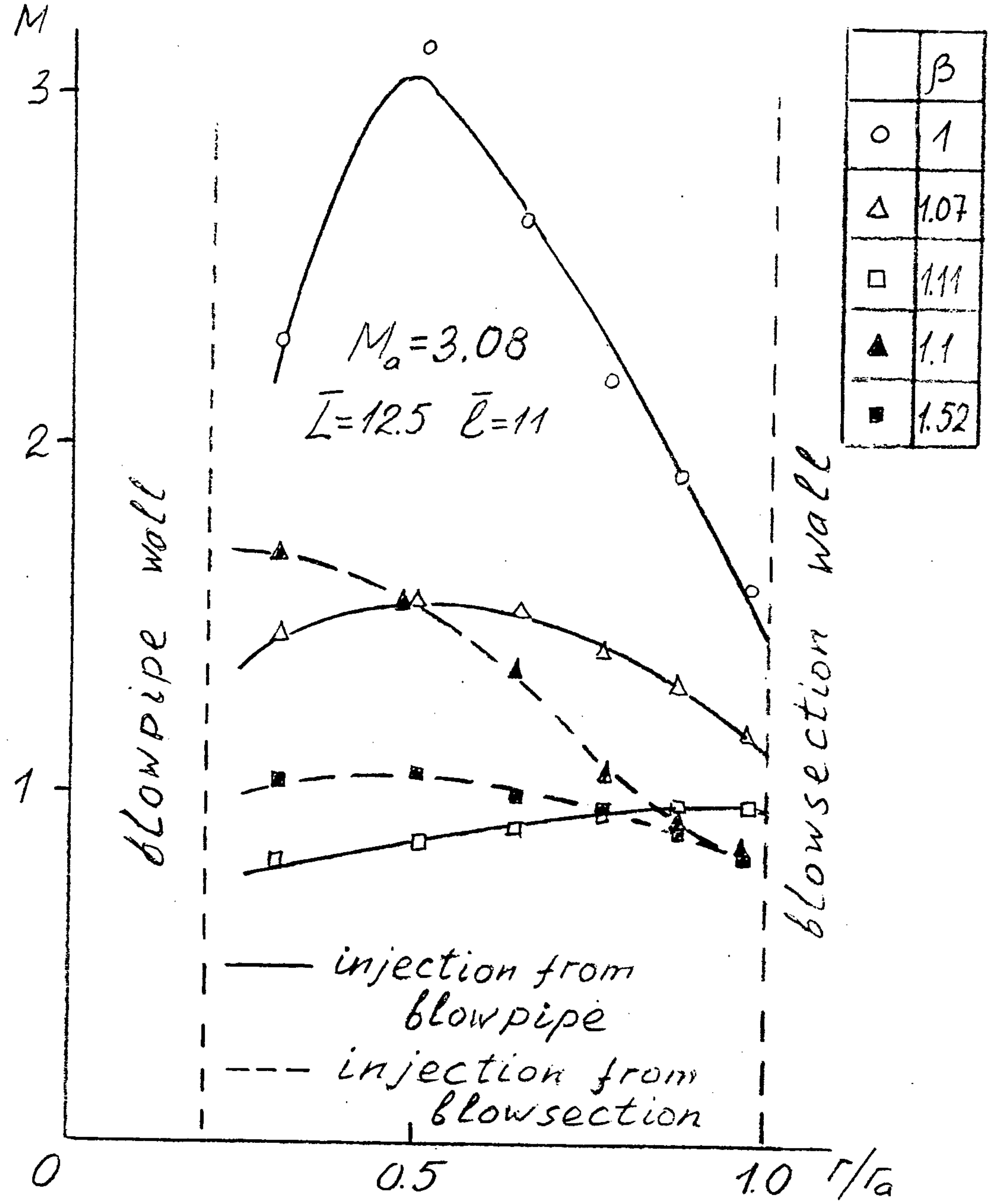

Fig. 4.2.12 Comparison of M-profiles at wall and blow pipe injection at different β

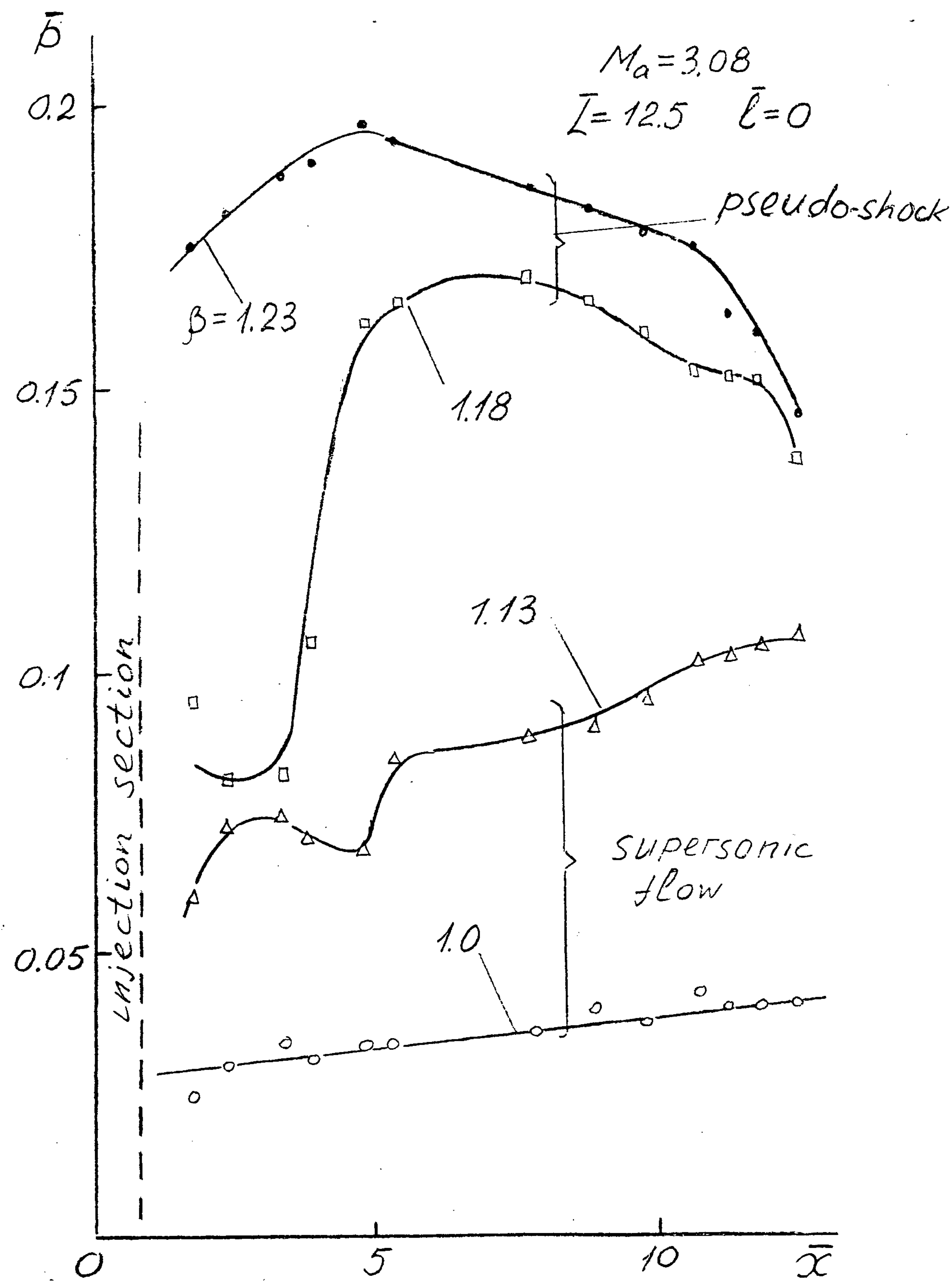

Fig. 4.2.13 Two types of perussure distribution depending on jet injection

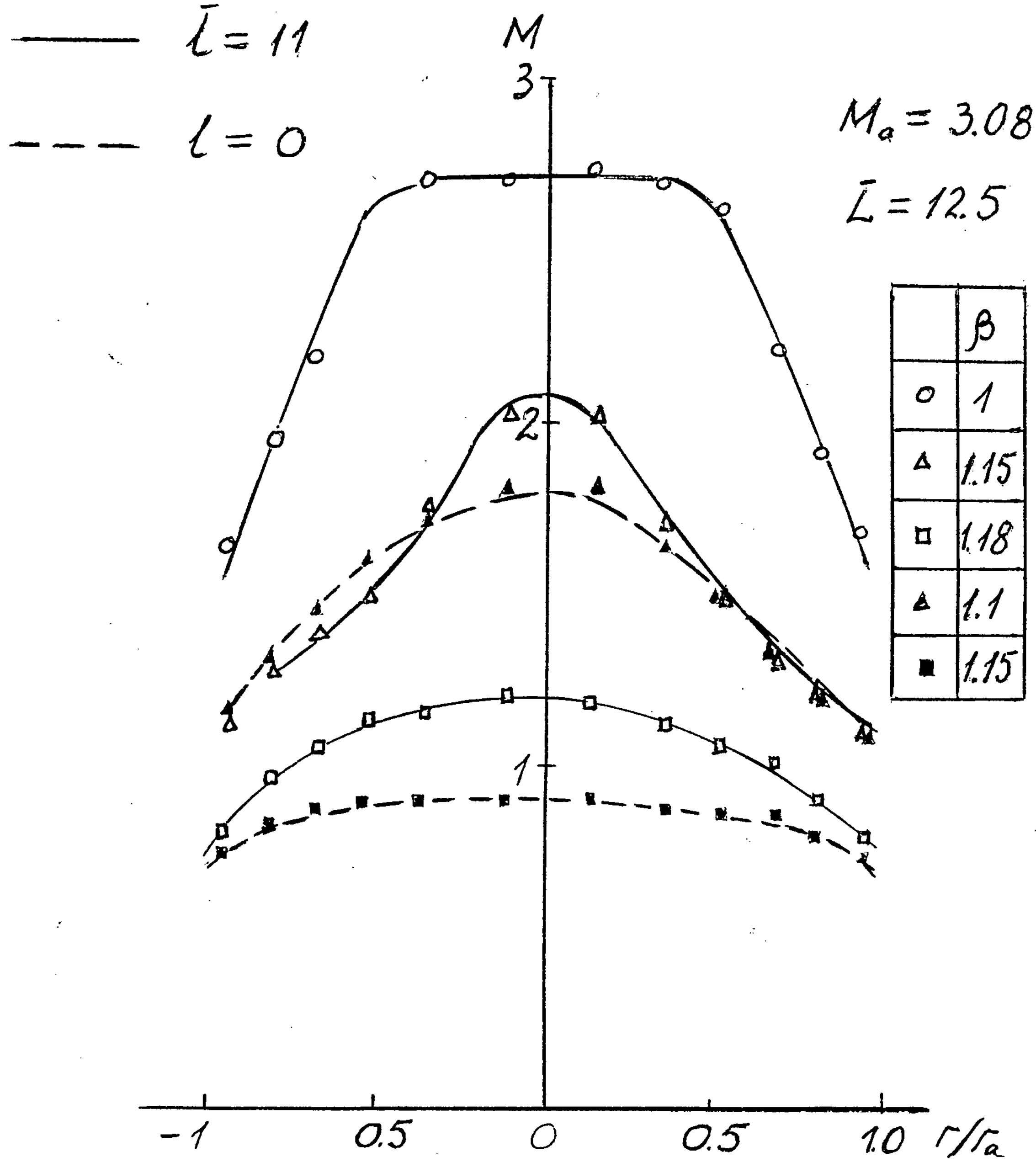

Fig. 4.2.14 Comparison of M-profiles at different β and distances of jet injection from nozzle

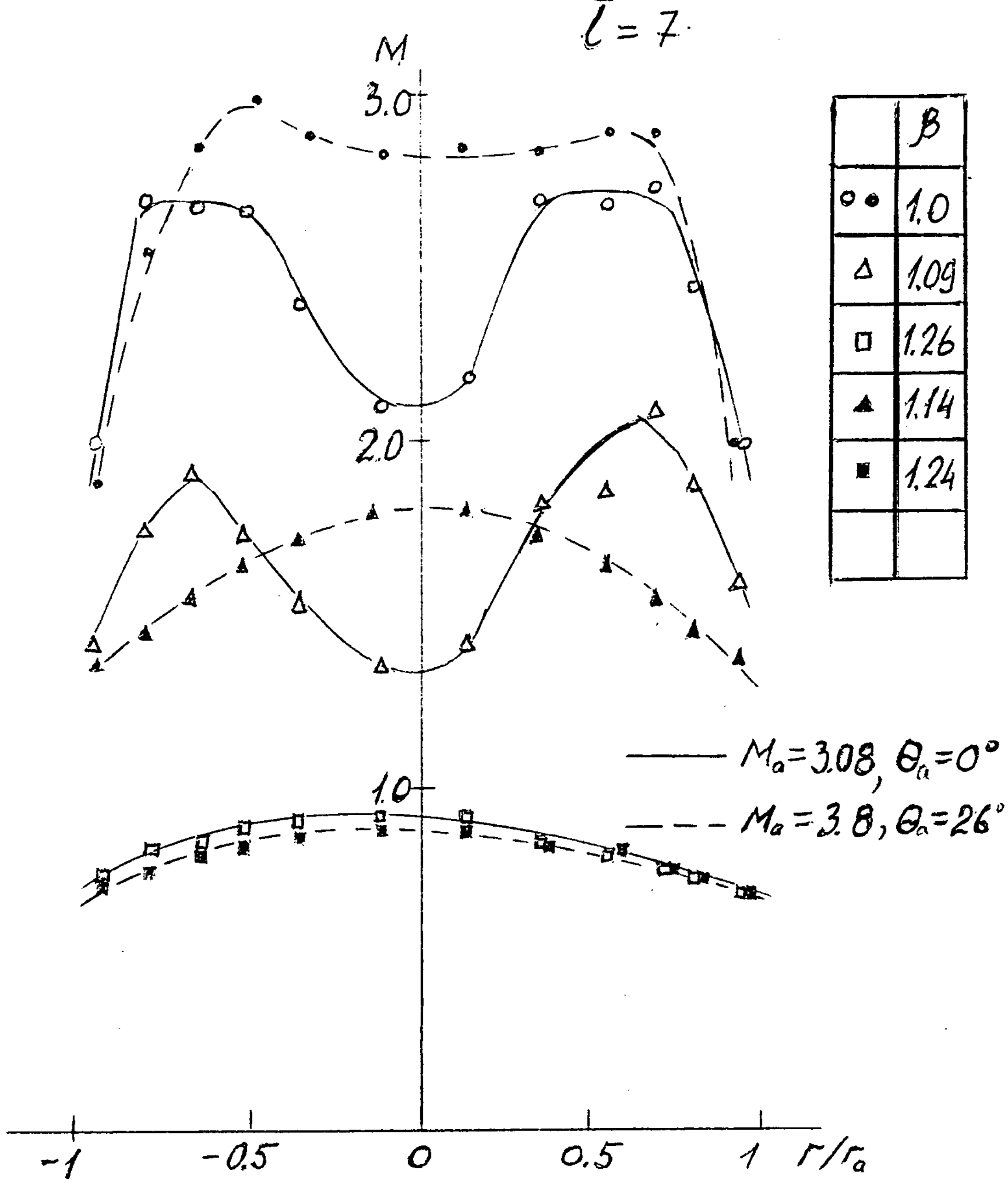

Fig. 4.2.15 Comparison of M-profiles at different β and types of nozzle

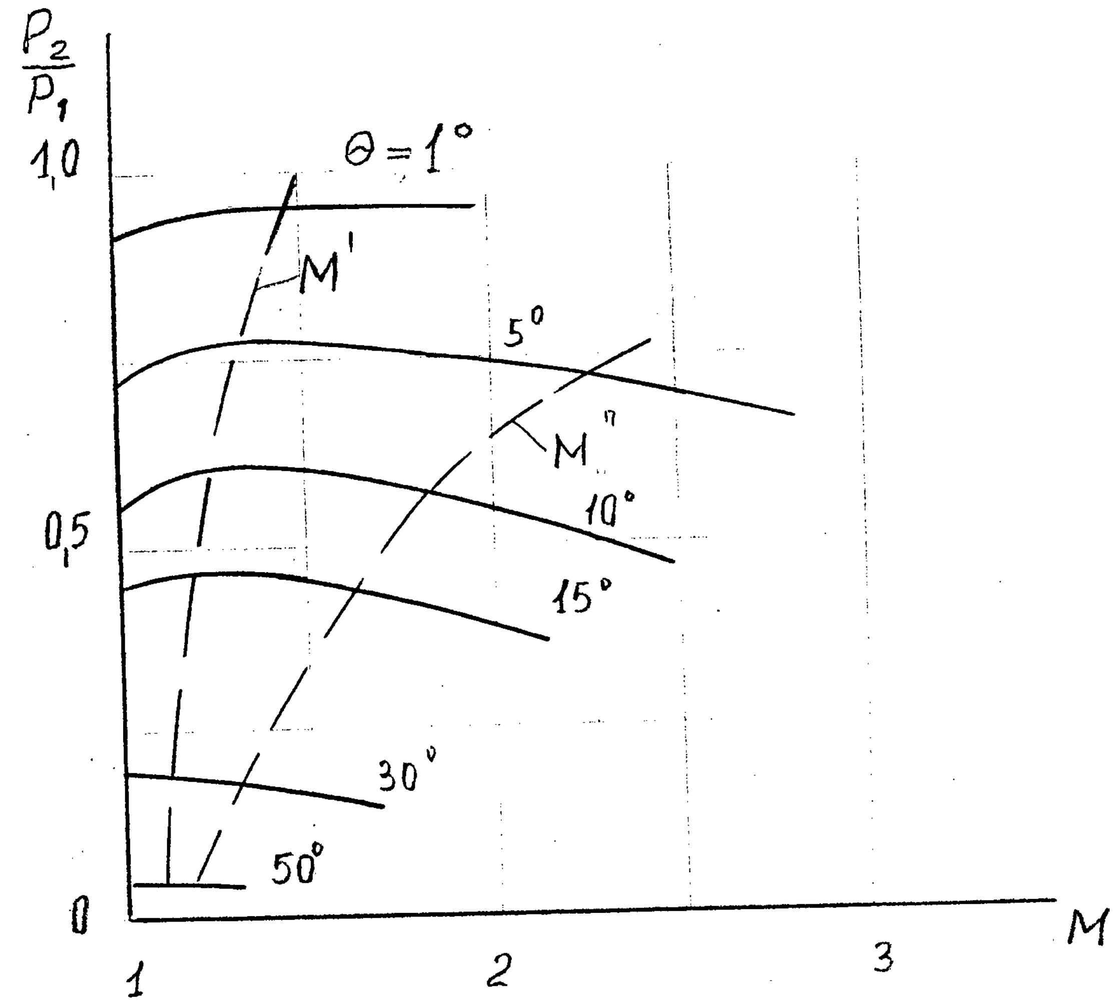

Fig. 4.2.16 Angular point pressure ratio dependence on M.

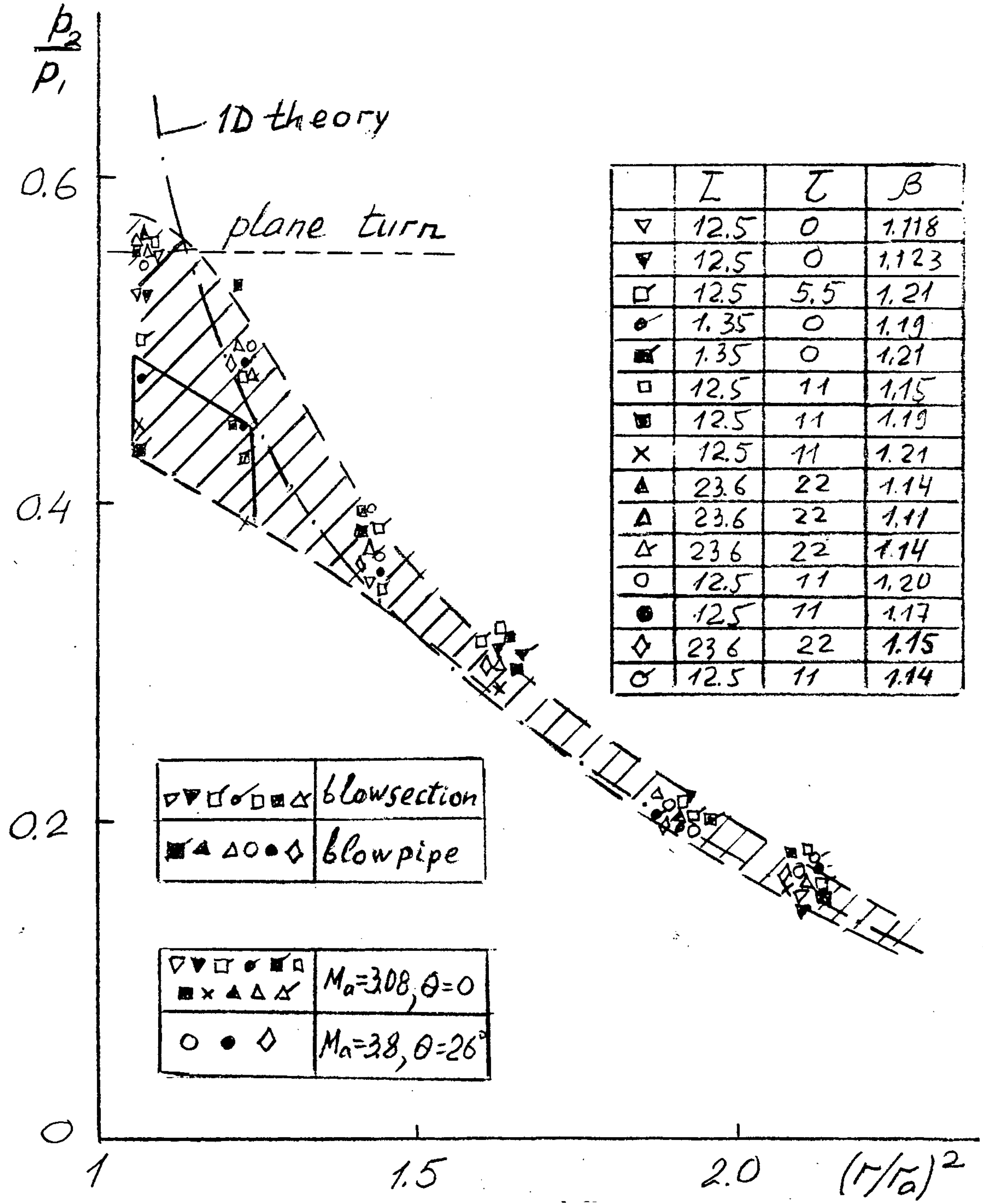

Fig. 4.2.17 Pressure distribution along conical section following cylindrical one with chocking regime created by different means

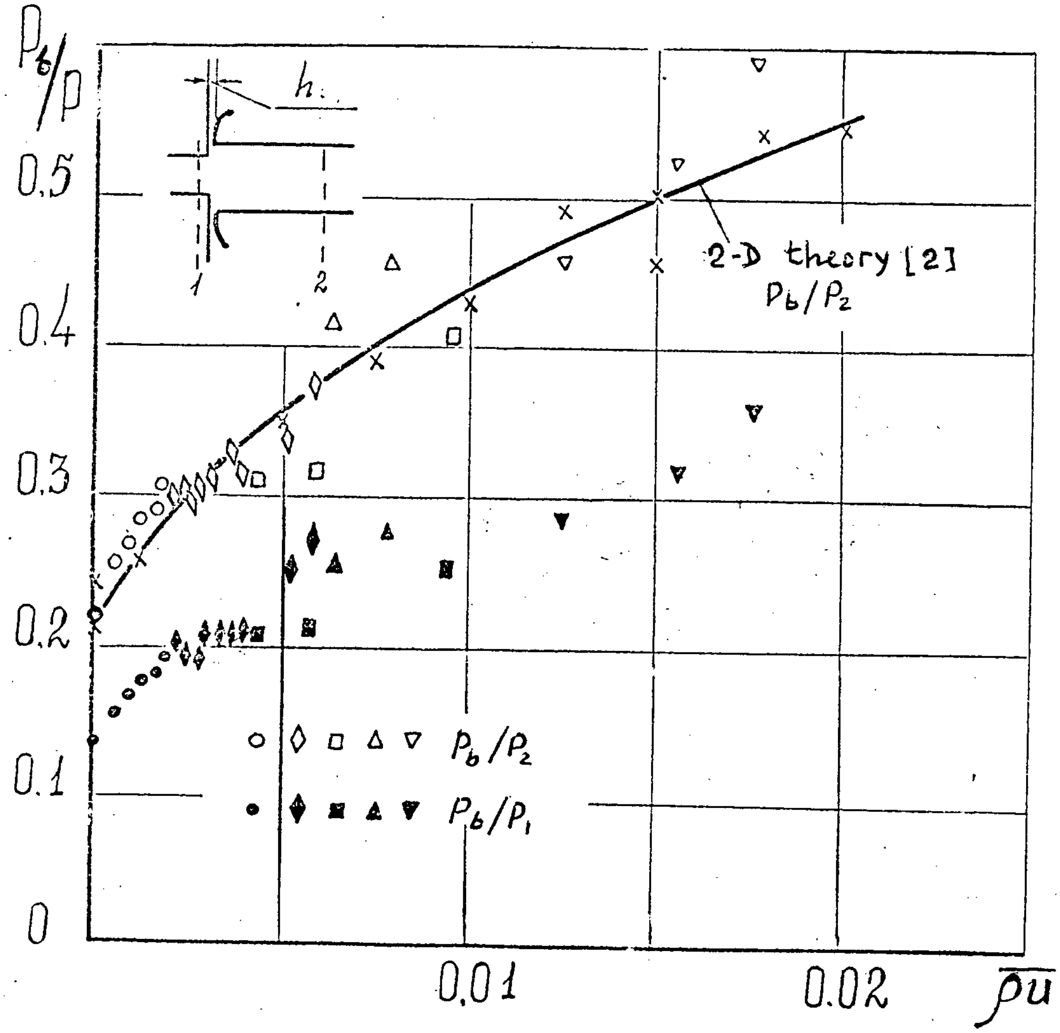

Fig. 4.2.18 Base pressure dependence on relative mass of jet injection into base region. Ma=2.6, f=1.51

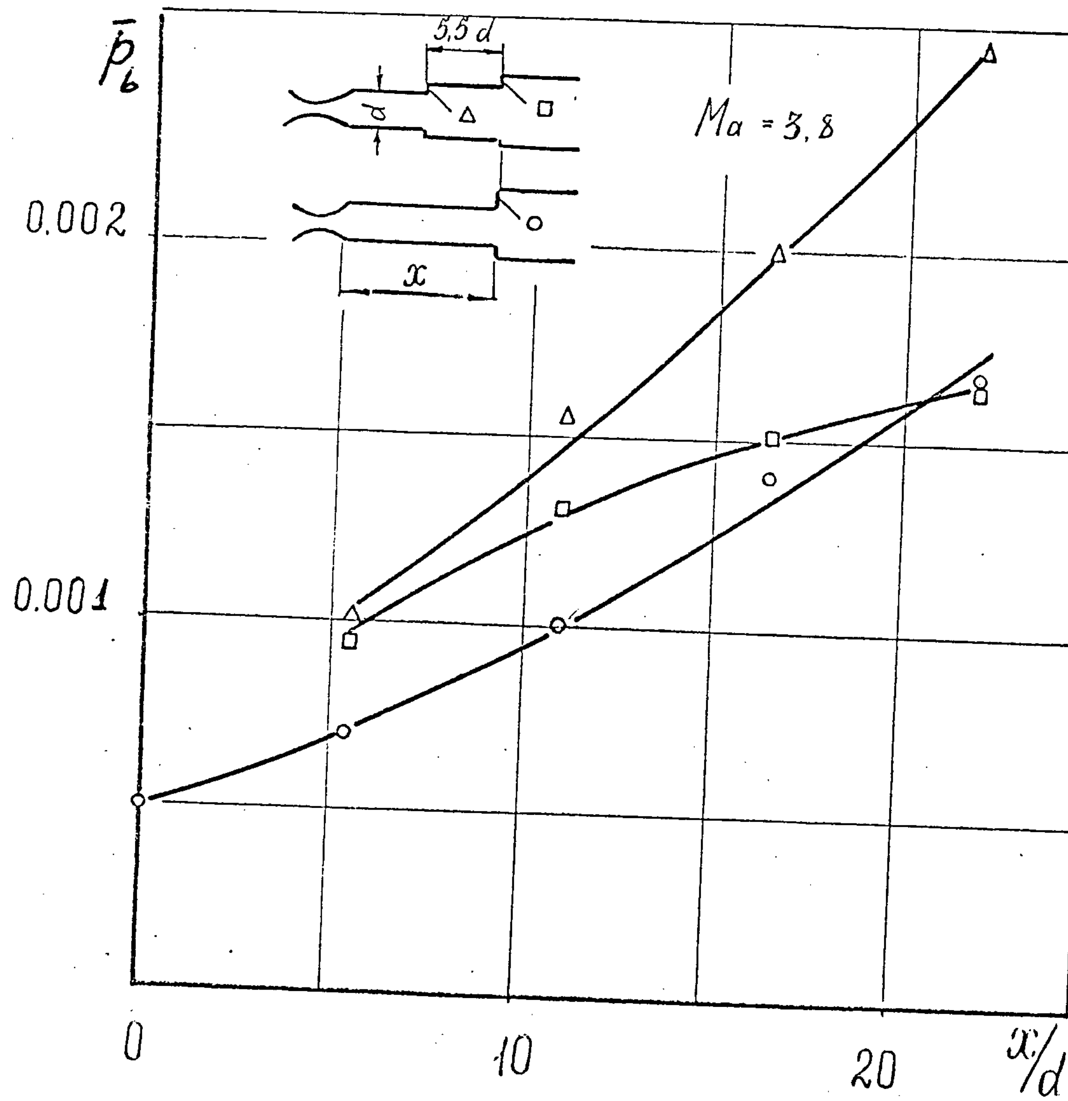

Fig. 4.2.19 Comparison of base pressures in ducts with one and two steps at different distances between step and nozzle

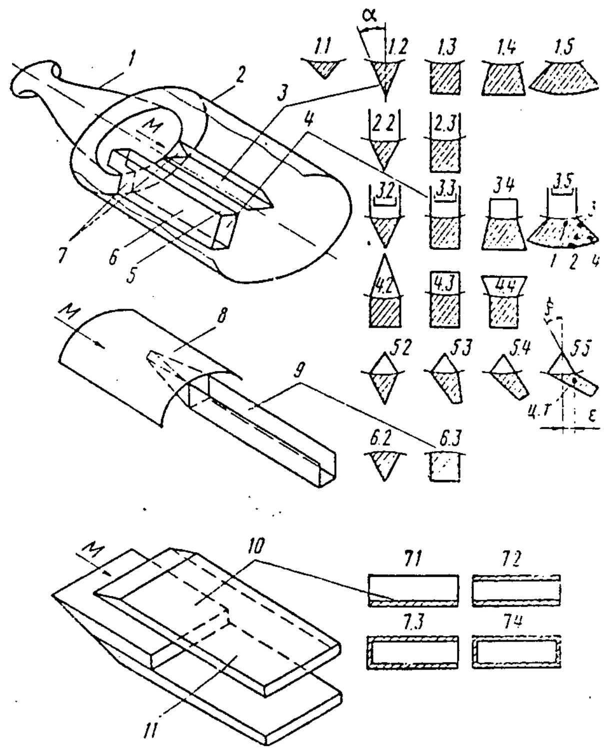

Fig. 4.3.1 Scemes of stepped ducts
1- contoured nozzle, 2- cylindrical tube, 3- opened duct, (shoot) with angle a=30 deg., 4- closed duct (a=0), 5- upper duct wall, 6- side wall, 7- step face, 8- cylindrical surface, 9- shoot with a=0, 10- wedge insert forming step, 11- upper and lower

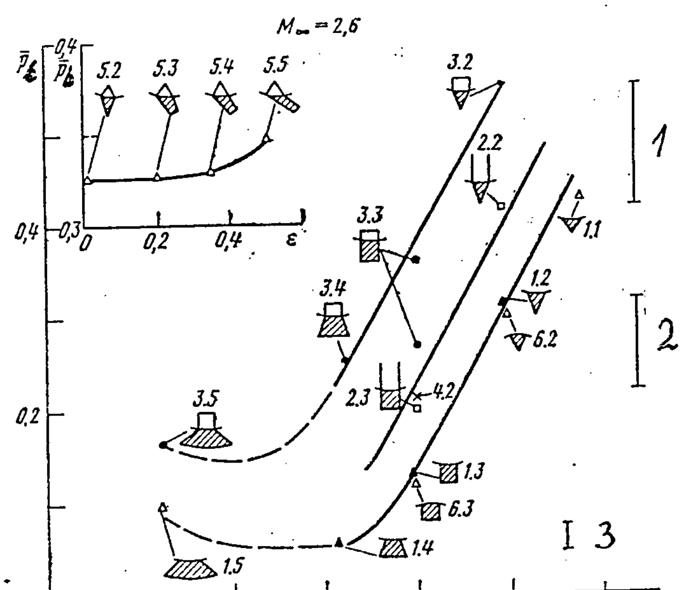

Fig. 4.3.2 Base pressure dependence on α, 1- axisymmetric towards axis, 2-plane, 3- axisymmetric outward axis

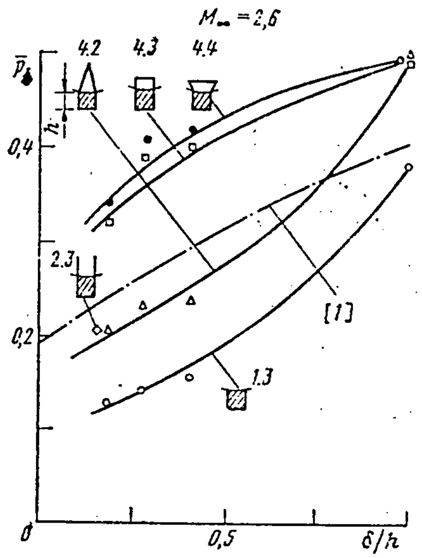

Fig.4.3.3 Base pressure dependence on δ/h

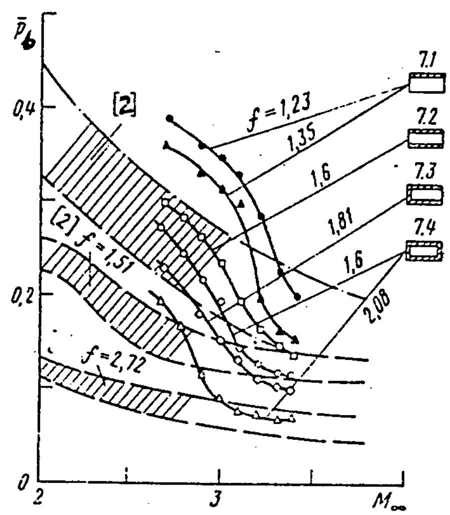

Fig. 4.3.4 Base pressure dependence on Ma

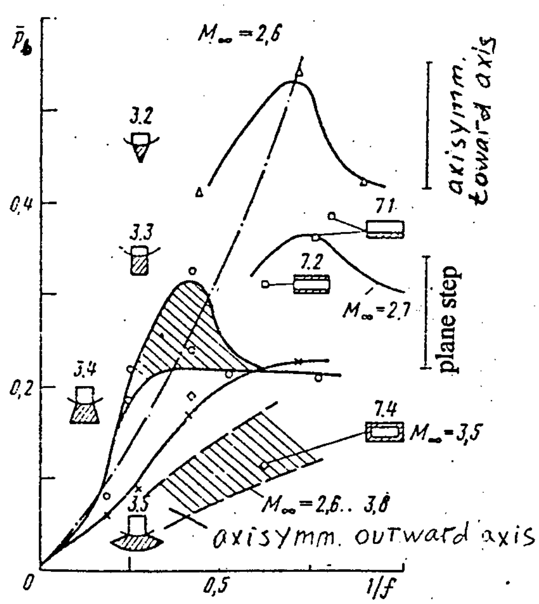

Fig. 4.3.5 Base pressure dependence on 1/f

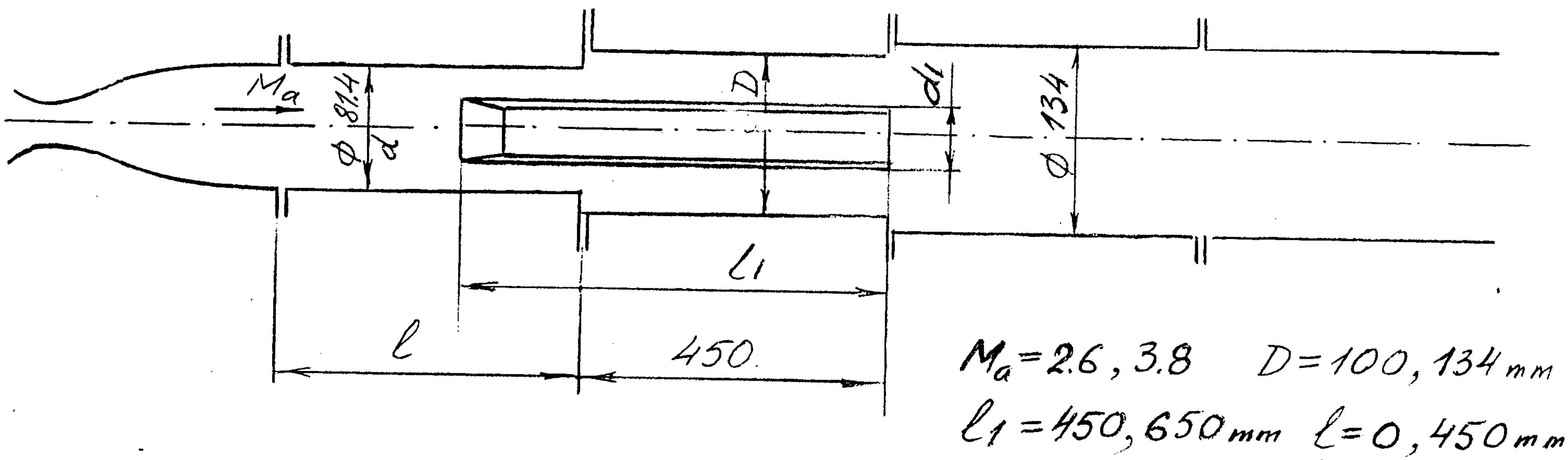

Fig. 4.4.1 Experimental modele schematic

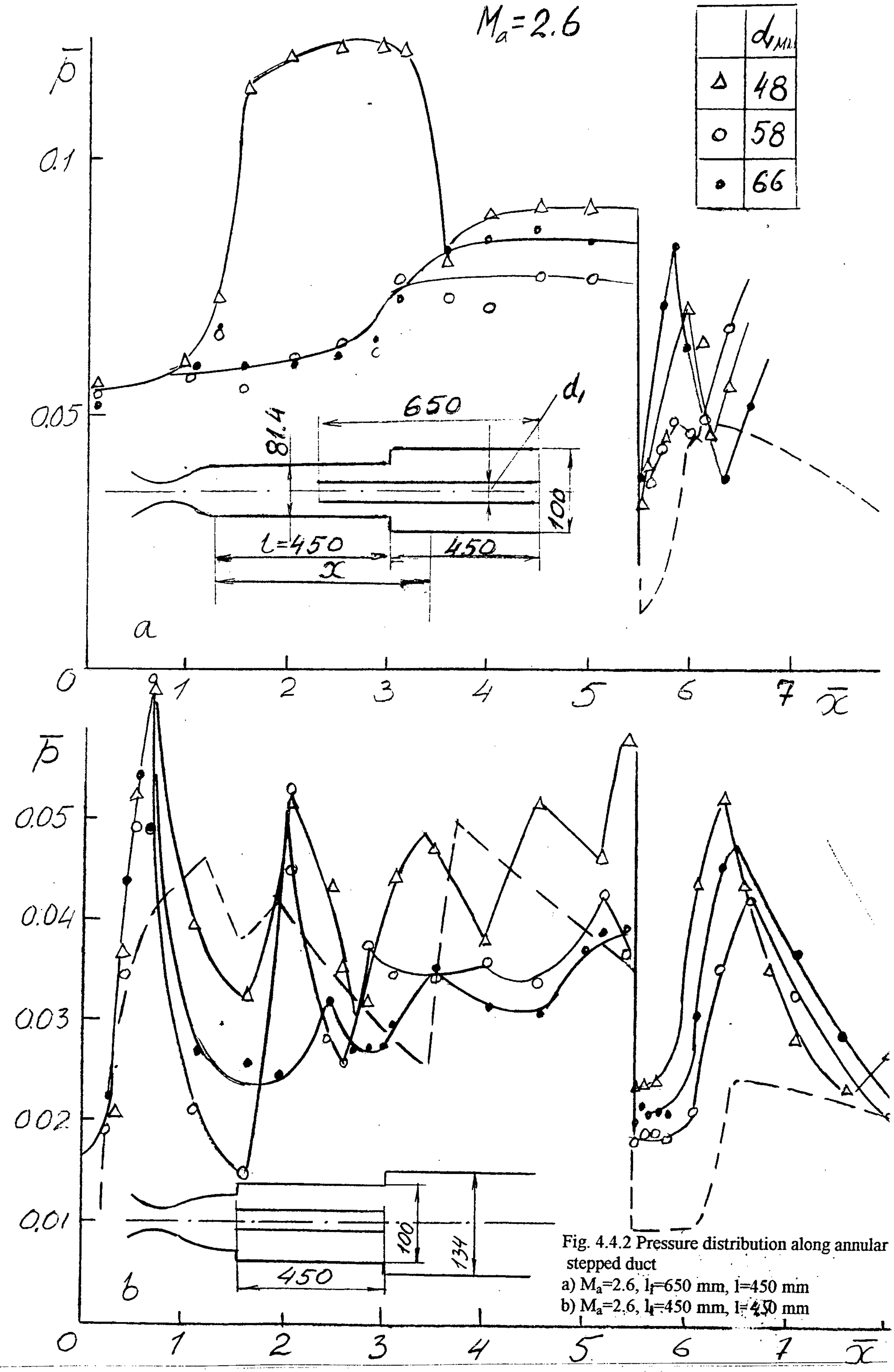

Fig. 4.4.2 Pressure distribution along annular stepped duct

a) M_a=2.6, l_1=650 mm, l=450 mm

b) M_a=2.6, l_1=450 mm, l=450 mm

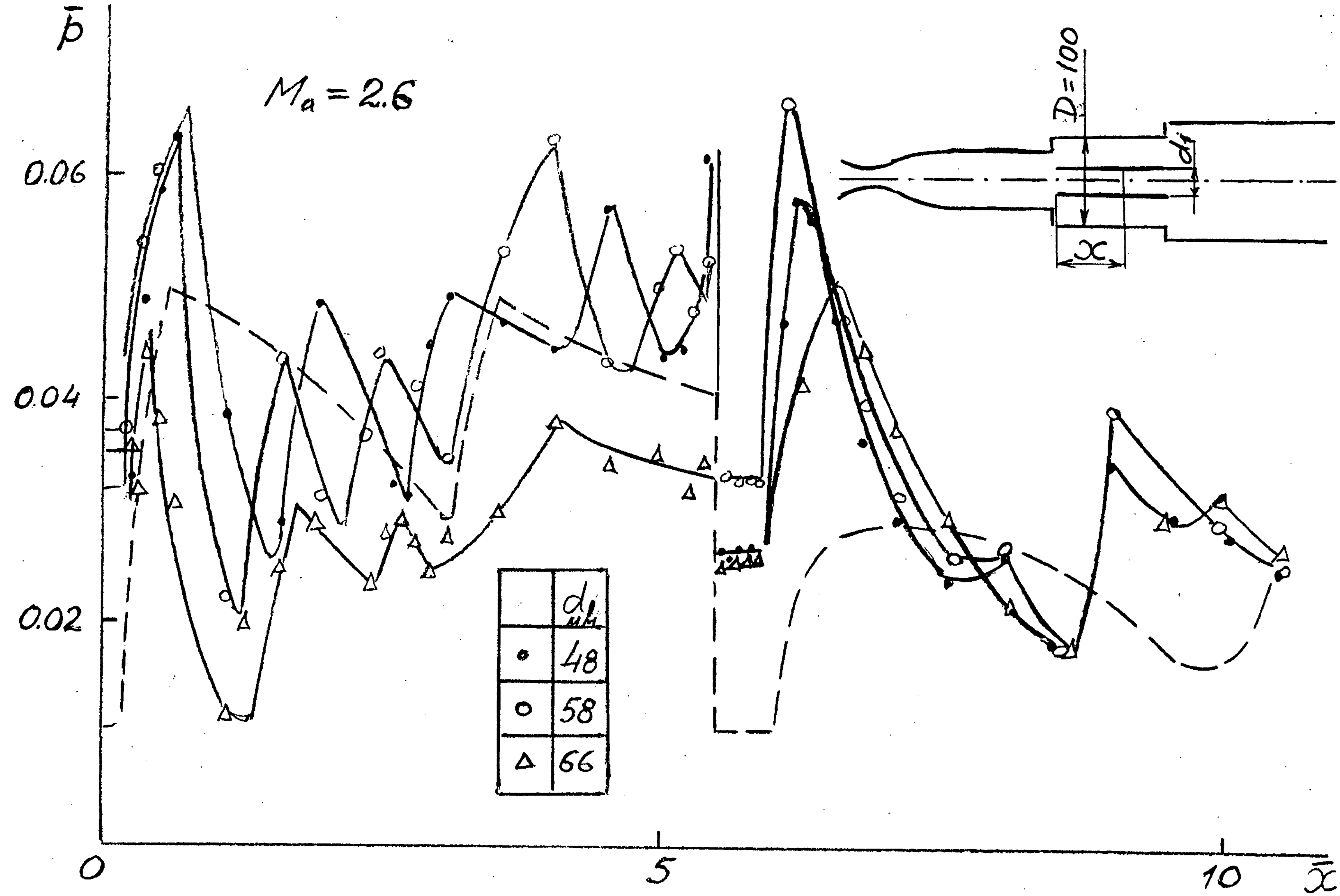

Fig. 4.4.3 Pressure distribution along annular stepped duct
Ma=2.6, l =450 mm, l_i=450 mm.

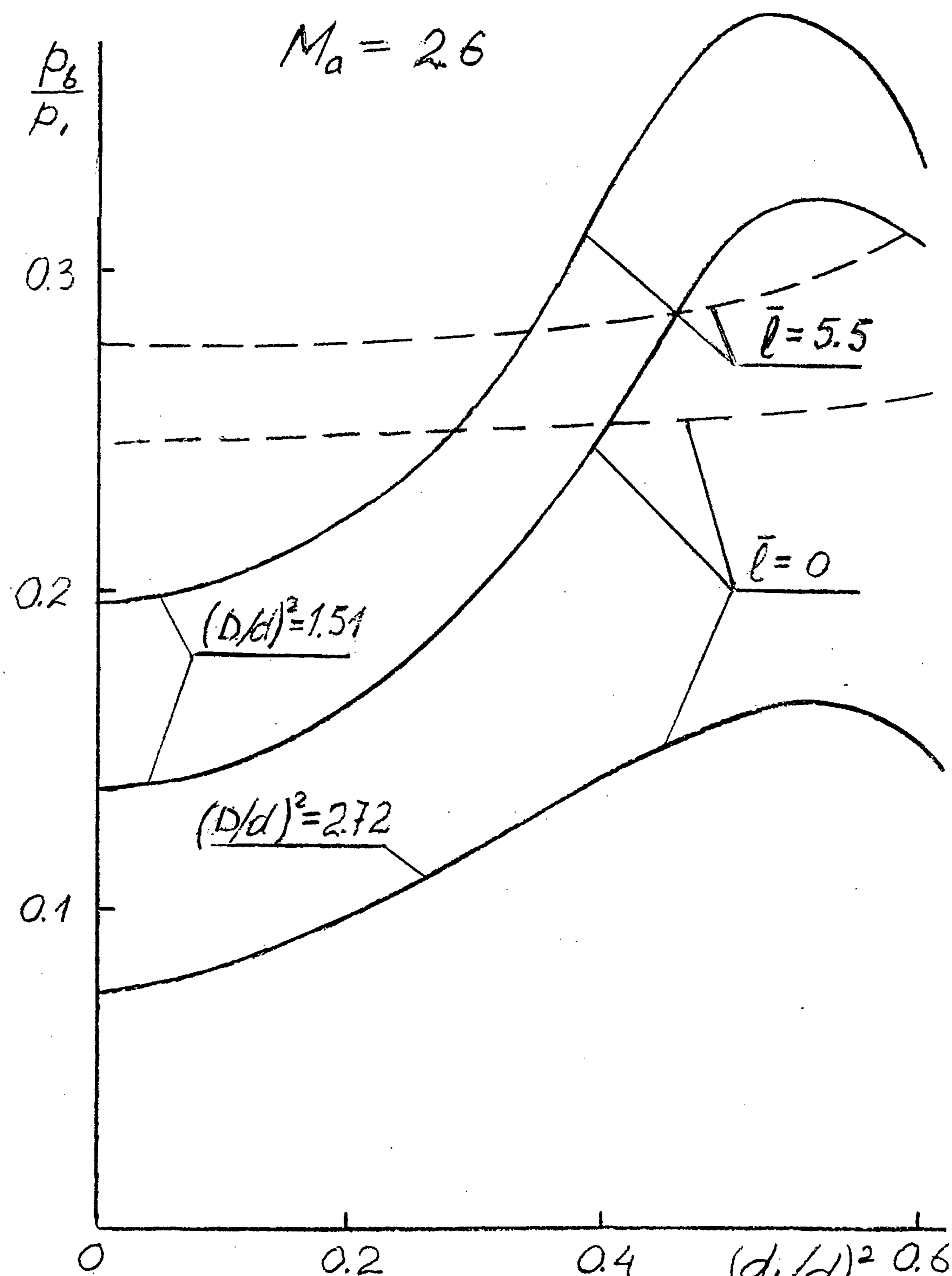

Fig. 4.4.4 **Annular duct base pressure dependence on $(d_1/d)^2$.**
M_a=2.6,—annular stepped duct, ----plane step

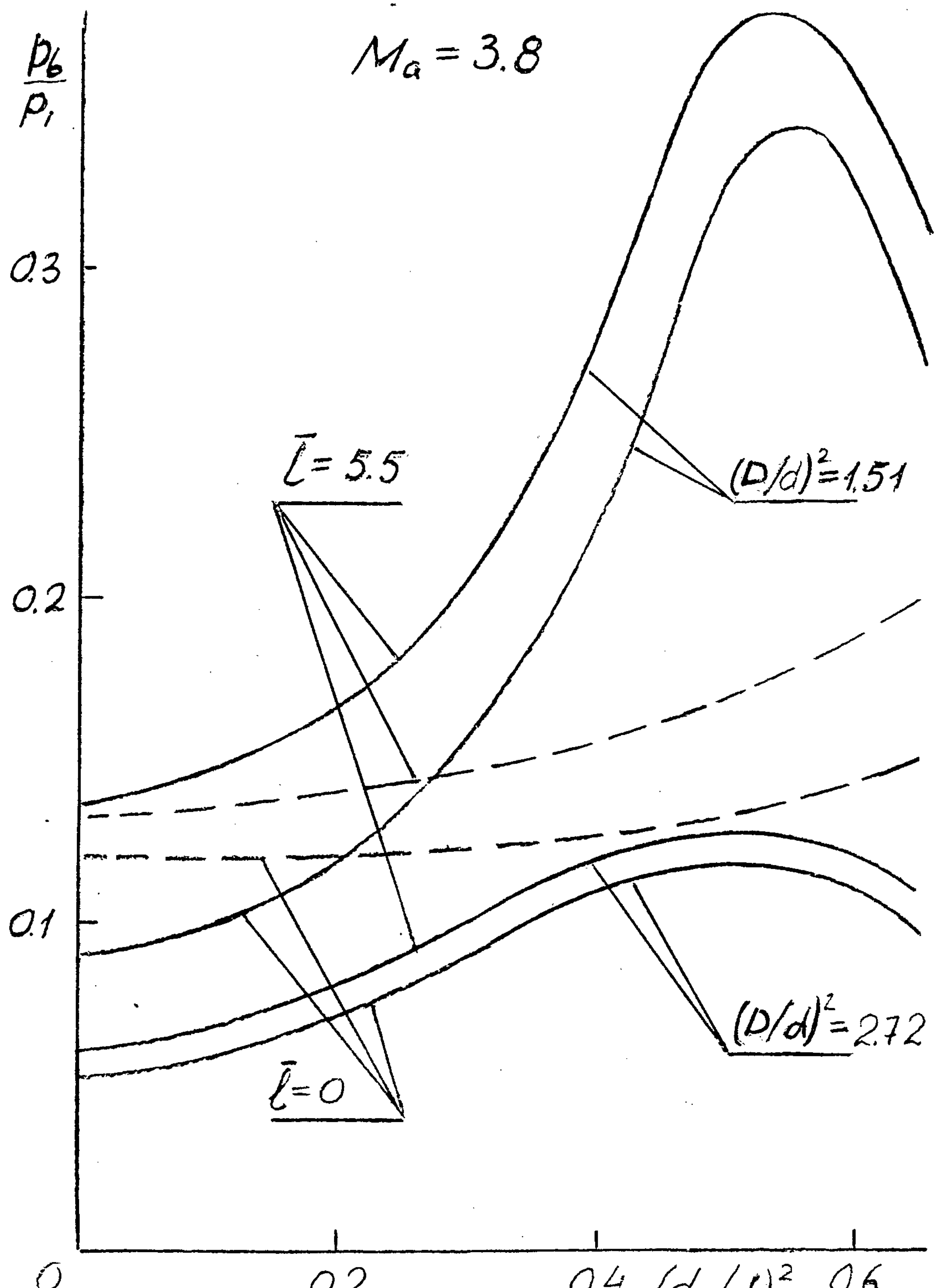

Fig. 4.4.5 Annular duct base pressure dependence on $(d_1/d)^2$
M_a=3.8,—annular stepped duct, ----plane step

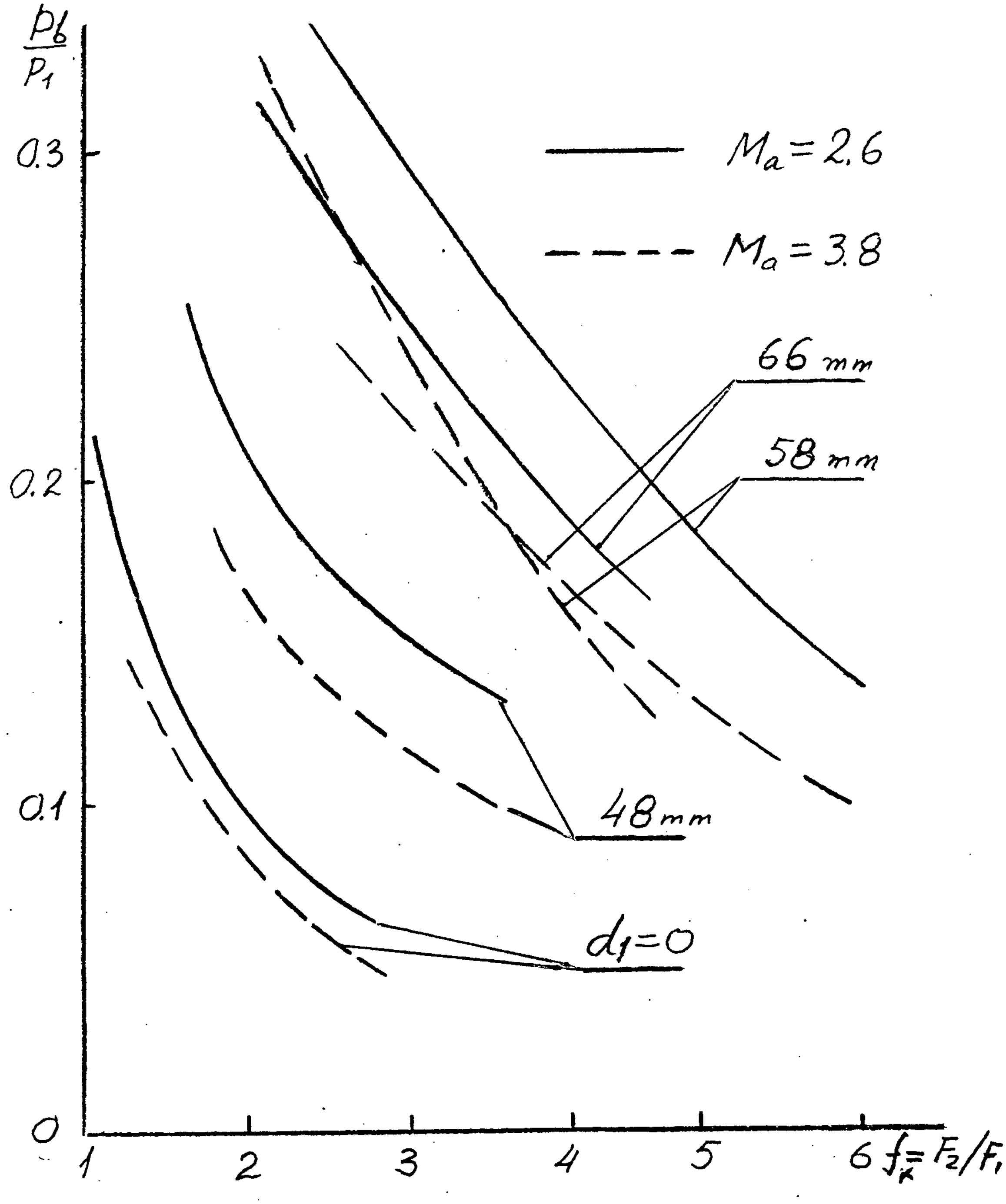

Fig. 4.4.6 Annular duct base pressure dependence on f_κ
Ma=2.6,—annular stepped duct,

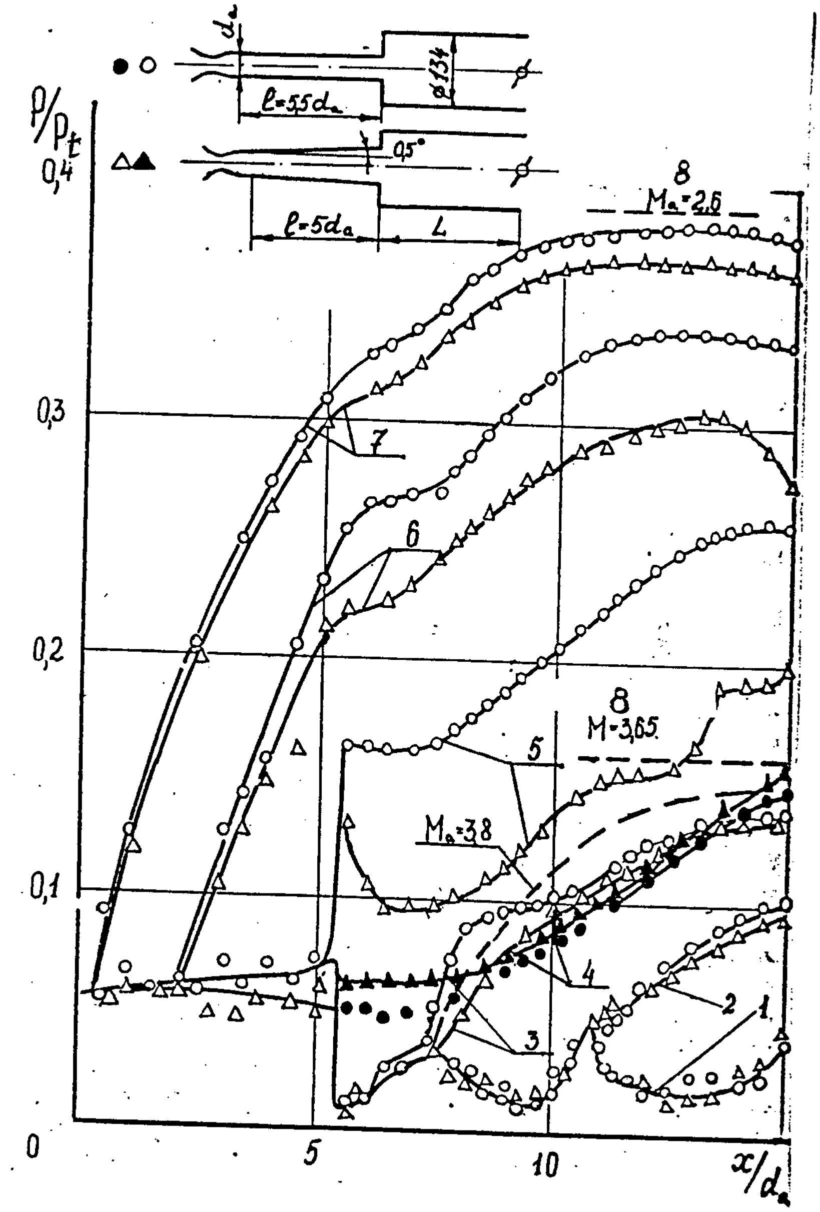

Fig. 4.5.1 Pressure distribution in stepped ducts at different back pressures. Ma=2.6, 1-7-numbers of regimes, 8-normal shock, M=2.65, 9- M=3.65

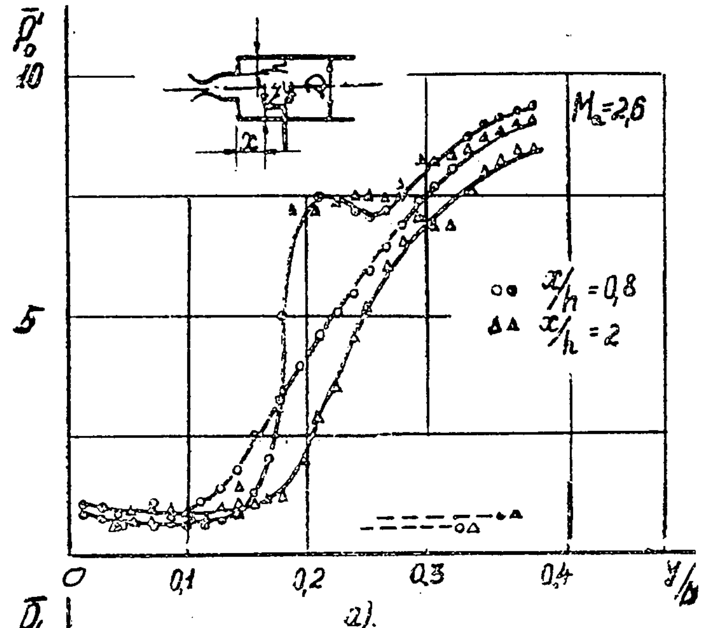

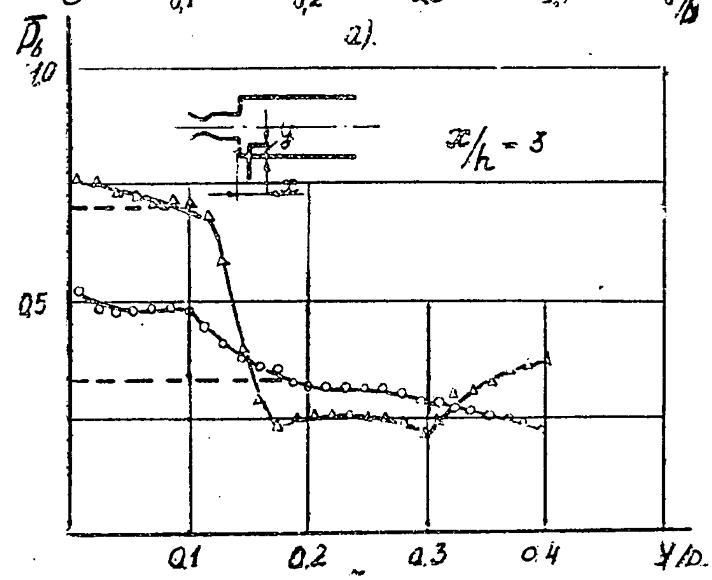

Fig. 4.5.2 Pressure profiles measured by Pitot tube downstream the step.

o Δ correspond to curves 3, ● ▲ -4 of Fig 4.5.1

Fig. 4.5.3 Pressure profiles measured by Pitot tube turned downstream

o correspond to curves 3, Δ -4 of Fig 4.5.1

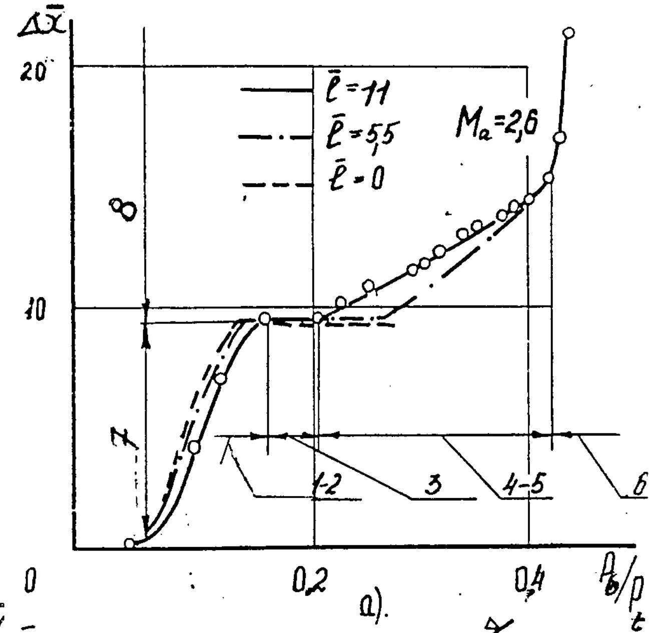

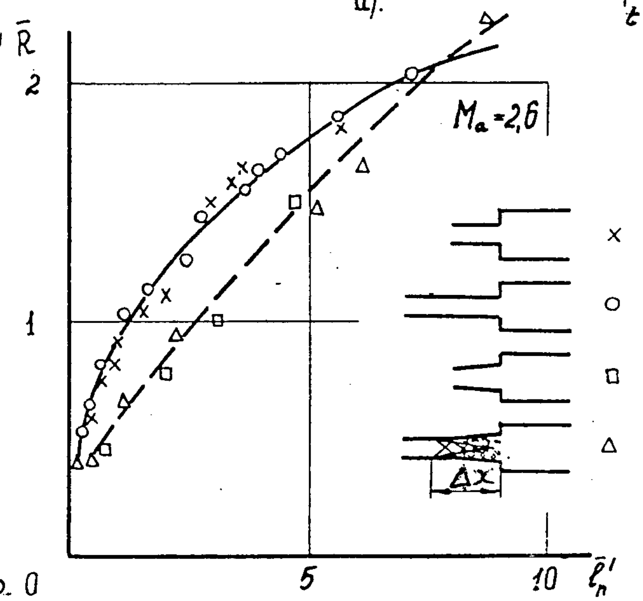

Fig. 4.5.4 Distances of upstream influence vs. back pressure

M_a=2.6, — l=11, ---- l=0, 1-6- numbers of regimes, 7-wide part, 8- narrow part of the stepped duct.

Fig. 4.5.5 Relative axial force imposed to the duct dependence on pseudo-shock length.

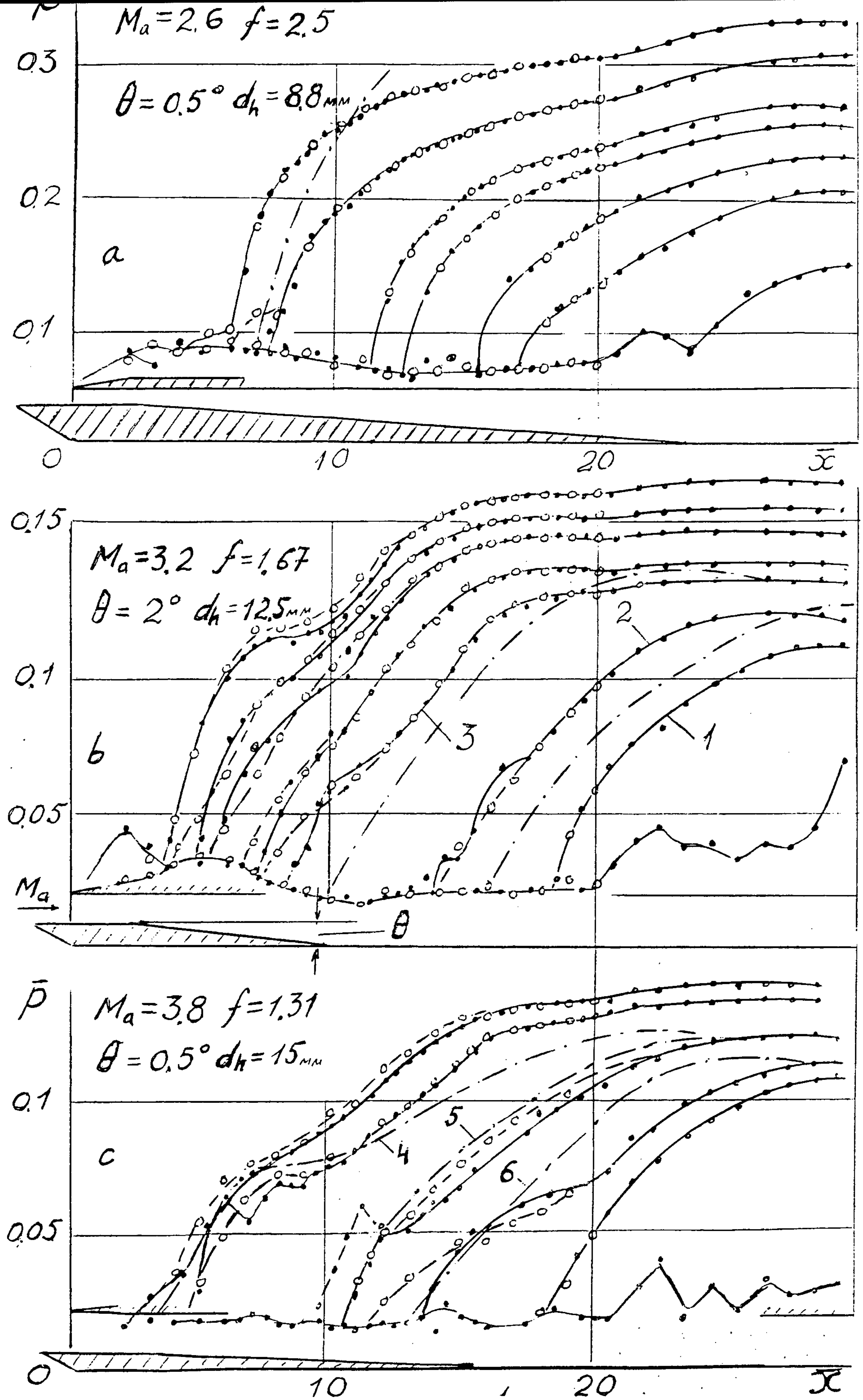

Fig. 4.6.1 Pressure distributions in rectangular diverging ducts. 1-6-flow regimes.

a)-M_a=2.6, f=2.5, $\theta=0.5^0$, d_h= 8.8 mm

b)-M_a=3.2, f=1.67, $\theta=2^0$, d_h=12.5 mm

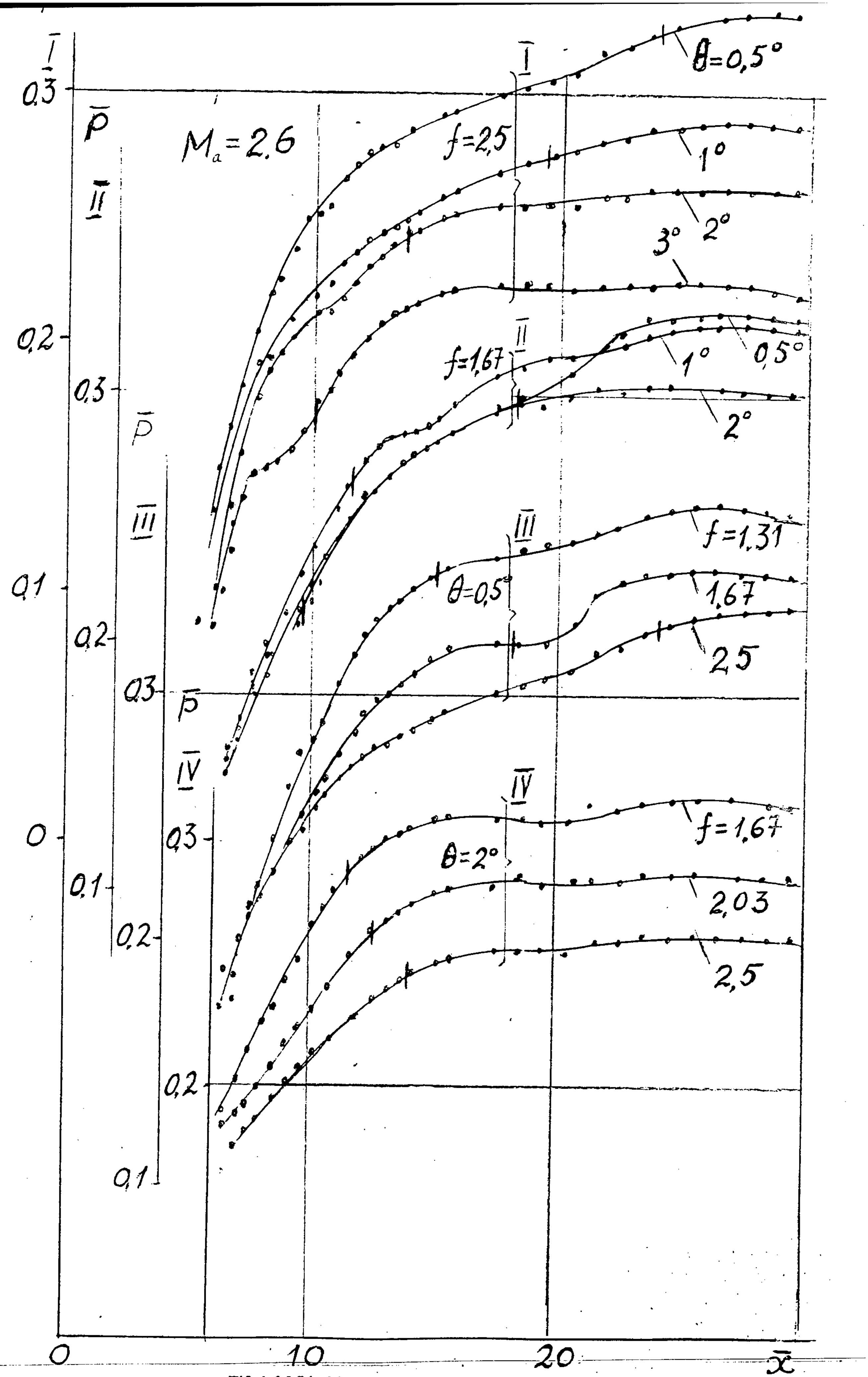

Fif. 4.6.2 Limiting pressure distributions in different

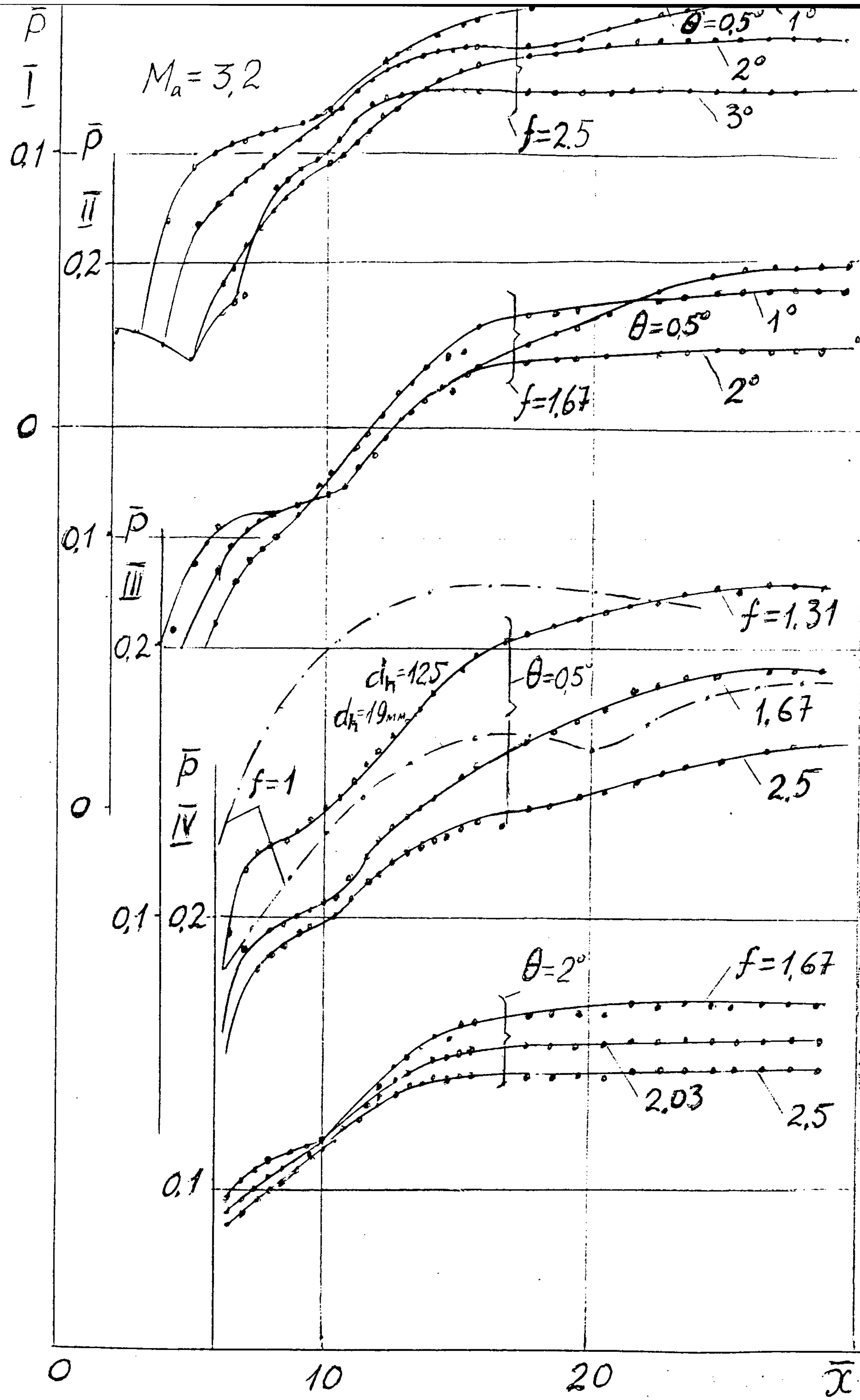

Fig.4.6.3 Limiting pressure distributions in different rectangular diverging ducts, M_a=3.2

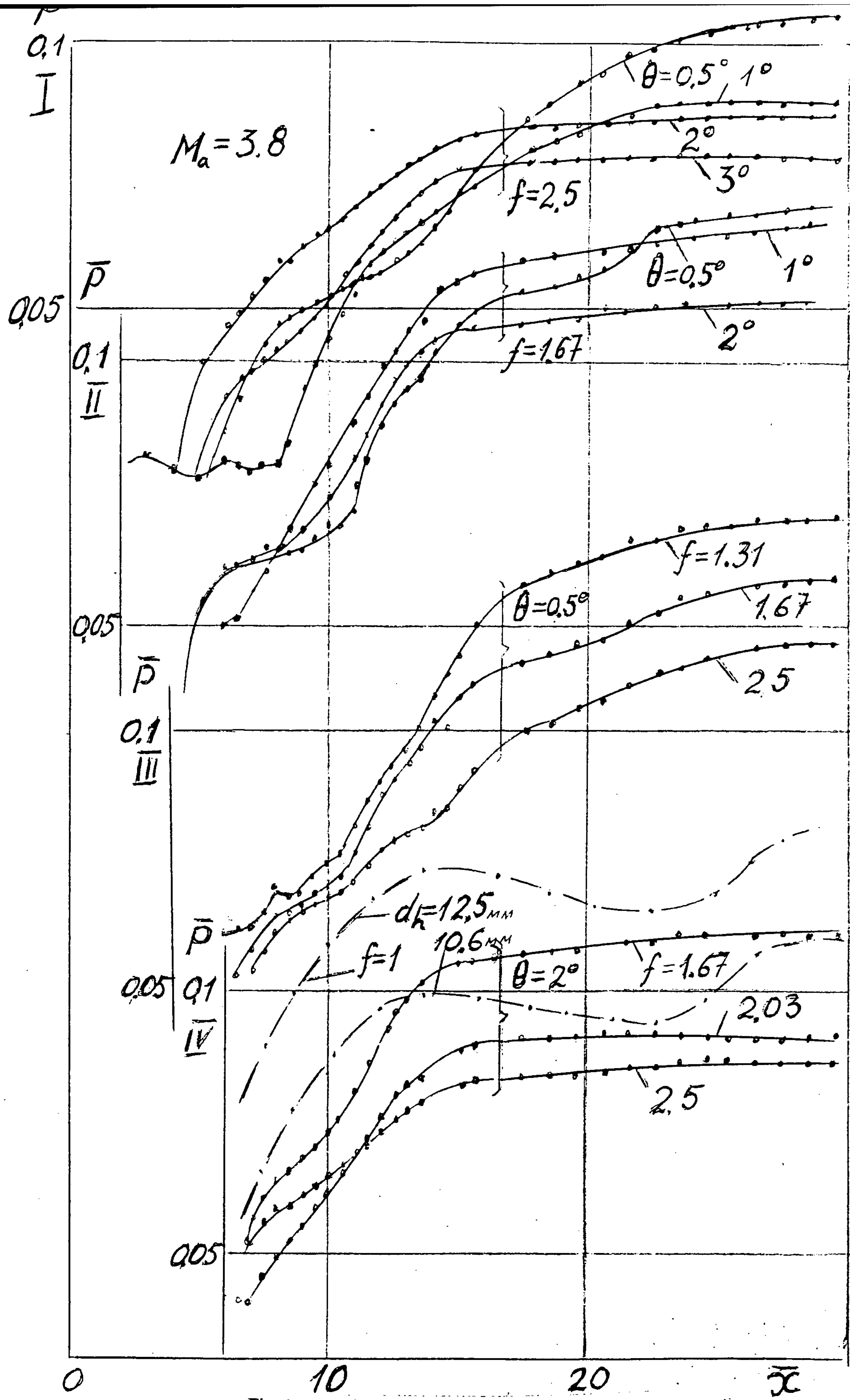

Fig. 4.6.4 Limiting pressure distributions in different rectangular diverging ducts, M_a=3.8

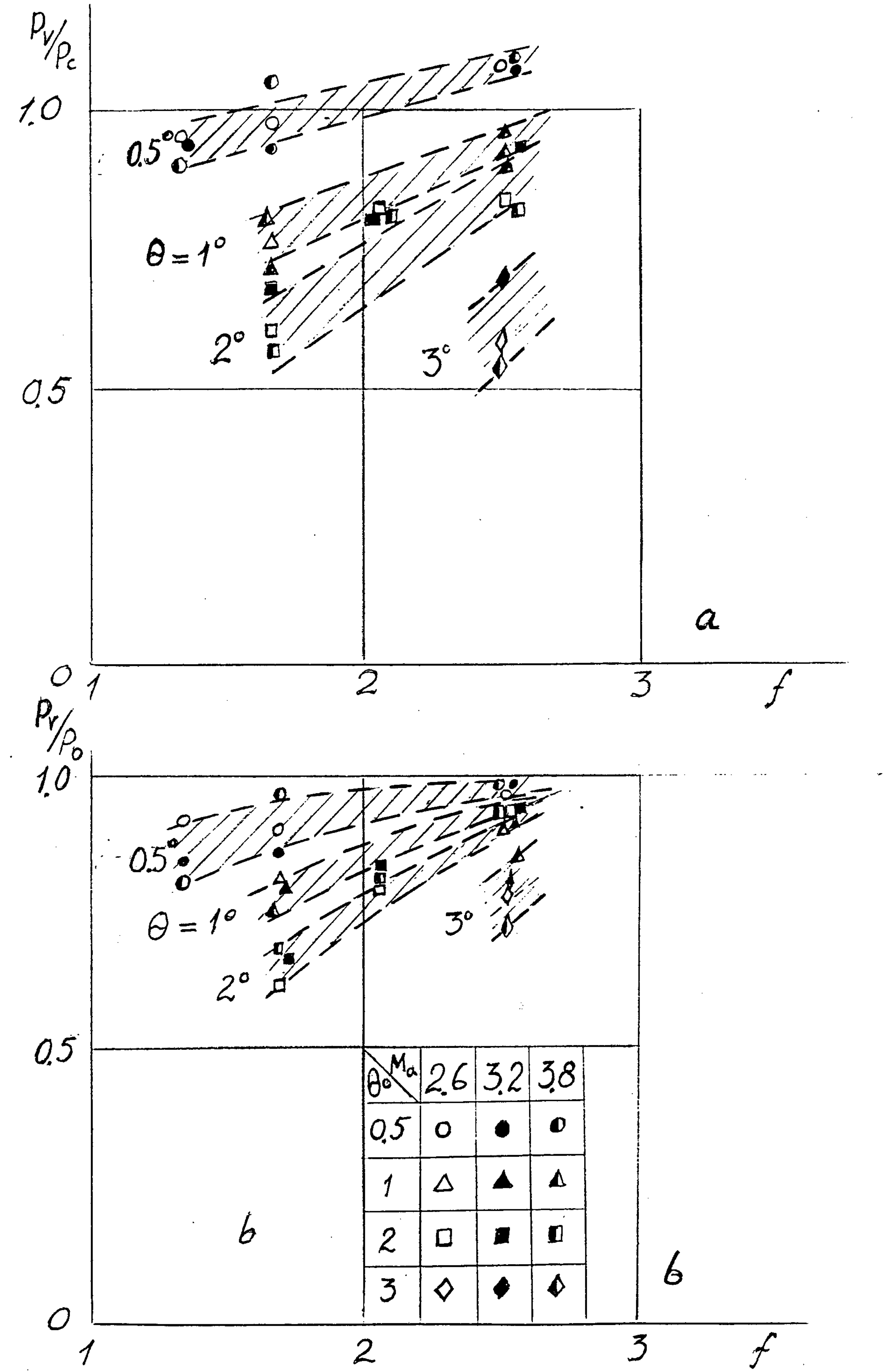

Fig. 4.6.5 f dependence on ratio of pressure recoveries
a)-diverging and constant area ducts,
b)-diverging and combined area ducts

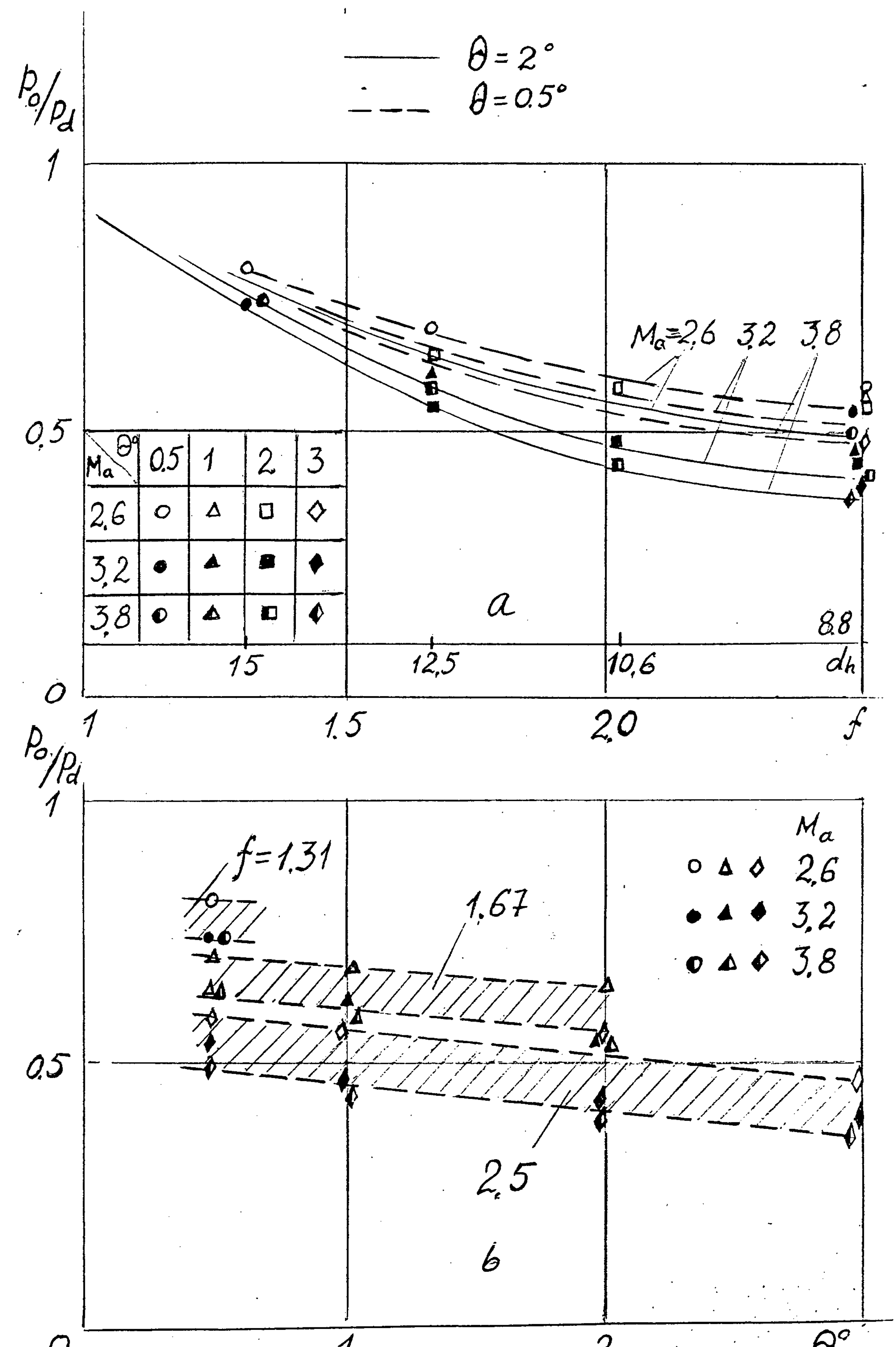

Fig. 4.6.6 Ratio of pressure recoveries in combined area ducts and theoretically maximal possible
a)-vs f, b)-vs θ

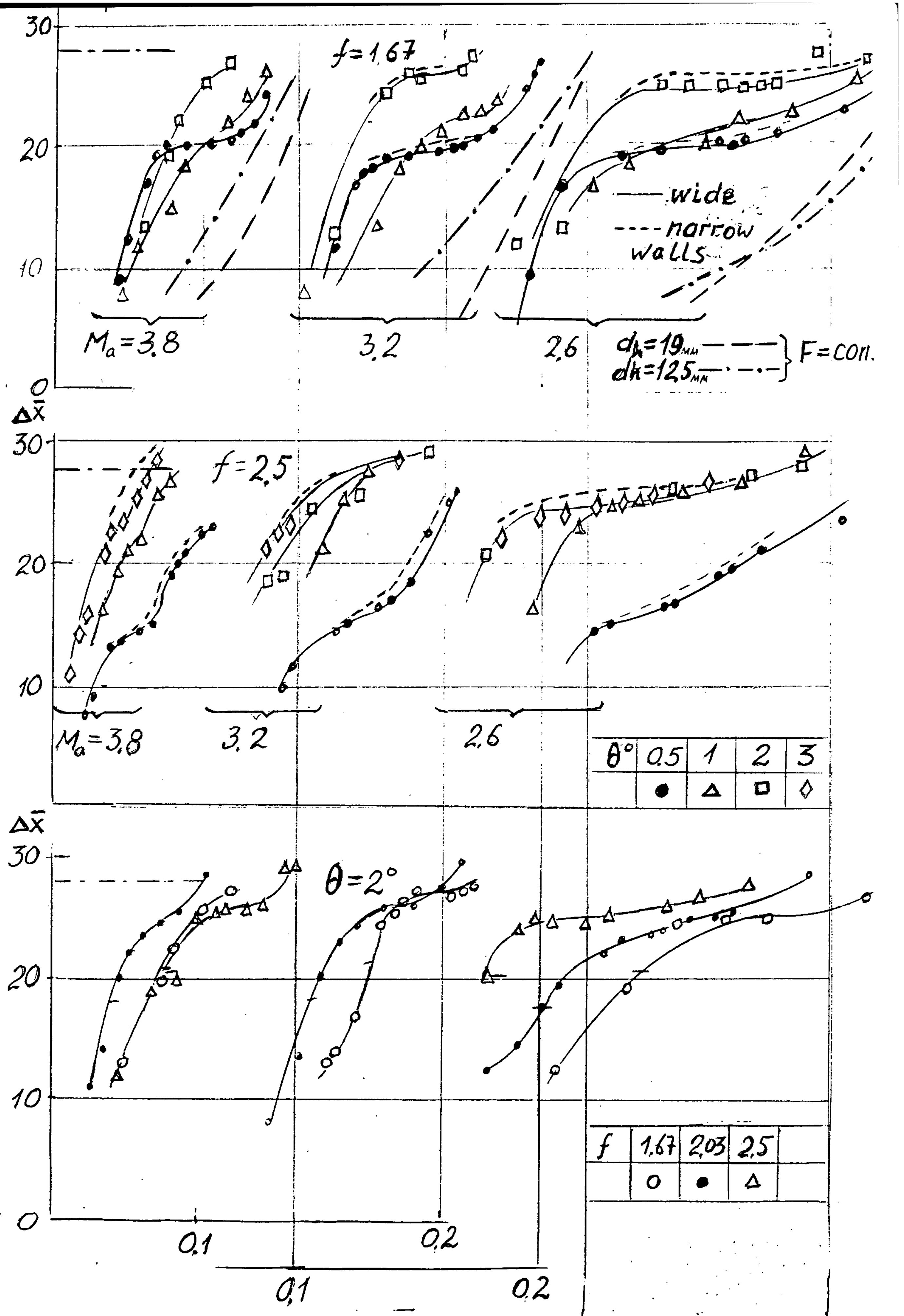

Fig. 4.6.7 Distancies of upstream influences vs. back pressure in rectangular diverging ducts at different M_a, f, θ

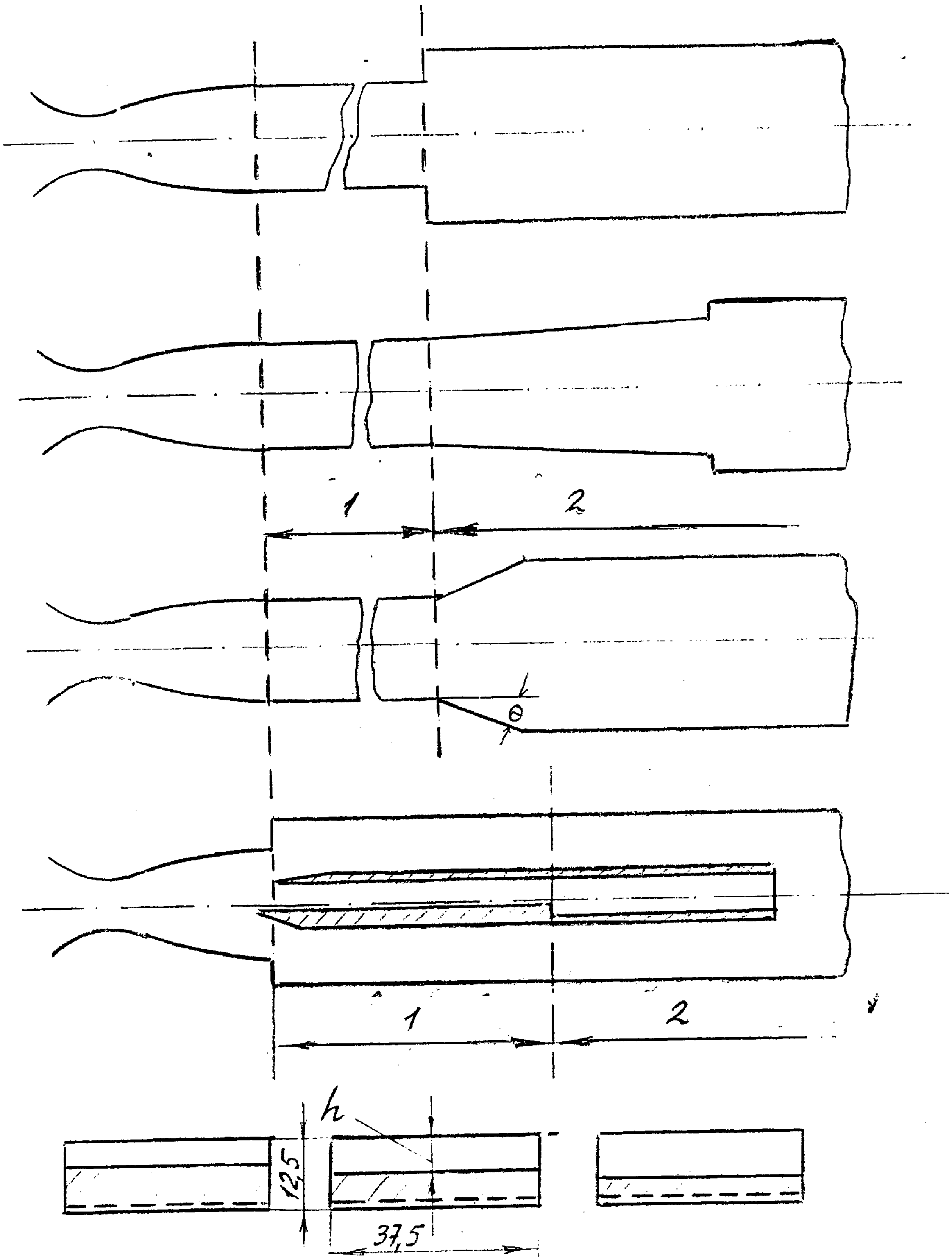

Fig. 4.7.1 Models schematic
1-supersonic, 2- subsonic diffusers

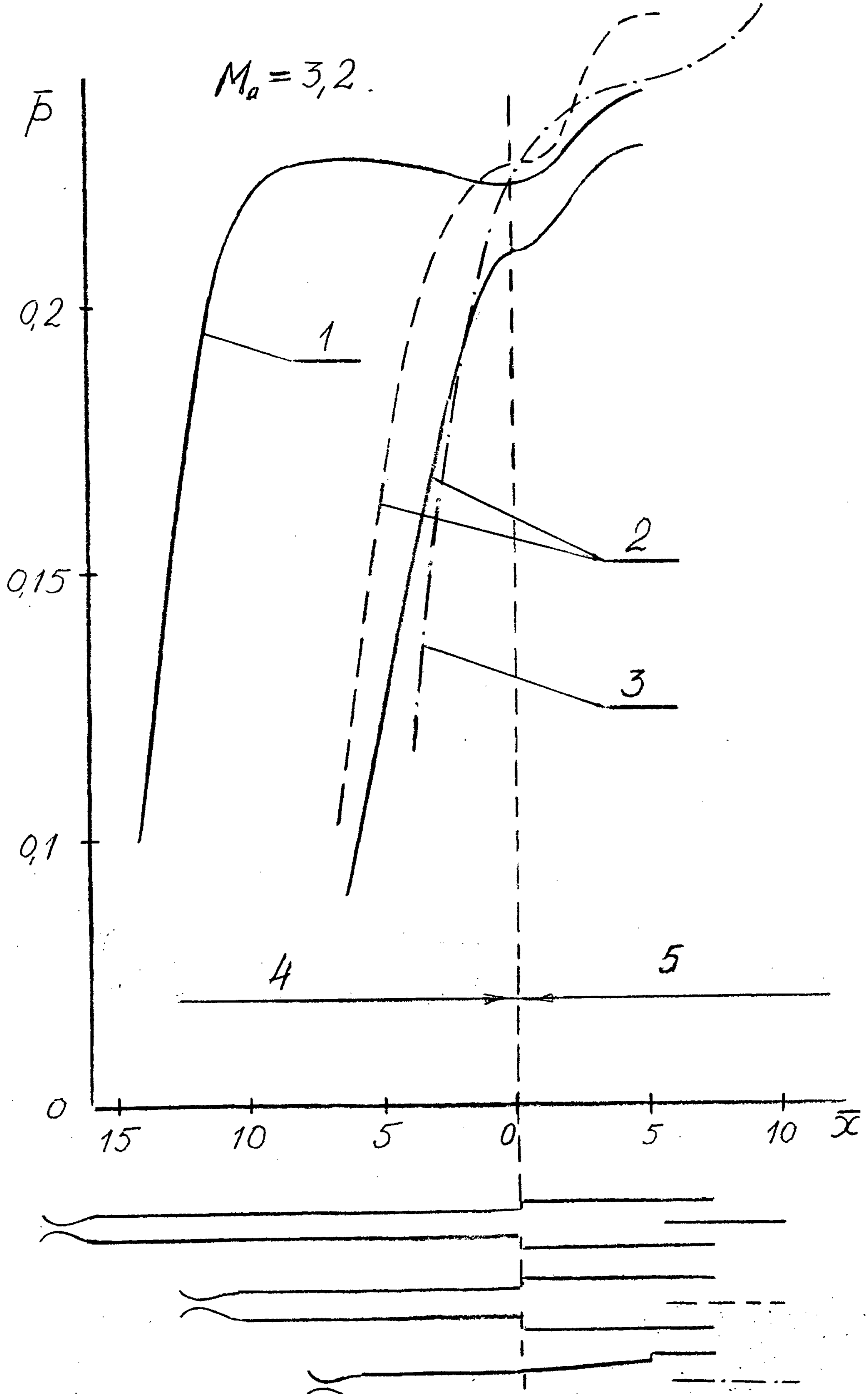

Fig. 4.7.2 Pressure distribution in circular supersonic/subsonic diffuser, M_a=3.21-3 flow

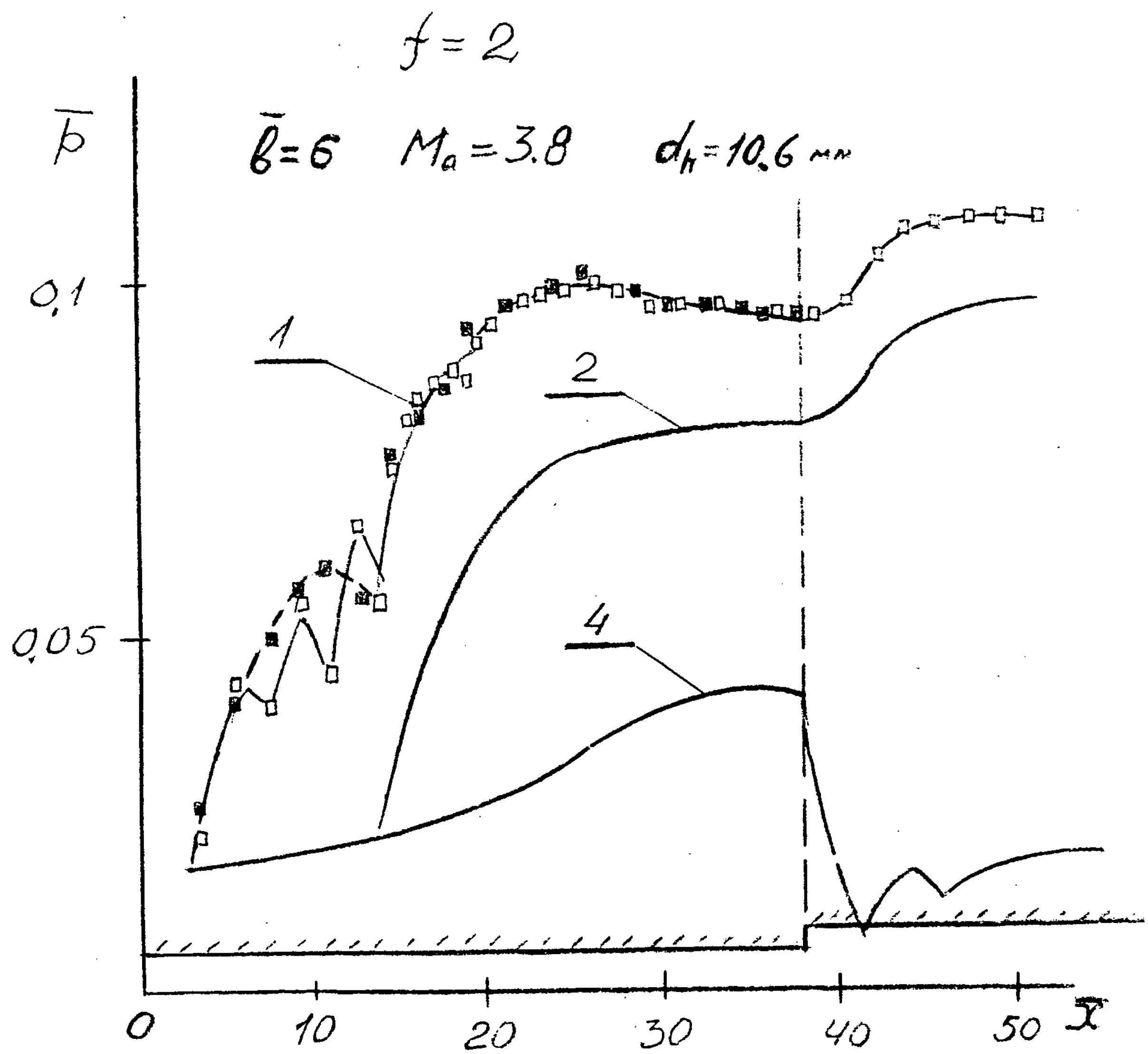

Fig. 4.7.3 Pressure distribution in rectangular supersonic/subsonic diffuser,
M_a=3.8, f=2, b=6, d_h=10.6 mm, 1-4 numbers of regimes

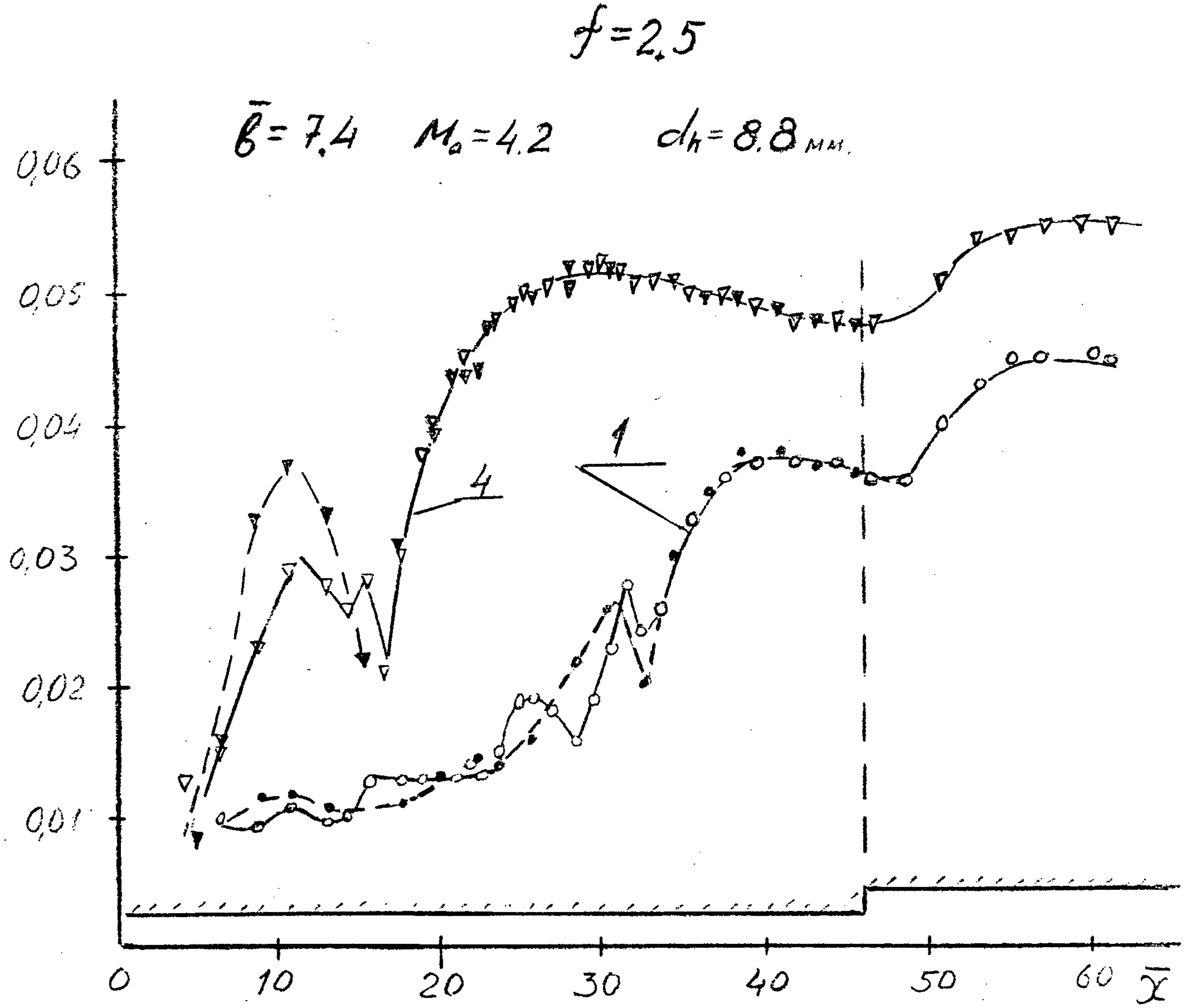

Fig. 4.7.4 Pressure distribution in rectangular supersonic/subsonic diffuser, M_a=4.25, f=2.5, b=7.4, d_h=8.8 mm, 1-4 numbers of regimes

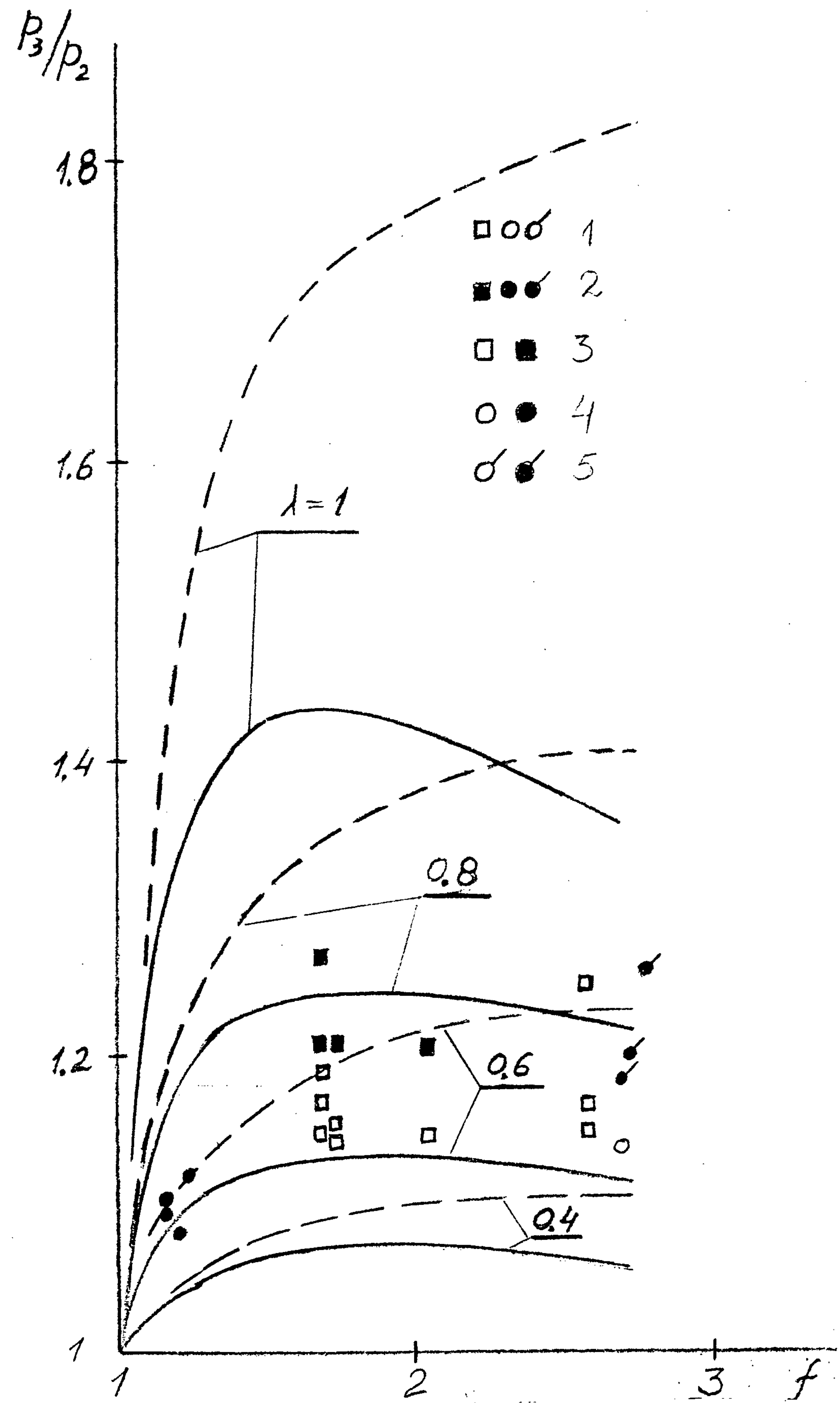

Fig. 4.7.5 Pressure recovery p_3/p_2 vs f in subsonic part of diffuser at different velocity coefficients λ in front of diverging section of the duct.
1-regime 1, 2-2, 3-rectangular, 4-circular ($\theta=90^0$, 0.5^0) ducts, 5-circular duct ($\theta=11^0$), theory:— step,---- isentropic.

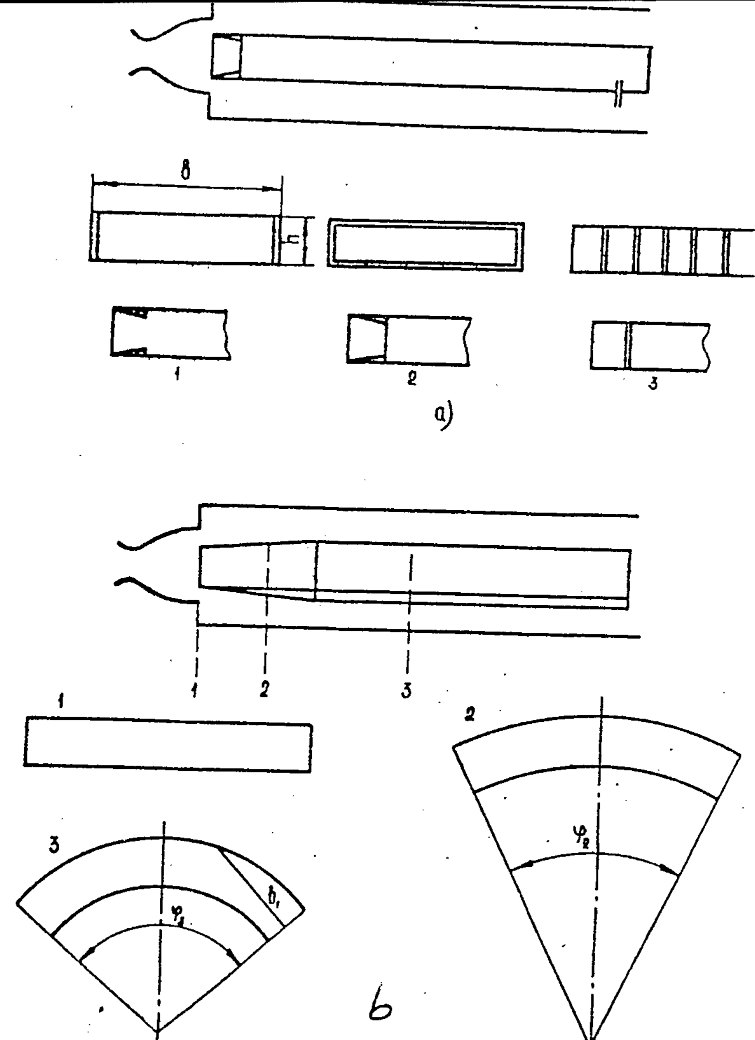

Fig 5.1 Models installation schematic
a)-rectangular ducts with wedges and wires
1- wedges on two walls, 2-on four walls
3-uniformly installed wires
b)-variable cross section duct
1-3-cross sections of the duct

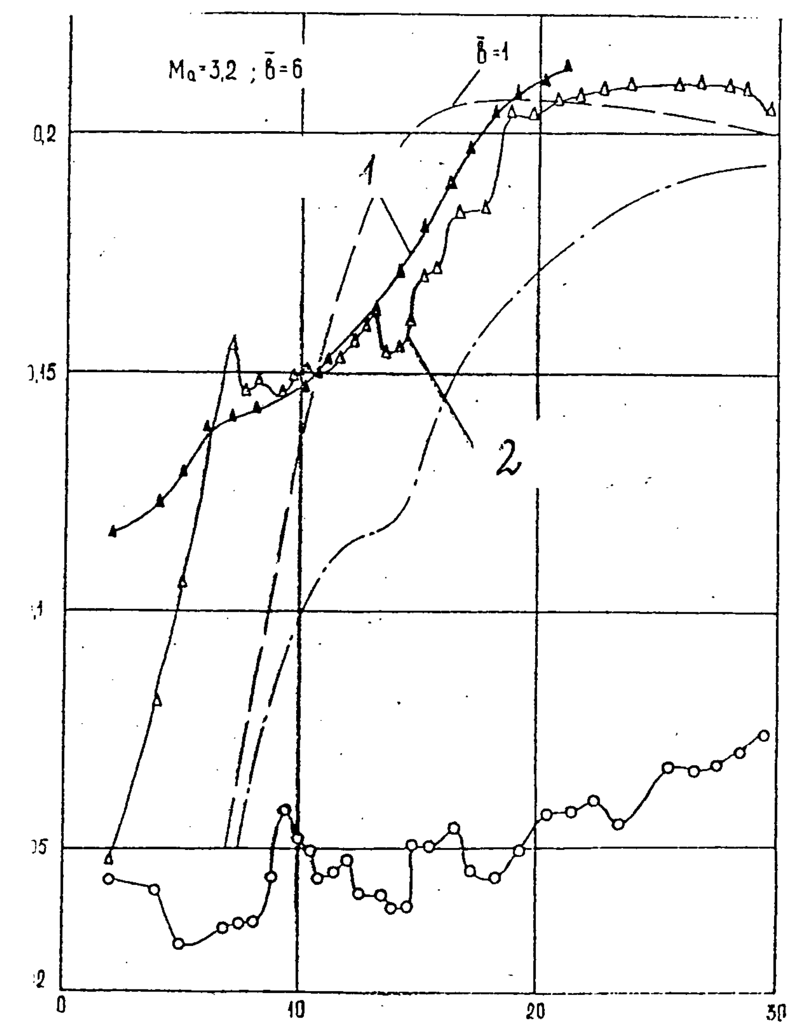

Fig.5.1.1 Pressure distribution along the rectangular duct, b=6 with wedges at the entrance. M_a=3.2
1-narrow, 2- wide walls

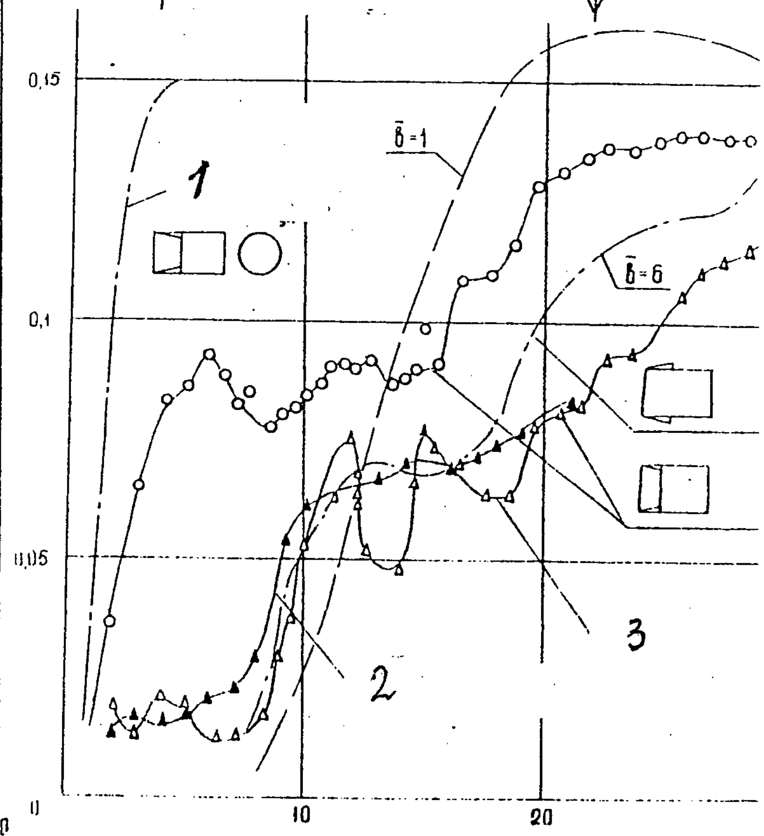

Fig. 5.1.2 Pressure distributions along rectangular ducts with wedges at the entrance, M_a=3.8
1-circular jut, 2- narrow, 3- wide walls.

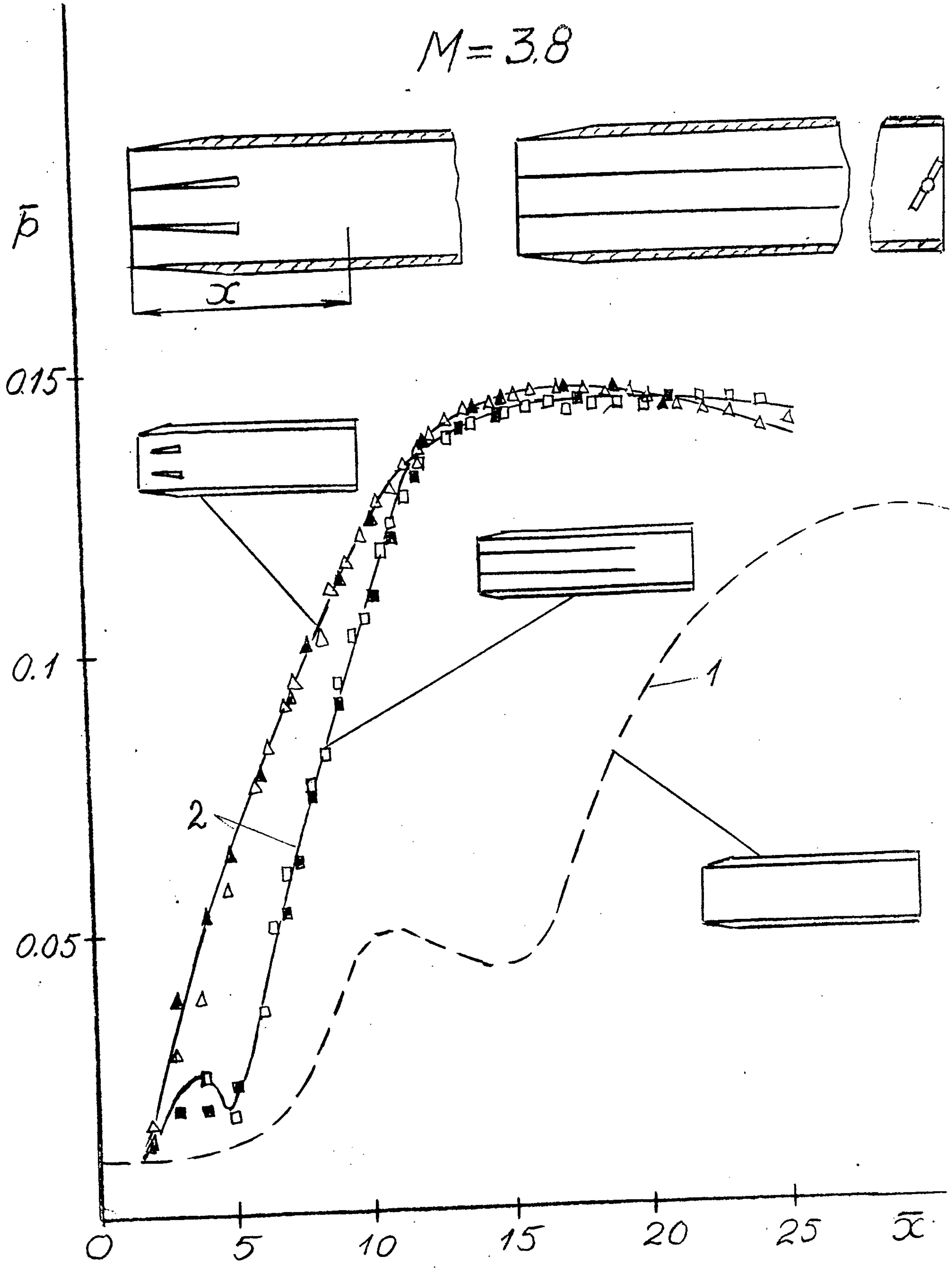

Fig. 5.1.3 Transformation of separation flow into pseudo-shock in rectangular duct, b=6, M_a=3.8 due to wedges and partitions installations.
1-separation flow, 2- pseudo-shock

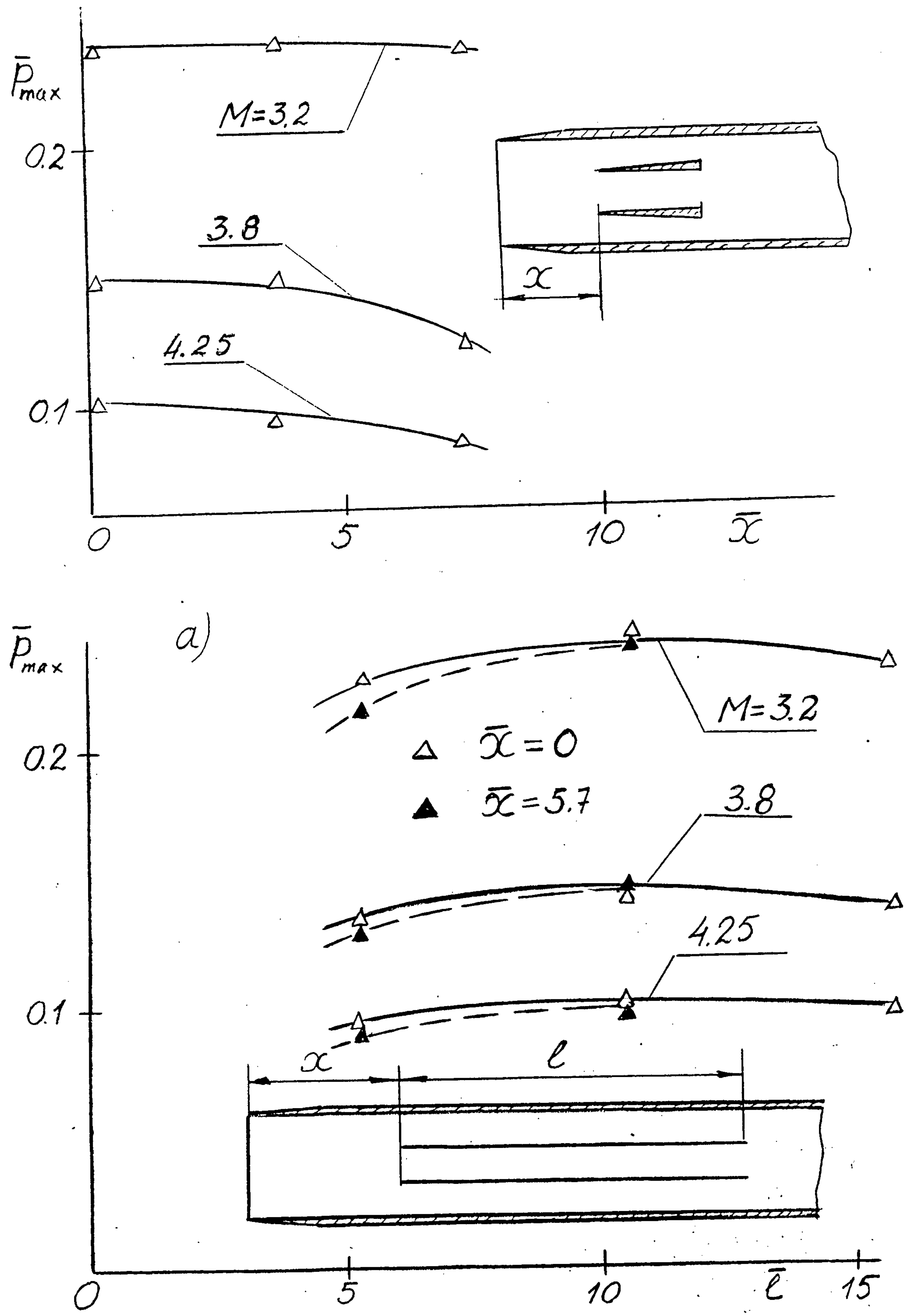

Fig. 5.1.4 Pressure recovery dependence on wedges and partitions disposition and length.

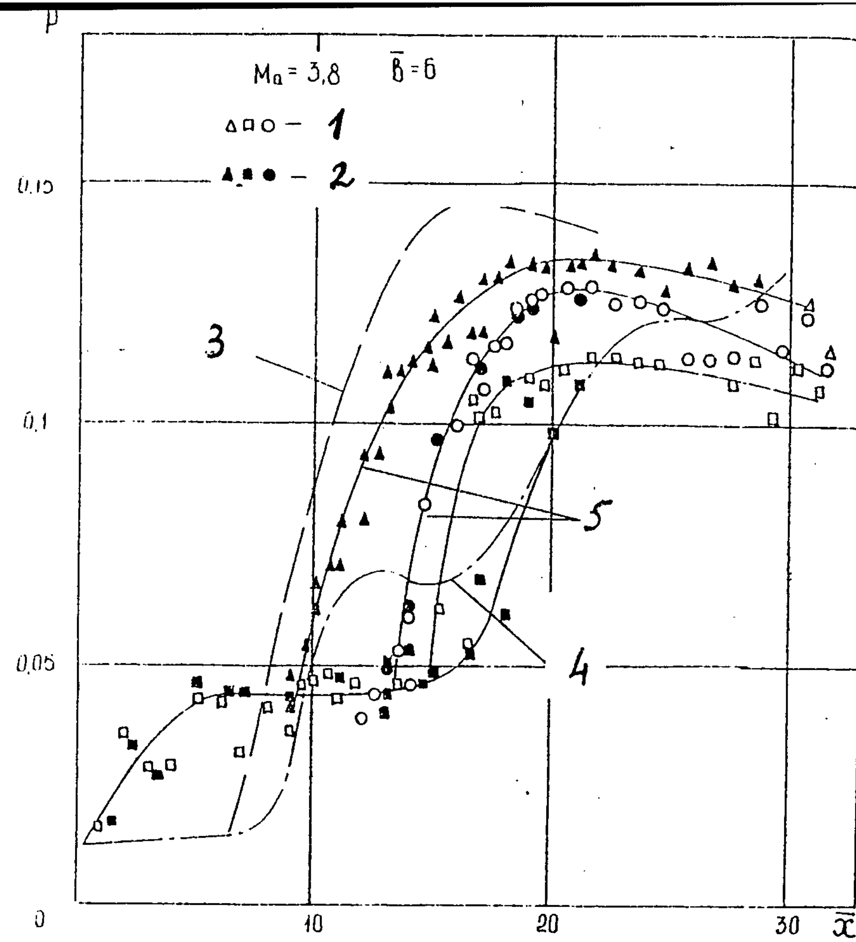

Fig. 5.2.1 Transformation of separation flow into pseudo-shock due to variation of cross section shape along the duct length, b=6, M_a=3.8
1-wide, 2-narrow walls, 3-circular, 4-rectangular duct

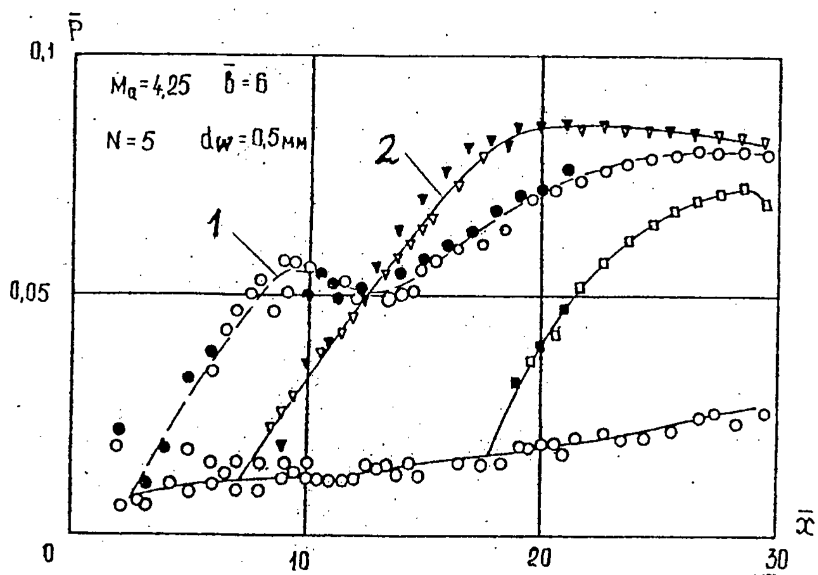

Fig. 5.3.1 Transformation of separation flow into pseudo-shock due to installation of 5 wires, 0.5 mm diameter into rectangular duct, b=6 at M_a=4.25
1-separation flow, 2- pseudo-shock

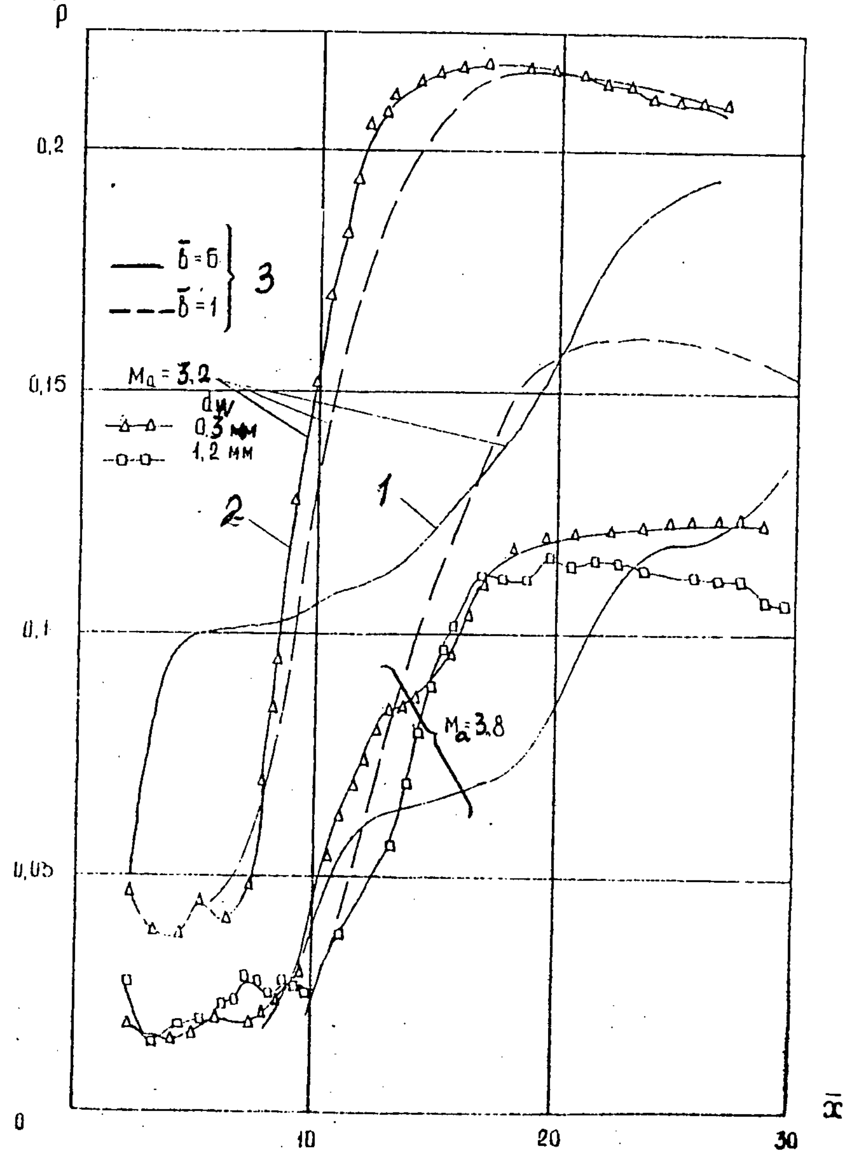

Fig. 5.3.2 Transformation of separation flow into pseudo-shock due to installation of 5 wires, 0.5 and 1.2 mm diameter into rectangular duct, b=6 at M_a=3.2 and 3.8
1-separation flow, 2- pseudo-shock, 3-smooth duct

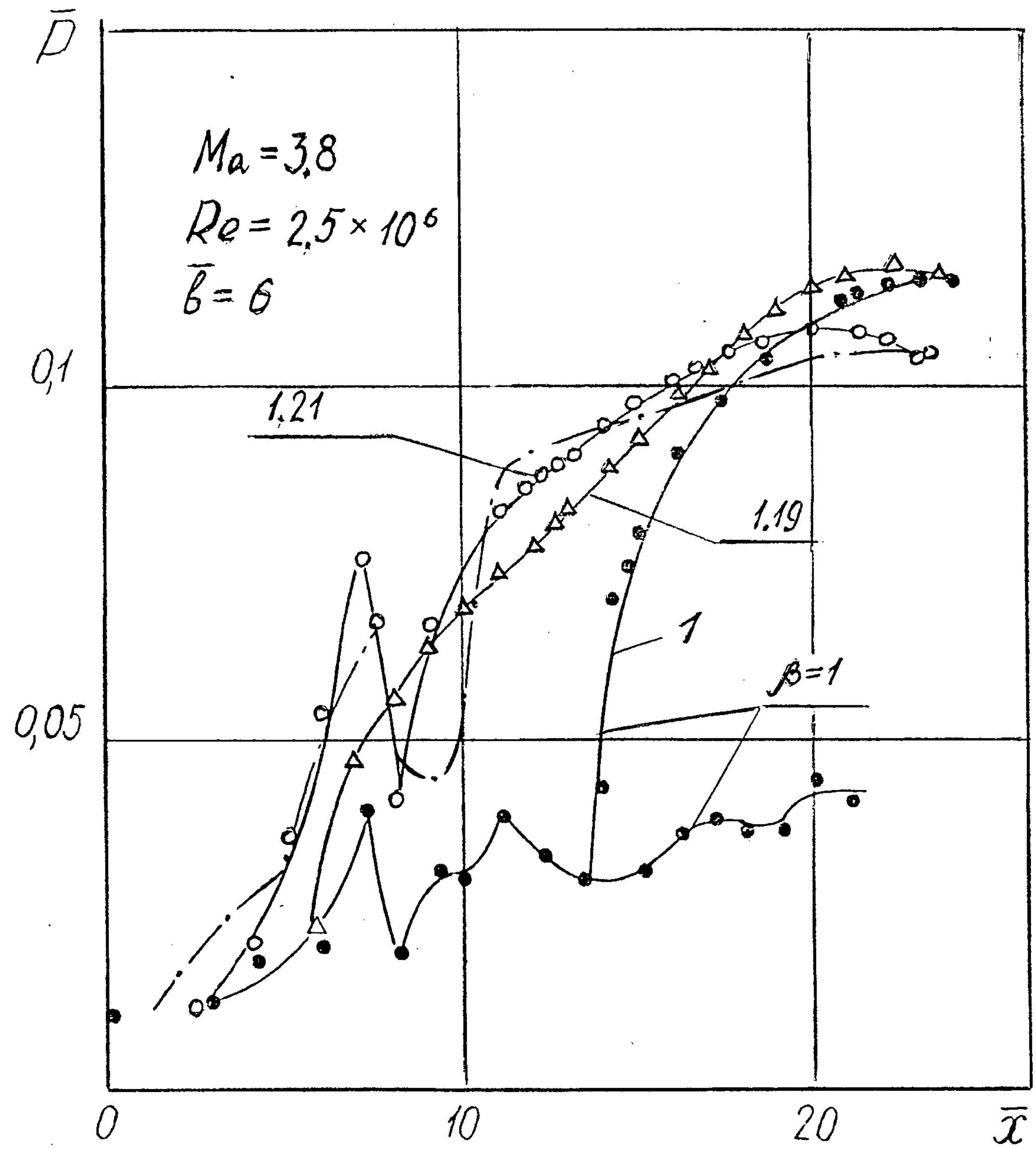

Fig 5.4.1 Pressure distribution in rectangular, b=6, duct at M_a=3.8 at different jet injections.

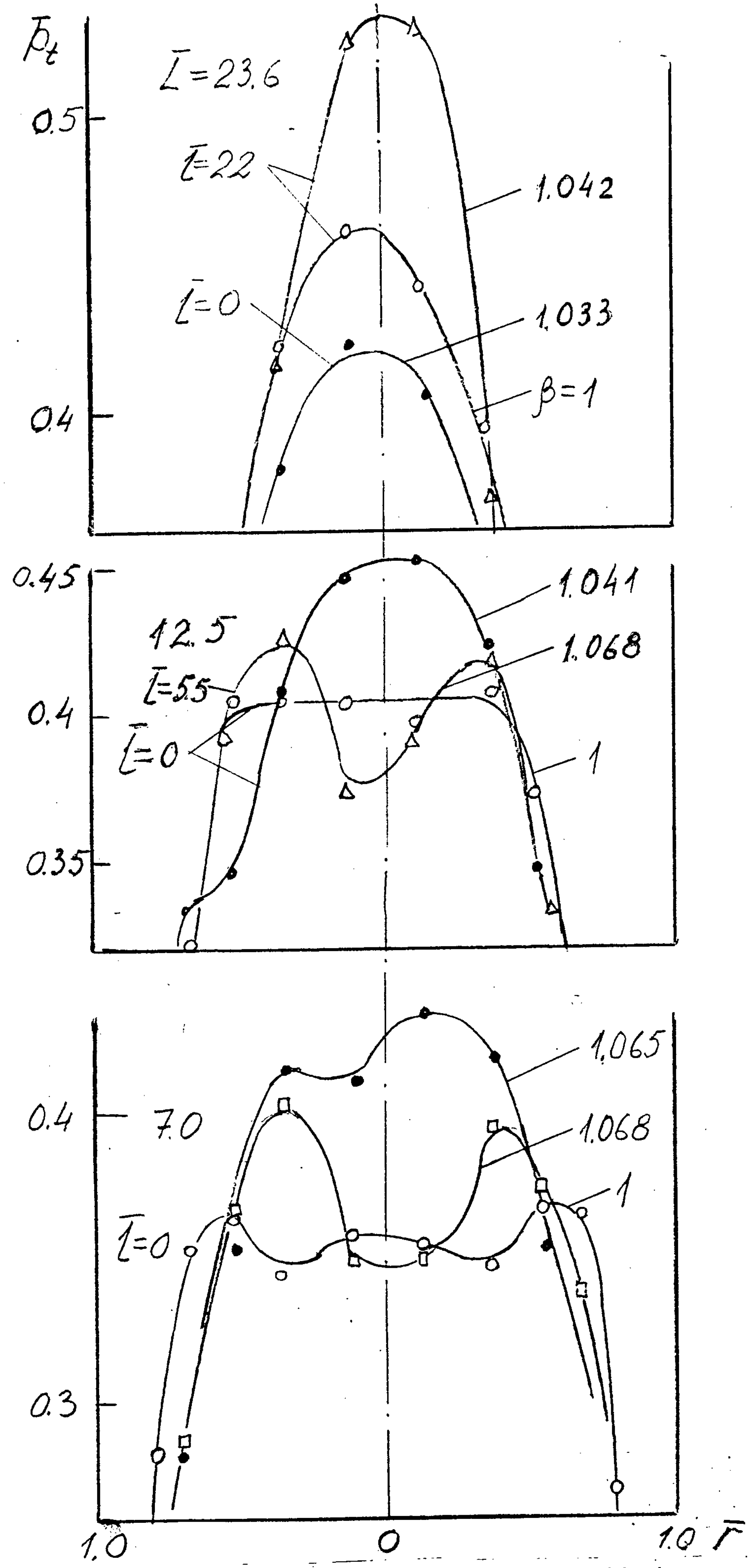

Fig. 6.1.1 Total pressure fields at the end of the pipe
Different jet injection. L-relative length of the pipe,

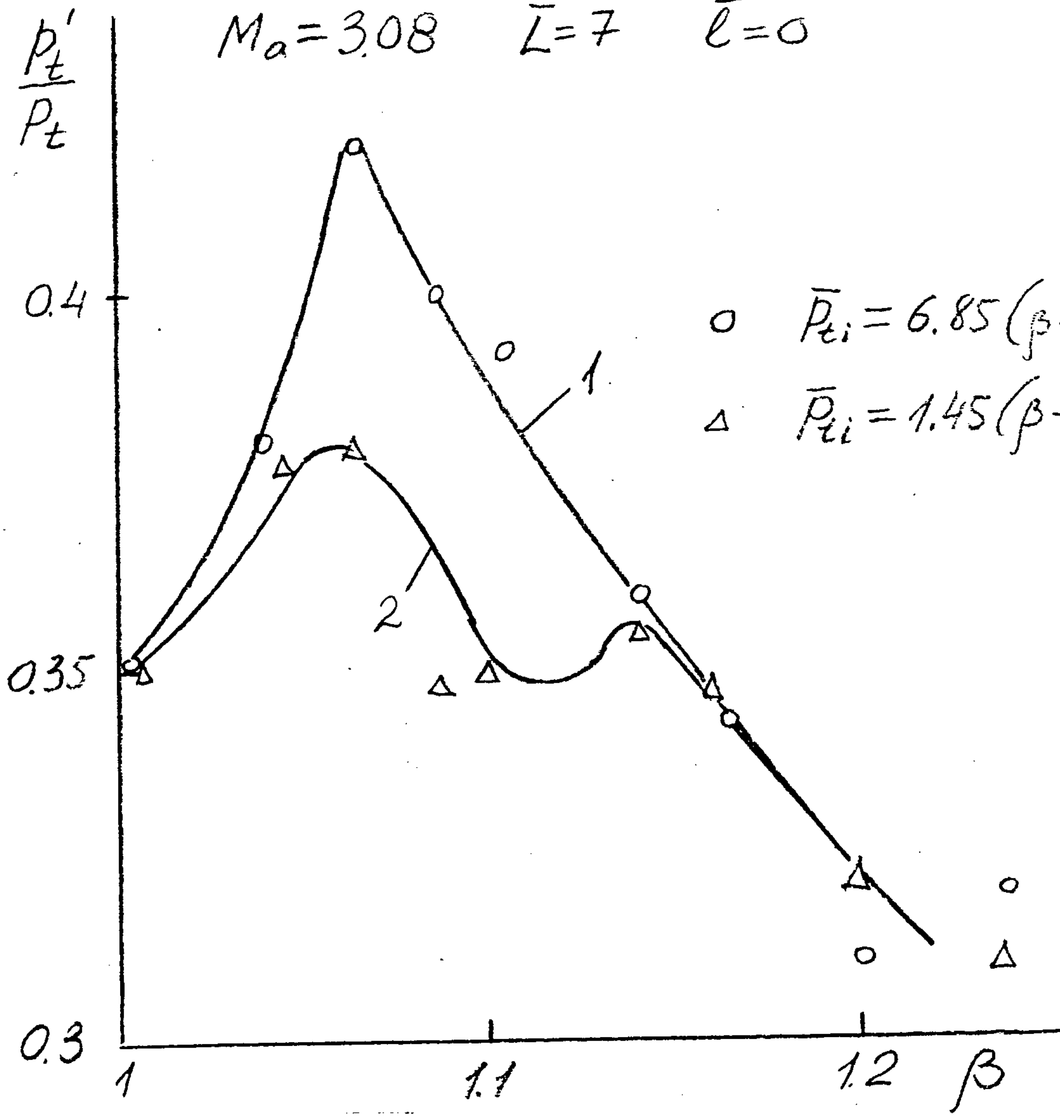

Fig. 6.1.2 Dependence of average Pitot tube pressure on β, M_a=3.08, L=7, l=0, 1-high pressure, 2-low pressure injection.

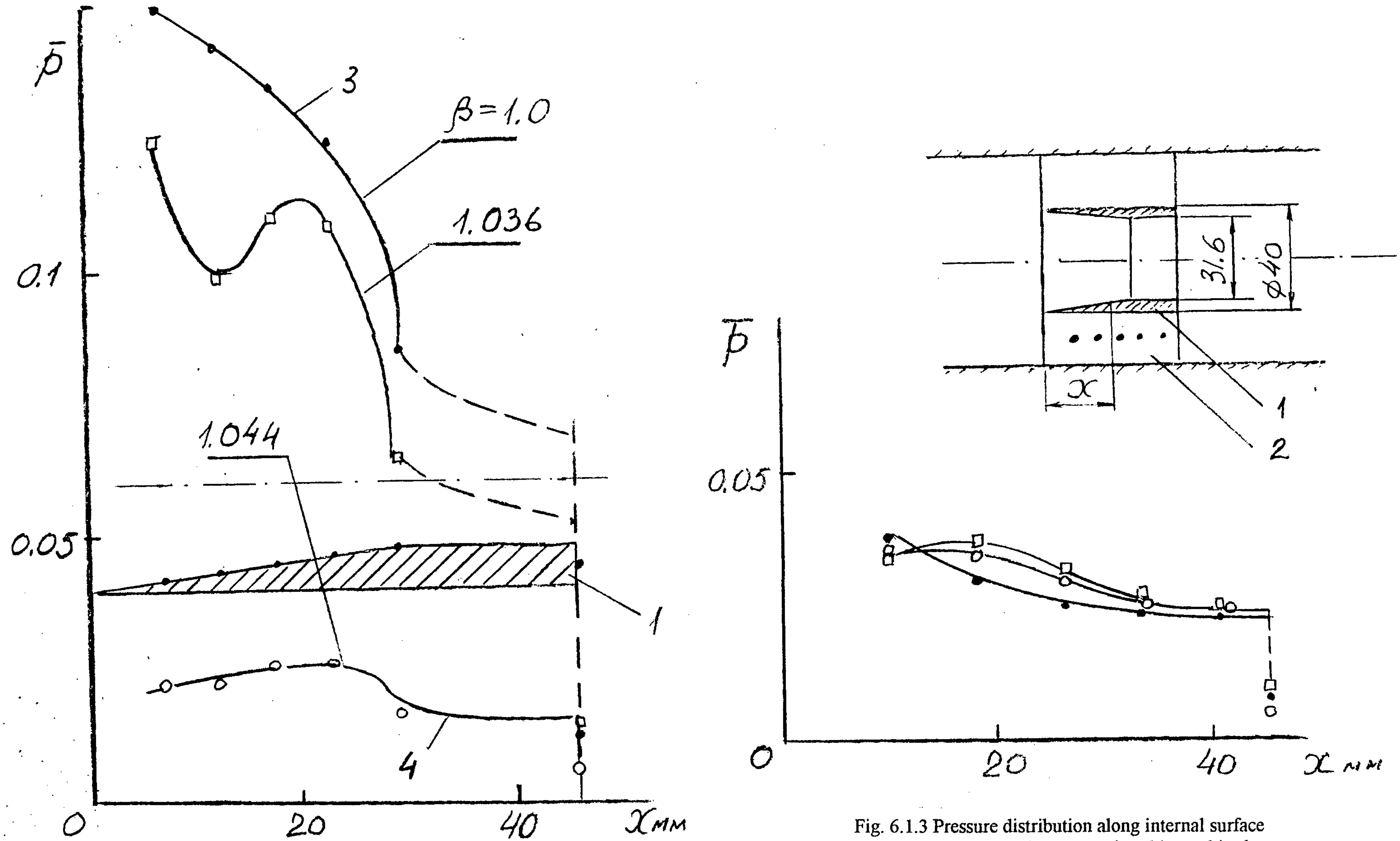

Fig. 6.1.3 Pressure distribution along internal surface of conical cowl and pylon supporting this cowl in the pipe at different jet injections. 1-cowl, 2-pylon, 3- non started channel, 4-started up channel.
● -β =1, □ -β =1.036, ○ -β =1.044

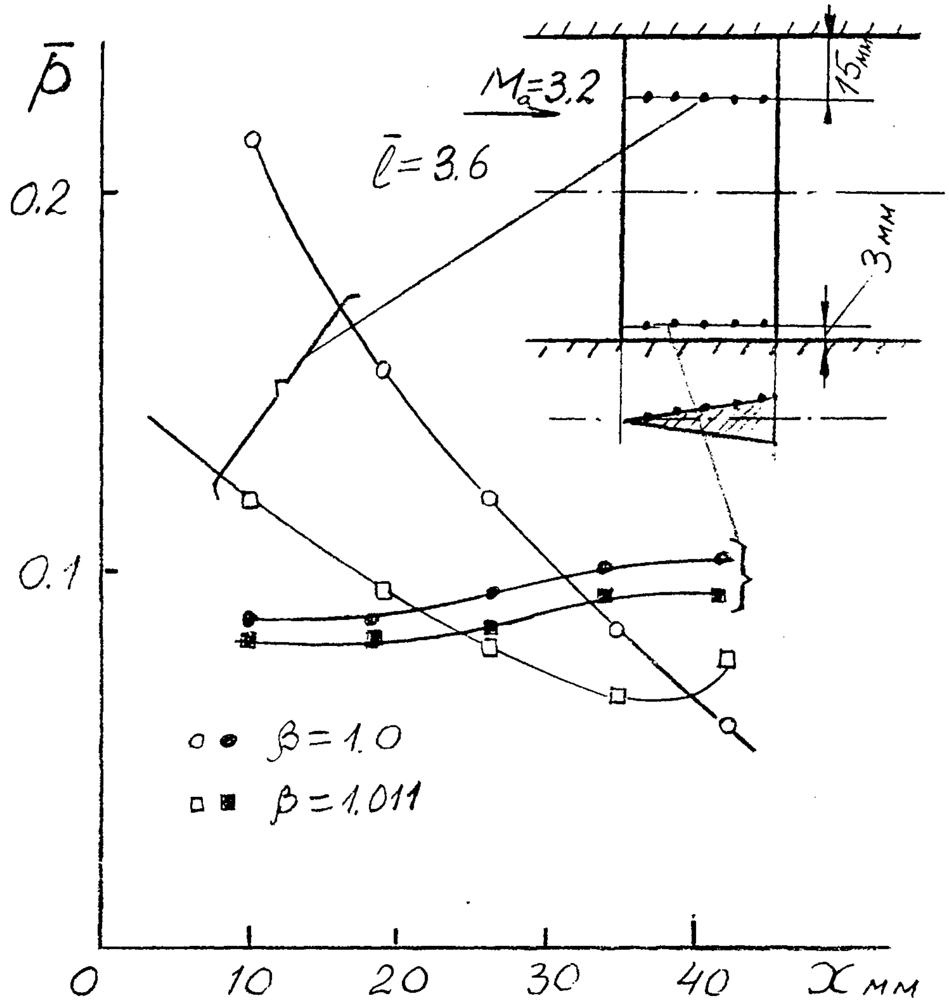

Fig. 6.1.4 Pressure distribution along wedge crossing the pipe at different jet injections

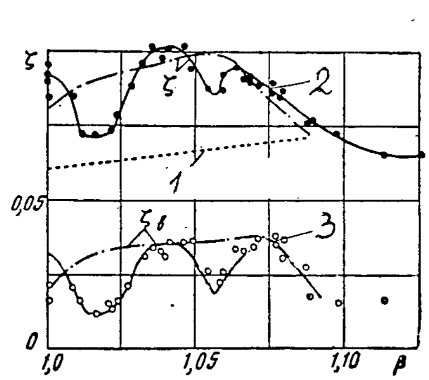

Fig. 6.2.1 Cavity Impulse loss coefficient ξ dependence on jet injection coefficient β
1-no cavity, 2-duct drag, 3-cavity drag.
— high pressure, — • —low pressure injecion

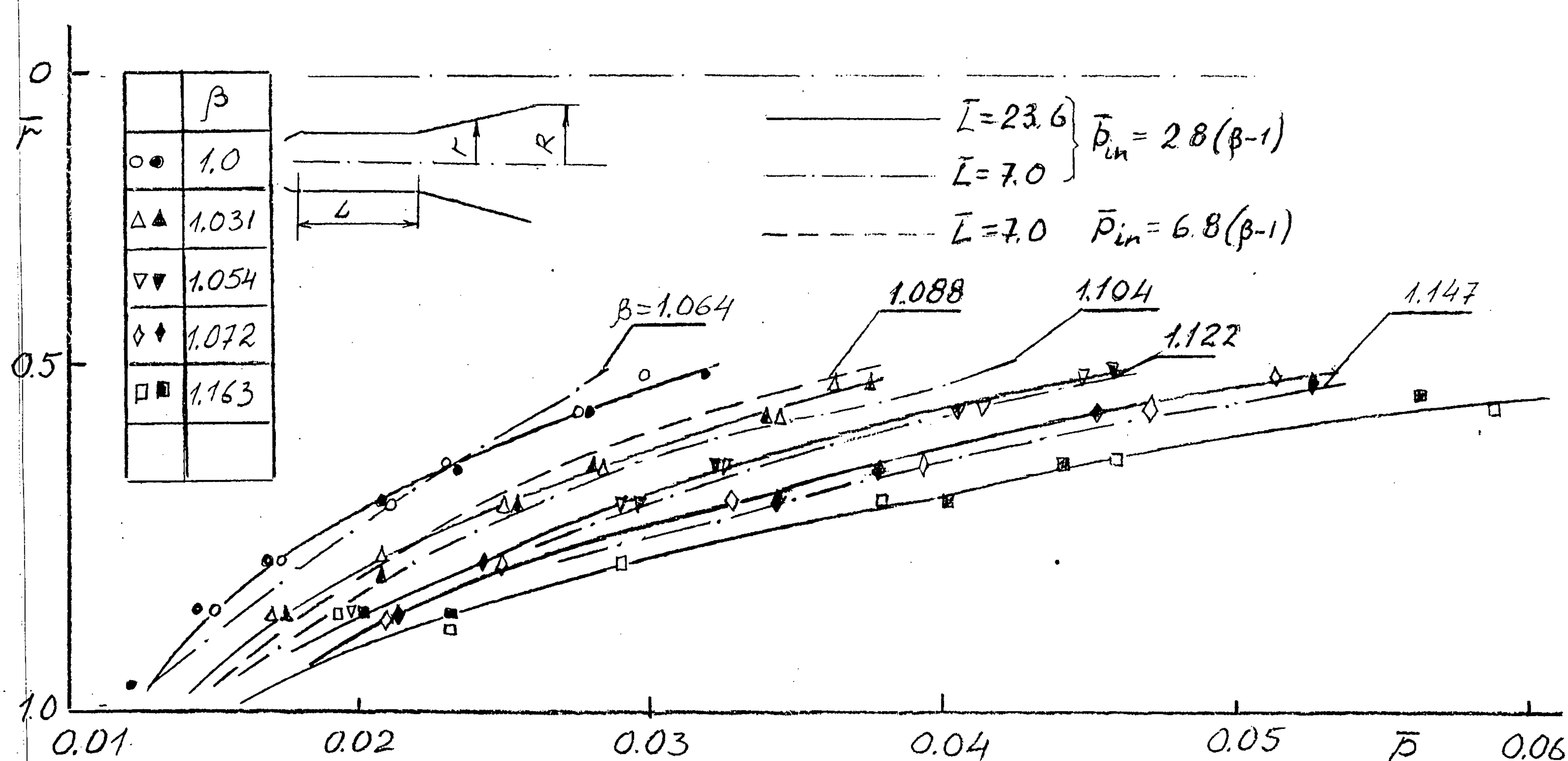

Fig. 6.2.2 Pressure distribution along conical duct at different jet injections and length of ducts.
— L=23.6, — • —l= 7, low pressure injection,
••—l=7, high pressure injection

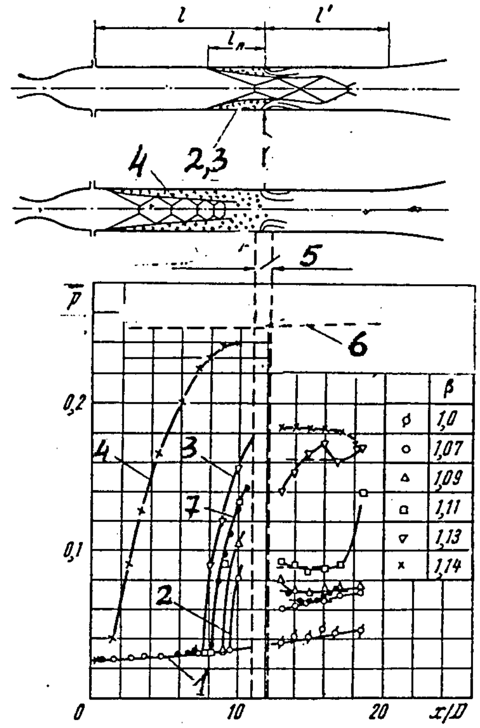

Fig.6.3.1 Comparison of pressure distributions along the pipe with annular jut and jet injection. M_a=3.08 , 1- msupersonic flow, 2-3-pseudo-shock arising, 4-developed pseudo-shock, 5-injection section, 6- pressure downstrem of normal shock M_a=2.8, 7,- upstream of annular jut.

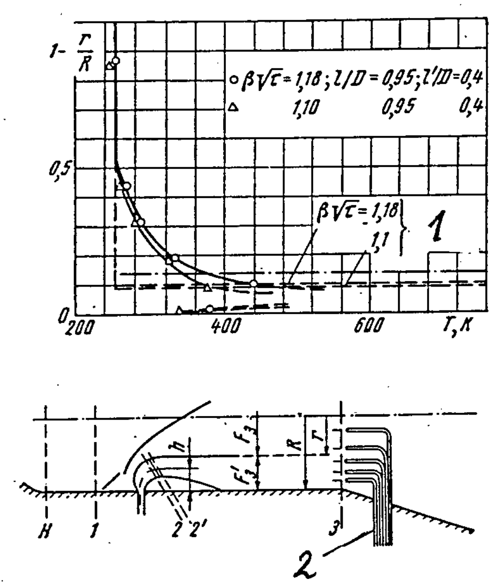

Fig. 6.3.2 Flow model schematic. Temperature profile for two values of jet injection pressure P_t T_{it}=750K, 1-theory, 2- rakes of P_t,T_t

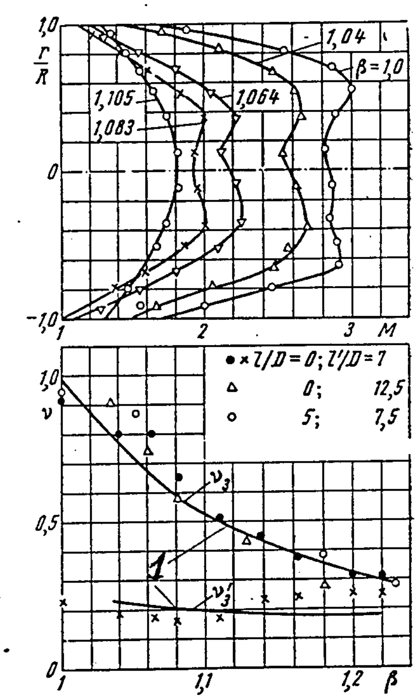

Fig. 6.3.3 M-profile and total pressure recovery coefficients dependences on jet injection. . 1-theory

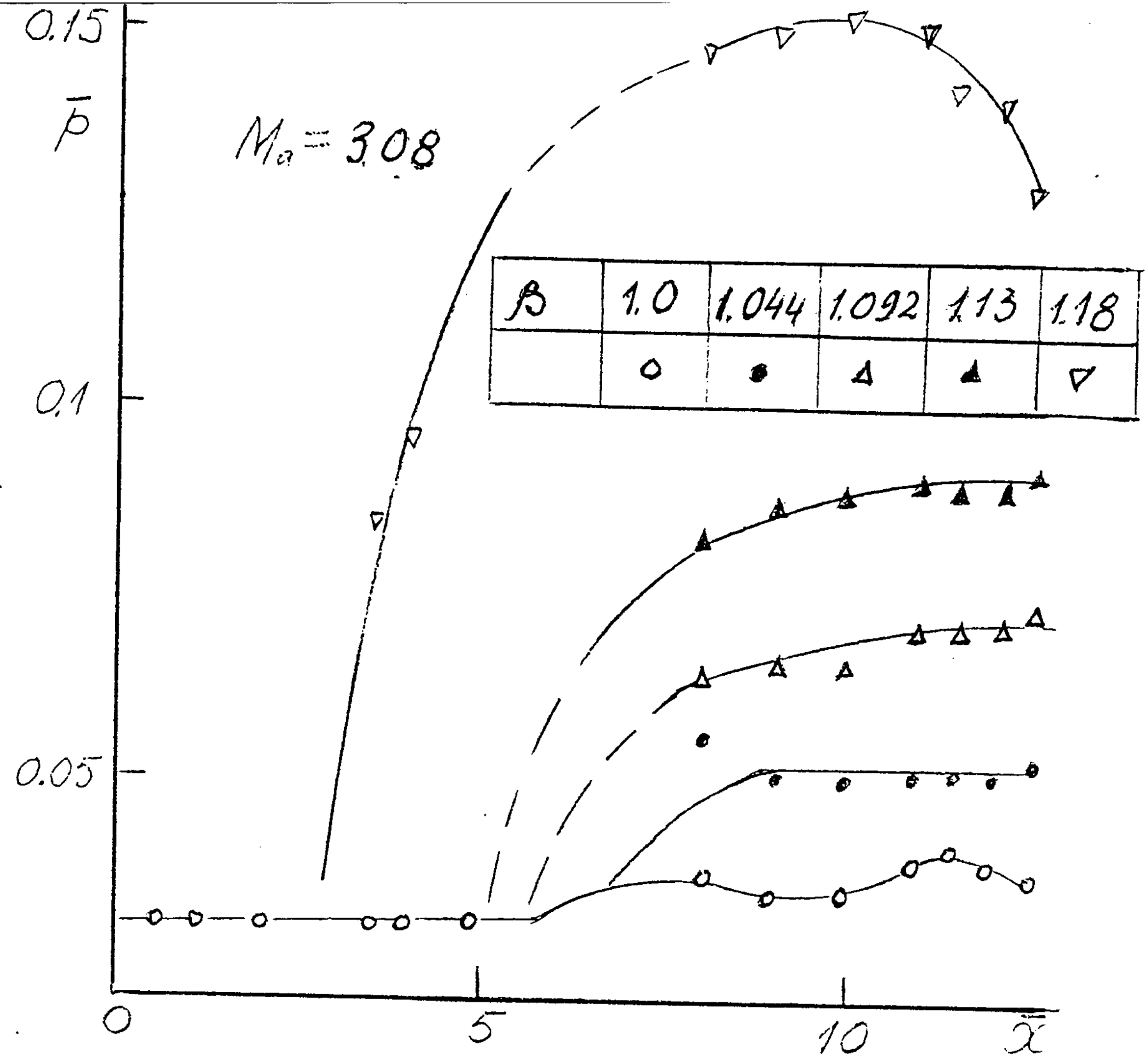

Fig. 6.4.1 Pressure distribution along the pipe at dispersed low pressure jet injection

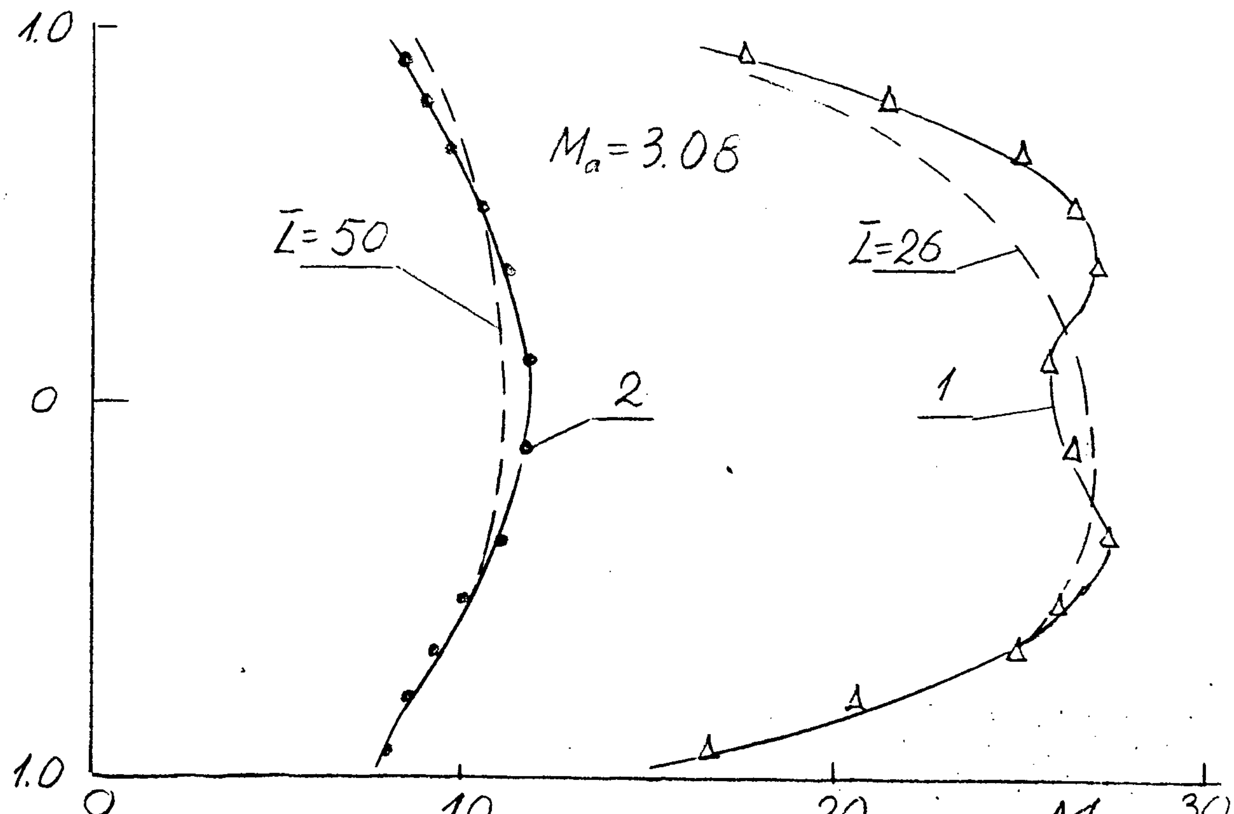

Fig. 6.4.2 Comparison of M-fields at the end of the long pipe (50d) without injection and short pipe (7d) with injection, $M_a = 3.08$

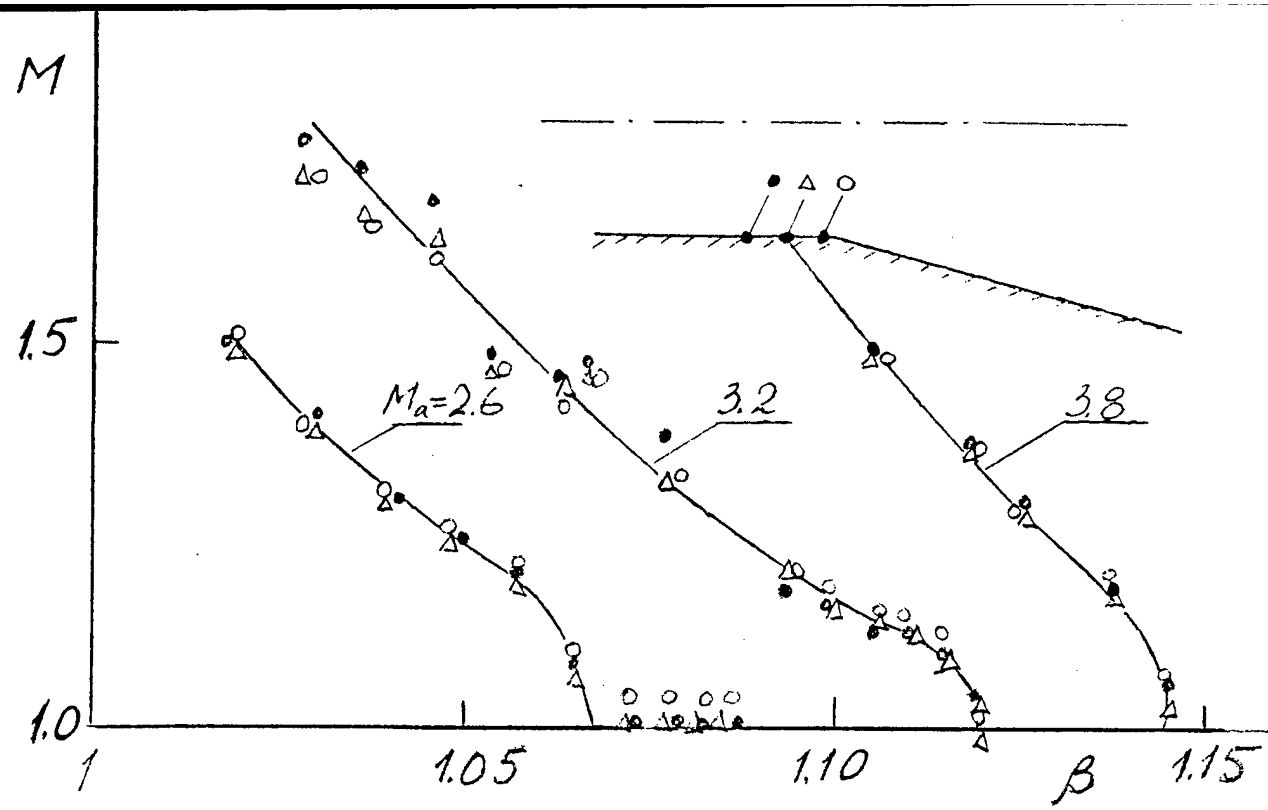

Fig. 6.4.3 Pipe end average M dependence on jet injection for different M_a,L= ,l=0

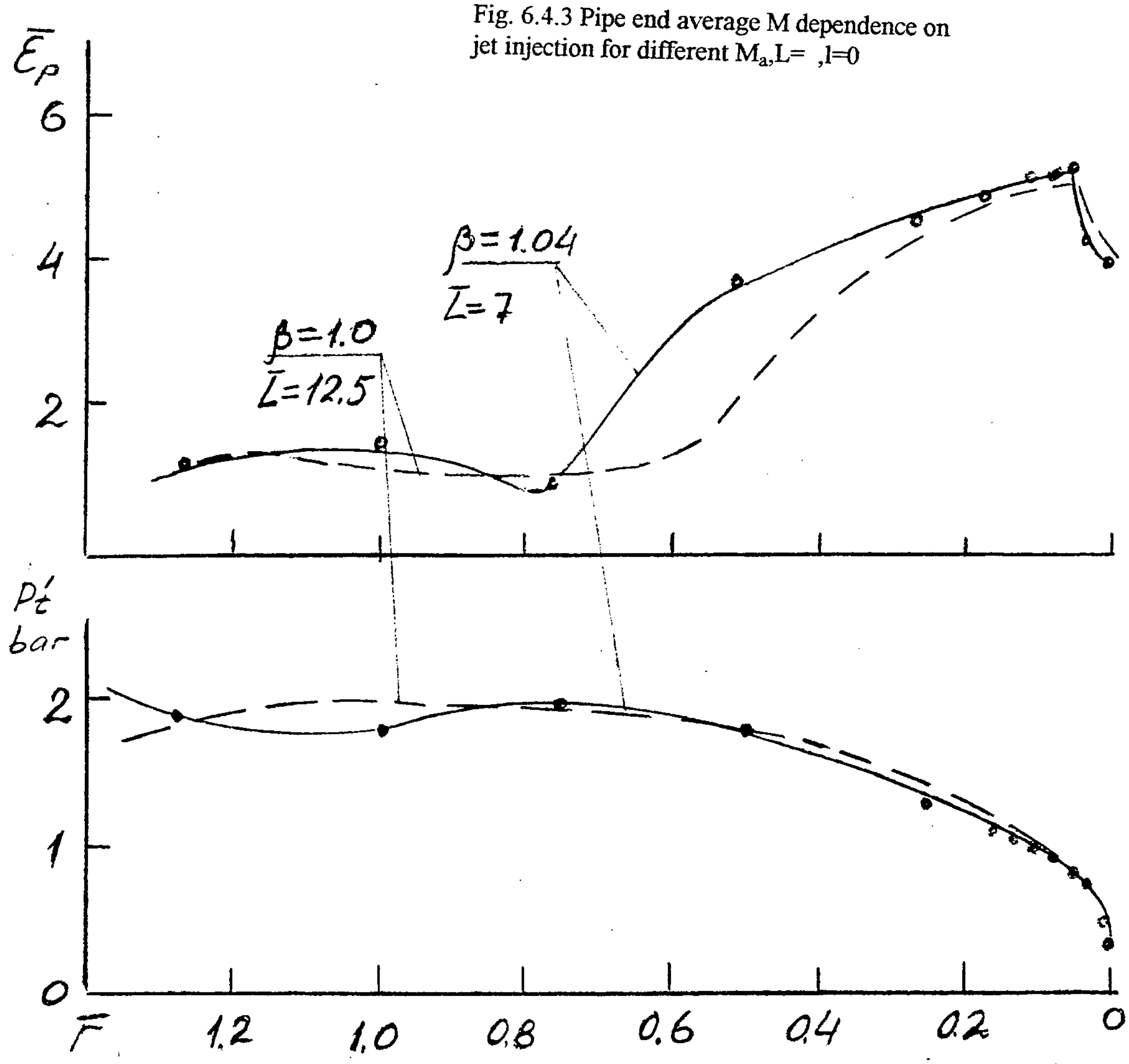

Fig. 6.4.4 Comparison of pulse characteristics in long pipe and short pipe with injection.
—-L=12.5, no injection — L=7, β=1.04

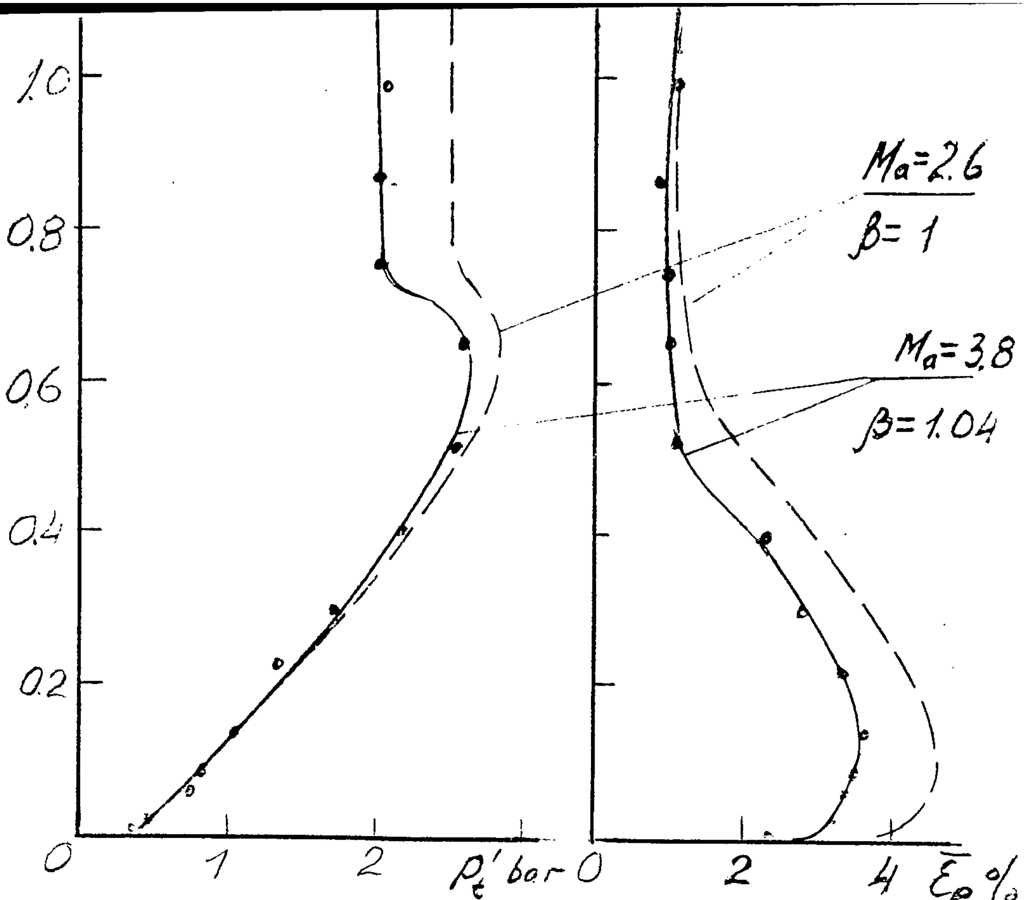

Fig. 6.4.5 Comparison of pulse characteristics
in pipe with different M_a and β
----M_a=2.6, β=1, — M_a=3.8, β=1.04, l=12.5

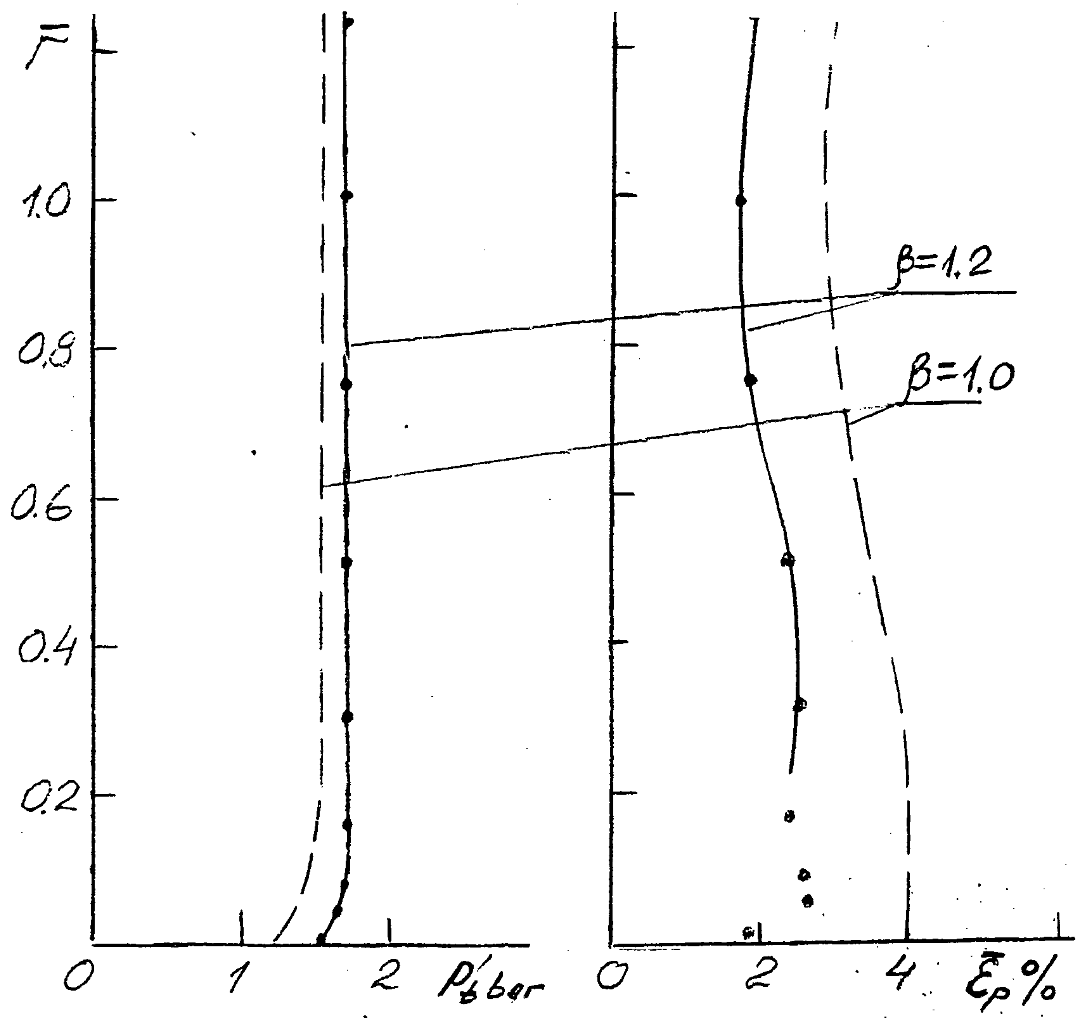

646

Fig. 6.4.6 Comparison of pulse characteristics
at the end of pseudo-shock, received by throttling
and jet injection, M_a=3.8, l=12.6